Genetic And Transcriptomic Approaches To Understanding And Engineering Terpenoid Biosynthesis In *Mentha x piperita*

Alistair Haris Fadzil Holland

A thesis submitted for the degree of
Doctor of Philosophy

Cardiff University

September 2025

Summary

Mentha × *piperita* cv. Black Mitcham is an economically important aromatic crop valued for its essential oil, particularly the monoterpenoid menthol. This thesis focuses on developing experimental platforms to investigate and engineer the menthol biosynthetic pathway. An efficient in vitro regeneration protocol utilising 1-naphthaleneacetic acid and thidiazuron was established, enabling rapid callus formation and de novo shoot induction. Three transformation strategies were explored, with biolistic delivery of exogenous DNA and direct injection of *Agrobacterium tumefaciens* yielding the most consistent transgene expression. Heterologous reconstitution of menthol biosynthesis was attempted in *Nicotiana benthamiana and Arabidopsis thaliana*. Transient and stable expression of *Mentha x piperita GERANYL DIPHOSPHATE SYNTHASE SMALL SUBUNIT, Picea abies LIMONENE SYNTHASE, and Mentha x piperita LIMONENE-3-HYDROXYLASE in Nicotiana benthamiana* enabled production of limonene and (–)-*trans*-isopiperitenol, while stable transformation in *Arabidopsis thaliana* generated additional intermediates. Additionally, increasing the supply of terpenoid precursors by co-expression of *Nicotiana tabacum 1-DEOXY-D-XYLULOSE 5-PHOSPHATE SYNTHASE* increased precursor availability, enhancing limonene production. Essential oil profiling revealed dynamic changes across development, with menthone and menthol displaying reciprocal changes between vegetative and reproductive growth phases. RNA-seq transcriptomic analysis was performed to link these compositional changes to gene expression. This transcriptomic survey provided a genome-wide view of developmental regulation, identifying developmental stage-specific expression patterns of key pathway genes. Clustering and promoter motif analysis further suggested candidate transcription factors that may regulate menthol biosynthesis, while additional genes encoding putative biosynthetic enzymes were uncovered. Together, this work delivered novel regeneration and transformation strategies for peppermint, established heterologous model systems for menthol biosynthesis pathway intermediate biosynthesis, and provided regulatory insights from transcriptomics, laying the foundation for metabolic engineering of menthol in *Mentha x piperita* cv. Black Mitcham and alternative plant hosts.

Table of Contents

Acknowledgements

I would like to express my deepest gratitude to my PhD supervisors Dr Simon Scofield and Prof. John Pickett for the guidance, support and knowledge offered throughout this journey. Id like to thank the Biotechnology & Biological Sciences Research Council and South West Biosciences Doctoral Training Partnership for funding this project. I'd like to thank Prof. John Harwood for his role in being on my review panel, and the support and advice provided at our progress monitoring meetings. I'd like to thank Dr Richard Ludlow and Dr Carsten Müller for allowing me access to the Cardiff University Small Molecules Hub to undertake my chemical analytics work, and for support, guidance and training for all chemistry related work. Many thanks to Dr Tamara Lechon Gomez for the support, guidance and training with the bioinformatics analysis. Thank you Dr Ryan Coates for the guidance, training and discussions for the transient expression work in tobacco. I'd like to thank the members of the W 3.10 lab, past and present, for making the work environment such an enjoyable experience. Many thanks to my friends and family, who have reminded me throughout this PhD journey that I am capable. Finally, I'd like to express my heartfelt gratitude to Emily Darby for her unwavering support throughout this PhD, and for the continued support in the journey ahead.

List of Abbreviations

Abbreviation	Meaning
DNA	Deoxyribonucleic acid
RNA	Ribonucleic acid
cDNA	Complementary deoxyribonucleic acid
mRNA	Messenger ribonucleic acid
UTR	Untranslated region
PCR	Polymerase chain reaction
RT-PCR	Reverse transcription polymerase chain reaction
RT-qPCR	Reverse transcription quantitative PCR
qPCR	Quantitative polymerase chain reaction
RNAseq	RNA sequencing
RNase	Ribonuclease
DNase	Deoxyribonuclease
ATP	Adenosine triphosphate
NAD / NADP	Nicotinamide adenine dinucleotide / phosphate
FW	Fresh weight
M. x piperita	*Mentha × piperita*
cv.	Cultivar
A. thaliana	*Arabidopsis thaliana*
N. benthamiana	*Nicotiana benthamiana*
N. tabacum	*Nicotiana tabacum*
A. tumefaciens	*Agrobacterium tumefaciens*
E. coli	*Escherichia coli*
P. putida	*Pseudomonas putida*
MBP	Menthol biosynthesis pathway
MEP	2-C-methyl-D-erythritol 4-phosphate
MVA	Mevalonate pathway
IPP	Isopentenyl diphosphate
DMAPP	Dimethylallyl diphosphate
GPP	Geranyl diphosphate

HMB-PP	(E)-4-hydroxy-3-methyl-but-2-enyl diphosphate
GPPS	Geranyl diphosphate synthase
GPPS.SSU	Geranyl diphosphate synthase, small subunit
GPPS.LSU	Geranyl diphosphate synthase, large subunit
LimS	(−)-limonene synthase
L3H	(−)-limonene 3-hydroxylase
L6H	(−)-limonene 6-hydroxylase
IPDH	(–)-trans-Isopiperitenol dehydrogenase
IPR	(–)-Isopiperitenone reductase
IPGI	(+)-cis-Isopulegone isomerase
PGR	(+)-Pulegone reductase
MMR	(–)-Menthone:(–)-menthol reductase
MNMR	(–)-Menthone:(+)-neomenthol reductase
MFS	(+)-Menthofuran synthase
KSI	Ketosteroid isomerase
PGRs	Plant Growth Regulators
TF	Transcription Factor
DEG	Differentially Expressed Gene

Chapter 1 - Introduction

1.1 Plant secondary metabolites – essential oils, monoterpenoids and their importance

The study of aromatic plants has been a focus of great interest, due to their global importance in the agricultural sector, both from an academic and industrial perspective. Interest in aromatic plants stems from the secondary metabolites they produce, which are small molecules produced by the plant to give them a competitive advantage in their own native environments (Teoh 2015). Plant secondary metabolites are involved in a variety of roles, such as growth, development, immunity, stress responses, pest and pathogen defence, plant-microbe signalling, insect attractants/repellents and shaping host-associated microbial communities (Piasecka et al. 2015; Guerrieri et al. 2019; Isah 2019; Yang et al. 2019b). Of these secondary metabolites, terpenoids (also known as terpenes or isoprenoids) represent one of the most chemically diverse group of natural products in nature, with over 80000 terpenoids found across the plant kingdom alone (Christianson 2017). Terpenoids are derived from C_5 isoprene units, which undergo head-to-tail coupling reactions to form higher order terpenoid structures (Poulter and Rilling 1978; Kellogg and Poulter 1997). They are categorised through the prefixes such as “mono-”, “sesqui-”, “di-”, “sester-” or “tri-”, according to the number of C_5 isoprene units making up the terpene backbone (Bergman and Phillips 2021) (Figure 1.1).

Classification	Carbon Atoms (Isoprene Units)	Chemical Structure
Monoterpenes	10 (2)	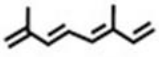
Sesquiterpenes	15 (3)	
Diterpenes	20 (4)	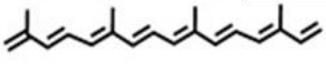
Sesterterpenes	25 (5)	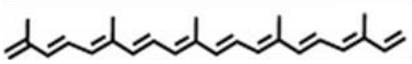
Triterpenes	30 (6)	

Figure 1.1. Outline of terpenoid classification and naming conventions. Figure adapted from (Mosquera et al. 2021)

Within the diverse terpenoid family, monoterpenes, derived from the coupling of two C_5 isoprene units to form a C_{10} backbone (Figure 1.1), hold particular economic and industrial significance in the flavour and fragrance sectors. Their low molecular weight and non-polar structures make them highly volatile compounds, a property central to their commercial value (Mołdoch et al. 2025). The baseline C_{10} backbone can be further modified by a range of chemical modifications such as cyclisation, reduction or decoration of their chiral sites with a host of different functional groups, all of which lead to an alteration in their biological properties (Ludwiczuk et al. 2017). These modifications can result in the modification of simple unsaturated hydrocarbons into constitutive alcohols, aldehydes or ketones (Singh 2007). Monoterpenes can be further classified as either acyclic, aliphatic, monocyclic or bicyclic (Mosquera et al. 2021). One of the most well characterised monoterpenoid pathways is that of the cyclic monoterpenoid (-)-menthol, which is known as the menthol biosynthesis pathway (MBP) (Croteau et al. 2005). Although menthol can exist as different stereoisomers, the (-)-menthol isomer is the most abundant in nature, and is of most commercial interest (Lawrence 2006; Patel et al. 2007). It is estimated that roughly 32000 metric tonnes of (-)-menthol is consumed annually, making (-)-menthol one of the most important flavouring products globally, just behind vanilla and citrus (Kamatou et al. 2013).

The (-)-menthol isomer forms a major constituent in the essential oil of *Mentha. x piperita* (*M. x piperita;* peppermint), and its use in a variety of commercial products from toothpastes to cigarettes highlights its commercial importance (Bergman and Phillips 2021). *M x piperita* essential oil can be defined as a volatile oil consisting of biologically active secondary metabolites formed from terpenoid derivatives, mainly including monoterpenes and sesquiterpenes (Dhifi et al. 2016; Muntean et al. 2019; Zhao et al. 2022). Outside of its widespread use in the flavouring industry, (-)-menthol has further been reported to have diverse biological properties that are applicable to the pharmaceutical, medical, cosmetic and even cleaning product industries (Nair 2001; Tucker and Naczi 2006; Eftekhari et al. 2021). The overall essential oil of *M. x piperita* has been reported to have a range of diverse properties such as insect repellent, anti-fungal, anti-microbial, anti-allergenic, anti-biofilm, anti-viral, anti-tumour promoting and anti-inflammatory, further highlighting the versatile properties and uses (Fuchs et al. 2022). The overall essential oil is composed of a

bouquet of other monoterpenes, such as (-)-limonene and (-)-menthone (intermediates in the MBP), which together contribute to the versatility of *M. x piperita* essential oil (Fazal et al. 2023). These diverse biological properties of *M. x piperita* essential oil and wide range of potential applications further cement the importance of studying the production of this high value natural product.

1.2 Black Mitcham (*M. x piperita*) as a model and industrial crop

The majority of global *M. x piperita* essential oil is sourced from the United States, where the cultivar Black Mitcham has been the predominantly grown cultivar since its introduction in the early 1800s (Lawrence 2006). Black Mitcham is also the most predominantly grown cultivar in Europe, however the European market represents a minor share of the global essential oil market (Vining et al. 2020). This has made the Black Mitcham essential oil a standard for commercial *M. x piperita* type essential oils, and has consequently become the "model" *M. x piperita* cultivar for research purposes (Tucker 2012; Kippes et al. 2025).

Black Mitcham peppermint possesses a complex allohexaploid genome, with chromosome counts of 2n = 6x = 72 reported based on karyotype studies, reflecting its origin through natural hybridisation between *Mentha aquatica* (*M. aquatica*) and *Mentha spicata* (*M. spicata*) (Harley and Brighton 1977). Despite its long history of cultivation, the precise genetic background of Black Mitcham remains debated (Vining et al. 2020). The prevailing hypothesis proposes two successive hybridisation events. First, diploid ancestors *Mentha longifolia* (*M. longifolia*) and *Mentha suaveolens* (*M. suaveolens*) hybridised to form the allotetraploid *M. spicata*, as demonstrated by phylogenetic analyses using amplified fragment length polymorphism (AFLP) and chloroplast markers (Gobert et al. 2002; Gobert et al. 2006). Subsequently, *M. spicata* hybridised with the octoploid *M. aquatica*, giving rise to the allohexaploid Black Mitcham (Tucker et al. 1980; Tucker and Naczi 2006). As AFLP data showed *M. x piperita* clustering closer to *M. aquatica* than to *M. spicata*, the prevailing model for the Black Mitcham sub genome structure is as follows: Four sets of chromosomes were inherited from *M. aquatica*, whilst one set of chromosomes each was inherited from *M. longifolia* and *M. suaveolens* through *M. spicata* (Talbot et al. 2024). In allopolyploids like *M. x piperita*, differential expression between sub genomes can result in genome dominance, where one parental sub genome contributes disproportionately to the total transcriptome (Woodhouse et al.

2014). This phenomenon has been documented across multiple plant allopolyploids, where one sub genome can dominant over another, contributing to higher gene expression, retention and stronger regulatory influence (Grover et al. 2012). A well documented example of this has been observed in the allopolyploid *Brassica napus*, where the A_n sub genome showed consistent dominance in transcript abundance over the C_n genome (Chalhoub et al. 2014). Considering the *M. x piperita* allohexaploid genome composition, it is plausible that one of the ancestral sub genomes and associated genes may show a greater propensity to influencing the total transcriptome.

The allohexaploid genetic background of *M. x piperita* cv. Black Mitcham, has rendered it sterile, and consequently is only clonally propagated (Tucker and Naczi 2006). This sterile nature has hindered the use of conventional breeding techniques for crop improvement of Black Mitcham. One of the earliest approaches to improving Black Mitcham was through gamma irradiation studies, which resulted in the discovery of two cultivars which had improved resistance to *Verticilum* wilt, ‘Todd’s Mitcham’ and ‘Murray Mitcham’ (Murray and Todd 1972; Todd et al. 1977). However, these cultivars have not been widely adopted, and subsequent irradiation based cultivar improvement strategies have not been pursued (Tucker 2012). Instead, the majority efforts for trait improvements in Black Mitcham have since been focused around genetic engineering approaches, primarily to improve essential oil yield and quality (Lange 2015).

Although *M x piperita* cv. Black Mitcham is clonally propagated and therefore genetically uniform, the agronomic performance and essential oil yield exhibit pronounced phenotypic plasticity through genotype x environment x management interactions. Environmental conditions such as temperature, soil type and climatic variation can heavily influence biomass accumulation and oil composition (Telci et al. 2011; Soltanbeigi et al. 2021). Management practices further modulate these environmental effects, which has been shown in the harvesting time, where the essential oil from the first harvest of the season is of a higher quality compared to subsequent harvests (Soltanbeigi et al. 2021). This is further compounded by management practices such as mulch treatments, fertilisation regimes and soil amendments having a significant impact on both biomass and essential oil yields (Fallah et al. 2024; Dragumilo et al. 2025). Taken together, even with a fixed

genotype, the environmental and management interaction can create substantial variation in yield and quality of *M. x piperita* essential oil. This variability complicates optimisation through agronomy practices alone, and highlights the value of a synthetic engineering approach by targeting intrinsic pathway regulation. Therefore, it may be possible to offset the environmental and management induced variation, to improve the consistency in essential oil yield and content, beyond what conventional agronomic optimisation can achieve.

1.2.1 Essential oil biosynthesis in Black Mitcham

The essential oil produced by Black Mitcham that makes it such a valuable commodity is both synthesised and stored in the peltate glandular trichomes (PGTs), distributed throughout the aerial surfaces of the plant, primarily on the leaf surface (Amelunxen 1965; Gershenzon et al. 1989; McCaskill et al. 1992). There are three types of trichomes which appear on Black Mitcham leaves: non-glandular trichomes (can be a multicellular or simple hair structure), capitate glandular trichomes (containing a singular secretory head cell) and PGTs (containing an eight celled apical disc of secretory cells) (Maffei et al. 1989; Brun et al. 1991). PGTs are characterised by a prominent sub-cuticular storage cavity, which arises from the separation of the cuticle from the apical walls of the disc cells and accumulates essential oil predominantly composed of monoterpenoids (Turner et al. 2000b). The lipophilic monoterpenes are stored in the extracellular sub-cuticular cavity, where they accumulate as a hydrophobic oil phase (Turner et al. 2000b). The cavity therefore functions as a passive storage reservoir for essential oils to accumulate, without disrupting the intracellular membrane integrity. There has been debate on whether the PGTs are the sole site of synthesis and storage of essential oil in Black Mitcham. The capitate glandular trichomes are known to have limited storage capacity, and the secretions mainly contain a complex mixture of proteins, carbohydrates and lipids (Werker et al. 1985; Ascensão and Pais 1998). However, the secretions have also been reported to contain minute amounts of monoterpenes typically present in the essential oil (Amelunxen 1965). Conversely, analyses of meristematic and leaf primordia, which lack PGTs, showed an absence of the monoterpenes characteristic of essential oil biosynthesis (Brun et al. 1991). Overall, PGTs are the predominant site of the majority of essential oil biosynthesis and storage in Black Mitcham.

The structural and physiological constraints of this storage system impose important limitations on metabolic flux. The finite volume of the sub cuticular cavity restricts total oil accumulation, whilst intracellular monoterpene intermediates are inherently membrane disruptive and potential cytotoxic (Gershenzon and Dudareva 2007). Efficient coordination between biosynthesis, export and accumulation is therefore essential to prevent feedback inhibition or cellular damage within the secretory cells. These constraints provide critical context for a push-pull-protect metabolic engineering strategy, whereby increasing precursor supply and enzymatic activity (“push”) must be matched by enhanced transport and accumulation capacity (“pull”), whilst protective mechanisms (“protect”) must be considered to mitigate cytotoxic stress induced by volatile intermediates.

PGTs are not unique to the *Mentha* genus, and are typically associated with terpenoid producing higher plant species (Booth et al. 2017; Huchelmann et al. 2017). Glandular trichomes in *Mentha* are thought to be involved in herbivory plant defence, however there is a lack of studies directly addressing their function with respect to the interaction of *Mentha* with its native environment (Langenheim 1994; Lange and Ahkami 2013). PGT initiation continues throughout leaf expansion, leading to a steady increase in gland number until growth ceases (Turner et al. 2000b). The formation of PGTs are spatially regulated, with prolonged initiation and higher densities occurring in the abaxial basal and mid-zones, whilst the early cessation in the apical region reflects the basipetal progression of epidermal maturation (Turner et al. 2000b). The development of PGTs during leaf maturation has been directly linked to essential oil biosynthesis, where the number of PGTs in the secretory phase was directly linked to monoterpene production rates (Gershenzon et al. 2000; McConkey et al. 2000; Turner et al. 2000a). The monoterpene content of leaves has also been shown to change over the developmental stage of the leaf. In younger leaves, the monoterpenes (-)-limonene and (-)-menthone form the majority of the essential oil, with (-)-limonene typically appearing first, corresponding with the onset of peltate glandular trichome development (Kjonaas and Croteau 1983; Brun et al. 1991; McConkey et al. 2000). Whereas in the process of leaf maturation, the levels of (-)-limonene and (-)-menthone decrease, with an increase in (-)-menthol attributed to the reduction of (-)-menthone to (-)-menthol, coinciding with flower initiation (Kjonaas et al. 1982; Brun

et al. 1991; McConkey et al. 2000; Croteau et al. 2005). In leaves approaching full maturation and at the onset of senescence, as well as in plants undergoing active flowering, levels of menthyl acetate increase (Brun et al. 1991; McConkey et al. 2000). This accumulation is attributed to the acetylation of (-)-menthol; however, the specific enzyme catalysing this reaction has not yet been identified (Croteau and Hooper 1978). However, the precise definitions of what constitutes a young or mature leaf, or a plant in mid-flowering or late-flowering are difficult to standardize between these studies, so there are still ambiguities in this respect.

1.3 The menthol biosynthesis pathway

The majority monoterpene composition in the essential oil of Black Mitcham stems from the menthol biosynthesis pathway (MBP), and the many intermediates that are produced in the build up to this product. The MBP is one of the most well characterised monoterpene biosynthetic pathways in plants. The entire process comprises of an eight step pathway to (-)-menthol from primary metabolism (Wise and Croteau 1999). The universal C_5 isoprene precursors isopentenyl diphosphate (IPP) and dimethylallyl diphosphate (DMAPP) used as precursors for the MBP are primarily derived from the plastidial 2-*C*-methyl-D-erythritol 4-phosphate (MEP) pathway (Figure 1.2) (McCaskill and Croteau 1995; Eisenreich et al. 1997).

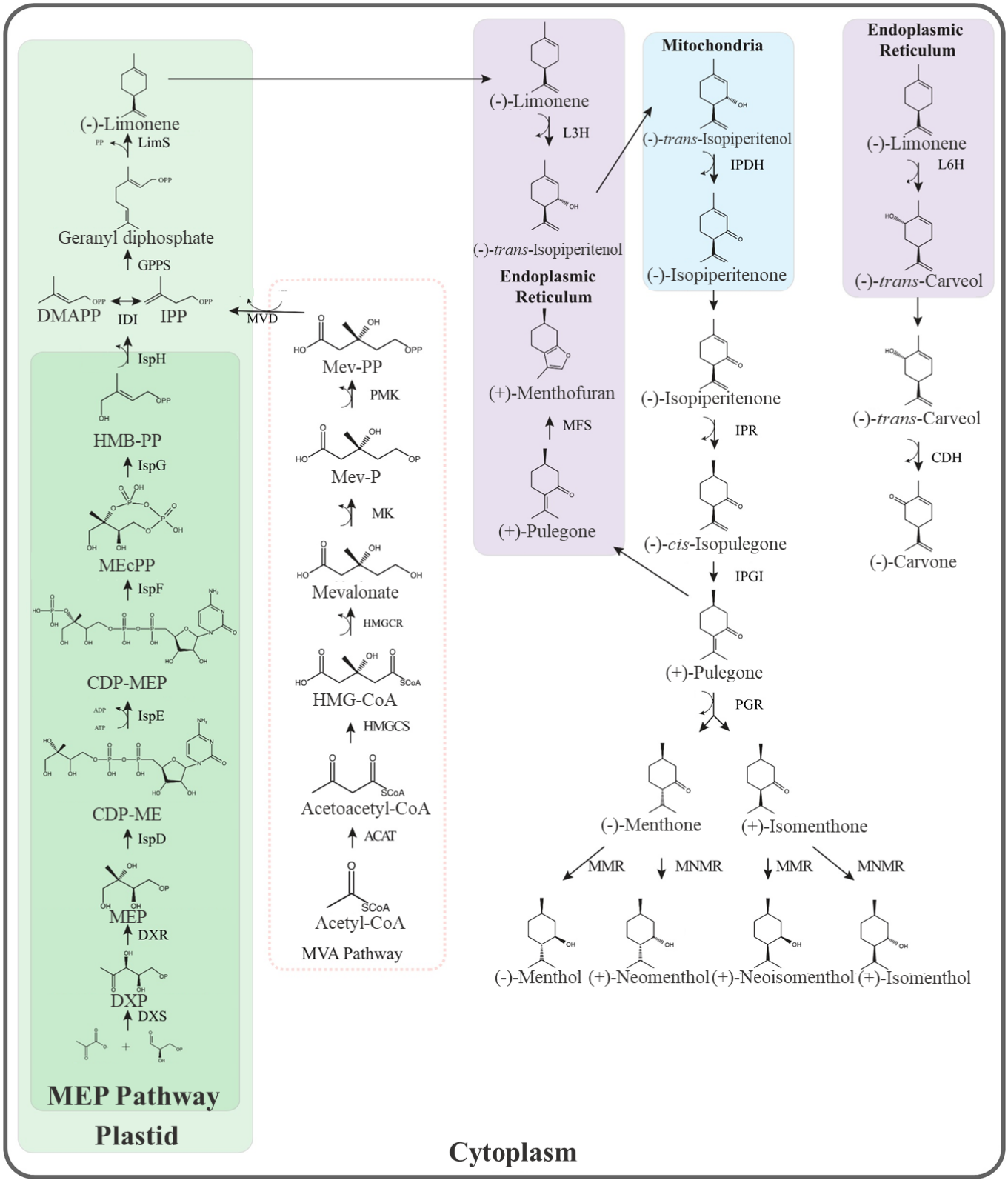

Figure 1.2. Monoterpene biosynthesis pathway in *Mentha*. Both the methyl erythritol phosphate (MEP) and the mevalonate (MVA) pathway are shown although the MVA pathway is non-functional in *M. x piperita* trichomes. ACAT, acetyl-coenzyme A acetyltransferases (Thiolase); HMGCS, hydroxymethylglutaryl-CoA synthase; HMGCR, 3-hydroxy-3-methylglutaryl-coenzyme A reductase; MK, mevalonate kinase; PMK, phosphomevalonate kinase; MCD, mevalonate diphosphate decarboxylase; DXS, 1-deoxy-D-xylulose 5-

phosphate synthase; DXR, 1-deoxy-D-xylulose 5-phosphate reductoisomerase; IspD, 2-C-methyl-D-erythritol 4-phosphate cytidylyltransferase; IspE, 4-(cytidine 5′-diphospho)-2-C-methyl-D-erythritol kinase; IspF, 2-C-methyl-D-erythritol 2,4-cyclodiphosphate synthase; IspG, 4-hydroxy-3-methylbut-2-en-1-yl diphosphate synthase; IspH, 4-hydroxy-3-methylbut-2-enyl diphosphate reductase; IDI, isopentenyl diphosphate isomerase; GPPS, geranyl diphosphate synthase; LimS, (–)-limonene synthase; L3H, (–)-4S-limonene-3-hydroxylase; IPDH, (–)-trans-isopiperitenol dehydrogenase; IPR, (–)-trans-isopiperitenone reductase; IPGI, (+)-cis-isopulegone isomerase; PGR, (+)-pulegone reductase; MFS:(+)-menthofuran synthase; MMR, (–)-menthone: (–)-menthol reductase; MNMR, (–)-menthone: (–)-neomenthol reductase; L6H, (–)-4S-limonene-6-hydroxylase; CDH, (+)-trans-carveol dehydrogenase. DXP, 1-Deoxy-D-xylulose-5-phosphate; MEP, 2-C-Methyl-D-erythritol-4-phosphate; CDP-ME, 4-Diphosphocytidyl-2-C-methylerythritol; CDP-MEP, 4-Diphosphocytidyl-2-C-methyl-D-erythritol 2-phosphate; MEcPP, 2-C-Methyl-D-erythritol-2,4-cyclopyrophosphate; HMB-PP, (E)-4-Hydroxy-3-methyl-but-2-enyl pyrophosphate The absolute stereochemistry, corresponding to the optical rotation signs, is provided structurally. Image adapted from Fuchs et al. 2022.

The MEP pathway begins with the condensation of glyceraldehyde-3-phosphate (D-Gap) and pyruvate by 1-Deoxy-D-xylulose 5-phosphate synthase (DXS) to form 1-deoxy-D-xylulose-5-phosphate (DXP), followed by a reductive isomerisation to (MEP) by DXP reducto-isomerase (DXR) (Figure 1.2) (Zhao et al. 2013). A series of further enzyme catalysed steps culminates in the conversion of (E)-4-Hydroxy-3-methyl-but-2-enyl pyrophosphate (HMB-PP) into IPP and DMAPP by 4-hydroxy-3-methylbut-2-enyl diphosphate reductase (IspH) (Figure 1.2). Therefore, pyruvate represents the link between central carbon metabolism (glycolysis) and the MBP (via the MEP pathway) (Sweetlove et al. 2025).

Although the cytosolic mevalonate (MVA) pathway also produces IPP and DMAPP in higher plants, the MVA and MEP pathway act in different compartments to provide precursor intermediates specific to separate groups of terpenoids (Phillips et al. 2008; Frank and Groll 2017). In *Mentha* trichomes, the MVA pathway is blocked at the 3-hydroxy-3-methylglutaryl-coenzyme A reductase (HMGCR) enzyme, rendering it non-functional for the production of monoterpene precursors (Figure 1.2) (McCaskill and Croteau 1995).

1.3.1.1 The menthol biosynthesis pathway – geranyl diphosphate synthase

Following the MEP pathway supplied IPP and DMAPP, these C_5 precursor isoprene intermediates are condensed into the universal monoterpene precursor geranyl diphosphate (GPP) by the action of plastid-localised geranyl diphosphate synthase (GPPS). GPPS is a member of the short chain prenyltransferase family and functions as a branch point enzyme to direct C_5 precursors into monoterpene

production, as opposed to higher order terpenoid production (Burke et al. 1999). This function is highlighted by the capability of GPPS to be only capable of a single condensation step to the C_{10} geranyl precursor, and inability to catalyse subsequent elongations to either the C_{15} farnesyl or C_{20} geranylgeranyl diphosphates (Burke et al. 1999).

M. x piperita GPPS (MpGPPS) exists as either a heterodimer or heterotetramer, comprised of a small subunit (GPPS.SSU) and a large subunit (GPPS.LSU), requiring a metal ion cofactor for catalysis (Burke and Croteau 2002b). The subunits have been shown to be non-functional alone, and prenyltransferase activity is only detected when both units are co-expressed (Burke et al. 1999; Burke et al. 2004). This mode of action has been further cemented by the resolution of a crystal structure for the native MpGPPS, that showed a heterotetrameric (GPPS.LSU · GPPS.SSU)$_2$-type (Chang et al. 2010). MpGPPS.LSU contains the aspartate-rich DD(X)$_n$D motif (where D indicates aspartate, X indicates any residue, n = 2 or 4), which is crucial for substrate and co-factor binding (Chang et al. 2010). The catalytically inactive MpGPPS.SSU lacks this motif, and instead functions to activate MpGPPS.LSU to restrict chain length elongation of terpenoids to specifically the C_{10} monoterpene terpenoid (Croteau et al. 2005). This ability of MpGPPS.SSU to restrict chain length elongation is not specific to *Mentha* GPPS.LSU. MpGPPS.SSU has been shown to restrict chain length elongation of C_{20} prenyltransferases from *Taxus canadensis* and *Abies grandis* to produce the C_{10} GPP (Burke and Croteau 2002b). Furthermore, when MpGPPS.SSU was co-expressed in *Nicotiana benthamiana* (*N. benthamiana*), an overall increase in GPP and monoterpene derivates was achieved, presumably through the modification of chain length specificity of the native *N. benthamiana* C_{20} prenyltransferase (Orlova et al. 2009; Yin et al. 2017). Heterodimeric GPPS have been reported in a variety of other plant species, such as in *Lavandula x intermedia, Antirrhinum majus* and *Populus trichocarpa* (Tholl et al. 2004; Lackus et al. 2019; Adal and Mahmoud 2020). Additionally, homodimerc forms of GPPS also exist, appearing in plant species such as *Picea abies*, *Lycopersicon esculentum* and *Catharanthus roses* (Van Schie et al. 2007; Schmidt et al. 2010; Rai et al. 2013).

1.3.1.2 The menthol biosynthesis pathway – limonene synthase

The first committed step towards (-)-menthol biosynthesis is the action of plastid localised (-)-limonene synthase (LimS) to cyclise GPP into (-)-limonene (Figure 1.2) (Kjonaas and Croteau 1983; Turner et al. 1999). The overall reaction can be summarised as a ionisation, isomerisation, ionisation, cyclisation and deprotonation steps (Davis and Croteau 2000) LimS exhibits properties typical to that of other terpenoid synthases from angiosperms, such as the requirement for a divalent metal ion cofactor (typically Mg^{2+} or Mn^{2+}) for catalysis activity (Davis and Croteau 2000). The first identified and biochemically characterised LimS was that of *M. spicata*, which was shown to have a nearly identical sequence similarity to that of *M. x piperita*, as well as identical biochemical functionality (Alonso et al. 1992; Colby et al. 1993). This is unsurprising as *M. spicata* is a parent of *M. x piperita*, together with *M. aquatica.* Similarly to GPPS, LimS contains the aspartate-rich $DD(X)_nD$ motif (Chen et al. 1994). Additionally, there is an N-terminal arginine pair (R58R59) that is involved in the isomerisation step of the overall cyclisation reaction (Williams et al. 1998; Hyatt et al. 2007). The action of LimS when in the presence of GPP forms (-)-limonene as the major product (~94%), with minor products of myrcene, (−)-α-pinene and (−)-β-pinene formed as side products (which are reported minor constituents of *Mentha* essential oils) (Alonso et al. 1992; Colby et al. 1993; Beigi et al. 2018). These minor side products are thought to arise from aberrant reaction cycles occurring during the overall cyclisation of GPP to (-)-limonene (Croteau et al. 2005).

1.3.1.3 The menthol biosynthesis pathway – limonene-3-hydroxylase

The next step of the MBP is the NADP- and O_2- dependant hydroxylation of (-)-limonene to (-)-*trans*-isopiperitenol by limonene-3-hydroxylase (L3H), and represents a typical cytochrome P450-dependent mixed function oxidase reaction (Figure 1.2) (Karp et al. 1990). L3H is similar in sequence (70% identity and 85% similarity) to limonene-6-hydroxylase (L6H), which catalyses the hydroxylation of (-)-limonene to (-)-*trans*-carveol in *M. spicata* (Figure 1.2) (Lupien et al. 1999). Both L3H and L6H contain elements of typical cytochrome P450 proteins, such as an oxygen binding domain, cytochrome p450 reductase docking site, the highly conserved heme-binding motif and an N-terminal membrane anchor for insertion of the enzyme into the endoplasmic reticulum (Croteau et al. 2005). Additionaly, immunogold labelling

studies demonstrated its localisation to the endoplasmic reticulum (Turner and Croteau 2004).

1.3.1.4 The menthol biosynthesis pathway - (−)-*trans*-isopiperitenol dehydrogenase

After hydroxylation of (-)-limonene to (-)-*trans*-isopiperitenol, a subsequent oxidation to (-)-isopiperitenone is catalysed by the NAD-dependant (-)-*trans*-isopiperitenol dehydrogenase (IPDH) (Figure 1.2) (Kjonaas et al. 1985). Immunogold labelling studies revealed the mitochondrial localisation of IPDH, highlighting the multi compartment transfer of intermediates from plastid, to endoplasmic reticulum to mitochondria, in the early stage intermediates of the MBP (Turner and Croteau 2004). Although the mechanism by which this multi compartment transfer are currently unknown, it was recently discovered that in *Catharanthus roseus,* a multidrug and toxic compound extrusion (MATE) family protein CrMATE1 is implicated in the transport of monoterpene indole alkaloid precursors from the cytoplasm to vacuole, and the nitrate peptide family transporter protein NPF2.9 is involved in the transport between vacuole to nucleus (Larsen et al. 2017; Li et al. 2024). This represents a better characterised multi compartmental biosynthetic pathway and associated transporter mechanisms, and therefore a similar mechanism could be found in *Mentha*.

IPDH shares >99% amino acid sequence similarity with (−)-*trans*-carveol dehydrogenase from *M. spicata*, which catalyses the oxidation of (−)-*trans*-carveol to (-)-carvone (Ringer et al. 2005). Both dehydrogenases are active in homodimeric and homotetrameric assemblies, and have similar enzyme kinetics and selectivity for their respective substrates (Kjonaas et al. 1985).

1.3.1.5 The menthol biosynthesis pathway - (−)-isopiperitenone reductase

(-)-Isopiperitenone is then reduced by (-)-isopiperitenone reductase (IPR) in an NADPH-dependent reaction to form (+)-*cis*-isopulegone (Figure 1.2) (Croteau and Venkatachalam 1986). IPR activity is highly efficient, as the monoterpene intermediate (-)-isopiperitenone is not found in substantial levels in the essential oil, typically only representing a very minor percentage (Croteau et al. 2005). Furthermore, IPR functions as a monomer, and lacks an N-terminal localisation signal, suggesting a cytosolic compartmentalisation (Lange et al. 2000). IPR bears a

characteristic NADPH cofactor binding motif, typical of enzyme families in the short-chain dehydrogenase/reductase superfamily (Ringer et al. 2003).

1.3.1.6 The menthol biosynthesis pathway - (+)-*cis*-isopulegone isomerase

The only uncharacterised enzyme of the MBP is (+)-*cis*-isopulegone isomerase (IPGI), which catalyses the isomerisation of (+)-*cis*-Isopulegone to (+)-pulegone (Figure 1.2) (Croteau and Venkatachalam 1986). There has also been evidence that (-)-isopiperitenone can be isomerised by IPGI to yield Piperitenone, another minor monoterpene constituent that is sometimes reported in *Mentha* essential oil (Croteau et al. 1991). The isomerisation catalysed by IPGI closely resembles that of a microbial ketosteroid isomerase (KSI) , however the lack of KSI homologues in plants has been a bottleneck in the discovery of the native *Mentha* IPGI (Talalay and Benson 1972; Croteau et al. 2005). A *Pseudomonas putida* (*P. putida*) KSI (PpKSI) was shown to function in *E. coli* catalysing the isomerisation of (+)-*cis*-Isopulegone to (+)-pulegone, however this was in a microbial system and no reports of similar reactions *in planta* have been reported (Currin et al. 2018). More recently, the identification of two putative *IPGI* genes were reported in *M. suaveolens* (an ancestor of *M. x piperita*) (Yang et al. 2024a). This was done by transcriptome mining for putative nuclear transport factor 2 (NTF2)-like family genes, of which the KSI enzyme family member (Li et al. 2018).

1.3.1.7 The menthol biosynthesis pathway – (+)-Pulegone reductase

The penultimate step in the MBP involves the NADPH-dependant reduction of (+)-pulegone to (-)-menthone and (+)-isomenthone, by the catalytic activity of (+)-pulegone reductase (PGR) (Figure 1.2) (Battaile et al. 1968; Ringer et al. 2003). The enzyme has a propensity to favour the production of (-)-menthone over (+)-isomenthone, which is also reflected in the final *M. x piperita* essential oil composition(~10:1 ratio of (-)-menthone to (+)-isomenthone) (Lawrence 1978; Ringer et al. 2003). PGR is localised to the cytoplasm, as evidenced by a lack of localisation signals, and immunolocalization studies implicating its location in the cytoplasm (Turner and Croteau 2004). PGR is a monomeric enzyme, harbouring a NADPH cofactor binding motif (Ringer et al. 2003). PGR is a member of the medium chain dehydrogenase/reductase enzyme family (Ringer et al. 2003). Interestingly, both PGR and IPR catalyse similar reactions and have similar substrates, yet share less than 12% at the amino acid level.

1.3.1.8 The menthol biosynthesis pathway - (-)-menthone: (-)-menthol reductase

The final step in the MBP is the reduction of (-)-menthone to yield (-)-menthol, by the NADPH-dependant reaction performed by (-)-menthone: (-)-menthol reductase (MMR) (Figure 1.2) (Kjonaas et al. 1982). The similar (-)-menthone: (+)-neomenthol reductase (MNMR) catalyses the reduction of (-)-menthone to (+)-neomenthol. Similarly, (+)-isomenthone is reduced to (+)-neoisomenthol and (+)-isomenthol by MMR and MNMR respectively (Croteau et al. 2005). Although MMR mainly reduces (-)-menthone or (+)-isomenthone to (-)-menthol or (+)-isomenthol respectively, there is a propensity to form minor amounts of (+)-neomenthol and (+)-isomenthol. Similarly, MNMR can form minor amounts of (-)-menthol and (+)-isomenthol. This reflects the promiscuous nature of these menthone reductases, and account for all the potential menthol isomers found in *Mentha* essential oil (Croteau et al. 2005).

1.3.1.9 The menthol biosynthesis pathway – (+)-Menthofuran synthase

The monoterpene intermediate (+)-pulegone represents a branch point in the MBP, by its transformation into (+)-menthofuran, a reaction catalysed by (+)-menthofuran synthase (MFS) (Battaile and Loomis 1961; Bertea et al. 2001). This diversion to the production of (+)-menthofuran instead of (-)-menthone is an unwanted side reaction, as high (+)-menthofuran content is indicative of a low quality essential oil (Figure 1.2) (Croteau et al. 2005). This transformation involves a hydroxylation, cyclisation, and finally a dehydration to produce the resulting (+)-menthofuran (Bertea et al. 2001). MFS has the structural characteristics typical of a cytochrome P450 and shares similarity with L3H, including an endoplasmic reticulum localization signal, but differs markedly in its putative substrate recognition sites (Bertea et al. 2001; Rios-Estepa et al. 2010).

1.4 Developmental regulation of the menthol biosynthesis pathway

Overall, the pathway to menthol represents a multi stage biosynthesis pathway, which co-ordinates production and transport of intermediates between specialised compartments within the cell, going from plastids, to endoplasmic reticulum, to the mitochondria, and finally the cytoplasm for the final biosynthesis of (-)-menthol.

The developmental and regulatory aspects of monoterpene biosynthesis and metabolism have been linked to two distinct phases in Black Mitcham essential oil

production (McConkey et al. 2000). The first phase occurs in younger plants, during the stage of leaf expansion and PGT filling, where there is a rapid peak in activity of the first seven enzymes (no direct evidence for IPGI – this was assumed) of the MBP (GPPS, LimS, L3H, IPDH, IPR, IPGI, PGR), culminating in the production of (-)-menthone (Brun et al. 1991; McConkey et al. 2000; Turner et al. 2000b). This rapid peak in activity of the early MBP enzymes is correlated with a sharp peak in the presence of (-)-menthone in the essential oil, suggesting monoterpene production is directly influenced by the corresponding enzyme activity (McConkey et al. 2000). The second phase occurs in older plants, at the stage of flower initiation and more mature leaves, where there is a steady decrease in the activity of the enzymes in the first phase (Brun et al. 1991; McConkey et al. 2000; Croteau et al. 2005). The decline of early MBP enzyme activity to near-negligible levels coincides with a sharp increase in the activity of the final MBP enzyme, MMR, which is accompanied by an increase in (–)-menthol and a decrease in (–)-menthone (McConkey et al. 2000). Taken together, this shows that the first phase is characterised by an accumulation of (-)-menthone in juvenile Black Mitcham essential oil, followed by an essential oil maturation stage where (-)-menthone is converted to (-)-menthol.

Although there is a clear correlation between enzyme activity and monoterpene content in the essential oil, the transcriptional regulation is less well understood. Early studies using RNA-blot analysis showed that the *GERANYL DIPHOSPHATE SYNTHASE* (*GPPS*), *LIMONENE SYNTHASE* (*LimS*) and *LIMONENE-3-HYDROXYLASE* (*L3H*) gene activity correlated with their respective enzyme activity (McConkey et al. 2000). However, no probes were available for the other genes at the time of the study, and there have been no reports following up on this. Furthermore, it is unclear if the probes used in the study were for the small or large subunit of *GPPS*.

Overall, there remains an incomplete understanding of the transcriptional regulation of the remaining MBP genes. The pioneering work to determine the biochemically characterised (and therefore canonical) MBP genes was performed by probing expressed sequence tag libraries, which in an allohexaploid genomic background such as Black Mitcham, may not have captured all potential homologs of the MBP genes (Lange et al. 2000). More recently, Ahkami et al. 2015 showed that there was a general decrease in *LimS, L3H, ISPD* and *IPR* activity and increase in *PGR* and

MMR activity going from “immature leaves” to “mature leaves”. However the developmental stages of the plant were not noted, and not all potential MBP gene homologs were accounted for.

1.5 Engineering menthol biosynthesis in *Mentha*

Genetic engineering of the menthol biosynthesis pathway in Black Mitcham has been enabled by the use of the *Agrobacterium tumefaciens* (*A. tumefaciens*) mediated co-cultivation transformation method to obtain stably regenerated plants (Berry et al. 1996; Caissard et al. 1996; Diemer et al. 1998; Niu et al. 1998; Li et al. 2001; Yu et al. 2022). Approaches to improve oil characteristics have been centred around the precursor supply genes (MEP pathway) and early MBP genes with a goal to increase carbon flux into the MBP pathway and subsequently improve oil content (Lange and Ahkami 2013).

Separate overexpression of *MpDXR, MpIDI* and *Abies grandis GPPS* resulted in a 44%, 26% and 18% increase in overall oil yield compared to wild types (Mahmoud and Croteau 2001; Lange et al. 2011). However, no appreciable monoterpene compositional changes in the oil yield were reported. Similarly, overexpression of *MpDXS* or *MpL3H* did not yield any appreciable changes in either oil yield or content (Mahmoud and Croteau 2001; Mahmoud 2004; Lange et al. 2011). Overexpression of *M. spicata LimS* has yielded conflicting results in the literature (Krasnyanski et al. 1999; Diemer et al. 2001; Mahmoud 2004; Lange et al. 2011). Krasnyanski et al (1999) reported an increase in (+)-pulegone, (+)-Menthofuran and (-)-Menthone, with a decrease in (-)-Menthol in transgenic *M. x piperita* overexpressing *LimS*, compared to wild type controls (Krasnyanski et al. 1999). In a similar study, Diemer et al. (2001) reported no changes in (-)-limonene content, however large variations in the overall monoterpene content was observed in the four transgenic lines presented (Diemer et al. 2001). Finally, Mahmoud et al. (2004) reported no appreciable change in monoterpene composition or yield in *LimS* overexpressing transgenic lines compared to wild type controls (Mahmoud 2004).

Suppression of *L3H*, which codes for the enzyme that converts (-)-limonene to (-)-*trans*-isopiperitenol, resulted in an accumulation of (-)-limonene and reduction in the downstream monoterpenes in the overall essential oil of transgenic Black Mitcham (Mahmoud 2004). Suppression of *MFS*, which codes for the enzyme that converts

(+)-pulegone to (+)-menthofuran, resulted in a decrease in (+)-menthofuran and (+)-pulegone, as well as an overall yield increase in the essential oil of transgenic Black Mitcham compared to wild type controls (Mahmoud and Croteau 2001). The unexpected yield increase was attributed to a generally higher level of PGTs on the leaves of transgenic lines, as determined by follow up studies utilising mathematical modelling (Rios-Estepa et al. 2010).

Genetic engineering approaches to improve essential oil quality and yield have been predominantly reported by the Lange/Croteau group, and have primarily focused on targeting the MBP genes directly. Genetic engineering approaches in *M. x piperita* var Black Mitcham outside of this group have been sparsely reported, with reports in other *Mentha* species focusing on potential transcriptional regulators of MBP genes, or increasing trichome count on leaves (Wang et al. 2016b; Reddy et al. 2017; Hwang et al. 2020; Qi et al. 2022; Yu et al. 2024). The *M. spicata YABBY5* (*MsYABBY5)* transcription factor (TF) was revealed to be an overall repressor of secondary metabolism in transgenic lines of *M. spicata*, *Ocimum basilicum* and *Nicotiana sylvestris* (Wang et al. 2016b). The *M. spicata* R2R3-MYB gene (*MsMYB*) was simiarily shown to be a negative regular of secondary metabolism in transgenic lines of *Ocimum basilicum* and *Nicotiana sylvestris,* and suppressed expression of the *MsGPPS.LSU* by binding to MYB transcription factor binding sites (TFBS) (Reddy et al. 2017). A basic leucine-zipper (bZIP) family transcription factor from *Mentha canadensis* (*M. canadensis*) (*McbZIP1*) was shown to bind to the *LimS* promoter, and transgenic *M. x piperita* lines overexpressing *McbZIP1* showed an increase in expression of *McGPPS*, *McLimS, McIPDH, McIPR* and *McPGR* (Yu et al. 2024). However, the authors did not specify which subunit of *McGPPS* was upregulated. Furthermore, although the authors reported an increase in menthol in transgenic lines, these findings were not statistically significant, and the exact enantiomer of menthol was not specified. In a similar study, the *M. canadensis* R2R3-MYB TF (*McMIXTA*) was revealed to have a role in increasing PGT density when overexpressed in *M. x piperita*, resulting in a 25% increase compared to wild type controls (Qi et al. 2022). This increase in PGT was thought to be induced by the positive regulation of the trichome development-related HD-ZIP IV TF by McMIXTA. In orange mint (*M. x piperita* f. *citrata*), overexpression of the *Nicotiana tabacum* (*N. tabacum*) *lipid transfer protein* (*NtLTP1*) resulted in the increase in size of the PGTs,

and an increase in volatile monoterpene emissions in transgenic lines, compared to wild type controls (Hwang et al. 2020).Genetic manipulation of *Mentha* to modulate the overall essential oil characteristics and yield has therefore been focused on directly targeting the MBP genes, targeting TFs which regulate MBP genes, or to increase PGT abundance to increase overall oil yields.

An additional consideration is that past genetic engineering approaches to modulate essential oil in have all relied on constitutive and ubiquitous promoters driving transgene expression. Care must be taken when constitutively expressing genes outside of their native cell type, as unexpected phenotypes can arise. When genes for ginsenoside saponin production in *N. tabacum* were constitutively overexpressed, this led to dwarfism, aberrant flower and pollen morphology, and failure to set seed (Gwak et al. 2017). A similar study overexpressing the genes to produce artemisinic acid in *N. tabacum* chloroplasts also resulted in dwarfism (Saxena et al. 2014). These phenotypes could be explained by both the depletion of terpenoid precursors (IPP/DMAPP) required for other essential processes, as well as the potential of the newly produced compounds being toxic to the plant when not contained in specialised cell types such as glandular trichomes. These detrimental effects caused by constitutive and ubiquitous overexpression could be circumvented by confining expression specifically to sites which would not impose a negative phenotype on the plant overall. Exerting cell-type specific expression for essential oil biosynthesis could be achieved through the use of trichome-specific promoters, an approach which has not yet been explored in Black Mitcham (Tissier 2012). The promoter sequences for the MBP genes from *M. x piperita* cv. ‘Cim-Madhuras’ have recently been characterised, and conferred trichome-specific expression in *N. tabacum* (Qamar et al. 2022). Trichome-specific promoters could therefore be utilised as a tool in MBP modulation, in both non-native plants and in Black Mitcham itself. However, although the *A. tumefaciens* co-cultivation stable transformation protocols for Black Mitcham are relatively viable at the experimental scale, the transformation efficiencies reported are generally low, and the desired phenotypes are often not clearly achieved (Lange 2015). For trichome-specific promoters to be effectively utilised in Black Mitcham, however, efficient and reliable transformation methods are required, and this remains a major limitation in the species.

1.5.1 Factors effecting stable transformation in *A. tumefaciens*-mediated plant transformation

A major bottleneck for plant biotechnology, both on a fundamental and practical level, is plant transformation. The recalcitrance of many commercial and minor crops to the introduction of genetic changes, and slow generation time of transgenics has slowed plant biotechnology progress, and Black Mitcham is no exception to this (Bélanger et al. 2024)The majority of reports utilising stable transformation of Black Mitcham have used some variation of the co-cultivation method developed by Niu et al (1998). This method involves co-cultivating explants with *A. tumefaciens* for gene transfer to occur, followed by the *in vitro* regeneration of the explants into whole new plants. However, the transformation efficiency has remained low, and represents a major bottle neck to the production of stably transformed Black Mitcham lines (Niu et al. 1998; Vining et al. 2017). The transformation efficiency of *A. tumefaciens* co-cultivation and subsequent regeneration can be influenced by a variety of factors such as plant species, genotype, type of explant, age of explant, plant growth regulator choice and ratio, antibiotic type, temperature, light, *A. tumefaciens* strain and cell density, presence or absence of chemical additives, and finally, control of *A. tumefaciens* overgrowth (Niu et al. 2000; Salas et al. 2001; Zambre et al. 2003; Pawar et al. 2013; Yu et al. 2022). Some of the major contributors to transformation efficiency are introduced below.

A. tumefaciens strains are named by both their chromosomal background and harboured disarmed Ti plasmid (Azizi-Dargahlou and pouresmaeil 2024). Some commonly utilised strains in plant biotechnology are the GV3101, EHA105 and AGL-1 strains, derived from the C58 chromosomal background (Wood et al. 2001), and the LBA4404 strain, derived from the Ach5 chromosomal background (Ooms et al. 1982). The pathogenicity of *A. tumefaciens* strains can greatly vary depending on the target plant species to be infected (Wang et al. 2019). When the *A. tumefaciens* strains GV3101, EHA105 and LBA4404 were tested for stable transformation efficiency in three different cultivars of *Nicotiana tabacum* (*N. tabacum*), LBA4404 was shown to have the highest transformation efficiency (Heidari Japelaghi et al. 2018). However, even between the cultivars tested, there was a range of reported transformation efficiencies reported for LBA4404, highlighting that the transformation efficiencies are cultivar specific. A similar investigation in *Panicum virgatum* L.

showed that between GV3101, EHA105 and LBA4404, EHA105 showed the highest transformation efficiency in this plant species, further highlighting the context dependent pathogenicity of different *A. tumefaciens* strains (Song et al. 2012). In Black Mitcham, two independent studies reported that EHA105 was the most virulent strain, although overall transformation efficiencies were still relatively low (1.0% and and 10%) (Diemer et al. 1998; Niu et al. 1998). Another study reported the testing of multiple *A. tumefaciens* strains, and found GV3101 to have the highest transformation efficiency (Krasnyanski et al. 1999). However, the authors stated this was done in preliminary experiments and did not show the actual data, nor did they state which other strains were compared against. More recent studies to optimise the transformation of Black Mitcham have reported a ~8% transformation efficiency using EHA105 (Yu et al. 2022).

One of the key prerequisites to a successful stable transformation protocol is the ability for plant regeneration following *A. tumefaciens* infection. The most widely reported method used for *Mentha* has relied on *in vitro* regeneration from explants following *A. tumefaciens*-mediated transformation (Niu et al. 1998; Niu et al. 2000; Yu et al. 2022). For *in vitro* regeneration, explants are used as starting material to develop regenerating callus, which through the use of tissue culture manipulations can regenerate into a whole plant (Dhar and Joshi 2005; Minutolo et al. 2020; Zlobin et al. 2020).

The explant source is an important determinant of regeneration frequency, which can vary between plant species and tissue types (Long et al. 2022). In *Mentha*, the explant sources reported for *in vitro* regeneration have been internodes, leaves and petiole segments (Diemer et al. 1998; Niu et al. 1998; Wang et al. 2009; Thul and Kukreja 2010; Yu et al. 2022). However, direct comparisons between these studies to determine the optimal explant source are difficult, due to the lack of standardisation in growth conditions and tissue culture used in these reports.

The age of the explant is also an important factor, with younger tissue typically having higher regeneration frequencies reported (Haliloglu and Aydin 2016; Chou et al. 2020). A study in *Solanum lycopersicum* (*S. lycopersicum*) cv. Micro-Tom looking at regenerative frequencies between explants at varying ages showed that younger tissue had a higher propensity towards callus induction and shoot regeneration

compared to older tissue, regardless of explant type tested (Lee et al. 2020). A similar study in *M. x piperita* showed that out of three groups of internode tissue (1-3 from youngest to oldest), group 2 showed the highest regeneration frequency (Wang et al. 2009).

Exogenous plant growth regulators (PGRs) such as auxins and cytokinins play a pivotal role in callus induction and subsequent regeneration in plant explants (Schwarz and Beaty 2000). The interaction between these exogenous PGRs and explant tissue can determine the regenerative efficiency of an explant, and relies on balancing the ratios of PGRs to induce regeneration (Bernula et al. 2020). A general ratio used to cause shoot regeneration from explants is a high ratio of cytokinin to auxin, although the exact ratios will vary between regeneration protocols (Skoog and Miller 1957). In *Mentha*, commonly reported auxins have been indole-3-acetic acid (IAA), indole-3-butyric acid (IBA) or 1-naphthaleneacetic acid (NAA), used in combination with the cytokinins 6-benzylaminopurine (BAP) , zeatin (ZT), kinetin (KIN) and/or thidiazuron (TDZ) to induce regeneration (Diemer et al. 1998; Niu et al. 1998; Wang et al. 2009; Yu et al. 2022). Furthermore, coconut water is typically added as an additional supplement to the regeneration medium due to the cytokinin content (Niu et al. 1998; Yong et al. 2009; Yu et al. 2022). However, one study reported that the removal of coconut water increased the survival rate of explants co-cultivated with *A. tumefaciens* (Niu et al. 2000).

The co-cultivation time of plant explants with *A. tumefaciens* solutions is a necessity for gene transfer to occur, however can result in overgrowth if left for too long, leading to explant death (Sutradhar and Mandal 2023). Overgrowth during the co-cultivation period can be controlled by optimising the cell density of the *A. tumefaciens* strain used, the temperature during co-cultivation and the duration at which co-cultivation is performed (Bhatt et al. 2021; Molina-Risco et al. 2021; Muppala et al. 2021). A fine balance between allowing sufficient time for gene transfer to occur without causing overgrowth is therefore key to achieving successful transformation and survival of explants.

Following co-cultivation, the removal of *A. tumefaciens* is typically performed by the transferal of explants to a growth medium supplemented with antibiotics (Wiebke et al. 2006). In *Mentha*, the antibiotics primarily reported are Timentin or Cefotaxime

sodium salts, however the exact concentrations used have not been standardised (Diemer et al. 1998; Niu et al. 1998; Yu et al. 2022). Additionally, additional selection is performed on the putatively transformed explants using an antibiotic specific to the resistance gene transferred into the explant. In *Mentha*, this antibiotic has been Kanamycin, although exact concentrations used have not been standardized (Diemer et al. 1998; Niu et al. 1998; Niu et al. 2000). The exact concentrations of antibiotics must be optimised according to the plant species, cultivar and specific growth conditions, as the interplay between these factors can have an impact on transformation efficiency and selection of putative transgenic plants (Azizi-Dargahlou and pouresmaeil 2024; Poormassalehgoo et al. 2025).

The main factor behind the ability of *A. tumefaciens* to perform gene transfer into plant cells lies in the virulence (*vir*) genes which mediate the DNA transfer through the transferred (T-DNA) region (Lee and Gelvin 2008). The activation of these genes (specifically the VirA/VirG two component system) was originally found to be activated by acetosyringone, which is a phenolic compound released by wounded plant cells (Stachel et al. 1985). Since this discovery, acetosyringone has been used to increase the pathogenicity of *A. tumefaciens* by exogenous supplementation in both dicot and monocot plants alike (Sheikholeslam and Weeks 1987; Ashrafi-Dehkordi et al. 2021; Ashrafi-Dehkordi et al. 2021; Niedbała et al. 2021; Du et al. 2022).

A phenomenon called “browning” can also occur post *A. tumefaciens* co-cultivation, and may be exacerbated by the addition of exogenous acetosyringone (Chakrabarty et al. 2002). This browning is thought to be induced by the release of phenolic compounds (such as acetosyringone) and can be detrimental to the survival of the explants (Permadi et al. 2024). To control this browning, chemical additives such as polyvinylpolypyrrolidone (PVPP), ascorbic acid, citric acid or activated charcoal (AC) are frequently added to the explant regeneration medium (Amente and Chimdessa 2021).

1.5.2 Alternative transformation approaches in Black Mitcham

As discussed above, the stable transformation of plants, especially non-model plants such as Black Mitcham, requires a variety of interconnecting factors to be considered. Even so, efficiencies reported for *A. tumefaciens* mediated stable

transformation of Black Mitcham remain consistently low overall (Lange 2015). Alternative transformation methods which circumvent the use of *A. tumefaciens* have explored direct gene transfer into protoplasts, or biolistic bombardment (Niu et al. 1998; Krasnyanski et al. 1999). Direct gene transfer into Black Mitcham protoplasts to generate stable transformants has only been shown by a single publication, and no follow up papers have been published replicating this method (Krasnyanski et al. 1999). Biolistic bombardment was able to induce transient gene expression in Black Mitcham, however stable transformants were unable to be recovered ,and no further reports utilising this technique in Black Mitcham have been published (Niu et al. 1998). More recently, a direct injection transformation method termed regenerative activity–dependent *in-planta* injection delivery (RAPID) has been developed, which has been successfully used to transform *Ipomoea pes-caprae* L. (bayhops), a plant which like Black Mitcham, is propagated vegetatively (Mei et al. 2023). The RAPID method does not require tissue culture manipulations and has yet to be tested in Black Mitcham. Therefore, this novel method represents a means to increase transformation efficiency in Black Mitcham. A summary of transformation strategies for Black Mitcham is shown in Table 1.1

Table 1.1. Summary of transformation strategies in Black Mitcham.

Transformation Approach	Method	Outcomes
Agrobacterium mediated transformation	Cocultivation with *Agrobacterium tumefaciens* strain EHA105	1% transformation efficiency. Eight transgenic plants regenerated (Niu et al. 1998).
Biolistic bombardment	Biolistic bombardment of leaf explants	No stable transgenics recovered after >20,000 bombardments (Niu et al. 1998).
Agrobacterium mediated transformation	Cocultivation with *Agrobacterium tumefaciens* strain EHA105	10% transformation efficiency (Diemer et al. 1998).

Agrobacterium mediated transformation	Cocultivation with *Agrobacterium tumefaciens* strain EHA105, with tobacco cell feeder layer	20% Transformation efficiency (Niu et al. 2000)
Direct DNA uptake into protoplasts	Polyethylene glycol - mediated protoplast transformation	Stable transgenics recovered – efficiency not reported (Krasnyanski et al. 1999).
Agrobacterium mediated transformation	Cocultivation with *Agrobacterium tumefaciens* strain GV3101	Stable transgenics recovered – efficiency not reported (Krasnyanski et al. 1999).
Agrobacterium mediated transformation	Cocultivation with *Agrobacterium tumefaciens* strain EHA105, with acetosyringone	Stable transgenics recovered – efficiency not reported (Mahmoud and Croteau 2001)
Agrobacterium mediated transformation	Cocultivation with *Agrobacterium tumefaciens* strain EHA105	~8% transformation efficiency (Yu et al. 2022)

1.5.3 Heterologous expression of menthol biosynthesis pathway genes outside of *Mentha*

An alternative strategy to overcome the low transformation efficiencies in Black Mitcham is the heterologous expression of MBP genes in non-native hosts. This approach not only enables the production of specific MBP-derived terpenoids, but also provides a platform to test whether genetic manipulations yield the desired effects before committing to stable transformation in Black Mitcham. The first reported MBP intermediate to be produced by heterologous expression was (-)-limonene. This was done by introducing the *Perilla frutescens LimS* gene into *N. tabacum*, with three different localisation signals: plastid, cytoplasm, and

endoplasmic reticulum (Ohara et al. 2003). The *Perilla frutescens LimS* gene localised to the plastids gave highest (-)-limonene levels, followed by cytoplasm, whilst no (-)-limonene was detected in endoplasmic reticulum localised *LimS*. This early study highlighted the importance of mimicking the native compartmentalisation when heterologously expressing genes outside of their native host. A similar study was able to produce (+)-limonene in *N.* tabacum, by the stable transformation of the *Citrus limon* L. Burm. f. *LimS* gene (Lücker et al. 2004b). In a follow up study, the additional transformation of a putative *L3H* from *M. spicata* L. 'Crispa', into the (+)-limonene producing *N. tabacum* resulted in the emission of (+)-*trans*-isopiperitenol (Lücker et al. 2004a). Curiously, the natural substrate for the *Mentha* derived L3H enzymes is the (-)-limonene enantiomer, which produces (-)-*trans*-isopiperitenol, an intermediate in the MBP. The ability for the *Mentha* derived L3H to produce (+)-*trans*-isopiperitenol from (+)-limonene suggests a degree of substrate promiscuity. More recently, attempts to increase (-)-limonene production in tobacco were achieved by the co-expression of *MpGPPS.SSU with Picea abies LimS* (*PaLimS*), which showed a 22-35 fold increase compared to when *PaLimS* was expressed alone (Yin et al. 2017). Co-expression of the MEP pathway gene *DXS* with *PaLimS* did not result in any appreciable change in (-)-Limonene, and no other studies have attempted the *in planta* co-expression of the other MEP pathway genes as a strategy to increase flux towards (-)-limonene production (Yin et al. 2017).

Further studies of downstream products past (-)-limonene in the MBP have yet to be reported, such as the production of (-)-*trans*-isopiperitenol and beyond. Attempts may have been discouraged due to the lack of a characterised *IPGI* gene for the MBP. However, the discovery that PpKSI can function as an IPGI-like enzyme in *E. coli* may allow complete heterologous expression in model hosts such as tobacco (*N. benthamiana* or *N. tabacum*) (Currin et al. 2018). Indeed, PpKSI has been used in both *Escherichia coli* (*E. coli*) *and Saccharomyces cerevisiae* for the synthesis of (-)-menthol from the biosynthetic precursor GPP, albeit in trace amounts (Lv et al. 2022b; Shou et al. 2022). The use of *E. coli* as an expression system for terpenoids may not be ideal when expressing plant derived P450 (such as *MpL3H*) and prenyltransferases (such as *MpGPPS*) leading to low expression or non-functionality (Chang et al. 2007; Wang et al. 2018). This may be attributed to the inability for eukaryotic post-translation modifications to be performed by *E. coli* (Kumari et al.

2024). In contrast, the use of *Saccharomyces cerevisiae* has circumvented these limitations, allowing successful production of monoterpenes such as limonene and (-)-menthol (Cheng et al. 2019; Ma et al. 2021; Lv et al. 2022b).

However, using microbes for heterologous expression of plant derived genes can still be detrimental due to the potential toxicity of the compounds being produced, lack of multiple subcellular compartments, inability to derive metabolic precursors from products of photosynthesis, lack of specialised storage structures that only exist in plants, unwanted flavour profile and use of fossil fuel feedstocks (Tremblay et al. 2010; Stephenson et al. 2020; Kumari et al. 2024; Roque et al. 2025). Furthermore, the processing of plants for monoterpene products typically requires less specialist equipment, and is more applicable to smaller industrial operations (Fuchs et al. 2022). However, a downside to consider in plants is their rich endogenous metabolic pathways, which may act on intermediate compounds produced by the heterologously expressed genes, resulting in dead-end product formation or lack of downstream products (Farré et al. 2014; Caputi et al. 2018). Moreover, metabolic flux through these pathways can be strongly influenced by environmental factors such as temperature, light intensity, and nutrient availability, which in turn affect precursor supply, enzyme activity, and ultimately the yield and quality of essential oils (Malik et al. 2023; Bourtsoukidis et al. 2024). However, standardising and generalising these variables remains a challenge across all plant systems. Taking all the above factors into consideration, this makes the heterologous expression of MBP genes in a plant system more amenable to transformation such as tobacco (*N. benthamiana* or *N. tabacum*), a desirable option to circumvent the low transformation efficiencies observed in Black Mitcham.

1.6 Alternative *in planta* chassis for menthol biosynthesis pathway reconstitution

Tobacco is a model chassis for metabolic engineering and synthetic biology studies, where *N. benthamiana* is typically used for transient expression and laboratory scale stable expression, and *N. tabacum* is used for scaling up resulting stable transgenics (Molina-Hidalgo et al. 2021). One of the defining characteristics of *N. benthamiana* is its amenability to rapid, transient expression, in a technique known as Agroinfiltration (Ma et al. 2012). This involves the introduction of *A. tumefaciens* carrying the genes or pathways of interest into the intracellular spaces in the leaf mesophyll, presumably

through the stomatal openings (Chincinska 2021). This introduction is performed either through the use of a needless syringe or a vacuum pump, and this process is termed ‘infiltration’ (Chen et al. 2013; Matsuo et al. 2016; Mad’ Atari and Folta 2019). Upon infiltration of the leaves, the *A. tumefaciens* transfers the genes or pathways of interest through the T-DNA segment into the leaf cells, and the infiltrated areas will transiently express the genes, until the expression tapers off due to plasmid degradation and/or quenching by RNA silencing (Voinnet et al. 2003; Ma et al. 2012; Fischer and Buyel 2020).

Transient expression in *N. benthamiana* has enabled the elucidation and reconstitution of a variety of complex biosynthetic pathways. The pyrethrin biosynthetic pathway from *Tanacetum cinerariifolium* was successfully reconstituted by the co-infiltration of four genes, to give rise to the monoterpenoids pyrethric acid or chrysanthemic acid (Xu et al. 2019a). In a similar study, the methylperillate biosynthetic pathway from *Salvia dorisiana* was successfully reconstituted, by the co-infiltration of four main pathway genes, and an additional *GPPS* to increase precursor formation, resulting in the production of methylperillate (Jongedijk et al. 2020). The reconstitution of the strictosidine pathway was achieved by co-infiltration of fourteen pathway genes, by combining genes from *Catharanthus roseus* and *Nepeta mussinii* (Dudley et al. 2022a). The authors also reported that mimicking the native *Catharanthus roseus* biosynthetic pathway subcellular compartmentalisation by the addition of compartment specific localisation signals resulted in maximum strictosidine production. To date, no similar studies employing the MBP genes from Black Mitcham have been reported; the only related work describes the co-infiltration of *MpGPPS* and *PaLimS*, which resulted in the production of (-)-limonene (Yin et al. 2017).

Transient co-expression enables the rapid testing of potential gene combinations to produce intermediate compounds, and reconstitution of entire biosynthetic pathways (Petrie et al. 2010; Garcia-Perez et al. 2026). However, stable transformation to integrate transgenes into the nuclear genome of plants can be a more favourable approach (Burnett and Burnett 2020). This is especially true for users without access to specialised equipment such as plant growth facilities or equipment for *A. tumefaciens* cultivation (Golubova et al. 2024). Other than the downsides of lengthy generation time and constantly shifting regulatory processes for stable transgenic

plants, field cultivation and harvest is relatively simple. In a study by Forestier *et al.* (2021b), the optimal gene combinations for producing the diterpenoid jolkinol C in *N. benthamiana* were first identified through transient expression studies. These optimal combinations of precursor and pathway genes were then introduced via stable transformation, demonstrating how transient and stable approaches can complement each other (Forestier et al. 2021b).

An alternative chassis for proof-of-concept metabolic engineering studies is the model plant *Arabidopsis thaliana* (*A. thaliana*). It has a relatively short lifespan (6-8 weeks), diploid genetic background, fully sequenced genome and wealth of bioinformatic resources, which makes it an attractive option as a chassis for metabolic engineering and synthetic biology applications (Leonelli 2007; Woodward and Bartel 2018). However, outside of proof-of-study applications, the small biomass of *A. thaliana* and low scalability are a key disadvantage (Holland and Jez 2018). Nonetheless, *A. thaliana* has been a cornerstone for metabolic engineering studies, particularly in stable transformation studies. A well-known example is the production of omega-3 fatty acids docosahexaenoic acid (DHA) and eicosapentaenoic acid (EPA) by reconstitution of the DHA and EPA biosynthesis pathways in *A. thaliana* (Petrie et al. 2012; Sayanova et al. 2012; Ruiz-Lopez et al. 2013). Reconstitution of bacterial biosynthetic pathways in *A. thaliana* has also been reported, where the reconstitution of four bacterial biosynthesis genes resulted in the production of Butanetriol (1,2,4-butanetriol) (Abdel-Ghany et al. 2013). A similar study transferred microbial genes involved in detoxification of polycyclic aromatic hydrocarbons into *A. thaliana,* and transgenic lines gained this *de-novo* functionality (Peng et al. 2014). These studies not only highlight the applicability of *A. thaliana* as a proof-of-concept chassis, but also the cross-species compatibility of microbial gene derived pathways functioning in plants.

1.6.1 Modular cloning as a system to facilitate rapid testing of single gene constructs for transient expression, and subsequent combination into multi-gene constructs

To complement the rapid testing of gene constructs through transient *A. tumefaciens* infiltration in *N. benthamiana*, a suitable cloning system is required. The modular cloning (MoClo) system, based on type IIS restriction site cloning, allows the rapid assembly of multi-gene constructs to be assembled from standardized genetic

elements (Weber et al. 2011; Marillonnet and Werner 2025). A simplified schematic is shown in Figure 1.3.

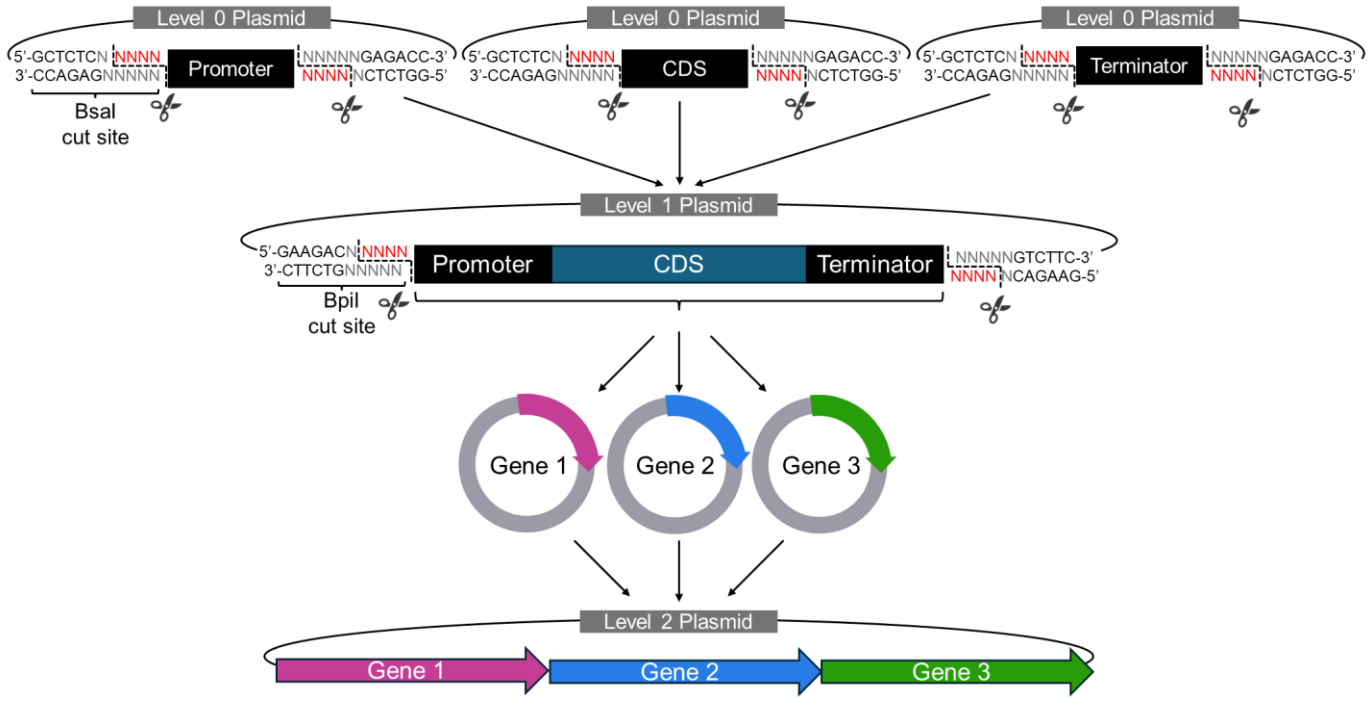

Figure 1.3. Simplified schematic for the Modular Cloning (MoClo) system. Level 0 plasmids contain gene parts, such as promoters, coding sequences (CDS) and terminators. Level 0 plasmids are flanked by BsaI cut sites, which are used to integrate multiple Level 0 plasmids into Level 1 plasmids. Level 1 plasmids represent single transcriptional units, consisting of a promoter, CDS and terminator in its most basic form. Level 1 plasmids are flanked by BpiI cut sites, which are used to integrate multiple Level 1 plasmids into a Level 2 plasmid. Level 2 plasmids represent multi-gene plasmids, containing multiple single transcriptional units. Figure uses elements from Biorender (BioRender.com).

The MoClo system is separated into level 0, level 1 and level 2 plasmids. Level 0 plasmids are gene parts, which include promoters, coding sequences and terminators at its most simplified level. These level 0 plasmids are then assembled into single transcriptional units as level 1 plasmids. The level 1 plasmids can then be used as they are for *A. tumefaciens* transformation (and subsequent plant transformation), or can be combined into multi-gene constructs as level 2 plasmids (Engler et al. 2014). The MoClo system has been utilized with great success in transient expression co-infiltration studies utilising level 1 plasmids, as well as transient and stable expression studies utilising the multi-gene level 2 plasmids (Forestier et al. 2021b; Dudley et al. 2022a). For stable transformation, using a single multi-gene level 2 plasmid ensures all genes are integrated into a single chromosomal site in the genome, which facilitates transmission to the next progeny

generation (Chen et al. 2006; Zhu et al. 2019). This strategy is generally more favourable than approaches relying on multiple single-gene vectors, such as co-transformation, retransformation, or genetic crossing. These single-gene vector methods often result in complex T-DNA integration patterns derived from multiple independent insertion events, which can cause unpredictable transgene expression and segregation in progeny, in addition to requiring considerably more time to obtain the desired multi-gene lines (Dafny-Yelin and Tzfira 2007).

Taken together, the combination of the MoClo system with transient and stable expression pipelines provides a powerful platform for reconstituting the menthol biosynthetic pathway (MBP) in *N. benthamiana* and *A. thaliana*. Transient co-infiltration using level 1 plasmids enables rapid assessment of gene combinations, from which the most effective set can be assembled into level 2 plasmids. These level 2 plasmids can first be tested transiently in *N. benthamiana* before proceeding to stable transformations in both *Arabidopsis* and *N. benthamiana*. This platform is summarised in Figure 1.4.

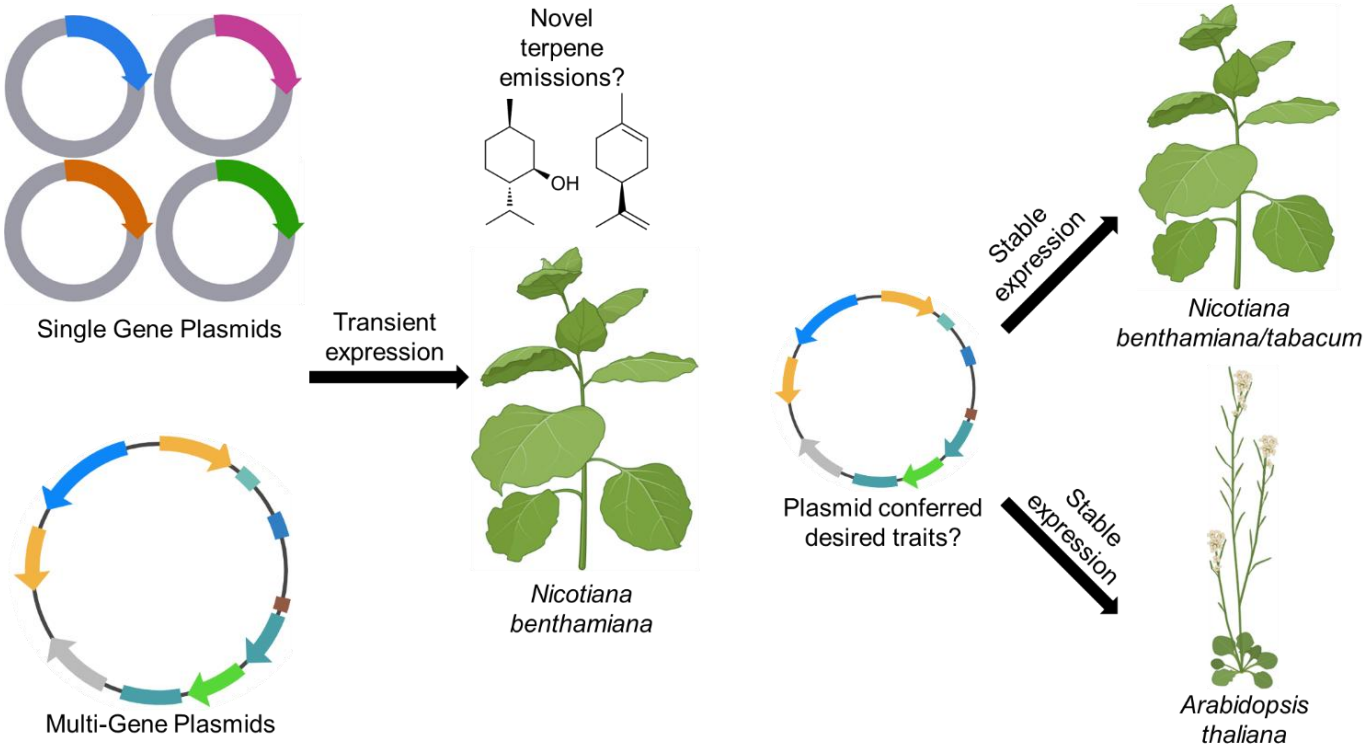

Figure 1.4. Platform for using the MoClo system to design, build and test plasmids in *Nicotiana benthamiana* and *A. thaliana*. Single gene (level 1) plasmids are tested by transient expression via co-infiltration in *Nicotiana benthamiana* for the desired phenotype (such as novel terpene emissions). The best combination of single gene plasmids are then combined into multi-gene (level 2) plasmids and tested through transient expression to

ensure plasmid functionality. If confirmed, the multi-gene plasmids are then stably transformed into both *Nicotiana benthamiana* or *A. thaliana*. Stable expression in *Nicotiana tabacum* is an option for further upscaling this process, but was not explored in this thesis. Figure uses elements from Biorender (BioRender.com).

A longer-term use of this platform would be to prototype gene combinations for modulating essential oil biosynthesis in Black Mitcham, prior to undertaking the more time-intensive process of generating stable mint transformants. This could also serve as a platform to test novel regulatory genes, such as transcription factors that increase trichome density or co-ordinate expression of multiple MBP enzymes, and, if discovered, to evaluate uncharacterised pathway genes such as the putative *MpIPGI*. However, identifying such regulatory factors and uncharacterised biosynthetic genes requires a comprehensive understanding of how the menthol biosynthetic pathway is expressed and controlled in *Mentha* itself.

Although developmental changes in enzyme activity and essential-oil composition have been well characterised, much less is known about the transcriptional regulation underlying these transitions. Early RNA-blot studies provided only limited evidence for correlation between transcript levels and enzyme activity, and subsequent analyses were constrained by probe availability, incomplete EST libraries, and the absence of a reference genome (Lange et al. 2000; McConkey et al. 2000; Ahkami et al. 2015). As a consequence, most MBP genes were not profiled comprehensively at the transcript level, and in the allohexaploid background of Black Mitcham, the presence of gene homologs was not accounted for (Ahkami et al. 2015; Upton et al. 2023). Furthermore, previous transcriptomic studies on developmental regulation have relied on *de novo* transcriptome assembly (Ahkami et al. 2015). With the recent release of the Black Mitcham genome, developmental regulation transcriptome studies with a direct reference genome will allow the previous pitfalls to be addressed (Talbot et al. 2024).

1.7 Transcriptomic studies in *Mentha*

To date, transcriptomic studies in *Mentha* have largely focused on chemotype variation, and responses to environmental or hormonal cues, with relatively little attention paid to developmental regulation (Qi et al. 2018; Yu et al. 2021; López-Hernández and Cortés 2022; An et al. 2023; Huang et al. 2025).

A study in *Mentha haplocalyx* (*M. haplocalyx*) Briq. looking at differences in gene expression in four different chemotypes, revealed that the TF families of basic helix-loop-helix (bHLH), basic leucine zipper domain (bZIP), apetela2/ethylene response factor (AP2/ERF), MYB and WRKY were highly correlated with chemotypes with high expression of *PGR, MMR* and *L3H* (An et al. 2023).

Certain *M. suaveolens* chemotypes form piperitenone oxide as the main monoterpene essential oil product, however the biosynthetic pathway for its formation is not known (Moreno et al. 2002). A transcriptomics approach was used to identify putative *CYP71D* (terpene epoxidase) and *IPGI* genes, which have yet to be characterised in *Mentha* (Yang et al. 2024a). This study is of a particular interest to Black Mitcham, as a similar approach could be utilised to discover the uncharacterised *MpIPGI*.

Environmental effects on trichome development and essential oil biosynthesis have been characterised in *Mentha* species. PGT densities and essential oil yields in *M. canadensis* were found to be decreased in low light conditions (Yu et al. 2021). This was also accompanied by a change in the monoterpene components of the essential oil, with a decrease in menthol, and increase in pulegone and piperitenone. There was also a decrease in the *GPPS.SSU, GPPS.LSU, LimS, L3H, IPDH, IPR* and *PGR* genes from the MBP, as well as sesquiterpenoid biosynthesis pathway genes, highlighting a direct link between expression of MBP genes and essential oil yield in *M. canadensis*.

The application of methyl jasmonate on *M. canadensis* leaves resulted in an enrichment of differentially expressed genes (DEGs) associated with monoterpene biosynthesis (Qi et al. 2018). Specifically, there was an upregulation of the *GPPS.SSU* and *IPDH* genes, whilst a downregulation of the *MFS* gene was observed. This highlighted the potential of using methyl jasmonate application to decrease expression of *MFS* (which codes for the enzyme involved in the production of (+)-menthofuran, an undesirable essential oil component), to improve essential oil quality in *M. canadensis*. However essential oil profiles in this study were not presented. A study in *M. arvensis* leaves treated with methyl jasmonate showed an increase in essential oil yield and PGT density (Huang et al. 2025). There was an increase in *GPPS.SSU, GPPS.LSU, LimS, L3H* and *IPR* genes, however there was

no significant change in the essential oil components after methyl jasmonate treatment.

Ahkami et al. (2015) looked at the differences in expression of the main homolog MBP genes (previously biochemically characterised) in ‘immature’ and ‘mature’ leaves in Black Mitcham, and found high expression of the early MBP genes in ‘immature’ leaves. Conversely, in ‘mature’ leaves, the expression of the early MBP genes decreased, and the expression of *MMR* (involved in the conversion of (-)-menthone to (-)-menthol) was only upregulated at this stage (Ahkami et al. 2015). However, the homolog MBP genes were not accounted for, and the leaves from this study were representative of the plant at only the flowering stage. Furthermore, no information regarding TF regulation of the MBP genes was presented.

The transcriptional control of MBP genes in relation to developmental stages and resulting change in essential oil profile in Black Mitcham have not been addressed, and this represents a key knowledge gap that this thesis aims to address.

1.8 Aims and objectives

The overarching aims of this thesis were to further understand and characterise the menthol biosynthesis pathway (MBP) in *M. x piperita* cv. Black Mitcham, to discover new ways to genetically manipulate Black Mitcham for metabolic engineering purposes by: (i) Developing and optimising robust regeneration and transformation methods for Black Mitcham to facilitate genetic manipulations (Chapter 3), (ii) Reconstitution of the menthol biosynthesis pathway through heterologous expression in non-native plant hosts, and characterisation of trichome- specific promoters (Chapter 4), and (iii) Analysing changes in expression of the menthol biosynthesis pathway genes and co-expressing transcription factors (TFs) in parallel with the change in production of essential oil components, using transcriptomic and metabolomic analysis methods (Chapter 5). These aims would provide a means to identify targets for metabolic engineering, a platform to validate and characterise monoterpene biosynthesis outside of the native host and provide new ways to genetically manipulate Black Mitcham for metabolic engineering purposes.

1.9 Chapter summaries

Chapter 3 involved the optimisation of an *in vitro* regeneration protocol in Black Mitcham, whilst exploring novel PGRs and assessing their suitability for Black Mitcham tissue culture. Attempts to transform Black Mitcham through *A. tumefaciens* co-cultivation were reported, as well as the utilisation of biolistic bombardment to rapidly test plasmid functionality in Black Mitcham. The use of a novel direct injection method, circumventing the need for *in vitro* regeneration, was also reported. The findings of this chapter will aid future transformation studies in the recalcitrant Black Mitcham.

Chapter 4 explored heterologous expression of MBP genes in *N. benthamiana* through transient expression of genes introduced through infiltration of *A. tumefaciens,* transformed with either single gene or multi-gene constructs. Gene combinations which showed the emission of novel terpenes were stably transformed into both *N. benthamiana* and *A. thaliana,* to determine suitability as novel terpene-producing transgenic plants. The characterisation of trichome-specific promoters, through GUS reporter gene fusions in *N. benthamiana* and *A. thaliana,* was performed to determine suitable promoters for use in future metabolic engineering studies. The findings of this chapter will firstly look to reconstitute the entire MBP in a non-native host for *in planta* monoterpene production, as well as serve as a platform to test plasmids before committing to the lengthy process of generating stable transformants in Black Mitcham.

Chapter 5 presented a transcriptomic study in leaves from Black Mitcham plants at different developmental stages (vegetative, early flowering, late flowering) to analyse how changes in gene expression of the MBP genes correlated to the changes in essential oil profiles. This was done by oil profile analysis of leaves from plants at different developmental changes and selecting leaves which had the greatest difference in monoterpene contents. The same leaves were then subjected to RNAseq, and identification and expression analysis of multiple homolog MBP genes was performed, together with promoter analysis, and finally identification of putative previously uncharacterised *IPGI* genes. The findings of this chapter will identify additional MBP gene homologs as targets for metabolic engineering, help determine the developmental regulation of MBP genes, and find the missing link in the MBP

(gene/enzyme responsible for the conversion of (-)-*cis*-Isopulegone to (+)-Pulegone – thought to be IPGI) that has before this thesis eluded researchers.

Chapter 2 - Materials and Methods

2.1 Plant Material and Growth

All soil used, unless otherwise stated, was comprised of 4 parts Levington Advance seed & modular F2 formula compost (Fargro, Cat no. LEVSM75) to 1 part Melcourt horticultural sharp sand (Melcourt, Cat no. 8003). The soil was then heat treated at 70^{o}C for 4 hours, and allowed to cool to room temperature prior to use. Unless otherwise stated, soil grown plants were grown in a growth room under long day conditions (16 hours light, 8 hours darkness). *Mentha* plants were generated from rhizome cuttings taken from established *M. x piperita* cv. Black Mitcham lines from the Scofield laboratory. *Mentha* plants for general purposes were grown in soil. *N. benthamiana* seeds were provided by the Scofield laboratory. *N. tabacum* cv. *SR1* seeds were kindly donated by the de Graaf laboratory. *Nicotiana* seeds were grown in soil.

2.1.1 Growth of *A. thaliana*

A. thaliana seeds (Col-0 ecotype) were washed in 1 mL 70% ethanol. Seeds were briefly vortexed and centrifuged at ~2,000 x g using a 5 second pulse in a benchtop centrifuge. The ethanol was removed, and the seeds rinsed with 1 mL sterile H2O. Seeds were again vortexed and centrifuged using a short pulse, and the water removed. They were then washed with 1 mL of 10% bleach solution containing 1% (v/v) Triton X-100 (Sigma Aldrich; Cat no. T8787), and incubated at room temperature for 10 minutes on a shaking incubator. Following this, seeds were then centrifuged using a short pulse and had the solution removed in a sterile flow hood using sterile pipette tips. 1 mL sterile water was used to rinse the seeds, vortexed, centrifuged using a short pulse, and removed again. This washing step was repeated twice. Seeds were then resuspended in a final 1 mL sterile water, and pipetted into rows onto growth medium plates (4.4 g/L Murashige and Skoog Medium with vitamins (Melford, Cat no. M0220), 0.5 g/L (2-(N-morpholino) ethanesulfonic acid) (MES) Buffer (Sigma, Cat no. M3671), 3% (w/v) Sucrose (Sigma, Cat no. S5390), 0.3g/L Micro Agar (Melford, Cat no. M1002), pH 5.8). These were then incubated in growth cabinets at 25°C in continuous light, before being transferred to soil once four true leaves had formed.

2.2 Plant Transformation and Regeneration

2.2.1 *Mentha in vitro* regeneration

In vitro grown Mentha lines were are already established in the Scofield laboratory. Repropagation was performed under sterile conditions in a laminar flow hood by excision of the shoot apex and first leaf pair from actively growing plants, and placing them into hormone free (HF) growth medium (4.4 g/L Murashige and Skoog Medium with vitamins (Melford, Cat no. M0220), 0.5 g/L (2-(N-morpholino)ethanesulfonic acid) (MES) Buffer (Sigma, Cat no. M3671), 3% (w/v) Sucrose (Sigma, Cat no. S5390), 0.3g/L Micro Agar (Melford, Cat no. M1002), pH 5.8).

Mentha explants were then excised from established *in vitro* stocks using a sterile scalpel, and placed onto hormone free (HF) growth medium, supplemented with plant growth regulators at different concentrations. Concentrations of plant growth regulators used are shown in Appendix Table 1. For control plates, only HF growth medium was used. Leaf explants were placed with the abaxial side in contact with the growth medium. Explants were then placed in a growth room at 25ºC under continuous light conditions.

2.2.2 Black Mitcham *A. tumefaciens*-mediated co-cultivation transformation

A. Tumefaciens strain EHA105 containing the pL2Kan:GUS plasmid was grown to an optical density (OD) of 1 in 50 mL LB medium supplemented with 20 µg/µL Rifampicin (*A. tumefaciens* specific antibiotic) and 50 µg/µL Kanamycin (pL2Kan:GUS specific antibiotic), in a 250 mL conical flask, at 28ºC in a shaking incubator set to 200 RPM. Black Mitcham internode and leaf explants were co-cultivated with *A. tumefaciens* strain EHA105 containing the pL2Kan:GUS plasmid for 30 minutes on a shaking platform. Explants were then blotted dry on sterile filter paper, and were then transferred to shoot induction medium (SIM) (0.5 µM NAA, 9 µM TDZ) for 4 days at 26ºC in the dark. Following this, explants were then transferred to SIM supplemented with 300 µg/µL Cefotaxime-sodium salts (Claforan, Duchefa, Cat no. C0111) and 10 µg/µL Kanamycin for *A. tumefaciens* removal and antibiotic selection. The explants were transferred to new medium every two weeks. Where different *A. tumefaciens* strains were used, the same growth conditions were used. When either activated charcoal (AC) or polyvinylpolypyrrolidone (PVPP) were

added, a concentration of 1g/L was used as a final concentration in the selection medium.

2.2.3 Black Mitcham RAPID transformation

A. tumefaciens strain EHA105 harbouring the pL2Kan:GUS plasmid was grown to an OD of 1. The cultures were spun down in a centrifuge at 4000 *x g* for 30 minutes, and resuspended in a wash buffer (10mM $MgCl_2$ and 100 µM Acetosyringone, pH 5.6). The cultures were spun down again at 4000 *x g* for 30 minutes and resuspended to a final OD of 0.5 with infiltration buffer (2.2 g/L Murashige and Skoog Medium with vitamins, 0.1 % (w/v) Sucrose, 100 µM Acetosyringone and 0.02% Silwet L-77 (v/v) (De Sangosse, Cat no. 0640), pH 5.6). Black Mitcham rhizome, stem and nodal tissue were injected with the suspension solution using a 1mL syringe until no further solution could be injected. For control samples, tissue was infiltrated with infiltration buffer without *A. tumefaciens*. The injected Black Mitcham was then buried in soil and placed in a growth room until new shoots with at least 4 leaf pairs had developed. GUS activity was then assayed as per section 2.2.8.

2.2.4 Biolistic bombardment

2.2.4.1 Microcarrier preparation

Biolistic bombardment was performed using a PDS-1000 | He™ System (BIO-RAD, Cat no. 1652257) with1.1 µm Tungsten particles used as the microcarrier. These were prepared by washing 30 mg of tungsten particles in 1 mL of 70% ethanol by vortexing for 5 minutes. Vortexed tungsten particles were then allowed to soak in the ethanol solution for 15 minutes. After 15 minutes, the soaked tungsten particles were centrifuged for 5 seconds at 20,800 x *g*, and the resulting supernatant was removed. Three washes using 1 mL of sterile H_2O were then performed. Following this, tungsten particles were washed three times by adding 1 mL nuclease-free water vortexing for 1 minute, allowing the suspension to stand for 1 minute, and pelleting by centrifugation at 20,800 × *g* for 5 seconds. The supernatant was then removed. Finally, 500 µL of 50% glycerol was added.

2.2.4.2 Pre-Bombardment cleaning

Prior to performing biolistic bombardment, 1100 psi rupture disks (BIO-RAD, Cat no. 1652329) were sterilised by briefly dipping in 70% isopropanol for 3 seconds. Stopping screens were sterilised by autoclaving (BIO-RAD, Cat no. 1652336). The

PDS-1000 | He™ System chamber was cleaned with 70% ethanol and allowed to dry before use.

2.2.4.3 Coating DNA onto tungsten particle microcarriers

Prepared tungsten particle microcarriers were vortexed for 5 min, and 50 µL of the suspension was transferred to a 1.5 mL microcentrifuge tube. While gently vortexing, 5 µL plasmid DNA (1 µg/µL) was added, followed by 50 µL of 2.5 M $CaCl_2$ and 20 µL of 0.1 M spermidine (free base, tissue culture grade), in that order. The mixture was vortexed continuously for 3 min, then allowed to stand for 1 min to permit microcarrier settling. Microcarriers were pelleted by centrifugation at 20,800 × g for 5 s, and the supernatant was removed. The pellet was washed once with 140 µL of 70% ethanol and once with 140 µL of 100% ethanol, with vortexing and settling between each wash. Finally, the microcarriers were resuspended in 48 µL of 100% ethanol.

2.2.4.4 Macrocarriers preparation and bombardment

Prior to loading microcarriers onto macrocarriers (BIO-RAD, Cat no. 1652335), an assembly holder was constructed by placing $CaCl_2$ desiccant in a 60 mm Petri dish, followed by a square piece of filter paper, the macrocarrier holder (BIO-RAD, Cat no. 1652322), and finally the microcarrier placed inside the holder. To load the macrocarriers, 6 µL of DNA-coated microcarriers were spread and left to evaporate. Plant material for bombardment was prepared by cutting leaves into disks using the cap of a 1.5 mL Eppendorf tube and four leaf disks placed in a 60 mm Petri dish filled with HF media. Prepared plant material was placed at level 3 in the bombardment chamber, which corresponds to 9 cm below the stopping screen. A sterile stopping screen was placed on the stopping screen, and samples were bombarded at 1100 psi, with each sample being bombarded twice. Following bombardment, plant tissue was incubated at 25^{o}C under continuous light conditions, and then assayed for GUS activity as described in section 2.2.8.

2.2.5 Stable transformation of *A. thaliana* by floral dipping

Floral dipping of *A. thaliana* was adapted from (Davis et al. 2009). Glycerol stocks of *A. tumefaciens* transformed with the plasmid of interest were used to inoculate a 50 mL culture of LB medium supplemented with the appropriate antibiotics and concentration, placed in a sterile 250 mL flask. The solution was then placed in a

shaking incubator at 28°C and 200 RPM for 48 hours. Following this, the solution was added into 450 mL of LB medium lacking antibiotics in a 2 L sterile flask and grown for 6 hours. Sucrose (12.5g) was then added and further incubated for 1 more hour. Immediately before dipping, solutions were transferred to a beaker and 250 µL of Silwet L-77 was added. Four- to five-week-old *A. thaliana* plants at flowering stage were used for dipping. To increase transformation efficiency, any siliques were removed prior to dipping. *A. thaliana* plants were dipped in the transformation solution for 10 seconds, with gentle agitation. Plants were then loosely covered by an autoclave bag and incubated at 25°C for 24 hours. After 24 hours, plants were removed from the bags, and placed in growth rooms at 25°C under long day conditions (16 hours light, 8 hours dark) and grown until the end of their life cycle, to be harvested for seeds.

For T1 plant selection, seeds from the T0 plants (primary transformants) were plated onto growth medium supplemented with 50 µg/mL kanamycin and 200 µg/mL cefotaxime. For T2 plant selection, seeds from T1 plants were plated onto growth medium supplemented with 50 µg/mL Kanamycin, and lines with a 3:1 segregation ratio of resistant to susceptible lines were used in further experiments.

2.2.6 Stable transformation of *Nicotiana benthamiana* by *A. tumefaciens* co-cultivation

For each transformation, 2-3 of the youngest but fully expanded leaves from 5-6 week old *N. benthamiana* were harvested. The leaves were then submerged in sterilisation solution (10% bleach, 0.01% (v/v) Tween) for 30 seconds, then washed twice in sterile H_2O with 0.01% (v/v) Tween, followed by storage in sterile H_2O. The sterilised leaves were then cut into ~1cm x 1cm squares using a sterile scalpel, whilst omitting the main vasculature of the leaf. To prepare the *A. tumefaciens* solution, cultures were grown for 48 hours in LB medium supplemented with the appropriate antibiotics, in a shaking incubator at 28°C and 200 RPM. The *A. tumefaciens* solutions were then spun down in a centrifuge at 4000 *x g* for 20 minutes, and resuspended in MMA medium (4.3 g/L Murashige and Skoog Medium with vitamins (Melford, Cat no. M0220), 10 mM (2-(N-morpholino)ethanesulfonic acid) (MES) Buffer (Sigma, Cat no. M3671), 20 µM Acetosyringone, 20 g/L Sucrose, pH 5.8) to a final OD of 0.8. Sterilised leaf segments were then co-cultivated in the *A. tumefaciens* solution for 30 minutes on a shaking platform. Leaf segments were then

transferred onto sterile filter paper placed in a square petri dish, which had been wet with sterile H_2O, stored in the dark at 25°C for 48 hours for *A. tumefaciens* co-cultivation.

Following co-cultivation, leaf segments were placed into a washing solution (sterile H2O supplemented with 100 µg/mL Kanamycin and 250 µg/mL Cefotaxime) for 3-5 minutes. The leaf segments were then placed onto shooting medium (4.3 g/L Murashige and Skoog Medium with vitamins (Melford, Cat no. M0220), 10 mM (2-(N-morpholino)ethanesulfonic acid) (MES) Buffer (Sigma, Cat no. M3671), 20 g/L Sucrose, 1 µg/mL 6-Benzylaminopurine (BAP), 0.1 µg/mL Naphthalene acetic acid (NAA), 100 µg/mL Kanamycin, 200 µg/mL Cefotaxime, pH 5.8) for callus and shoot formation to occur. Well defined shoots were excised from the callus body using a sterile scalpel, and transferred to rooting medium (4.3 g/L Murashige and Skoog Medium with vitamins (Melford, Cat no. M0220), 10 mM (2-(N-morpholino)ethanesulfonic acid) (MES) Buffer (Sigma, Cat no. M3671), 20 g/L Sucrose, 100 µg/mL Kanamycin, 200 µg/mL Cefotaxime, pH 5.8) for roots to develop. Once roots had developed, whole plants were transferred into soil and grown to maturity.

2.2.7 Transient transformation of *N. benthamiana*

A. tumefaciens strains transformed with the plasmid of interest were grown in liquid LB medium supplemented with the appropriate antibiotic were grown for 48 hours at 28°C in a shaking incubator at 200 RPM. The saturated cultures were then centrifuged at 4000 *x g* for 30 minutes, and the supernatant discarded. The cells were then resuspended in infiltration buffer (10mM $MgCl_2$, 10mM MES, 200 µM Acetosyringone, pH 5.6), and incubated at 28°C for 2 hours at 200 RPM in a shaking incubator. Following incubation, cells were diluted in infiltration buffer to a final OD of 1, and then mixed such that each *A. tumefaciens* strain was at a final OD of 0.2 in the final infiltration solution. For all infiltrations, a separate *A. tumefaciens* strain containing the P19 suppressor of gene silencing from the Tomato Bushy Stunt Virus (TBSV) which is known to increase heterologous expression was included (Sainsbury et al. 2009). *N. benthamiana* plants with at least 4 fully expanded true leaves were infiltrated in the abaxial side of the leaf using a 1 mL needleless syringe, to the point of saturation which was visually monitored. Following infiltration, plants

were grown in a growth room for a period of 3 days, or as dictated by the experimental conditions, and leaves were harvested for subsequent analysis.

2.2.8 GUS reporter gene assay

Detection of transformation success where a β-glucuronidase (GUS) reporter gene was present in the construct was performed by a GUS assay. This assay works on the basis of the GUS enzyme hydrolysing the 5-bromo-4-chloro-3-indolyl glucuronide (X-Gluc) substrate into 5,5'-dibromo-4,4'-dichloro-indigo (diX-indigo) which is a blue product that can be visually observed. Transformed plant tissue samples were first washed in 90% ice-cold acetone for 20 minutes, followed by 3 washes with sterile H_2O. Then sterile H_2O was then removed and replaced with GUS substrate solution (0.16 mg/mL X-Gluc, 50mM sodium phosphate buffer pH 7, 0.4 mM potassium ferrocyanide, 0.4 mM potassium ferricyanide, 0.1% (v/v) Triton X-100), and vacuum infiltrated for 3 minutes. Samples were then incubated at 37^{o}C for 16 hours. Following incubation, samples were cleared with repeated incubations with 70% ethanol at room temperature until samples were decolourised.

2.3 Molecular Biology and Cloning

2.3.1 Gene Synthesis

Unless otherwise specified, DNA sequences were synthesised as gene fragments from GeneWiz® using their PriorityGene Service. For non-plant derived DNA coding sequences, codon optimisation using the Benchling® (https://www.benchling.com) codon optimisation tool was used. Coding sequences were domesticated by introducing silent mutations to remove internal BsaI or BpiII restriction sites. Sources for the sequences used are shown in Table 2.1. For the *PpKSI* coding sequence, no nucleotide sequence was available, so the published amino acid sequence (UnitProt ID PO7445) was reverse translated using Benchling. To reverse translate, the amino acid sequence was loaded into Benchling, and the “Back translate” function was used.

2.3.2 DNA extraction

Liquid nitrogen frozen plant tissue was ground in with a sterile mortar and pestle, using liquid nitrogen to keep the tissue frozen during grinding. Ground tissue (0.1g) was added to a sterile 1.5 mL Eppendorf, and 500 µL of CTAB buffer (2% (w/v)

Hexadecyltrimethylammonium bromide (Sigma, Cat no. H5882), 100 mM Tris-HCl, 20mM EDTA, 1.4 M NaCl,1% (w/v) PVP, pH 8) was added and mixed. β-mercaptoethanol (BME) (5 µL) was then added, and the solution incubated at 65^{o}C for 30 minutes with agitation (800 RPM). Following incubation, 500 µL of CIA (24 parts chloroform to 1 part isoamyl alcohol) were added and mixed for 10 minutes at 800 RPM. The solution was then centrifuged for 20,800 *x g* for 5 minutes at 4^{o}C. Following centrifugation, the upper aqueous phase was transferred to a fresh 1.5mL Eppendorf tube, ensuring not to disturb the interphase or organic phase layer. An additional 500 µL of CIA was added, and the solution was mixed for 10 minutes at 800 RPM, and the aqueous layer was transferred to a fresh 1.5 mL Eppendorf tube. An equal volume to the aqueous layer of ice cold isopropanol was then added, and the mixture was incubated for 1 hour at -20^{o}C. Following incubation, the mixture was centrifuged at 20,800 *x g* for 5 minutes, and the supernatant was discarded. The resulting pellet was washed with 1 mL of 70% ethanol and allowed to dry in a laminar flow hood to remove residual ethanol. The pellet was then dissolved in 50 µL nuclease free water that had been prewarmed to 65^{o}C.

2.3.3 Q5 Amplification of DNA fragments

Cloning of the *Mald1* and *CPS2* promoters was performed from genomic DNA of *N. tabacum* using Q5 DNA polymerase, according to the manufacturer's instructions (NEB, Cat no. M0491S), with slight modifications. In brief, 0.25 µL of Q5 high-fidelity DNA polymerase, 4 µL of 5 x buffer, 1 µL 10 mM dNTPs mix (NEB, Cat no. N0447S), 1 µL of each 10 µM forward and reverse primers, 100 ng of template DNA, and nuclease free H_2O to a final volume of 20 µL was added to a PCR tube. Thermocycler conditions used were an initial denaturation of 95°C for 2 minutes, followed by 30 cycles of 95°C denaturation for 10 seconds, 55-60°C annealing for 10 seconds, and 72°C amplification for 30 seconds per kilobase of target amplicon, followed by a final extension step of 72°C for 10 minutes, and a final hold of 4°C.

2.3.4 Golden Gate Cloning

The MoClo toolkit (Addgene, Kit #1000000044) and MoClo Plant Parts Kit (Addgene, Kit # 1000000047) were used to assemble level 0 (basic modules), level 1 (single gene constructs) or level 2 (multi-gene constructs). Golden Gate cloning was achieved by mixing 1.5 µL of T4 DNA ligase buffer, 1 µL Type IIS restriction

endonuclease (BsaI for level 1 constructs (Thermofisher, Cat no. ER0291) or BpiI for level 0 and level 2 constructs (Thermofisher, Cat no. ER1012)), 1 µL of T4 DNA ligase (NEB, Cat no. M0202S), vector: insert in a 1:3 molar ratio, and nuclease free H_2O to a total volume of 15 µL. These were placed in a thermocycler for 99 cycles of 37°C for 5 minutes, then 16°C for 5 minutes, followed by a final 37°C cutting step for 10 minutes, then a 55°C followed 80°C denaturation step, each for 10 minutes, with a final hold of 4°C. The reaction mix (5 µL) was used to transform competent *E. coli* cells. Validation of the plasmids was performed by miniprep to purify the plasmids as described in section 2.3.5, followed by sequencing as described in section 2.3.14. Resulting sequence files were aligned to the plasmid sequence in Benchling.

2.3.5 Plasmid DNA extraction

Plasmid DNA was extracted using the QIAprep Spin Miniprep Kit (Qiagen, UK, Cat no. 27104), according to manufacturer instructions with some modifications. 5 mL of bacterial culture grown at 37ºC for 16 hours was centrifuged at 4,000 x *g* for 10 minutes. The supernatant was discarded, and the resulting pellet was resuspended in 250 µL of resuspension buffer (50 mM Tris·HCl, 10 mM EDTA, 100 µg/mL RNase A, pH 8). Lysis buffer (250 µL; 200 mM NaOH, 1% SDS (w/v)) was added and the solution was gently inverted 10 times, and then incubated at room temperature for 2 minutes. Neutralisation buffer (350 µL; 4.2 M Gu-HCl, 0.9 M KOAc, pH 4.2) was then added and the tube was inverted 3 times to mix. Samples were then centrifuged for 10 minutes at 20,800 x *g*. The resulting supernatant (typically ~800 µL) was transferred to a spin column placed in a collection tube, centrifuged for 1 minute at 20,800 x *g* and the flow through was discarded. Wash buffer (750 µL; 10 mM Tris·HCl, 80% ethanol (v/v)) was added to the spin column and centrifuged at 20,800 x *g* for 1 minute, and the flow through discarded. A second spin under identical conditions was performed to remove residual wash buffer. The spin column was then transferred to a sterile 1.5 mL Eppendorf tube and 30-50 µL of 65ºC nuclease free water (Sigma, UK, Cat no. W4502-1L) was added, and the column was incubated at room temperature for 1 minute. To elute the DNA, the spin column and Eppendorf tube were centrifuged at 20,800 x *g* for 1 minute.

2.3.6 Gel Electrophoresis

Agarose gel electrophoresis was carried out using a 0.8-1.5% agarose Tris-acetate-EDTA (TAE) gel (40 mM Tris base, 20 mM glacial acetic acid, 1 mM EDTA), supplemented with SafeView (NBS Biologicals, Cat no. NBS-SV1-C) for visualisation. Either a 1kb+ ladder (NEB, Cat no. N0469S) or Smartladder (Eurogentec, Cat no. MW-1700-02) was used as a molecular weight marker. Where necessary, samples were mixed with 6x NEB purple loading dye (NEB, Cat no. B7025). Gels were run at between 40-100 V for 20-60 minutes depending on the gel % used and size of fragments to be separated.

2.3.7 DNA extraction from an agarose gel

The Zymoclean Gel DNA recovery kit (Zymoresearch, Cat no. D4001/D4002) was used to extract DNA from agarose gels according to the manufacturer instructions. The DNA band of interest was excised using a sharp scalpel or razor blade and placed into an Eppendorf tube and weighed. Three volumes (w/v) of Agarose Dissolving Buffer (ADB) were added to the tube, followed by heating in a heating block at 50^{o}C for 5-10 minutes, until no solid agarose remained. The sample was then transferred to the provided spin columns, and centrifuged at 20,800 x *g* for 1 minute, and the flow through was discarded. The spin column was then washed twice with 200 µL of wash buffer (10 mM Tris·HCl, 80% ethanol (v/v)), involving centrifugation at 20,800 x *g* for 1 minute, followed by discarding the flow through. The spin column was transferred to a sterile 1.5 mL Eppendorf tube, and 30 µL of 65^{o}C nuclease free water (Sigma, Cat no. W4502-1L) was added and incubated at room temperature for 1 minute. The DNA was then eluted by centrifuging at 20,800 x *g* for 1 minute.

2.3.8 Nucleic acid quantification

Nucleic acid quantification was performed on a Nanodrop 1000 Spectrophotometer (Thermo Scientific, UK). Prior to each measurement, the Nanodrop was blanked with a solvent matching the sample to be measured. A 1 µL of sample was applied directly to the measurement pedestal, and absorbance was recorded at 260 nm. Sample purity was assessed by monitoring the A260/A280 ratios to detect protein or phenolic compound contamination, and the A260/A230 ratios to detect salt, carbohydrate, or residual organic solvents (guanidine, phenol etc) contamination.

2.3.9 *E. coli* transformation

Chemically competent *E. coli* (strain DH5α, Zymoresearch, Cat no. T3007) were transformed according to manufacturer's instructions, with some slight modifications as follows. In brief, cells were thawed on ice for 10 minutes, and had either 1 µL DNA (purified DNA) or 5 µL golden gate reaction mix added to 50 µL aliquots of competent cells. These were left on ice for 15-30 minutes. Cells then had 200 µL of overgrowth medium (Zymobroth, Zymoresearch, Cat no. M3015-100) added and were incubated at 37°C at 200 rpm for 1 hour. Cells were then plated onto agar plates containing appropriate antibiotics, and IPTG and X-gal if blue-white screening was used. Plated cells were then grown at 37ºC for 16 hours for single colonies to develop.

2.3.10 Blue-White Screening of Colonies

E. coli colonies transformed with plasmids containing a *LacZ* selection part were screened using blue-white selection on agar plates containing the appropriate antibiotic, 100 µM isopropyl β-d-1-thiogalactopyranoside (IPTG) and 40 µg/mL 5-bromo-4-chloro-3-indolyl-β-D-galactopyranoside (X-gal). For level 1 plasmids, white colonies were positive transformants, whilst blue colonies were negative transformants. For level 2 plasmids, blue colonies were positive transformants, whilst white or orange colonies were negative transformants.

2.3.11 *A. tumefaciens* transformation

A. tumefaciens strains GV3101:pMP90 were provided by the Scofield Laboratory. *A. tumefaciens* strains LBA4404 and EHA105 were kindly donated by the Rogers Laboratory. Aliquots (50 µL) of *A. tumefaciens* were thawed on ice for 10 minutes. 150 ng of purified plasmid DNA was added to each aliquot. The solution was then added into a BIO-RAD Gene Pulser® Cuvette (Cat no. 165-2086), and the cells were electroporated (2.4 kV, 25 µF, 200 ohms) by applying a pulse for 1-2 seconds, as indicated by the BIO-RAD MicroPulser™ machine, for a pulse constant of 4.5 – 4.7 ms. 1 mL of LB medium (20 g/L, pH 7.2 (Melford; catalogue number: L24060)) was then added to the cuvette, and the resulting solution was poured into a 1.5 mL Eppendorf tube. The solution was then placed in a shaking incubator at 28°C and 200 RPM for 2 hours. Cells were then plated onto LB agar plates containing rifampicin (20 µg/mL), and depending on the *A. tumefaciens* strain and transformed

plasmid used, and either/or gentamycin (20 µg/ml), kanamycin (50 µg/mL), carbenicillin (100 µg/mL).

2.3.12 Colony PCR

Colony PCRs for screening were carried out using 1 x PCRBIO Taq Mix Red (PCRBiosystems, Cat no. PB10.13-02), forward and reverse primer (0.5 µM), and nuclease free H_2O were added to a total volume 15 µL. The target colony was picked into the PCR mix and placed in a thermocycler. Thermocycling conditions used were 95°C for 2 minutes, then 35-40 cycles of 95°C denaturation for 15 seconds, 55-60°C annealing for 15 seconds, and 72°C amplification for 20 seconds per kilobase of amplicon DNA, followed by a final amplification stage of 72°C for 2 minutes. Where *A. tumefaciens* was used as a template, an additional step of heating at 95ºC for 10 minutes was included prior to the above thermocycling conditions.

2.3.13 Glycerol stocks

Glycerol stocks of bacterial cultures were produced by mixing 500 µL of saturated culture (~16 hours growth for *E. coli*, ~48 hours growth for *A. tumefaciens*) with 500 µL of sterile 50% glycerol. These were then stored at -80ºC.

2.3.14 Sequencing

DNA sequencing was performed using either the TubeSeq Supreme or ONT Lite Whole Plasmid Sequencing services from Eurofins Genomics. For TubeSeq Supreme, plasmids were normalised to a concentration of 50 ng/µL in a total volume of 20 µL, and sequencing primers were normalised to 10 µM in a total volume of 20 µL. For ONT Lite Whole Plasmid Sequencing, plasmids were normalised to a concentration of 60 ng/µL in a total volume of 30 µL.

Table 2.1. General level 1 construct parts list. Sources of DNA sequences are shown in brackets, with either the MoClo part ID or NCBI ID shown.

Level 1 Constructs				
Construct ID	Backbone	Promoter	Coding Sequence	Terminator
pL1NtDXS	Level 1 Acceptor	2xCaMV35S + 5'UTR TMV(pICH51288)	*Nicotiana tabacum DXS*	AtuNos (pICH41421)

	Position 2 (pICH47742)		(NCBI ID: EU650419)	
pL1MpDXR	Level 1 Acceptor Position 2 (pICH47742)	2xCaMV35S + 5'UTR TMV(pICH51288)	*Mentha x piperita DXR* (NCBI ID: AF116825)	AtuNos (pICH41421)
pL1AtIspD	Level 1 Acceptor Position 2 (pICH47742)	2xCaMV35S + 5'UTR TMV(pICH51288)	*A. thaliana IspD* (NCBI ID: AF230737.1)	AtuNos (pICH41421)
pL1AtIspE	Level 1 Acceptor Position 2 (pICH47742)	2xCaMV35S + 5'UTR TMV(pICH51288)	*A. thaliana IspE* (NCBI ID: NM_128250.4)	AtuNos (pICH41421)
pL1AtIspF	Level 1 Acceptor Position 2 (pICH47742)	2xCaMV35S + 5'UTR TMV(pICH51288)	*A. thaliana IspF* (NCBI ID: NM_180640.3)	AtuNos (pICH41421)
pL1AtIspG	Level 1 Acceptor Position 2 (pICH47742)	2xCaMV35S + 5'UTR TMV(pICH51288)	*A. thaliana IspG* (NCBI ID: NM_180902.5)	AtuNos (pICH41421)
pL1AtIspH	Level 1 Acceptor Position 2 (pICH47742)	2xCaMV35S + 5'UTR TMV(pICH51288)	*A. thaliana IspH* (NCBI ID: AY168881.1)	AtuNos (pICH41421)
pL1AtIDI	Level 1 Acceptor Position 2 (pICH47742)	2xCaMV35S + 5'UTR TMV(pICH51288)	*A. thaliana IDI* (NCBI ID: NM_121649.6)	AtuNos (pICH41421)
pL1MpGPPS.SSU	Level 1 Acceptor Position 2 (pICH47742)	2xCaMV35S + 5'UTR TMV(pICH51288)	*Mentha x piperita GPPS.SSU* (NCBI ID: AF182827.1)	AtuNos (pICH41421)

pL1PaLimS	Level 1 Acceptor Position 2 (pICH47742)	AtuNos + 5'UTR TMV (pICH87633)	*Picea abies LimS* (NCBI ID: AY473624)	AtuNos (pICH41421)
pL1MpL3H PM2	Level 1 Acceptor Position 2 (pICH47742)	AtuMas (pICH85281)	*Mentha x piperita L3H* PM2 (NCBI ID: AF124817.1)	AtuNos (pICH41421)
pL1MpIPDH	Level 1 Acceptor Position 2 (pICH47742)	AtuOcs (pICH88103)	*Mentha x piperita IPDH* (NCBI ID: AY641428)	AtuNos (pICH41421)
pL1MpIPR	Level 1 Acceptor Position 2 (pICH47742)	*AtAct2* + 5'UTR TMV (pICH87644)	*Mentha x piperita IPR* (NCBI ID: AY300162)	AtuNos (pICH41421)
pL1PpKSI	Level 1 Acceptor Position 2 (pICH47742)	2xCaMV35S + 5'UTR TMV(pICH51288)	*Pseudomonas putida KSI* (Uniprot ID: P07445)	AtuNos (pICH41421)
pL1MpPGR	Level 1 Acceptor Position 2 (pICH47742)	AtuMas (pICH85281)	*Mentha x piperita PGR* (NCBI ID: AY300163)	AtuNos (pICH41421)
pL1MpMMR	Level 1 Acceptor Position 2 (pICH47742)	AtuOcs (pICH88103)	*Mentha x piperita MMR* (NCBI ID: AY288138)	AtuNos (pICH41421)
pL1TBSVp19	Level 1 Acceptor Position 2 (pICH47742)	2xCaMV35S + 5'UTR TMV(pICH51288)	Tomato bushy stunt virus *p19* suppressor of gene silencing (pICH44022)	AtuNos (pICH41421)
pCamV35S::GUS	Level 1 Acceptor	2xCaMV35S + 5'UTR TMV(pICH51288)	*E. coli β-glucuronidase* with two plant	AtuOcs (pICH41432)

	Position 2 (pICH47742)		introns (pICH7511)	
pAtuOcs::GUS	Level 1 Acceptor Position 2 (pICH47742)	AtuOcs (pICH88103)	*E. coli β-glucuronidase* with two plant introns (pICH7511)	AtuOcs (pICH41432)
pAtuMas::GUS	Level 1 Acceptor Position 2 (pICH47742)	AtuMas (pICH85281)	*E. coli β-glucuronidase* with two plant introns (pICH7511)	AtuMas (pICH77901)
pAtuNos::GUS	Level 1 Acceptor Position 2 (pICH47742)	AtuNos + 5'UTR TMV (pICH87633)	*E. coli β-glucuronidase* with two plant introns (pICH7511)	AtuNos (pICH41421)
pAtAct::GUS	Level 1 Acceptor Position 2 (pICH47742)	*AtAct2* + 5'UTR TMV (pICH87644)	*E. coli β-glucuronidase* with two plant introns (pICH7511)	*AtAct2* (pICH44300)
pNtMald1::GUS	Level 1 Acceptor Position 2 (pICH47742)	*Nicotiana tabacum MALD1* (NCBI ID: MG493458.1)	*E. coli β-glucuronidase* with two plant introns (pICH7511)	AtuNos (pICH41421)
pNtCPS2::GUS	Level 1 Acceptor Position 2 (pICH47742)	*Nicotiana tabacum CPS2* (NCBI ID: HE588139.1)	*E. coli β-glucuronidase* with two plant introns (pICH7511)	AtuNos (pICH41421)
pMpLimS::GUS	Level 1 Acceptor Position 2 (pICH47742)	*Mentha x piperita LimS* (NCBI ID: OP527754)	*E. coli β-glucuronidase* with two plant	AtuNos (pICH41421)

			introns (pICH7511)	
pMpL3H::GUS	Level 1 Acceptor Position 2 (pICH47742)	*Mentha x piperita L3H* (NCBI ID: OP527758)	*E. coli β-glucuronidase* with two plant introns (pICH7511)	AtuNos (pICH41421)
pMpPGR::GUS	Level 1 Acceptor Position 2 (pICH47742)	*Mentha x piperita PGR* (NCBI ID: OP527757)	*E. coli β-glucuronidase* with two plant introns (pICH7511)	AtuNos (pICH41421)
pMpIPDH::GUS	Level 1 Acceptor Position 2 (pICH47742)	*Mentha x piperita IPDH* (NCBI ID: OP527756)	*E. coli β-glucuronidase* with two plant introns (pICH7511)	AtuNos (pICH41421)
pL1P1F_MpGPPS.SSU	Level 1 Acceptor Position 1 (pICH47732)	2xCaMV35S + 5'UTR TMV(pICH51288)	*Mentha x piperita GPPS.SSU* (NCBI ID: AF182827.1)	AtuNos (pICH41421)
pL1P3F_MpL3H	Level 1 Acceptor Position 3 (pICH47751)	AtuMas (pICH85281)	*Mentha x piperita L3H* PM2 (NCBI ID: AF124817.1)	AtuNos (pICH41421)
pL1P1FKan	Level 1 Acceptor Position 1 (pICH47732)	*AtAct2* + 5'UTR TMV (pICH87644)	*E. coli nptII* (pICH86966)	*AtAct2* (pICH44300)
KN03	Level 1 Acceptor Position 3 (pICH47751)	Kanamycin resistance part from MoClo kit. Has *AtuNos* promoter, *E. coli NptII* coding sequence, *AtuOcs* terminator (pICSL70004)		
KN04	Level 1 Acceptor Position 4	Kanamycin resistance part from MoClo kit. Has *AtuNos* promoter, *E. coli NptII* coding sequence, *AtuOcs* terminator (pICSL70004)		

	(pICH47761)	

Table 2.2. General level 2 construct parts list. Where applicable, sources of DNA sequences used as parts are shown in brackets as the MoClo ID.

Level 2 Constructs					
Construct ID	Position 1	Position 2	Position 3	Position 4	Position 5
pL2_LimS	Level 2 Acceptor (pAGM4673)	pL1P1F_MpGPPS.SSU	KN03	Level 2 end-linker 3 (pICH49277)	N/A
pL2_L3H	Level 2 Acceptor (pAGM4673)	pL1P1F_MpGPPS.SSU	pL1P3F_MpL3H	KN04	Level 2 end-linker 4 (pICH49283)
pL2Kan:GUS	Level 2 Acceptor (pAGM4673)	pL1P1FKan	pAtuNos::GUS	Level 2 end-linker (pICH49266)	N/A
pL2Mald1:GUS	Level 2 Acceptor (pAGM4673)	pL1P1FKan	pNtMald1::GUS	Level 2 end-linker (pICH49266)	N/A
pL2CPS2:GUS	Level 2 Acceptor (pAGM4673)	pL1P1FKan	pNtCPS2::GUS	Level 2 end-linker (pICH49266)	N/A
pL2LimS:GUS	Level 2 Acceptor (pAGM4673)	pL1P1FKan	pMpLimS::GUS	Level 2 end-linker (pICH49266)	N/A

pL2L3H:GUS	Level 2 Acceptor (pAGM4673)	pL1P1FKan	pMpL3H::GUS	Level 2 end-linker (pICH49266)	N/A
pL2IPDH:GUS	Level 2 Acceptor (pAGM4673)	pL1P1FKan	pMpIPDH::GUS	Level 2 end-linker (pICH49266)	N/A
pL2PGR:GUS	Level 2 Acceptor (pAGM4673)	pL1P1FKan	pMpPGR::GUS	Level 2 end-linker (pICH49266)	N/A

Table 2.3. Whole menthol biosynthesis pathway level 1 construct parts list. Sources of DNA sequences are shown in brackets, with either the MoClo part ID or NCBI ID shown.

Whole Menthol Biosynthesis Pathway Construction – Level 1 constructs				
Construct ID	Backbone	Promoter	Coding Sequence	Terminator
KN01	Level 1 Acceptor Position 1 (pICH47732)	Kanamycin resistance part from MoClo kit. Has *AtuNos* promoter, *E. coli NptII* coding sequence, *AtuOcs* terminator (pICSL70004)		
MM02	Level 1 Acceptor Position 2 (pICH47742)	*AtLHB1B2* (pICH45131) + 5'UTR TMV chloroplast transit peptide (pICH78133)	*Abies grandis GPPS* (NCBI ID: AF513112.1)	AtuNos (pICH41421)
MM05	Level 1 Acceptor Position 3 (pICH47751)	*AtLHB1B1* (pICH45125) + 5'UTR TMV chloroplast transit peptide (pICH78133)	*Picea abies LimS* (NCBI ID: AY473624)	AtuNos (pICH41421)
MM06	Level 1 Acceptor Position 4 (pICH47761)	*AtRbcsS1B* (pICH45234)	*Mentha x piperita L3H* PM2 (NCBI ID: AF124817.1)	CaMV35S (pICH41414)

MM07	Level 1 Acceptor Position 5 (pICH47772)	*SlRbcs1* (pICH71292)	*Mentha x piperita IPDH* (NCBI ID: AY641428)	AtuNos (pICH41421)
MM08	Level 1 Acceptor Position 6 (pICH47781)	*SlRbcs3A* (pICH71311)	*Mentha x piperita IPR* (NCBI ID: AY300162)	CaMV35S (pICH41414)
MM09	Level 1 Acceptor Position 7 (pICH47791)	*AtRbcS2B* (pICH45195)	*Pseudomonas putida KSI* (Uniprot ID: P07445)	AtuNos (pICH41421)
MM10	Level 1 Acceptor Position 1 (pICH47732)	*SlRbcs2* (pICH71301)	*Mentha x piperita PGR* (NCBI ID: AY300163)	CaMV35S (pICH41414)
MM11	Level 1 Acceptor Position 2 (pICH47742)	*AtuMas* (pICH85281)	*Mentha x piperita MMR* (NCBI ID: AY288138)	AtuNos (pICH41421)

Table 2.4. Whole menthol biosynthesis pathway level 2 construct parts list. Sources of DNA sequences are shown in brackets with the MoClo part ID shown.

Whole Menthol Biosynthesis Pathway Construct – Level M/P							
Construct ID	Position 1	Position 2	Position 3	Position 4	Position 5	Position 6	Position 7
CMM17 – M1	Level M Acceptor Position 1 (pAGM8031)	KN01	MM02	MM05	MM06	MM07	Level M end-linker 5 (pICH50914)
CMM17 – M2	Level M Acceptor Position 6 (pAGM8081)	MM08	MM09	MM10	MM11	Level M end-linker 2 (pICH50881)	N/A
ppL2_MBP	Level P Acceptor (pICH82094)	CMM17 – M1	CMM17 – M2	Level P end-linker 2 (pICH79264)	N/A	N/A	N/A

2.4 Metabolite Extraction and Chemical Analysis

2.4.1 Solvent extraction of Black Mitcham leaves

Black Mitcham leaves were ground in hexane spiked with decane at a concentration of 0.1mg/mL to account for losses during extraction (> 99%, Sigma-Aldrich) for 2 minutes using a glass rod. The amount of hexane used was standardised to the weight of leaf tissue, at a ratio of 1 mL hexane per 0.1g of leaf tissue. Leaf extracts were filtered to remove leaf material and debris, and blown down to a volume of 300 µL under a nitrogen stream.

2.4.2 Solvent extraction *Nicotiana benthamiana* leaves

N. benthamiana leaf tissue was first surface extracted with dichloromethane with enough to cover the leaf surface, then the leaves were ground in liquid nitrogen until homogenised, and further extracted with dichloromethane. Leaf extracts were filtered to remove leaf material and debris, and solvent extracts were blown down to a volume of 300 µL under a nitrogen stream.

2.4.3 Dynamic headspace sampling

2.4.3.1 Preparation of Porapak Q filters

Porapak Q adsorbent filters (“Porapak tubes”) were prepared using glass tubes (~8 cm in length) packed sequentially with glass wool (1.5 cm), Porapak Q (0.048–0.052 g), and a final 1.5 cm plug of glass wool. All tubing, vials, and forceps used in filter preparation were pre-rinsed with diethyl ether. Prior to use, Porapak tubes were cleaned by rinsing three times with diethyl ether (≥99%) and conditioned at 132 °C under nitrogen flow for 2 h. Following use, tubes were re-cleaned and reconditioned before storage in sealed Falcon tubes.

2.4.3.2 Air entrainment of whole plants

Volatile organic compounds were collected using an air entrainment system (Webster et al. 2008; Ferretti et al. 2025). Charcoal-filtered air was introduced into an oven-treated plastic bag (previously heated at 60 °C for ≥12 h to reduce background contamination) at a flow rate of 1000 mL min^{-1}. Air was withdrawn through a Porapak Q adsorbent filter (50 mg, 50/80 mesh, Supelco) at 400 mL min^{-1}, creating a slight positive pressure within the bag to prevent contamination from ambient air and

eliminating the need for an airtight seal. Plant samples were enclosed individually in bags, and entrainment was performed for 24 hours.

2.4.3.3 Collection and elution of volatiles

After entrainment, Porapak filters were carefully removed and volatiles were desorbed by elution with 1 mL of HPLC-grade diethyl ether (99.9%) through each tube using a needle and syringe, and eluates were collected in GC–MS vials. All samples were stored at −20°C prior to GCMS analysis

2.4.4 Liquid sample GCMS conditions

Samples were injected into a Thermo Trace 1300 gas chromatograph fitted with a Thermo TG-5MS column (30 m × 0.25 mm × 0.25 µm) and detected using a Thermo ISQ LT mass spectrometer. The injection port was operated at 200 °C, into which 1 µL of the sample was injected and loaded onto the column at a 1:5 split ratio, with the column being operated at 1 mL min^{-1} He carrier gas. The GC oven was run with a ramped temperature profile; initial temperature 50 °C for 2 min, ramp at 5 °C min^{-1} to 230 °C and held for 12 min. The mass spectrometer was operated with a transfer line temperature of 250 °C, an ion source temperature of 230 °C and a mass scan range of 35–350, with a 2 min solvent delay.

2.4.5 SPME extraction and GCMS conditions

Volatile compounds were analysed using headspace solid phase microextraction (SPME) coupled with gas chromatography–mass spectrometry (GC–MS). A 50/30 µm divinylbenzene/carboxen/polydimethylsiloxane (DVB/CAR/PDMS) fibre (Supelco, Cat no. 57328-U) was used for volatile collection. Before use, the fibre was conditioned according the manufacturer instructions.

For collection of volatiles, leaf tissue was placed into 20 mL headspace vials (Agilent, Cat no. 5182-0839) and placed in a 60°C water bath. The SPME fibre was then inserted into the vial, and volatile adsorption onto the fibre was performed for 30 mins. The fibre was then desorbed in the front inlet of the GCMS machine at 230 °C for 2 min equipped with a Restek Topaz SPME liner (0.75 mm × 6.35 mm × 78.5 mm) (Restek, Cat no. 23434). Between injections, fibres were conditioned in the front inlet at 230°C for 10–30 min to minimize carryover.

GC–MS analyses were carried out on a Thermo Trace 1300 gas chromatograph fitted with a Thermo TG-5MS capillary column (30 m × 0.25 mm × 0.25 µm) and coupled to a Thermo ISQ LT mass spectrometer. The injection port was operated in split mode at 230 °C with a carrier pressure of 55.68 kPa, a column flow of 1 mL min^{-1} He, a purge flow of 5 mL min^{-1}, and a split flow of 10 mL min^{-1}. The oven was programmed with an initial temperature of 50 °C for 2 min, ramped at 5 °C min^{-1} to 230 °C, and held for 12 min.

2.4.6 GC-MS data processing

GC–MS data were processed using Chromeleon (Version 7.2 SR4; Thermo Scientific, USA) and the deconvolution and integration of signal peaks occurred in AMDIS (NIST, 2014). Where available, authentic standards of (-)-limonene, (+)-pulegone, (-)-menthone, (-)-menthol and (+)-menthofuran were used to compare retention time and m/z spectra of compounds putatively identified by NIST.

2.4.7 SPME volatile semi-quantification and analysis

A standard curve for (-)-limonene was produced by spiking 10 µL of ethanol-diluted analytical standards (>99%, Sigma Aldrich) into samples, corresponding to added masses of 3.125, 31.25, 62.5, 125, 250, 500, and 1000 ng of (-)-limonene. Adsorption onto the fibre was performed as in 2.4.5, and the areas under peaks for (-)-limonene were used to generate a standard curve. Semi-quantification of limonene in plant tissue samples was performed by comparison of the areas under putatively identified limonene peaks to that of the standard curve. The corresponding mass of limonene in the unknown plant tissue samples was then normalised against the weight of the leaf tissue being analysed to give the limonene content as ng/g of fresh weight (FW). The measurements from three biological replicates were used to calculate the mean and standard deviation.

2.4.8 Black Mitcham essential oil semi-quantification and analysis

The peak area for all identified peaks (excluding decane) were normalised against the peak area for decane to calculate the normalised peak area. The normalised peak area was then normalised against the weight of the leaf sample to calculate normalised peak area by leaf mass. The normalised peak area by leaf mass for all identified peaks was summed, and results expressed as relative abundance (%) of

each compound within a sample. Three biological replicates were used for each analysis, and results presented as the mean and standard deviation.

2.5 RNA extraction, cDNA synthesis and transcript detection

2.5.1 RNA extraction

RNA extraction was performed using the RNeasy® Plant Mini Kit (Qiagen, Cat no. 74903). Plant tissue was that had been flash frozen in liquid nitrogen and stored at -80ºC was ground in a sterilised mortar and pestle, using liquid nitrogen to keep tissue frozen at all times. Ground tissue (50 mg) was then added to an RNase-free, liquid nitrogen cooled 2 mL Eppendorf tube, and 450 µL of Buffer RLC (supplemented with β-mercaptoethanol (BME) to a final concentration of 1% (v/v)) was immediately added, and vortexed vigorously. The resulting lysate was transferred to a QIAshredder spin column placed in a 2 mL collection tube, and centrifuged at 20,800 *x g* for 2 minutes. The supernatant of the flow-through was carefully transferred to a sterile 1.5 mL Eppendorf tube, and 0.5 volume of 100% ethanol was added and mixed by pipetting. The entire solution (typically ~600-650 µL) was then transferred to an RNeasy Mini spin column in a 2 mL collection tube, and centrifuged at 10,000 *x g* for 15 seconds, and the flow through then discarded. 700 µL of Buffer RW1 was then added to the spin column, centrifuged at 10,000 *x g* for 15 seconds and the flow through then discarded. 500 µL of Buffer RPE was then added to the spin column, centrifuged at 10,000 *x g* for 15 seconds and the flow through then discarded. An additional 500 µL of Buffer RPE was then added to the spin column, centrifuged at 10,000 *x g* for 2 minutes, and the flow through discarded. Then spin column was then placed in a new 2 mL collection tube and centrifuged at 20,800 *x g* for 1 minute to remove any residual buffer. The spin column was then placed in a sterile 1.5 mL Eppendorf tube, and 30 µL of sterile nuclease free water, preheated to 65ºC was added to the spin column membrane, and incubated at room temperature for 1 minute. Following incubation, the spin column was centrifuged at 10,000 *x g* for 1 minute to elute the RNA.

2.5.2 DNAse Treatment of RNA

DNA contamination in RNA samples was removed using the DNA-*free*™ DNA Removal Kit (Invitrogen, Cat no. AM1906). For a 50 µL total reaction mix, 44 µL of RNA was mixed with 5 µL of 10X DNase I Buffer, and 1 µL of DNase Enzyme. The

reaction mix was then incubated at 37ºC for 20 minutes. Following incubation, 5.5 µL of DNase Inactivation Agent was added to the reaction mix, and the tube was flicked periodically during an incubation at room temperature for 2 minutes. The reaction mix was then centrifuged at 10,000 *x g* for 30 seconds at 25ºC, and the resulting supernatant was transferred to a sterile 1.5 mL Eppendorf tube.

2.5.3 cDNA synthesis

DNA-free RNA was reverse transcribed using a ProtoScript® II First Strand cDNA Synthesis Kit (NEB, Cat no. E6560S). Ideally, 1µg of RNA in 6 µL total volume was used as input. Where this was not possible due to low RNA concentrations, the maximum amount of RNA that could be obtained from 6 µL of the lowest concentration RNA sample was used as the input, and other RNA samples in the same experiment would then use this same RNA amount. In a PCR tube containing the 6 µL RNA sample, 2 µL dNTPs (Oligo d(T)23 VN) was added to anneal to the poly(A) tail of mRNA, and the solution was incubated at 65ºC for 5 minutes. The solution was briefly centrifuged to remove condensation build up in the lid of the PCR tube, and placed on ice. Protoscript II Reaction Mix (10 µL), followed by 2 µL of Protoscript Enzyme Mix was added to the tube. The tube was then flicked to mix the reagents, and briefly centrifuged to bring the reagents to the bottom of the tube. The reaction mixes were then incubated at 42ºC for 1 hour, followed by incubation at 80ºC for 10 minutes to deactivate the enzyme.

2.5.4 Reverse transcriptase PCR

For reverse transcriptase (RT) PCR, the resulting cDNA was diluted 1 in 10 with nuclease free water. To perform RT-PCR, 0.1 µL of cDNA template was added to a final PCR reaction volume of 15 µL (1X PCRBIO Taq Mix Red (PCRBiosystems, Cat no. PB10.13-02), 0.5 µM forward primer, 0.5 µM reverse primer). Thermocycling conditions used were 95˚C for 2 minutes, then 35 cycles of 95°C denaturation for 10 seconds, 55°C annealing for 10 seconds, and 72°C amplification for 20 seconds per kilobase of amplicon DNA, followed by a final amplification stage of 72°C for 2 minutes.

2.6 RNAseq analysis

2.6.1 Library preparation, sequencing and data analysis

Black Mitcham plants for the RNAseq work were grown at the Talybont green houses (Cardiff, UK) between the months of January to March 2025, supplemented with artificial light (Kroptek Sunstream). Plants were grown in a potting mix consisting of 15 parts Levington Advance M2, 1 part sharp sand, 1 part perlite standard grade and 1 part vermiculite medium grade. Leaves were harvested from individual plants at three different developmental stages termed ‘Vegetative’, ‘Early flowering’ and ‘Late flowering’. Three biological replicates were taken for each leaf pair harvested. Leaves were then excised from the plant, petiole removed and then cut length-wise. For each leaf, half of the leaf was subjected to oil profile analysis, and the other half was frozen in liquid nitrogen for RNA extraction. RNA extraction and DNAse treatment was performed as in section 2.5.1 and section 2.5.2.

RNA was normalised to 225 ng total RNA as quantified by a Qubit fluorometer, and RNA quality was checked using a TapeStation D1000. The libraries were then prepared using a directional NEB RNA ultra ii prep with an upfront polyA module. Libraries were then sequenced on an Illumina NovaSeq 6000 platform in paired end mode, with read lengths of 2 x 150 bp, and to a sequencing depth of 60 million reads.

Reads were assessed using FastQC (v0.11.9), and fastp (0.23.4 – mr6qifo) was used to removed remove adaptor sequences and low quality sequences. MultiQC (1.9) was then used to aggregate the results of FastQC to analyse reads before and after fastp quality control. Reads were aligned to the *M. x piperita* cv. Black Mitcham genome (NCBI Genome Assembly ID: ASM4114648v1) (Talbot et al. 2024) using STAR (2.7.6a) (Dobin et al. 2012). The BAM files outputted from STAR were then sorted by genomic coordinates using samtools (1.17), and duplicates were marked using picard (3.0.0 – cnu7rdq). Basic alignment statistics (e.g. total reads, mapped reads, read length distribution, and duplicate read counts) were obtained using bamtools (v2.5.1) for each BAM file. These metrics were used to assess sequencing quality and to compare data before and after duplicate marking or removal. Read counts per gene were obtained using *featureCounts* the Subread package (2.0.6-abbqxcc), and summarised at the gene level using the gene_id attribute. The

resulting read counts were used as input for analysis using the DESeq2 module (Love et al. 2014),and downstream data analysis was performed in R (version 4.5.0). Three files of pairwise comparisons (late flowering vs vegetative, early flowering vs vegetative, and late flowering vs early flowering) were generated, which contained information for normalised gene counts and relative expression (in the form of Log_2 Fold Change (Log_2FC) values) of DEGs. A cutoff p adjusted (padj, as determinted by the Benjamini-Hochberg correction method used by DESeq2) of < 0.05, and a Log_2FC >1 or <-1 was implemented on DEGs, and only DEGs which passed this threshold were used in subsequent downstream analysis.

To assess sample quality and global expression patterns, data were variance-stabilised using the regularised log (rlog) transformation. Sample-to-sample distances were visualised with hierarchical clustering and heatmaps (pheatmap v1.0.12; RColorBrewer v1.1-2). Principal component analysis (PCA) was performed to examine variance structure across conditions (ggplot2 v3.3.5). Additional exploratory plots included boxplots of transformed counts and dendrograms of hierarchical sample clustering.

Functional gene annotation was performed by using command line BLASTx from the Blast+ module (2.12.0) against both the *A. thaliana* (taxid: 3702) and *Lamiaceae* (taxid: 4136) NR databases (NCBI non-redundant protein sequences). The settings used in the BLASTx were - max_target_seqs 1, -max_hsps 1 and -evalue 1E-5. The output format (outfmt) was "6 qseqid sseqid pident salltitles length mismatch gapopen qstart qend sstart send evalue bitscore".

2.6.2 Promoter analysis

Promoter analysis was performed using PlantTFDB v5.0 using the species *Salvia miltiorriza* (Jin et al. 2017). Promoters were chosen as either the intergenic region between the translational start site of the gene and the start or end of the next gene, or as the 2000 bp intergenic region upstream from the translational start site. The counts for each transcription factor binding site (TFBS) family per promoter sequence were visualised using ggplot2 v3.3.5.

2.6.3 Functional enrichment analysis

Functional enrichment analysis was performed using g:Profiler g:GOSt (version *e113_eg59_p19_f6a03c19*) (Kolberg et al. 2023), using *A. thaliana* as the

organism, and with a g_SCS threshold of 0.05 applied. Only DEGs which had a corresponding *A. thaliana* ID from BLASTx annotation could be used for this analysis. For Gene Ontology Terms (GO:MF, GO:CC, GO:BP), only driver terms were highlighted. Visualisation was performed using ggplot2 v3.3.5.

2.6.4 K-means clustering

Normalised gene expression data from DESeq2 for each developmental stage were first imported into R (version 4.5.0) and organized with genes as rows and samples as columns. For each gene, the mean expression across biological replicates was calculated for three stages: Vegetative, Early Flowering, and Late Flowering.

To make expression profiles comparable across genes, the data were row-scaled: for each gene, the mean expression across stages was subtracted and divided by the standard deviation, producing a matrix of standardized values. This ensures that clustering reflects the relative expression patterns of each gene across stages rather than absolute expression levels.

The optimal number of clusters (k) was assessed using three complementary approaches: the Elbow method, silhouette analysis, and the gap statistic, implemented with the factoextra (version 1.0.7) R package. K-means clustering was then performed on the scaled expression data using the kmeans function with 25 random starts (nstart = 25) to improve convergence and reproducibility. Genes were assigned to clusters according to the resulting cluster centroids.

Cluster-specific mean expression profiles were calculated by averaging scaled expression values across all genes within each cluster. These profiles were visualized using line plots and faceted plots showing both individual gene trajectories and cluster means, with standard deviation shading to illustrate intra-cluster variation.

2.6.5 Heatmaps of menthol biosynthesis genes

Heatmaps of menthol biosynthesis genes were produced in R (version 4.5.0) using pheatmap (v1.0.12), using the log_2FC values as an input. For visualisation purposes, log_2FC values that had ‘NA’ as a value were changed to 0.

2.6.6 Venn diagrams

Venny (v2.1) (Oliveros 2015) was used to compare gene lists between developmental stage comparisons and generate Venn diagrams.

2.6.7 Reverse transcriptase quantitative PCR

Validation of RNAseq data was performed by RT-qPCR. RT-qPCR was conducted on the Rotorgene 6000 RT-PCR machine (Qiagen) using qPCRBIO SyGreen Lo-Rox Mix (PCR Biosystems) and *MpBetaActin* (BMitcham.V1_g90804) as reference. Although the use of multiple validated reference genes is recommended to maximise normalisation accuracy, due to practical constraints, *MpBetaActin* has been previously used as a single reference gene under similar conditions (Rieu and Powers 2009; Ahkami et al. 2015). cDNA was first diluted from 20 µL to 150 µL with nuclease free water, and 2.5 µL of cDNA was added to 5 µL qPCRBIO SyGreen Lo-Rox Mix mastermix, with 2.5 µL of primer mix (1.25 µM forward and reverse primer mixed together). Thermocycler conditions were as follows: 95^{o}C for 10 mins, followed by 45 cycles of 95^{o}C for 5 seconds, then 60^{o}C for 30s. Acquisition was performed on the green channel at the end of the 30s 60^{o}C of each cycle. After 45 cycles, temperature increased from 50-95^{o}C to perform melt analysis to ensure single products produced. Data was analysed using the $\Delta\Delta$CT method (Livak and Schmittgen 2001). One biological replicate and three technical replicates were used to generate average relative expression and standard deviation (error bars).

2.7 Microscopy

Imaging was performed using a Nikon dissecting microscope and images captured using a GXCAM Hi Chrome-SMII camera. Post image processing was performed using ImageJ.

2.8 Statistical analysis

Statistical analyses were performed in R (version 4.5.0). Data manipulation and visualisation were carried out using the tidyverse (version 2.0.0) (Wickham et al., 2019). Assumptions of normality were assessed using the Shapiro–Wilk test and visual inspection of Q–Q plots and histograms of residuals, as these are standard, complementary approaches for detecting deviations from normality in model residuals. Homogeneity of variance was tested using Levene's test from the car package (version 3.1-3), which is robust to deviations from normality and widely

recommended for evaluating equality of variances in biological data. Where assumptions were satisfied, one-way or two-way ANOVA (base R) was conducted to test for overall treatment and factor effects, and, where the global F-test was significant, pairwise treatment differences were explored using Tukey's Honest Significant Difference (HSD) post-hoc tests to obtain all pairwise comparisons while controlling the family-wise error rate. Although the routine use of multiple comparison procedures has been questioned, their application is appropriate when the primary aim is to compare all treatment means rather than a small number of pre-planned contrasts; in this context, Tukey's HSD provides a transparent and reproducible way to identify which groups differ while maintaining a controlled Type I error rate across comparisons. Where data violated assumptions, the non-parametric Kruskal–Wallis test (base R) was used as a rank-based alternative to ANOVA, followed by Dunn's post-hoc tests implemented using the FSA package (version 0.10.0) to allow multiple pairwise comparisons with appropriate p-value adjustment under non-parametric conditions. Compact letter displays for post-hoc comparisons were generated using multcompView (version 0.1-10) to summarise groups that did and did not differ significantly. For visualisation, ggplot2 (version 3.5.2) and ggpubr (version 0.6.1) were used to generate boxplots and bar plots with error bars, and Microsoft Excel was used to generate bar graphs where no statistical analysis was performed. Statistical significance was defined at $p < 0.05$.

2.8.1 Statistical analysis – *in vitro* regeneration (chapter 3)

Regeneration frequencies obtained from independent in vitro culture experiments (chapter 3) were compared across explant types and hormone treatments using a two-way ANOVA to test for main effects and their interaction.

2.8.2 Statistical analysis – transformation efficiency (chapter 4)

Regeneration frequencies obtained from independent transformation experiments (chapter 4) were compared across *Agrobacterium* strains using a one-way ANOVA.

2.8.3 Statistical analysis – metabolite concentration (chapter 4 and 5)

Limonene concentrations obtained from independent experimental replicates were compared across samples using a one-way ANOVA (chapter 4). Essential oil compound concentrations were compared across developmental stages using a one-way ANOVA for each compound (chapter 5).

Chapter 3 - Optimizing *in vitro* regeneration of *M. x piperita* cv. Black Mitcham and approaches towards genetic engineering

3.1 Introduction

3.1.1 Regeneration and transformation techniques and approaches used for *Mentha*

M. x piperita cv. Black Mitcham is a cultivar of peppermint commonly grown for both commercial use and research (Tucker 2012). Black Mitcham is thought to be a natural hybrid of *M. aquatica* and *M.* spicata, where Black Mitcham has chromosome numbers of 2n = 6x = 72 based on karyotype data (Harley and Brighton 1977). Consequently, Black Mitcham is a sterile hybrid, and thus is not amenable to conventional breeding techniques to allow introgression of desirable genetic traits. Black Mitcham is prized commercially for its essential oil content which is rich in monoterpenoids such as menthol and menthone (Schmidt et al. 2009; Ludwiczuk et al. 2016). However, the essential oil composition can also vary over developmental stage, and depending on growth conditions can produce unwanted monoterpenes such as menthofuran which imparts an “off” taste to the oil (Benn 1998; Abdi et al. 2019). Thus, genetic engineering approaches have looked at approaches to alter the essential oil composition by targeting the genes responsible for essential oil biosynthesis (Lange et al. 2011). However, genetic engineering of plants requires a robust transformation method, and many plants are recalcitrant to this approach (Bélanger et al. 2024).

Plant transformation techniques can be broadly classified into direct and indirect gene transfer (Low et al. 2018). Direct gene transfer involves the introduction of exogenous DNA directly into the plant genome (Paszkowski et al. 1984). This is typically done through physical or chemical means, including but not limited to particle bombardment, PEG or electroporation (Su et al. 2023). Direct gene transfer methods in *Mentha* have been seldom reported, and have not seen widespread use in the literature. PEG mediated transformation of Black Mitcham protoplasts has been reported only once, with no follow up work or other authors reporting its use (Krasnyanski et al. 1999). Attempts to transform Black Mitcham utilizing biolistic bombardment were reported in a single publication, where no stable transgenic

plants were recovered from over 22,000 leaf explants (Niu et al. 1998). The authors did however report the presence of transient *uidA* gene expression, hinting at the utility of biolistic bombardment being used as a potential platform to rapidly test construct activity in Black Mitcham.

Indirect gene transfer involves the use of an intermediate biological vector to carry the exogenous DNA and insert it into the plant genome (Bélanger et al. 2024). The biological vector of choice for stable integration is typically the use of *A. tumefaciens* (Gelvin 2017). *A. tumefaciens*-mediated transformation is the most widely used option in many plant species (Hao et al. 2024). *A. tumefaciens*-mediated transformation has been reported for the *Mentha* species, including Black Mitcham (Diemer et al. 1998; Niu et al. 1998; Krasnyanski et al. 1999; Lange et al. 2011; Yu et al. 2022). Therefore, for the purposes of this thesis, *A. tumefaciens*-mediated transformation was chosen as the means to introduce genetic changes into Black Mitcham. Due to the varied approaches taken in the literature in *A. tumefaciens*-mediated transformation of mint, and the varied transformation efficiencies reported, one of the aims of this chapter was to develop a standardized protocol. There were several factors to consider in standardizing this procedure, such as *A. tumefaciens* strain, concentration of *A. tumefaciens* cells (typically measured by OD_{600}), explant source, type, *A. tumefaciens* co-cultivation time, explant preculture on callus induction medium, means to enhance *A. tumefaciens* virulence (typically done by addition of Acetosyringone) and addition of chemical additives (such as AC or PVPP) (Aboofazeli et al. 2024). A summary of successful *A. tumefaciens* mediated transformation of Black Mitcham is shown in

Table 3.1. Summary of successful *Agrobacterium mediated* transformation protocols from the literature.

Source	*Agrobacterium* Strain	OD	Explant Source	Explant Type	Basal Medium	Co-cultivation medium	*Agrobacterium* and explant cocultivation time	*Agrobacterium* co-cultivation conditions	Selection Medium	Shoot Elongation Medium	Chemical Additives
Niu et al. 1998	EHA105	1	3–6-week-old *in-vitro* plants	Leaf with petiole (1cm or less in length)	MS salts, 100 mg/L myo-inositol, 0.4 mg/L thiamine, 7.5 g/L agar and 30 g/L sucrose, and 0.1 mg/L BAP, pH 5.8	25% coconut water, 2 mg/L TDZ	30 minutes	4 - 5 days in darkness at 26°C	25% coconut water, 2 mg/L TDZ, 20 mg/L kanamycin, 200mg/L Ticar	15 mg/L Kanamycin, 100 mg/L Ticar	N/A
Niu et al. 2000	EHA105	1	3–6-week-old *in-vitro* plants	Leaf with petiole (1cm or less in length)	MS salts, 100 mg/L myo-inositol, 0.4 mg/L thiamine, 7.5 g/L agar and 30 g/L sucrose, and 0.1 mg/L BAP, pH 5.8	2 mg/L TDZ	30 minutes	4 - 6 days in darkness at 26°C	2 mg/L TDZ, 30 mg/L Kanamycin, 200mg/L Ticar	0.01 mg/L NAA, 2 mg/L TDZ, 30 mg/L Kanamycin, 200mg/L Ticar	Tobacco liquid cell suspensions
Krasnyanski et al. 1999	GV3101	0.8-1	*In-vitro* plants - age not specified	Internode segments (5-7mm)	MS salts with Gamborg vitamins, 2% sucrose and 0.35% Phytagel (Sigma), pH 5.7	25% coconut water, 2 mg/L BAP, 3 mg/L TDZ	20-30 minutes at 28°C in darkness	2 days in darkness at 25°C	300 mg/L timentin, 20 mg/L Kanamycin	N/A	N/A
Mahmoud and Croteau 2001	EHA105	1	Not specified, cites Niu 1998, 2000	Not specified, cites Niu 1998, 2000	Not specified, cites Niu 1998, 2000	Not specified, cites Niu 1998, 2000	Not specified, cites Niu 1998, 2000	Not specified, cites Niu 1998, 2000	Not specified, cites Niu 1998, 2000	Not specified, cites Niu 1998, 2000	0.2 mM Acetosyringone
Yu et al. 2022	EHA105	0.6	4-week-old *in-vitro* plants	Internode segments (2mm)	Murashige and Skoog (MS) (Murashige and Skoog 1962) 2% (w/v) sucrose, 1% agar pH 5.8	25% coconut water, 3 mg/L TDZ 0.2 mg/L IAA	30 minutes	4 days at 2°6C	25% coconut water, 3 mg/L TDZ, 0.2 mg/L Indole-3-acetic acid, 3 mg/L Hygromycin, 125 mg/L cefotaxime	5 mg/L Hygromycin, 125 mg/L cefotaxime	N/A

A. tumefaciens-mediated transformation works on the basis of T-DNA integration from the *A. tumefaciens* into the plant cell nucleus (Gelvin 2017). This occurs during the co-cultivation of *A. tumefaciens* with the plant explants, where individual cells are infected. The regeneration of a whole transformed plant, therefore relies on the totipotency of the plant cells to regenerate a whole new plant arising from a single, infected plant cell (Shiboleth and Tzfira 2012). This not only emphasises the importance of the choice of explant type, but also the need to have a robust *in vitro* regeneration protocol.

Reports for *in vitro* regeneration of *M. x piperita* are extensive within the literature (Niu et al. 1998; Bhat et al. 2002; Wang et al. 2009; Thul and Kukreja 2010; Fejér et al. 2018; Yu et al. 2022). However, making direct comparisons between these reports is difficult due to the difference in growth medium, explant types used, PGRs used, growth conditions and how the authors deemed the most “optimal” conditions were. This is not an uncommon finding in TC practice, where well established, standardized TC protocols are often missing in agricultural plants (Bennur et al. 2025). *In vitro* regeneration typically proceeds through either direct or indirect somatic embryogenesis, and direct or indirect *de novo* organogenesis (Hill and Schaller 2013). Irrespective of the route taken towards regeneration of a new plant, some factors to consider when optimizing such a protocol are explant source, explant age, PGRs and basal growth medium composition (Long et al. 2022).

In terms of PGRs used to induce regeneration from Black Mitcham explants, the cytokinins TDZ, ZT, BAP and KIN, and the auxins NAA, IBA and IAA have commonly been used in different proportions and combinations to each other (Diemer et al. 1998; Niu et al. 1998; Wang et al. 2009; Fejér et al. 2018; Yu et al. 2022). In addition, coconut water was commonly added to the TC medium, which is thought to aid in the induction of plant regeneration due to its cytokinin type activity (George and Sherrington 1984). There are also a wide variety of cytokinins present in coconut water, with the kinetins and zeatins thought to impart its cytokinin-like properties with respect to plant TC (Yong et al. 2009). However when addressing the problem of optimizing a TC protocol, the inherent biological variability introduced from adding coconut water to a growth medium presents issues as the exact concentrations of the chemical constituents will vary. Coconut water is typically added into growth media in terms of percentages, however this again introduces variability as the

coconut water itself is still biologically variable. Furthermore, it was also found that in terms of Black Mitcham *A. tumefaciens*-mediated transformation and regeneration, coconut water inhibited the regenerative, and subsequent transformation efficiency of Black Mitcham explants (Niu et al. 2000). Therefore, for the purposes of this chapter to develop an optimised regeneration protocol, coconut water was excluded from the medium.

The genotype of the explant is also of particular importance, which has been exemplified in studies on agricultural crops such as soybean and maize, where genotype differences showed considerable variation in both regeneration and transformation potential (Frame et al. 2006; Song et al. 2013; Yang et al. 2016). Taken together, there is much need for an optimised *in vitro* regeneration, and subsequent *A. tumefaciens*-mediated transformation protocol for Black Mitcham.

Besides *A. tumefaciens*-mediated transformation, there have been no recent reports of the use of more novel techniques as a mechanism to transform Black Mitcham, or even any other *Mentha* species. As Black Mitcham is a sterile hybrid which is clonally propagated and does not produce seed, this removes the option of trialling any form of germline transformation such as floral dipping or pollen transformation (Clough and Bent 1998; Eapen 2011). The fact that Black Mitcham is clonally propagated, and reproduces vegetatively does however lead to the interesting possibility of utilizing a novel “direct injection” method (Mei et al. 2023). The Regenerative Activity-dependent in Planta Injection Delivery (RAPID) method relies on direct injection of an *A. tumefaciens* solution containing a construct of interest into a plant cutting, and subsequently regenerating a potential transgenic plant from either adventitious root or shoot formation. In the context of *M. x piperita,* this would rely on regeneration from transformed rhizomes, and subsequently, new plants resulting from the potential transgenic rhizomes. This was therefore trialled in this thesis as potential preliminary work towards a novel transformation method.

3.1.2 Aims and Objectives

The overarching aims of this chapter were to address two major shortcomings in the literature regarding the potential genetic manipulation of Black Mitcham: (1) The lack of a standardized and reproducible *in vitro* regeneration system, and (2) the low

transformation efficiency and reliability of *A. tumefaciens*-mediated transformation with respect to Black Mitcham. These aims were explored by:

1. Evaluating the regenerative capacity of different explant types under different PGR regimes in Black Mitcham
2. Exploring the use of PGR regimes optimised for Black Mitcham in other *Mentha* species
3. Trialling the use of 2,4-D in callus and subsequent regeneration in Black Mitcham
4. Characterizing the effects of the use of the novel PGR FPX for applications towards *in vitro* regeneration of Black Mitcham
5. Developing an optimised *A. tumefaciens*-mediated transformation protocol for Black Mitcham through the optimisation of key parameters
6. Investigating the use of the novel RAPID technique applied to Black Mitcham
7. Investigating the potential of biolistic bombardment to test construct efficacy in Black Mitcham

3.2 Results

3.2.1 Black Mitcham explant choice optimisation

An initial goal was to standardize the explant source that offered the best balance between ease of dissection, availability, and regenerative capacity. Since Black Mitcham propagates vegetatively and does not produce seed, a baseline source first had to be established. This was achieved by excising the shoot apex and first leaf pair from Black Mitcham stock plants maintained in sterile tissue culture vessels and transferring it into fresh vessels (Figure 3.1). Creating this baseline ensured that the age of the plant tissue and subsequent explant sources could be accounted for in the downstream optimisation steps. This also helped to standardize the starting material to ensure only a single primary shoot was taken as an explant source.

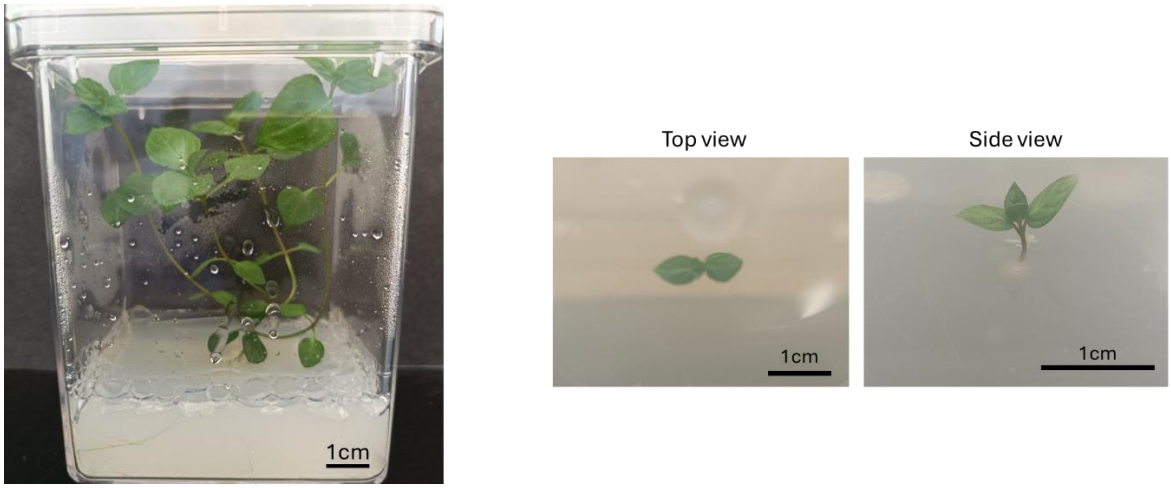

Figure 3.1. Propagation of Black Mitcham stock plants. Pictured above are Black Mitcham stock plants housed in sterile Magenta vessels. New stock plants are propagated by excision of actively growing shoot apexes together with a single leaf pair, and transferring them into fresh Magenta vessels with fresh growth medium to establish a new plant.

With the starting stock material standardized to minimise the effects of biological variation from the Black Mitcham plants themselves, an appropriate explant source now had to be determined. This was done by growing the plants until at least 4 leaf pairs, excluding the shoot apex and starting leaf pair, were present. It was it this stage where the plants were dissected and divided into their respective explant types (Figure 3.2).

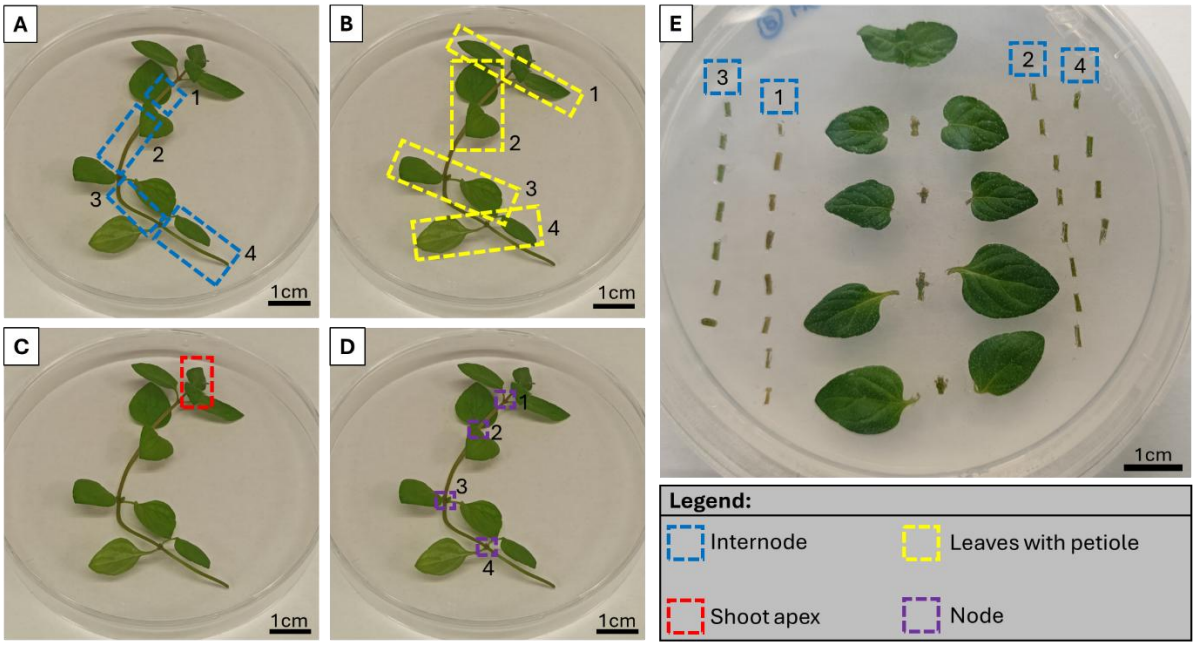

Figure 3.2. Outline of dissection process for Black Mitcham explants. A. Internode explants (shown with a blue box) were labelled from 1 – 4, from youngest to oldest tissue. B. Leaf explants (shown with a yellow box) with the petiole still attached were labelled from 1 – 4, from youngest to oldest tissue. C. Shoot apex explant (shown with a red box). D. Nodal explants (shown with a purple box) were labelled 1 – 4, from youngest to oldest. E. Representative layout for scoring explant callus development. Internode explants were further split into roughly 5mm segments.

To account for differences in age, explants were categorised from 1-4, were 1 was the youngest tissue and 4 was the oldest tissue. The explants were separated into internode 1-4 (Figure 3.2 A), leaf including petiole (henceforth to be referred to as leaf) 1-4 (Figure 3.2 B), shoot apex (Figure 3.2 C) and internodes 1-4 (Figure 3.2 D). Internode segments were further split into roughly 5mm segments, and an example layout is shown in Figure 3.2 E, which shows one ‘replicate’ plate.

The development of an optimised *in vitro* regeneration protocol was to be ultimately used as a means for *A. tumefaciens*-mediated transformation of explants. Therefore the suitability of explants to be used should only have regenerative capacity upon treatment with PGRs. This would allow the timing of regenerative capacity of the explants to be controlled. Additionally, resulting regenerated plants would have arisen from a single dedifferentiated and subsequently re-differentiated cell. In the context of *A. tumefaciens*-mediated transformation, this would assume that any successfully transformed cell would give rise to a transgenic plant derived from a single cell type. To this end, potential explants were first cultured on basal, hormone

free growth medium (henceforth referred to as HF growth medium) to rule out explant sources which already have a basal regenerative capacity (Figure 3.3)

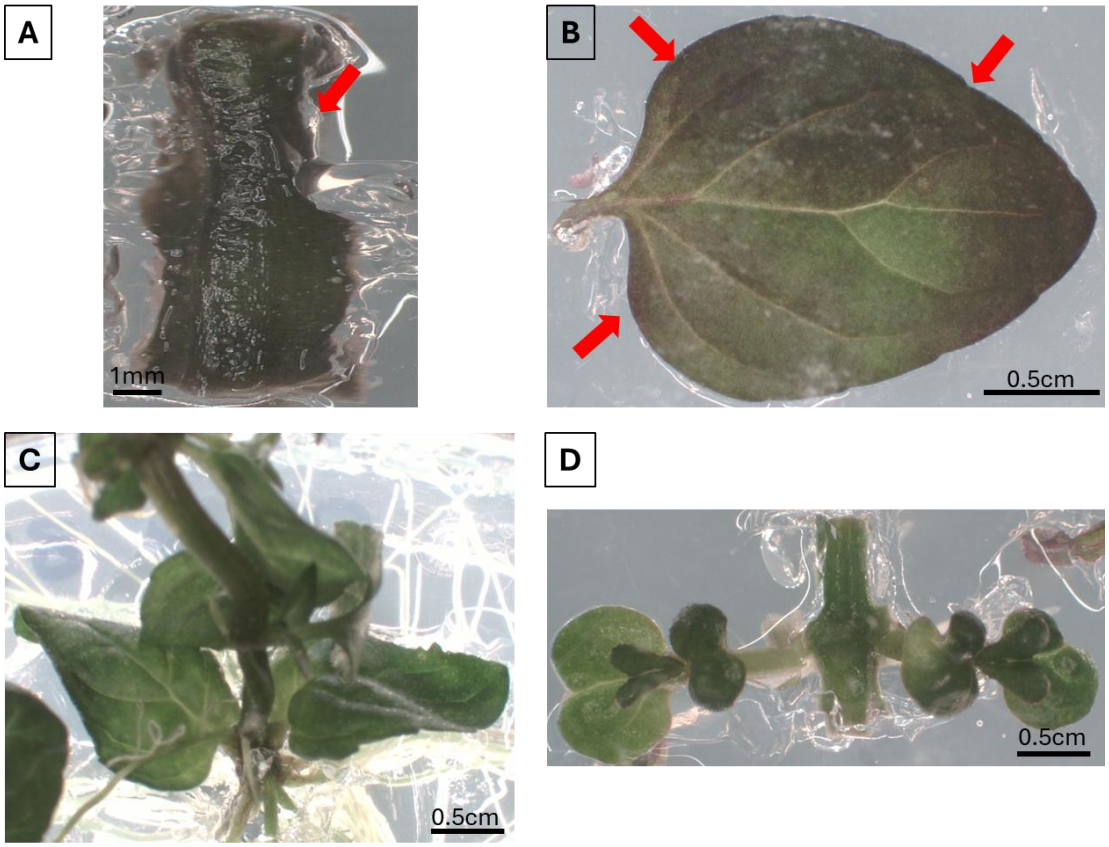

Figure 3.3. Representative images of explants cultured on HF growth medium at stages of either 2 weeks or 6 weeks post culture. A. Internode explant after culture for 6 weeks on HF growth medium. Red arrow indicates tissue necrosis as shown by browning. B. Leaf explant after culture for 6 weeks on HF growth medium. Red arrows indicate tissue necrosis shown by onset of browning. C. Shoot apex explant after 6 weeks on HF growth medium. D. Nodal segment after 2 weeks on HF growth medium.

Time points for taking the representative images were taken at either after 2 or 6 weeks of culture. Internode explants showed no obvious signs of growth, and showed a browning and necrosed phenotype after culture for 6 weeks (Figure 3.3A). Leaf explants showed no obvious signs of growth after 6 weeks, from neither the leaf surface or the leaf petiole (Figure 3.3B). Signs of chlorosis and necrosis can also be observed, as indicated by the onset of browning on the outer leaf edge. Shoot apex segments showed both rooting and shooting after 6 weeks of culture (Figure 3.3C). As expected, nodal segments showed shooting even after just 2 weeks of growth (Figure 3.3D). Taken together, the findings of Figure 3.3 allowed the nodal and shoot apex explants to be discarded from consideration for use as an explant type, as they

showed clear regeneration without supplementation of exogenous PGRs. The explants of choice were therefore either internode explants, or leaf explants.

3.2.2 Preliminary determination of optimal plant growth regulator concentration for regeneration from explants

Having determined the optimal explant source, the next factor to consider was the use of which PGRs to use to induce the highest regenerative capacity. The term “regenerative capacity” for this thesis was deemed as any explant which showed any form of callus production. The cytokinins TDZ, BAP and KIN were investigated by varying the concentration used to supplement the explant growth medium. The PGRs were also supplemented with the auxin NAA, and this was kept at a constant concentration. Three different concentrations of cytokinins were tested, and were chosen based on what was commonly used in the literature with respect to regeneration of Black Mitcham. For each condition chosen condition, a control condition of explants grown on HF growth medium was included to ensure that it was the supplementation of PGRs to the growth medium that was causing callus formation. This was also used as a comparison point for explant cultured on PGR supplemented medium that did not show callus formation. The first chosen PGR combination was NAA and TDZ, with concentrations of 0.5 µM NAA supplemented with either 4.5 µM, 9 µM or 13.62 µM TDZ chosen. The counts were taken after a 6 week period of culture. This was compared for both internode segment explants (Figure 3.4) and leaf explants (Figure 3.5) from different positions on the donor plant.

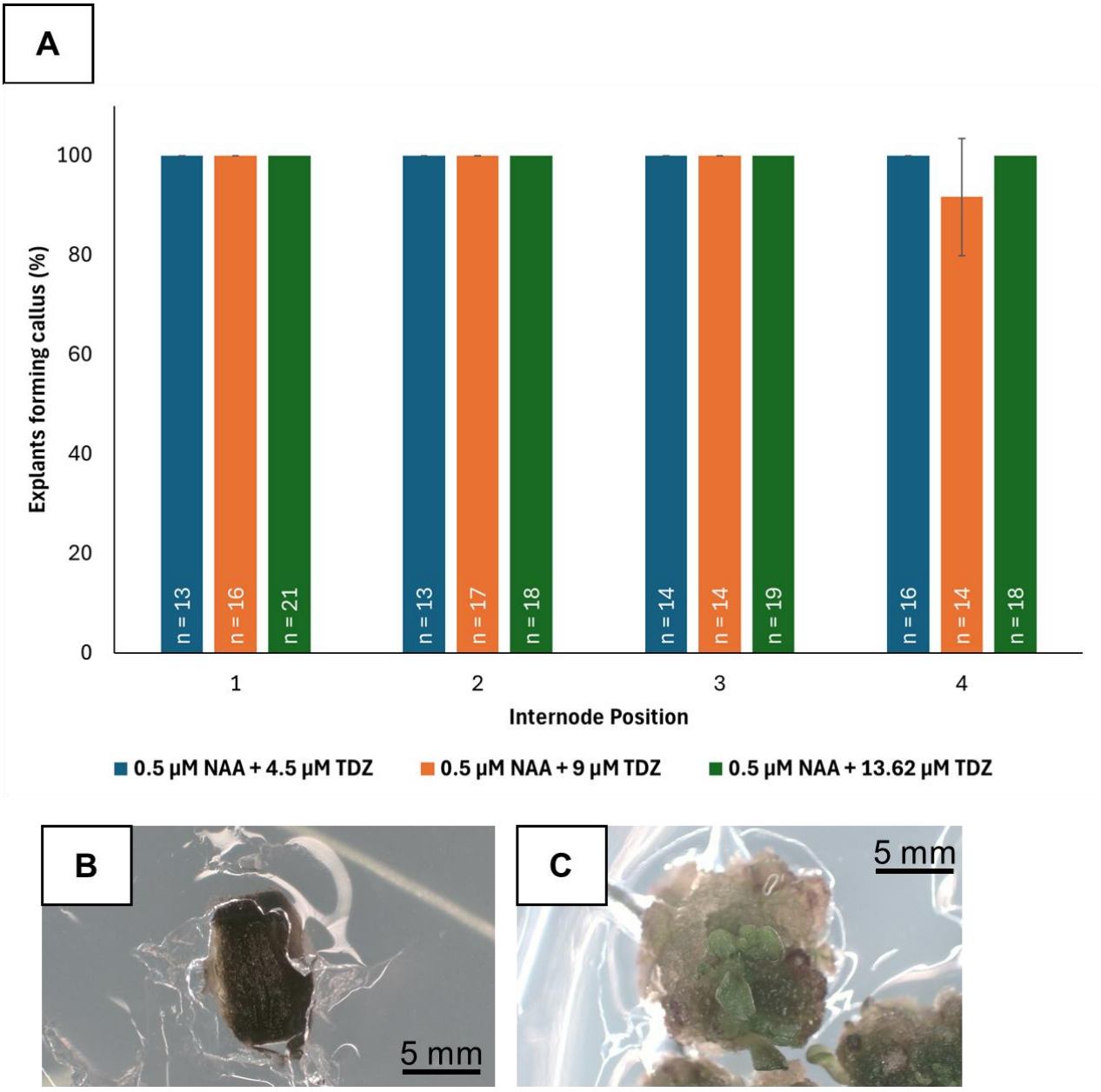

Figure 3.4. Regenerative capacity of Black Mitcham internode explants cultured on different concentrations of TDZ after 6 weeks. A. Three combinations of increasing concentrations of TDZ were used to evaluate either the presence or absence of callus formation. Internode segments from youngest (1) to oldest (4) are shown by internode position. The y axis shows the percentage of explants forming callus. Bars represent mean ± standard deviation of 3 biological replicates (each "biological replicate" are composed of multiple explants in a single petri dish) , with the total number of explants given as n. B. Representative image of internode explant classed as no callus formation. Scale bar shown in black. C. Representative image of internode segment classed as callus formation. Scale bar shown in black.

Internode segments cultured on all concentrations of TDZ showed high callus formation capacity (Figure 3.4 A). Age of the tissue seemingly had little influence on callus formation capacity, with only 0.5 µM NAA + 9 µM TDZ in the oldest internode

(4) showing a a 91.7% callus formation capacity compared to 100% observed in all other internode positions.

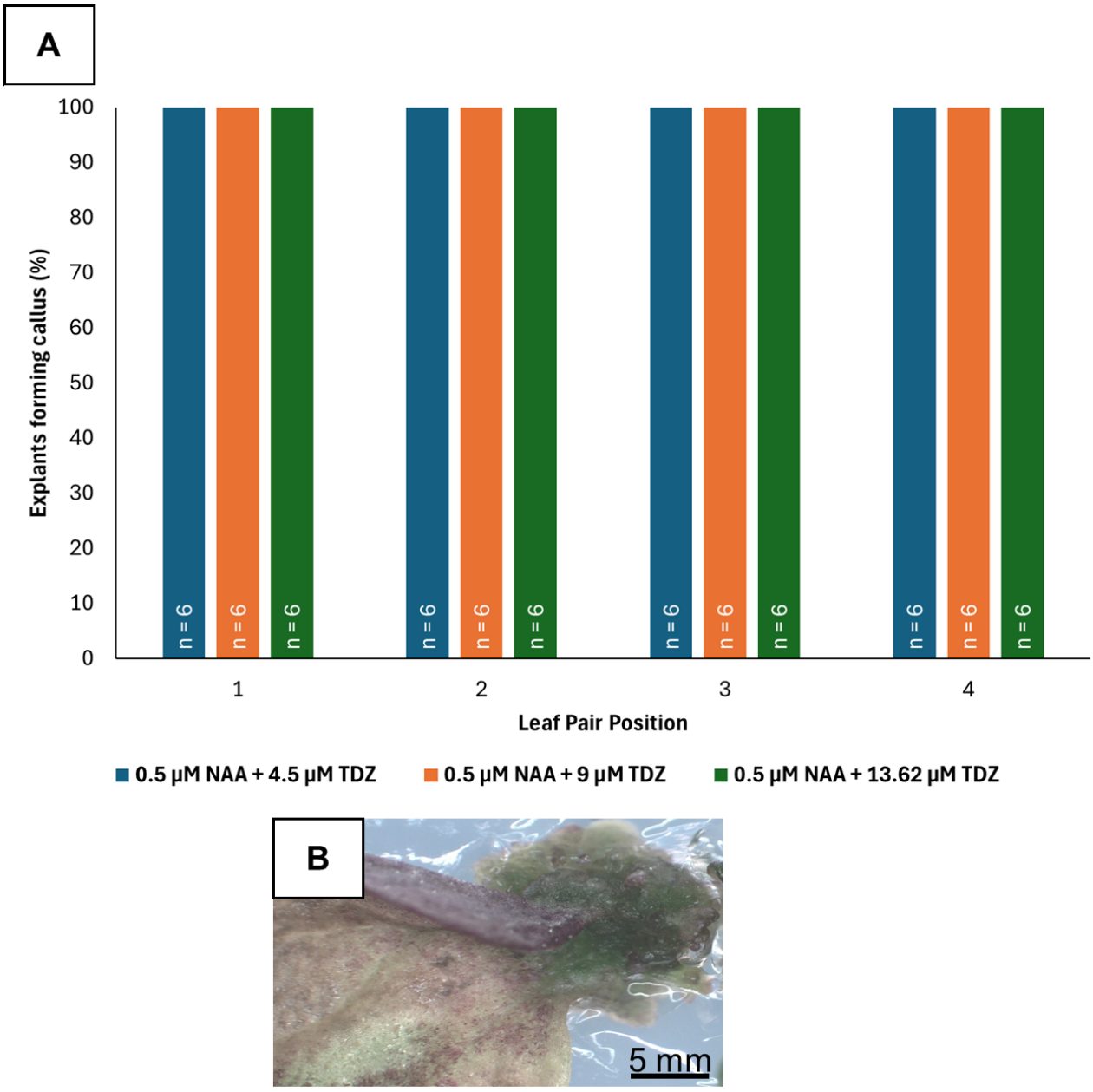

Figure 3.5 Regenerative capacity of Black Mitcham leaf explants cultured on different concentrations of TDZ after 6 weeks. A. Three combinations of increasing concentrations of TDZ were used to evaluate either the presence or absence of callus formation. Leaf explants from youngest (1) to oldest (4) are shown by leaf pair position. The y axis shows the percentage of explants forming callus. Bars represent mean ± standard deviation of 3 biological replicates, with the total number of explants given as n. B. Representative image of a leaf explant classed as callus formation. Scale bar shown in black.

A similar trend can be observed with leaf explants, where all leaf positions (leaves taken from leaf positions outlined in Figure 3.2 B) showed a 100% callus formation

(Figure 3.5 A). Callus only formed on the petiole of the leaf explants (Figure 3.5 B). Similarly, this experiment was repeated with BAP, of concentration of 13.32 µM, 17.76 µM and 22.2 µM (Figure 3.6 and Figure 3.7).

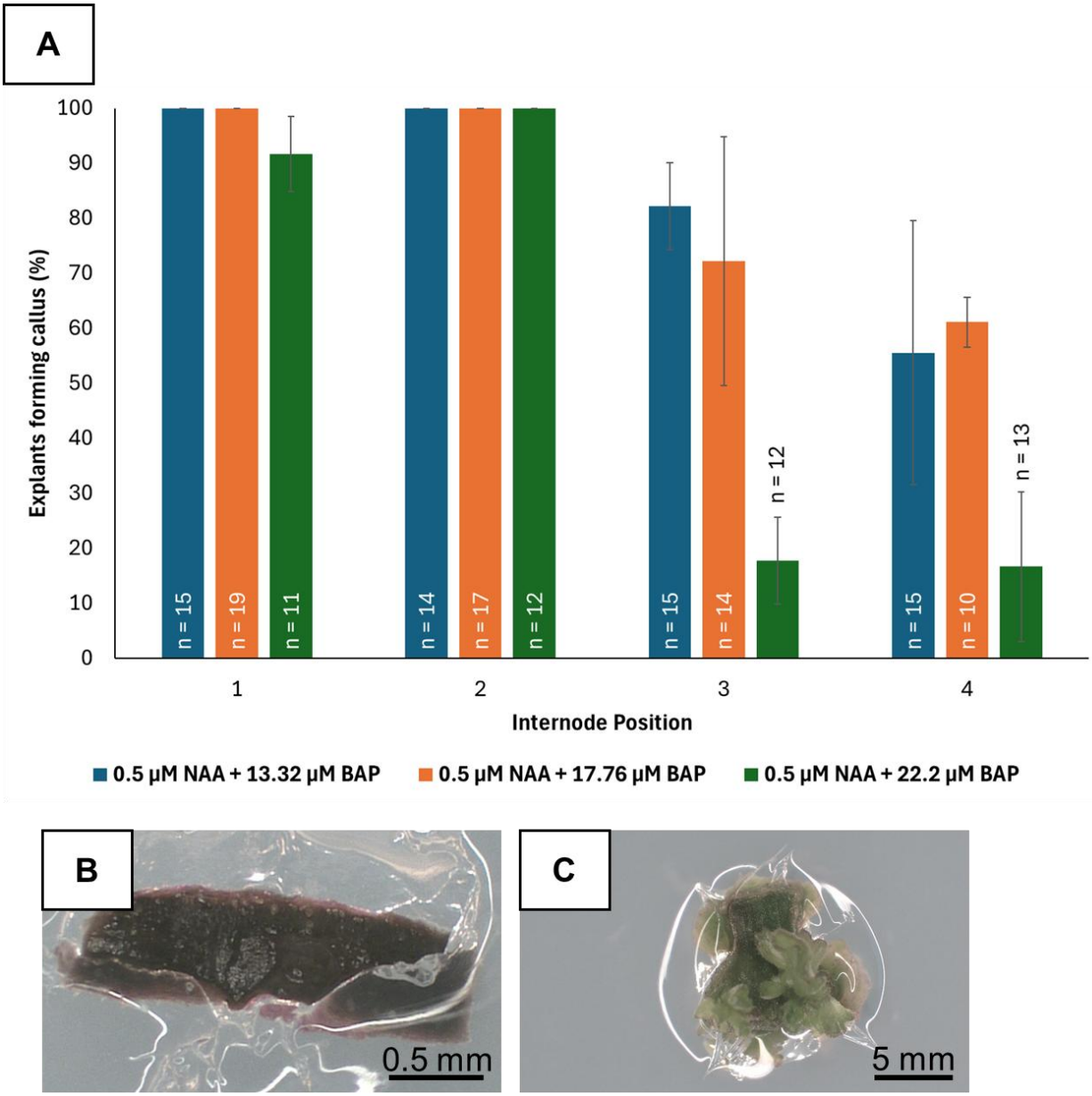

Figure 3.6. Regenerative capacity of Black Mitcham internode explants cultured on different concentrations of BAP after 6 weeks. A. Three combinations of increasing concentrations of BAP were used to evaluate either the presence or absence of callus formation. Internode segments from youngest (1) to oldest (4) are shown by internode position. The y axis shows the percentage of explants forming callus. Bars represent mean ± standard deviation of 3 biological replicates, with the total number of explants given as n. B. Representative image of internode explant classed as no callus formation. Scale bar shown in black. C. Representative image of internode segment classed as callus formation. Scale bar shown in black.

For internodes cultured on 13.32 µM BAP, internodes (1) and (2) showed the greatest percentage of callus formation per explant at 100% and 100%. Internodes (3) and (4) showed a decrease to 82% and 56% (Kruskal-Wallis test confirmed significant position effects ($H=9.87$, $p=0.007$, $df=3$). Dunn's post-hoc showed internodes 3 vs internodes 1/2 as $p=0.08$, internodes 4 vs internodes 1/2: $p<0.01$). For internodes cultured on 17.76 µM BAP, internodes (1) and (2) once again showed the greatest percentage of callus formation at 100% and 100%. Internodes (3) and (4) showed similar percentages of 72% and 61% respectively. For internodes cultured on 22.2 µM BAP, internodes (2) showed the highest percentage of callus formation of 100%, followed by internodes (1) at 92%. Internodes (3) and (4) showed a drop in percentage of callus formation at 18% and 17% respectively.

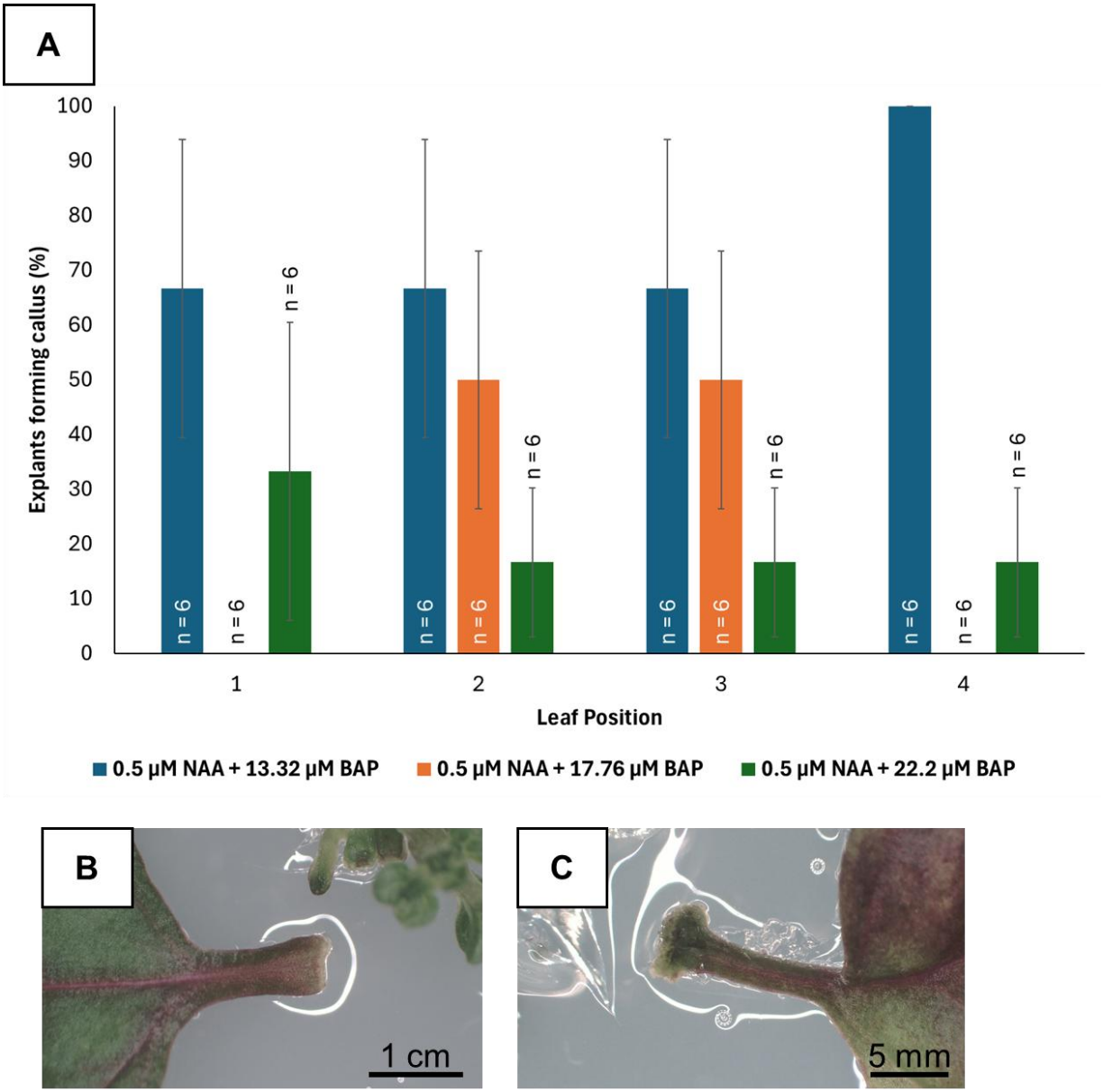

Figure 3.7. Regenerative capacity of Black Mitcham leaf explants cultured on different concentrations of BAP after 6 weeks. A. Three combinations of increasing concentrations of BAP were used to evaluate either the presence or absence of callus formation. Leaf explants from youngest (1) to oldest (4) are shown by internode position. The y axis shows the percentage of explants forming callus. Bars represent mean ± standard deviation of 3 biological replicates, with the total number of explants given as n. B. Representative image of a leaf explant classed as no callus formation. Scale bar shown in black. C. Representative image of a leaf explant classed as callus formation. Scale bar shown in black.

Leaf explants cultured on 13.32 µM BAP at positions (1), (2), (3) and (4) showed a percentage of callus formation value of 67%, 67%, 67% and 100%, respectively. Leaf explants cultured on 17.76 µM BAP at positions (2) and (3) showed values of 50% and 50%, whilst positions (1) and (4) did not show any formation of callus. Leaf petiole explants cultured on 22.2 µM BAP at position (1), (2), (3) and (4) showed a percentage of callus formation value of 33%, 17%, 17% and 17% respectively.

Finally, internode and leaf explants were cultured on KIN supplemented growth medium at concentrations of 4.65 µM, 9.3 µM and 13.95 µM. However, after 6 weeks of culture, the formation of callus was unclear in comparison to the explants cultured on TDZ or BAP. Therefore, all explants cultured on KIN supplemented growth medium could not be reliably scored in this assay. Representative images of the internode and leaf explants after 6 weeks of culture on KIN supplemented medium are shown in Figure 3.8.

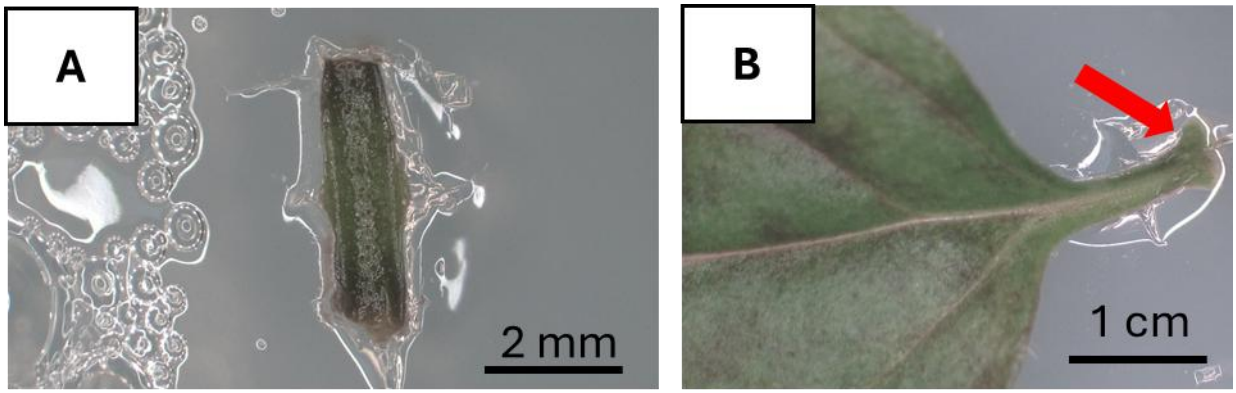

Figure 3.8. Representative images of explants cultured on different concentration of KIN after 6 weeks. A. Internode explants. B. Leaf explants. A red arrow indicates swelling of the cut end of the petiole, which could be classed as callus formation Scale bar is shown as a black bar.

Slight formation of callus at the cut end of the petiole of the leaf explant can be observed (Figure 3.8 B), however this assay was classed as no callus formation due to leaf explants cultured on TDZ and BAP showing a much more obvious callus formation phenotype. Therefore, although in this assay KIN was classed as being unable to induce callus formation due to an unclear phenotype, it is still capable of inducing callus, but may need a longer period of culture in comparison to TDZ and BAP induced explants.

3.2.3 Determination of optimal regeneration protocol based on phenotypic differences of explants cultured on TDZ, BAP or KIN

Following on from these preliminary experiments, the type of callus produced was classified according to the phenotypes observed. Additionally, increased replicates were included to more accurately reflect the amount of explants typically used for a *A. tumefaciens*-mediated transformation as this was ultimately the end goal of optimizing an *in vitro* regeneration protocol. Furthermore, the timeframe of these experiments was increased from 6 weeks (time frame of assays performed in 3.2.2)

to 8 weeks. The decision to increase the timeframe was to allow the development of clearer phenotypes to be produced, as for example a 6 week time period was insufficient to distinguish callus formation in KIN cultured explants (Figure 3.8). Additionally, the specific number of 8 weeks was chosen as this was the rough time frame observed in the literature where Black Mitcham callus tended to start to differentiate into defined structures (Niu et al. 1998; Niu et al. 2000).

This set of experiments was performed to inform the optimal plant growth regulator, the concentration of chosen PGR, explant type and phenotypes of explants treated with the plant growth regulators. The phenotype was of particular importance to consider as the plant growth regulator chosen would have to induce a large number of shoots, which would ultimately increase the chances of more viable transformants.

Firstly, any explants which showed some form of visible healthy callus formation, were classed as green callus. The explants were then subclassed depending on the observed phenotype. If a callus showed a visible shoot growth, this was classed as a shoot-like callus, and a representative image of what was classed as a shoot-like callus is shown in Figure 3.9 A. To reduce the ambiguity of what was classed as a 'shoot-like' callus, a comparison to *N. tabacum* regenerative callus from the literature was used (Figure 3.9 B) (Pathi et al. 2013). Alternatively, if an explant showed any rhizome/root-like structures, this was classed as a rhizome/rooting phenotype. Of important note, is that TDZ cultured internode explants also showed a variety of shoot-like callus phenotypes, with varied degrees of elongation (Figure 3.9 C).

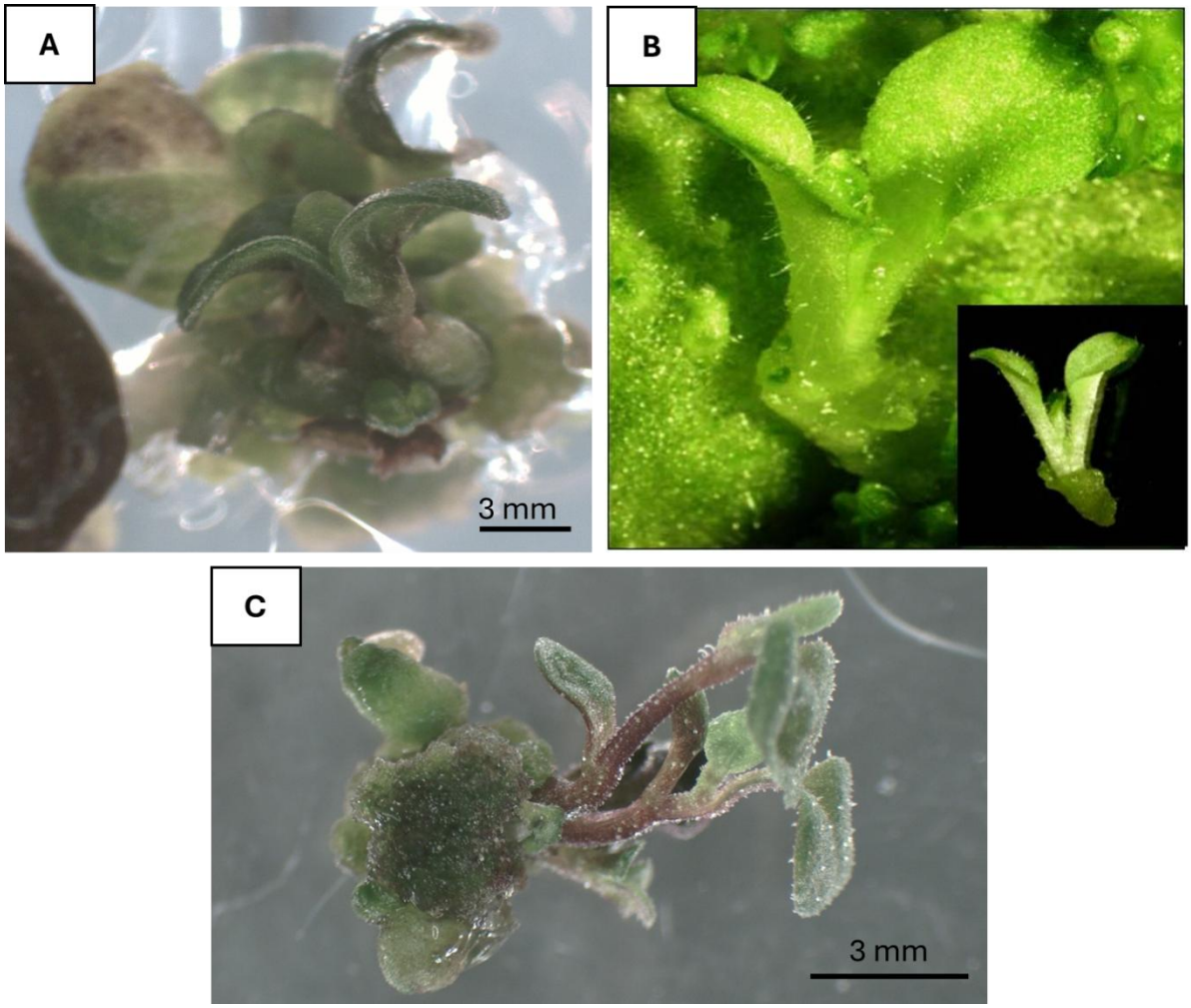

Figure 3.9. Scoring system used to determine "shoot-like callus". A. Black Mitcham internode explant cultured on 0.5 µM NAA and 9 µM TDZ to induce callus formation. Leaf structures can be observed protruding from the callus mass. B. *Nicotiana tabacum* callus tissue showing leaf structures protruding from the callus mass. This was used as comparison against Black Mitcham shoot like callus. Image adapted from Pathi et al. 2013. C. Elongated shoot callus phenotype. This was observed in varying degrees in Black Mitcham internodes. Scale bar shown in black.

The concentrations of PGRs used going forward were 0.5 µM NAA and either 9 µM TDZ, 13.32 µM BAP, or 4.65 µM KIN. For explant sources, only explants from positions (1) or (2) were used. A variety of phenotypes were observed in both internode and leaf explants cultured on growth medium supplemented with either TDZ, BAP or KIN, with representative images of each phenotype being shown in Figure 3.10.

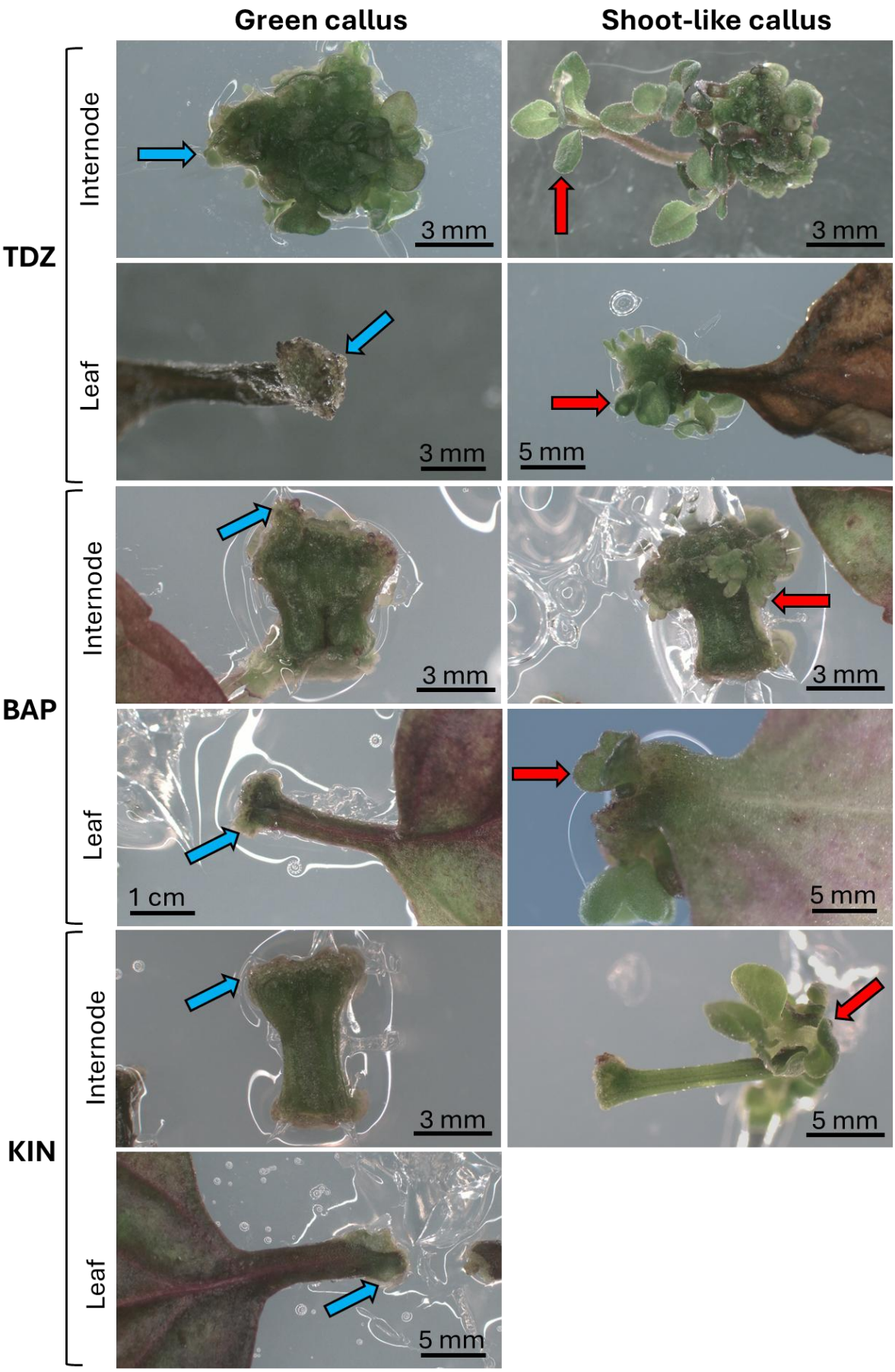
Green callus
Shoot-like callus
TDZ
BAP
KIN
Internode
Leaf
3 mm
5 mm
1 cm

Figure 3.10. Phenotypes of Black Mitcham internode or leaf explants cultured on growth medium supplemented with 0.5 µM NAA and either 9 µM TDZ, 13.32 µM BAP, or 4.65 µM KIN. Phenotypes were separated into green callus or shoot-like callus. Blue arrows highlight areas of green callus formation, which classes an explant in the green callus phenotype. Red arrows highlight areas of shoot-like callus formation, which classes an explant in the shoot-like callus phenotype. Scale bars are indicated as a black bar, with the scale indicate above in either cm or mm units.

Explants cultured on 0.5 µM NAA and 9 µM TDZ showed either a green callus or shoot-like callus phenotype (Figure 3.10). Internode explants in the shoot-like callus phenotype category also showed highly distinguishable shooting structures, with elongated stems. This phenotype was only observed in the 0.5 µM NAA and 9 µM TDZ phenotypes. The leaf explants showed shoot-like structures, but were not as elongated as the structures observed from the internodes. Explants cultured on 0.5 µM NAA and 13.32 µM BAP similarly showed either a green callus or shoot-like callus phenotype (Figure 3.10). The shoot-like callus phenotype observed here was distinguished from the green callus phenotype by the presence of leaf structures developing from the callus mass. The shoot-like callus phenotype in the internode explants had a fasciated appearance, with a lack of shoot elongation observed. Explants cultured on 0.5 µM NAA and 4.65 µM KIN showed the green callus and shoot-like callus phenotype (Figure 3.10). The shoot-like callus phenotype observed here had more well defined leaf structures, was less fasciated than those cultured on BAP, but similarly, did not show any elongation. An additional rhizome/root-like phenotype was also observed in KIN cultured internodes as identified by the development of rhizome or root like structures protruding from the internode body (Appendix Figure 1). Of note, the root or rhizome like structure did not originate from a site of callus. The appearance of either the green callus or shoot-like callus phenotype was quantified, and is shown in Figure 3.11.

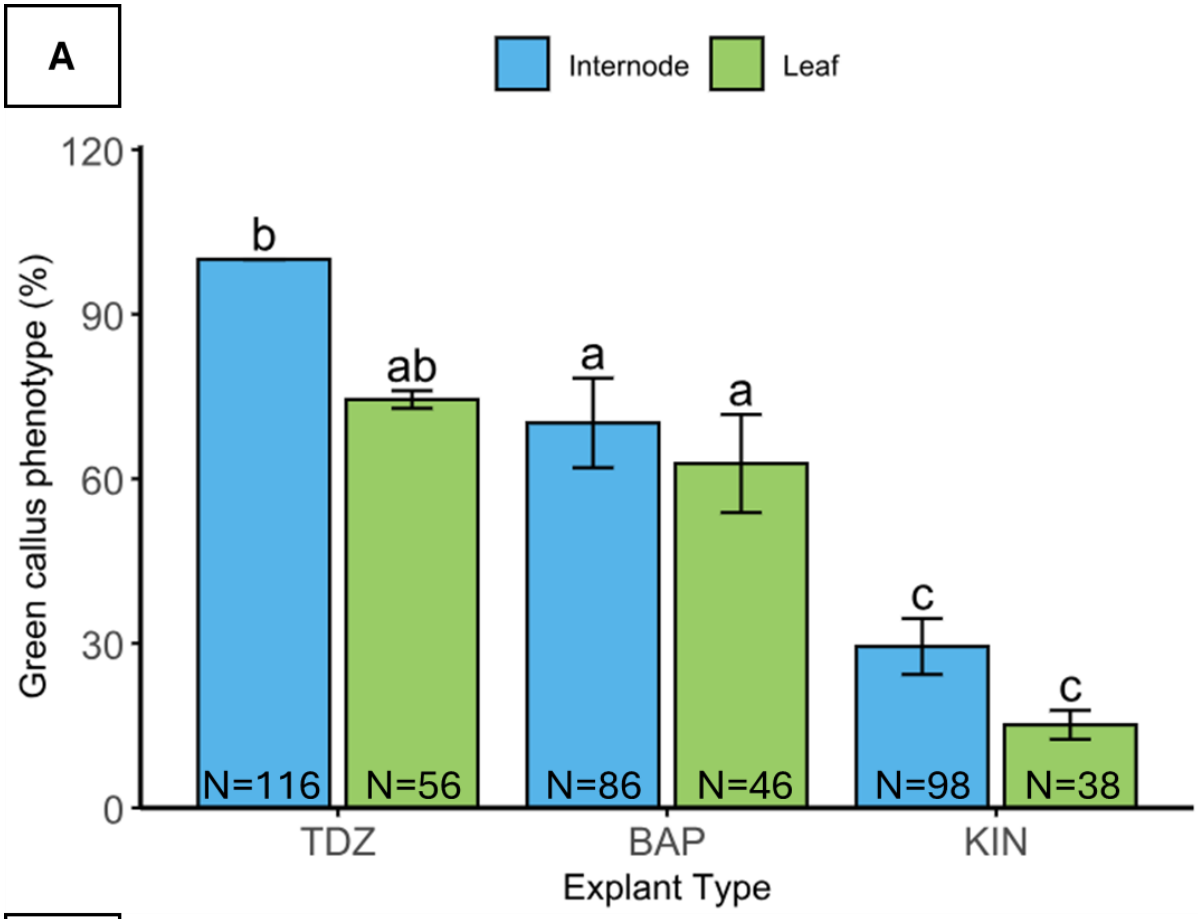
A
Internode
Leaf
Green callus phenotype (%)
120
90
60
30
0
b
ab
a
a
c
c
N=116
N=56
N=86
N=46
N=98
N=38
TDZ
BAP
KIN
Explant Type

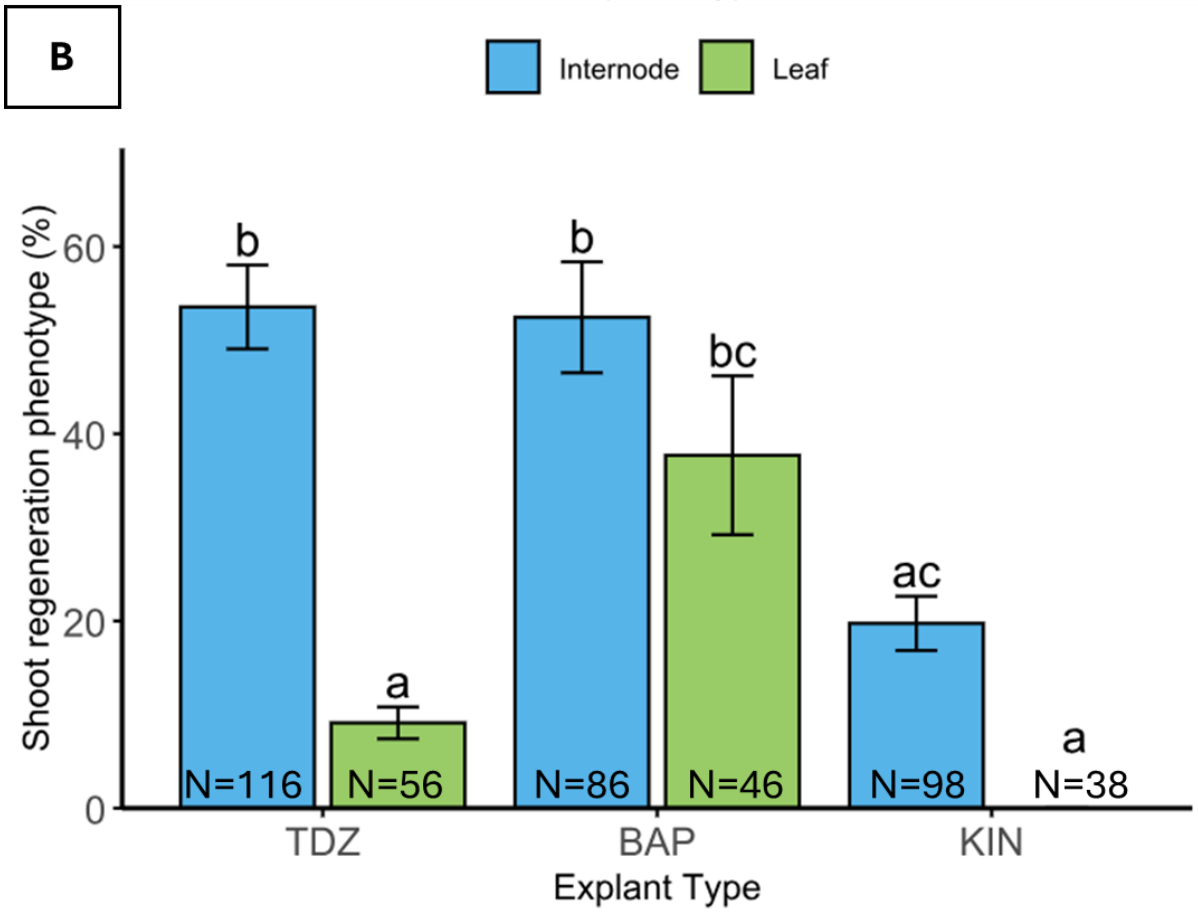
B
Internode
Leaf
Shoot regeneration phenotype (%)
60
40
20
0
b
a
b
bc
ac
a
N=116
N=56
N=86
N=46
N=98
N=38
TDZ
BAP
KIN
Explant Type

Figure 3.11. Comparison of callus types across all tested PGR combinations. A. Comparison of green callus phenotype frequency of internode and leaf explants cultured on 0.5 µM NAA and either 9 µM TDZ, 13.32 µM BAP or 4.65 µM KIN. B. Comparison of shoot regeneration phenotype frequency of internode and leaf explants cultured on 0.5 µM NAA and either 9 µM TDZ, 13.32 µM BAP or 4.65 µM KIN. For both A and B, bars represent mean phenotype frequencies (%) and error bars represent standard deviation. Statistical differences were determined by Tukey's HSD post-hoc test following two-way ANOVA. Letters above bars indicate significant differences based on explant type, PGR treatment and their interaction ($p < 0.05$); groups sharing the same letter are not significantly different. N indicates total number of explants.

Black Mitcham explants cultured on 0.5 µM NAA and 9 µM TDZ produced a green callus phenotype in 100% of internode explants and 74% of leaf explants (Figure 3.11 A). From these, 54% of internodes and 9% of leaves developed shoot-like callus or showed some degree of shoot elongation (Figure 3.11 B). When cultured on 0.5 µM NAA and 13.32 µM BAP, green callus formation occurred in 70% of internodes and 62% of leaves (Figure 3.11 A). Of these, 52% of internodes and 38% of leaves developed shoot-like callus (Figure 3.11 B). A third treatment, 0.5 µM NAA and 4.65 µM KIN, resulted in green callus in 29% of internodes and 15% of leaves (Figure 3.11 A). From these, 24% of internodes developed shoot-like callus, while leaves did not progress beyond green callus (Figure 3.11 B). An additional phenotype—rhizome-like or rooting structures—was observed in ~20% of internodes, all of which also displayed either green or shoot-like callus. Leaves did not exhibit this phenotype (Appendix Figure 1).

Overall, internode explants consistently showed higher frequencies of both green callus and shoot regeneration compared with leaf explants. Statistically, only TDZ-treated explants showed a significant difference between internodes and leaves for green callus formation. Across PGR treatments, TDZ induced the highest frequency of green callus, followed by BAP and then KIN. Shoot regeneration frequencies also followed this trend. Internodes generally regenerated at higher rates than leaves, and this difference was statistically significant. TDZ and BAP induced similar regeneration frequencies in internodes, while KIN was least effective. In leaves, however, BAP significantly outperformed TDZ, and KIN failed to induce regeneration.

Internode explants were therefore more suitable than leaves as regeneration sources: they were more abundant per plant, could be sectioned into smaller pieces (maximizing culture space), and had larger regenerative areas compared to leaves, which regenerated only from the petiole. Among PGRs, TDZ produced the highest

callus induction and comparable shoot regeneration to BAP, but with a desirable elongated shoot phenotype. In contrast, BAP only produced fasciated shoots. Taken together, 0.5 µM NAA and 9 µM TDZ was identified as the most effective regeneration medium and is henceforth referred to as shoot induction medium (SIM).

3.2.4 Applicability of shoot induction medium for use in other *Mentha* species

The applicability of SIM was then tested against other *Mentha* species, including *Mentha aquatica, Mentha arvensis, Mentha spicata* and *Mentha Longifolia* (Figure 3.12).

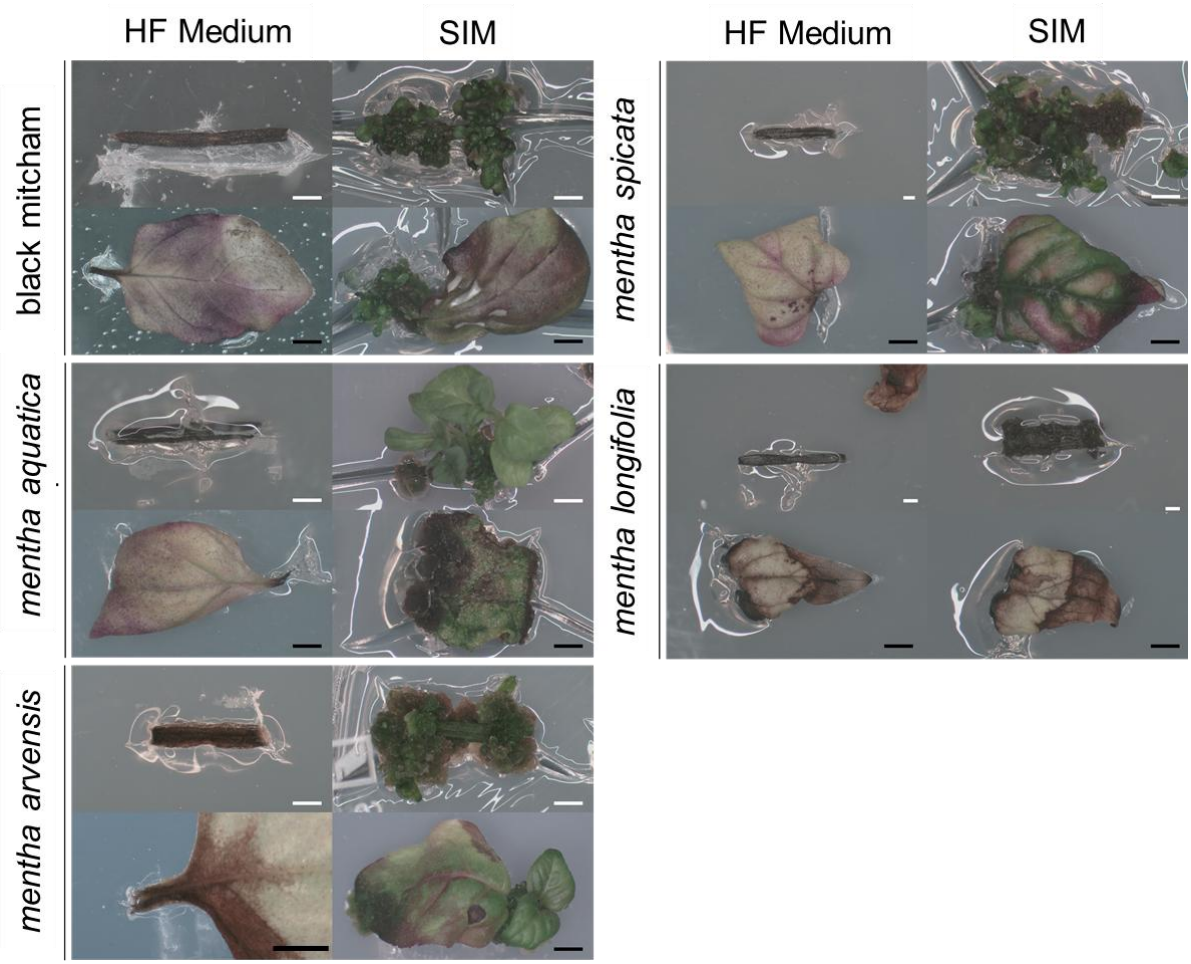

Figure 3.12. Explants from Black Mitcham, *Mentha spicata, Mentha aquatica, Mentha longifolia and Mentha arvensis* cultured on SIM. Internode and leaf explants were cultured on growth medium supplemented with 0.5 µM NAA + 9 µM TDZ to induce callus and shoot induction. The same explants were cultured on hormone free (HF) medium as a control. Representative images are presented. All *Mentha* species except *Mentha longifolia* showed shoot regeneration. Black scale bars are 1 cm. White scale bars are 1 mm.

Mentha longifolia did not appear to respond to the PGR treatment, with both internode and leaf explants turning necrotic, similar to the phenotype observed on HF-medium (Figure 3.12). Black Mitcham, *Mentha arvensis* and *Mentha spicata* internodes showed a similar callus phenotype (Figure 3.12). *Mentha aquatica* internodes showed a higher degree of shoot elongation from the shoot-like callus mass (Figure 3.12). Black Mitcham and *Mentha spicata* leaf explants showed a similar phenotype, where callus formed solely at the petiole (Figure 3.12). *Mentha*

aquatica leaf explants showed a green callus phenotype with a lack of obvious shoot like structures observed, with callus regenerating from not just the petiole but the entire leaf surface (Figure 3.12). *Mentha arvensis* showed a shoot green callus formation from both the petiole and the leaf surface, and well defined shoot regeneration could be observed at the regenerating petiole (Figure 3.12). Overall this showed that there is no universal plant growth regulator combination for inducing regeneration in *Mentha* species, and thorough optimisation needs to be done for each species.

3.2.5 Black Mitcham explants cultured on shoot induction medium show shoot elongation and rooting upon transfer to hormone free medium

To complete the protocol for Black Mitcham regeneration from explants, it was found that transferring the shoot regenerating callus to HF-medium encouraged shoot elongation and rooting (Figure 3.13 B).

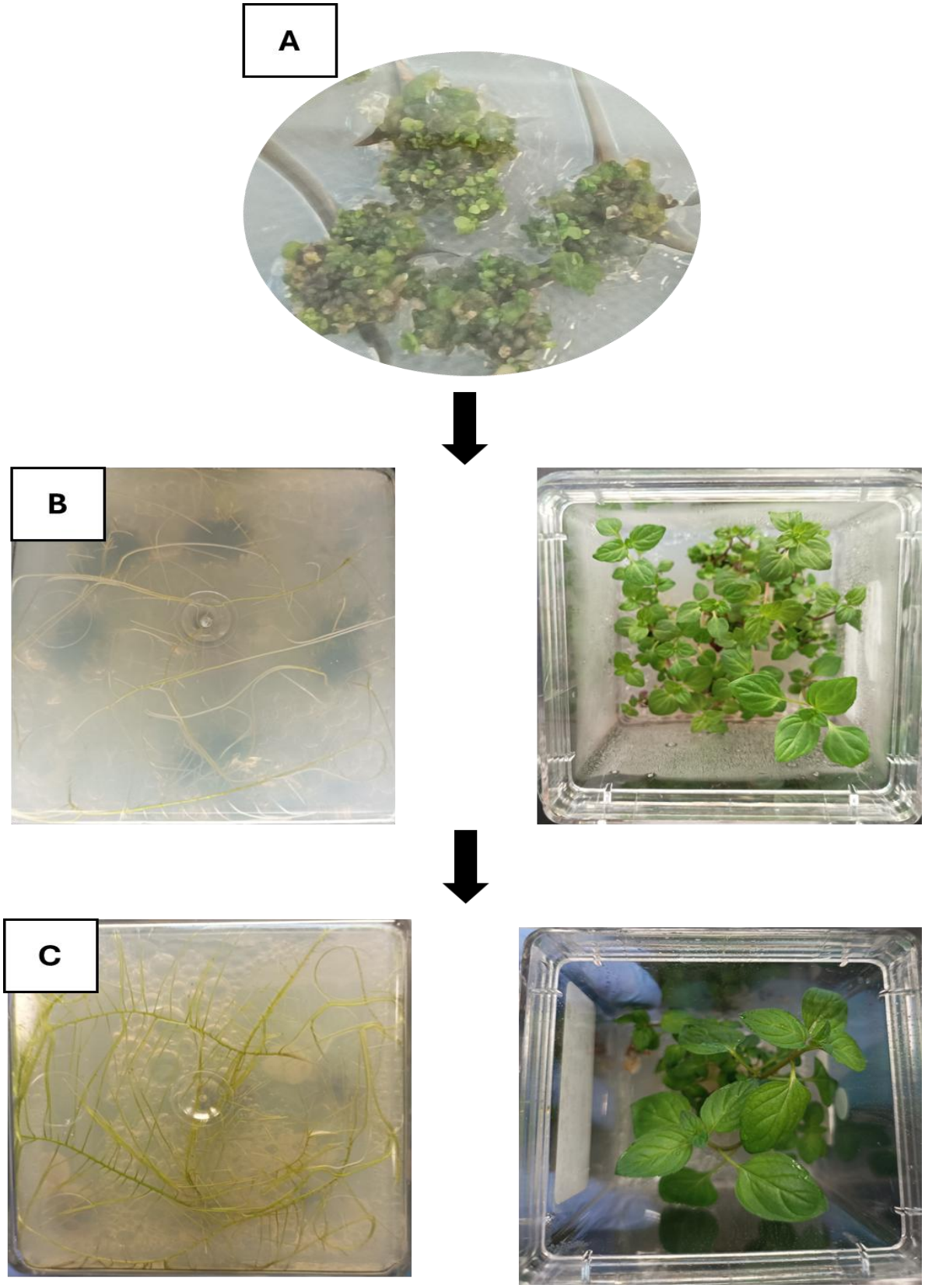

Figure 3.13. Regeneration process to produce new whole plants from shoot-like callus. A. Explants are cultured on SIM until shoot-like callus are observed. B. Shoot-like callus are transferred to HF medium for shoot elongation and root induction. C. Elongated shoots are excised from the shoot-like callus and transferred to HF medium for rooting and further shoot elongation.

The entire process for regenerating Black Mitcham from internode segments is shown in Figure 3.13. This first involved generation of shoot regenerating callus on SIM (Figure 3.13 A). This was followed by transferring onto HF medium which induced simultaneous rooting and shoot elongation (Figure 3.13 B). Sufficiently elongated shoots were then excised from the callus mass and placed in fresh HF medium for further rooting to occur (Figure 3.13 C). This completed the regeneration process, and ensured that each new plant originated from a single shoot.

3.2.6 Exploration of novel plant growth regulator 2,4-D for the *in vitro* regeneration of Black Mitcham

Although an optimised SIM had been developed for Black Mitcham, an alternative regeneration protocol was aimed to be developed using separate callus induction, followed by shoot regeneration induction on separate plant growth regulator supplemented growth mediums. An indirect regeneration route via a callus phase was investigated because auxin-induced dedifferentiation can increase the pool of competent cells for subsequent shoot organogenesis. 2,4-Dichlorophenoxyacetic acid (2,4-D) is a synthetic auxin widely used to promote callus formation and friable callus morphology in many dicot species, due to its stability and strong inductive effect on cell proliferation (Zheng and Konzak 1999; Long et al. 2022; Mahood et al. 2022). To test this, 2,4-D was tested for its ability to induce callus formation in Black Mitcham explants. Concentrations of 2.26 µM, 4.52 µM and 9.05 µM were trialled (Figure 3.14).

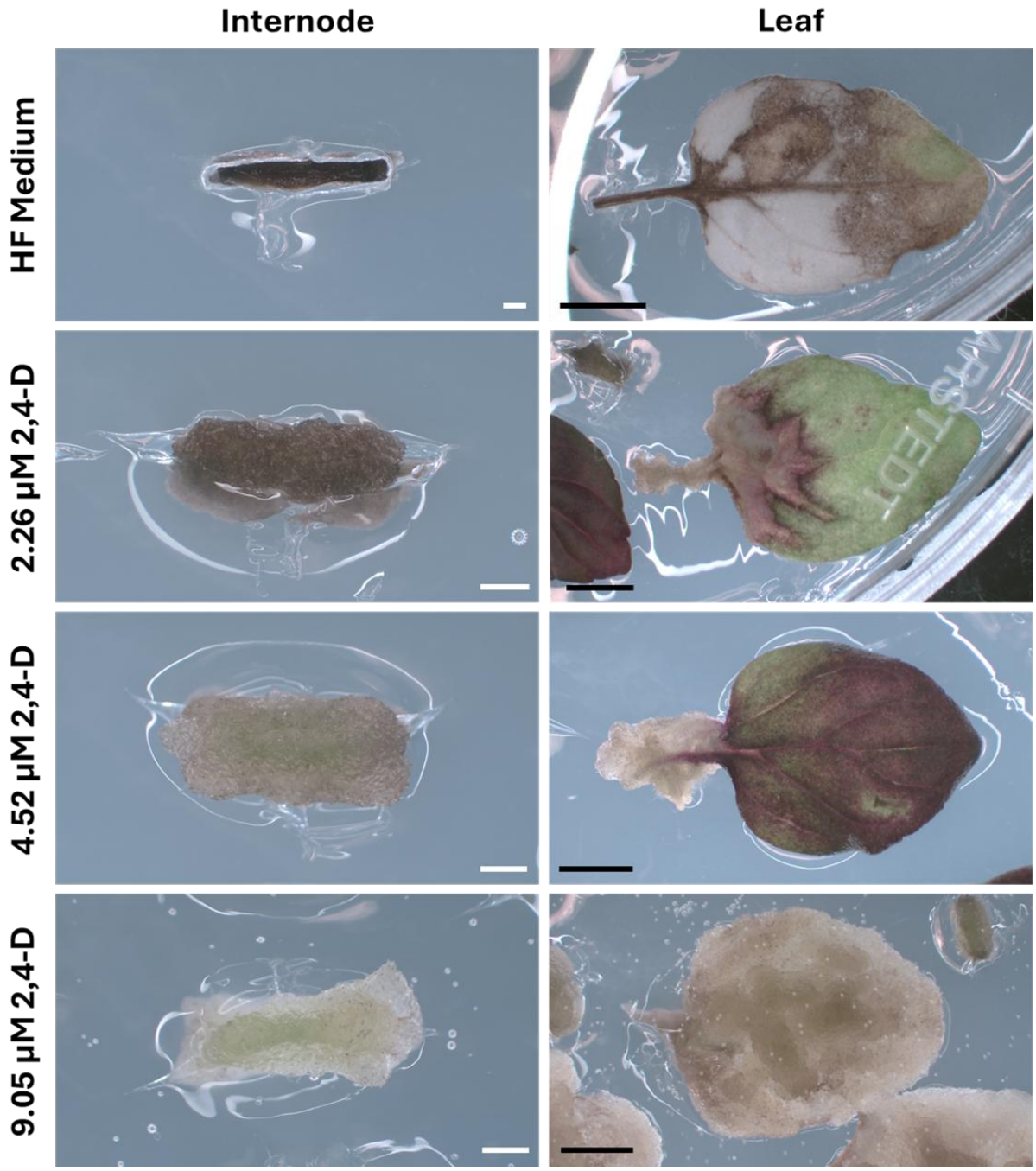

Figure 3.14. Explants from Black Mitcham cultured on growth medium with increasing 2,4-D concentrations. Callus produced shows a creamy, friable type. Explants were cultured for 4 weeks. Black scale bars are 1 cm. White scale bars are 1 mm.

Explants at all concentrations tested showed creamy, friable callus growth (Figure 3.14). In internode explants, 2.26 µM 2,4-D showed darker, friable callus, whilst at increasing concentrations (4.52 µM and 9.05 µM) the callus colour appeared lighter. Leaf explants at 2.26 µM and 4.52 µM 2,4-D showed creamy, friable callus originating from the leaf petiole. Whilst at 9.06 µM 2,4-D, creamy friable callus was observed at all surfaces of the leaf. Representative images were taken at the 4 week

time point as exceeding this amount of time on 2,4-D the callus turned necrotic (data not shown).

To test if the callus induced on 2,4-D could differentiate into shoot tissue, callus that had been cultured for 4 weeks onto 2,4-D was transferred to SIM and monitored for any shoot formation (Figure 3.15).

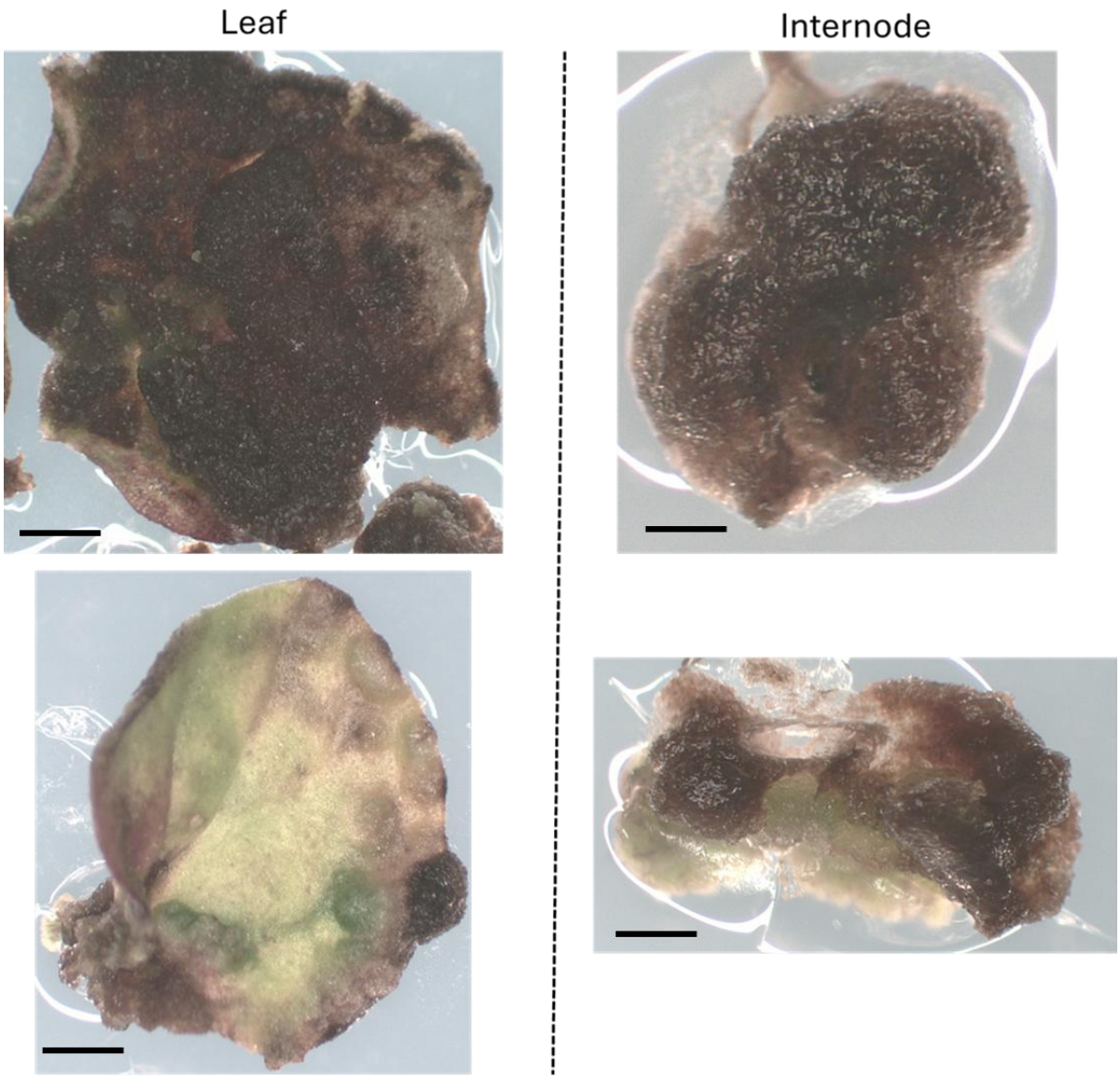

Figure 3.15. Explants from Black Mitcham cultured on 9.05 µM 2,4-D for 4 weeks, then transferred over to 0.5 µM NAA + 9 µM TDZ. Representative photos are shown of callus after 2 weeks of culture. Scale bar for leaf explants are 1 cm. Scale bar for internode explants are 1 mm.

A concentration of 9.05 µM 2,4-D was chosen as the embryogenic callus looked the healthiest in terms of colour and callus proliferation (Figure 3.14). After 2 weeks of culture on SIM, the callus appeared to turn necrotic and no signs of shoot regeneration could be observed (Figure 3.15). This showed that 2,4-D induced Black Mitcham callus was not regenerative, and thus not suitable for the *in vitro* regeneration of Black Mitcham.

3.2.7 Exploration of the novel plant growth regulator fipexide for the *in vitro* regeneration of Black Mitcham

Fipexide (FPX) is a novel chemical inducer that promotes callus formation and shoot regeneration in many plant species, acting as a plant growth regulator (Nakano et al. 2018). FPX has not previously been used for *in vitro* regeneration of Black Mitcham, and has been shown to have varying callus induction effects on different plant species, such as rice, poplar, soybean, tomato and cucumber (Nakano et al. 2018). It was therefore trialled with Black Mitcham explants to test what the observed effects would be, and if it could be applied to *in vitro* regeneration of Black Mitcham. Concentrations of 10, 20 and 50 µM FPX were chosen based on typical concentration ranges used in the literature (Nakano et al. 2018) (Figure 3.16).

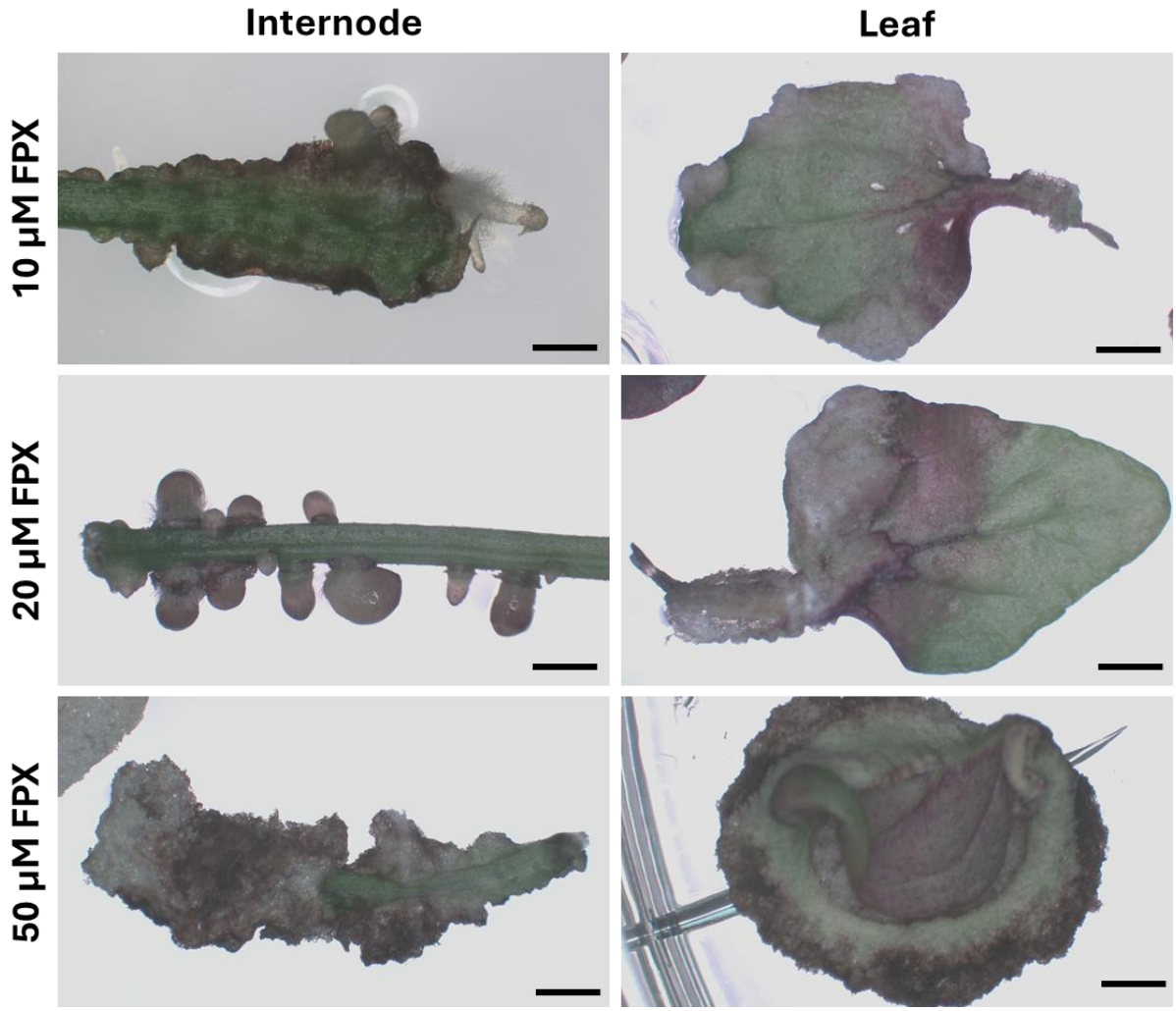

Figure 3.16. Explants from Black Mitcham cultured on growth medium with increasing concentrations of FPX. Representative photos after 4 weeks of culture are shown. Scale bars for internode explants represent 1 mm. Scale bars for leaf explants represent 1 cm

FPX at 10 µM induced a mix of dedifferentiated callus tissue throughout the surface of the internode, together with hairy root like rhizome structures. At 10 µM in leaf explants, masses of dedifferentiated callus developed at the petiole and throughout the surface of the leaf. At 20 µM in internode explants, lateral root-like growths can be seen protruding from the sides of the explant. In leaf explants at 20 µM, further masses of dedifferentiated cells can be observed mainly from the petiole. At 50 µM in internode explants, dedifferentiated callus tissue can be observed protruding throughout the internode. In leaf explants at 50 µM, the entire leaf appears to show dedifferentiated callus formation, with signs of browning and necrotic callus occurring (Figure 3.16). FPX induced callus was then transferred to SIM and scored after a period of 4 weeks, to deduce if the dedifferentiated callus could differentiate into shoot-like tissue (Figure 3.17).

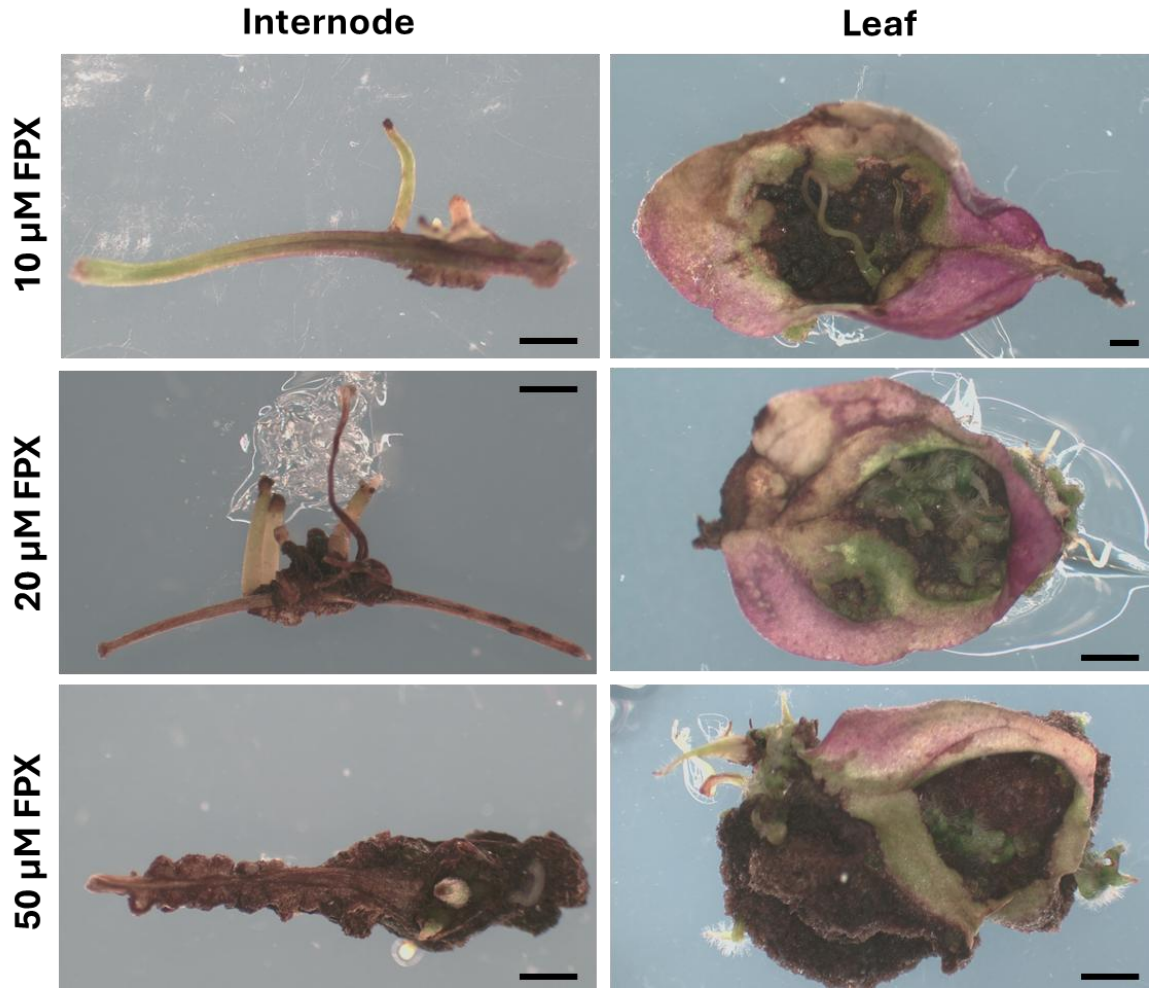

Figure 3.17. Explants from Black Mitcham cultured on growth medium with increasing concentrations of FPX for 4 weeks, followed by culture on SIM for 4 weeks.

Representative images are shown. Scale bars for internode explants represent 1 mm. Scale bars for leaf explants represent 1 cm.

In all concentrations of FPX tested after culture on SIM for 4 weeks, there appeared to be an induction of rhizome-like structures from both types of explants (Figure 3.17). Callus originating from explants cultured at 50 µM showed less well elongated rhizome-like structures, with a higher degree of callus browning and necrosis. Lower concentrations (10 µM and 20 µM) showed a lower degree of browning or necrosis, and more well-defined rhizome-like structures (Figure 3.17). Ultimately, neither 2,4-D or FPX induced callus could be differentiated into shoot-like structures. Therefore, the original *in vitro* regeneration protocol culturing explants directly on SIM was chosen as the most optimal.

3.2.8 Optimisation and troubleshooting of *A. tumefaciens*-mediated transformation in Black Mitcham

With an optimised *in vitro* regeneration protocol for Black Mitcham developed, *A. tumefaciens*-mediated transformation would now be attempted as a means to stably transform Black Mitcham. As the transformation protocol would involve an antibiotic selection step, the SIM was supplemented with increasing concentrations of kanamycin to determine a range which was inhibitory to callus formation and growth (Figure 3.18).

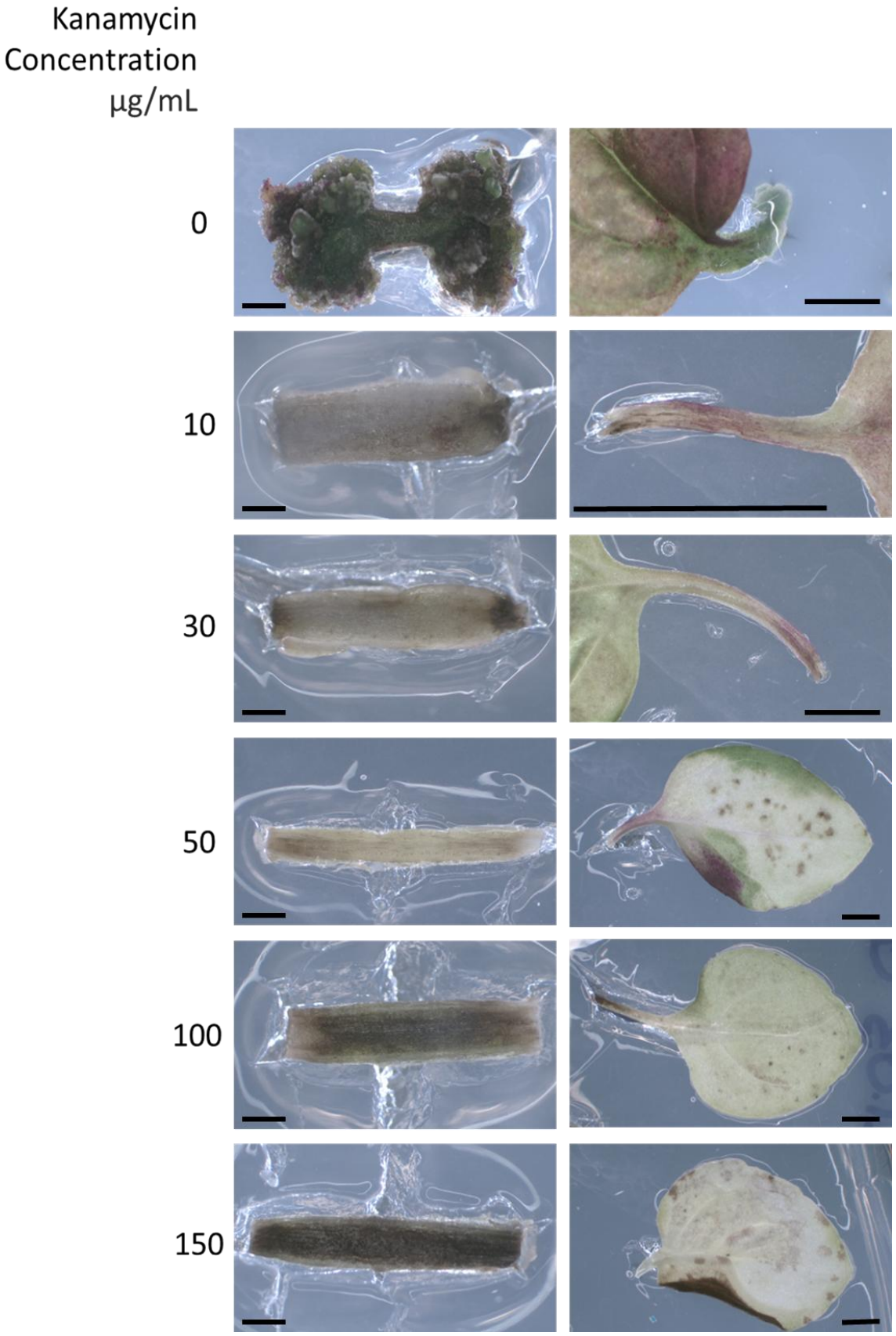

Figure 3.18. Black Mitcham explants cultured on SIM supplemented with increasing concentrations of Kanamycin. Representative images after 6 weeks are shown. Black scale bars for internodes represent 1mm. Black scale bars for leaf explants represent 1cm.

In the absence of kanamycin, both explant types showed some formation a callus or shoot regeneration (Figure 3.18). At the first concentration of kanamycin tested (10 µg/mL), neither internode or leaf explants show a capacity for callus formation even after 6 weeks of culture (Figure 3.18). This showed that even at relatively small quantities, kanamycin was sufficient to select against non-transformed explants and prevent escapes. Following this, a series of *A. tumefaciens*-mediated transformation attempts were performed, as summarised in Table 3.2.

Table 3.2. Summary of optimisation procedures performed on *A. tumefaciens*-mediated transformation protocol. SM = selection medium. SIM = shoot induction medium.

Baseline Condition: Cocultivation with EHA105 *A. tumefaciens* solution at 1 OD for 30 minutes, incubated on SIM plates for 4 days at 26°C in the dark, selection on SM plates		
Optimisation Factor	**Variable Conditions**	**Additional notes**
Co-cultivation time in *A. tumefaciens*	5, 15, 30 minutes of co-cultivation with EHA105 *A. tumefaciens*	
Co-cultivation duration on plates	1, 2, 3, 4, 5 days	
Co-cultivation temperature	20, 26, 28°C	
A. tumefaciens strain	GV3101::pMP90, LBA4404, EHA105	
Acetosyringone concentration	0, 100, 500 µM	Cocultivation with EHA105 *A. tumefaciens* solution with variable Acetosyringone added for 30 minutes
Chemical additives	Activated Charcoal, PVPP	Selection on SM plates supplemented with chemical additives (1g/L)

A. tumefaciens strains were transformed with the pL2Kan:GUS vector (Table 2.2) to select for regenerative tissue based on both kanamycin resistance and GUS activity, to give a clear indication of transformed tissue. The pL2Kan:GUS vector contains the kanamycin resistance gene *nptII* driven by the *A. thaliana ACT2* promoter, and the GUS reporter gene *uidA* driven by the *A. tumefaciens nos* promoter, making it suitable to select for transformed tissue based on the above selection parameters. This vector was kept standard throughout the troubleshooting attempts. A minimum of 100 young internode explants (sourced from positions (1) and (2)) were used for each transformation attempt, together with a variable number of leaf explants. Explants were moved to fresh SM plates every 2 weeks, which were supplemented with 10 µg/mL kanamycin and 300 µg/mL cefotaxime. No regenerating explants were recovered from any of these troubleshooting attempts, with representative images at 4 weeks of culture shown in Figure 3.19.

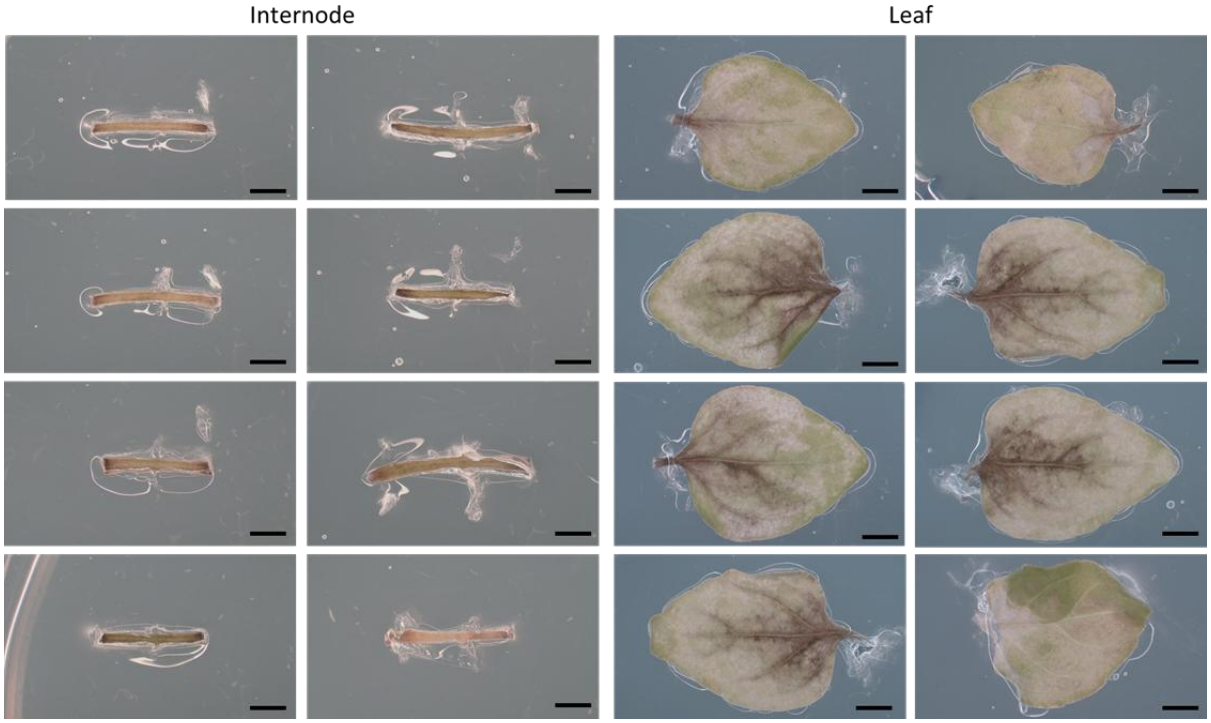

Figure 3.19. Explants from Black Mitcham co-cultivated with *A. tumefaciens* and cultured on SIM with antibiotics. Representative images were taken after 4 weeks of culture, where no callus could be observed. Scale bars for internode explants are 5 mm. Scale bars for leaf explants are 1 cm.

In all transformation attempts, explants showed no visible signs of regeneration, and after 4 weeks all explants showed obvious signs of chlorosis (Figure 3.19). Explants were nonetheless transferred to fresh SM medium every 2 weeks, until the 16 week

mark, where all explants had gone necrotic, and the experiment was terminated (data not shown).

The addition of chemical additives was performed to reduce callus and growth medium browning that occurred during TC, which was thought to be a possible cause of transformation failure. Activated charcoal supplemented SM plates showed caused an increased overgrowth of *A. tumefaciens* around the explants, causing death (Figure 3.20).

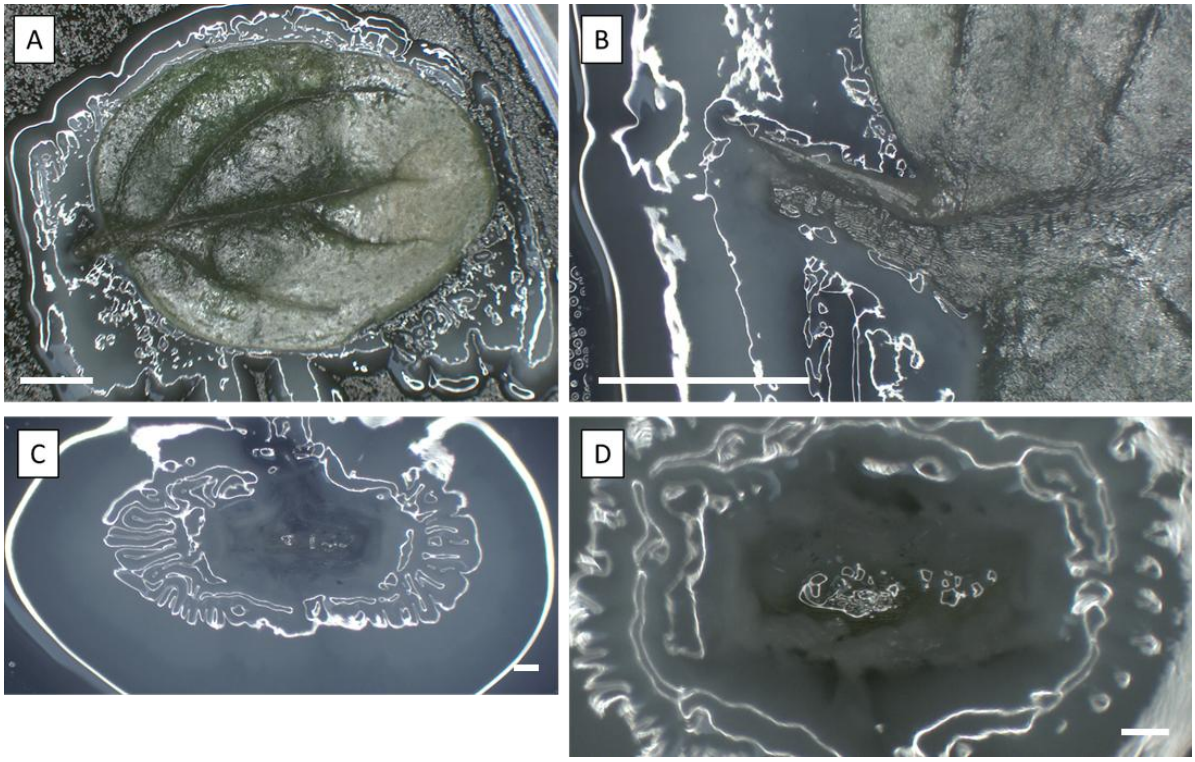

Figure 3.20. Black Mitcham internode and leaf explants cultured on selection medium supplemented with activated charcoal. A. Leaf explants showing overgrowth of *A. tumefaciens* around the leaf surface. Scale bar is a white bar and represents 1cm. B. Petiole from leaf explant showing overgrowth of *A. tumefaciens*. Scale bar is a white bar and represents 1 cm. C, D. Internode explants showing overgrowth of *A. tumefaciens*. Scale bar is a white bar and represents 1 mm.

Addition of PVPP to the SM also showed no improvement to transformation, as no obvious callus growth was observed (Figure 3.21).

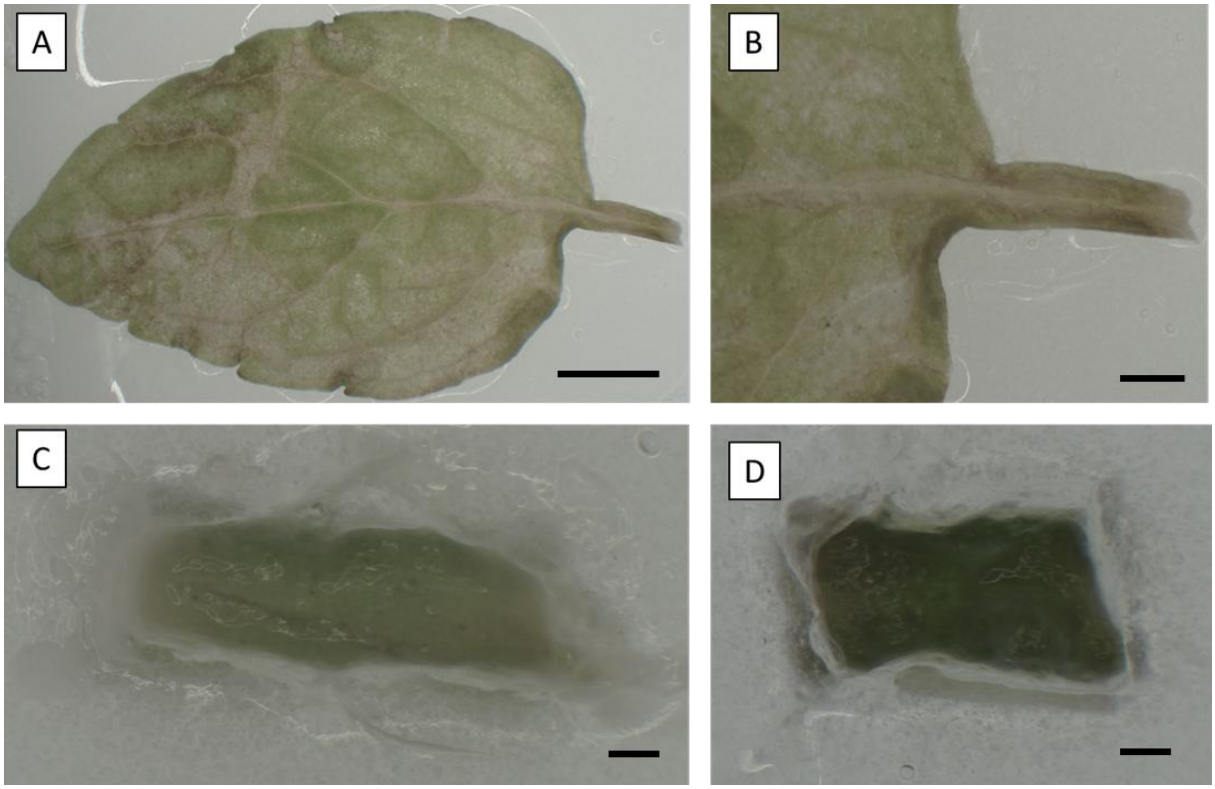

Figure 3.21. Black Mitcham internode and leaf explants cultured on SM for 4 supplemented with PVPP, for 4 weeks. A. Leaf explants showing lack of callus formation and signs of chlorosis. Scale bar is a black bar and represent 1cm. B. Petiole from a leaf explant showing lack of callus formation. Scale bar is a black bar and represents 1cm. C, D. Internode explants showing a lack of callus formation. Scale bar is a black bar and represents 1 mm.

At this stage, it was speculated whether the antibiotic selection was too strong, so a baseline condition transformation protocol (Table 3.2) was trialled whilst omitting kanamycin from the SM. The experiment was run until elongated shoots could be recovered, and then all plant material was harvested and stained for GUS activity. This is summarized in Figure 3.22.

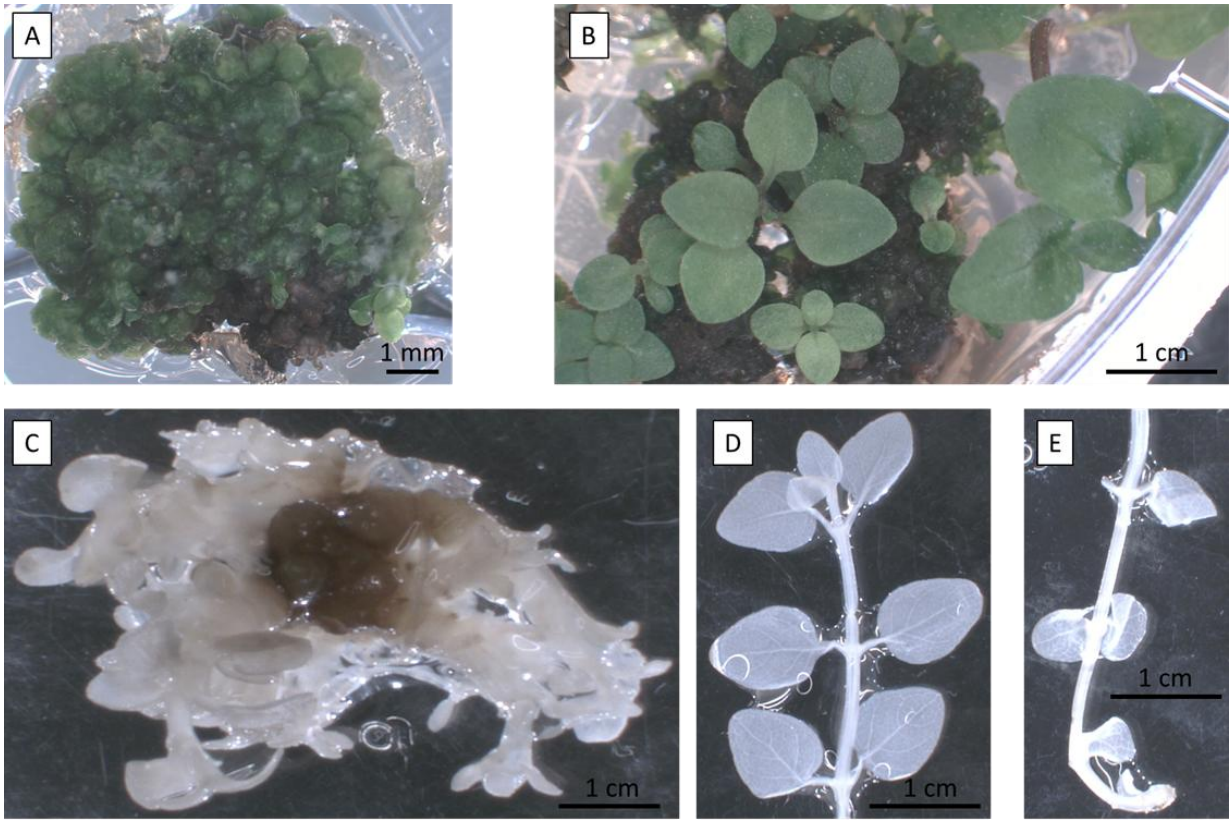

Figure 3.22. Explants from Black Mitcham co-cultivated with A. tumefaciens and cultured on SM without antibiotics. A. Shoot-like callus formed on internode explants after co-cultivation with A. tumefaciens and cultured on SM. B. Elongated shoots forming on HF medium. C. Shoot-like callus mass after GUS staining and tissue clearing. D/E. Elongated shoots after GUS staining and tissue clearing.

Explants developed callus and proliferated shoots after co-cultivation with *A. tumefaciens* strain EHA105 (Figure 3.22 A), and subsequently shoots were able to elongate on HF medium (Figure 3.22 B). Both callus masses (Figure 3.22 C) and elongated shoots (Figure 3.22 D/E) were stained for GUS activity, where none could be detected in the >100 internode explants grown. Alongside this experiment, *A .thaliana* and *N. benthamiana* were transformed alongside, using the same culture of *A. tumefaciens* strain EHA105 harbouring the pL2Kan:GUS vector. This was done as a control to test if the *A. tumefaciens* strain EHA105 or the pL2Kan:GUS vector were capable of stable transformation in plant species at all (Figure 3.23).

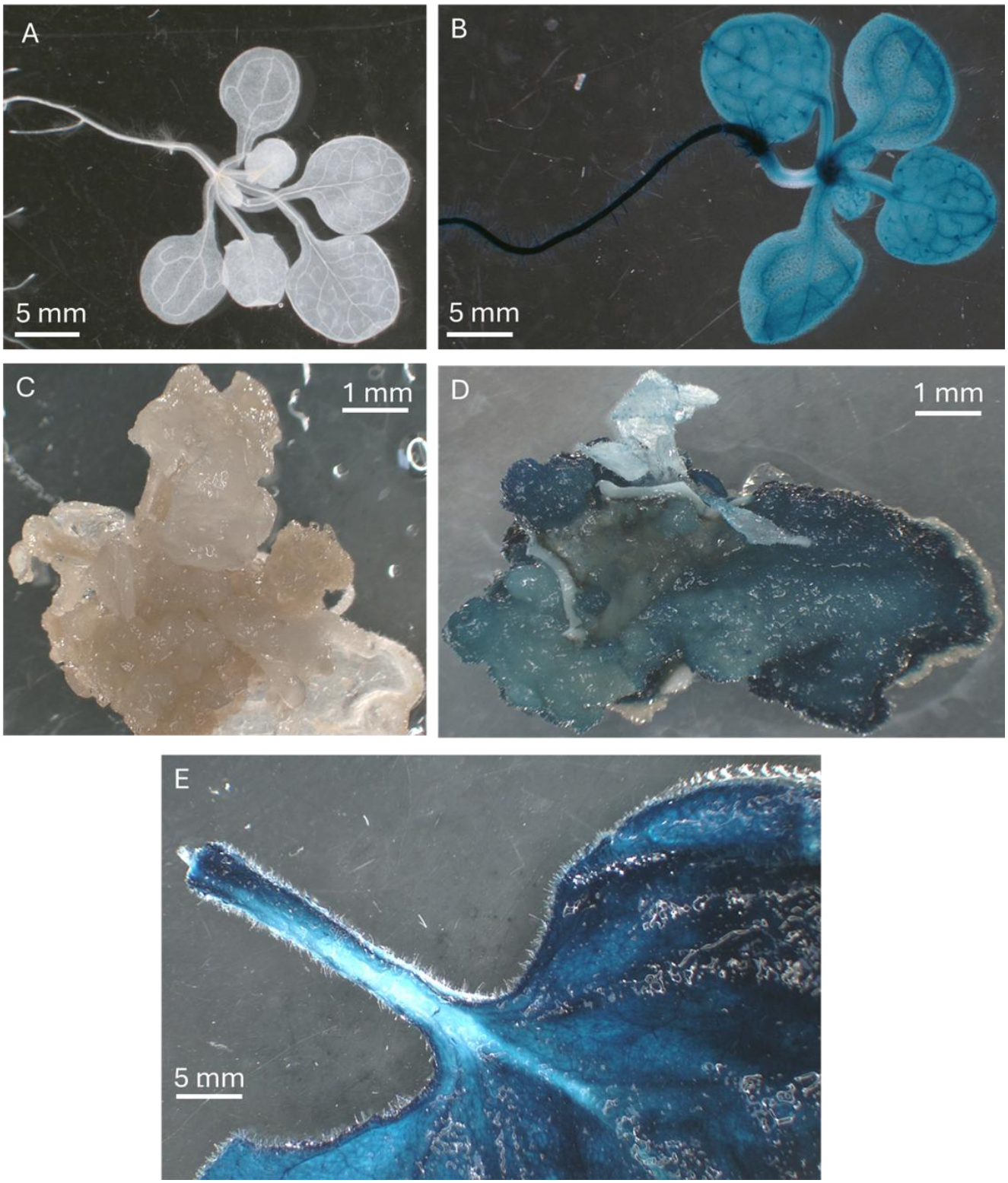

Figure 3.23. *A. thaliana* and *N. benthamiana* transformed with *A. tumefaciens* strain EHA105 harbouring the pL2Kan:GUS vector. A. Untransformed *A. thaliana* post GUS staining and clearing. B. T1 transformant *A. thaliana* post GUS staining and clearing. C. Untransformed *N. benthamiana* callus post GUS staining and clearing. D. Transformed *N. benthamiana* callus post GUS staining and clearing. E. Transformed T0 *N. benthamiana* leaf post GUS staining and clearing. Scale bars are shown as white bars.

T1 *A. thaliana* plants recovered after floral dipping showed constitutive GUS activity in all of the tissue (Figure 3.23 B). An untransformed WT was included as a control to rule out any endogenous GUS activity (Figure 3.23A). *N. benthamiana* were transformed in a similar manner to Black Mitcham, with an *A. tumefaciens*-mediated cocultivation of leaf disc explants with kanamycin selection. Resulting callus was stained for GUS activity as a comparison point to Black Mitcham callus, and GUS activity was observed throughout the callus mass (Figure 3.23 D). An untransformed callus, induced on callus induction medium for *N. benthamiana* was GUS stained and used as a control to rule out any endogenous GUS activity resulting from callus formation (Figure 3.23 C). T0 *N. benthamiana* plants resulting from the transformant callus were grown to a full plant structure, and a leaf was stained for GUS activity, which again showed GUS activity throughout the tissue (Figure 3.23). As a final quality control check on the pL2Kan:GUS plasmid, *N. benthamiana* leaves were transiently transformed and stained for GUS activity (Figure 3.24).

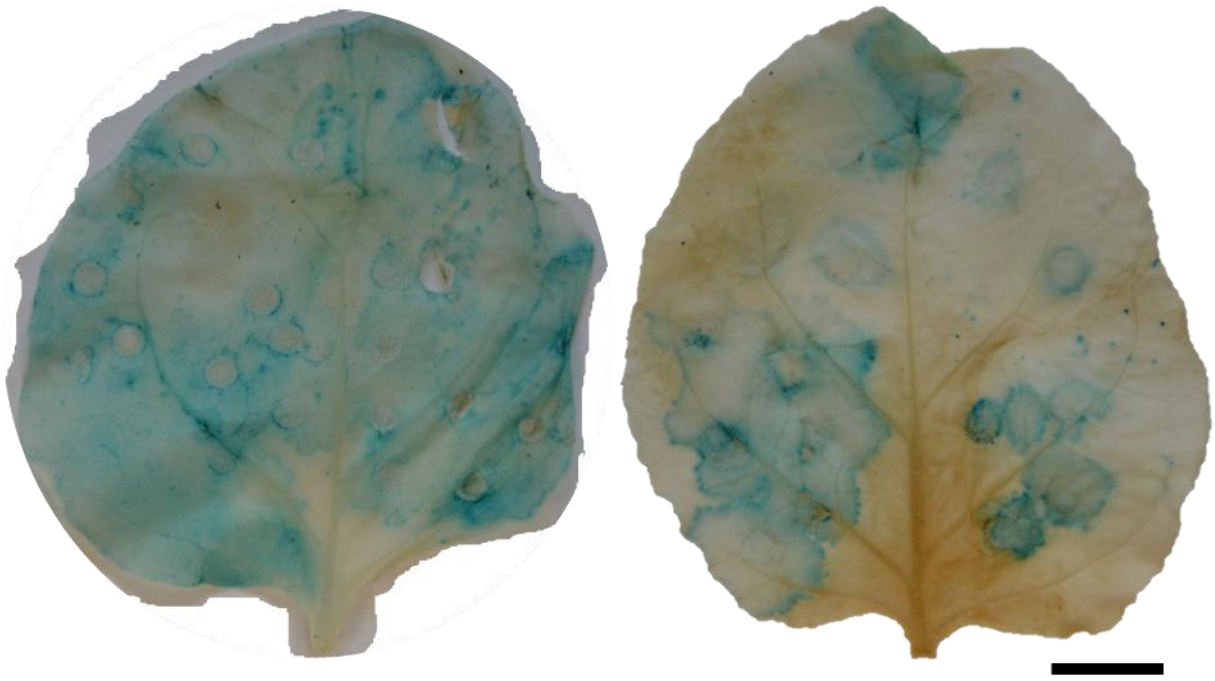

Figure 3.24. *N. benthamiana leaves* injected with *A. tumefaciens* strain EHA105 harbouring the pL2Kan:GUS plasmid. Representative images are shown of leaves stained for GUS activity and cleared of chlorophyl. Scale bar in black is 2cm.

With the transiently expressed *N. benthamiana* leaves, GUS activity can be observed throughout the tissue, radiating from the sites of injection (Figure 3.24). Taken together, this gives strong evidence that both the *A. tumefaciens* strain EHA105 and the pL2Kan:GUS plasmid are functional.

Finally, alternative approaches to the *A. tumefaciens*-mediated co cultivation transformation were trialled as an exploratory approach to alternative methods of transformation. A novel “RAPID” method was trialled which involved injection the *A. tumefaciens* strain EHA105 harbouring the pL2Kan:GUS plasmid directly into Black Mitcham rhizome, shoot tissue and nodes. The injected Black Mitcham were grown in soil until new shoots had emerged. Resulting plants were then stained for GUS activity, as shown in Figure 3.25.

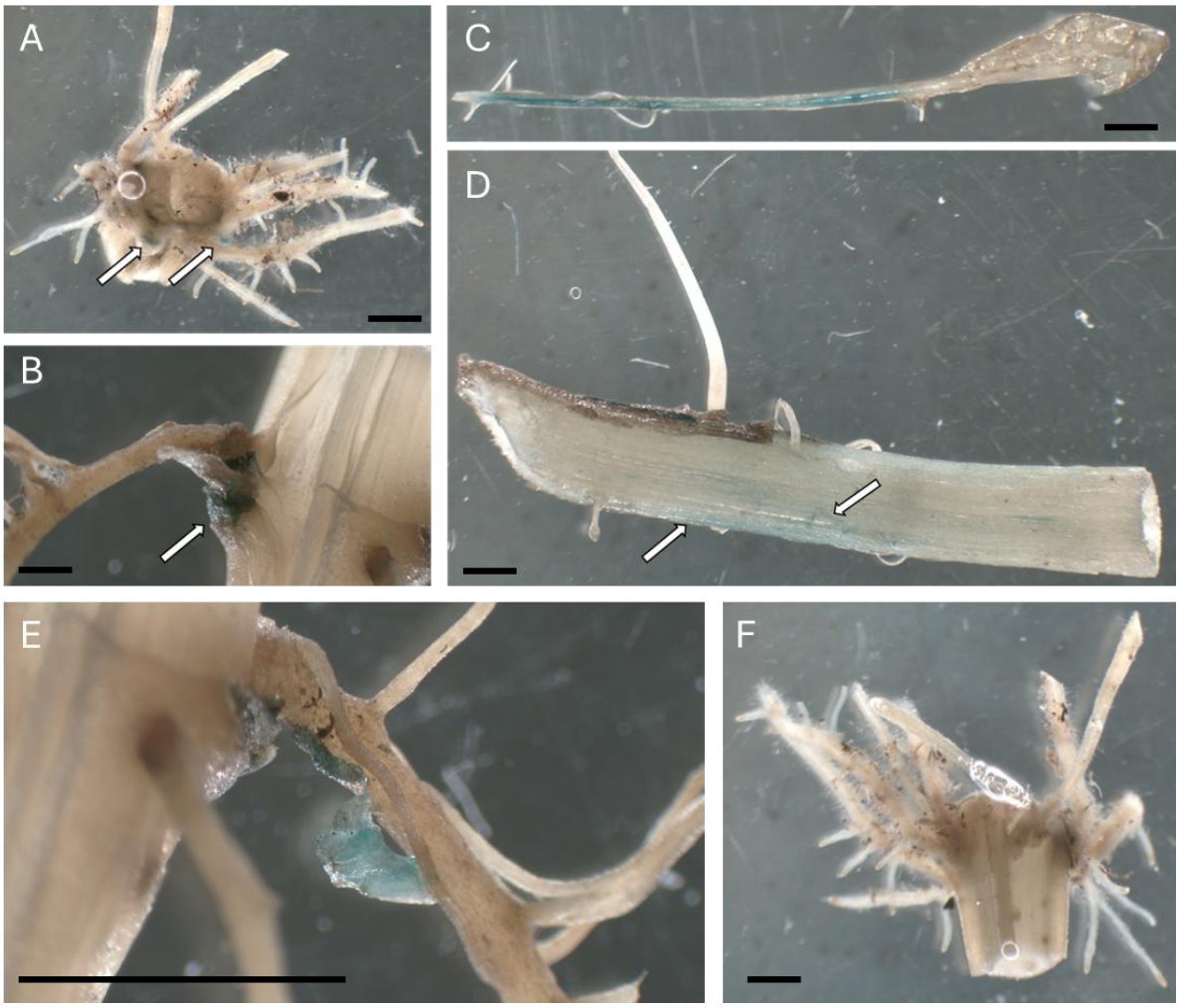

Figure 3.25. Black Mitcham plant segments showing GUS activity after RAPID transformation using *A. tumefaciens* strain EHA105 harbouring the pL2Kan:GUS plasmid. A. Mass of roots and rhizomes showing GUS activity indicated by the white arrows. Scale bar is shown as a black bar and represents 2 cm. B. Rhizome segment showing GUS activity at the site of injection, as shown by the white arrow. Scale bar is shown as a black bar and represents 1 cm. C. Root segment showing GUS activity throughout the tissue. Scale bar is shown as a black bar and represents 1 mm. D. Rhizome segment showing diffuse GUS activity throughout the tissue, as highlighted by white arrows. Scale bar is shown as a black bar and represents 1 cm. E. GUS activity from roots originating from injected rhizome tissue. Scale bar is shown as a black bar and represent 1 cm. F. Control rhizome segment injected with a buffer solution. Scale bar is shown as a black bar and represents 1 cm.

GUS activity was observed primarily around the injection sites of the rhizome tissues (Figure 3.25 A, B). GUS activity was also observed in some of the root tissues (Figure 3.25 C). Diffuse GUS activity was observed in some of the rhizome segments, separate from the sites of injection (Figure 3.25 D). Stronger GUS activity was observed in root tissue originating from injected rhizome segments (Figure 3.25 E). Overall, RAPID transformation of Black Mitcham rhizomes showed GUS activity around injection sites as well as newly grown tissue, highlighting the applicability of this technique in Black Mitcham.

In parallel, biolistic bombardment of Black Mitcham tissue was trialled as a means to evaluate if pL2Kan:GUS was functioning in Black Mitcham tissue (Figure 3.26).

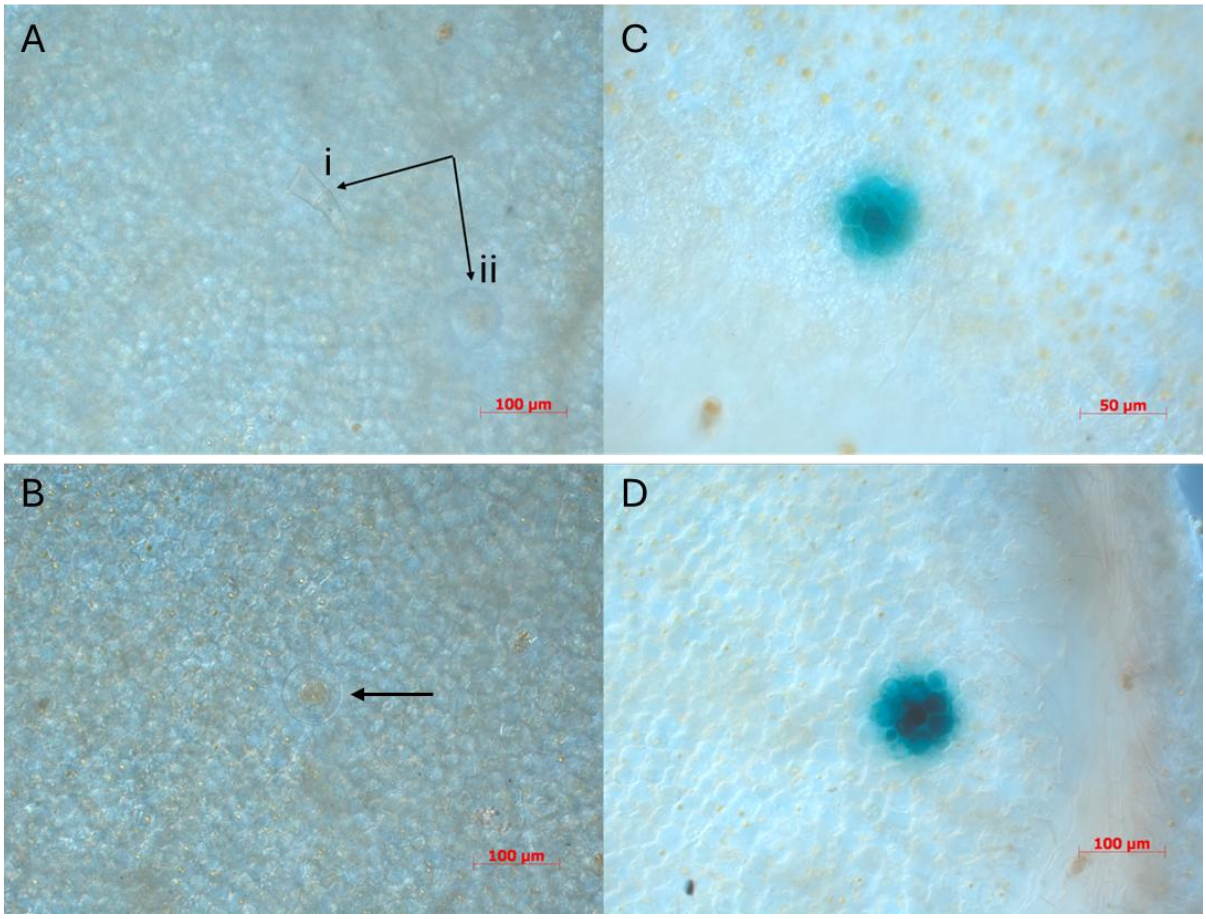

Figure 3.26. Mentha leaf tissue stained for GUS activity following biolistic bombardment. A. Non-glandular trichomes (i) and glandular peltate trichomes (ii) on surface on mint leaf shown by black arrows. Identification is based on Vaidya et al. 2019. B. Untransformed glandular peltate trichome shown by a black arrow. C,D. GUS activity on the leaf surface of Black Mitcham. Scale bars are shown as red bars.

Biolistic bombardment of Black Mitcham leaf tissue with the pL2Kan:GUS vector showed the ability to confer GUS activity in the leaf tissue (Figure 3.26 C,D). It also

appears to be localised around the site of impact, potentially even from a glandular peltate trichome.

3.4 Conclusions

Chapter 3 aimed to establish the foundational tools and methodologies required for genetic manipulation of Black Mitcham by developing an efficient *in vitro* regeneration system and assessing the feasibility of several transformation approaches.

The regeneration protocol developed here demonstrated that young internode segments cultured on a medium supplemented with 0.5 µM NAA and 9 µM TDZ produced the most robust and consistent regeneration response. The omission of coconut water from the medium simplified the protocol, and allowed for a clearer interpretation of the effects of each PGR tested in this study. The final optimised protocol did not require a separate callus and shoot induction phase, which removed unneeded TC manipulation, thus reducing the chance of contamination. The protocol developed in this chapter provides a reliable platform for downstream genetic transformation protocol requiring an explant mediated regeneration step.

The regenerative capacity of PGRs 2,4-D and FPX were also explored but ultimately did not show the ability to induce regenerative callus. FPX induced the unexpected capability to produce multiple rhizome-like structures from both internode and leaf callus, and this novel finding shows promise in future studies in rhizome development in Black Mitcham.

Despite extensive troubleshooting, *A. tumefaciens*-mediated transformation failed to produce regenerative callus in the Black Mitcham cultivar used in this study. This prompted the investigation of the RAPID transformation protocol in Black Mitcham. Direct injection of *A. tumefaciens* solution into vegetatively propagating rhizomes yielding promising results. GUS staining was observed at both the injection sites and from adventitious roots originating from the injection sites. This novel finding has laid the foundation for future studies of *in-planta* regeneration from Black Mitcham, offering a potential route to substantially speed up the delivery of exogenous DNA for genetic engineering purposes.

Biolistic bombardment was also investigated as a DNA delivery strategy as a means to test functionality of MoClo derived plasmids in Black Mitcham tissue. Preliminary results showed GUS staining originating from a glandular peltate trichome, highlighting this as a potential system to rapidly prototype plasmids before

committing to longer stable transformation procedures. The transformation strategies trialled in this chapter are summarised in Table 3.3.

Table 3.3. Summary of transformation strategies trialled for Black Mitcham

Transformation Approach	Variables Tested	Outcome
A. tumefaciens co-cultivation	5, 15 and 30 minutes co-cultivation in *A. tumefaciens* solution	All explants necrotic after 12 weeks on selection medium
A. tumefaciens co-cultivation	1, 2, 3, 4 and 5 days of post co-cultivation incubation on non-selective medium, prior to transfer to selection medium	All explants necrotic after 12 weeks on selection medium
A. tumefaciens co-cultivation	20°C, 26°C and 28°C temperature for post co-cultivation incubation on non-selective medium, prior to transfer to selection medium	All explants necrotic after 12 weeks on selection medium
A. tumefaciens co-cultivation	*A. tumefaciens strains* GV31091::pMP90, LBA4404 and EHA105 used for transformation	All explants necrotic after 12 weeks on selection medium
A. tumefaciens co-cultivation	Acetosyringone concentrations of 100μM and 500μM added during co-cultivation	All explants necrotic after 12 weeks on selection medium
A. tumefaciens co-cultivation	Activated charcoal and PVPP at concentrations of 1g/L added to selection medium	All explants necrotic after 12 weeks on selection medium
A. tumefaciens co-cultivation	Kanamycin removed from selection medium	Explants developed into callus and subsequently formed shoots. No GUS expression detected in any of the tissue.
A. tumefaciens direct injection	*A. tumefaciens* EHA105 strain directly injected into rhizomes, shoots and nodal tissue.	New, regenerated tissue showed GUS expression localised to injection sites. Trace GUS expression observed away from sites of injection
Biolistic bombardment	pL2Kan:GUS plasmid bombarded onto leaf tissue	GUS expression localised around bombardment sites.

Taken together, chapter 3 highlights both the challenges and opportunities of working with a non-novel plant species such as Black Mitcham, and in-depth discussion of these findings is found in Chapter 6. Although relatively well understood, the perturbation of the menthol biosynthetic pathway in Black Mitcham has taken many years to develop transgenic lines, often with unexpected changes. A more tractable experimental system is needed to be able to design, build and test the various potential genetic changes. This gap can be met by the reconstitution of the menthol biosynthesis pathway in less recalcitrant and more well understood model plant species such as *A. thaliana* and *N. benthamiana*. Chapter 4 therefore aims to shift the focus to the heterologous expression of menthol biosynthesis genes in both these plant species to evaluate pathway functionality and establish proof-of-concept production for menthol and its precursors outside of the native host using MoClo derived plasmids.

Chapter 4 - Heterologous expression of menthol biosynthetic pathway genes in non-native plant hosts

4.1 Introduction

4.1.1 The *M. x piperita* menthol biosynthesis pathway: Missing links and past approaches to heterologous gene expression in non-native hosts

The MBP begins with the universal monoterpene C_{10} precursor GPP which is formed by the condensation of the universal C_5 isoprenoid precursors IPP and DMAPP by GPPS (Eisenreich et al. 1997; Burke et al. 1999). The C_5 precursors are solely derived from the plastidial MEP pathway in *M. x piperita* trichomes (Eisenreich et al. 1997). The *M. x piperita* GPPS is comprised of a small subunit (MpGPPS.SSU) and a large subunit (MpGPPS.LSU), representing a family of heteromeric GPP synthases (Burke et al. 1999). The MpGPPS.SSU has been shown to modify the chain length specificities of phylogenetically distant C_{20} prenyltransferase geranylgeranyl diphosphate synthases (GGPPS) to favour the production of the C_{10} GPP instead (Burke and Croteau 2002a). This chain length modification ability was also seen in *Antirrhinum majus GPPS.SSU*, and overexpression of *AmGPPS.SSU* in *N. tabacum* increased IPP flux into monoterpene production whilst reducing flux into sesquiterpene production (Orlova et al. 2009)

The first committed step of the MBP is the cyclization of GPP to (-)-limonene by the enzyme (-)-limonene synthase (LimS) (Kjonaas and Croteau 1983) (Figure 1.2). This is followed by the hydroxylation of (-)-limonene to (-)-*trans*-isopiperitenol by the enzyme limonene-3-hydroxylase (MpL3H) (Lupien et al. 1999). The production of the products (-)-limonene and (-)-*trans*-isopiperitenol in non-native plant hosts has been demonstrated in the literature through a combination of both transient and stable expression approaches.

The production of (-)-limonene in the non-native host organism *N .benthamiana* has been demonstrated through transient co-expression of the *M. x piperita GPPS small subunit* gene (*MpGPPS.SSU*) and *Picea abies (-)-limonene synthase* gene (*PaLimS)* (Yin et al. 2017). It was found that transient expression of *PaLimS* alone only produced (-)-limonene in trace amounts, and these findings were replicated in stable transformants of *N. tabacum* (Yin et al. 2017). The production of (+)-trans-

isopiperitenol, an enantiomer of (-)-*trans*-isopiperitenol has been produced in stable transformants of *N. tabacum* (Lücker et al. 2004a). This was done by stably expressing the *Citrus limon* (L.) Burm.f. *(+)-limonene synthase* (*LimS*) gene, together with the *Mentha spicata* L. 'Crispa' L3H in *N. tabacum,* which resulted in (+)-limonene, the enantiomer of (-)-limonene, and (+)-trans-isopiperitenol (Lücker et al. 2004a). These findings represent the feasibility of expressing the early pathway genes of the *M. x piperita* MBP in non-native plant hosts such as *N. benthamiana*.

The later steps of the *M. x piperita* MBP involve the allylic oxidation of (-)-*trans*-isopiperitenol to (-)-isopiperitenone by (−)-trans-isopiperitenol dehydrogenase (MpIPDH), followed by the reduction of (-)-isopiperitenone to (+)-*cis*-isopulegone by (−)-isopiperitenone reductase (MpIPR) (Kjonaas et al. 1985; Croteau and Venkatachalam 1986). Following this, a double bond migration is required to convert (+)-*cis*-isopulegone into (+)-pulegone, presumed to be carried out by a (+)-*cis*-isopulegone isomerase (MpIPGI) (Croteau and Venkatachalam 1986). The (+)-*cis*-isopulegone isomerase has yet be characterised however, and remains the only uncharacterised enzyme in the *M. x piperita* MBP. The mechanism of the isomerisation of (+)-*cis*-isopulegone to (+)-pulegone is thought to mimic the action of a microbial ketosteroid isomerase (KSI) (Talalay and Benson 1972). (+)-pulegone is then reduced to either (−)-menthone or (+)-isomenthone at a ratio of 10:1 by the action of (+)-pulegone reductase (MpPGR) (Battaile et al. 1968; Ringer et al. 2003). (−)-menthone is finally reduced to (-)-menthol by the action of menthone-menthol reductase (MpMMR) (Davis et al. 2005).

A recent discovery of a KSI from *P. putida* (PpKSI) showed the capability to act as an IPGI, causing the isomerization of (+)-*cis*-isopulegone to (+)-pulegone (Currin et al. 2018). This novel PpKSI was also shown to function with the downstream MpPGR and MpMMR to generate (-)-menthol in *Escherichia coli* (*E. coli*) (Currin et al. 2018). As PpKSI mimics the action of MpIPGI, and was shown to accomplish the isomerization of (+)-*cis*-isopulegone to (+)-pulegone without the need for co-factors, this represented a unique opportunity to explore the action of PpKSI in a plant host system. Taken together, this would allow research to be built upon the expression of the early *M. x piperita* MBP genes in non-native plant hosts, by extending this to the expression of the entire *M. x piperita* MBP, using PpKSI as a proxy for MpIPGI.

4.1.2 Synthetic biology approaches and strategies towards full pathway reconstruction

Full pathway reconstruction of the MBP in a non-native host requires the ability to design, build, and test synthetic constructs to drive expression of the various MBP genes. The Modular Cloning (MoClo) system has been widely adopted in plant synthetic biology due to its capacity for rapid assembly of genetic elements into both single-gene and multi-gene constructs (Weber et al. 2011; Engler et al. 2014).

While MoClo enables fast design and assembly of constructs, testing their effects in stable transgenic plants remains a major bottleneck. As demonstrated in the previous chapter, generating stable transformants in non-model plant species is often hindered by persistent technical challenges and may even render certain experimental approaches unfeasible. Transformation of model species such as *A. thaliana* or *N. benthamiana* is generally more reliable, but still requires months before construct activity can be evaluated.

Transient expression in *N. benthamiana* offers a more rapid alternative, as transformed plants can be assayed within days. This approach aligns well with the MoClo design–build–test cycle. The development of single-gene constructs enables co-infiltration strategies, which have been used to reconstruct biosynthetic pathways of up to 16 genes (Schultz et al. 2019). This made co-infiltration an attractive strategy to trial in the reconstitution of the MBP described in this chapter.

Furthermore, single-gene constructs can be seamlessly combined into multi-gene constructs within the MoClo system. These multi-gene constructs can be tested via transient expression from a single *A. tumefaciens* T-DNA insertion and are readily applicable to downstream stable transformation. Overall, the MoClo system enables rigorous quality control of constructs via transient assays before committing to the time-intensive process of stable plant transformation.

In terms of the strategy to reconstruct the MBP in *N. benthamiana* in this chapter, it was already shown from previous studies that (-)-limonene could be produced through the transient expression of *MpGPPS.SSU* and *PaLimS* (Yin et al. 2017). The next product in the MBP, (-)-*trans*-isopiperitenol, had not been previously demonstrated to be produced in *N. benthamiana*, only its enantiomer (+)-trans-isopiperitenol. This too was produced by a different combination of genes sourced

from different organisms, and by a stable transformation approach (Lücker et al. 2004a). Thus, a key aim of this chapter was to determine whether stepwise co-expression of MBP genes in *N. benthamiana* could yield successive pathway intermediates, culminating in the production of (-)-menthol. A further objective was to assess whether these results could be replicated using multi-gene constructs transiently, and whether such constructs could ultimately be used for stable transformation to produce MBP products.

Another approach was to evaluate if metabolic flux into the reconstituted pathway could be increased by transient expression of the MEP pathway genes. Certain studies have shown that transient overexpression of MEP genes can increase terpenoid content (Forestier et al. 2021a; Forestier et al. 2021b; Park et al. 2022). Expectedly, the first committed step in the MEP pathway gene *DXS* was a common MEP gene used in these studies to increase metabolic flux. However, these studies used *DXS* genes sourced from different plant species (*N. tabacum* and *A. thaliana*), and were not performed in the context of increasing MBP related products. Curiously, when another study overexpressed the *DXS* gene from *S. lycopersicum* together with *PaLimS*, there was no change in the levels of (−)-limonene (Yin et al. 2017). This observation highlighted the potential for gene-specific and context-dependent effects, and underscored the need for a systematic evaluation of individual MEP pathway genes on MBP product accumulation—an additional objective addressed in this chapter.

4.1.3 Considerations for stable expression in non-native plant hosts

When transitioning from transient to stable expression, there are a variety of factors to consider for construct design, such as expression cassette orientation, inclusion of proper termination sequence and stop codons and non-coding spacer regions, all of which can minimize read through and aberrant transcripts (Aydın Akbudak and Srivastava 2017). For large multigene constructs, stability also becomes a major factor, as positional or structural effects can lead to uneven expression between transgenes (Rajput et al. 2025). Large multi gene constructs have been reported to be stably integrated into *Nicotiana*, however assessing long term stability remains a challenge (Buntru et al. 2013). Furthermore, transcript expression for each gene in a multi gene construct can vary (Aydın Akbudak and Srivastava 2017). Cellular compartmentalisation of introduced transgenes (enzyme targeting and the use of

transporters) is also am important parameter to consider when introducing new metabolic pathways, as this can influence access to metabolic pools (substrate availability) for the newly introduced enzymes (Heinig et al. 2013).

Another important consideration in construct design is the avoidance of repeated use of the same promoter sequence to drive multiple transgenes. Repetition of identical promoter regions within a single construct increases the risk of homology-dependent gene silencing, particularly in stable transformants (Park et al. 1996). To address this, the plant MoClo system used in this chapter provides access to a broad set of constitutive promoters suitable for expression of transgenes, enabling greater flexibility in promoter selection and improved transgene stability (Engler et al. 2014). The MoClo system also enables constructs to be designed with tailored genetic parts, control of directionality and the option to introduce localisation signals for compartmentalisation.

Whilst constitutive expression of transgenes is typically suitable for transient expression studies, for stable transformation the spatial control of expression is an important parameter to consider. In the context of engineering terpenoid biosynthetic pathways, the use of constitutive promoters can cause adverse effects such as chlorosis, dwarfism, decreased seed production and a general detrimental impact on the plants other essential biosynthesis pathways (Saxena et al. 2014; Gwak et al. 2017). The adverse effects arise from the cytotoxicity of these compounds when they accumulate ectopically in tissues where they are not typically synthesized. One option to circumvent these detrimental effects are to restrict the biosynthesis of potentially cytotoxic metabolites to specialised tissues and/or organ types where these metabolites are naturally produced, such as in the PGTs (Huchelmann et al. 2017). The monoterpenes derived from the MBP in *M. x piperita* are produced in the PGTs of the leaves (Gershenzon et al. 1989). It has been shown that the monoterpene products of the MBP are toxic to non-specialised plant tissues, with limonene specifically showing the greatest toxicity (Brown et al. 1987).

Taken together, there is a need to generate a suite of trichome-specific promoters for use in the MoClo system, which can be applied to other plant species, such as the model *A. thaliana* and *N. benthamiana*, for the expression of genes which code for potentially cytotoxic products. A caveat of integrating sequences into the MoClo

system is that they cannot have any internal *BsaI* or *BpiI* restriction sites. Internal restrictions sites within coding regions are typically removed through silent mutations that preserve the amino acid sequence due to the redundancy of the genetic code, in a process called domestication (Marillonnet and Grützner 2020). In contrast, domestication is not feasible for promoter sequences as nucleotide changes are more unpredictable and may result in the disruption of TF binding motifs, potentially altering or abolishing activity altogether. Therefore, a subset of *M. x piperita* promoters from genes from the MBP which are specifically expressed in the PGTs were chosen for characterization of expression in *A. thaliana* and *N. benthamiana*. These promoters were from the genes *MpIPDH*, *MpL3H*, *MpLimS* and *MpPGR*, derived from the Madhuras cultivar of *M. x piperita* (Qamar et al. 2022). Two additional genes from *N. tabacum* that have previously shown expression restriction to trichomes in *N. tabacum* were also chosen (Pottier et al. 2020). These promoters were from the genes *MAJOR ALLERGEN MAL D 1.0501* (*NtMALD1*) and *COPAL-8-OL DIPHOSPHATE SYNTHASE 2* (*NtCPS2*) (Pottier et al. 2020). These promoters were characterised by fusion to a *uidA* gene (Table 2.1) to observe where GUS activity would localise in *A. thaliana* and *N. benthamiana*, as this had not been done previously. This would inform which promoters would be suitable for trichome-specific expression in both model plant species for future stable transformation studies.

4.1.4 Volatile sampling methodologies applicable to this study

The monoterpenes produced by the MBP are typically volatile, and require the development of an extraction technique to analyse them. Although methods for the extraction of monoterpenes from *M. x piperita* have been established, this chapter aims to reconstitute the MBP outside of its host organism (Gershenzon et al. 2000; Radivojac et al. 2021). This introduces additional confounding variables, such as where the potentially produced monoterpenes would be originating from. In terms of transient expression, which is induced in the leaf tissue in *N. benthamiana*, this could mean that the monoterpenes could be being produced anywhere from the inner mesophyll tissue, the outer surface tissue and even the trichomes themselves.

Typical volatile extraction procedures can include solvent extractions, which uses a non-polar solvent to extract the non-polar terpenes. As this method involves a liquid solvent to extract, this allows an internal standard to be added which allows both the

downstream quantification of the volatiles and extraction efficiency to be accounted for (Jiang et al. 2016). A downside of this method is that the use of a solvent can dilute the extracted volatiles, which necessitates the downstream concentration of the sample, leading to the loss of lower molecular weight volatiles (Killiny and Jones 2017). Furthermore, if the volatiles being produced are at a low concentration, this could lead to the failure to detect the volatiles entirely. This is where the use of alternative extraction methods such as headspace solid phase microextraction (HS-SPME), which extracts emitted volatiles from the surrounding air of the plant tissue onto an ab/adsorbent material, which can be later desorbed for analysis (Tholl et al. 2006). This technique can be applied on whole plants, using a “push-pull” method, which allows the non-destructive sampling of volatiles from all plant tissues (Tholl et al. 2006). This has the benefit of the ad/absorbent material having the capability for the volatiles to be desorbed using a liquid solvent of choice, which allows the use of an internal standard for downstream quantification purposes (Yin et al. 2017). However, this method can be prone to picking up contamination from the surrounding environment and apparatus, and may be less sensitive to lower abundance volatiles (Tholl et al. 2006). An alternative approach to using whole plants for HS-SPME is the use of detached leaves in smaller contained vials to aid in the detection of lower abundance volatiles (Wong et al. 2019). This method termed static HS-SPME works by placing a detached leaf in a sealed sample vial, followed by the insertion of an ab/absorbative fibre which collects the headspace, which is then desorbed directly onto the injection port of a gas chromatography (GC) device (Jeleń et al. 2000). The downsides of this method however, are that an internal standard in the sample vial for downstream quantification purposes may have inherent inaccuracies. This is due to each volatile having a different affinity for the fibre, and the internal standard used will not have the same properties as the analyte being measured for (Lytovchenko et al. 2009). Therefore, for downstream quantification, an external standard using the same analyte of interest can be employed, and has been shown to adequately reflect volatile compositions in plant tissue (Ruiz-Hernández et al. 2018).

The extraction method is therefore a critical parameter, as inappropriate methodology can lead to false negatives, where an analyte of interest is undetected not due to absence, but due to methodological limitations. Accordingly, an additional

aim of this chapter was to evaluate different extraction strategies to reliably detect monoterpenes, thereby complementing the reconstitution of the MBP outside its native host. Therefore, solvent extractions, “push-pull” HS-SPME and static HS-SPME were trialled to determine which method could most readily detect the expected volatiles from the MBP, as well as give a measure to quantify how much of a particular volatile was being produced.

4.1.5 Aims and objectives

The overall aim of this chapter was to reconstruct the MBP outside of its native host and evaluate the production of pathway intermediates and final products using transient and stable expression systems. This would allow the optimal combination of genetic elements to be determined in more amenable systems before committing to the long and arduous stable transformation associated with non-model plant species such as Black Mitcham. The objectives were therefore:

1. To assess whether stepwise transient co-expression of MBP genes in *N. benthamiana* can lead to the accumulation of successive pathway intermediates, culminating in the expression of (-)-menthol
2. To determine whether multi-gene constructs assembled using the MoClo system can replicate the results of co-expression studies in transient expression assays
3. To test the feasibility of using these multi-gene constructs in stable transformation for longer-term MBP expression
4. To evaluate the impact of co-expression of downstream MEP pathway genes on MBP product yields
5. To characterise *M. x piperita* and *N. tabacum* derived trichome specific promoters in *A. thaliana* and *N. benthamiana*
6. To identify a suitable analytical method for detecting volatiles in transformed plant tissues by trialling solvent extraction, “push-pull” HS-SPME and static HS-SPME

4.2 Results

4.2.1 Validation of the MoClo toolkit in *N. benthamiana*

An initial early step was to validate the chosen parts from the MoClo toolkit. This was achieved by creating a series of single transcriptional unit constructs, termed as Level 1 in the MoClo nomenclature, to validate a series of different promoters as well as the *uidA* gene included in the MoClo kit. The Level 1 (L1) constructs all had the same *uidA* gene driven by either the Cauliflower Mosaic Virus (CamV) 35S promoter with the Tobacco Mosaic Virus (TMV) 5'UTR (pCamV35S::GUS), the *A. tumefaciens octopine synthase* (*ocs*) promoter (pAtuOcs::GUS), the *A. tumefaciens mannopine synthase* (*mas*) promoter (pAtuMas::GUS), the *A. tumefaciens nopaline synthase* (*nos*) promoter with the TMV 5'UTR (pAtuNos::GUS) or the *A. thaliana ACTIN2* (*act*) promoter with the TMV 5'UTR (pAtAct::GUS) (Figure 4.1).

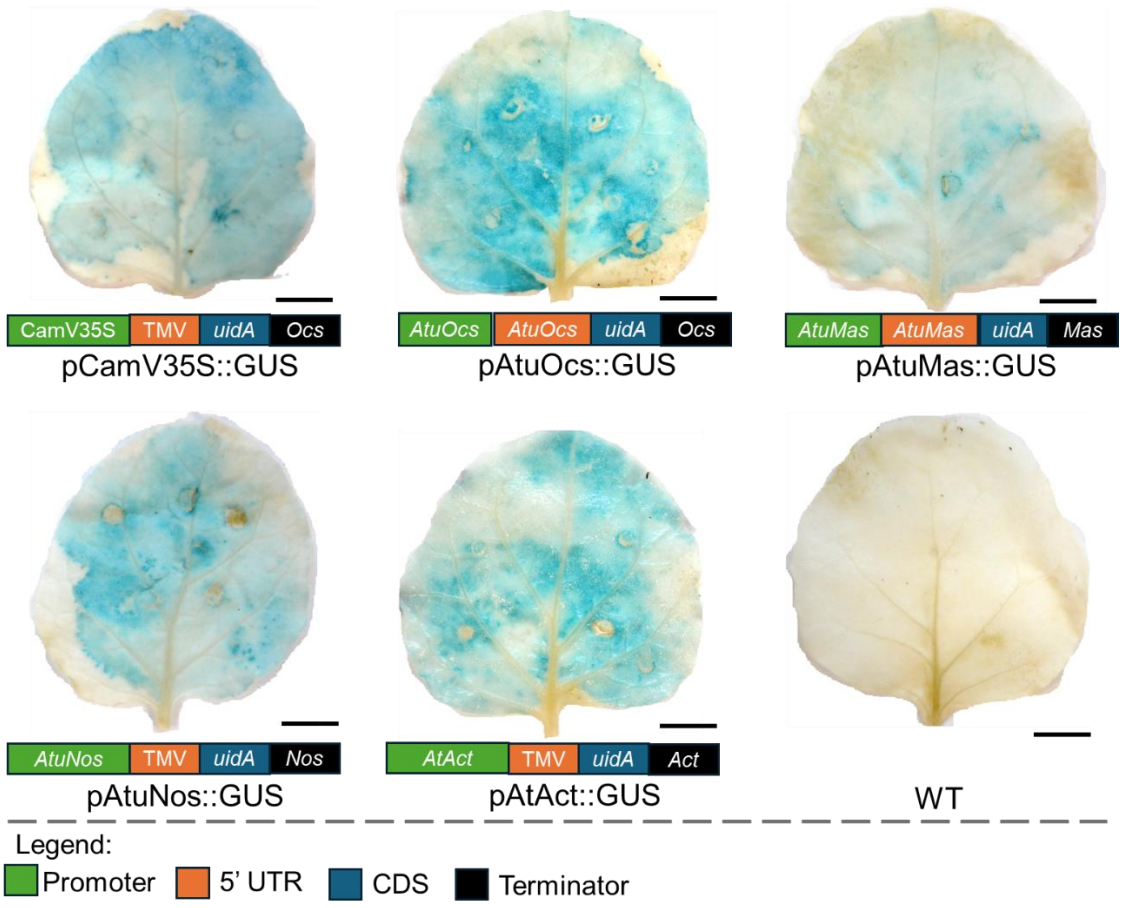

Figure 4.1 Representative images of *N. benthamiana* leaves showing transient GUS activity driven by different promoters from the MoClo tool kit. Level 1 constructs were transformed into A. tumefaciens strain GV3101:pMP90 and injected into leaves of *N. benthamiana*. GUS activity was visualised at 3 dpi. Scale bar is shown as a black line and represents 2cm.

The different L1 constructs were transformed into *A. tumefaciens* strains GV3101:pMP90 and subsequently injected into *N. benthamiana* leaves to assess if *uidA* expression could be observed. Leaves were assayed for *uidA* expression 3 days post infiltration (dpi), and all L1 constructs tested functioned as intended, as indicated by the formation of blue pigment in the leaf (Figure 4.1). This confirmed the suitability of the tested promoter parts for use in constructing the other constructs made in this thesis. It should be noted that the pL2Kan:GUS plasmid used in Chapter 3 was built using these same MoClo parts.

Learning from the troubleshooting performed in Chapter 3 with transformations of Black Mitcham, a *N. benthamiana* stable transformation protocol was also developed as part of this chapter. A key parameter tested was the strain of *A. tumefaciens* used, as this was known to have an impact on transformation efficiency in stable transformants. The strain GV3101:pMP90 has been routinely used in the Scofield lab for stable *A. thaliana* transformations, but not for *N. benthamiana*. Therefore, the strains EHA105 and LBA4404 were tested against GV3101:pMP90 for transformation efficacy. An initial quality control check to see if the EHA105 and LBA4404 *A. tumefaciens* strains used in this thesis were even functional, was to perform transient expression in *N. benthamiana* using the pL2Kan:GUS plasmid (Figure 4.2).

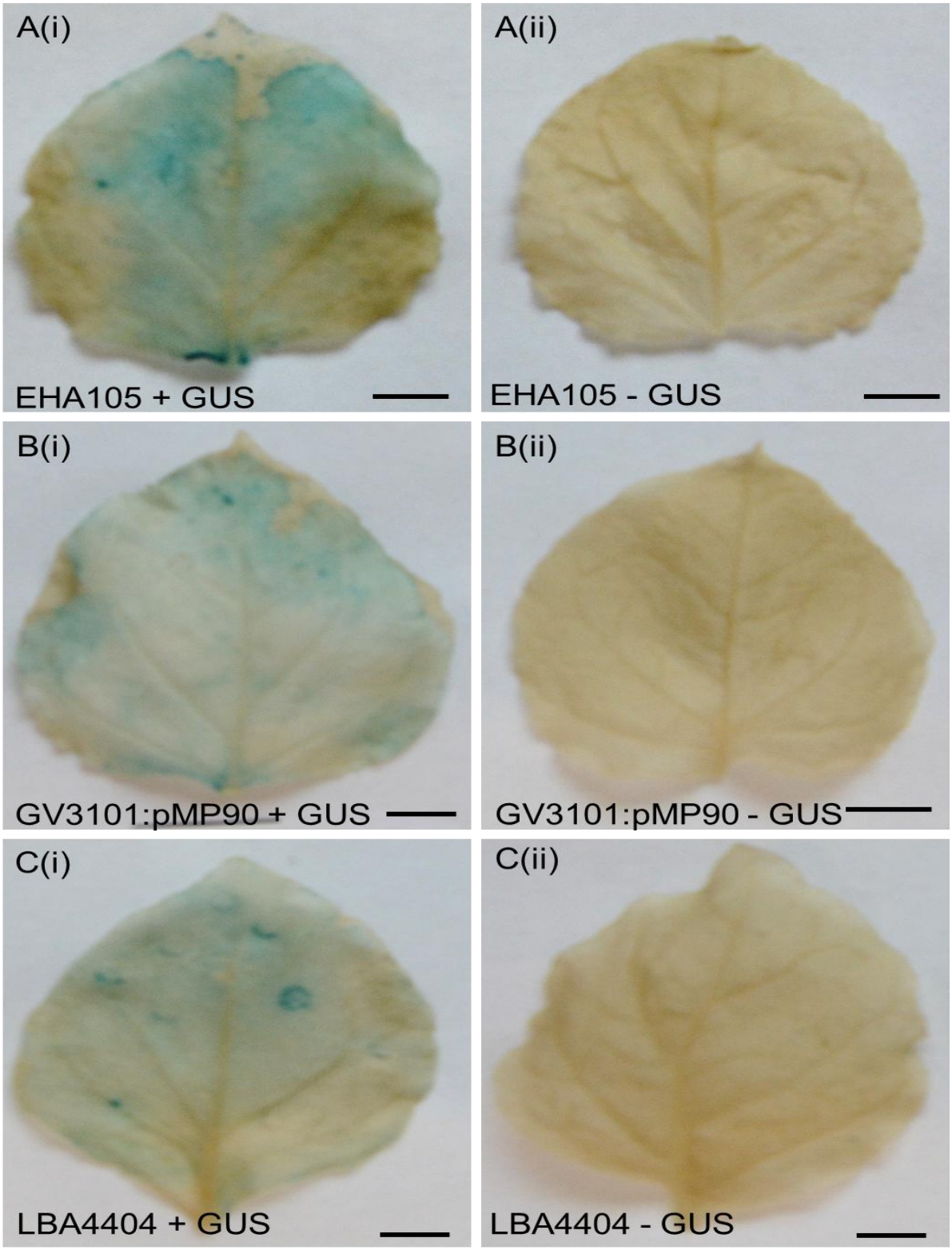

Figure 4.2 Transient expression in *N. benthamiana* leaves following infiltration with *A. tumefaciens* strains carrying the pL2Kan:GUS construct.
(A) Strain EHA105: (i) transformed with pL2Kan:GUS construct; (ii) untransformed control.
(B) Strain GV3101:pMP90: (i) transformed with pL2Kan:GUS construct; (ii) untransformed control.
(C) Strain LBA4404: (i) transformed with pL2Kan:GUS construct; (ii) untransformed control.
Images show GUS staining 5 days post-infiltration. Scale bars = 1 cm.

All 3 transformed *A. tumefaciens* strains were able to confer transient GUS activity in *N. benthamiana* leaves, whilst the corresponding untransformed controls showed no GUS activity (Figure 4.2). This confirmed the capability of all three strains to transiently transform *N. benthamiana* and showed that the GUS activity was conferred solely by the pL2Kan:GUS plasmid, ruling out the possibility of endogenous GUS activity.

Next, the *A. tumefaciens* strains were characterised for stable expression in *N. benthamiana*. This experiment aimed to validate whether the *nptII* gene (Kanamycin resistance, from the MoClo kit) was sufficient to support *in vitro* callus regeneration in *N. benthamiana*, and whether the *uidA* (GUS) reporter gene would persist in stable transformants. To do so, leaf explants from *N. benthamiana* were stably transformed and plated on selection medium. The explants were cultured for 60 days, at which point they were scored for either regeneration frequency (%) or shoot transformation frequency (%) (Figure 4.3A).

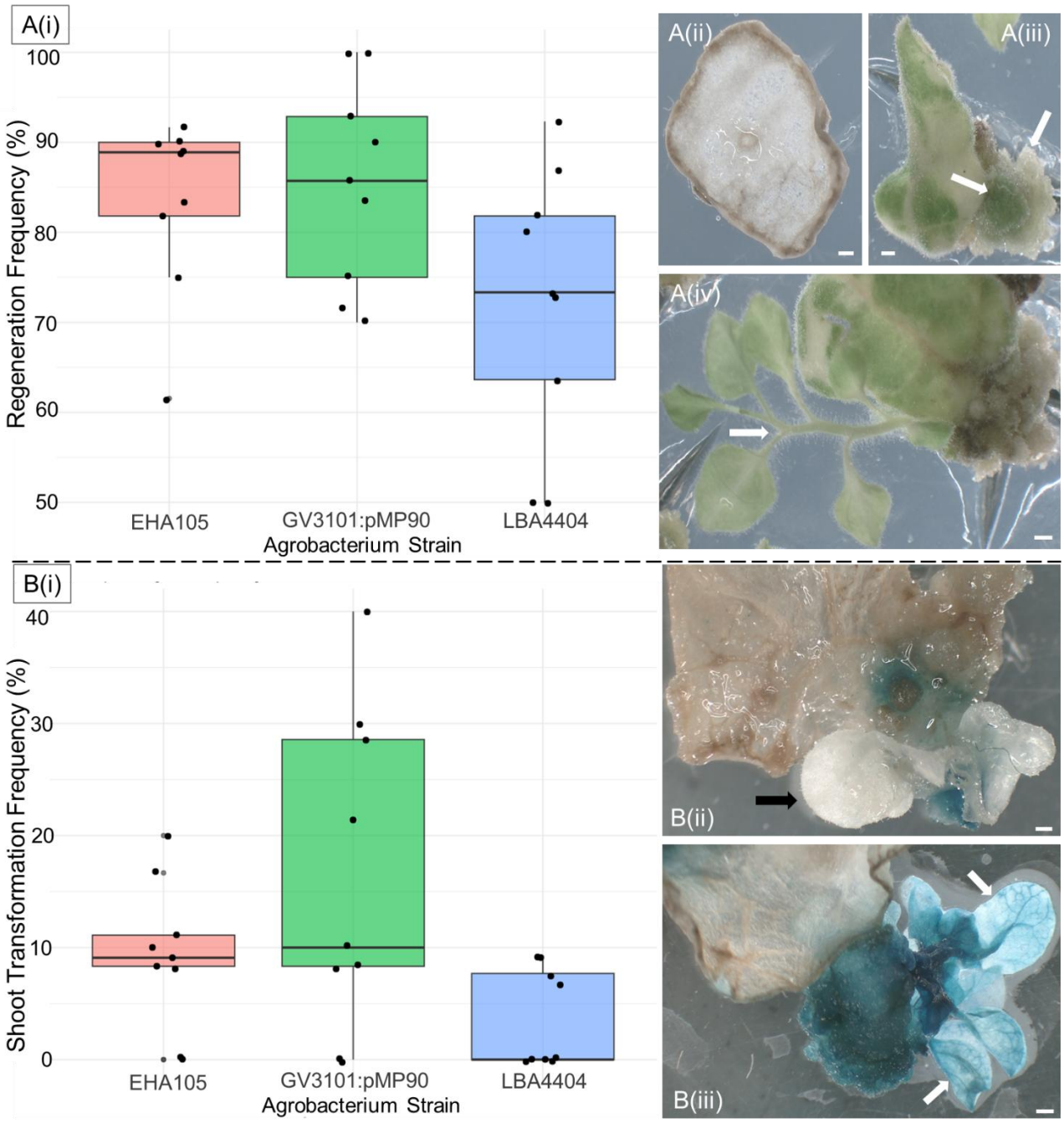

Figure 4.3. *A. tumefaciens* strain characterization in stable *N. benthamiana* transformants. A(i) Regeneration frequency of *N. benthamiana* leaf explants stably transformed with either EHA105, GV3101:pMP90, or LBA4404. Data are shown as boxplots with individual replicate values overlaid. Individual replicates represent the mean of 8–15 leaf explants cultured on a single selection medium plate. Data were analysed using one-way ANOVA followed by Tukey's HSD post hoc test.
A(ii) Representative image of a non-regenerative leaf explant.
A(iii) Representative image of callus regeneration from a leaf explant. White arrows indicate areas of callus formation.
A(iv) Representative image of shoot regeneration derived from a regenerating callus body. White arrows indicate defined shoot structures.
B(i) Shoot transformation frequency (%) of *N. benthamiana* leaf explants stably transformed with either EHA105, GV3101:pMP90, or LBA4404. Data are shown as boxplots with individual replicate values overlaid. Data were analysed using Welch's ANOVA followed by

Games–Howell post hoc tests.
B(ii) Representative image of regenerative shoots showing no GUS activity (black arrow).
B(iii) Representative image of regenerative shoots showing GUS activity (white arrows).
Scale bar for A(ii), A(iii), A(iv), B(ii), and B(iii) = 1 cm.

Regeneration frequency (Figure 4.3A (i)) was defined as the percentage of explants forming any callus or new growth originating from the explant (Figure 4.3A (iii–iv)). All three *A. tumefaciens* strains tested were able to deliver the pL2Kan:GUS construct and confer kanamycin resistance to *N. benthamiana* leaf explants. A one-way ANOVA found no significant differences in regeneration frequency among strains ($p = 0.12$). Tukey's HSD post hoc test also detected no pairwise differences (adjusted $p > 0.05$), although the comparison between GV3101:pMP90 and LBA4404 approached significance ($p = 0.082$).

Shoot transformation frequency (Figure 4.3 B(i)) was defined as the percentage of regenerating shoots showing GUS activity (Figure 4.3B (iii)), excluding cases where expression was limited to the callus body (Figure 4.3B (ii)). A one-way Welch's ANOVA indicated a significant strain effect ($F(2, 14.1) = 4.60$, $p = 0.029$), but Games–Howell post hoc tests did not identify significant pairwise differences (adjusted $p > 0.05$). The comparison between GV3101:pMP90 and LBA4404 again approached significance ($p = 0.07$).

Although there was no clear statistically better or worse *A. tumefaciens* strain to use for future experiments, this experiment revealed no fundamental flaws in both the *A. tumefaciens* strains used and the pL2Kan:GUS plasmid. As preliminary transformation of the various constructs produced in this thesis had already begun in strain GV3101:pMP90, there was no strong rationale to switch to another strain from this experiment. Therefore going forward, the GV3101:pMP90 was used for all subsequent transient and stable transformation work in *N. benthamiana*. Henceforth, when *A. tumefaciens* is mentioned in this chapter, it is referring to the GV3101:pMP90 strain.

4.2.2 Construction of Menthol Biosynthesis Pathway genes using the MoClo system

The MBP genes were first assembled into L1 MoClo constructs as single transcriptional units for preliminary testing. The *Tomato bushy stunt virus* (TBSV) suppressor of silencing gene *p19* was also included in this initial pipeline to suppress

post-transcriptional gene silencing of the introduced transgenes (Lombardi et al. 2009). As part of the routine QC process, all assembled constructs (Table 2.1) were first transformed into *E. coli* and then sequenced to confirm their identity. The constructs were then transformed into *A. tumefaciens* to be used for transient infiltration of *N. benthamiana*. As *A. tumefaciens* produces the transformed plasmids at a low copy number, further plasmid sequencing from the transformed *A. tumefaciens* is not generally viable. Therefore as the final QC step, transformed *A. tumefaciens* were subjected to colony PCR to reconfirm the successful transformation of the L1 constructs, by amplification of the entire construct (Figure 4.4)

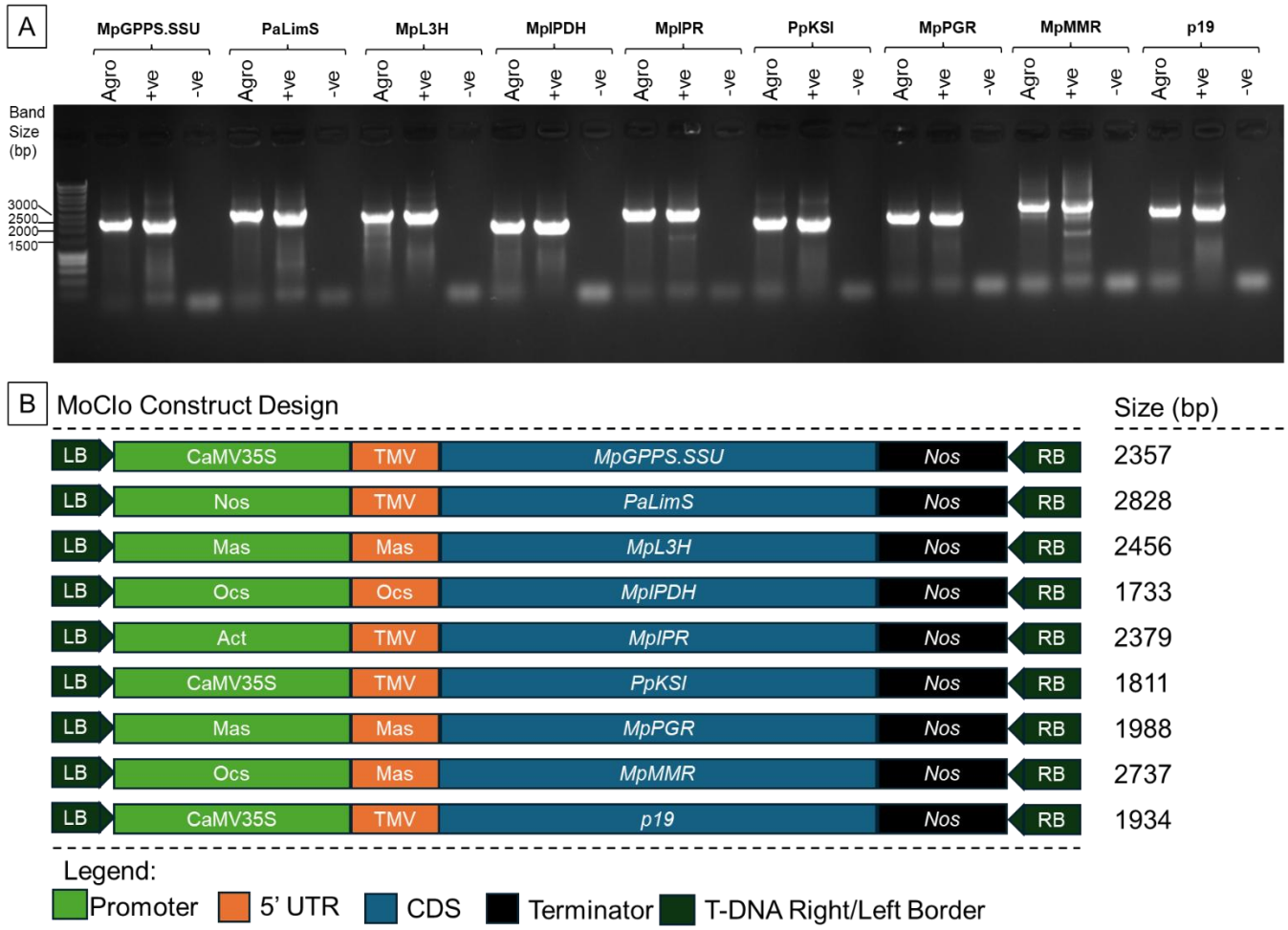

Figure 4.4 Menthol Biosynthesis Gene construction and final validation in *A. tumefaciens*. A. Colony PCR from transformed *A. tumefaciens* (Agro) containing p19 or the various menthol biosynthesis pathway genes. The positive control (+ve) is the corresponding plasmid used for transformation. The negative control (-ve) is a no template control. B. Design schematic of the constructs, with the expected sizes for the amplified fragments shown.

In each transformant tested, the amplified DNA band was of the expected size (Figure 4.4B), and matched that of the positive control (Figure 4.4A). No bands could be detected in the negative control in all cases (Figure 4.4A). There were some non-specific bands in the positive control for L1 PaLimS, MpIPR and L1 MpMMR, which may be attributable to a high number of PCR cycles. Overall, as the plasmids had been confirmed by sequencing, and the transformed *A tumefaciens* colony PCRs showed the expected products, these strains highly likely contained the correct plasmids, and were used in the next sections of this chapter to reconstitute the MBP.

4.2.3 Co-expression of *MpGPPS.SSU* and *PaLimS* into *N. benthamiana* to determine tissue sampling points

The next steps were to transiently express the MBP genes in *N. benthamiana* by step-wise expression, culminating in the reconstitution of the entire pathway. Transient expression in *N. benthamiana* is performed by injection of the *A. tumefaciens* solution into the abaxial side of the leaves, which enters through its stomatal openings and spreads throughout the leaf tissue (Stephenson et al. 2018). Before this however, an important parameter to consider was how many days post infiltration the leaves should be harvested for analysis. There is no optimal established time in the literature for this, and typically must be performed empirically for each experiment (Bach et al. 2014; Norkunas et al. 2018; Yamamoto et al. 2018; Grützner et al. 2024). Furthermore, the age of the leaf can effect both the susceptibility to infiltration and gene expression capability (Wydro et al. 2006). From early preliminary work done to form this chapter, the physical infiltration of the leaves was the least successful in either the oldest leaves or the youngest leaves. Thus, for all transient infiltration studies in this chapter, the third youngest leaf was used (Figure 4.5A)

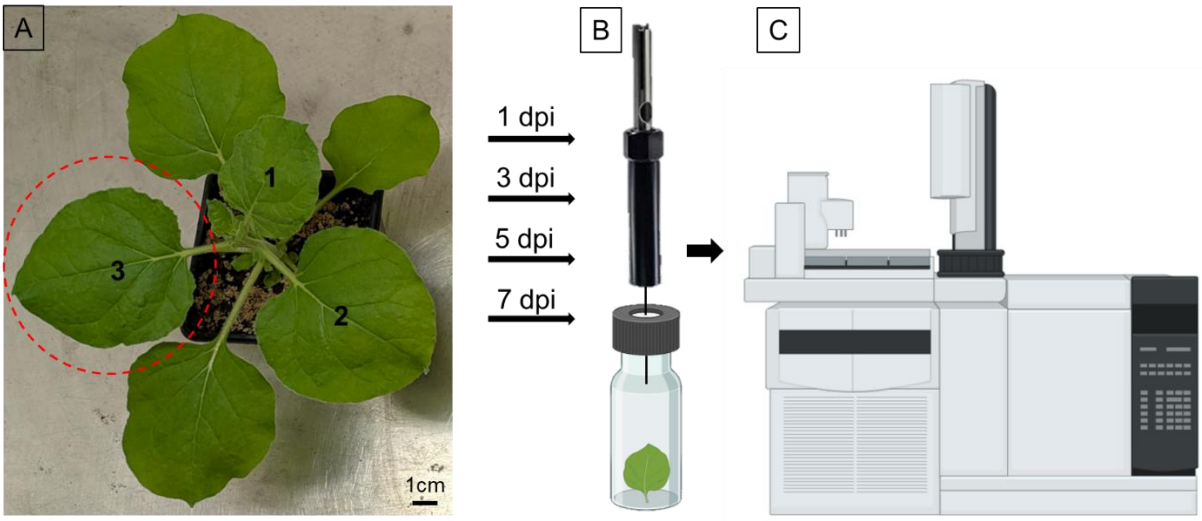

Figure 4.5 Schematic for preliminary transient expression studies in *N. benthamiana*. A. Representative photo of the developmental stage of *N. benthamiana* used for transient expression work. The 1st, 2nd and 3rd leaf are numbered, with the 3rd leaf which was used for infiltrations circled in red. The infiltrated leaves are then harvested at 1, 3, 5 or 7 dpi. B. Schematic for volatile detection using static headspace SPME. The volatiles are adsorbed onto a fibre from the headspace surrounding the leaf. C. The fibres with the adsorbed volatiles are desorbed onto the GCMS for analysis.

As a prerequisite to determine the best sampling time, infiltrated leaves were harvested at 1, 3, 5 and 7 dpi (Figure 4.5A). Preliminary experiments with leaves expressing *MpGPPS.SSU* and *PaLimS* showed that static HS-SPME could detect the volatile Limonene (Appendix Figure 2). This was therefore used as a starting point for volatile collection at different dpi time points (Figure 4.5B). It should also be noted, that for all transient co-expression studies, p19 was always included in the transformation mixture. For the GCMS chromatograms being presented below, 3 replicates for each co-expression sample were performed, with a single representative replicate being shown for clarity.

At 1dpi, the expected product Limonene could not be detected from *N. benthamiana* leaves co-infiltrated with *MpGPPS.SSU and PaLimS* (Figure 4.6) (additional replicates shown in Appendix Figure 4).

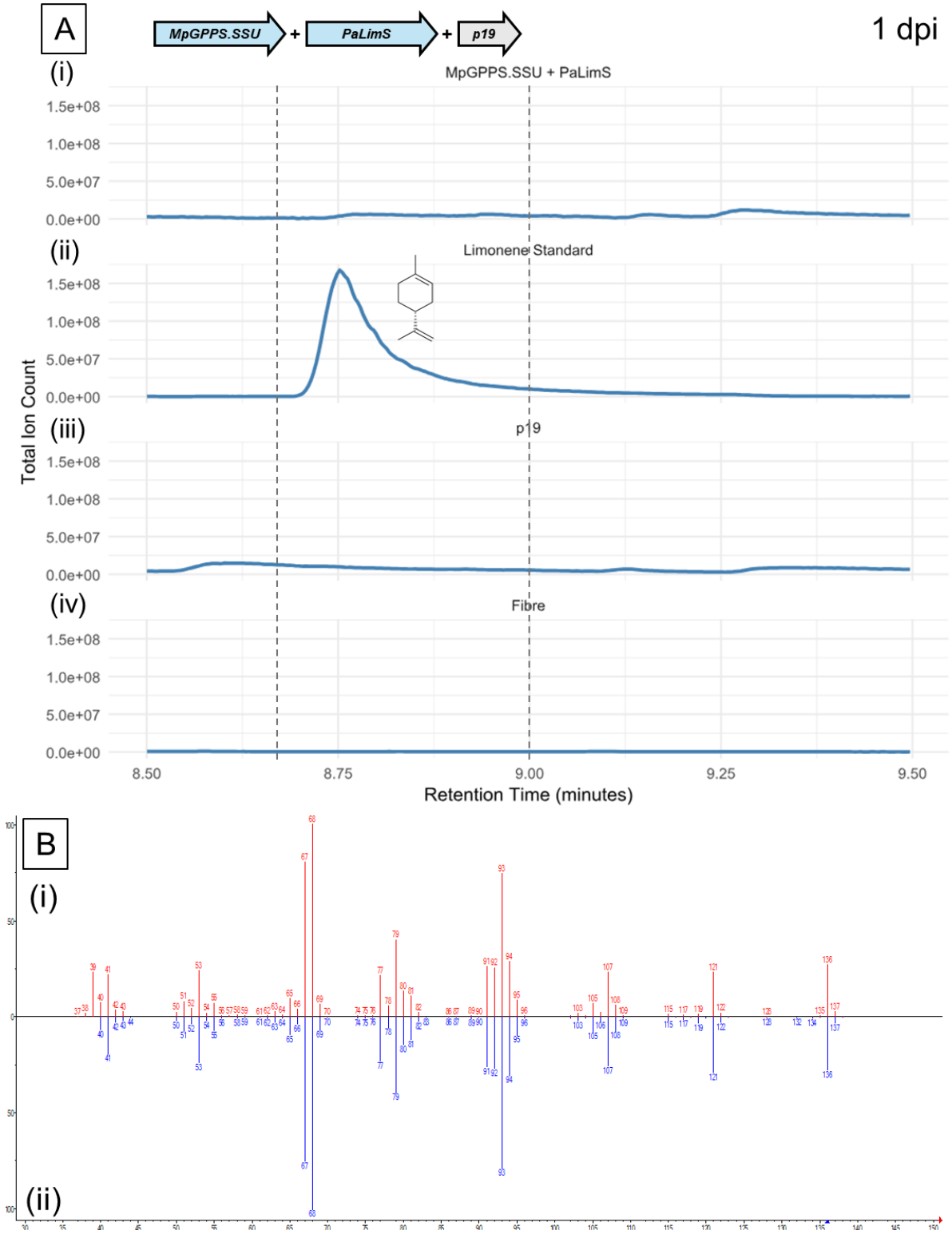

Figure 4.6 Co-infiltration of *MpGPPS.SSU* + *PaLimS* + *p19* in *N. benthamiana* at 1 dpi. A. Chromatograms obtained by GCMS analysis showing Total Ion Count on the y-axis, and Retention Time (minutes) on the x axis for: (i) *N benthamiana* co-infiltrated with *MpGPPS.SSU* + *PaLimS* + *p19*. (ii) Limonene standard. The chemical structure of (-)-Limonene is shown (iii) *N benthamiana* infiltrated with p19 only. (iv) SPME fibre only. B (i) Head-to-tail plots of (-)-limonene standard from A(ii) (red) vs library (blue) mass spectra using NIST mass spectral library search version 2.2 (NIST 2014). Y-axis = relative abundance for each ion, X-axis = mass to charge ratio (m/z).

A (-)-limonene standard was included as a comparison point to determine at what retention time the product should have been expected at, and to supplement identification of any putatively identified products by the NIST database (Figure 4.6A (i) and B). Mass spectral deconvolution using AMDIS and subsequent identification using NIST were able to correctly identify the Limonene standard (Figure 4.6 B). Distinguishing between limonene enantiomers was not possible due to a non-chiral GC column being used, and is a limitation of the hardware used in this chapter. A control was included as leaves infiltrated with the *p19* containing *A. tumefaciens* solution only (p19) (Figure 4.6 (iii)). This was done to account for any metabolic changes resulting from general *A. tumefaciens* infiltration and infection, as well as the p19 protein itself. An additional control of the SPME fibre incubated in a collection vial under identical conditions in the absence of a leaf (Fibre) was included to account for any contaminants from the surrounding air and vial headspace (Figure 4.6 (iv)). Overall, no peak was observed for *MpGPPS.SSU* + *PaLimS* infiltrated leaves at 1 dpi, and no mass spectra for compounds resembling Limonene could be deconvoluted and identified (Figure 4.6 A (i)).

In tissues co-infiltrated with *MpGPPS.SSU* + *PaLimS* analysed at 3 dpi, a peak can be observed (≈ 8.75 minutes), putatively identified as limonene, similar to that of the external limonene standard (Figure 4.7) (additional replicates shown in Appendix Figure 4).

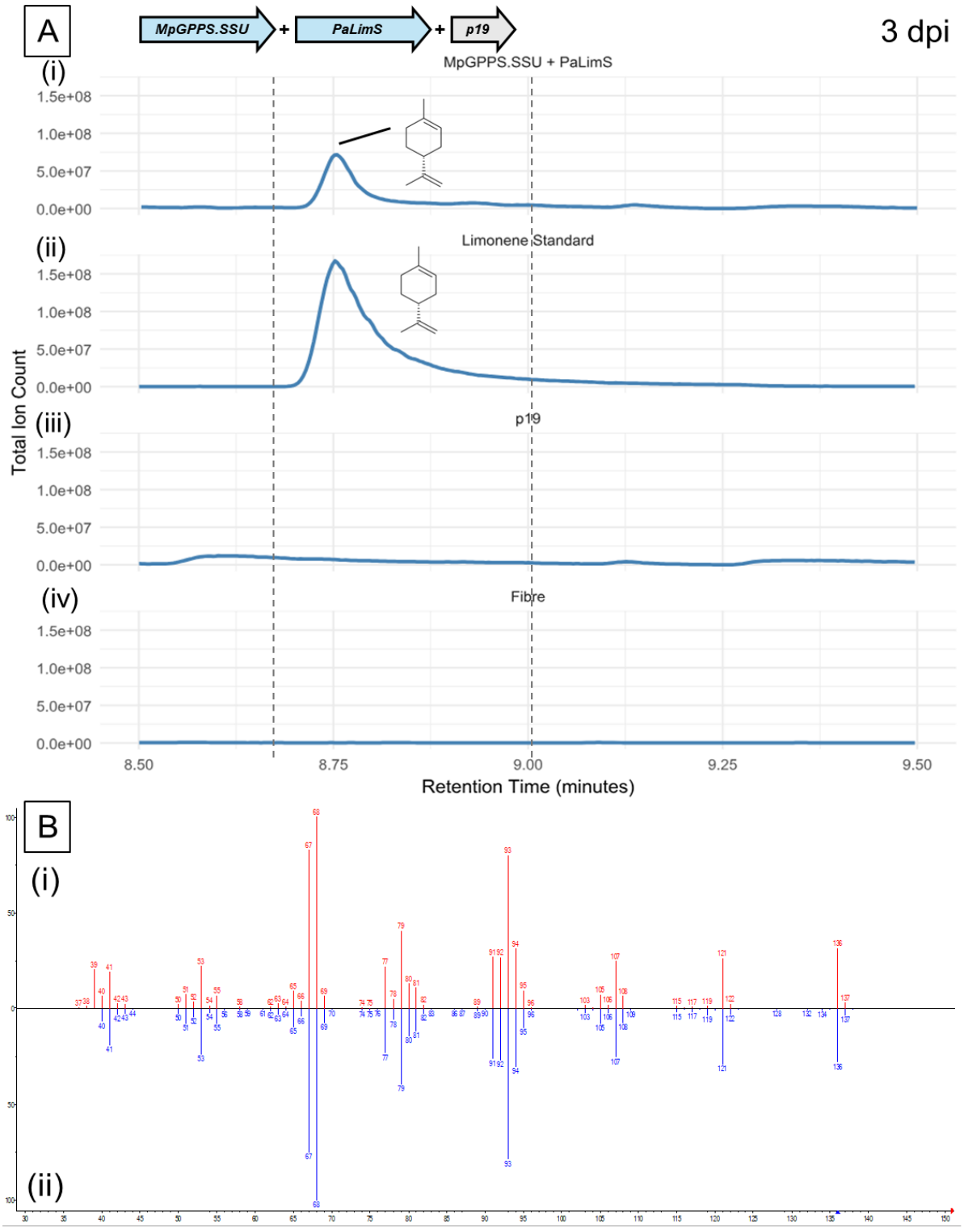

Figure 4.7 Co-infiltration of *MpGPPS.SSU* + *PaLimS* + *p19* in *N. benthamiana* at 3 dpi. A. Chromatograms obtained by GCMS analysis showing Total Ion Count on the y-axis, and Retention Time (minutes) on the x axis for: (i) *N benthamiana* co-infiltrated with *MpGPPS.SSU* + *PaLimS* + *p19*. Putatively identified limonene is shown by a black line and chemical structure (ii) Limonene standard. The chemical structure of (-)-Limonene is shown (iii) *N benthamiana* infiltrated with p19 only. (iv) SPME fibre only. B (i) Head-to-tail plots of the identified compound from A(i) (red) vs library match for limonene (blue) mass spectra using NIST mass spectral library search version 2.2 (NIST 2014). Y-axis = relative abundance for each ion, X-axis = mass to charge ratio (m/z).

This GCMS chromatogram was further deconvoluted by AMDIS, and the mass spectra was identified against the NIST library as limonene (Figure 4.7B). Taken together, this provides evidence towards the putative peak being limonene, the first committed monoterpene intermediate in the MBP.

Analysis of tissue co-infiltrated with *MpGPPS.SSU* + *PaLimS* was also conducted at 5dpi, to determine if emissions of limonene were increasing or had begun to decline (Figure 4.8) (additional replicates shown in Appendix Figure 4).

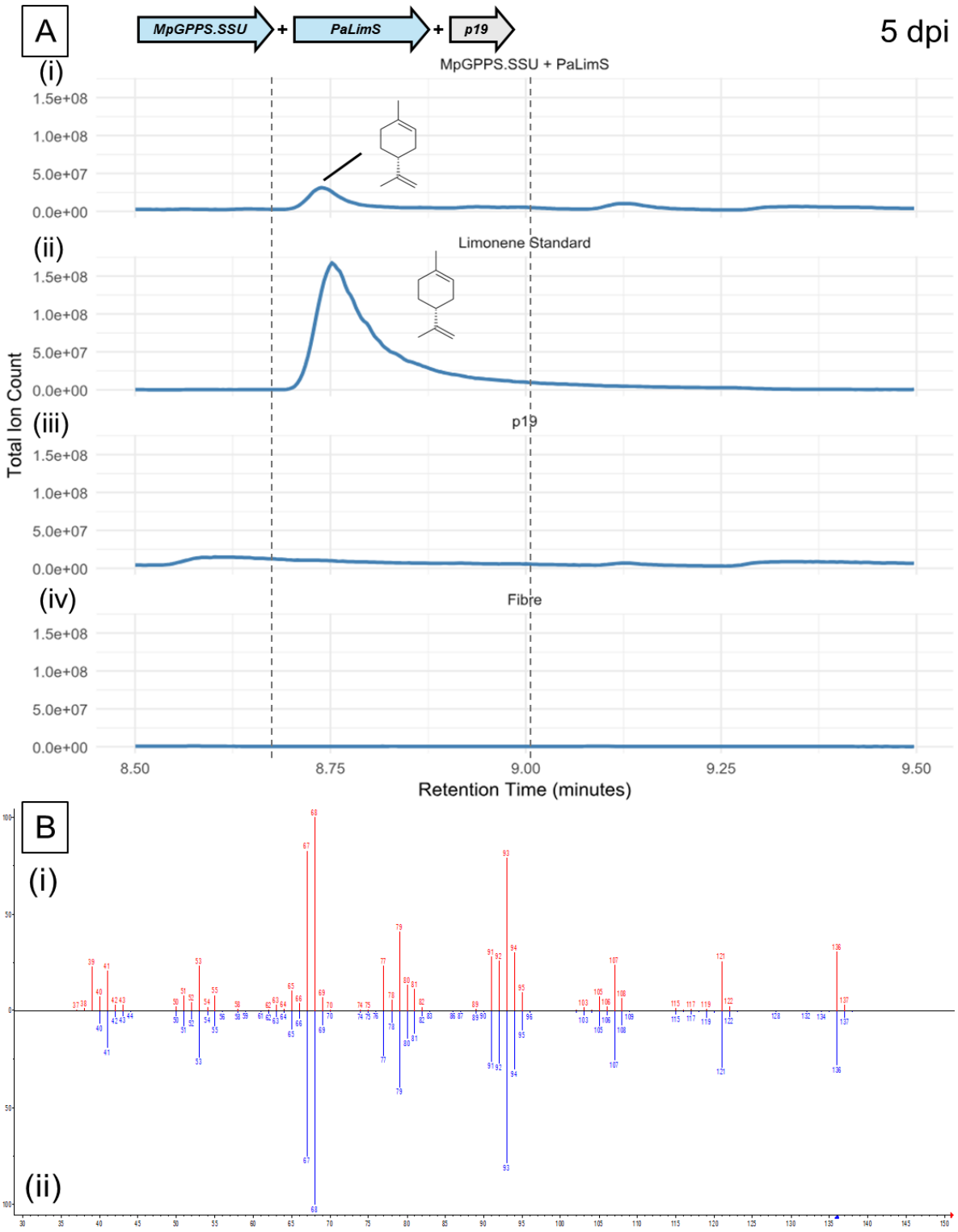

Figure 4.8 Co-infiltration of *MpGPPS.SSU* + *PaLimS* + *p19* in *N. benthamiana* at 5 dpi. A. Chromatograms obtained by GCMS analysis showing Total Ion Count on the y-axis, and Retention Time (minutes) on the x axis for: (i) *N benthamiana* co-infiltrated with *MpGPPS.SSU* + *PaLimS* + *p19*. Putatively identified limonene is shown by a black line and chemical structure (ii) Limonene standard. The chemical structure of (-)-Limonene is shown (iii) *N benthamiana* infiltrated with p19 only. (iv) SPME fibre only. B (i) Head-to-tail plots of the identified compound from A(i) (red) vs library match for limonene (blue) mass spectra using NIST mass spectral library search version 2.2 (NIST 2014). Y-axis = relative abundance for each ion, X-axis = mass to charge ratio (m/z).

Similarly to at 3dpi, tissues co-infiltrated with *MpGPPS.SSU* + *PaLimS* at 5dpi showed a similar putative peak in the GCMS chromatogram (Figure 4.8A (i)). This peak was deconvoluted in AMDIS and compared against the NIST library, and was similarly identified as limonene (Figure 4.8B). The size of the peak compared to the limonene standard appears smaller, suggesting a reduction in limonene emissions (Figure 4.8 A (i) and (ii)). This shows that although limonene is still being detected at 5dpi, there may be a decrease in limonene compared to 3dpi (Figure 4.7).

Tissues co-infiltrated with *MpGPPS.SSU* + *PaLimS* were further analysed at 7 dpi, to determine if limonene emissions still persisted or would have begun to taper off (Figure 4.9) (additional replicates shown in Appendix Figure 4).

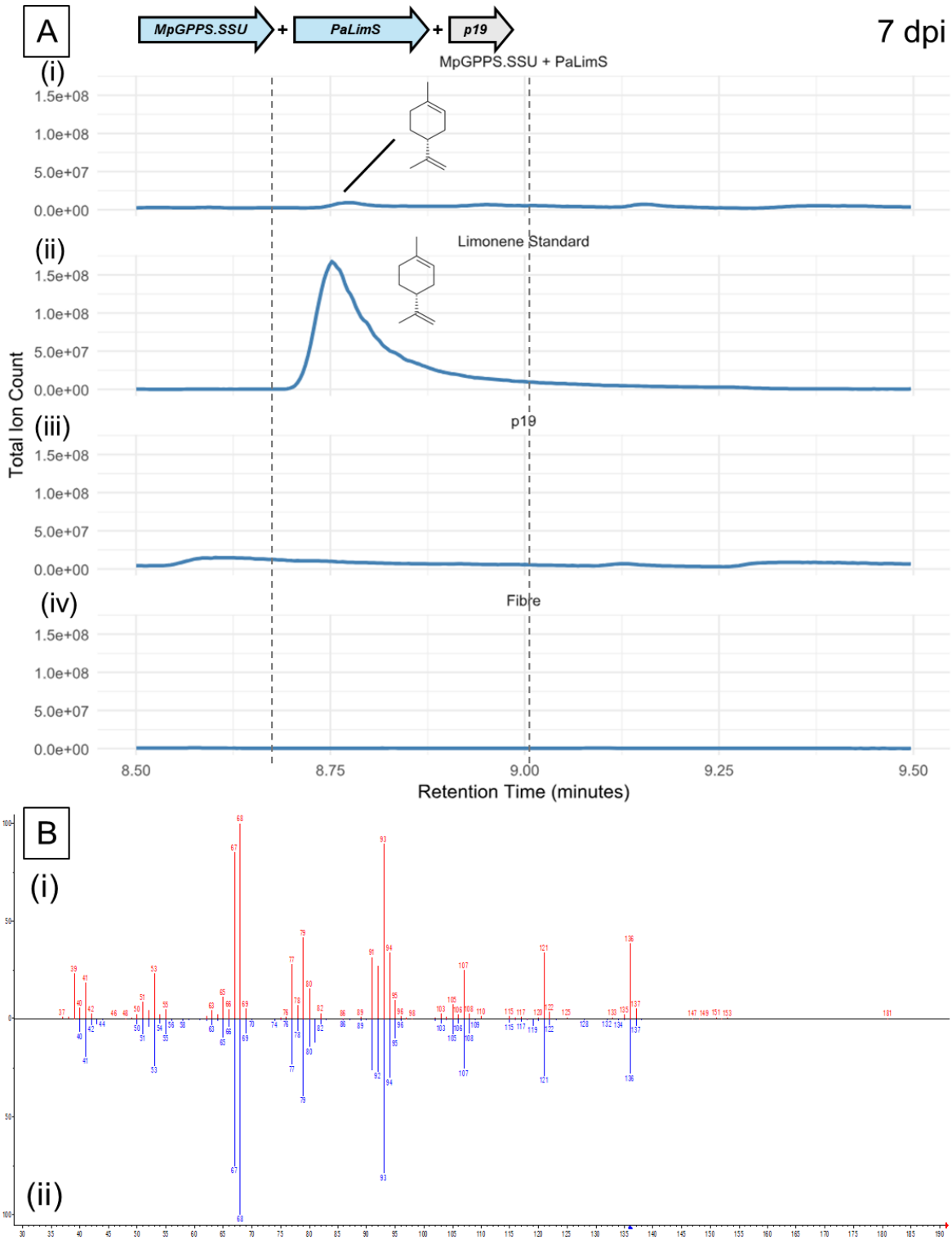

Figure 4.9 Co-infiltration of *MpGPPS.SSU* + *PaLimS* + *p19* in *N. benthamiana* at 7 dpi. A. Chromatograms obtained by GCMS analysis showing Total Ion Count on the y-axis, and Retention Time (minutes) on the x axis for: (i) *N benthamiana* co-infiltrated with *MpGPPS.SSU* + *PaLimS* + *p19*. Putatively identified limonene is shown by a black line and chemical structure (ii) Limonene standard. The chemical structure of (-)-Limonene is shown (iii) *N benthamiana* infiltrated with p19 only. (iv) SPME fibre only. B (i) Head-to-tail plots of the identified compound from A(i) (red) vs library match for limonene (blue) mass spectra using NIST mass spectral library search version 2.2 (NIST 2014). Y-axis = relative abundance for each ion, X-axis = mass to charge ratio (m/z).

Tissue co-infiltrated with *MpGPPS.SSU* + *PaLimS* at 7 dpi shows a similar putative limonene peak, although it appears barely detectable in comparison to the limonene standard (Figure 4.9A (i) and (ii)). This suggested that emissions of limonene at 7 dpi are the lowest, and that this time point may be too late to harvest tissue for volatile emission analysis.

4.2.4 Development of a quantitative method for detecting volatiles in *N. benthamiana*

Overall, comparison of putative limonene peaks compared to a limonene standard has qualitatively shown that between 3 and 5 dpi may be the most suitable time to analyse tissue for volatile emissions in co-infiltrated *N. benthamiana*. However, the development of a quantitative measure would more accurately determine the optimum dpi for analysis. As previously introduced, static HS-SPME on solid leaf tissue samples inherently prevents the use of internal standards being used for quantification purposes. Therefore, development of a semi-quantitative static HS-SPME method was performed. This was performed by first creating an external calibration curve for limonene to observe if increasing limonene mass would lead to a linear increase in peak areas as detected by the GCMS (Figure 4.10A).

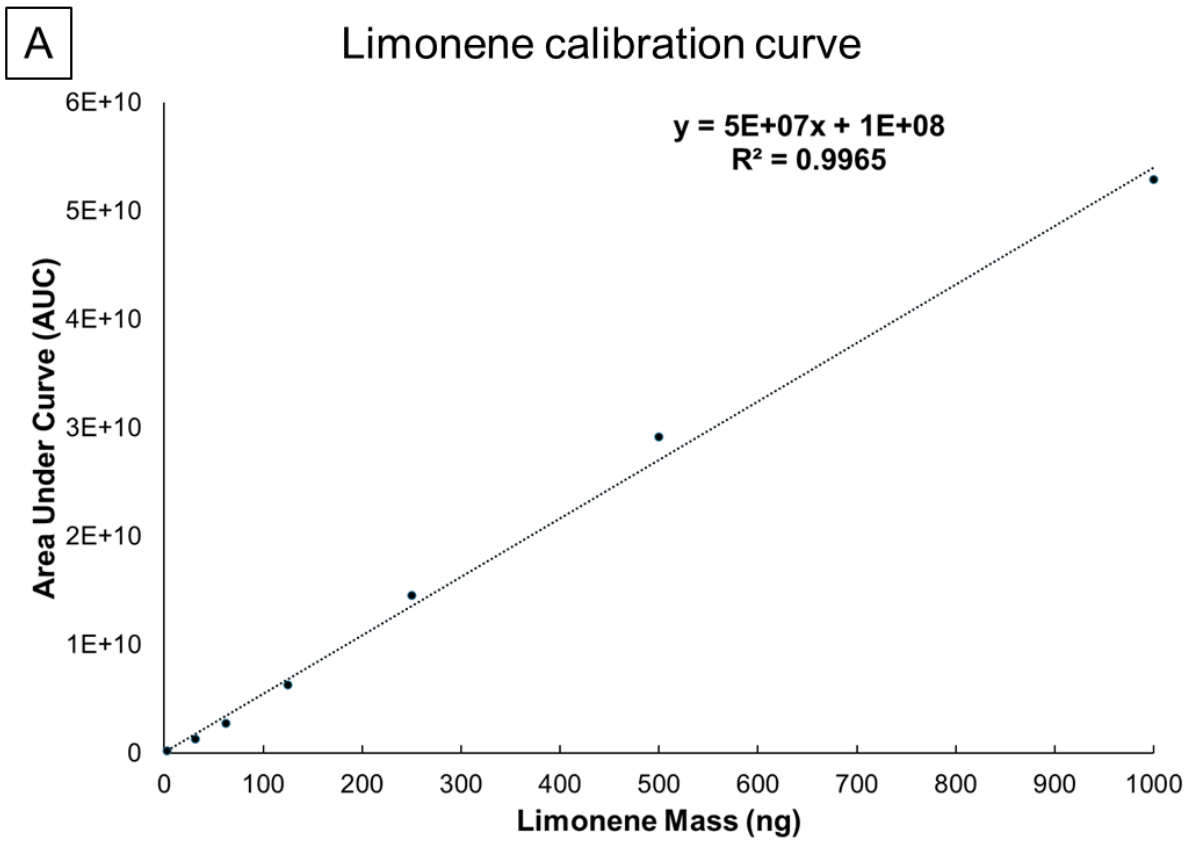
A
Limonene calibration curve
y = 5E+07x + 1E+08
R² = 0.9965
Area Under Curve (AUC)
6E+10
5E+10
4E+10
3E+10
2E+10
1E+10
0
0
100
200
300
400
500
600
700
800
900
1000
Limonene Mass (ng)

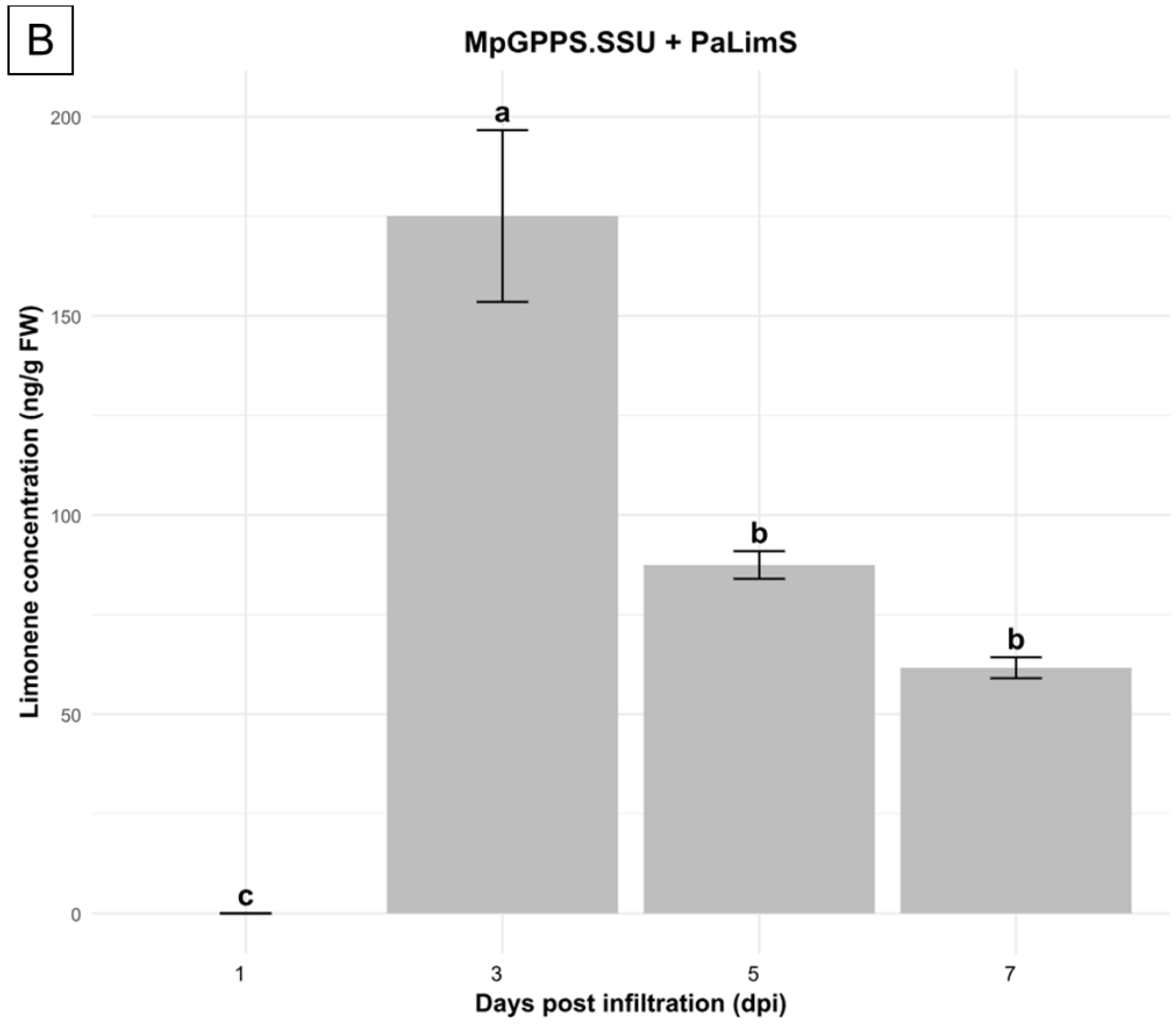
B
MpGPPS.SSU + PaLimS
Limonene concentration (ng/g FW)
200
150
100
50
0
a
b
b
c
1
3
5
7
Days post infiltration (dpi)

Figure 4.10. Development of quantitative static HS-SPME for limonene. A. Standard calibration curve showing the linear relationship between known limonene masses (ng) (x-axis) and the area under the curve for the corresponding limonene peak (y-axis). The equation of the line is $y = 5 \times 10^7 x + 1 \times 10^8$, with a coefficient of determination $R^2 = 0.9965$. B. Quantification of limonene concentration (ng/g fresh weight(FW)) in *MpGPPS.SSU* + *PaLimS* infiltrated samples measured at 1, 3, 5, and 7 dpi (dpi). Data represent mean values ± standard deviation (SD) from three biological replicates (n = 3). Statistical significance was assessed using one-way ANOVA followed by Tukey's Honest Significant Difference (HSD) post-hoc test. Different letters above the bars indicate groups that are significantly different from each other at $p < 0.05$.

The addition of limonene at increasing masses to the static HS-SPME system showed a strong linear response with respect to the corresponding peak area under curve (AUC) (Figure 4.10A). This allowed the quantification of GCMS data from tissue samples co-infiltrated with *MpGPPS.SSU* + *PaLimS* at different dpi's to further inform on the most optimal day to sample volatiles (Figure 4.10 B). There was a statistically significant difference between 3 dpi and 5 dpi (p_adj = 0.0022), and 7 dpi (p_adj = 0.00039) (Figure 4.10B). There was a also a statistically significant difference between 1 dpi and all 3 other time points. Biologically speaking, sampling leaves at 3 dpi is the most optimal time point as the leaves appear to be actively producing limonene. Therefore, 3 dpi was chosen as the time point for subsequent co-infiltration experiments.

Alternative methods utilizing the use of solvents to extract the leaf tissue volatiles were also trialled. This was done as extractions into a liquid medium are inherently more accurate compared to solely relying on an external standard as in static HS-SPME. Solvent extraction using dichchloromethane (DCM) was trialled as an extraction method for leaves co-infiltrated with *MpGPPS.SSU* + *PaLimS* harvested at 3 dpi, with the surface of the leaves being extracted (Figure 4.11) (additional replicates shown in Appendix Figure 5).

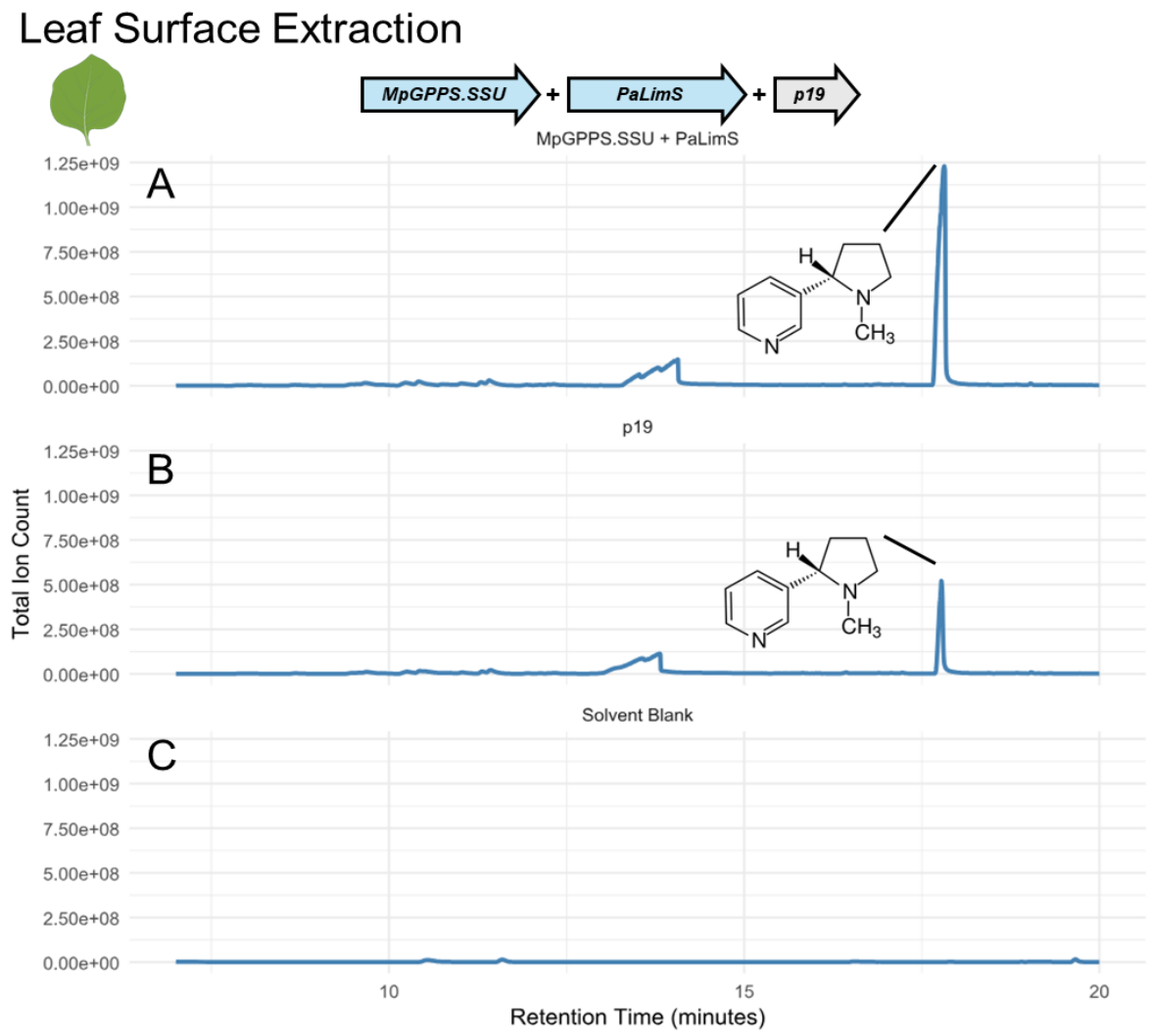

Figure 4.11. Leaf surface dichloromethane extraction at 3 dpi of *N. benthamiana* leaves co-infiltrated with *MpGPPS.SSU* + *PaLimS* + *p19*. Chromatograms obtained by GCMS analysis showing Total Ion Count on the y-axis, and Retention Time (minutes) on the x axis for: A. *N. benthamiana* leaves co-infiltrated with *MpGPPS.SSU* + *PaLimS* + *p19* surface extracted with dichloromethane. B. *N. benthamiana* leaves co-infiltrated with *p19* surface extracted with dichloromethane. C. Dichloromethane Blank. The structure for Nicotine is shown and the corresponding peak is highlighted by a black line.

The expected peak of limonene or other putative monoterpene metabolites were not detected in either the GCMS traces for leaves co-infiltrated with *MpGPPS.SSU* + *PaLimS* + *p19* surface extracted with dichloromethane (Figure 4.11A) , or in the control (Figure 4.11B). The metabolite nicotine could be detected in both leaf samples, indicating the success of the solvent extraction method itself from the leaf surface (Figure 4.11A, Figure 4.11B). To account for limonene or other putative monoterpene metabolites being compartmentalised in the inner mesophyll tissue, the leaf samples were subsequently homogenized in liquid nitrogen and further extracted

with dichloromethane (Figure 4.12) (additional replicates shown in Appendix Figure 5).

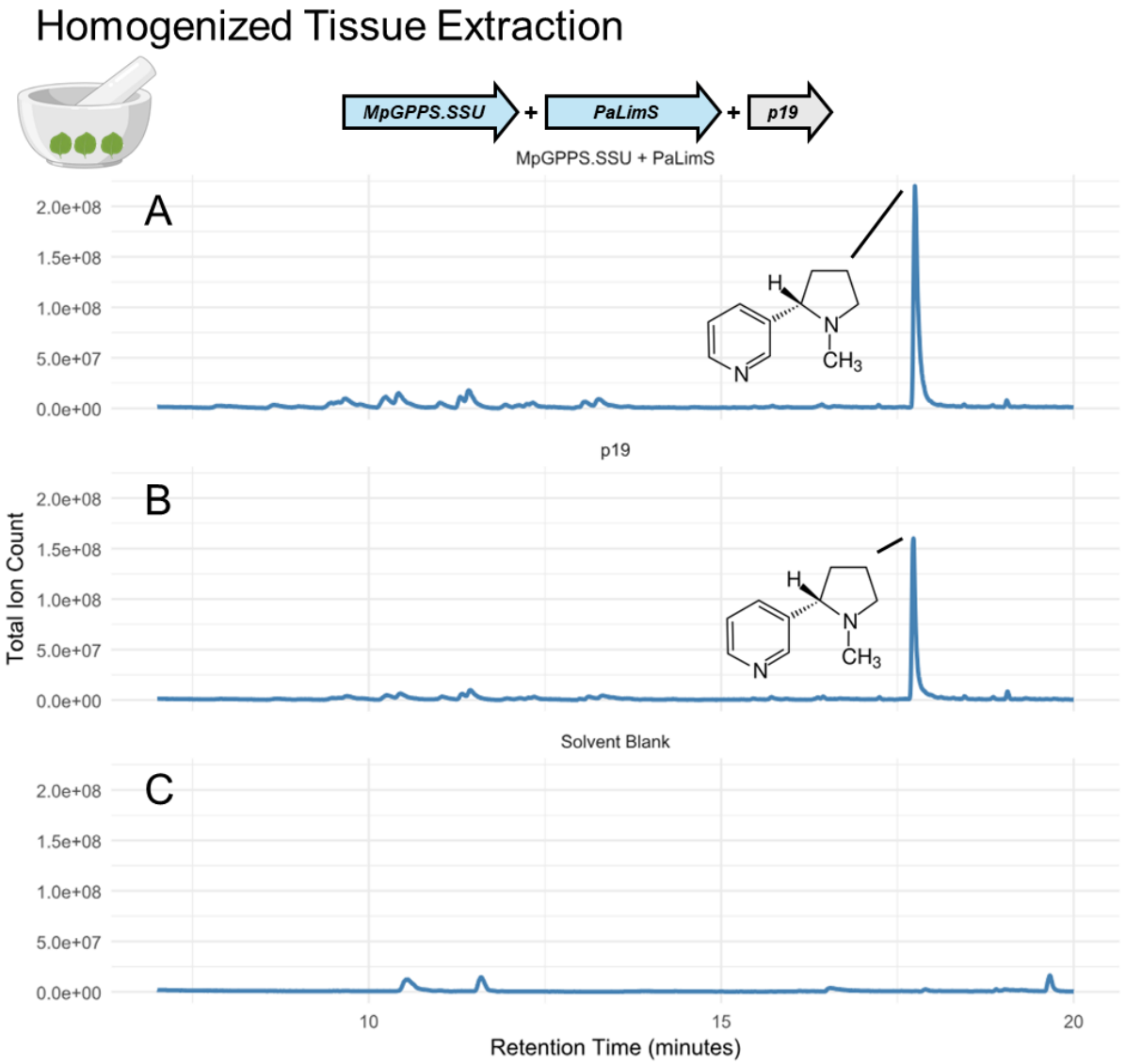

Figure 4.12. Homogenized leaf tissue dichloromethane extraction at 3 dpi of *N. benthamiana* leaves co-infiltrated with *MpGPPS.SSU* + *PaLimS* + *p19*. Chromatograms obtained by GCMS analysis showing Total Ion Count on the y-axis, and Retention Time (minutes) on the x axis for: A. *N. benthamiana* leaves co-infiltrated with *MpGPPS.SSU* + *PaLimS* + *p19,* homogenized and extracted with dichloromethane. B. *N. benthamiana* leaves co-infiltrated with *p19,* homogenized and extracted with dichloromethane. C. Dichloromethane Blank. The structure for Nicotine is shown and the corresponding peak is highlighted by a black line.

Dichloromethane extraction of the homogenized leaf tissue co-infiltrated with *MpGPPS.SSU* + *PaLimS* + *p19* did not show any of the expected limonene or other putative monoterpene metabolites (Figure 4.12A). The metabolite Nicotine could be detected in both leaf samples, indicating the success of the solvent extraction

method itself from the homogenized leaf tissue (Figure 4.12A, Figure 4.12B). Overall, solvent extraction of the leaves was largely unsuccessful in terms of detecting limonene. The next tested method was dynamic HS-SPME, which would involve metabolite collection onto an absorbent material which could then be eluted off using a liquid solvent thus allowing a liquid extraction to be performed (Figure 4.13) (additional replicates shown in Appendix Figure 6).

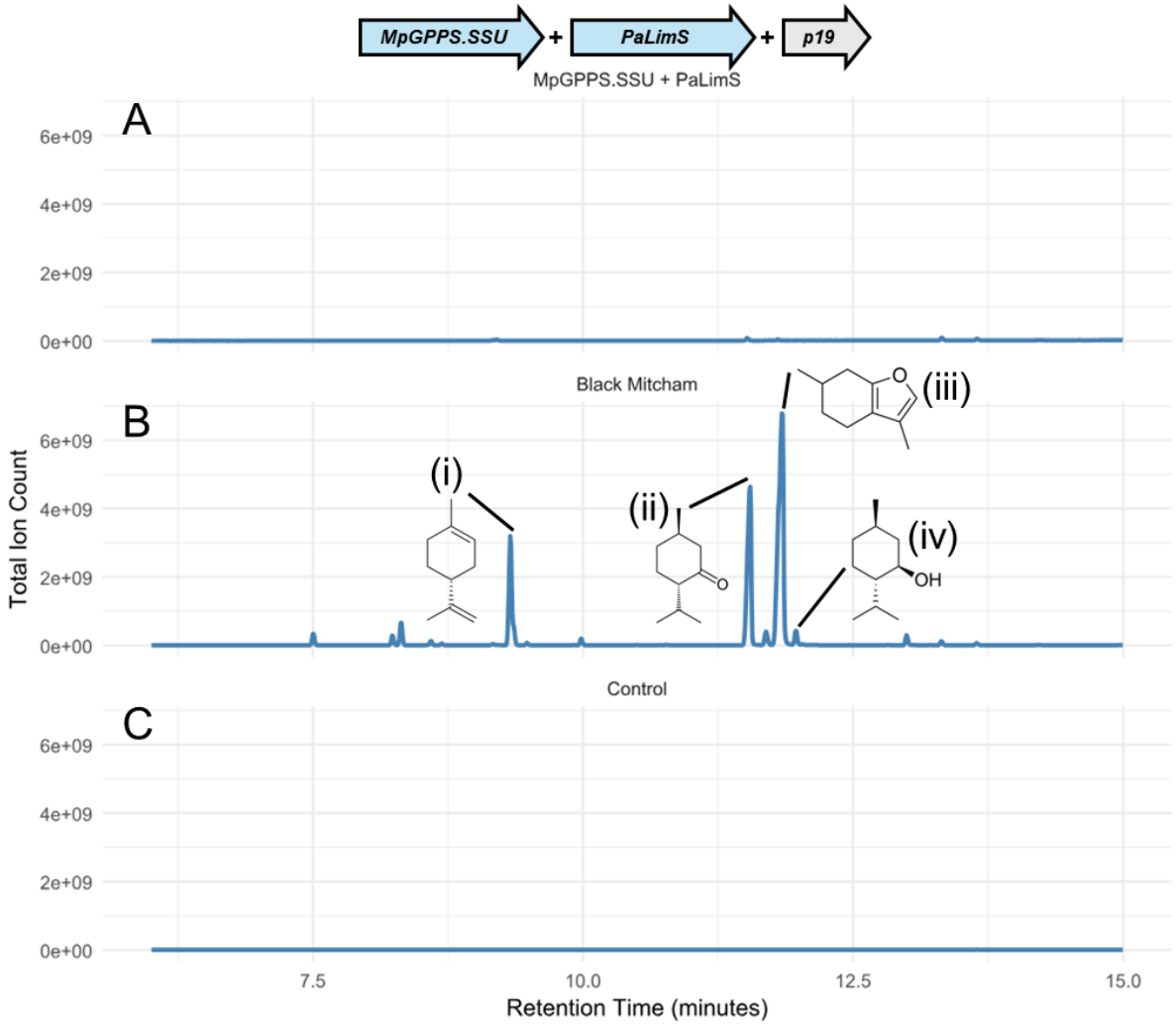

Figure 4.13. Dynamic HS-SPME of *N. benthamiana* leaf tissue co-infiltrated with *MpGPPS.SSU* + *PaLimS* + *p19* at 3 dpi. Chromatograms obtained by GCMS analysis showing Total Ion Count on the y-axis, and Retention Time (minutes) on the x axis for: A. *N. benthamiana* with leaves co-infiltrated with *MpGPPS.SSU* + *PaLimS* + *p19* after 24 hours of dynamic HS sampling of above ground tissues. B. Wild type Black Mitcham after 24 hours of dynamic HS sampling of above ground tissues. Putatively identified menthol biosynthesis pathway monoterpene products are shown as the chemical structure and highlighted by black lines: (i) Limonene. (ii) Menthone. (iii) Menthofuran. (iv) Menthol. C. Empty headspace vessel after 24 hours of dynamic HS sampling.

For dynamic HS-SPME of *N. benthamiana*, all leaves which were at the correct developmental stage to be amenable to infiltration, were co-infiltrated with

MpGPPS.SSU + *PaLimS* + *p19*, to increase the likelihood of detecting limonene in the dynamic headspace (Figure 4.13 A). No monoterpene products were detected in *N. benthamiana* aerial tissue after headspace sampling for 24 hours (Figure 4.13 A). A positive control of a Black Mitcham plant was also performed here, and clear peaks of putative monoterpene products (limonene, menthone, menthofuran and menthol) of the menthol biosynthesis pathway can be observed (Figure 4.13 B), indicating the dynamic HS-SPME method used was capable of trapping volatiles. Overall, of the three sampling methods tested, only static HS-SPME was able to capture limonene from the headspace, and subsequently allowed the quantification using an external limonene calibration curve (Figure 4.10). Therefore, this static headspace sampling was used for all qualitative, and where applicable, quantitative analysis going forward.

4.2.5 Step-wise transient co-expression of menthol biosynthesis pathway genes in *N. benthamiana*

With a means to reliably detect the products from co-infiltrated *N. benthamiana* leaves, step-wise co-infiltration of subsequent MBP genes could now be performed. The next combination performed was *MpGPPS.SSU* + *PaLimS* + *MpL3H* + *p19,* shown in Figure 4.14 (additional replicates shown in Appendix Figure 7).

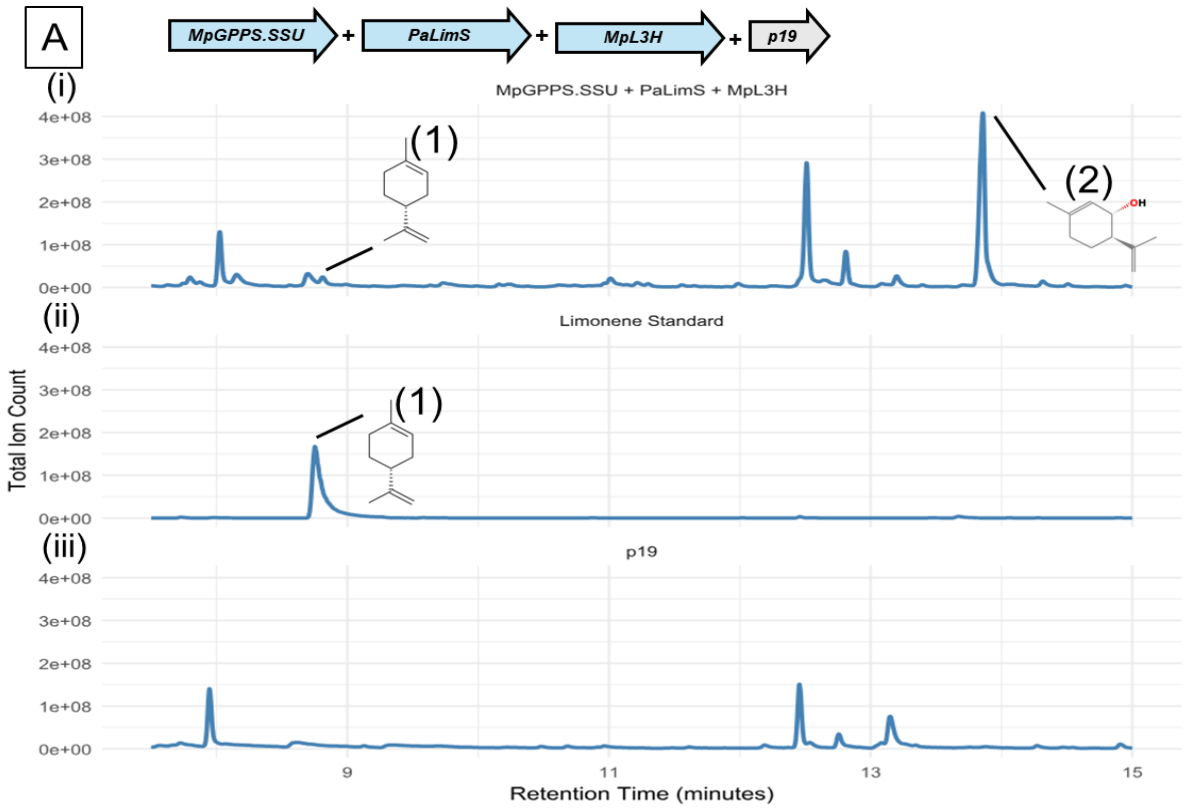
A
MpGPPS.SSU
+
PaLimS
+
MpL3H
+
p19
(i)
MpGPPS.SSU + PaLimS + MpL3H
(1)
(2)
OH
(ii)
Limonene Standard
(1)
(iii)
p19
Total Ion Count
4e+08
3e+08
2e+08
1e+08
0e+00
9
11
13
15
Retention Time (minutes)

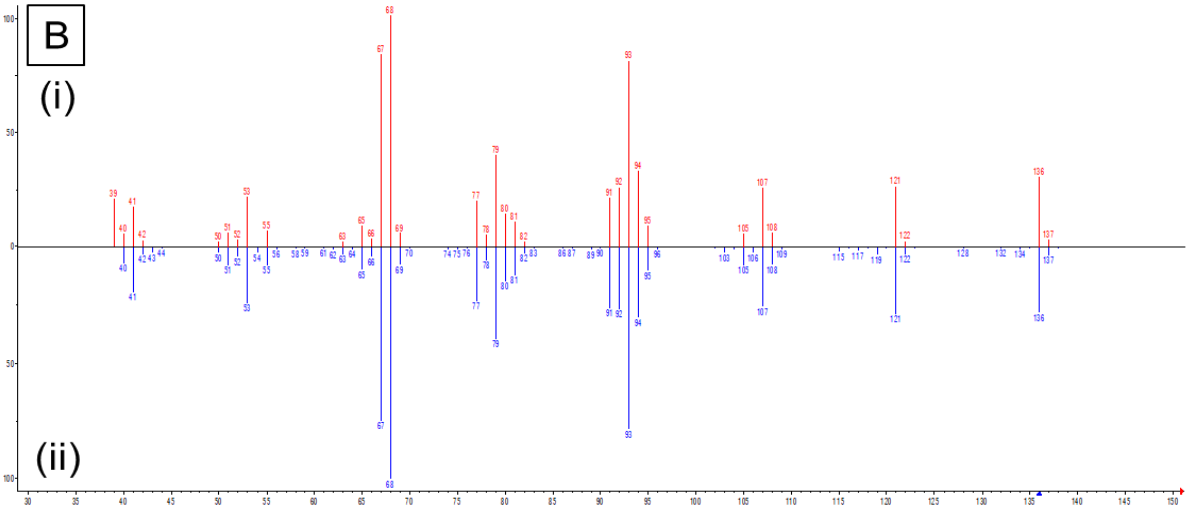
B
(i)
(ii)

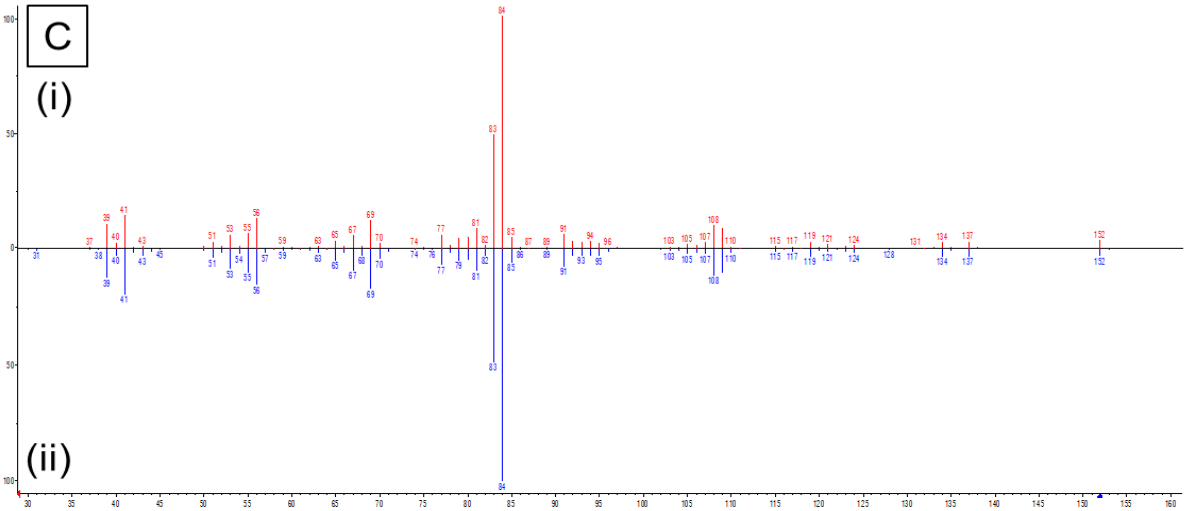
C
(i)
(ii)

Figure 4.14. Co-infiltration of *MpGPPS.SSU* + *PaLimS* + *MpL3H* + *p19* in *N. benthamiana*. A. Chromatograms obtained by GCMS analysis showing Total Ion Count on the y-axis, and Retention Time (minutes) on the x axis for: (i) *N benthamiana* co-infiltrated with *MpGPPS.SSU* + *PaLimS* + *MpL3H* + *p19*. Putatively identified limonene is shown by a black line and chemical structure (1). Putatively identified trans-isopiperitenol is shown by a black line and chemical structure (2). (ii) Limonene standard. Putatively identified limonene is shown by a black line and chemical structure (1). (iii) *N benthamiana* infiltrated with p19 only. B. (i) Head-to-tail plots of the identified compound from A(i)(1) (red) vs library match for limonene (blue) mass spectra using NIST mass spectral library search version 2.2 (NIST 2014). Y-axis = relative abundance for each ion, X-axis = mass to charge ratio (m/z). C. (i) Head-to-tail plots of the identified compound from A(i)(2) (red) vs library match for (-)-trans-Isopiperitenol (blue) mass spectra using NIST mass spectral library search version 2.2 (NIST 2014). Y-axis = relative abundance for each ion, X-axis = mass to charge ratio (m/z).

Co-infiltration of *MpGPPS.SSU* + *PaLimS* + *MpL3H* + *p19* in *N. benthamiana* leaves resulted in an additional peak on the GCMS chromatogram (Figure 4.14 A (i) (2)), which was identified by NIST as trans-isopiperitenol (Figure 4.14 C). Limonene was also detected (Figure 4.14 A (i)), which was identified by NIST (Figure 4.14 B) and corroborated with a limonene standard (Figure 4.14 A (ii)). The trans-isopiperitenol peak was not detected in the *p19* only control (Figure 4.14 A (iii).

RT-PCR was also performed to determine active gene expression of the co-infiltrated genes for the combination *MpGPPS.SSU* + *PaLimS* and *MpGPPS.SSU* + *PaLimS* + *MpL3H* (Figure 4.15).

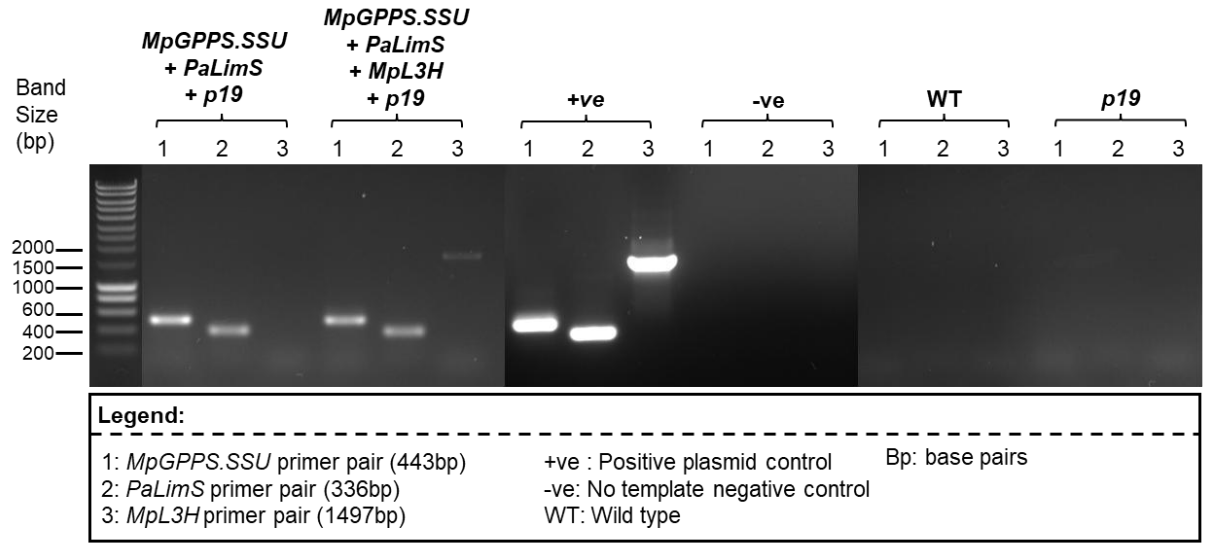

Figure 4.15. RT-PCR analysis of *MpGPPS.SSU*, *PaLimS* and *MpL3H* expression in infiltrated *N. benthamiana* leaf tissue. RT-PCR was performed using cDNA from *N. benthamiana* leaves co-infiltrated with either *MpGPPS.SSU* + *PaLimS* + *p19, MpGPPS.SSU* + *PaLimS* + *MpL3H*, or *p19 alone*. Wild type *N. benthamiana* leaves were also analysed as an additional negative control. Expected product sizes for primer pairs used are shown in the legend. The presence of bands at the expected band size indicates successful transcription in the tissue samples. *N. benthamiana* leaf tissue was harvested at 3dpi. Gel image is a

composite of the same gel, cropped together for ease of viewing (unedited gel in Appendix Figure 18).

cDNA from samples co-infiltrated with *MpGPPS.SSU* + *PaLimS* + *p19* showed an amplified band at the expected size for *MpGPPS.SSU* (443 bp) and *PaLimS* (336 bp), but the absence of a band for *MpL3H* (1497 bp) (Figure 4.15). cDNA from samples co-infiltrated with *MpGPPS.SSU* + *PaLimS* + *MpL3H* + *p19* showed bands at the expected sizes for *MpGPPS.SSU, PaLimS* and *MpL3H* (Figure 4.15). The amplified bands also matched those in the positive plasmid control which contained the same respective genes (Figure 4.15). There was an absence of bands in the lanes corresponding to cDNA from the wild type *N. benthamiana* leaf tissue and the *p19* only infiltrated tissue indicating the bands observed in the co-infiltrated tissue are solely derived from the transiently expressed genes (Figure 4.15). Finally, in the no template control lane, there was a lack of amplified bands indicating a lack of contamination in the RT-PCR reaction (Figure 4.15).

With confirmation that the early MBP could be reconstituted up to the production of the intermediate trans-isopiperitenol in *N. benthamiana*, further step-wise co-infiltration of the next genes (*MpIPDH, MpIPR, PpKSI* (acting as a *MpIPGI* homolog*)*, *MpPGR* and *MpMMR*)) in the MBP was performed (Figure 4.16) (additional replicates shown in Appendix Figure 8).

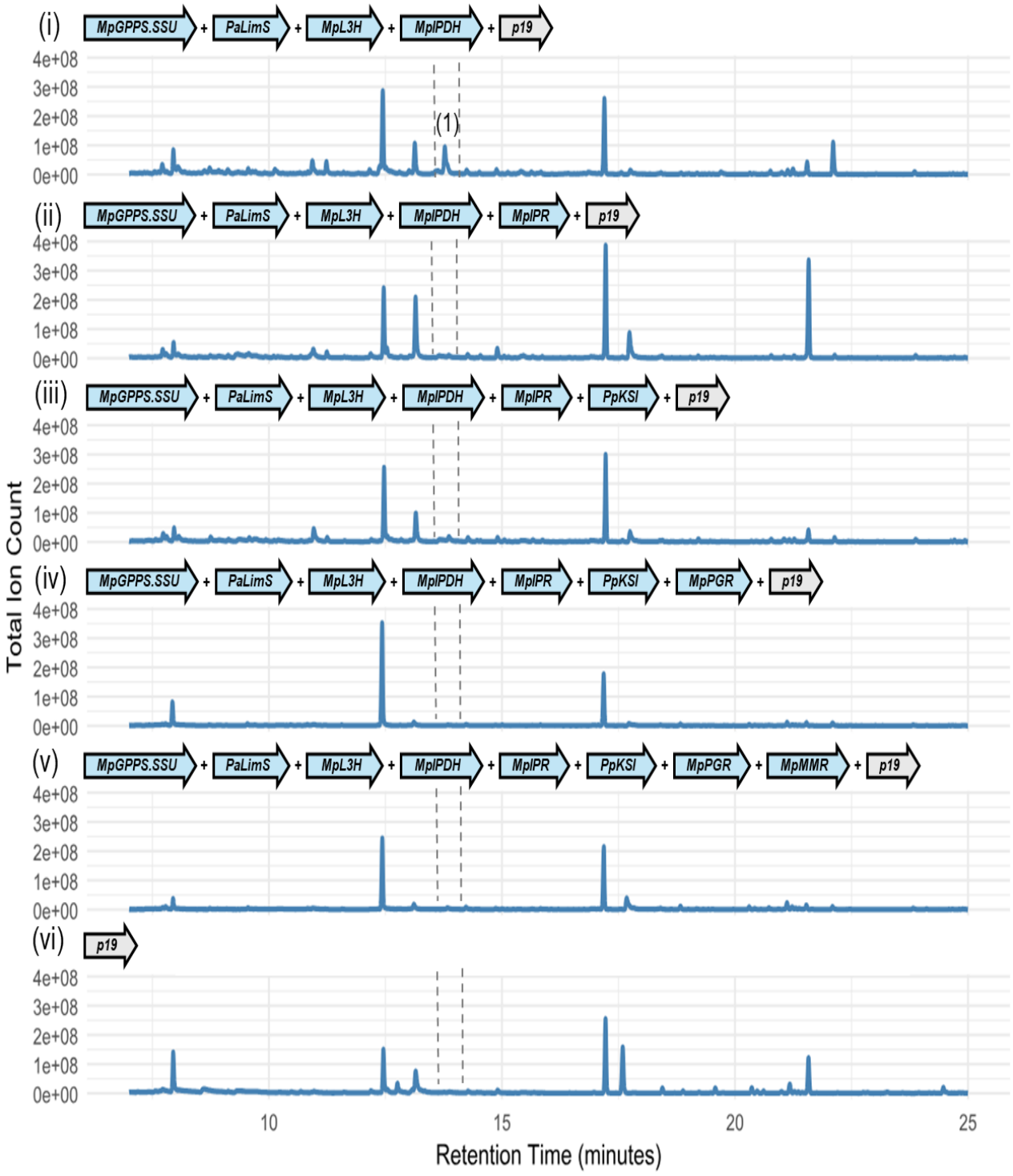

Figure 4.16. Step-wise co-infiltration of menthol biosynthesis pathway genes in *N. benthamiana*. Chromatograms obtained by GCMS analysis showing Total Ion Count on the y-axis, and Retention Time (minutes) on the x axis for *N. benthamiana* leaves:
(i) *Co*-infiltrated with *MpGPPS.SSU* + *PaLimS* + *MpL3H* + *MpIPDH* + *p19*. Putatively identified trans-isopiperitenol peak is shown in (1). (ii) Co-infiltrated with *MpGPPS.SSU* + *PaLimS* + *MpL3H* + *MpIPDH* + *MpIPR* + *p19*. (iii) Co-infiltrated with *MpGPPS.SSU* + *PaLimS* + *MpL3H* + *MpIPDH* + *MpIPR* + *PpKSI* + *p19*. (iv) Co-infiltrated with *MpGPPS.SSU* + *PaLimS* + *MpL3H* + *MpIPDH* + *MpIPR* + *PpKSI* + *MpPGR* + *p19*. (v) Co-infiltrated with *MpGPPS.SSU* + *PaLimS* + *MpL3H* + *MpIPDH* + *MpIPR* + *PpKSI* + *MpPGR* + *MpMMR* + *p19*. (vi) Infiltrated with *p19*.

No additional peaks corresponding to the expected downstream monoterpenes were observed following co-infiltration of the respective pathway genes (Figure 4.16). The infiltration of *MpIPDH* was expected to result in the conversion of (–)-*trans*-Isopiperitenol to (–)-Isopiperitenone, but no corresponding peaks were detected (Figure 4.16 (i)). Similarly, co-infiltration of *MpIPR* was intended to produce (–)-cis-Isopulegone from (–)-Isopiperitenone, yet this compound was not detected (Figure 4.16 (ii)). Infiltration of *PpKSI*, acting as an *MpIPGI* homolog, was expected to convert (–)-*cis*-Isopulegone to (+)-pulegone, but again, no new peaks were observed (Figure 4.16 (iii)). The conversion of (+)-pulegone to (–)-Menthone by *MpPGR* (Figure 4.16 (iv)), and the subsequent reduction of (–)-Menthone to (–)-Menthol by *MpMMR* (Figure 4.16 (v)), also failed to yield any additional peaks corresponding to the expected products.

These findings led to a hypothesis that the downstream intermediates may be being produced, but at too low of an abundance to be detected. This would still rely on the successful transcription of the downstream MBP genes. To confirm this, RT-PCR was performed on cDNA from *N. benthamiana* co-infiltrated with every gene in the MBP to assess if the gene could be detected (Figure 4.17).

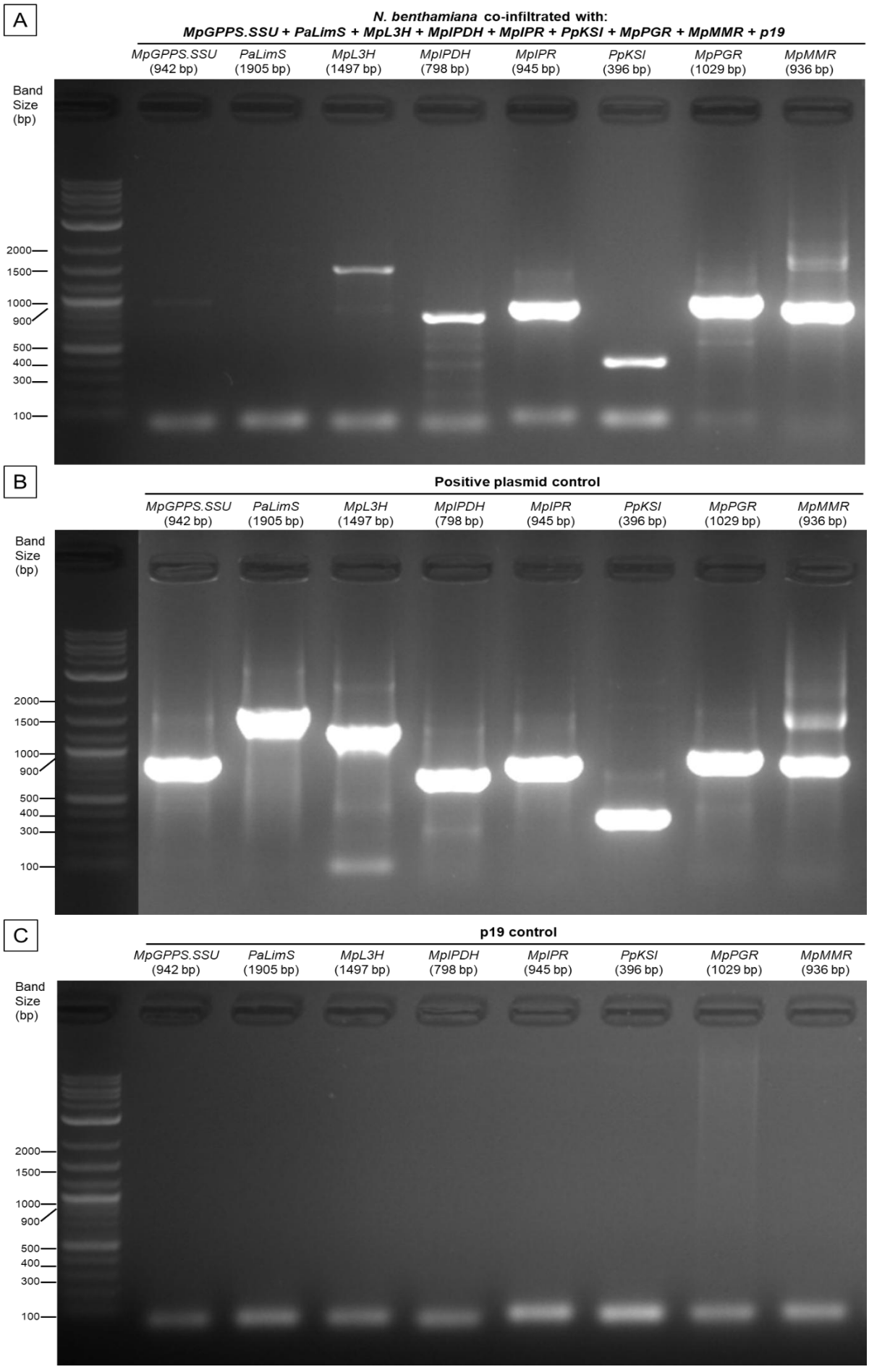
A
N. benthamiana co-infiltrated with:
MpGPPS.SSU + PaLimS + MpL3H + MpIPDH + MpIPR + PpKSI + MpPGR + MpMMR + p19
MpGPPS.SSU (942 bp)
PaLimS (1905 bp)
MpL3H (1497 bp)
MpIPDH (798 bp)
MpIPR (945 bp)
PpKSI (396 bp)
MpPGR (1029 bp)
MpMMR (936 bp)
Band Size (bp)
2000
1500
1000
900
500
400
300
100
B
Positive plasmid control
MpGPPS.SSU (942 bp)
PaLimS (1905 bp)
MpL3H (1497 bp)
MpIPDH (798 bp)
MpIPR (945 bp)
PpKSI (396 bp)
MpPGR (1029 bp)
MpMMR (936 bp)
Band Size (bp)
2000
1500
1000
900
500
400
300
100
C
p19 control
MpGPPS.SSU (942 bp)
PaLimS (1905 bp)
MpL3H (1497 bp)
MpIPDH (798 bp)
MpIPR (945 bp)
PpKSI (396 bp)
MpPGR (1029 bp)
MpMMR (936 bp)
Band Size (bp)
2000
1500
1000
900
500
400
300
100

Figure 4.17. RT-PCR analysis of *MpGPPS.SSU, PaLimS, MpL3H, MpIPDH, MpIPR, PpKSI, MpPGR, and MpMMR* in: A. cDNA from *N. benthamiana* leaves co-infiltrated with *MpGPPS.SSU, PaLimS, MpL3H, MpIPDH, MpIPR, PpKSI, MpPGR, MpMMR and p19*. B. Plasmids with corresponding gene sequences used for co-infiltration. C. cDNA from *N. benthamiana* infiltrated with *p19*. Bp = base pairs. Expected product sizes for the primer pairs used are shown in brackets under the name of each corresponding gene. *N. benthamiana* leaf tissue was harvested at 3dpi. Gel image is a composite of the same gel, cropped for ease of viewing (unedited gel in Appendix Figure 19).

The corresponding band for each gene from the MBP was detected in cDNA from *N. benthamiana* co-infiltrated with *MpGPPS.SSU, PaLimS, MpL3H, MpIPDH, MpIPR, PpKSI, MpPGR, MpMMR* and *p19* harvested at 3dpi (Figure 4.17 A). These bands match those observed in the positive controls, which represent the same plasmids used for co-infiltration (Figure 4.17 B). A clearer band is shown for *PaLimS* in an adjusted image (Appendix Figure 3). Non-specific bands can be observed in both co-infiltrated *N. benthamiana* cDNA and positive control lanes, indicating non-specificity of the primer pairs used for detection or as an artefact of high cycle numbers used in the thermocycler reaction. No bands are observed in the cDNA from *N. benthamiana* infiltrated with *p19* harvested at 3dpi (Figure 4.17 C). Overall, this RT-PCR analysis has confirmed the detection of each gene in the MBP, confirming that the co-infiltrated genes are being transcribed in *N. benthamiana* leaf tissue.

4.2.6 Substrate feeding assay in *N. benthamiana* leaves

With the confirmation of MBP gene activity detected, but lack of the expected monoterpene products shown, it was hypothesized that the downstream gene products of the MBP were non-functional in the *N. benthamiana* co-infiltration assay used in this thesis. A likely candidate would be *PpKSI,* which was acting as a *MpIPGI* homolog, whose enzyme product may not have been functional in *N. benthamiana* in the production of (+)-pulegone. This would explain the lack of further downstream (-)-menthone and (-)-menthol being formed (the products of *MpPGR* and *MpMMR* respectively), as if these volatile monoterpenes were being produced, they should have been readily detected by HS-SPME (Figure 4.13 B). Therefore, a substrate feeding assay was performed, where (+)-pulegone was co-infiltrated into leaves together with *MpPGR* and *MpMMR* (Figure 4.18). The expected products were menthone, caused by the conversion of pulegone by *MpPGR*, and menthol, cause by the conversion of menthone by *MpMMR*.

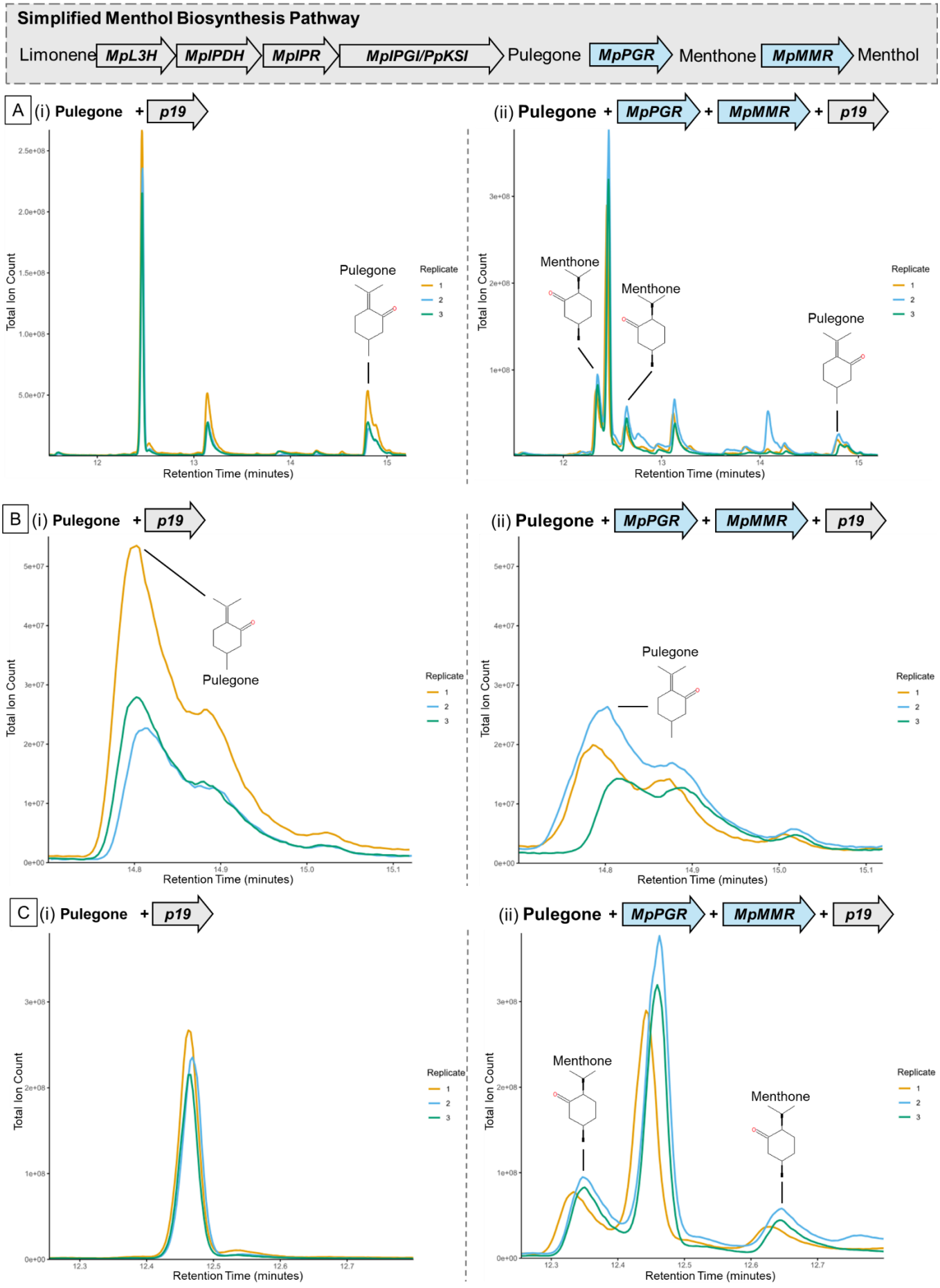
Simplified Menthol Biosynthesis Pathway
Limonene
MpL3H
MpIPDH
MpIPR
MpIPGI/PpKSI
Pulegone
MpPGR
Menthone
MpMMR
Menthol
A
(i) Pulegone + p19
(ii) Pulegone + MpPGR + MpMMR + p19
B
(i) Pulegone + p19
(ii) Pulegone + MpPGR + MpMMR + p19
C
(i) Pulegone + p19
(ii) Pulegone + MpPGR + MpMMR + p19
Total Ion Count
Retention Time (minutes)
Replicate
Pulegone
Menthone

Figure 4.18. HS-SPME analysis of *N. benthamiana* leaves co-infiltrated with pulegone as a substrate, together with either *MpPGR* + *MpMMR* + *p19* or *p19* alone..
Chromatograms show Total Ion Count (y-axis) versus Retention Time (minutes, x-axis). Leaves were infiltrated with (+)-pulegone and: (A, i) *p19* alone, (A, ii) *MpPGR* + *MpMMR* + *p19*. Panels B and C show magnified chromatograms at the retention times of pulegone and menthone, respectively, for (i) p19 and (ii) MpPGR + MpMMR + p19. Chemical structures of putatively identified compounds are shown, with black lines indicating their corresponding peaks. Three biological replicates are displayed as overlaid chromatograms. (+)-Pulegone was injected at 2 dpi, and leaves were sampled at 3 dpi. A simplified menthol biosynthesis pathway is shown for reference, highlighting the parts of the pathway involved in the substrate feeding assay.

(+)-Pulegone substrate feeding in *N. benthamiana* leaves infiltrated with *p19* (control) showed the presence of pulegone in the headspace at 3dpi (Figure 4.18 A (i)). This indicated the exogenously supplied (+)-pulegone was persisting in the leaf even after 24 hours, and the absence of any new peaks shows the lack of endogenous *N. benthamiana* enzymes metabolising the (+)-pulegone to menthone, as observed in Figure 4.18 C (i).

When the same experiment was repeated with *N. benthamiana* leaves co-infiltrated with *MpPGR* + *MpMMR* + *p19*, the presence of 2 new peaks, both identified as menthone by AMDIS and NIST were observed (Figure 4.18 A (ii), Figure 4.18 C (ii)). A peak for pulegone is also still observed (Figure 4.18 A (ii), Figure 4.18 B (ii)). This showed that it was the presence of *MpPGR* causing the conversion of (+)-pulegone to the newly observed peaks. The addition of *MpMMR* did not yield the predicted product of menthol, which would have been from the conversion of menthone to menthol by MpMMR. Therefore, the bottleneck appears to be between *MpIPDH* and *PpKSI*.

4.2.7 Upregulation of MEP precursor pathway genes to increase flux into the MBP

A line of experimentation that was performed in parallel to reconstitution of the MBP in *N. benthamiana*, was the co-expression of MEP genes to increase the amount of precursors available for monoterpene biosynthesis. However, the production of a quantifiable intermediate from the MBP was first needed. This was achieved in this chapter by means of a static HS-SPME method, using (-)-limonene as the quantifiable monoterpene (Figure 4.10). (-)-limonene was chosen as it was readily available as a commercial standard. Furthermore, an optimal sampling point of 3dpi was also determined, specifically for the detection of limonene from *N. benthamiana*

co-infiltrated with *MpGPPS.SSU* + *PaLimS* + *p19* (Figure 4.10). Therefore, singular genes from the entire MEP pathway were co-infiltrated with *MpGPPS.SSU* + *PaLimS* + *p19* to determine if flux into the reconstituted MBP could be increased (Figure 4.19).

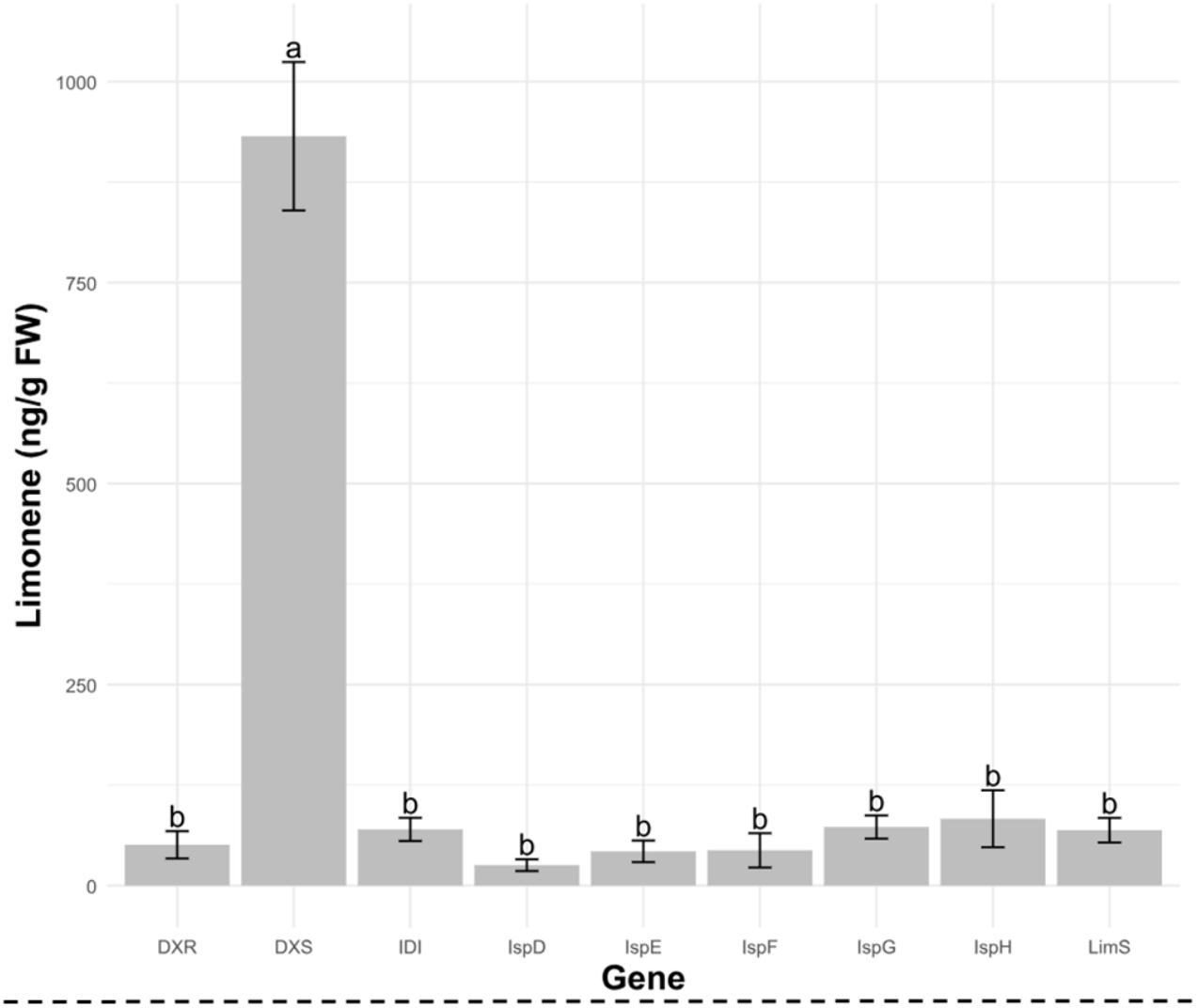

Legend:

DXR: *MpDXR* + *MpGPPS.SSU* + *PaLimS* + *p19*

DXS: *NtDXS* + *MpGPPS.SSU* + *PaLimS* + *p19*

IDI: *AtIDI* + *MpGPPS.SSU* + *PaLimS* + *p19*

IspD: *AtIspD* + *MpGPPS.SSU* + *PaLimS* + *p19*

IspE: *AtIspE* + *MpGPPS.SSU* + *PaLimS* + *p19*

IspF: *AtIspE* + *MpGPPS.SSU* + *PaLimS* + *p19*

IspG: *AtIspG* + *MpGPPS.SSU* + *PaLimS* + *p19*

IspH: *AtIspH* + *MpGPPS.SSU* + *PaLimS* + *p19*

LimS: *MpGPPS.SSU* + *PaLimS* + *p19*

Figure 4.19. Effect of co-infiltration of MEP genes together with *MpGPPS.SSU* + *PaLimS* + *p19* in *N. benthamiana* leaf tissue on limonene concentration. Bars represent the mean ± standard deviation (SD) of n = 3 biological replicates. A one-way ANOVA indicated significant difference among sample groups ($F(8, 18) = 202.2$, $p < 0.001$). Post-hoc comparisons were made using Tukey's Honestly Significant Difference (HSD) test. Groups not sharing a letter differ significantly at $p < 0.05$. Limonene concentration (ng/g FW) is shown on the y-axis, whilst the gene combination is shown on the x axis. The legend below the graph shows the gene names and combinations.

All of the MEP genes tested were driven by the 2xCaMV35S promoter (Table 2.1). Among the combinations tested, co-infiltration of NtDXS with MpGPPS.SSU + PaLimS + MpL3H yielded the highest limonene emission (~932 ng/g FW), which was significantly greater ($p < 0.05$) than all other constructs (Figure 4.19). By contrast, co-infiltration with other MEP genes produced much lower amounts (~25-83 ng/g FW), comparable to the baseline combination of MpGPPS.SSU + PaLimS (~69 ng/g FW). (Figure 4.19). The other gene combinations appear to have no statistically significant effect on limonene concentration (Figure 4.19). Overall, this experiment has revealed the potential of the co-infiltration of *NtDXS* as a key enzyme to increase flux into the MBP.

4.2.8 Transient expression of L2 MoClo constructs in *N. benthamiana*

Co-infiltration of multiple L1 MoClo constructs was shown to reconstitute the early parts of the MBP in *N. benthamiana*, proven by the detection of limonene and (-)-*trans*-isopiperitenol. The next step was to assess the feasibility of combining L1 MoClo constructs into a multi-gene L2 MoClo construct. Therefore, a L2 MoClo construct was produced, which combined *MpGPPS.SSU* and *PaLimS* into a single multi-gene construct, given the designation ppL2_LimS (Table 2.2). As this L2 construct was intended for use in stable expression, a kanamycin resistance gene driven by the *AtuNos* promoter was also included (Table 2.2). For transient expression experiments to first test the construct, *p19* was also co-infiltrated. Therefore, the ppL2_LimS construct was infiltrated into *N. benthamiana* leaves to determine if the previously seen product limonene could be transiently produced (Figure 4.20) (additional replicates shown in Appendix Figure 9).

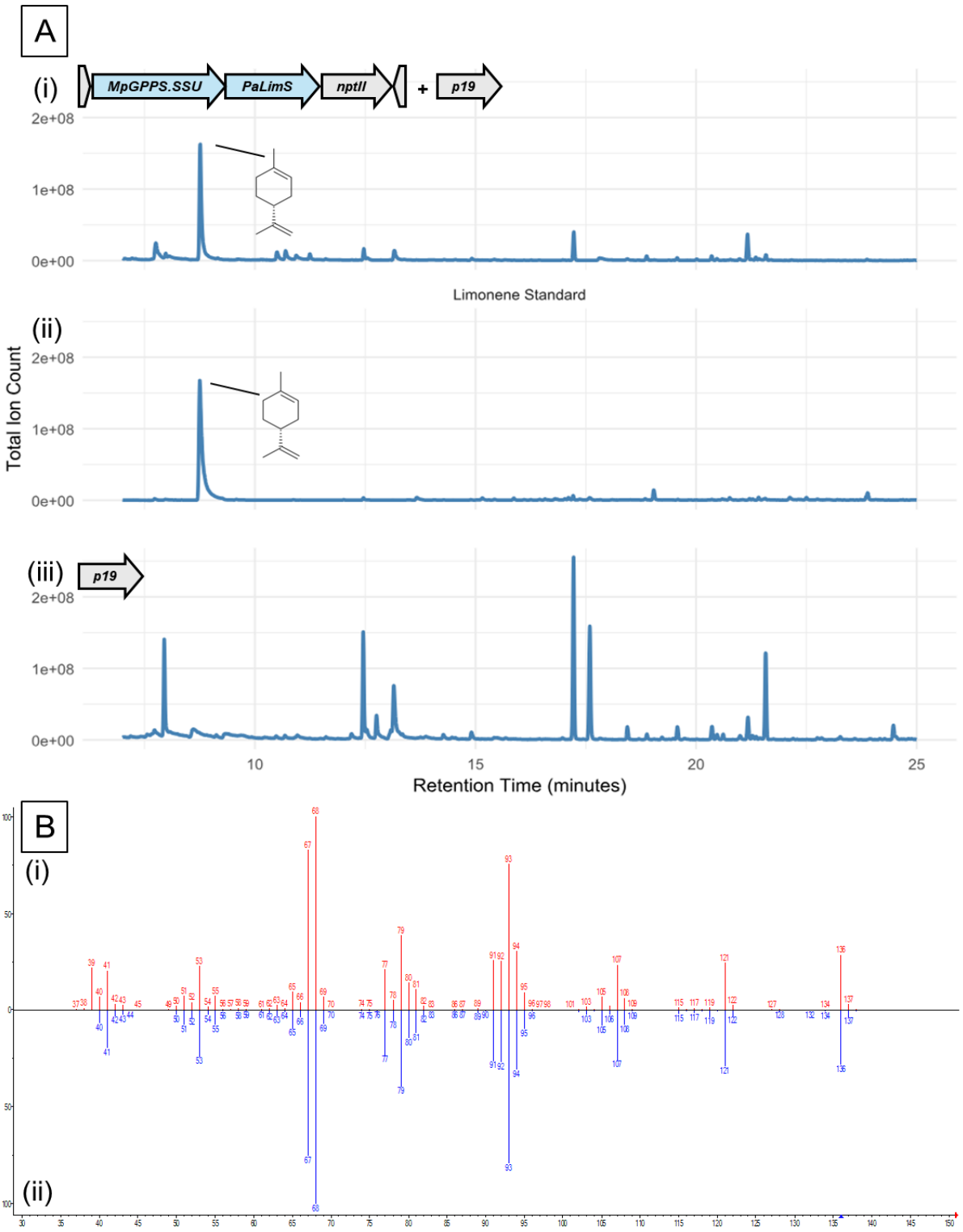

Figure 4.20. Infiltration of *N. benthamiana* leaves with the pL2_LimS construct containing *MpGPPS.SSU* and *PaLimS* in a single construct. A. Chromatograms obtained by GCMS analysis at 3dpi showing Total Ion Count on the y-axis, and Retention Time (minutes) on the x axis for: (i) *N benthamiana* co-infiltrated with pL2_LimS + *p19*. Putatively identified limonene is shown by a black line and chemical structure (ii) Limonene standard. The chemical structure of (-)-Limonene is shown (iii) *N benthamiana* infiltrated with *p19* only. B (i) Head-to-tail plots of the identified compound from A(i) (red) vs library match for limonene (blue) mass spectra using NIST mass spectral library search version 2.2 (NIST 2014). Y-axis = relative abundance for each ion, X-axis = mass to charge ratio (m/z).

Infiltrated *N. benthamiana* leaves were harvested for analysis by static HS-SPME at 3 dpi (Figure 4.20). Infiltration of pL2_LimS into *N. benthamiana* leaves showed the presence of a peak on the GCMS trace (Figure 4.20 A (i)) which was putatively identified as limonene by comparison to the NIST database (Figure 4.20 B). The retention time of the peak was corroborated by sharing a similar mass spectra (data not shown) and retention time as a (-)-limonene standard (Figure 4.20 A (ii)). The putative limonene peak was absent in *N. benthamiana* leaves infiltrated with only *p19,* even after chromatogram deconvolution with AMDIS(Figure 4.20 A (iii)). This result shows that the pL2_LimS construct is capable of transiently inducing the production of limonene in *N. benthamiana* leaves at 3 dpi.

The next L2 MoClo construct produced combined *MpGPPS.SSU, PaLimS* and *MpL3H* into a single multi-gene construct, designated pL2_L3H. Similarly, this construct also contained a kanamycin resistance gene, as it was intended to be used for stable transformation. The *p19* construct was also co-infiltrated for with pL2_L3H for transient expression (Figure 4.21) (additional replicates shown in Appendix Figure 10).

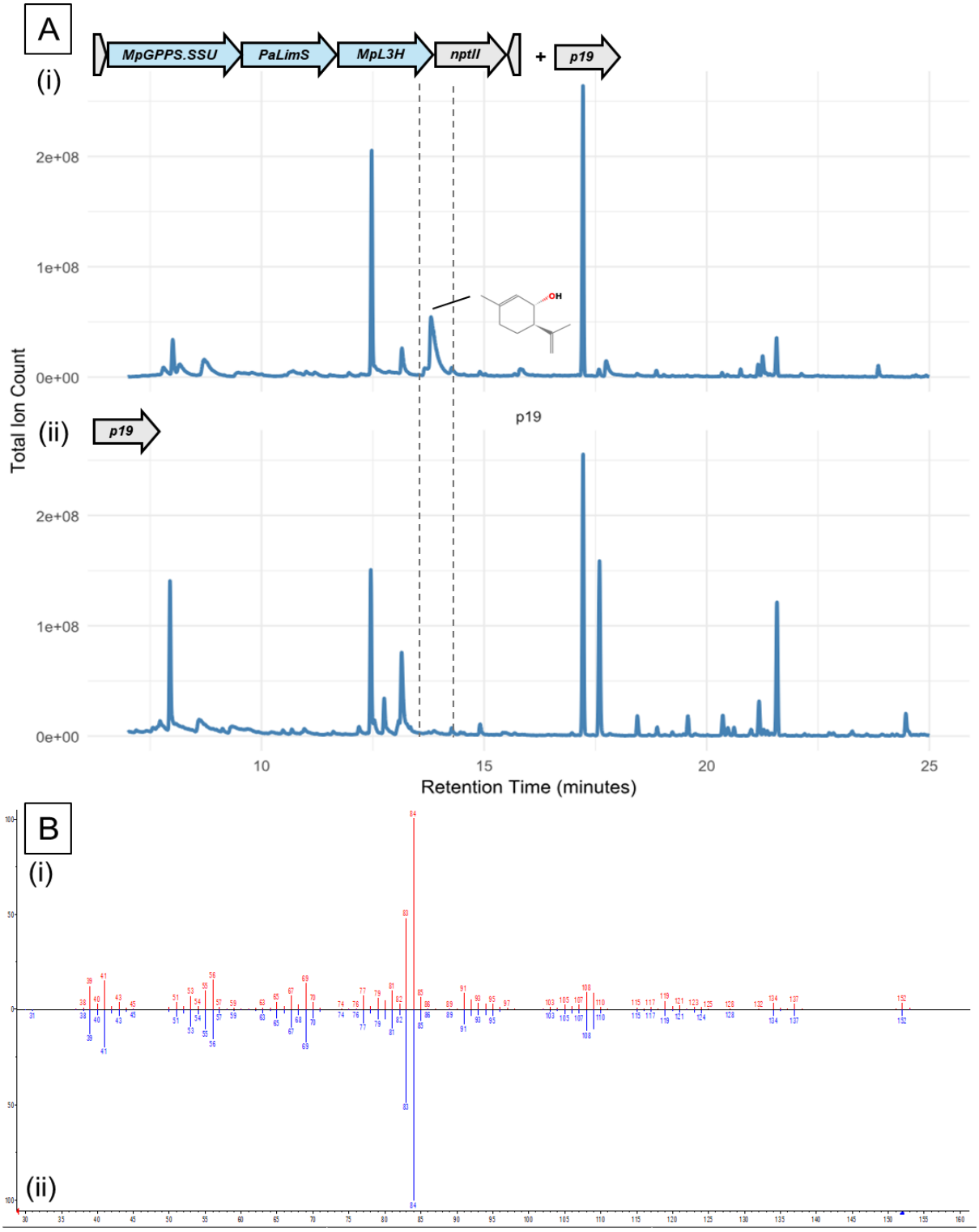

Figure 4.21. Infiltration of *N. benthamiana* leaves with the pL2_L3H construct containing *MpGPPS.SSU, PaLimS* and *MpL3H* in a single construct. A. Chromatograms obtained by GCMS analysis at 3 dpi showing Total Ion Count on the y-axis, and Retention Time (minutes) on the x axis for: (i) *N benthamiana* co-infiltrated with pL2_L3H + *p19*. Putatively identified trans-isopiperitenol is shown by a black line and chemical structure (ii) *N benthamiana* infiltrated with *p19* only. B (i) Head-to-tail plots of the identified compound from A(i) (red) vs library match for (-)-trans-Isopiperitenol (blue) mass spectra using NIST mass spectral library search version 2.2 (NIST 2014). Y-axis = relative abundance for each ion, X-axis = mass to charge ratio (m/z).

Infiltrated *N. benthamiana* leaves were harvested at 3 dpi for analysis by static HS-SPME. *N. benthamiana* leaves infiltrated with pL2_L3H showed a peak (Figure 4.21 A (i)) which was putatively identified by the NIST database as (-)-*trans*-isopiperitenol (Figure 4.21 B). This same peak was absent in *N. benthamiana* leaves infiltrated with only *p19* (Figure 4.21 A (ii)), even after stringent (increasing the sensitivity levels) deconvolution of the chromatogram using AMDIS (data not shown). Overall, this result shows that the multi-gene construct pL2_L3H was able to transiently induce the production of (-)-*trans*-isopiperitenol in *N. benthamiana* leaves at 3 dpi.

Finally, an additional L2 MoClo construct termed pL2_MBP was tested for transient expression in *N. benthamiana* leaves. This construct was created by Dr. Lorenz Fuchs and was created prior to the work of this PhD thesis. The pL2_MBP construct contained all the same coding sequences for every gene in the MBP, with the exception of a homodimeric *Abies grandis GPPS* (*AgGPPS*) in place of the heterodimeric *MpGPPS.SSU*. The regulatory sequences also differed, and full information of the parts used for construction are detailed in Table 2.3 and

Table 2.4.

Prior to working with pL2_MBP, the whole construct was sequenced to confirm its identity. The pL2_MBP was infiltrated into *N. benthamiana* leaves and harvested at 3 dpi for analysis (Figure 4.22) (additional replicates shown in Appendix Figure 11).

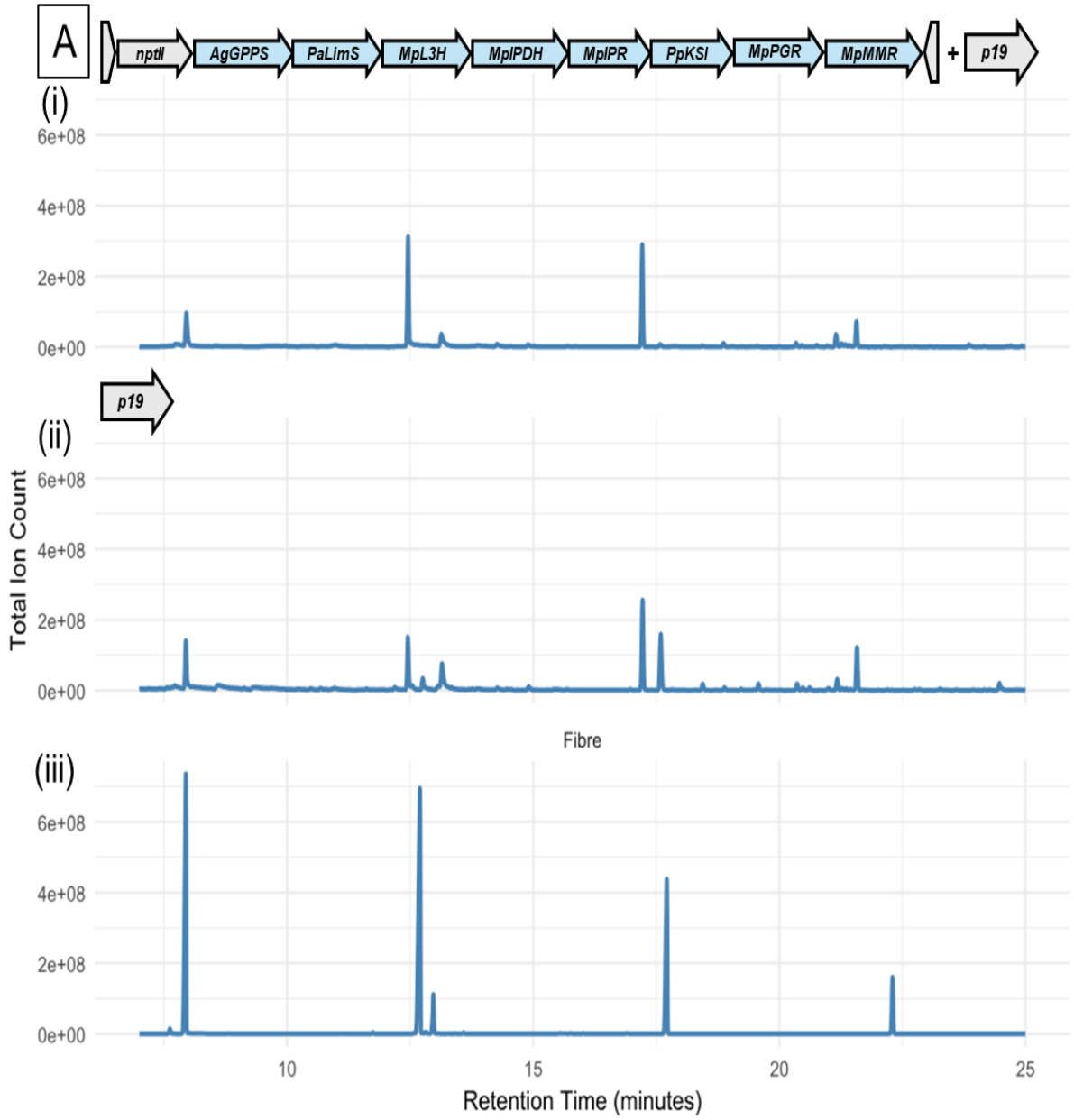

Figure 4.22. Infiltration of *N. benthamiana* leaves with the pL2_MBP construct containing *AgGPPS, PaLimS*, *MpL3H, MplPDH, MplPR, PpKSI, MpPGR* and *MpMMR* in a single construct. A. Chromatograms obtained by GCMS analysis at 3 dpi showing Total Ion Count on the y-axis, and Retention Time (minutes) on the x axis for: (i) *N. benthamiana* leaves co-infiltrated with pL2_MBP and *p19*. (ii) *N. benthamiana* leaves co-infiltrated with *p19*. (iii) An SPME fibre used for static HS-SPME in an empty collection vessel.

No additional peaks corresponding to the expected MBP products were observed from *N. benthamiana* leaves infiltrated with pL2_MBP and analysed at 3 dpi (Figure 4.22 A). Even after increasing the sensitivity of the scrutiny of AMDIS for peak deconvolution, no MBP related pathway products could be detected (data not shown). This shows that the combination of genes used in pL2_MBP may not be suitable for the transient production of MBP products in *N. benthamiana*.

4.2.9 Stable transformation of L2 MoClo constructs into *N. benthamiana* and *A. thaliana*

Transient expression of pL2_LimS resulted in the production of limonene (Figure 4.20), whilst transient expression of pL2_L3H resulted in the production of both limonene and (-)-*trans*-isopiperitenol (Figure 4.21). This showed the utility of transient expression systems in *N. benthamiana* leaves to rapidly test constructs for intended activity before committing to the lengthier process of generating stable transformants. Earlier in this chapter, a stable transformation protocol was optimised for *N. benthamiana* and a means to generate stable transformants was presented (Figure 4.3). Taken together, this allowed the pL2_L3H construct to be used in generating stable transformants in *N. benthamiana*, to assess if the results obtained through transient expression could be replicated stably. Three primary stable *N. benthamiana* transformants (T0) for pL2_L3H were grown to a flowering state. For each independent transformant, alternate leaves was harvested and pooled together in an SPME vial, and were subsequently analysed by static HS-SPME for analysis (Figure 4.23) (all three independent T0 lines shown in Appendix Figure 12).

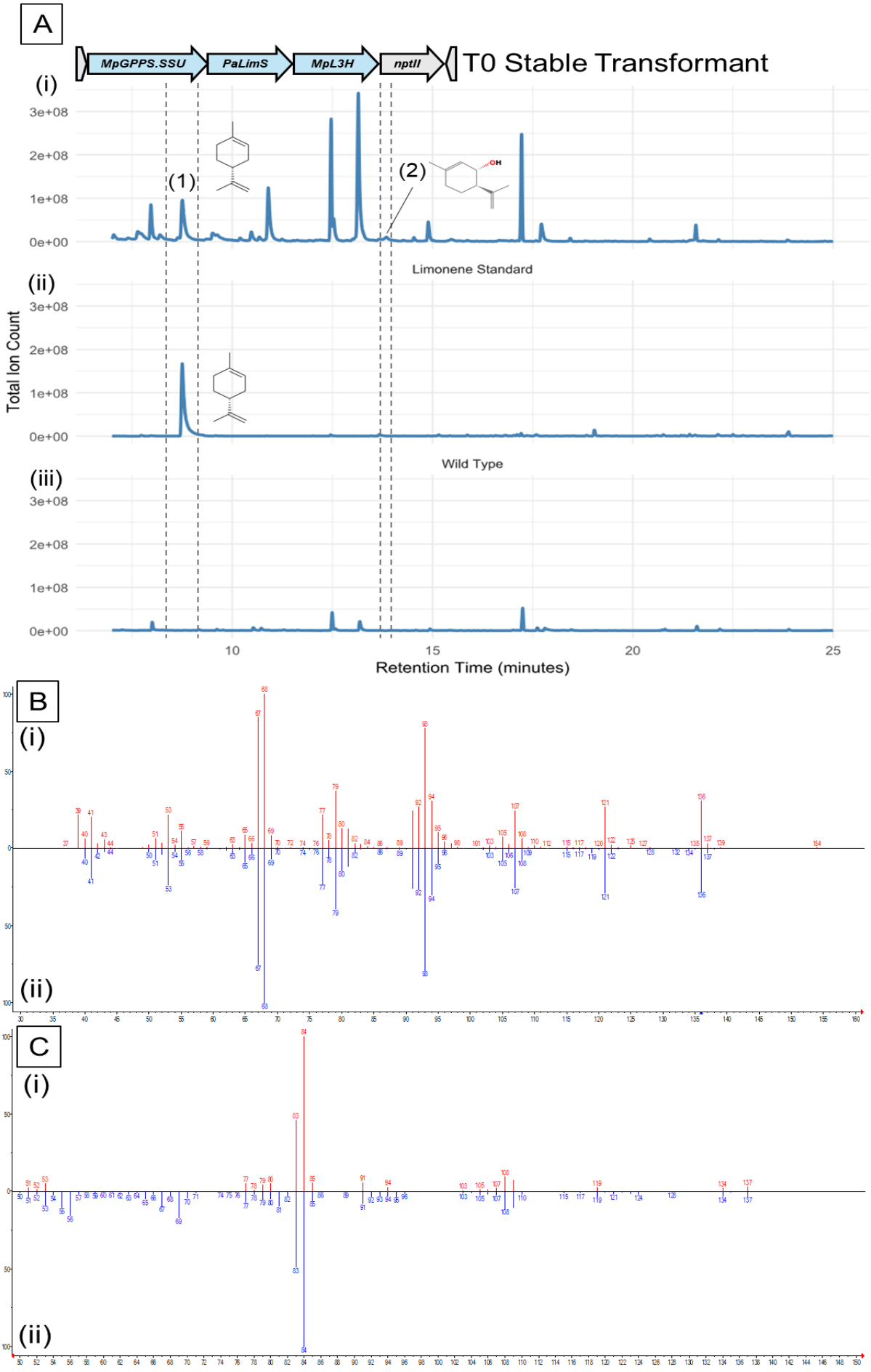
A
MpGPPS.SSU
PaLimS
MpL3H
nptII
T0 Stable Transformant
(i)
(1)
(2)
OH
Limonene Standard
(ii)
Wild Type
(iii)
Total Ion Count
3e+08
2e+08
1e+08
0e+00
10
15
20
25
Retention Time (minutes)
B
(i)
(ii)
C
(i)
(ii)

Figure 4.23. Stable transformation of pL2_L3H in *N. benthamiana* A. Chromatograms obtained by GCMS analysis showing Total Ion Count on the y-axis, and Retention Time (minutes) on the x axis for: (i) T0 stable transformants of *N benthamiana* transformed with the pL2_L3H construct. Putatively identified limonene is shown alongside the chemical structure (1). Putatively identified (-)-trans-Isopiperitenol is highlighted by a black line and shown alongside the chemical structure (2). (ii) Limonene standard. (iii) Wild type untransformed *N. benthamiana.* B (i) Head-to-tail plots of the identified compound from A(i)(1) (red) vs library match for limonene (blue) mass spectra using NIST mass spectral library search version 2.2 (NIST 2014). Y-axis = relative abundance for each ion, X-axis = mass to charge ratio (m/z). C. (i) Head-to-tail plots of the identified compound from A(i)(2) (red) vs library match for (-)-trans-Isopiperitenol (blue) mass spectra using NIST mass spectral library search version 2.2 (NIST 2014). Y-axis = relative abundance for each ion, X-axis = mass to charge ratio (m/z).

Chromatograms resulting from static HS-SPME of T0 transformants of *N. benthamiana* transformed with pL2_L3H showed additional peaks compared to the untransformed wild type comparison (Figure 4.23). Two peaks were observed that are related to the MBP, putatively identified as limonene and (-)-trans-isopiperitenol by the NIST database, respectively. The head-to-tail plots for the mass spectra from the peak identified as limonene match closely to that of the NIST database (Figure 4.23 B). The head-to-tail plots for the mass spectra from the peak identified as (-)-trans-isopiperitenol match primarily in the peaks 84 and 83 against the mass spectra from the NIST database (Figure 4.23 C). The peak on the chromatogram for the putatively identified (-)-trans-isopiperitenol is also barely above the background noise, indicating only trace amounts are present. Overall, stable T0 pL2_L3H *N. benthamiana* transformants were able to produce limonene, and trace amounts of (-)-trans-Isopiperitenol (Figure 4.23). This finding has demonstrated a proof-of-concept for the use of MoClo multi-gene vectors in producing early intermediates of the MBP.

Next, the pL2_MBP construct was stably transformed into *N. benthamiana*, and the resultant T0 transformants were analysed as above.

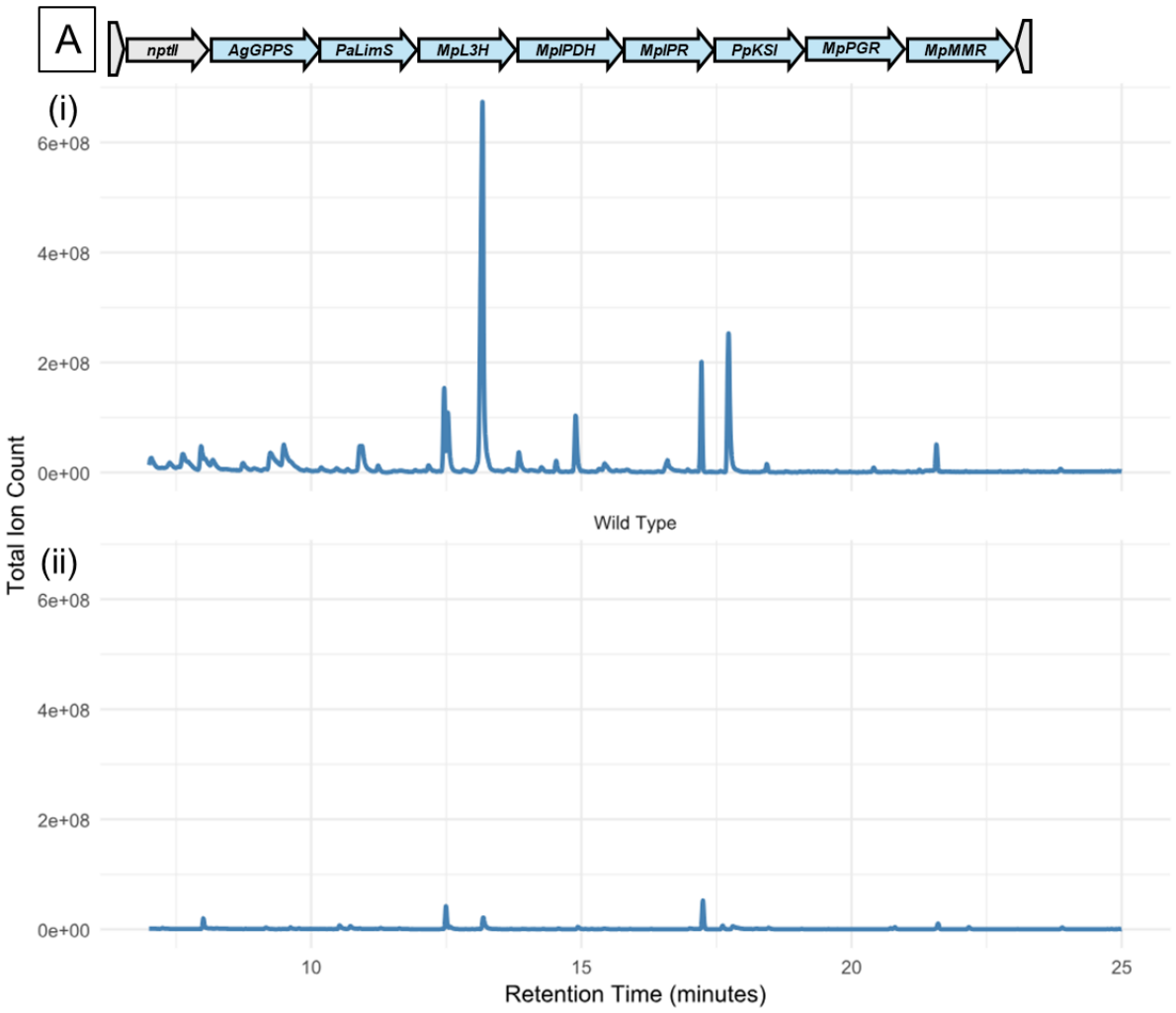

Figure 4.24. Stable transformation of pL2_MBP in *N. benthamiana.* A. Chromatograms obtained by GCMS analysis showing Total Ion Count on the y-axis, and Retention Time (minutes) on the x axis for: A (i) T0 stable transformants of *N benthamiana* transformed with the L2_MpMBP construct. (ii) Wild type untransformed *N. benthamiana.*

Stable transformation of pL2_MBP into *N. benthamiana* failed to produce any of the expected monoterpene intermediate products, or the final product (-)-menthol (Figure 4.24). Although there is the appearance of additional peaks in comparison to the wild type control, this is purely due to the use of more tissue material being used for the analysis of the transformed *N. benthamiana* compared to the wild type (Figure 4.24 B). It can be concluded from the GCMS analysis at least, that the stable pL2_MBP *N. benthamiana* transformants are not producing any MBP related monoterpenes as intended. This further highlights the importance of prototyping constructs transiently as an initial quality control check before committing to the production of stable transformants. Nonetheless, the stable transformants of pL2_L3H in *N. benthamiana* (Figure 4.23) showed promise as a construct to produce both limonene and (-)-*trans*-

isopiperitenol. The pL2_L3H construct was additionally transformed into *A. thaliana,* and T2 stable lines (which are a mix of homozygous and heterozygous transgene insertion lines) were harvested at an early developmental stage (formation of >3 rosette leaves). Static HS-SPME on the headspace of between 10-20 plants pooled together in a single vial, per T2 line, and the lines with the most detected additional monoterpene products are presented below (Figure 4.25 and Figure 4.26).

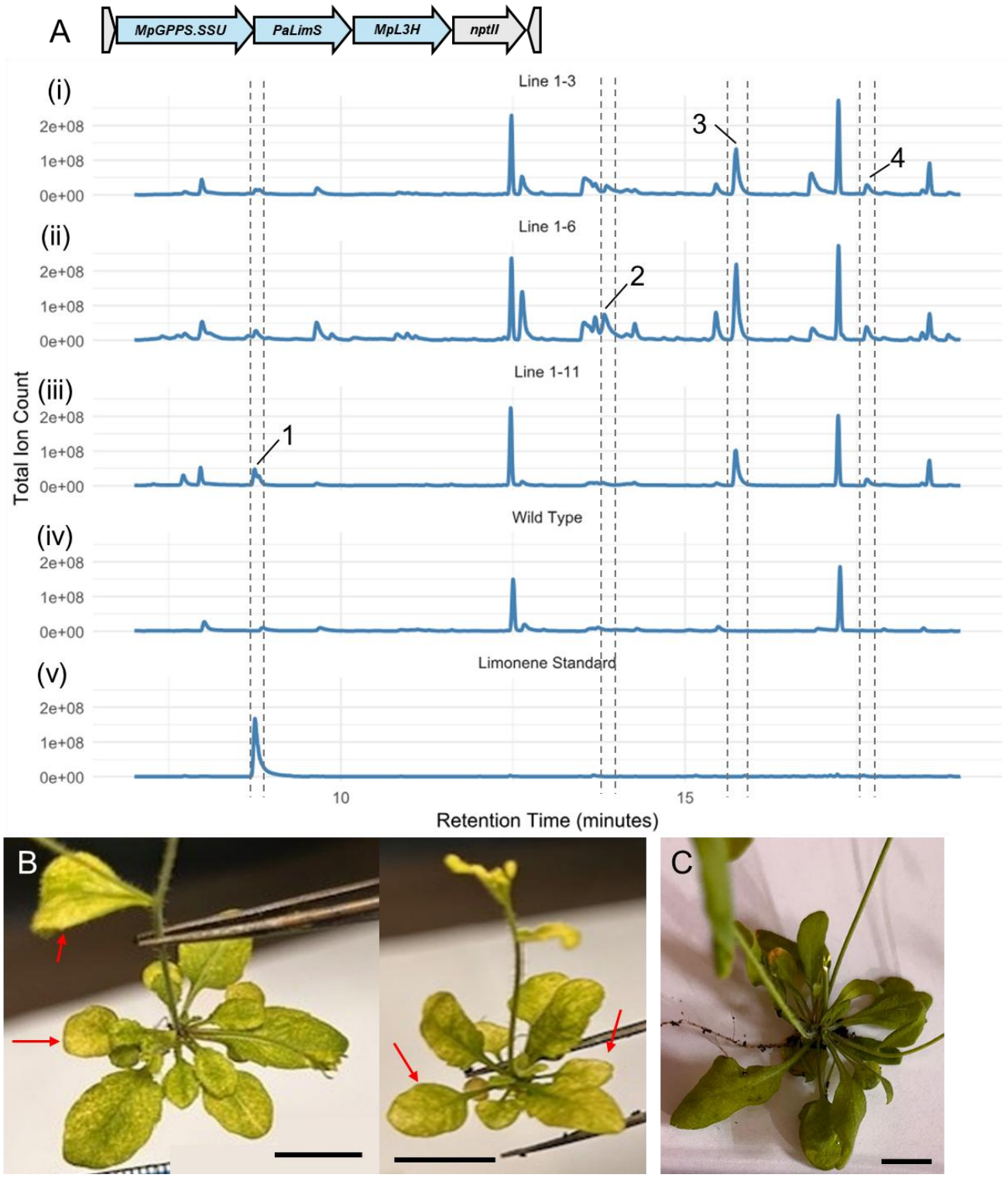

Figure 4.25. T2 stable *A. thaliana* transformed with pL2_L3H. A. Chromatograms obtained by GCMS analysis showing Total Ion Count on the y-axis, and Retention Time (minutes) on the x axis for: (i) T2 Line 1-3, (ii) T2 Line 1-6, (iii) T2 Line 1-11, (iv) Wild Type, (v) (-)-Limonene Standard. Numbers indicate putatively identified monoterpene compounds: 1 = Limonene, 2 = (-)-trans-isopiperitenol, 3 = Isopiperitenone, 4 = Piperitenone. B. Representative images of transgenic *A. thaliana* lines after being taken off selection medium and grown on soil until the flowering developmental stage. Red arrows indicate leaves with signs of chlorosis. C. Representative image of a wild type *A. thaliana* at flowering developmental stage. Black scale bar is 1 cm.

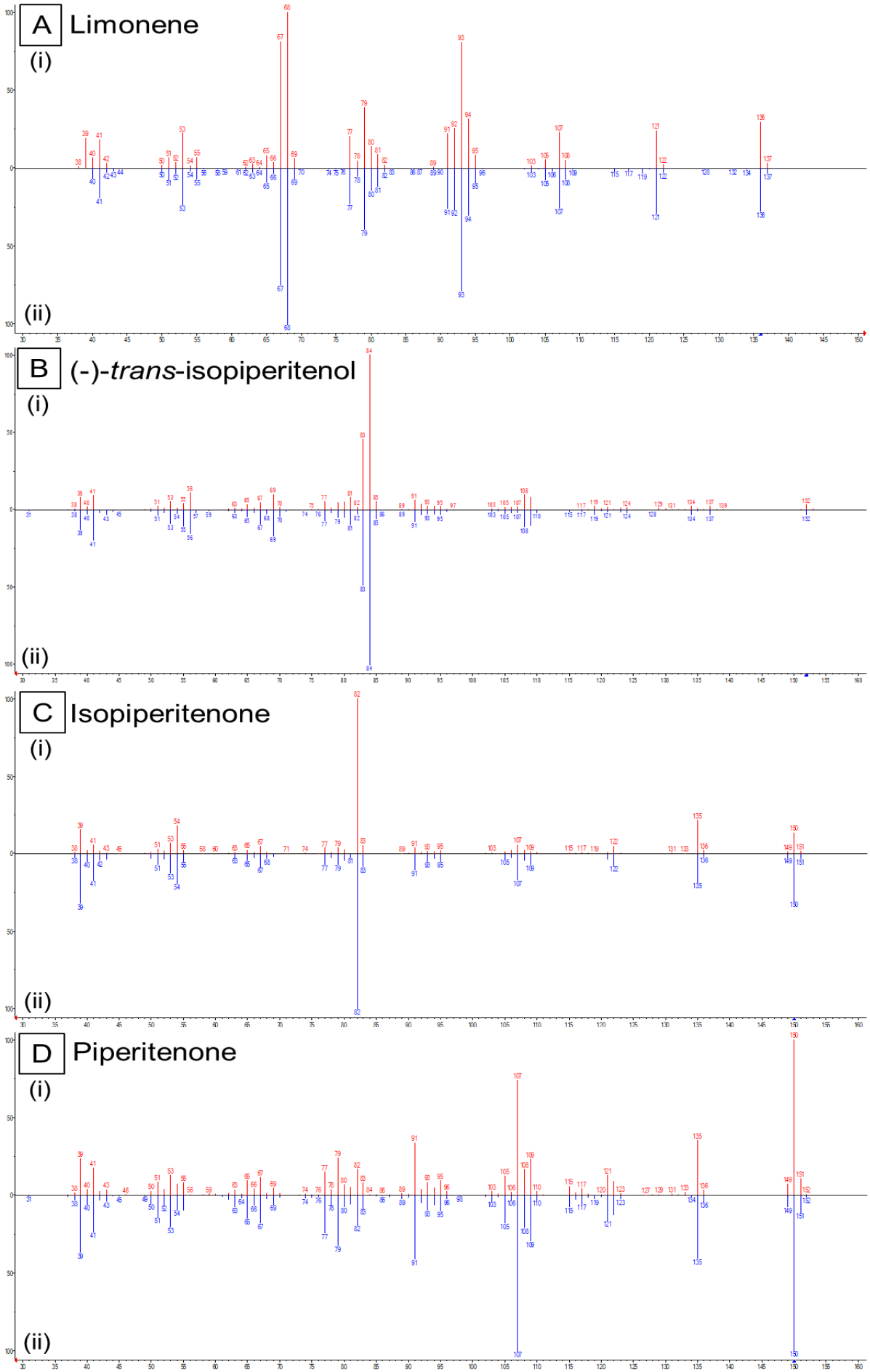
A Limonene
(i)
(ii)
B (-)-trans-isopiperitenol
(i)
(ii)
C Isopiperitenone
(i)
(ii)
D Piperitenone
(i)
(ii)

Figure 4.26. Head-to-tail plots of the identified compounds from Figure 4.25. A Head-to-tail plot for: (i) Peak 1 from Figure 4.25 (red) vs (ii) library match for limonene (blue). B. Head-to-tail plot for: (i) Peak 2 from Figure 4.25 (red) vs (ii) library match for (-)-*trans*-isopiperitenol. C. Head-to-tail plot for: (i) Peak 3 from Figure 4.25 (red) vs (ii) library match for Isopiperitenone. D. Head-to-tail plot for: (i) Peak 4 from Figure 4.25 (red) vs (ii) library match for Piperitenone. Y-axis = relative abundance for each ion, X-axis = mass to charge ratio (m/z). Library match represents mass spectra from the NIST mass spectral library search version 2.2 (NIST 2014).

T2 *A. thaliana* stably transformed with pL2_L3H showed the addition of 4 monoterpene compound peaks which were not present in the wild type control sample (Figure 4.25). The first putative peak matched a similar retention time to a chemical standard of (-)-limonene, and the mass spectra had a high similarity match to limonene identified by the NIST library (Figure 4.26 A). The peaks 2, 3 and 4 (Figure 4.25) were identified as (-)-*trans*-isopiperitenol, Isopiperitenone and Piperitenone by the NIST library, with similar mass spectra matches (Figure 4.26 B, C, and D). The observed peaks for limonene and (-)-*trans*-isopiperitenol were expected products as the pL2_L3H construct showed similar results in both transient and stable expression of *N. benthamiana*. The peaks for Isopiperitenone and Piperitenone were unexpected, and may be due to the action of endogenous *A. thaliana* enzymes causing the conversion of (-)-*trans*-isopiperitenol to Isopiperitenone, and subsequent conversion to piperitenone. Additionally, when transgenic lines showed a leaf chlorosis phenotype on selection medium, and this persisted when taken off selection medium and grown in soil until maturity (Figure 4.25 B). This suggests the newly emitted volatiles may be causing toxicity to the plant.

4.2.10 Characterisation of trichome-specific promoters in *N. benthamiana* and *A. thaliana*

The constructs used to generate stable transformants in this chapter were driven by constitutively expressing promoters, which are inherently non tissue specific. As glandular trichomes are known as the sites of synthesis of terpenes, targeting gene expression to specifically the trichomes was an intended aim of this chapter (Markus Lange and Turner 2013). This was aimed to be achieved by the use of trichome-specific promoters driving expression of the MBP genes. However, although trichome-specificity in the native host plant may be driving by their respective trichome-specific promoter, it is unknown how they would function when endogenously transformed into other plant hosts. To this end, a selection of

glandular trichome-specific promoters were selected from the literature, which were compatible with the MoClo system, were fused to the *uidA* gene and had the expression characterised by localisation of GUS activity. These promoters were from the genes *NtMald1*, *NtCPS2, MpL3H, MpLimS, MpIPDH and MpPGR*. This was first done in *A. thaliana*, which themselves do not possess glandular trichomes, to determine if trichome-specificity would still be conferred (Figure 4.27).

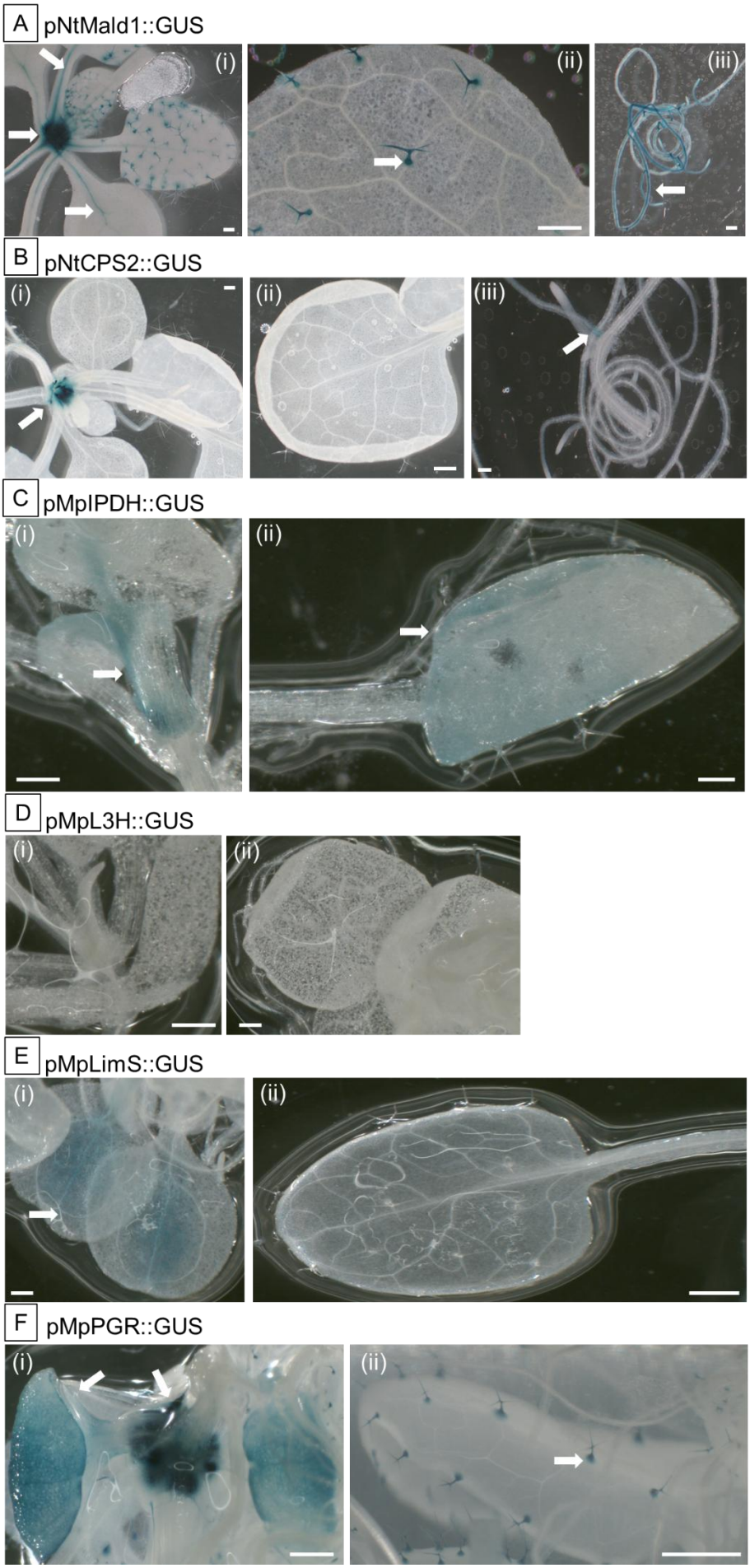
A pNtMald1::GUS
(i)
(ii)
(iii)
B pNtCPS2::GUS
(i)
(ii)
(iii)
C pMpIPDH::GUS
(i)
(ii)
D pMpL3H::GUS
(i)
(ii)
E pMpLimS::GUS
(i)
(ii)
F pMpPGR::GUS
(i)
(ii)

Figure 4.27. T2 stable *A. thaliana* transformed with glandular trichome-specific promoters driving the *uidA* gene and stained for GUS activity. A. pNtMald1::GUS. B. pNtCPS2::GUS. C. pMpIPDH::GUS. D. pMPL3H::GUS. E. pMpLimS::GUS. F. pMpPGR::GUS. White arrows indicate areas of GUS activity as determined by blue pigment formation. White scale bar = 1 mm.

The *NtMald1* promoter showed GUS activity in the shoot apex, leaf petiole vasculature, shoot vasculature (Figure 4.27A (i)), non-glandular trichomes (Figure 4.27A (ii)), roots and lateral roots (Figure 4.27A (iii)). The *NtCPS2* promoter showed GUS activity in the shoot apex, and slight activity in the lateral roots (Figure 4.27 B (i)(iii), but no activity in the non-glandular trichomes (Figure 4.27 B (ii)). The *MpIPDH* promoter showed faint GUS activity in the shoot apex, surrounding petiole tissue (Figure 4.27 C (i)) and leaf tissue (Figure 4.27 C (ii)). No detectable GUS activity was conferred by the *MpL3H* promoter (Figure 4.27 D). The *MpLimS* promoter showed faint GUS activity throughout the cotyledon leaves (Figure 4.27 E (i)), but not in the non-glandular trichomes (Figure 4.27 E (ii)). The *MpPGR* promoter showed strong expression in the shoot apex, cotyledon leaves (Figure 4.27 (i)) and non-glandular trichomes (Figure 4.27 F (ii)).

Overall, the promoters from *NtMadl1* and *MpPGR* showed the ability to confer strong trichome expression in the non-glandular trichomes of young *A. thaliana* plants, although this was not purely trichome-specific. The other tested promoters failed to confer expression to the trichomes, suggesting unsuitability for use in trichome-specific metabolic engineering studies in *A. thaliana*. The same set of promoters were also characterised in *N. benthamiana* T0 transformants to determine potential differences in spatial expression patterns between species (Figure 4.28)

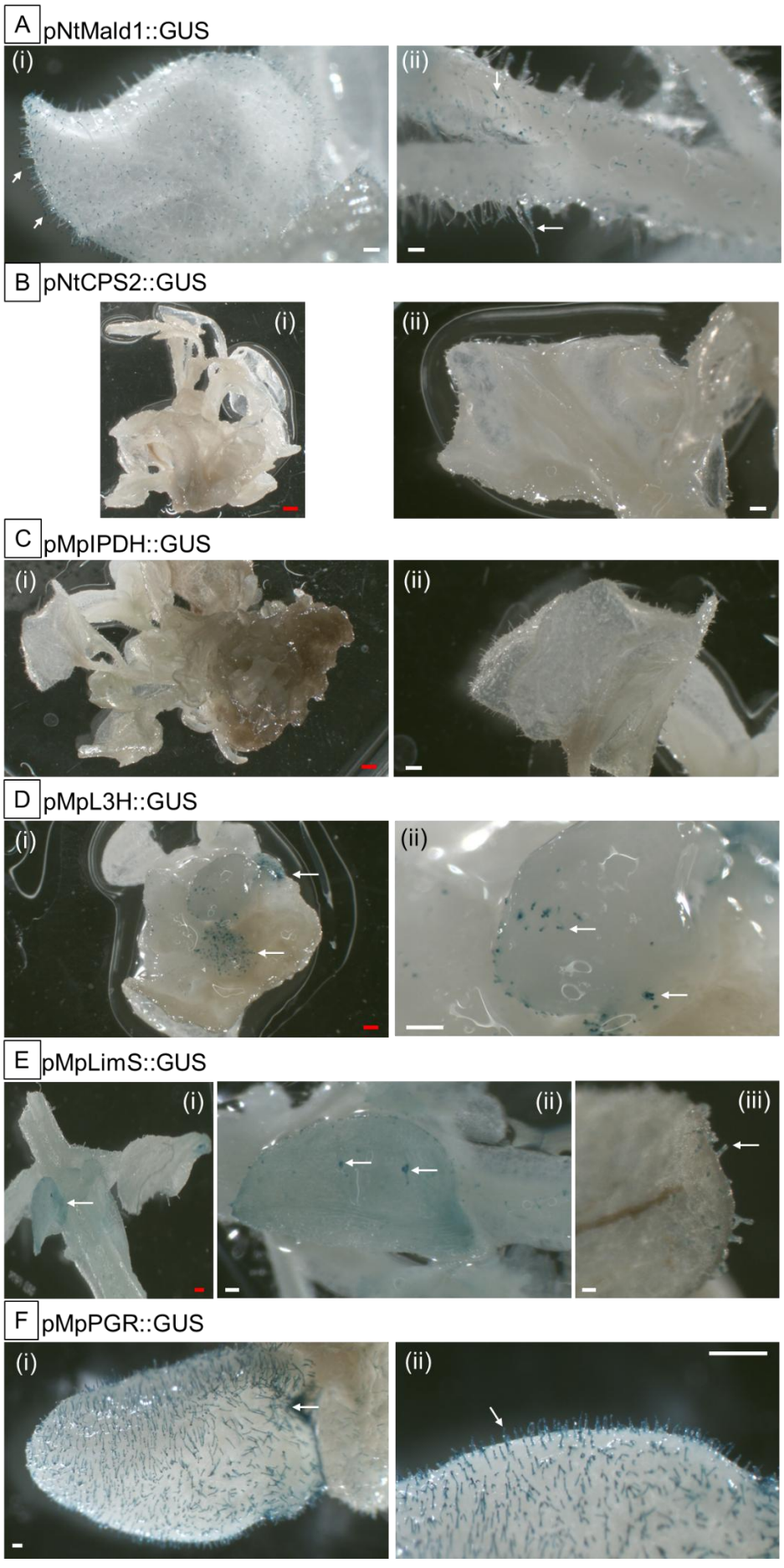
A pNtMald1::GUS
(i)
(ii)
B pNtCPS2::GUS
(i)
(ii)
C pMpIPDH::GUS
(i)
(ii)
D pMpL3H::GUS
(i)
(ii)
E pMpLimS::GUS
(i)
(ii)
(iii)
F pMpPGR::GUS
(i)
(ii)

Figure 4.28. T0 stable *N. benthamiana* transformed with glandular trichome-specific promoters driving the *uidA* gene and stained for GUS activity. A. pNtMald1::GUS. B. pNtCPS2::GUS. C. pMpIPDH::GUS. D. pMPL3H::GUS. E. pMpLimS::GUS. F. pMpPGR::GUS. White arrows indicate areas of GUS activity as determined by blue pigment formation. White scale bar = 1 mm. Red scale bar = 1cm.

In *N. benthamiana,* the *NtMald1* promoter conferred strong GUS activity in the glandular trichomes on both the leaves (Figure 4.28 A (i)) and stem (Figure 4.28 A (ii)). The *NtCPS2* promoter did not confer any GUS activity in any of the tissues of *N. benthamiana* (Figure 4.28 B). The *MpIPDH* promoter showed a lack of GUS activity in any of the tissues (Figure 4.28 C). The *MpL3H* promoter conferred GUS activity in the glandular trichomes of emerging leaf structures from the callus body (Figure 4.28 D). The *MpLimS* promoter showed faint GUS activity throughout the leaf tissue, and in the glandular trichomes (Figure 4.28 E). The *MpPGR* promoter conferred strong GUS activity in the glandular trichomes of emerging leaf structures from the callus body (Figure 4.28 F).

Of the trichome specific promoters tested in *N. benthamiana*, *NtMald1* and *MpPGR* show promise for use in future metabolic engineering studies, by driving the expression MBP genes in the glandular trichomes. Furthermore, *NtMald1* and *MpPGR* would be ideal candidates for metabolic engineering studies in *A. thaliana* to compartmentalise expression to the non-glandular trichomes.

4.3 Conclusions

The work done in chapter 4 has provided the groundwork for the production of early MBP monoterpenes in both transient and stable expression platforms in *N. benthamiana*, and an in-depth discussion will be presented in chapter 6. Both limonene and (-)-*trans*-isopiperitenol could be detected in both transiently and stably expression *N. benthamiana* transformed with *MpGPPS.SSU* + *PaLimS* + *MpL3H*. Stable transformation of *MpGPPS.SSU* + *PaLimS* + *MpL3H* in *A. thaliana* resulted in the additional unexpected products of isopiperitenone and piperitenone. A means to semi-quantify limonene in a static HS-SPME system was developed and leveraged to show that that co-expression of *NtDXS* with *MpGPPS.SSU* + *PaLimS* led to an increase in limonene emissions. Finally, a selection of trichome-specific promoters were characterised in *N. benthamiana* and *A. thaliana*, where *NtMald1* and *MpPGR* promoters showed the strongest trichome expression. Although full reconstitution of the MBP pathway did not result in the production of any further intermediates downstream from (-)-*trans*-isopiperitenol, this highlighted the possibility that there may be additional cofactors, partner proteins or additional novel genes needed to reconstitute the MBP outside of its native host. This is addressed in chapter 5, which aims included the identification of potential co-expressed TFs in the native host *M. x piperita*, by analysis of RNA-seq data from Black Mitcham at three developmental stages.

Chapter 5 – Integrating essential oil profiling and transcriptomics to explore the regulation of menthol biosynthesis in *M. x piperita* cv. Black Mitcham

5.1 Introduction

Monoterpenes represent a diverse class of plant secondary metabolites, with key roles in plant defence, ecological interactions and commercial applications (Qasim et al. 2024). Among these monoterpenes, the cyclic monoterpene menthol and its derivatives produced by *M. x piperita* is of substantial interest due to their widespread use in the flavour, fragrance and pharmaceutical industries (Kamatou et al. 2013; Zielińska-Błajet and Feder-Kubis 2020; Guzmán and Lucia 2021). The biochemical pathway responsible for menthol biosynthesis (MBP) has been well characterised at the enzymatic level, comprising of a series of transformations beginning with the cyclisation of GPP to (-)-limonene and culminating in the formation of (-)-menthol through a sequence of hydroxylation, isomerisation and reductive steps (Croteau et al. 2005). The most widely grown cultivar of *M. x piperita* is Black Mitcham, and thus most agricultural interest is focused around this cultivar (Lawrence 2006). (-)-menthol and it's derivatives are present in the essential oils produced by Black Mitcham, which are produced in specialised appendages known as the peltate glandular trichomes (PGT), where the majority of essential oil biosynthesis occurs (McCaskill et al. 1992). The PGTs are situated mainly on the leaves, where the composition of the essential oils produced are thought to be influenced by the developmental stage of the leaf. In general, younger leaves have a higher composition of menthone and intermediate monoterpenes, whilst mature leaves have a higher composition of menthol (Gershenzon et al. 2000) (Figure 5.1).

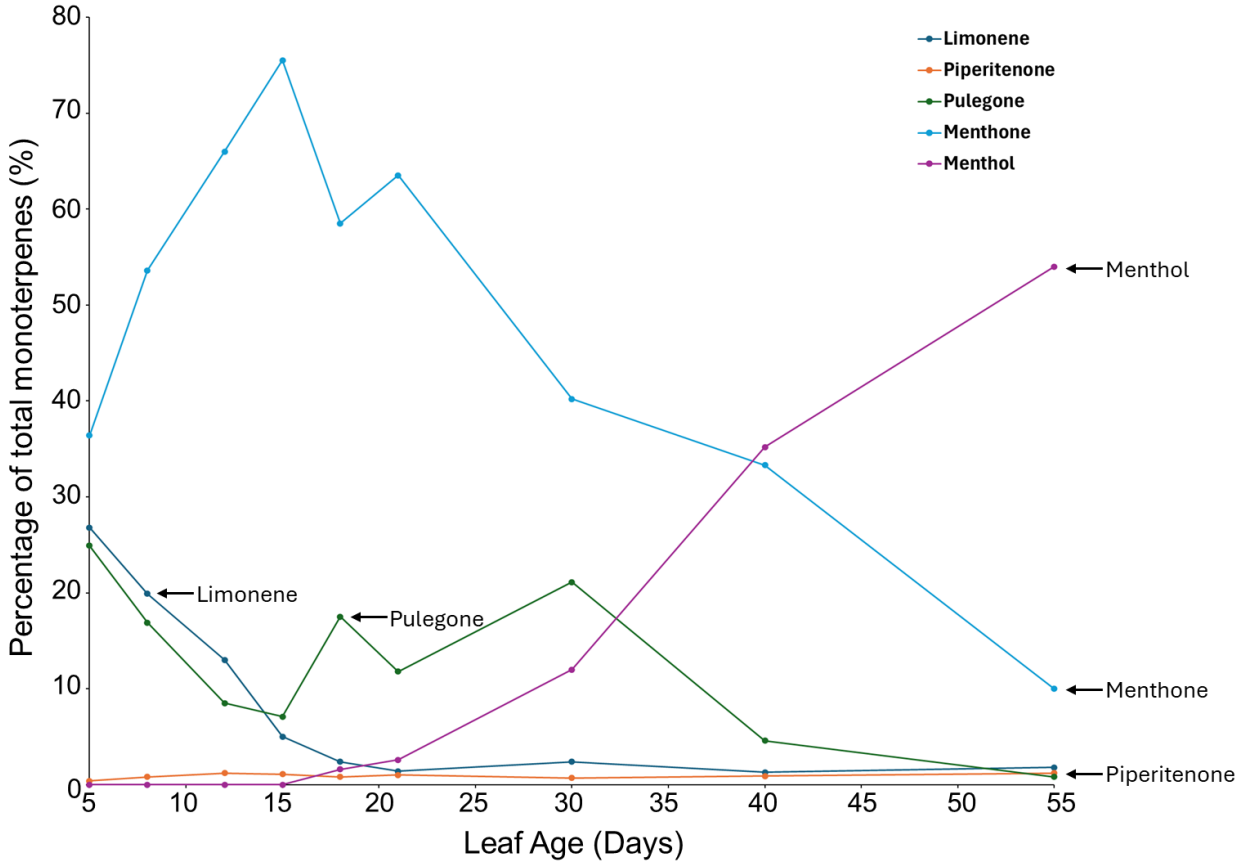

Figure 5.1. Black Mitcham essential oil composition from leaves at increasing ages. Y-axis shows each component expressed as a percentage of total monoterpenes. X-axis showed the age of the leaf in days. Each data point is the mean value of at least 3 independent replicates. This data is reanalysed from Gershenzon et al. 2000. Raw replicate data was not available to present standard deviations.

The change in essential oil compounds over the developmental stage of a leaf from young to mature is believed to be attributed to the activity of the MBP enzymes, which are developmentally regulated at the level of gene expression (McConkey et al. 2000). However, much less is known about the overall gene regulatory networks that the MBP exists in, and other key gene products that may be required for the activity of the MBP enzymes.

Chapter 4 of this thesis revealed that reconstitution of the MBP pathway in *N. benthamiana* using only the MBP enzymes was only successful using a combination of the first two enzymes, LimS and L3H, to generate (-)-*trans*-isopiperitenol. Further step-wise expression did not result in the production of further MBP products, highlighting that additional partner genes may be required for the activity of the downstream MBP enzymes. To increase the understanding of the regulation of the

MBP pathway and the potential additional regulatory mechanisms, further studies in the native host are required to elucidate previously uncharacterised mechanisms.

5.1.1 Transcriptional control of the menthol biosynthesis pathway in Black Mitcham

Transcriptional control of plant secondary metabolism is widely recognised as a main regulatory factor of terpenoid production. The transcript abundance of MBP genes was strongly correlated with the metabolite accumulation in Black Mitcham (McConkey et al. 2000). This observation was further confirmed by later transcriptomic studies on Black Mitcham, which saw similar trends of MBP gene transcript expression correlating with metabolite profiles in the essential oil (Ahkami et al. 2015). A similar trend has also been observed in other plant species, such as the production of artemisinin biosynthesis pathway in *Artemisia annua* (Lange and Ahkami 2013). The transcriptional control of the main genes of plant secondary metabolite pathways are orchestrated by TFs, which are known to tightly regulate the spatiotemporal expression of secondary metabolite pathway genes (Colinas and Goossens 2018). *Artemesia annua* is a well-studied example of this, where the TF families WRKY, APETALA2/ethylene-responsive factor (AP2/ERF), basic leucine zipper (bZIP) and basic helix–loop–helix (bHLH) have been implicated in directly regulating the expression of the artemisinin biosynthesis pathway genes (Shen et al. 2016).

The TFs involved in the direct regulation of MBP genes in Black Mitcham are unknown, with no publications available as of the writing of this thesis. There have however been reports of TF regulation of secondary metabolite pathway genes in other *Mentha species.* The bZIP family TF *McbZIP1* from *M. canadensis* has been reported to bind to the *McLimS* promoter, and when overexpressed in *M. x piperita*, was shown to cause an increase in menthol accumulation (Yu et al. 2024). In *M. haplocalyx*, the MYB family TFs *MhMYB1* and *MhMYB2* have been shown to both interact with the promoters of *MhMMR* and *MhPGR* by positive regulation, which showed a change in the (-)-menthone and (-)-menthol components of the essential oils when assayed by virus-induced gene silencing (VIGS) (An et al. 2024). Although not directly regulating a secondary metabolite pathway, the MYB family TF *McMIXTA* has also been implicated in playing a role as a positive regulator of peltate glandular trichome development (the site of essential oil biosynthesis) in *M. haplocalyx* (Qi et

al. 2022). In *Mentha spicata* (*Ms*), the *MsMYB* was shown to be a negative regulator of *MsGPPS.LSU*, and overexpression of *MsMYB* showed a generalised decrease in the monoterpenes (-)-limonene and (-)-carvone (Reddy et al. 2017). The YABBY TF family *MsYABBY5* was also shown to be an overall negative regulator of monoterpene production in *Mentha spicata*, which was shown by increased levels of (-)-limonene and (-)-carvone in *MsYABBY5* RNAi silenced lines (Wang et al. 2016b). With respect to Black Mitcham however, there is a clear gap in the literature for elucidating potential TFs regulating the MBP genes. The available literature from related *Mentha* species has narrowed down the focus to MYB, bZIP and YABBY TF families, however other TF families such as the WRKY, AP2/ERF, NAC and bHLH have been involved in the transcriptional control of secondary metabolite pathways in other plant species such as *Artemesia annua*, *Catharanthus roseus*, *Camellia oleifera* and *Panax ginseng* (Liu et al. 2023; Singh et al. 2024). Therefore, this knowledge gap highlights the need for integrated RNA-seq and chemotype analyses in Black Mitcham to identify potential TFs regulating the MBP.

5.1.2 Exploration of the Black Mitcham transcriptome comparing leaves at different developmental stages

Outside of the singular paper looking at the Black Mitcham transcriptome at two different developmental stages (Ahkami et al. 2015), there have been no other reports of transcriptome analysis aimed at the differences in developmental stages in Black Mitcham. Furthermore, the aforementioned study was focused on a cursory analysis of multiple *Mentha* varieties, and did not perform substantial analysis on the potential co regulatory network that may influence the MBP in Black Mitcham specifically. The work in this chapter aims to further improve upon this, by looking at leaves from Black Mitcham at different developmental stages to correlate the change in oil profiles with the change in gene expression of the key MBP genes by RNA-sequencing (RNA-seq). RNA-seq involves converting RNA into complementary DNA (cDNA), which is then used as input for sequencing to generate short sequence reads (Deshpande et al. 2023). These reads are mapped to reference genes, and the number of reads assigned to each gene provides a measure of its expression level. By comparing gene expression across different sample types or experimental conditions, genes that show significant changes in expression can be identified. These are known as differentially expressed genes (DEGs) and they are determined

using statistical methods that test whether observed differences are unlikely to have arisen by chance (Rosati et al. 2024). These identified DEGs can then be used to identify candidate genes in transcriptomic studies, and in the context of this chapter, to identify candidate DEGs that change between the different developmental stages of Black Mitcham.

Previous transcriptomic studies in Black Mitcham have relied on *de-novo* transcriptome assembly (Ahkami et al. 2015). When working in a polyploid species such as Black Mitcham (an allohexaploid), the presence of homologs can complicate assembly and downstream analysis (Payá-Milans et al. 2018). Most *de-novo* assemblers, such as Trinity (used in Akhami et al. 2015), use de Bruijn graphs, which reconstruct sequences by breaking reads into overlapping kmers and connecting them through shared (k-1)-mers (Compeau et al. 2011; Grabherr et al. 2011). Assembly accuracy depends on k, where short kmers improve coverage but risk mis assembly from shared sequences, while long kmers reduce ambiguity but may fragment assemblies. These issues are intensified in polyploid transcriptomes such as Black Mitcham, where highly similar alleles and homologs greatly increase graph complexity and error rates in the transcriptome assembly (Voshall and Moriyama 2020). This causes inaccuracies downstream when estimating gene expression values, and to accurately distinguish between homologs, reads must be mapped to a full polyploid reference genome (Voshall and Moriyama 2020). These short comings of previously used *de-novo* transcriptome assembly for RNA-seq studies in Black Mitcham were addressed in this chapter by mapping the RNA-seq data to the newly released Black Mitcham reference genome (Talbot et al. 2024).

As the study in this chapter is focused around correlating changes in oil expression with gene expression, a key aspect of the methodology for leaf sampling was changed. The sampled leaves were harvested by excising the leaves from the petiole, and cutting vertically along the leaf midrib, where one half of the leaf would be harvested for RNA-seq, and the other half would be harvested for essential oil profiling. This method accounts for the varied distribution of PGTs on the leaf, which are known to show a developmental change from the base to the apex of the leaf (Turner et al. 2000b). This sampling method also ensured that the same leaf was used for both types of analysis, thus reducing the biological variability that could arise from using separate leaves at roughly similar developmental stages. Thus, the

work from this chapter represents the first report of a preliminary exploratory transcriptome study of the Black Mitcham genome, aimed at exploring the changes in gene expression with changes in the essential oil profiles.

One of the main aims was to identify potential TFs which may be regulating the MBP pathway to facilitate the changes in oil profile changes over changes in development. To this end, co-expression analysis represents an ideal option to achieve this aim, where groups of DEGs are classified according to their gene expression pattern (van Dam et al. 2018). In the context of TFs potentially regulating the key MBP genes, this approach can be applied to identify TF DEGs that share the same expression pattern and thus identify putative regulatory TFs. Ideally, identification of TFs which could activate or repress multiple genes in the MBP would make excellent targets for metabolic engineering strategies (Grotewold 2008; Iwase et al. 2009). These regulatory TFs could then be tested in both the native Black Mitcham, as well as the non-native *N. benthamiana* or *A. thaliana* through heterologous expression, to build upon the work of the previous chapter (Chapter 4).

An additional aim from this chapter was to explore if the transcriptome generated in this thesis could be used to identify the previously uncharacterised *MpIPGI* from the MBP. IPGI catalyses the isomerisation of (+)-*cis*-isopulegone to (+)-pulegone, and is the only uncharacterised enzyme in the MBP to date (Croteau et al. 2005). It has been reported that the Δ5-3-ketosteroid isomerase from *P. putida* (*PpKSI*) possesses IPGI activity, from *in vitro* studies performed in *E. coli* (Currin et al. 2018). However, attempts to characterize its activity *in-planta* in the previous chapter (Chapter 4) by heterologous expression together with the upstream MBP genes failed to produce the expected formation of (+)-*cis*-isopulegone. Therefore, the identification of the native IPGI using the transcriptome data from this chapter would identify new potential targets for heterologous expression studies. As there have been no reports of ketosteroid isomerases of plant origin showing IPGI activity, and no obvious *MpIPGI* homologues in the literature, this has severely hampered the discovery and characterisation of the *MpIPGI* gene. However, the Δ5-3-ketosteroid isomerase enzyme forms a part of the larger nuclear transport factor (NTF2) like superfamily, and this could be used as a means to narrow down potential *MpIPGI* targets by using a co-expression approach (Li et al. 2018). Recently, this approach has been utilised to find putative *IPGI* genes in *Mentha suaveolens,* where two putative NTF2

family genes were shown to co-express with the early MBP genes *L3H* and *ISPD* (Yang et al. 2024a). Therefore, this approach is promising for finding the *MpIPGI* in the transcriptome dataset generated in this chapter.

5.1.3 Aims and objectives

The aims of this chapter were to address how transcriptional changes correlate with essential oil composition changes in Black Mitcham, focusing on elucidating potential TFs and uncharacterised *MpIPGI* that may follow similar expression patterns. The objectives were therefore:

1. Characterisation of the changes in essential oil profiles of leaves at three different developmental stages by GCMS analysis
2. Analysis of the global transcriptome dynamics across the different developmental stages
3. Evaluation of the expression patterns of key genes involved in the MBP
4. Correlation analysis of changes in gene expression with changes in essential oil profiles
5. Identification of TFs co-expressed with MBP genes to determine potential regulators
6. Exploration of potential NTF2 like family genes which co-express with MBP genes to identify putative *IPGI* genes

5.2 Results

5.2.1 Determination of leaf samples with different in essential oil profiles

The first step in this study was to determine suitable developmental stages for sampling the leaves of Black Mitcham. As the plant is sterile and is propagated vegetatively, actively growing plants were cut back to restore a pre-vegetative state of growth, and this was taken as the starting stock material. The plants were then grown until three distinct developmental stages, where the formation of flowers was used to determine at what stage of development the plant was in. These developmental stages were termed “Vegetative”, “Early Flowering” and “Late Flowering”, and are outlined in Figure 5.2.

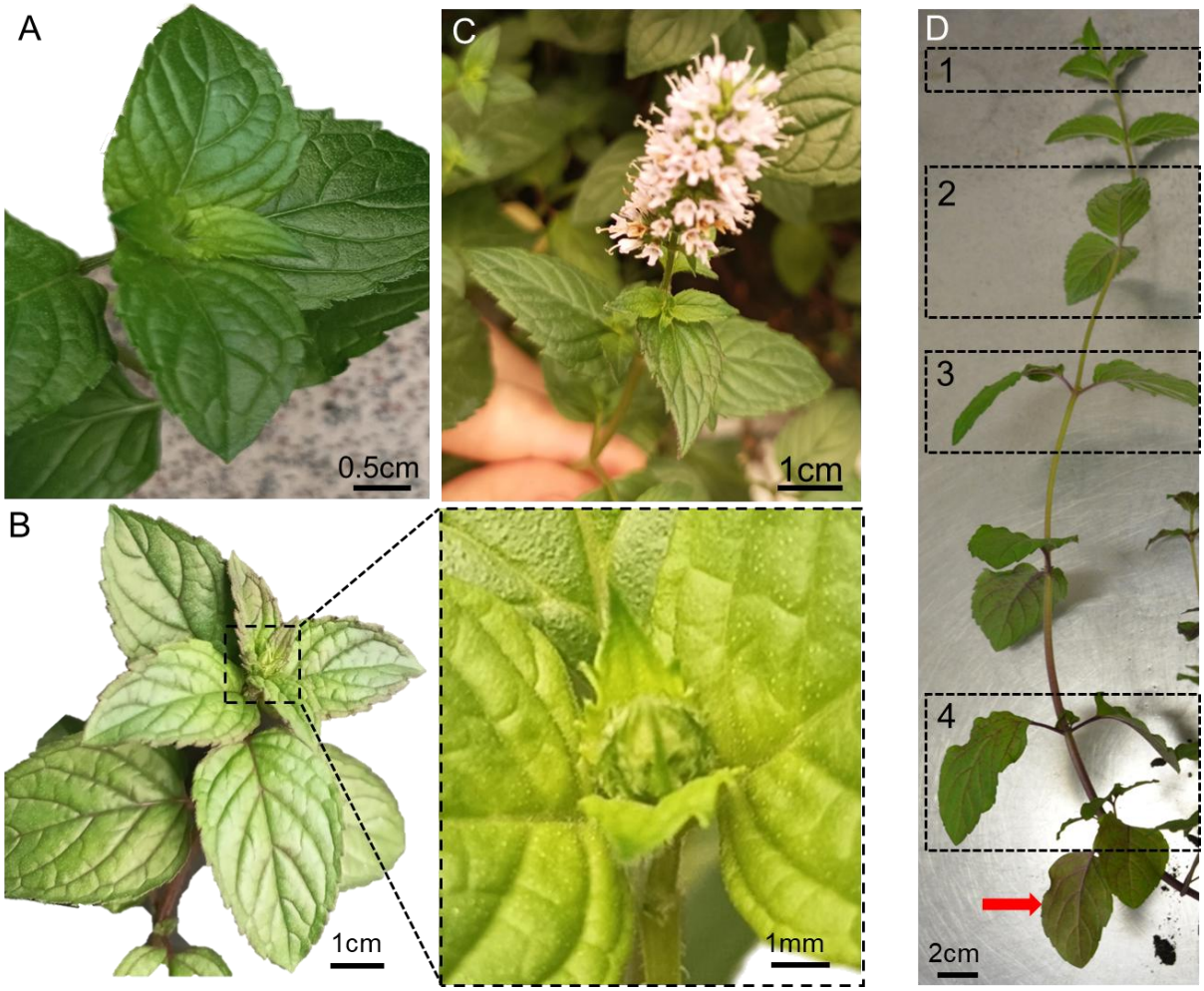

Figure 5.2. Black Mitcham developmental stages chosen for this study. A. Vegetative stage. The lack of flower development indicated the plant was in a vegetative state, and therefore termed “Vegetative”. B. Early Flowering stage. The onset of floral development is observed, with a zoomed image showed as an inset. C. Late Flowering stage. The development of a fully blooming flower with open buds indicated the late flowering stage. D. Sampling methodology for leaf pairs. Only leaves greater than 0.5 cm were classed as leaves, and the first leaf pair from the shoot apex was termed as leaf pair 1. Alternating leaf pairs were then harvested. Leaves with signs of senescence (indicated by red arrows) were discarded from the sampling.

To determine the set of leaf pairs which would show the widest range in essential oil profiles, leaf pairs labelled 1 - 4 from plants at the three developmental stages were harvested as outlined in Figure 5.2 D. The leaf pairs were subsequently extracted for their essential oil, and GCMS analysis was performed to find the leaf pairs with the most distinct oil profile from each other based on the most abundant monoterpenes menthone and menthol (Figure 5.3).

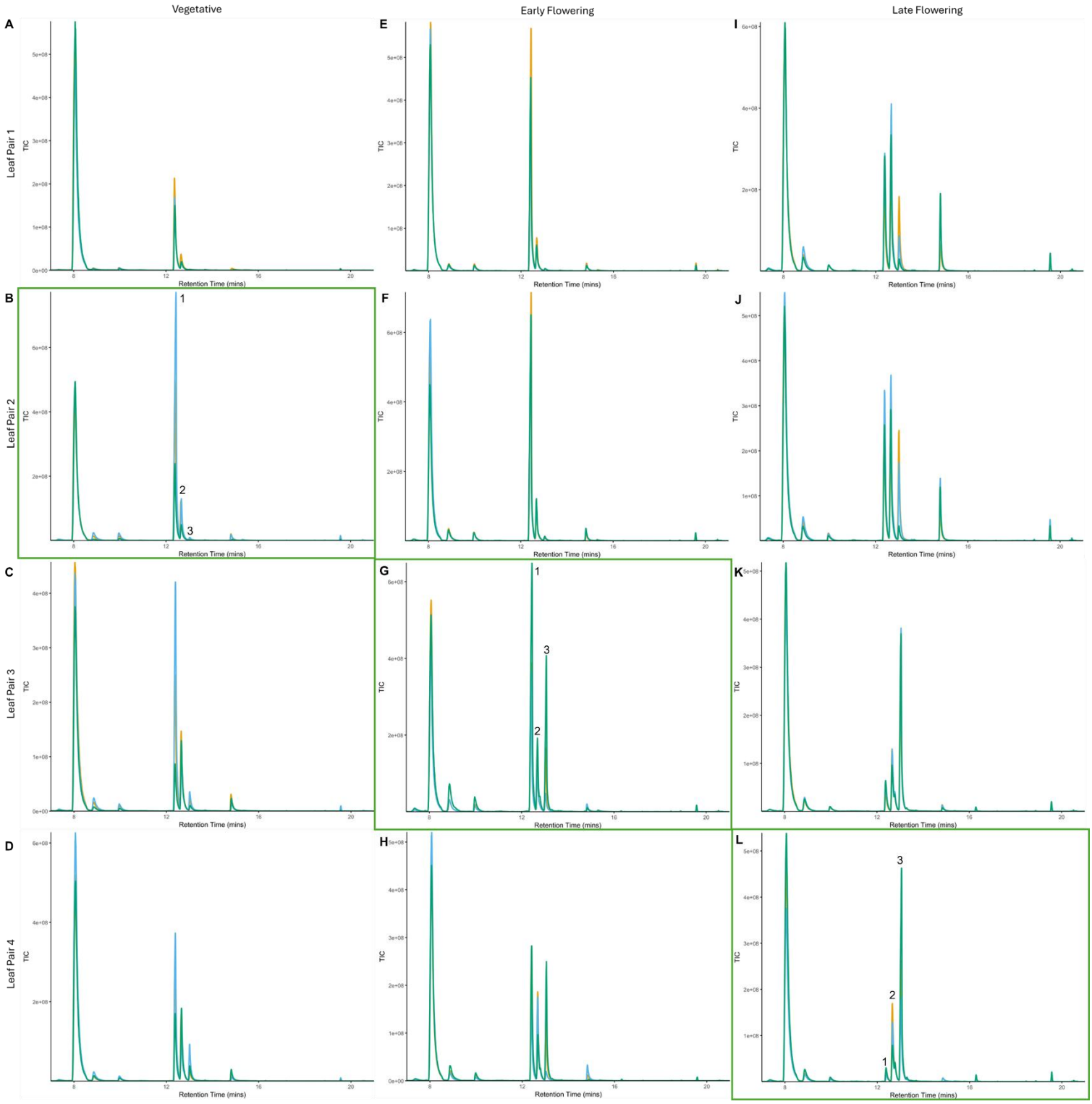

Figure 5.3. GCMS analysis of essential oil from all leaf pairs from all developmental stages of Black Mitcham. A-D: Vegetative samples leaf pair 1 - 4, E-H: Early Flowering samples leaf pair 1 - 4. I-L: Late Flowering samples leaf pair 1 - 4. The x-axis represents the retention time in minutes. The y-axis represents the total ion count (TIC). Peaks were deconvoluted by AMDIS, and identified by NIST (2014). Where available, mass spectra of NIST identified peaks were compared against authentic standards. Three representative replicates are plotted on the GCMS chromatograms and are distinguished by different colours as indicated in the figure. Green boxes highlight leaf pairs that were taken forward for further analysis, and are fully annotated in Figure 5.4. The main peaks are labelled as 1 = menthone, 2= menthofuran, 3 = menthol.

In leaf pairs from the vegetative stage plants (Figure 5.3 A – D), menthone is the major component in all leaf pairs, with increasing amounts of menthofuran detected in leaf pairs 3 to 4. Trace amounts of menthol can also be detected in vegetative stage plants leaf pair 4 (Figure 5.3 D). In leaf pairs from the early flowering stage plants, menthone remains abundant, but menthofuran and menthol are detected in greater abundance in leaf pairs 3 and 4 (Figure 5.3 E – H). In late flowering stage plants, menthone, menthofuran and menthol are relatively similar in abundance in leaf pairs 1 – 2 (Figure 5.3 I – J). In leaf pairs 3 – 4, menthol becomes more prominent in relation to menthone and menthofuran. From these leaf pairs, leaf pair 2 was chosen to represent the “Vegetative” stage, leaf pair 3 represented the “Early Flowering” stage, and leaf pair 4 represented the “Late Flowering” stage. The GCMS analysis of the essential oil components of the chosen samples are shown in Figure 5.4.

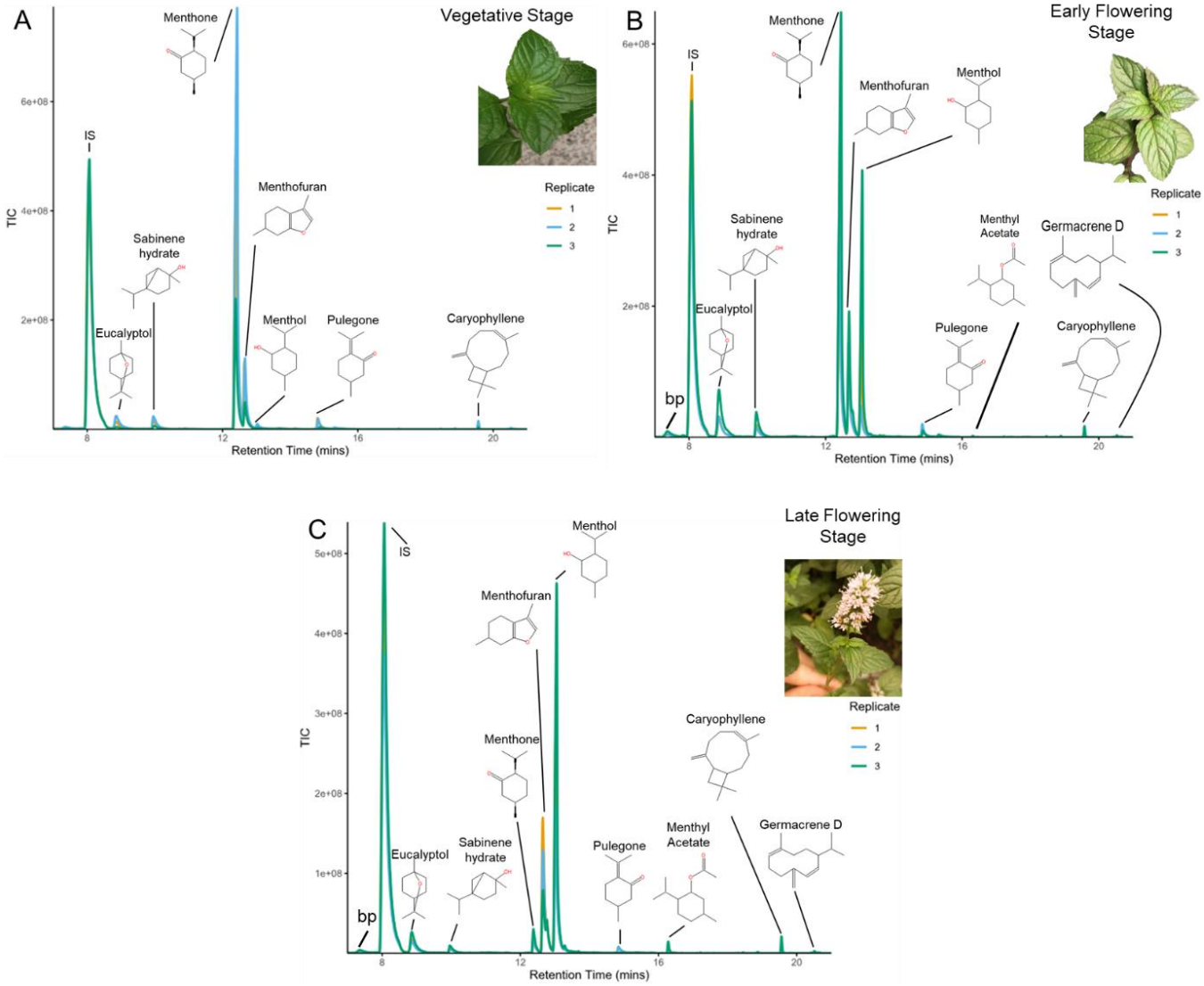

Figure 5.4. GCMS analysis of essential oil components from Black Mitcham leaves at three different developmental stages. A. Vegetative stage samples. B. Early flowering stage samples. C. Late flowering stage samples. The x-axis represents the retention time in minutes. The y-axis represents the total ion count (TIC). Peaks are annotated by the name, chemical structure and highlighted by a black line pointing towards the peak. Bp = beta-pinene. IS = Internal standard, Decane. Peaks were deconvoluted by AMDIS, and identified by NIST (2014). Where available, mass spectra of NIST identified peaks were compared against authentic standards. Three representative replicates are plotted on the GCMS chromatograms, labelled as 1, 2 and 3, and are distinguished by different colours as indicated in the figure.

The main components of Black Mitcham essential oil are menthone, menthol and menthofuran, whilst minor components include eucalyptol, limonene, pulegone, sabinene, caryophyllene, germacrene D and menthyl acetate (Gershenzon et al. 2000; Hudz et al. 2023). In the Vegetative stage samples, large peaks for menthone and menthofuran were detected, whilst minor peaks for eucalyptol, sabinene hydrate, menthol, pulegone and caryophyllene were present (Figure 5.4 A). It should

be noted that AMDIS detected the presence of limonene co-eluting at a similar retention time to eucalyptol, but as eucalyptol was detected as the main component of the GCMS peak, the peak was annotated as solely eucalyptol. In Early flowering stage samples, large peaks were detected for menthone, menthofuran and menthol, whilst minor peaks for eucalyptol, sabinene hydrate, beta-pinene, pulegone, caryophyllene, menthyl acetate and germacrene D were present (Figure 5.4 B). In Late flowering stage samples, large peaks for menthofuran and menthol were detected, whilst minor peaks for eucalyptol, sabinene hydrate, beta-pinene, menthone, pulegone, caryophyllene, menthyl acetate and germacrene D were detected (Figure 5.4 C). The results of this qualitative GCMS analysis indicated that the components detected in the oil profile of Black Mitcham at different developmental stages in this study were in-line with what has typically been reported in the literature. However, as the overall aim of this study was to correlate changes in oil profiles with changes in gene expression, it was important to determine if the levels of individual components of the essential oil was different between developmental stages. This was determined semi-quantitatively by measuring the relative abundance of the essential oil components across the developmental stages. The relative abundance of the main essential oil components is outlined in Figure 5.5.

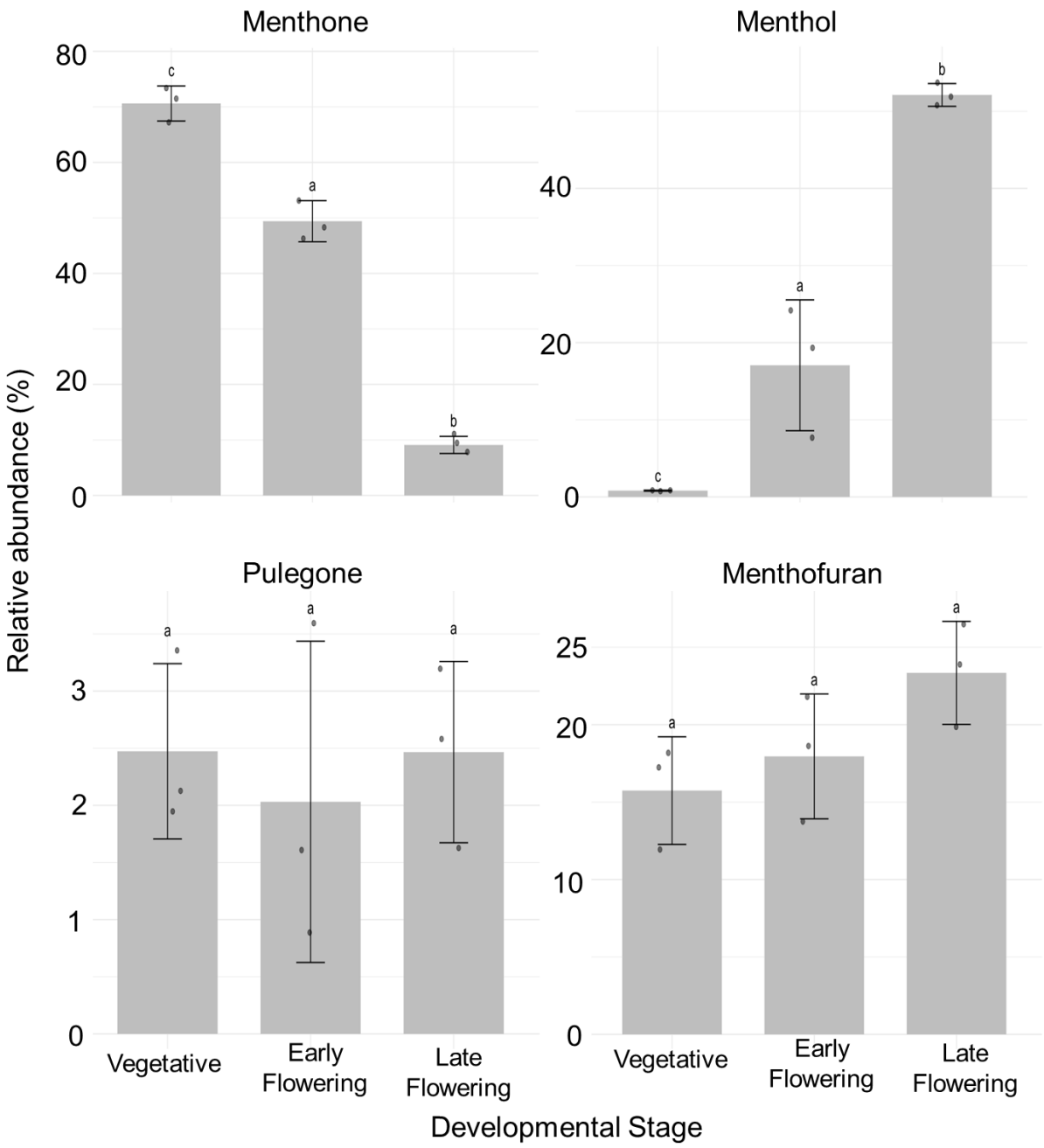

Figure 5.5. Relative abundance of menthone, menthol, pulegone and menthofuran in Black Mitcham at Vegetative, Early Flowering and Late Flowering stages. The x-axis shows the three developmental stages, and the y-axis shows the relative abundance of each compound, expressed as a percentage. Bars represent the mean of three biological replicates, and error bars indicate the standard deviation. Statistically significant differences among developmental stages were assessed using one-way ANOVA followed by Tukey's Honestly Significant Difference (HSD) post-hoc test. Different letters above the bars indicate significant differences ($p < 0.05$).

There is a trend of a decrease in the relative abundance of menthone from Vegetative, Early flowering and Late flowering, which is also statistically significant ($p < 0.05$) between the samples (Figure 5.5). Conversely, there is a trend of an increase in the relative abundance of menthol from Vegetative, Early flowering and Late flowering, which is also statistically significant ($p < 0.05$) between the samples (Figure 5.5). For pulegone and menthofuran, there appears to be no significant changes in relative abundance between the different developmental stages. Overall, in terms of the main MBP components, there is a trend of decreasing menthone and increasing menthol in the essential oil profile of Black Mitcham leaves as the leaves get older. This indicates that the samples used in this study reflect the predicted change in oil profiles as the leaves progress through different developmental stages. The balanced ratio of menthone and menthol in Early flowering samples also indicate that this stage represents a transitionary stage between Vegetative and Late flowering. The other detected oil components were also semi-quantified, as shown in Figure 5.6.

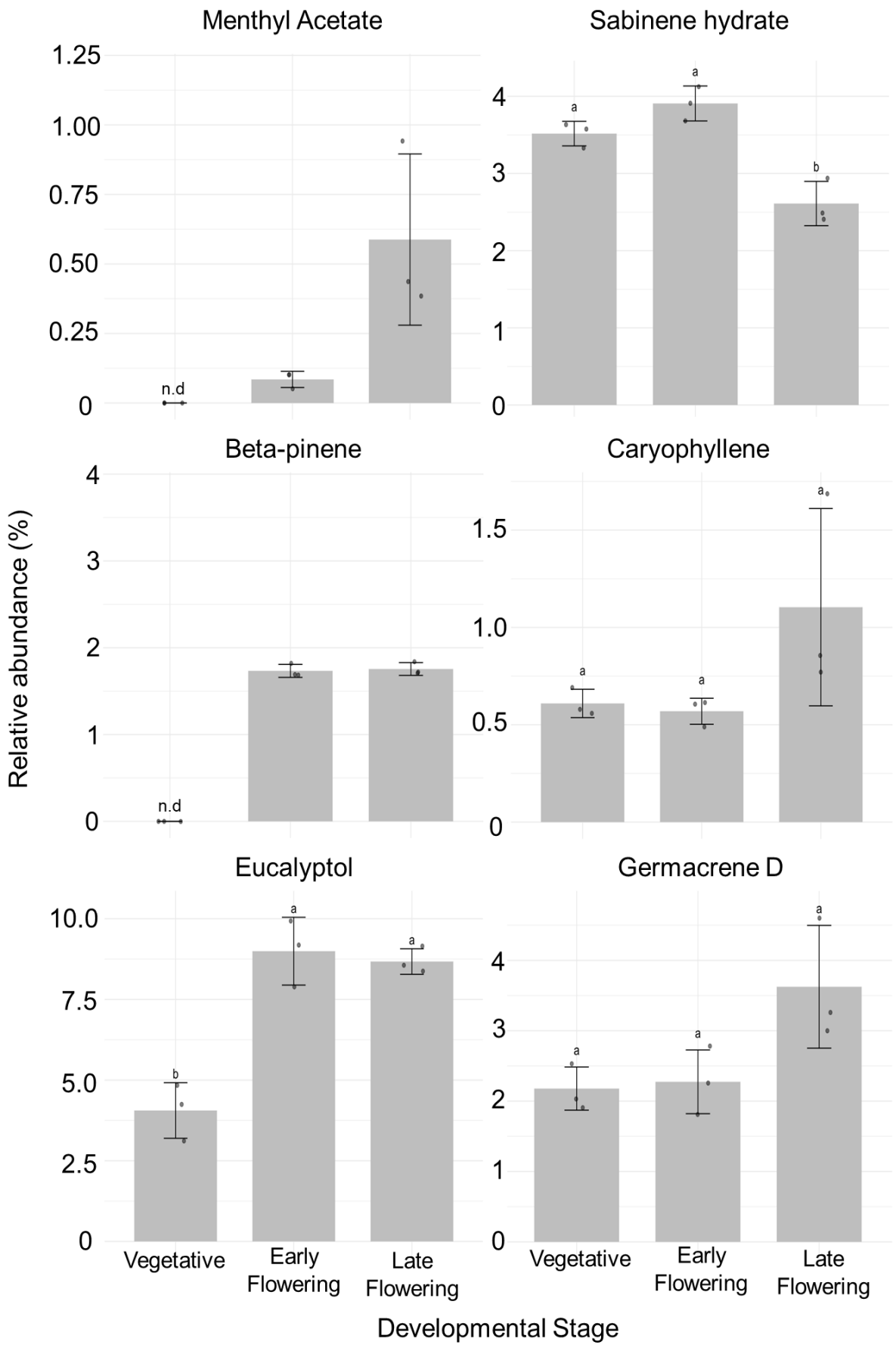
Menthyl Acetate
Sabinene hydrate
Beta-pinene
Caryophyllene
Eucalyptol
Germacrene D
Relative abundance (%)
n.d
Vegetative
Early Flowering
Late Flowering
Developmental Stage

Figure 5.6. Relative abundance of menthyl acetate, sabinene hydrate, beta-pinene, in Black Mitcham at Vegetative, Early Flowering and Late Flowering stages. The x-axis shows the three developmental stages, and the y-axis shows the relative abundance of each compound, expressed as a percentage. Bars represent the mean of three biological replicates, and error bars indicate the standard deviation. Where the compound was detected in all three developmental stages, statistically significant differences among developmental stages were assessed using one-way ANOVA followed by Tukey's Honestly Significant Difference (HSD) post-hoc test. Different letters above the bars indicate significant differences ($p < 0.05$). n.d = not detected.

Sabinene-hydrate showed a decrease in relative abundance in the Late flowering stage compared to Vegetative and Early flowering stage, which was statistically significant ($p < 0.05$) (Figure 5.6). Eucalyptol showed a decrease in relative abundance at the Vegetative stage when compared to both Early and Late flowering stages, which was also statistically significant ($p < 0.05$) (Figure 5.6). Both germacrene D and caryophyllene showed no changes in relative abundance between the different developmental stages (Figure 5.6). Both menthyl acetate and beta-pinene were only detectable in the Early and Late flowering stages (Figure 5.6). The presence of menthyl acetate in only the Early and Late flowering stages indicate that the leaf samples are of sufficient maturity difference compared to the vegetative stages, as menthyl acetate is thought to only be present in older leaves and after flowering has occurred (Croteau and Hooper 1978).

Taken together, based on the essential oil profile analysis, the Vegetative and Late flowering samples represent the greatest difference in essential oil profiles, representing "young" and "mature" essential oil profiles. The Early flowering samples represent a "transitionary" essential oil profile, which reflects the changes in oil profiles at the shift from a vegetative state to a flowering state. With the essential oil profile changes determined by GCMS, the next step was to determine if extraction of RNA was feasible, particularly in the older leaf pairs with higher levels of secondary metabolites, phenolics and polysaccharides.

5.2.2 RNA extraction troubleshooting

As Black Mitcham leaf tissue contains a high level of secondary metabolites and phenolics which can interfere with the RNA extraction process (Ghawana et al. 2011; Afkar 2023), a variety of RNA extraction methods were tested. The most promising RNA extraction was the use of the Qiagen RNeasy plant mini kit combined with the RLC buffer (information on the buffer is not available as public information). This

method was used to extract RNA from the samples that were chemotyped in section 5.2.1 (Figure 5.7).

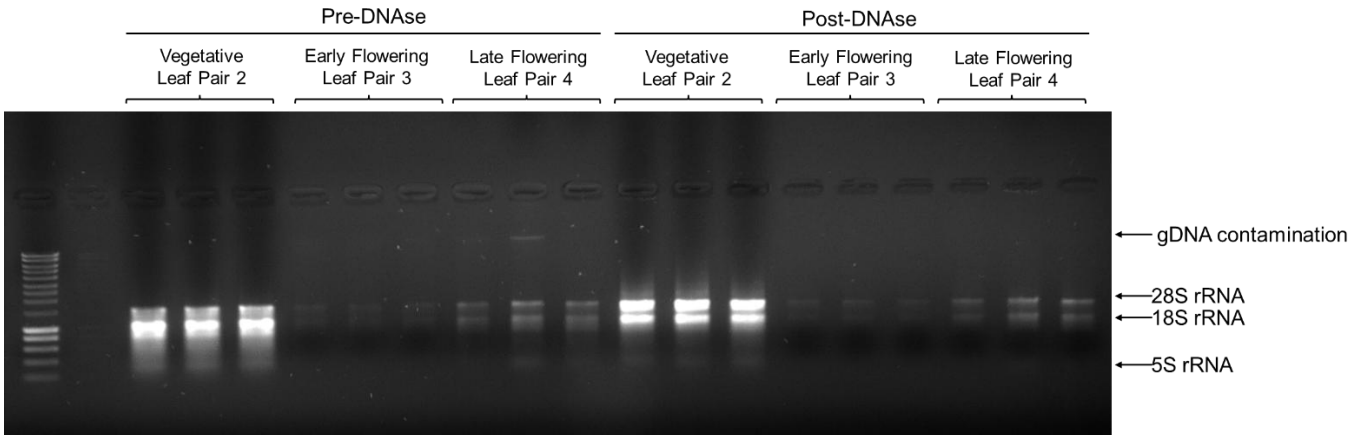

Figure 5.7 RNA extraction of samples from section 5.2.1. Vegetative, Early flowering and Late flowering samples are shown before and after DNAse treatment. Bands for 28S and 18S rRNA are present in all samples. The DNA ladder used is Eurogentec Smartladder.

Use of the Qiagen RNeasy plant mini kit was effective in extracting RNA from the vegetative, early flowering and late flowering leaf samples (Figure 5.7). Overall, this RNA extraction method was optimal for plant tissue samples with high levels of secondary metabolites and phenolics such as Black Mitcham. The extracted RNA was of sufficient quality to proceed to cDNA library preparation and sequencing, which was performed by the Cardiff University Genomics Hub. The resulting sequencing data comprised of three biological replicates for each developmental stage, for a total of 9 samples was then subjected to downstream quality control processes.

5.2.3 Quality control of RNA sequencing data

Raw sequencing reads were pre-processed by fastp to filter low quality reads, remove adaptors and correct erroneous bases (Chen et al. 2018). The results were summarised by MultiQC (Ewels et al. 2016). Summary statistics of sequencing reads before and after pre-processing are shown in Table 5.1.

Table 5.1. MultiQC report showing read statistics before and after fastp. R = Replicate. PE = Paired End. % Dups = Percentage of duplicate reads. % GC = Percentage of guanine-cytosine bases. M Seqs = Number of sequencing reads in millions.

	Before fastp			After fastp		
Sample Name	**% Dups**	**% GC**	**M Seqs**	**% Dups**	**% GC**	**M Seqs**
Vegetative R1 PE1	69.0%	50%	65.6	69.0%	50%	65.0
Vegetative R1 PE2	71.0%	50%	65.6	71.2%	50%	65.0
Vegetative R2 PE1	67.7%	50%	61.5	67.6%	50%	61.0
Vegetative R2 PE2	69.8%	50%	61.5	69.9%	50%	61.0
Vegetative R3 PE1	68.6%	50%	74.6	68.6%	50%	73.9
Vegetative R3 PE2	70.3%	50%	74.6	70.5%	50%	73.9
Early Flowering R1 PE1	58.0%	48%	67.9	57.9%	47%	67.4
Early Flowering R1 PE2	60.4%	48%	67.9	60.4%	47%	67.4
Early Flowering R2 PE1	60.9%	47%	71.8	61.0%	47%	71.2
Early Flowering R2 PE2	63.5%	48%	71.8	63.8%	47%	71.2
Early Flowering R3 PE1	60.0%	47%	77.8	60.0%	47%	77.1
Early Flowering R3 PE2	62.9%	48%	77.8	63.0%	47%	77.1
Late Flowering R1 PE1	62.5%	47%	71.9	62.4%	47%	71.4
Late Flowering R1 PE2	65.2%	47%	71.9	65.2%	47%	71.4
Late Flowering R2 PE1	64.1%	48%	65.8	64.1%	47%	65.3
Late Flowering R2 PE2	66.7%	48%	65.8	66.8%	48%	65.3
Late Flowering R3 PE1	59.0%	48%	59.1	58.9%	47%	58.6
Late Flowering R3 PE2	62.4%	48%	59.1	62.4%	47%	58.6

In general, there is a high level of sequence duplication (~60 - 70% duplicates) across all samples, which is expected in transcriptomic analyses. The GC content falls between ~47-50%, which is similar to the average range reported for *Mentha* species (López-Hernández and Cortés 2022). There is a slight drop in read counts after trimming (eg. 65.6 M Seqs to 65.0 M Seqs), indicative of the removal of some low quality reads (Table 5.1). In general, these statistics show that the data is of good quality and with sufficient reads to ensure good coverage of the whole transcriptome. Following on from this, the sequence reads were aligned against the Black Mitcham genome (Talbot et al. 2024), using the STAR aligner (Dobin et al. 2013). Key mapping statistics of the alignment are summarised in Table 5.2.

Table 5.2. Summary of STAR alignment statistics for RNA-seq samples. Each replicate corresponds to one paired-end library. The table shows the number of input reads, average read length, number and percentage of uniquely mapped reads, and the average length of mapped reads. R = Replicate

Sample	Number of input reads	Average input read length	Uniquely mapped reads number	Uniquely mapped reads (%)	Average mapped length
Vegetative R 1	65,036,849	273	45,056,074	69.28%	275.91
Vegetative R 2	60,990,693	270	42,218,442	69.22%	273.41
Vegetative R 3	73,882,111	272	52,100,396	70.52%	275.39
Early Flowering R 1	67,382,922	270	48,012,065	71.25%	273.16
Early Flowering R 2	71,235,809	276	51,063,591	71.68%	278.5
Early Flowering R 3	77,144,555	274	55,433,759	71.86%	276.9
Late Flowering R 1	71,351,832	270	50,622,971	70.95%	273.98
Late Flowering R 2	65,269,273	271	46,333,285	70.99%	274.31
Late Flowering R 3	58,600,628	272	41,629,971	71.04%	275.14

RNA-seq libraries from vegetative, early flowering, and late flowering stages were sequenced to a depth of ~59-77 million reads per sample, with an average read length of ~270 bp. Sequencing depth reflects the total number of reads generated, and higher depths improve sensitivity for detecting low abundance transcripts and increase the accuracy of expression quantification. The chosen depth therefore provided sufficient coverage to enable robust comparisons of transcriptional profiles across developmental stages, including the detection of transcripts expressed at low levels or restricted to a single stage (Patterson et al. 2019; Illumina 2024).

The average read length of ~270 bp further contributed to data quality by increasing the proportion of uniquely mapped reads, particularly in a plant genome where closely related paralogs are common. Longer reads also facilitated the identification of splice junctions and alternative isoforms, features known to be developmentally regulated (Chhangawala et al. 2015). With sequencing depths exceeding 55 million reads, previous studies have shown that most splice junctions can be reliably captured indicating that the dataset generated here provided comprehensive transcriptome coverage (Williams et al. 2014).

After alignment with STAR, between 69-72% of reads mapped uniquely to the reference Black Mitcham genome, corresponding to ~42-55 million uniquely mapped reads per sample. The average mapped read length was ~274 bp across all samples. These mapping rates are consistent across biological replicates and reflect good-quality RNA-seq data suitable for downstream differential expression analysis. Finally, the markduplicates function of the Picard tool was used to identify duplicate reads in the RNA-seq samples, as shown in Table 5.3.

Table 5.3. Duplicate read counts and percentages identified by Picard MarkDuplicates for each RNA-seq library. Values represent the number of duplicate reads and the corresponding percentage of total mapped reads. R = replicate

Sample	Duplicates
Vegetative R 1	38,970,825 (30.7386%)
Vegetative R 2	35,668,268 (29.9036%)
Vegetative R 3	47,592,492 (32.8998%)
Early Flowering R 1	23,360,582 (17.565%)
Early Flowering R 2	30,102,782 (21.4727%)
Early Flowering R 3	30,593,522 (20.1077%)
Late Flowering R 1	32,306,883 (22.8773%)
Late Flowering R 2	32,053,098 (24.8511%)
Late Flowering R 3	23,236,112 (20.0484%)

Duplicate read levels varied across developmental stages. Vegetative libraries showed the highest duplication rates (~30-33%), while early and late flowering libraries had lower duplication (~17-25%). Overall, the duplication rates are at the lower end of what is typically reported for RNA-seq experiments (~30-90%), and therefore the sequencing reads are of high quality and will allow for reliable quantification of gene expression in downstream analysis (Ji and Sadreyev 2018). Prior to differential expression analysis using DESeq2 the overall similarity between biological replicates and the separation of samples by developmental stage was assessed (Love et al. 2014). Clustering patterns between replicates were determined by sample-to-sample distances, calculated using variance stabilised counts (Figure 5.8 A).

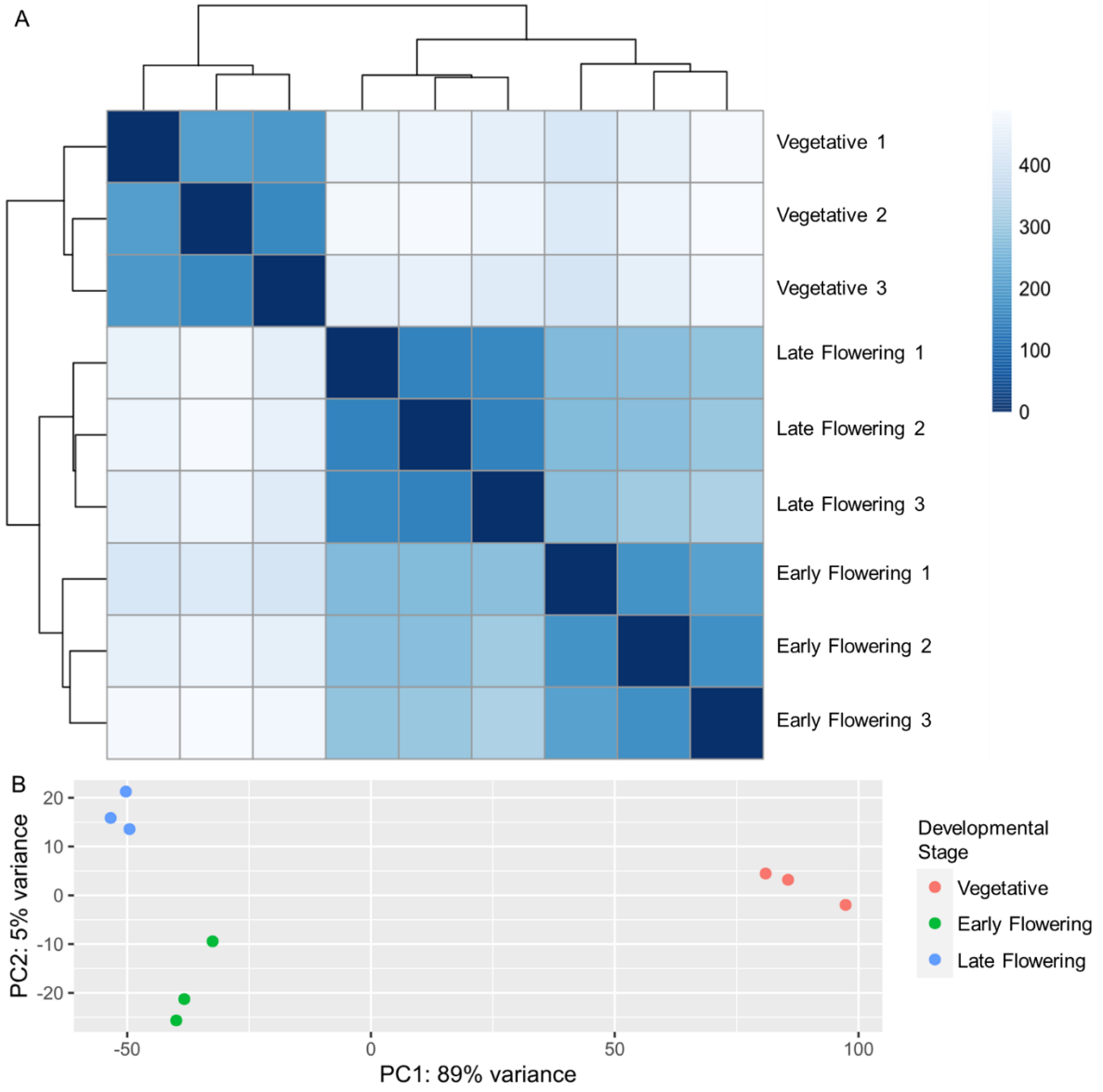

Figure 5.8. A. Heatmap of sample-to-sample distances based on variance-stabilized counts, showing clustering of biological replicates within developmental stages of vegetative, early flowering and late flowering. B. Principal component analysis (PCA) plot of variance-stabilized counts. The first principal component (x-axis) separates samples by developmental stage, while the second component (y-axis) captures residual variance between replicates.

The sample-to-sample distance heatmap indicated that the biological replicates clustered tightly together according to developmental stage. The vegetative samples clustered into their own distinct cluster, whilst the early and late flowering samples grouped into a larger cluster that contained a separate subcluster for each stage (Figure 5.8 A). In addition, principal component analysis (PCA) was conducted to reduce the dimensionality of the dataset and visualise the overall effect of experimental covariates and batch effects (Figure 5.8 B). The PCA plot showed that

the first principal component (PC1) separated samples according to developmental stage, accounting for the majority of variance in the dataset (89% variance), whilst the second principal component explained the residual variation between the replicates (5% variance) (Figure 5.8 B). Finally, outliers within each sample which may affect downstream analysis were checked by calculating the Cooks distance, which measures how much a single sample is influencing the fitted coefficients for a gene, and the value of Cooks distance represents the outlier count (Love et al. 2014). The Cooks distances were plotted as a boxplot of transformed counts, to visualise if there were large differences in Cooks distances between sample replicates (Figure 5.9).

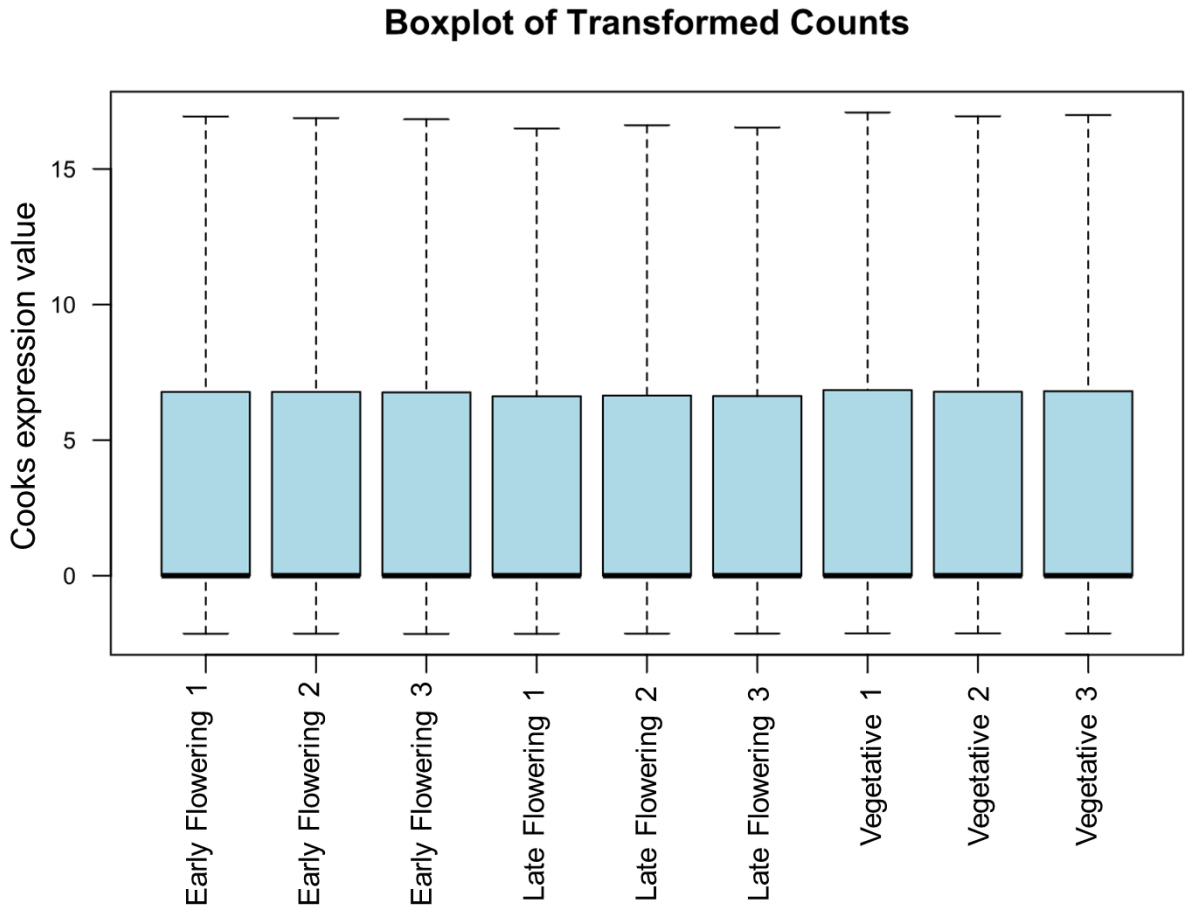

Figure 5.9 Cook's distance boxplot for RNA-seq samples. Boxplots show the distribution of Cook's distances across all genes for each sample, as estimated by DESeq2. Cook's distance reflects the influence of a sample on the fitted model for a given gene, with higher values indicating greater influence. The x-axis indicates the sample and replicate. The y-axis indicates the Cooks distance value

Cook's distance boxplots showed that all samples and replicates had highly similar distributions, with median values close to zero and the majority of data within the ~0-

7 range. A small number of outliers were observed (extending up to ~17), consistent with occasional gene-level influences, but no single replicate exerted disproportionate influence on the model (Figure 5.9). Taken together, the QC and data quality assessment showed that the RNA-seq data was fit for purpose of downstream differential gene expression analysis.

5.2.4 Exploration of the Black Mitcham transcriptome across the different developmental stages

The Black Mitcham structural genome annotation describes a total of 247,493 protein coding genes in the genome (Talbot et al. 2024). A total of 54,446 DEGs (DEGs) were identified that showed a difference across all pairwise comparisons of the developmental stages after a cutoff of log2fc > 1 or <-1, and adjusted p-value (padj) < 0.05 was applied. Of the 54,446 DEGs, 52290 had a functional annotation attached after performing a BLASTx search against both the *A. thaliana* and *Lamiaceae* protein database, with a E-value cutoff of 1.0×10^{-5}. Comparing early flowering vs vegetative, 17978 genes were upregulated, whilst 21879 genes were downregulated (Figure 5.10 A).

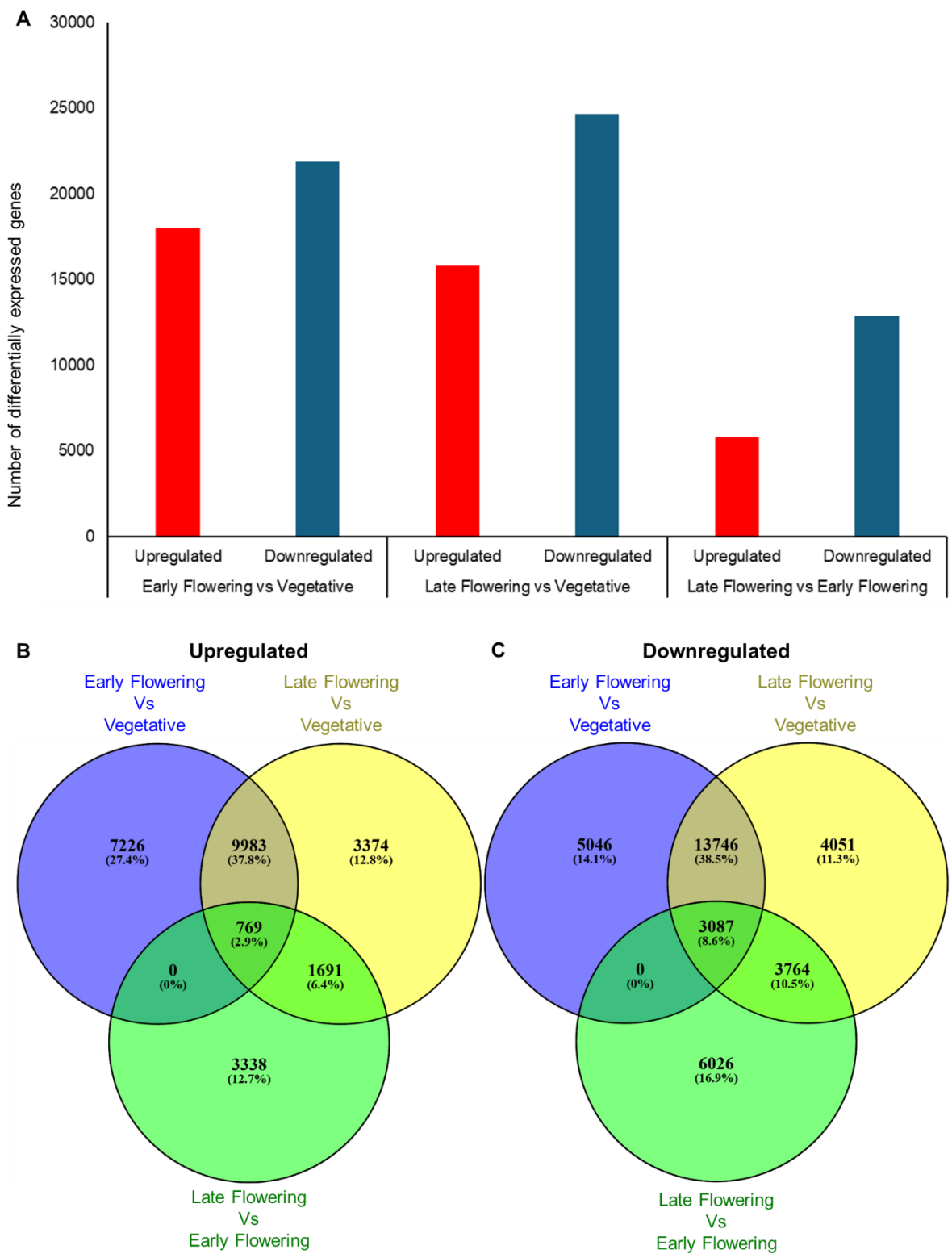

Figure 5.10. Summary of DEGs across all pairwise comparisons of developmental stage samples after cutoff values of log2fc > 1 and padj < 0.05 were applied. A. Bar graph showing a comparison of upregulated and downregulated genes between pairwise comparisons. X-axis shows the comparison type. Y-axis shows the number of DEGs (DEGs). B. Venn diagrams of upregulated and C. downregulated DEGs between all pairwise comparisons, highlighting shared DEGs that exist between comparisons.

In the late flowering vs vegetative comparison, 15817 genes were upregulated, whilst 24648 genes were downregulated (Figure 5.10 A). Comparing late flowering vs early flowering, 5798 genes were upregulated, whilst 12877 were downregulated (Figure 5.10 A).

Examination of the overlap in upregulated DEGs across the three developmental stage comparisons revealed both shared and stage-specific transcriptional responses (Figure 5.10 B). A total of 10,752 genes were upregulated in both the early flowering vs vegetative and late flowering vs vegetative contrasts, suggesting that many expression changes initiated during the transition to early flowering are maintained into late flowering. In contrast, 2,460 genes were commonly upregulated in the late flowering vs vegetative and late flowering vs early flowering comparisons, indicating transcriptional changes specific to the later stages of plant maturity. Interestingly, no DEGs were shared exclusively between the early vs. vegetative and late vs. early flowering comparisons, suggesting that most expression changes between the vegetative and early flowering stages are not preserved between early and late flowering. Only 769 genes were consistently upregulated across all three pairwise comparisons, representing a small core set of genes whose expression increases steadily throughout development.

Analysis of downregulated DEGs across the developmental stage comparisons revealed a similar pattern of overlap (Figure 5.10 C). A total of 16,833 genes were downregulated in both the early flowering vs vegetative and late flowering vs vegetative contrasts, indicating that many genes repressed during the transition from vegetative to early flowering remain suppressed in late flowering. In addition, 6,851 genes were downregulated in both the late flowering vs vegetative and late flowering vs early flowering comparisons, reflecting transcriptional repression that is more specific to the late stages of floral development. A total of 3,087 genes were consistently downregulated across all three comparisons, representing a core set of genes whose expression decreases progressively as development advances. As with the upregulated DEGs, no genes were exclusively shared between the early flowering vs vegetative and late flowering vs early flowering contrasts, suggesting that transcriptional changes distinguishing early from late flowering are largely distinct from those underpinning the initial vegetative to flowering transition.

The core set of 769 genes showed a consistent upregulation, and the core set of 3087 genes which showed a consistent downregulation (from vegetative, to early flowering, to late flowering) were further interrogated by gene ontology (GO) enrichment analysis (Figure 5.11).

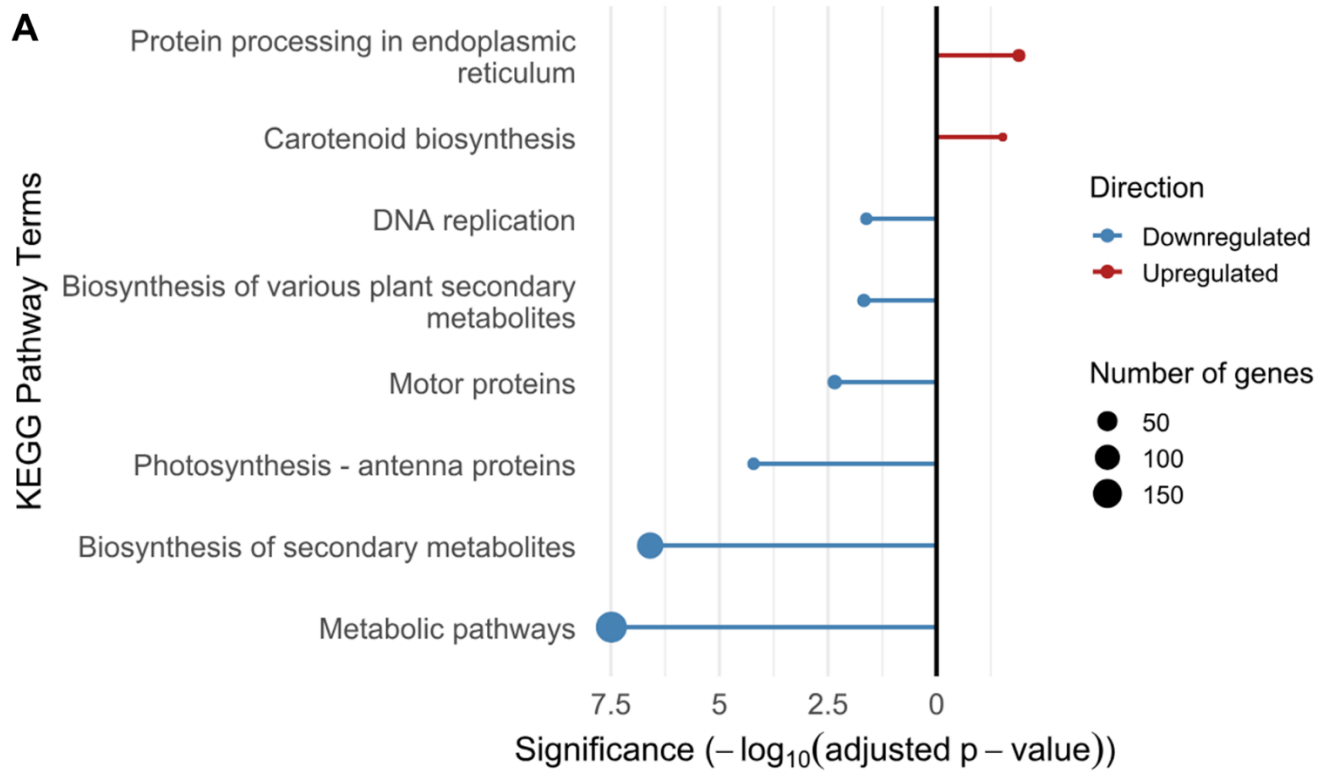
A
Protein processing in endoplasmic reticulum
Carotenoid biosynthesis
DNA replication
Biosynthesis of various plant secondary metabolites
Motor proteins
Photosynthesis - antenna proteins
Biosynthesis of secondary metabolites
Metabolic pathways
KEGG Pathway Terms
7.5
5
2.5
0
Significance (−log10(adjusted p−value))
Direction
Downregulated
Upregulated
Number of genes
50
100
150

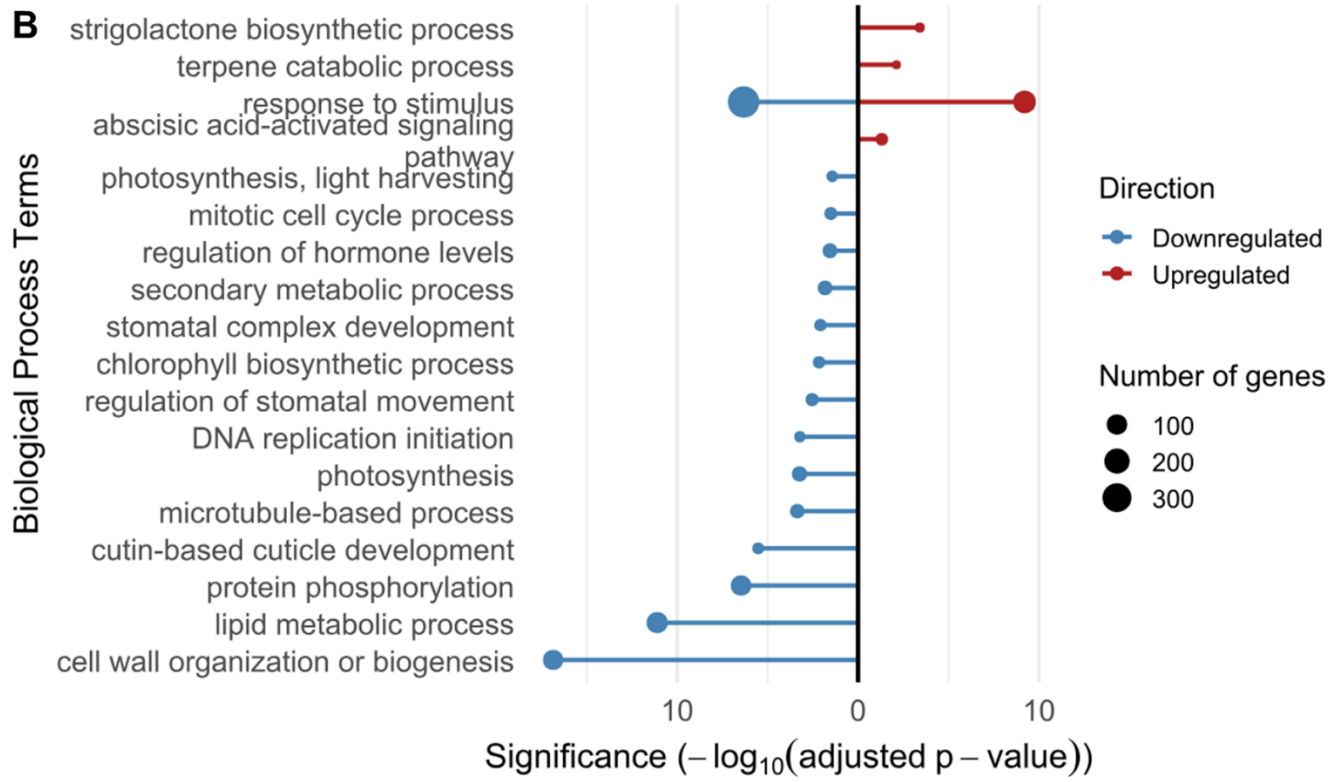
B
strigolactone biosynthetic process
terpene catabolic process
response to stimulus
abscisic acid-activated signaling pathway
photosynthesis, light harvesting
mitotic cell cycle process
regulation of hormone levels
secondary metabolic process
stomatal complex development
chlorophyll biosynthetic process
regulation of stomatal movement
DNA replication initiation
photosynthesis
microtubule-based process
cutin-based cuticle development
protein phosphorylation
lipid metabolic process
cell wall organization or biogenesis
Biological Process Terms
10
0
10
Significance (−log10(adjusted p−value))
Direction
Downregulated
Upregulated
Number of genes
100
200
300

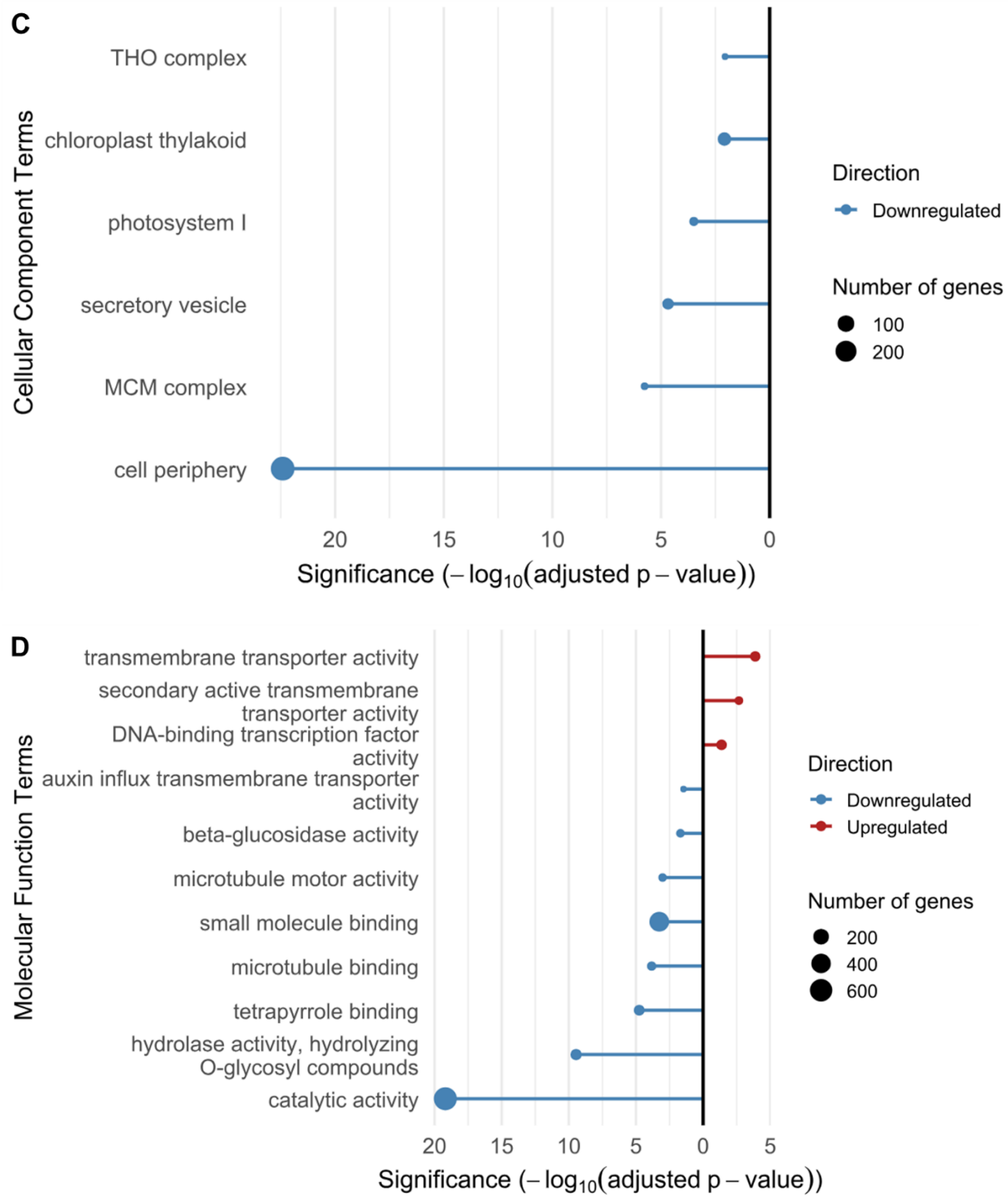

Figure 5.11. Gene ontology enrichment analysis for the DEGs which were showed consistent upregulation or downregulation in early flowering vs vegetative, late flowering vs vegetative and late flowering vs early flowering, arranged by terms from the: A. KEGG pathway. B. Biological process. C. Cellular components. D. Molecular function. Upregulated genes are shown in red. Downregulated genes are shown in blue. The size of the circle corresponds to the number of genes with the respective term. X-axis shows the significance. Y -axis shows the specific gene ontology terms.

The core sets of consistently upregulated or downregulated genes are expected to contain TFs with at least two distinct functional roles. One group likely comprises TFs that primarily regulate developmental programs, whilst a second group likely consist of TFs which more directly regulate the MBP. These groups of TFs could be separated by integrating TF expression profiles with MBP gene co-expression and metabolite measurements, allowing identification of TFs whose activity is tightly coupled to the MBP flux rather than general developmental programs (Kajla et al. 2023; Zhang et al. 2023a). Moreover, the coordinated downregulation of subsets pathway process (terpene, strigolactone, lipid etc.) is consistent with possible metabolic feedback inhibition, whereby accumulation of pathway intermediates or end products feeds back to down regulate biosynthetic genes and limit further production (Figure 5.11 B) (Li et al. 2025a).

DEGs which were consistently upregulated were associated with the carotenoid biosynthesis and protein processing in endoplasmic reticulum terms from the KEGG pathway (Figure 5.11 A). Downregulated DEGs include biosynthesis of secondary metabolites and metabolic pathways, which may represent the decrease in metabolic activity as a leaf ages and approaches senescence. Upregulated DEGs associated with biological process terms include strigolactone biosynthetic process, terpene catabolic process and abscisic acid-activated signalling pathway, whilst downregulated DEGs included terms such as cell wall organisation or biogenesis, and secondary metabolic process (Figure 5.11 B). There were no upregulated DEGs associated with cellular component terms, whilst a large number of downregulated genes were associated with cell periphery (Figure 5.11 C). Upregulated DEGs associated with molecular function terms included transmembrane transport activity and DNA binding transcription factor activity, whilst downregulated DEGs were primarily associated with catalytic activity (Figure 5.11 D). The above GO analysis revealed a variety of functions associated with core sets of DEGs which are either progressively upregulated or downregulated as the plant transitions from a vegetative state, to an early flowering state, to a late flowering state. Next, DEGs which were upregulated or downregulated in either the early flowering vs vegetative, late flowering vs vegetative, and late flowering vs early flowering were subject to GO analysis to explore their biological significance in each comparison.

When comparing early flowering vs vegetative DEGs, upregulated genes associated with the KEGG pathway terms include plant-pathogen interaction, MAPK signalling pathway – plant, and plant hormone signal transduction (Figure 5.12 A).

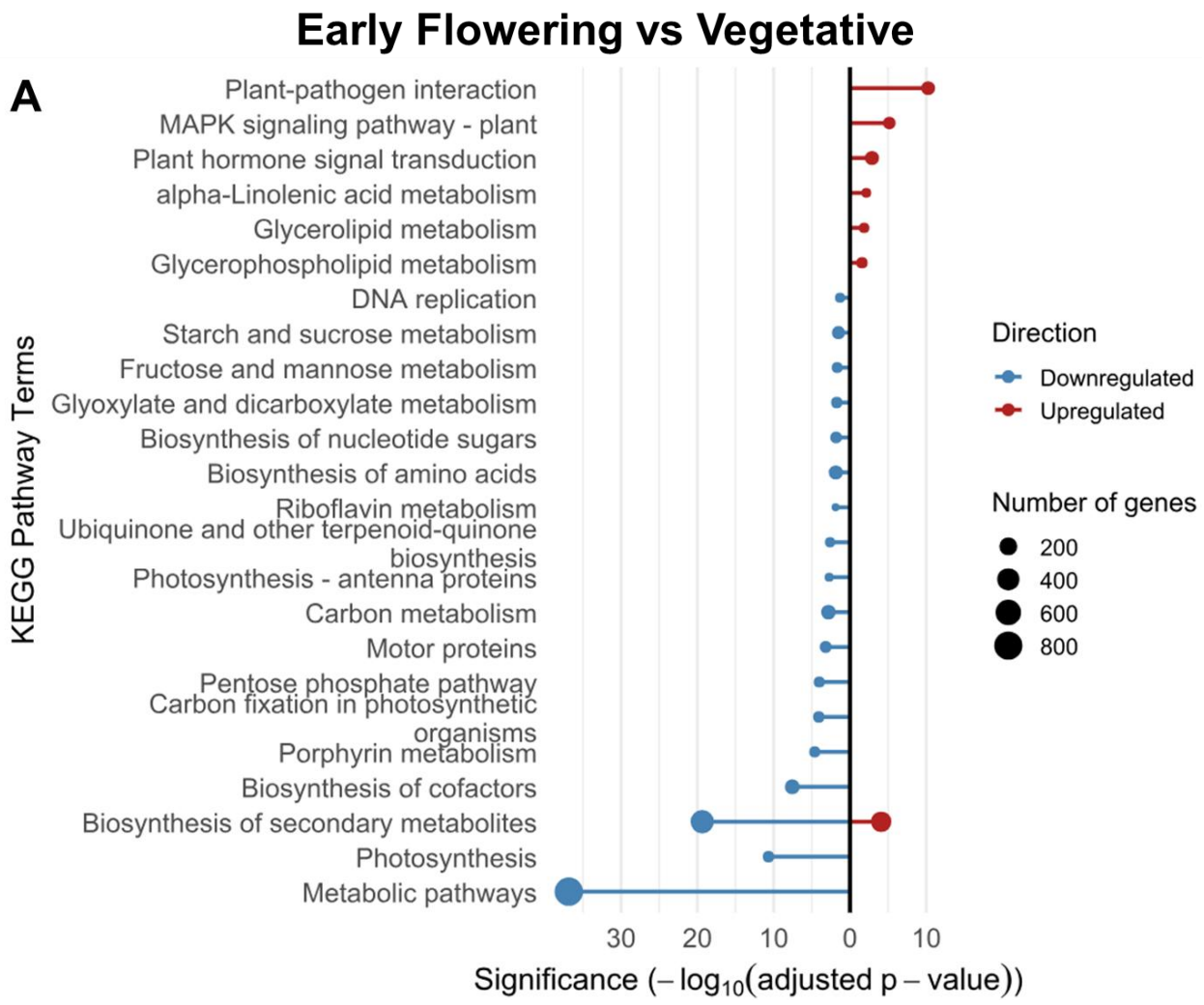
Early Flowering vs Vegetative
A
KEGG Pathway Terms
Plant-pathogen interaction
MAPK signaling pathway - plant
Plant hormone signal transduction
alpha-Linolenic acid metabolism
Glycerolipid metabolism
Glycerophospholipid metabolism
DNA replication
Starch and sucrose metabolism
Fructose and mannose metabolism
Glyoxylate and dicarboxylate metabolism
Biosynthesis of nucleotide sugars
Biosynthesis of amino acids
Riboflavin metabolism
Ubiquinone and other terpenoid-quinone biosynthesis
Photosynthesis - antenna proteins
Carbon metabolism
Motor proteins
Pentose phosphate pathway
Carbon fixation in photosynthetic organisms
Porphyrin metabolism
Biosynthesis of cofactors
Biosynthesis of secondary metabolites
Photosynthesis
Metabolic pathways
30
20
10
0
10
Significance (−log10(adjusted p−value))
Direction
Downregulated
Upregulated
Number of genes
200
400
600
800

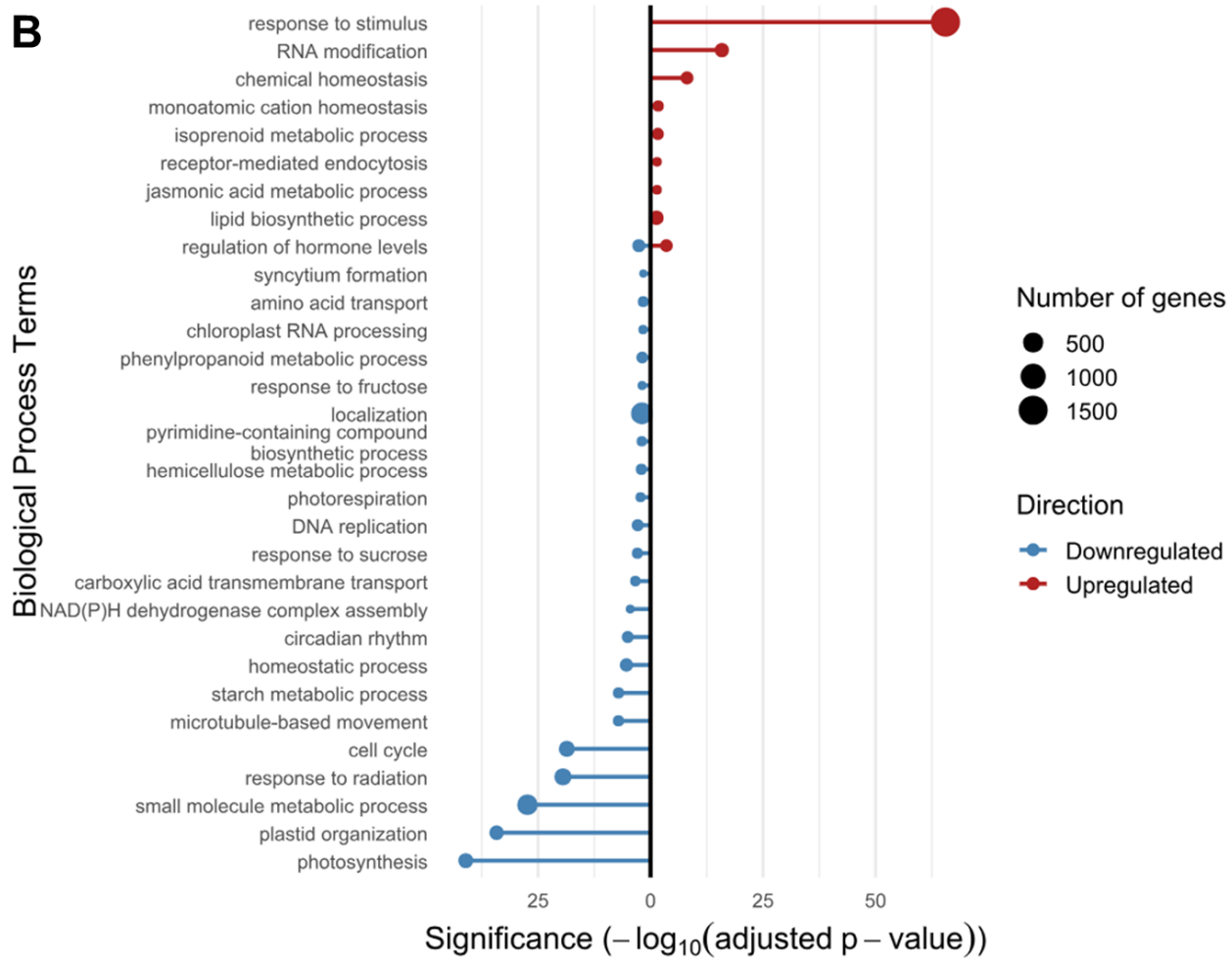
B
response to stimulus
RNA modification
chemical homeostasis
monoatomic cation homeostasis
isoprenoid metabolic process
receptor-mediated endocytosis
jasmonic acid metabolic process
lipid biosynthetic process
regulation of hormone levels
syncytium formation
amino acid transport
chloroplast RNA processing
phenylpropanoid metabolic process
response to fructose
localization
pyrimidine-containing compound biosynthetic process
hemicellulose metabolic process
photorespiration
DNA replication
response to sucrose
carboxylic acid transmembrane transport
NAD(P)H dehydrogenase complex assembly
circadian rhythm
homeostatic process
starch metabolic process
microtubule-based movement
cell cycle
response to radiation
small molecule metabolic process
plastid organization
photosynthesis
Biological Process Terms
25
0
25
50
Significance (−log10(adjusted p−value))
Number of genes
500
1000
1500
Direction
Downregulated
Upregulated

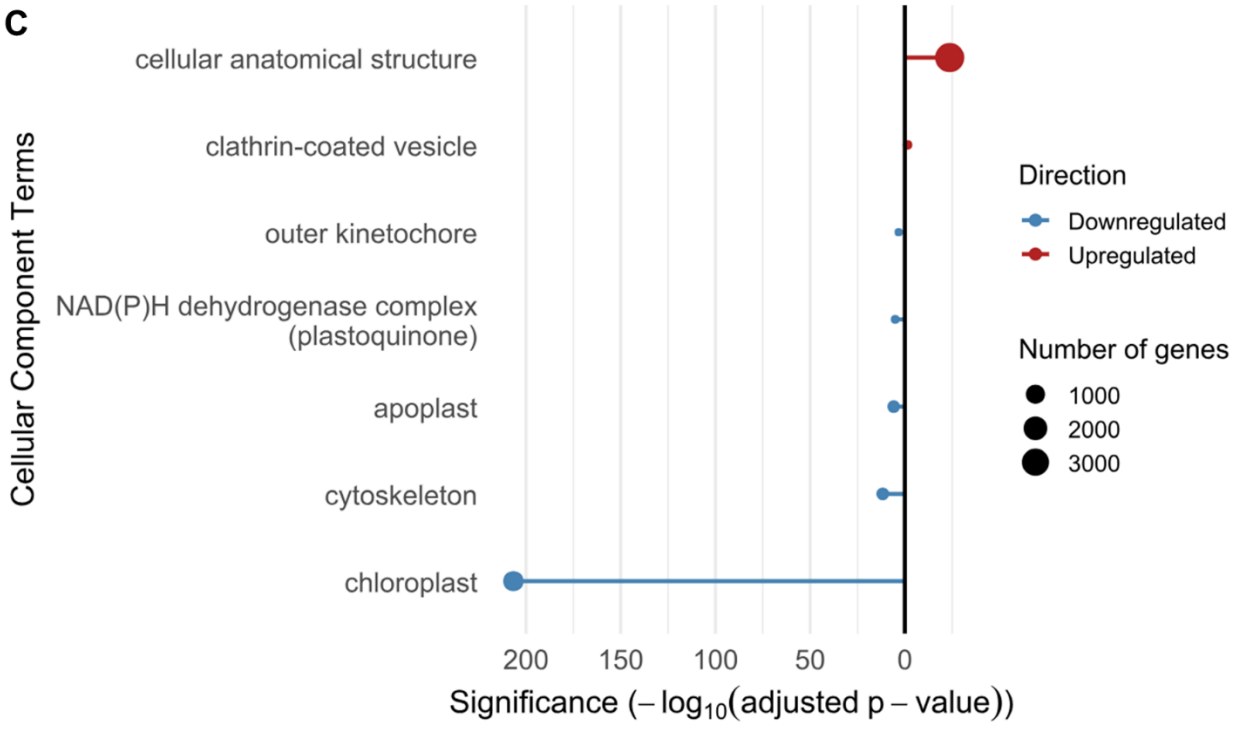
C
cellular anatomical structure
clathrin-coated vesicle
outer kinetochore
NAD(P)H dehydrogenase complex (plastoquinone)
apoplast
cytoskeleton
chloroplast
Cellular Component Terms
200
150
100
50
0
Significance (−log10(adjusted p−value))
Direction
Downregulated
Upregulated
Number of genes
1000
2000
3000

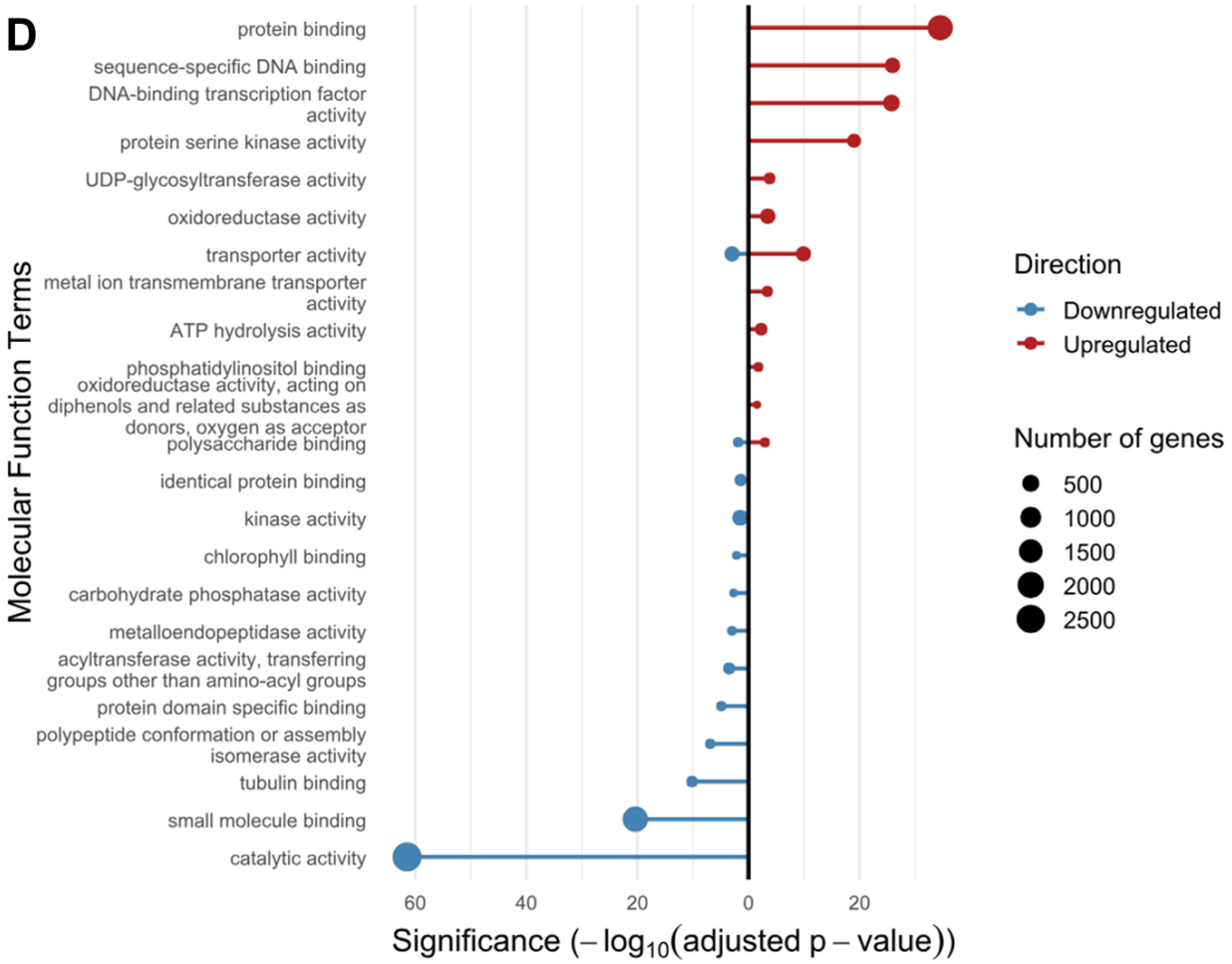

Figure 5.12. Gene ontology enrichment analysis for early flowering vs vegetative DEGs, arranged by terms from the: A. KEGG pathway. B. Biological process. C. Cellular components. D. Molecular function. Upregulated genes are shown in red. Downregulated genes are shown in blue. The size of the circle corresponds to the number of genes with the respective term. X-axis shows the significance. Y -axis shows the specific gene ontology terms.

KEGG terms associated with downregulated DEGs included metabolic pathways and biosynthesis of secondary metabolites (Figure 5.12 A). Biosynthesis of secondary metabolites was seen in both upregulated and downregulated DEGs, which may represent the change in MBP gene expression associated with a change in oil profile. For biological process, terms associated with upregulated DEGs included isoprenoid metabolic process and jasmonic acid metabolic process, whilst the top three terms associated with downregulated genes were photosynthesis, plastid organization and small molecule metabolic process (Figure 5.12 B). The top cellular components term for upregulated DEGs was cellular anatomical structure, and downregulated DEGs was chloroplast (Figure 5.12 C). For molecular function, the top 3 terms associated with upregulated DEGs were protein binding, sequence-

specific DNA binding and DNA-binding TF activity (Figure 5.12 D). The top three terms associated with downregulated DEGs were catalytic activity, small molecule binding and tubulin binding. The terms transporter activity and polysaccharide binding were shared between up and downregulated DEGs. The comparison of early flowering vs vegetative DEGs represents the transition from the leaves of plants in a vegetative state to an early flowering state, and the terms from the GO analysis may reflect those specific transcriptional changes.

In the late flowering vs vegetative comparison, upregulated genes associated with terms from the KEGG pathway included plant-pathogen interaction, ribosome biogenesis in eukaryotes, protein processing in endoplasmic reticulum and pyruvate metabolism (Figure 5.13 A).

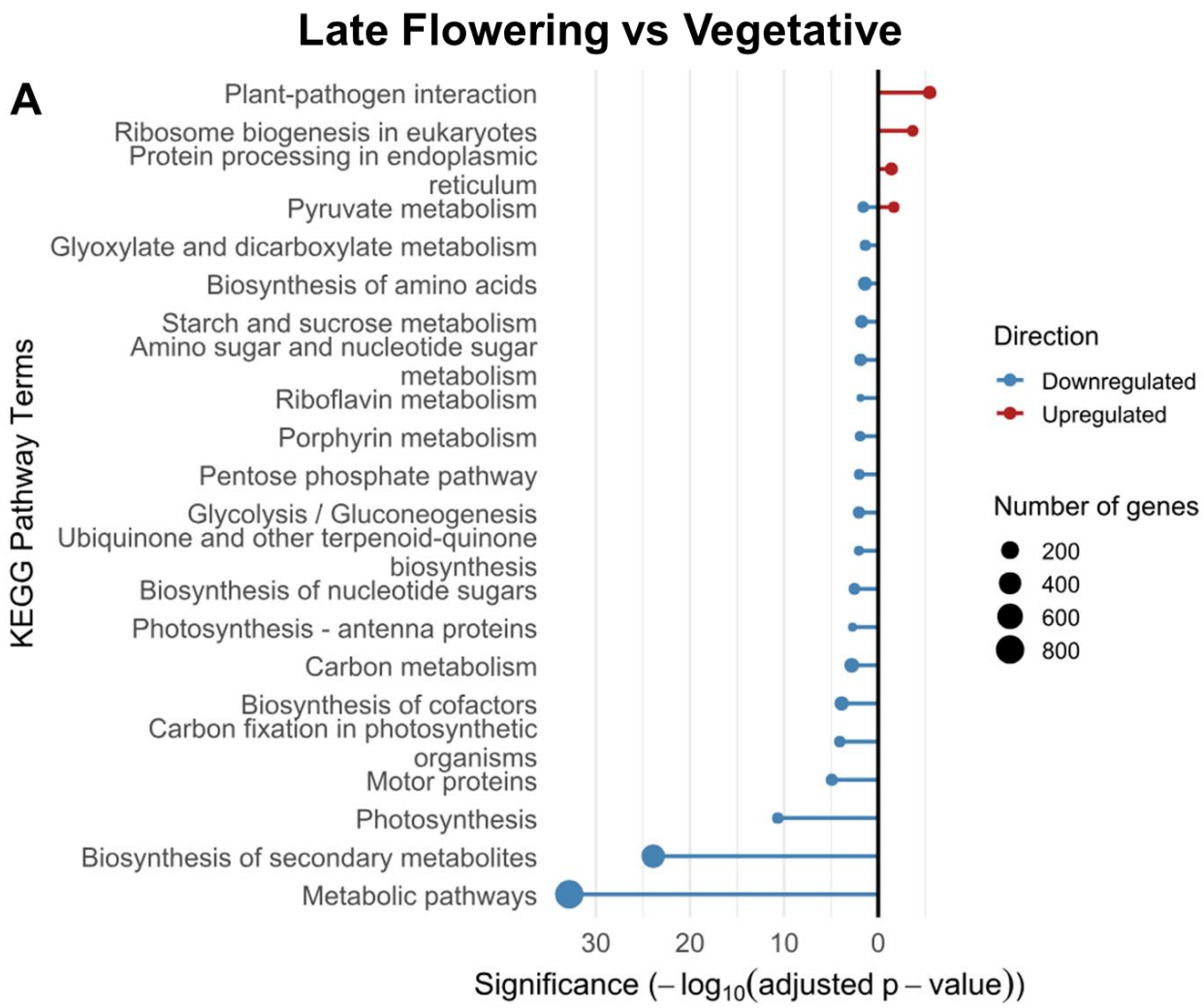
Late Flowering vs Vegetative
A
KEGG Pathway Terms
Plant-pathogen interaction
Ribosome biogenesis in eukaryotes
Protein processing in endoplasmic reticulum
Pyruvate metabolism
Glyoxylate and dicarboxylate metabolism
Biosynthesis of amino acids
Starch and sucrose metabolism
Amino sugar and nucleotide sugar metabolism
Riboflavin metabolism
Porphyrin metabolism
Pentose phosphate pathway
Glycolysis / Gluconeogenesis
Ubiquinone and other terpenoid-quinone biosynthesis
Biosynthesis of nucleotide sugars
Photosynthesis - antenna proteins
Carbon metabolism
Biosynthesis of cofactors
Carbon fixation in photosynthetic organisms
Motor proteins
Photosynthesis
Biosynthesis of secondary metabolites
Metabolic pathways
30
20
10
0
Significance (−log10(adjusted p−value))
Direction
Downregulated
Upregulated
Number of genes
200
400
600
800

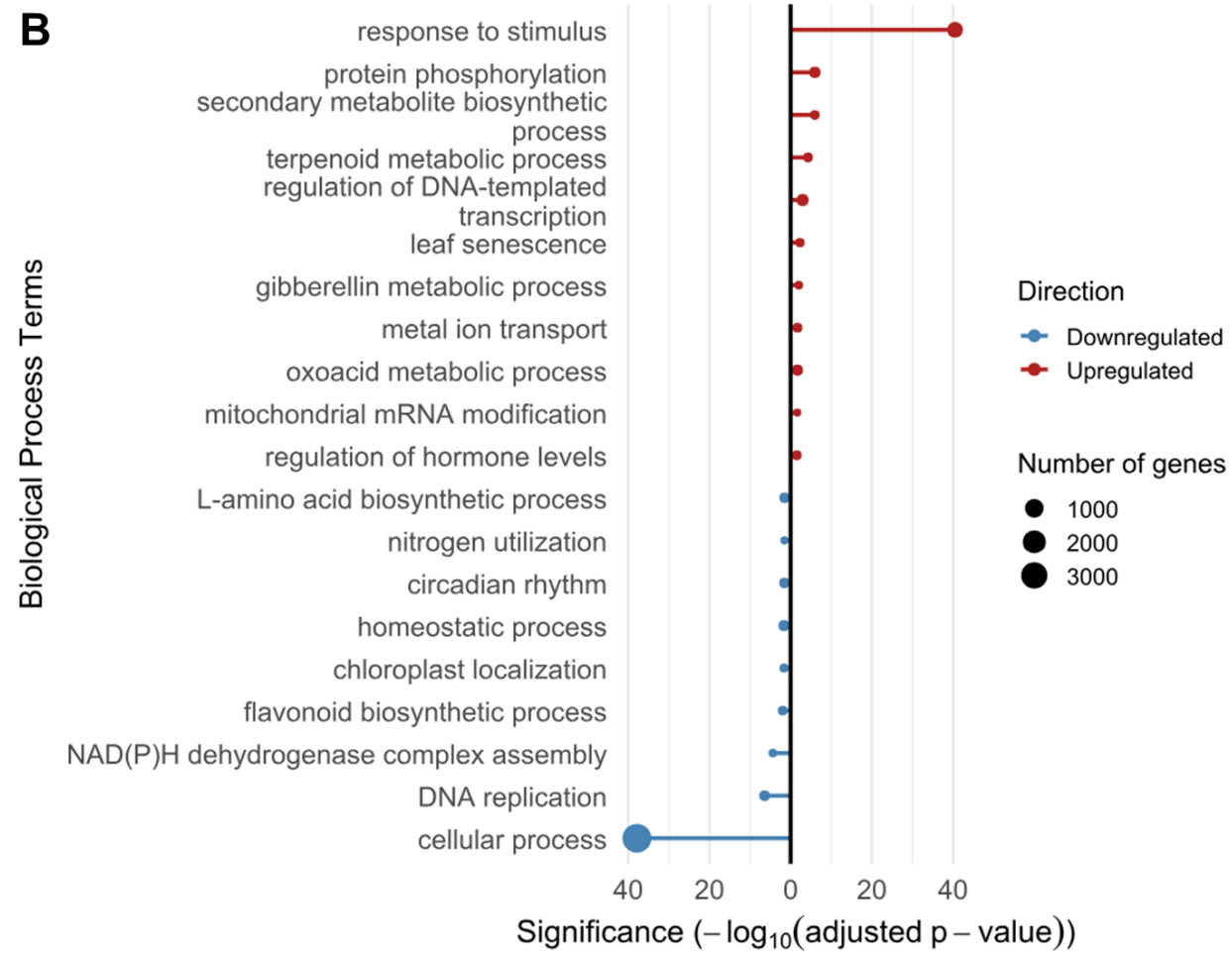
B
response to stimulus
protein phosphorylation
secondary metabolite biosynthetic process
terpenoid metabolic process
regulation of DNA-templated transcription
leaf senescence
gibberellin metabolic process
metal ion transport
oxoacid metabolic process
mitochondrial mRNA modification
regulation of hormone levels
L-amino acid biosynthetic process
nitrogen utilization
circadian rhythm
homeostatic process
chloroplast localization
flavonoid biosynthetic process
NAD(P)H dehydrogenase complex assembly
DNA replication
cellular process
Biological Process Terms
40
20
0
20
40
Significance (−log10(adjusted p−value))
Direction
Downregulated
Upregulated
Number of genes
1000
2000
3000

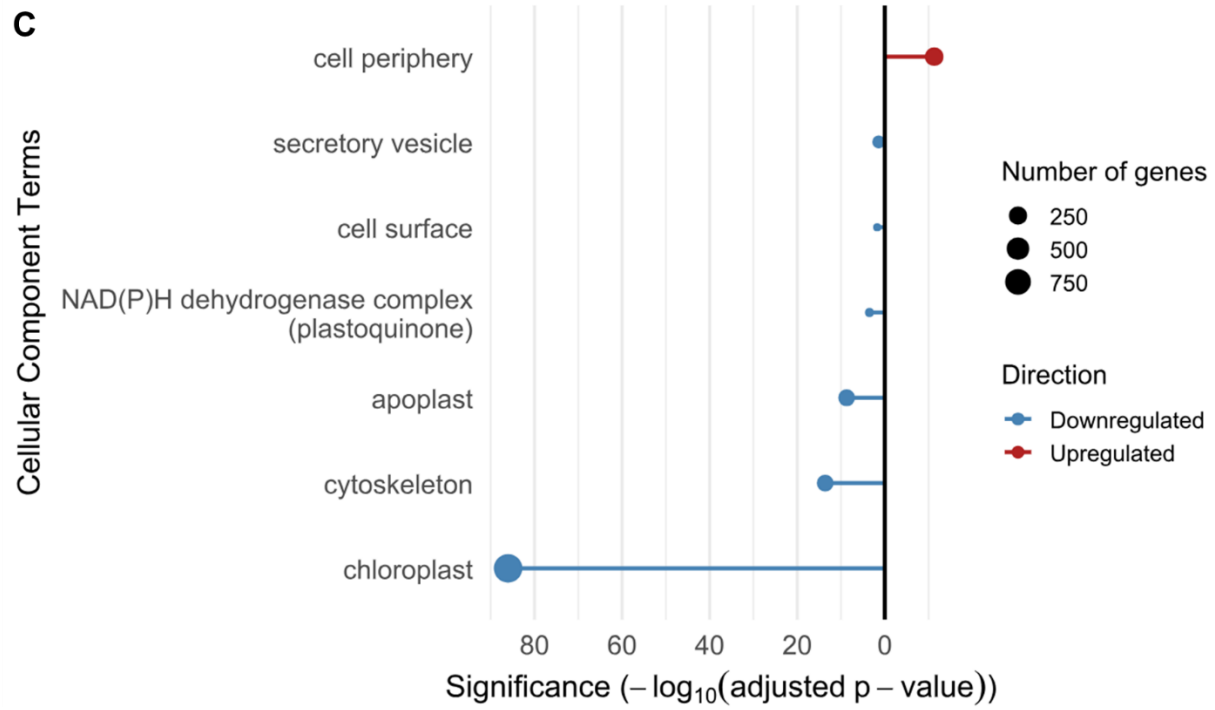
C
cell periphery
secretory vesicle
cell surface
NAD(P)H dehydrogenase complex (plastoquinone)
apoplast
cytoskeleton
chloroplast
Cellular Component Terms
80
60
40
20
0
Significance (−log10(adjusted p−value))
Number of genes
250
500
750
Direction
Downregulated
Upregulated

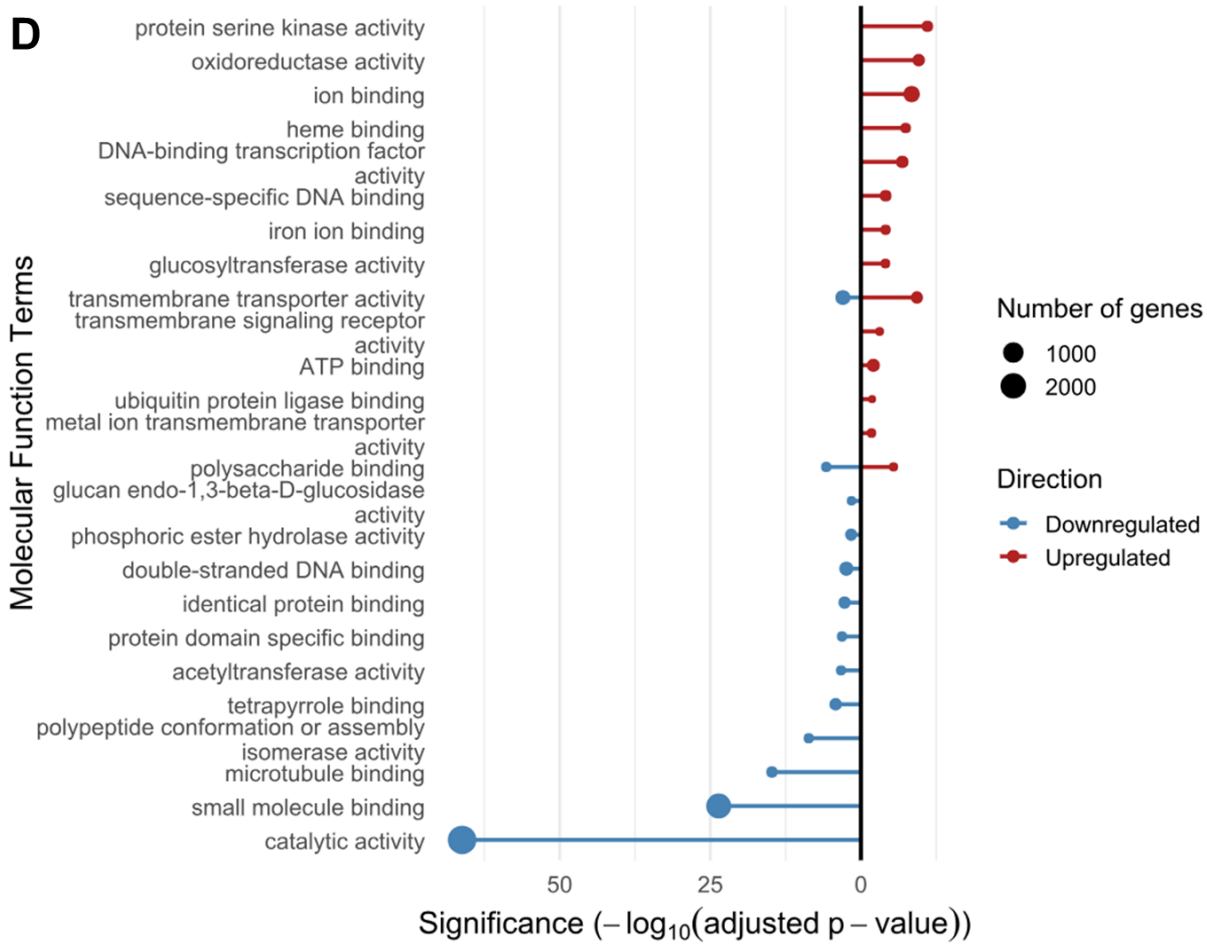

Figure 5.13. Gene ontology enrichment analysis for late flowering vs vegetative DEGs, arranged by terms from the: A. KEGG pathway. B. Biological process. C. Cellular components. D. Molecular function. Upregulated genes are shown in blue. Downregulated genes are shown in red. The size of the circle corresponds to the number of genes with the respective term. X-axis shows the significance. Y -axis shows the specific gene ontology terms.

The top two KEGG pathway terms from downregulated DEGs were metabolic pathways and biosynthesis of secondary metabolites (Figure 5.13 A). The biological process terms associated with upregulated DEGs included secondary metabolite biosynthetic process, terpenoid metabolic process, whilst the top term associated with downregulated genes was cellular process (Figure 5.13 B). The top cellular component term for upregulated DEGs was cell periphery, whilst for downregulated DEGs was chloroplast (Figure 5.13 C). The molecular function terms shared transmembrane transporter activity and polysaccharide binding between the upregulated and downregulated DEGs (Figure 5.13 D). The top 3 terms associated with upregulated DEGs were protein serine kinase activity, oxidoreductase activity and ion binding, whilst for downregulated DEGs was catalytic activity, small molecule

binding and microtubule binding. The comparison of late flowering vs vegetative represents the furthest apart developmental stages, and the differences in associated terms may represent the broad transcriptional reprogramming between leaves from a younger vegetative plant and a mature late flowering stage plant.

Finally, DEGs from late flowering vs early flowering were explored, to highlight potential transcriptional changes specific to only the most mature developmental stage of the plant after the transitioning to flowering has occurred (Figure 5.14).

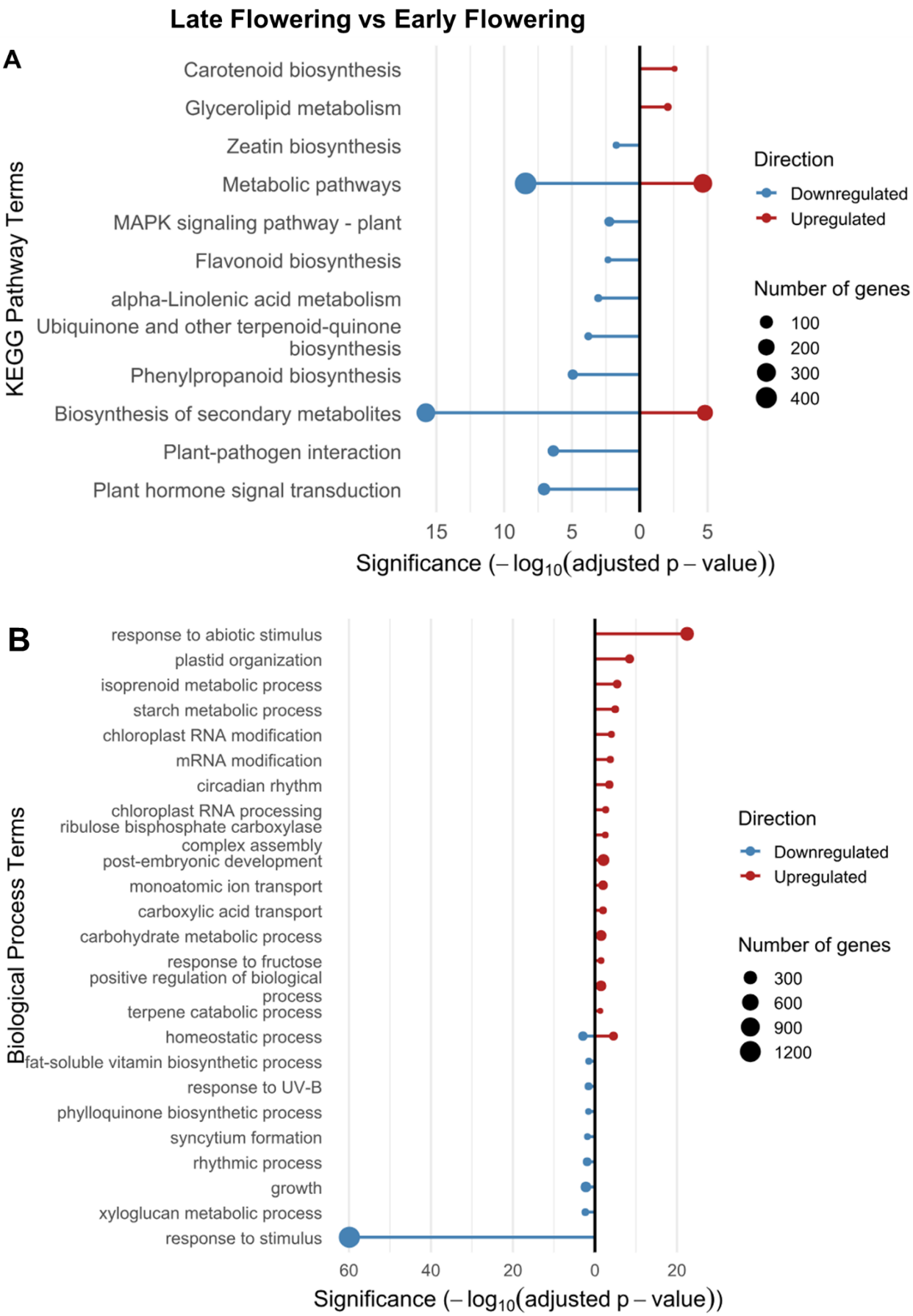
Late Flowering vs Early Flowering
A
KEGG Pathway Terms
Carotenoid biosynthesis
Glycerolipid metabolism
Zeatin biosynthesis
Metabolic pathways
MAPK signaling pathway - plant
Flavonoid biosynthesis
alpha-Linolenic acid metabolism
Ubiquinone and other terpenoid-quinone biosynthesis
Phenylpropanoid biosynthesis
Biosynthesis of secondary metabolites
Plant-pathogen interaction
Plant hormone signal transduction
15 10 5 0 5
Significance (– log10(adjusted p – value))
Direction
Downregulated
Upregulated
Number of genes
100
200
300
400
B
Biological Process Terms
response to abiotic stimulus
plastid organization
isoprenoid metabolic process
starch metabolic process
chloroplast RNA modification
mRNA modification
circadian rhythm
chloroplast RNA processing
ribulose bisphosphate carboxylase complex assembly
post-embryonic development
monoatomic ion transport
carboxylic acid transport
carbohydrate metabolic process
response to fructose
positive regulation of biological process
terpene catabolic process
homeostatic process
fat-soluble vitamin biosynthetic process
response to UV-B
phylloquinone biosynthetic process
syncytium formation
rhythmic process
growth
xyloglucan metabolic process
response to stimulus
60 40 20 0 20
Significance (– log10(adjusted p – value))
Direction
Downregulated
Upregulated
Number of genes
300
600
900
1200

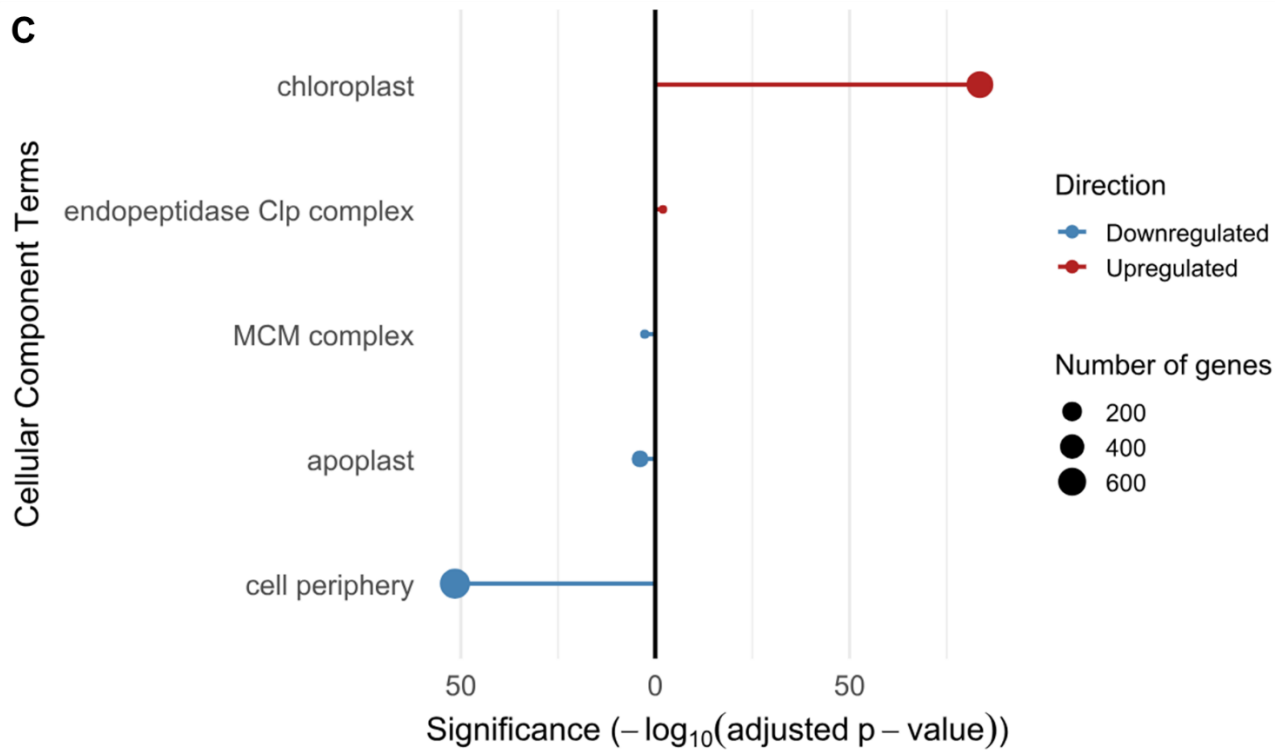
C
Cellular Component Terms
chloroplast
endopeptidase Clp complex
MCM complex
apoplast
cell periphery
50
0
50
Significance (−log10(adjusted p − value))
Direction
Downregulated
Upregulated
Number of genes
200
400
600

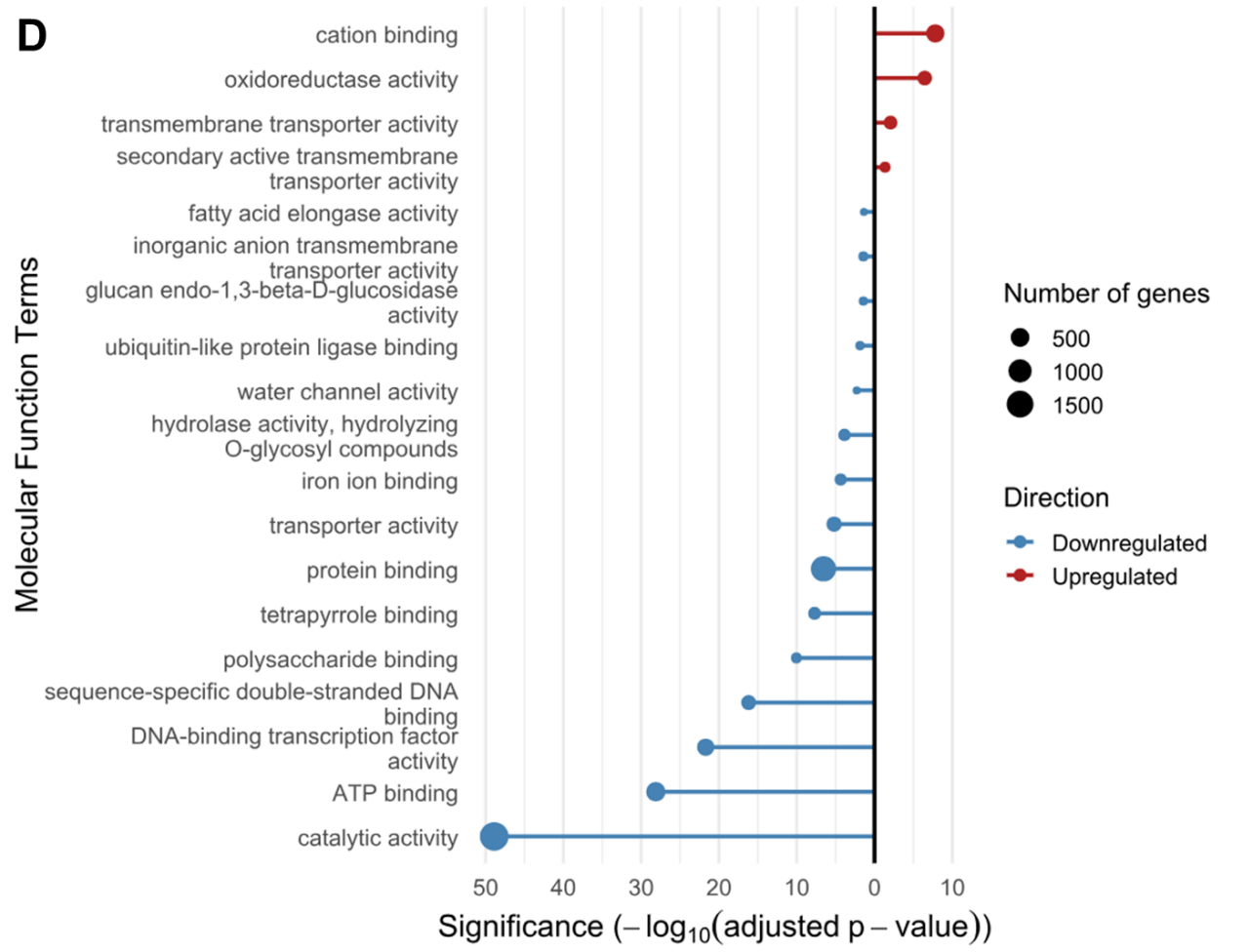
D
Molecular Function Terms
cation binding
oxidoreductase activity
transmembrane transporter activity
secondary active transmembrane transporter activity
fatty acid elongase activity
inorganic anion transmembrane transporter activity
glucan endo-1,3-beta-D-glucosidase activity
ubiquitin-like protein ligase binding
water channel activity
hydrolase activity, hydrolyzing O-glycosyl compounds
iron ion binding
transporter activity
protein binding
tetrapyrrole binding
polysaccharide binding
sequence-specific double-stranded DNA binding
DNA-binding transcription factor activity
ATP binding
catalytic activity
50
40
30
20
10
0
10
Significance (−log10(adjusted p − value))
Number of genes
500
1000
1500
Direction
Downregulated
Upregulated

Figure 5.14. Gene ontology enrichment analysis for late flowering vs early flowering DEGs, arranged by terms from the: A. KEGG pathway. B. Biological process. C. Cellular components. D. Molecular function. Upregulated genes are shown in blue. Downregulated genes are shown in red. The size of the circle corresponds to the number of genes with the respective term. X-axis shows the significance. Y -axis shows the specific gene ontology terms.

For KEGG pathway terms, both metabolic pathways and biosynthesis of secondary metabolites were associated with upregulated and downregulated DEGs (Figure 5.14 A). Downregulated DEGs also included the MAPK signalling pathway – plant. Biological process terms associated with upregulated DEGs included isoprenoid metabolic process and terpene catabolic process, whilst the top term associated with downregulated DEGs was response to stimulus (Figure 5.14 B). For cellular component terms, the top term for upregulated and downregulated DEGs was chloroplast and cell periphery, respectively (Figure 5.14 C). For molecular function terms, the top 3 terms associated with upregulated DEGs were cation binding, oxidoreductase activity and transmembrane transporter activity, whilst for downregulated DEGs, the top 3 terms were catalytic activity, ATP binding and DNA TF activity (Figure 5.14 D).

Overall, GO analysis has revealed the changes in the transcriptional landscape that may be occurring between the three developmental stages. Terms that may relate to the MBP such as metabolic pathways and biosynthesis of secondary metabolites showed a change between developmental stages, suggesting that there is a transcriptional change occurring between stages. The next stage of analysis involved the identification and characterisation of any Black Mitcham genes which could be putative MBP genes.

5.2.5 Identification and characterisation of menthol biosynthesis pathway genes and transcriptional changes

Identification of menthol biosynthesis pathway genes from the Black Mitcham genome gene IDs was first performed by BLASTn of MBP genes which have been biochemically characterised in the literature. The returning matches were then used as queries for BLASTx against the *Lamiaceae* protein database. Canonical genes were chosen based on which Black Mitcham gene ID had the highest similarity match to its respective biochemically characterised gene (Appendix Table 3). No p-value cut off value was applied for this analysis, to characterise all potential genes

related to the MBP. Differences in gene expression (expressed as normalised counts from DESeq2) of the identified MBP genes were first grouped into genes which did not have a corresponding oil profile product detectable from the oil profile characterisation in 5.2.1. These MBP genes were MpGPPS.SSU (BMitcham.V1_g162906), MpGPPS.LSU (BMitcham.V1_g208413), MpLimS (BMitcham.V1_g195282), MpL3H PM2 (BMitcham.V1_g117376), MpL3H PM17 (BMitcham.V1_g195283), MpIPDH (BMitcham.V1_g12076) and MpIPR (BMitcham.V1_g146769), and their respective changes in expression are shown between vegetative, early flowering and late flowering, quantified as the mean of normalised counts from three biological replicates (

Figure 5.15).

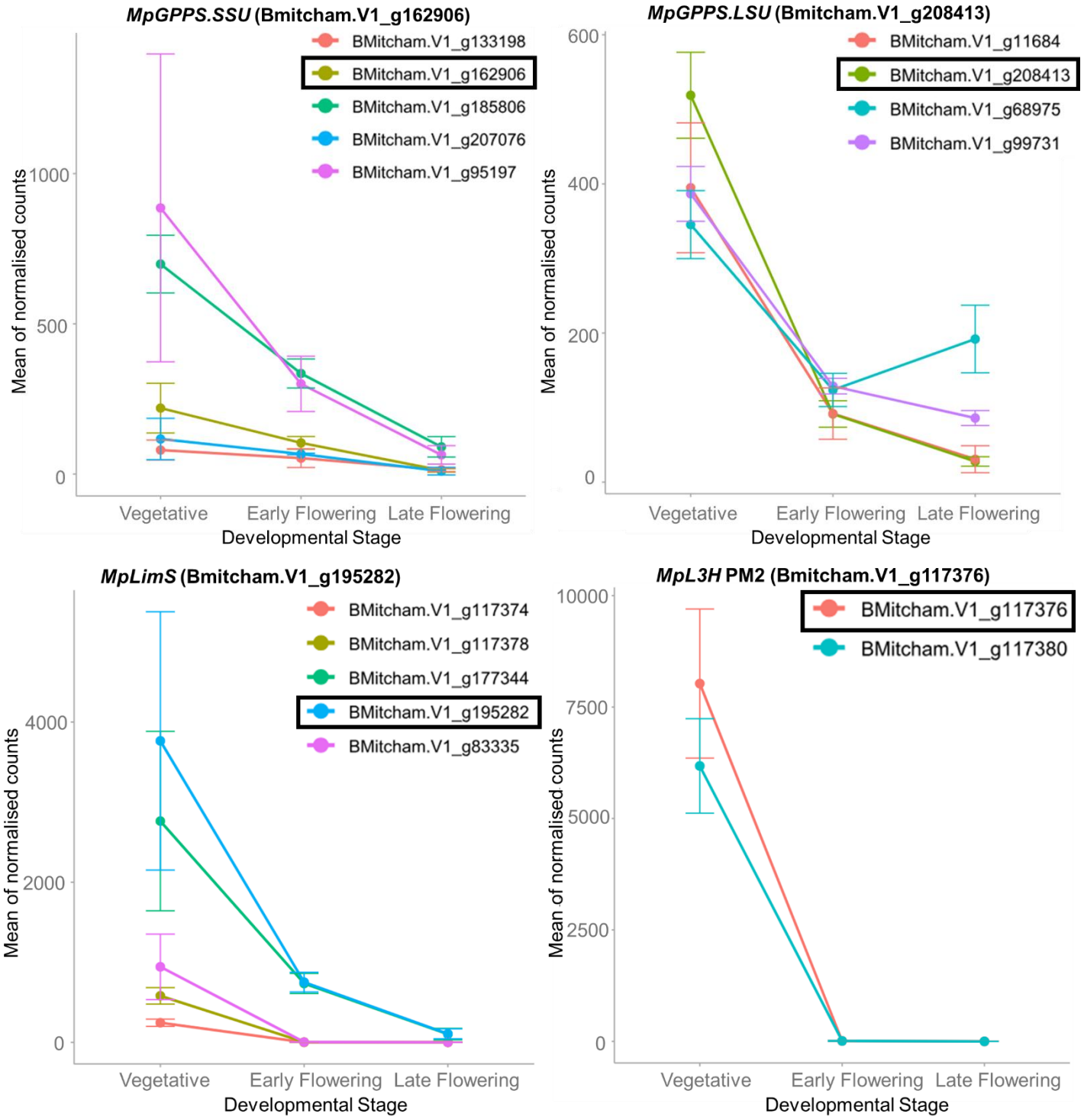
MpGPPS.SSU (Bmitcham.V1_g162906)
BMitcham.V1_g133198
BMitcham.V1_g162906
BMitcham.V1_g185806
BMitcham.V1_g207076
BMitcham.V1_g95197
Mean of normalised counts
0
500
1000
Vegetative
Early Flowering
Late Flowering
Developmental Stage
MpGPPS.LSU (Bmitcham.V1_g208413)
BMitcham.V1_g11684
BMitcham.V1_g208413
BMitcham.V1_g68975
BMitcham.V1_g99731
Mean of normalised counts
0
200
400
600
Vegetative
Early Flowering
Late Flowering
Developmental Stage
MpLimS (Bmitcham.V1_g195282)
BMitcham.V1_g117374
BMitcham.V1_g117378
BMitcham.V1_g177344
BMitcham.V1_g195282
BMitcham.V1_g83335
Mean of normalised counts
0
2000
4000
Vegetative
Early Flowering
Late Flowering
Developmental Stage
MpL3H PM2 (Bmitcham.V1_g117376)
BMitcham.V1_g117376
BMitcham.V1_g117380
Mean of normalised counts
0
2500
5000
7500
10000
Vegetative
Early Flowering
Late Flowering
Developmental Stage

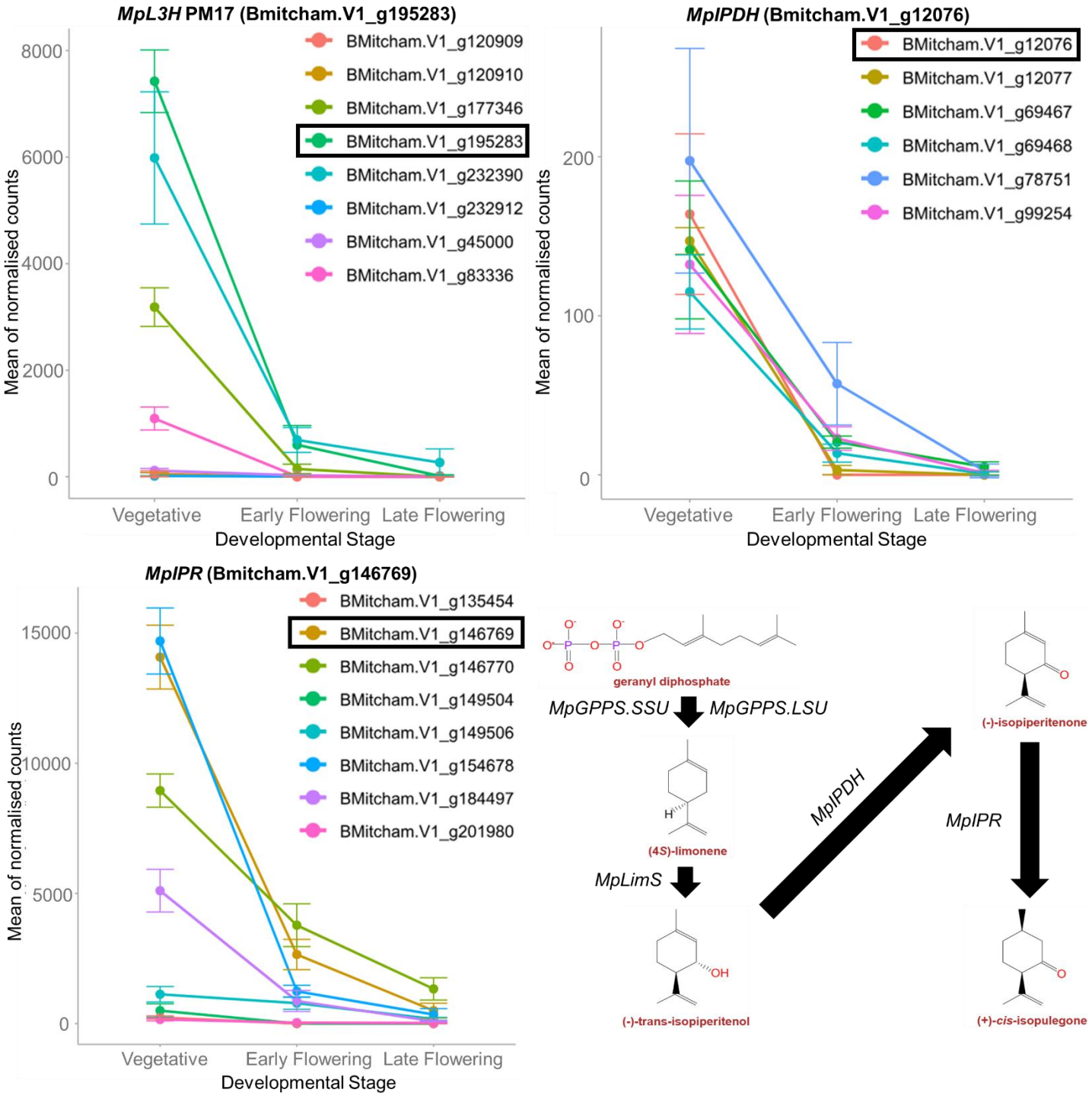

Figure 5.15. Change in gene expression of menthol biosynthesis pathway genes across vegetative, early flowering and late flowering samples. For each enzyme, putative homologs are shown as different coloured lines, with a key in the top right to indicate gene ID. The transcript with the strongest match to the biochemically characterised reference is labelled for each respective graph, and is also indicated by a black box surrounding the gene ID. Points show the mean of normalised counts from three biological replicates, with error bars indicating ±1 SD. The role of each gene within the menthol pathway is indicated as a simplified pathway for reference. Y-axis shows the mean of normalised counts. X-axis shows the developmental stage.

Each of the genes show a general decrease in expression from vegetative to early flowering to late flowering (

Figure 5.15). There are two biochemically characterised isoforms of *MpL3H*, PM2 and PM17 (Lupien et al. 1999). The PM2 isoform (BMitcham.V1_g117376) only showed expression during the vegetative stage, whilst the PM17 isoform (BMitcham.V1_g195283) was expressed in both the vegetative and early flowering stage. *MpIPDH* (BMitcham.V1_g12076) was only expressed in the vegetative stage.

MpPGR (BMitcham.V1_g26993), which catalyses the reduction of (+)-pulegone, showed a distinct expression pattern in the canonical gene, where expression was high in the vegetative stage, dropped to low expression in the early flowering stage, and further increased in the late flowering stage. (Figure 5.16)

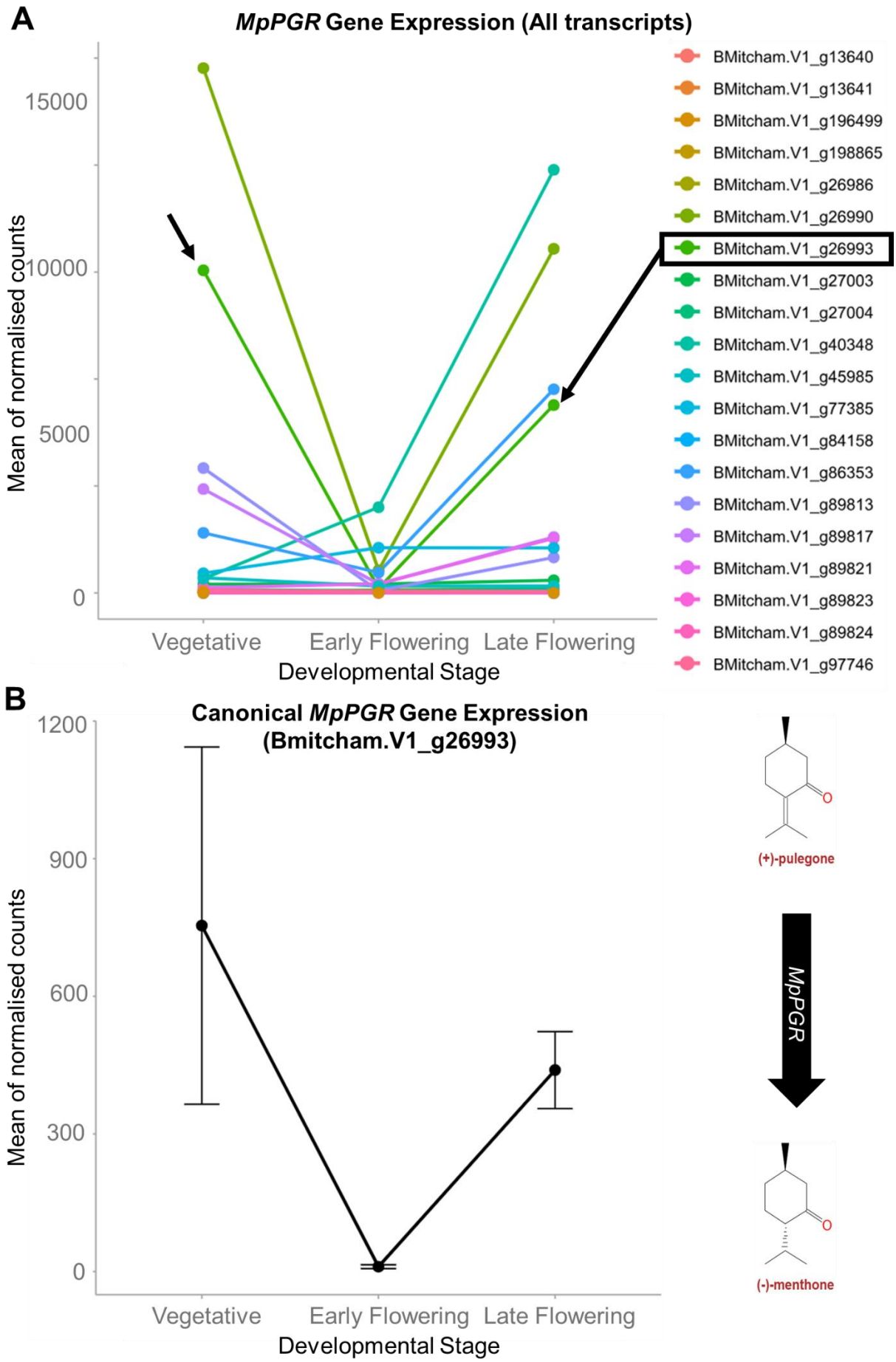
A
MpPGR Gene Expression (All transcripts)
Mean of normalised counts
15000
10000
5000
0
Vegetative
Early Flowering
Late Flowering
Developmental Stage
BMitcham.V1_g13640
BMitcham.V1_g13641
BMitcham.V1_g196499
BMitcham.V1_g198865
BMitcham.V1_g26986
BMitcham.V1_g26990
BMitcham.V1_g26993
BMitcham.V1_g27003
BMitcham.V1_g27004
BMitcham.V1_g40348
BMitcham.V1_g45985
BMitcham.V1_g77385
BMitcham.V1_g84158
BMitcham.V1_g86353
BMitcham.V1_g89813
BMitcham.V1_g89817
BMitcham.V1_g89821
BMitcham.V1_g89823
BMitcham.V1_g89824
BMitcham.V1_g97746
B
Canonical MpPGR Gene Expression
(Bmitcham.V1_g26993)
Mean of normalised counts
1200
900
600
300
0
Vegetative
Early Flowering
Late Flowering
Developmental Stage
O
(+)-pulegone
MpPGR
O
(-)-menthone

Figure 5.16 Change in gene expression of all identified *M. x piperita pulegone reductase (MpPGR)* genes across vegetative, early flowering and late flowering. A. All putative *MpPGR* homologs are shown as different colours, with a key in the top right to indicate gene ID. The canonical *MpPGR* is indicated by black arrows for clarity, and the gene ID is indicated by a surrounding black box. B. The canonical *MpPGR* shown on its own graph for clarity, with error bars indicating ±1 SD. Data points are representative of the mean of normalised counts from 3 biological replicates. A portion of the menthol biosynthesis pathway where *MpPGR* in involved is also shown for reference.

MpMMR (BMitcham.V1_g135464), which catalyses the reduction of (-)-menthone to (-)-menthol, showed an increase from vegetative to early flowering to late flowering for the canonical gene (Figure 5.17).

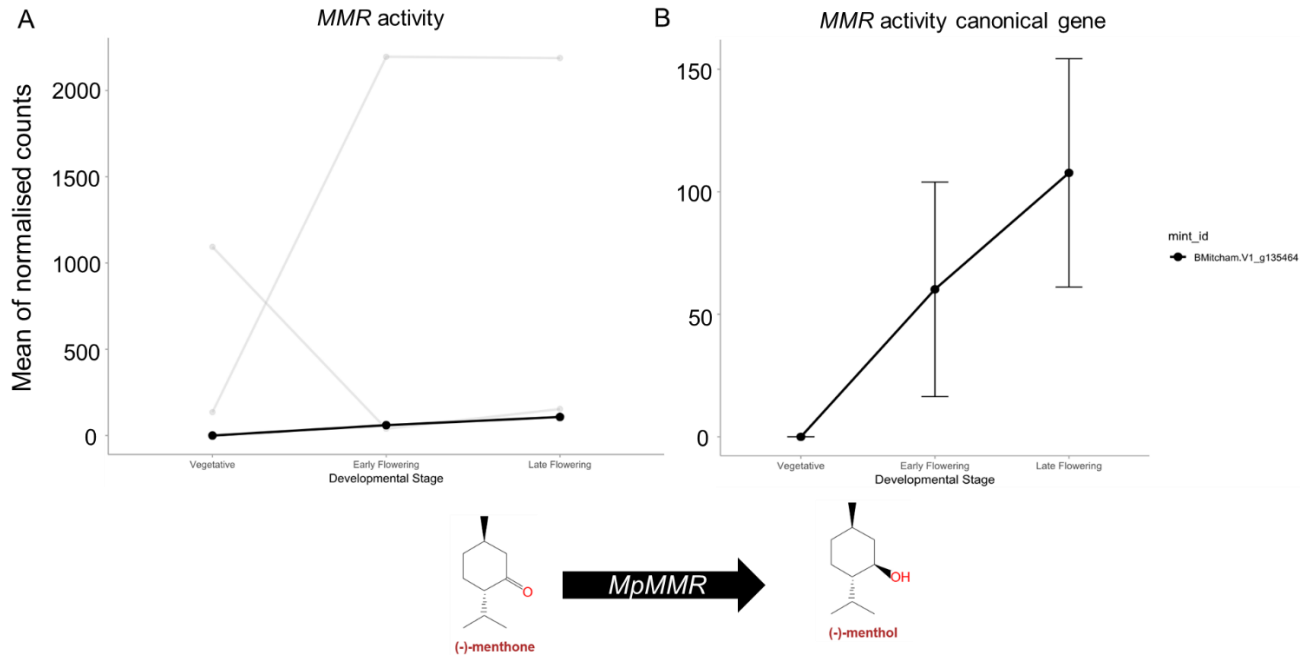

Figure 5.17. Change in gene expression of all identified *M. x piperita menthone reductase (MpMMR)* genes across vegetative, early flowering and late flowering. A. All the putative *MpMMR* genes are shown, with the best matching to the canonical *MpMMR* shown as a black line, whilst the other genes are shown as a grey line. B. The canonical *MpMMR* shown in its own graph for clarity, with error bars indicating ±1 SD. Data points are representative of the mean of normalised counts from 3 biological replicates .

There were two other putative *MpMMR* genes, where one showed an increase in expression from vegetative to early flowering to late flowering (BMitcham.V1_g184503), whilst the other showed high expression in vegetative, which was then reduced in the early flowering and late flowering stage (BMitcham.V1_g184498) (Figure 5.17 A).

The *MpMNMR* catalyses the reduction of (-)-menthone to (+)-neomenthol, and the best matching gene to the biochemically characterised *MpMNMR* (BMitcham.V1_g135458) showed an expression pattern of high in the vegetative

stage, low in the early flowering stage, and further increasing in the late flowering stage (Figure 5.18).

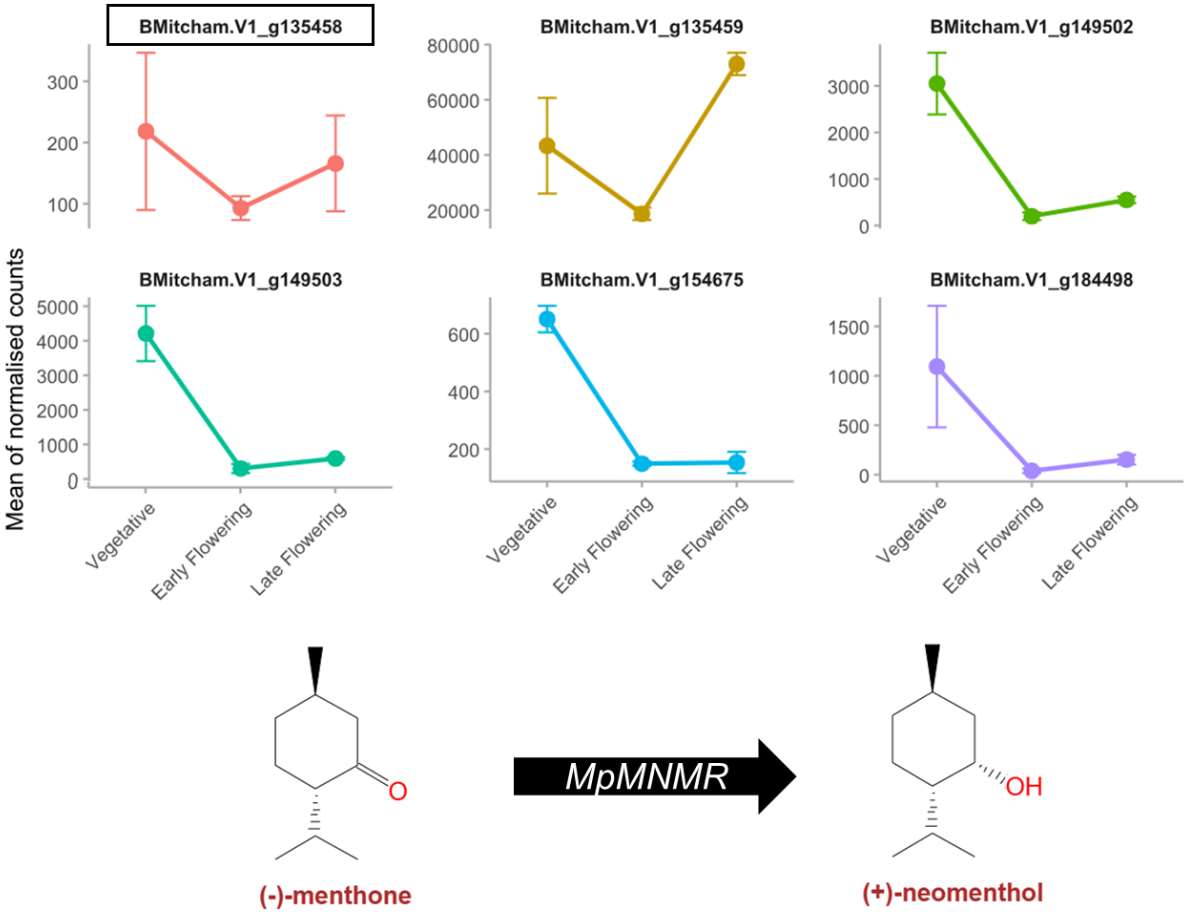

Figure 5.18. Change in gene expression of all identified *M. x piperita menthone neomenthol reductase (MpMNMR)* genes across vegetative, early flowering and late flowering. All the putative *MpMMR* genes are shown in different colours, with the gene which had the highest similarity match to the canonical *MpMNMR* highlighted by a black box. The data points represent the mean of normalised counts from 3 biological replicates, with error bars indicating ±1 SD.

For the *MpMFS* gene, which catalyses the hydroxylation of (+)-pulegone to (+)-menthofuran, there were a total of 6 putative genes which matched to the biochemically characterised *MpMFS* gene (Appendix Table 3). Of the 6 genes, 4 genes (BMitcham.V1_g199648, BMitcham.V1_g199649, BMitcham.V1_g199650, BMitcham.V1_g199652 showed an equal level of similarity to the canonical gene, and shared a similar expression pattern of being highly expressed in the vegetative stage, which then decreased in the early flowering and late flowering stages (Figure 5.19).

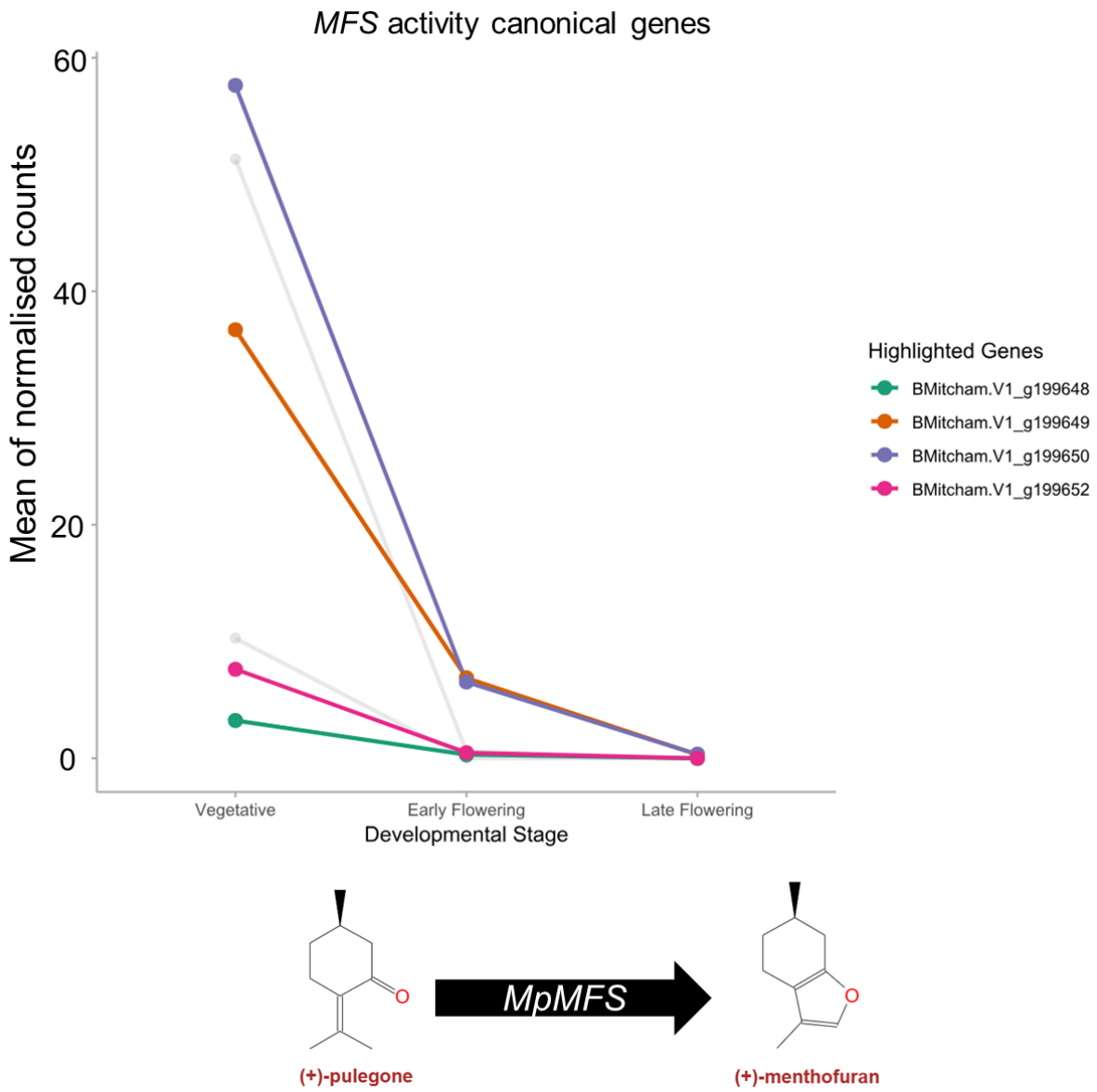

Figure 5.19. Change in gene expression of all identified *M. x piperita menthofuran synthase(MpMFS)* genes across vegetative, early flowering and late flowering. The four putative genes which had an equally similar match to the canonical *MpMFS* are shown as coloured lines, whilst the other two matches are shown in grey. Each data point represents the mean of normalised counts from three biological replicates.

To determine the overall gene expression profiles of all of the putative MBP genes, the log fold change between all developmental stages was used to generate heatmaps based on the log_2fc (with a cutoff of log_2fc >1 or <-1) to map against the menthol biosynthesis pathway, to identify the overall changes in gene expression of key MBP genes (Figure 5.20).

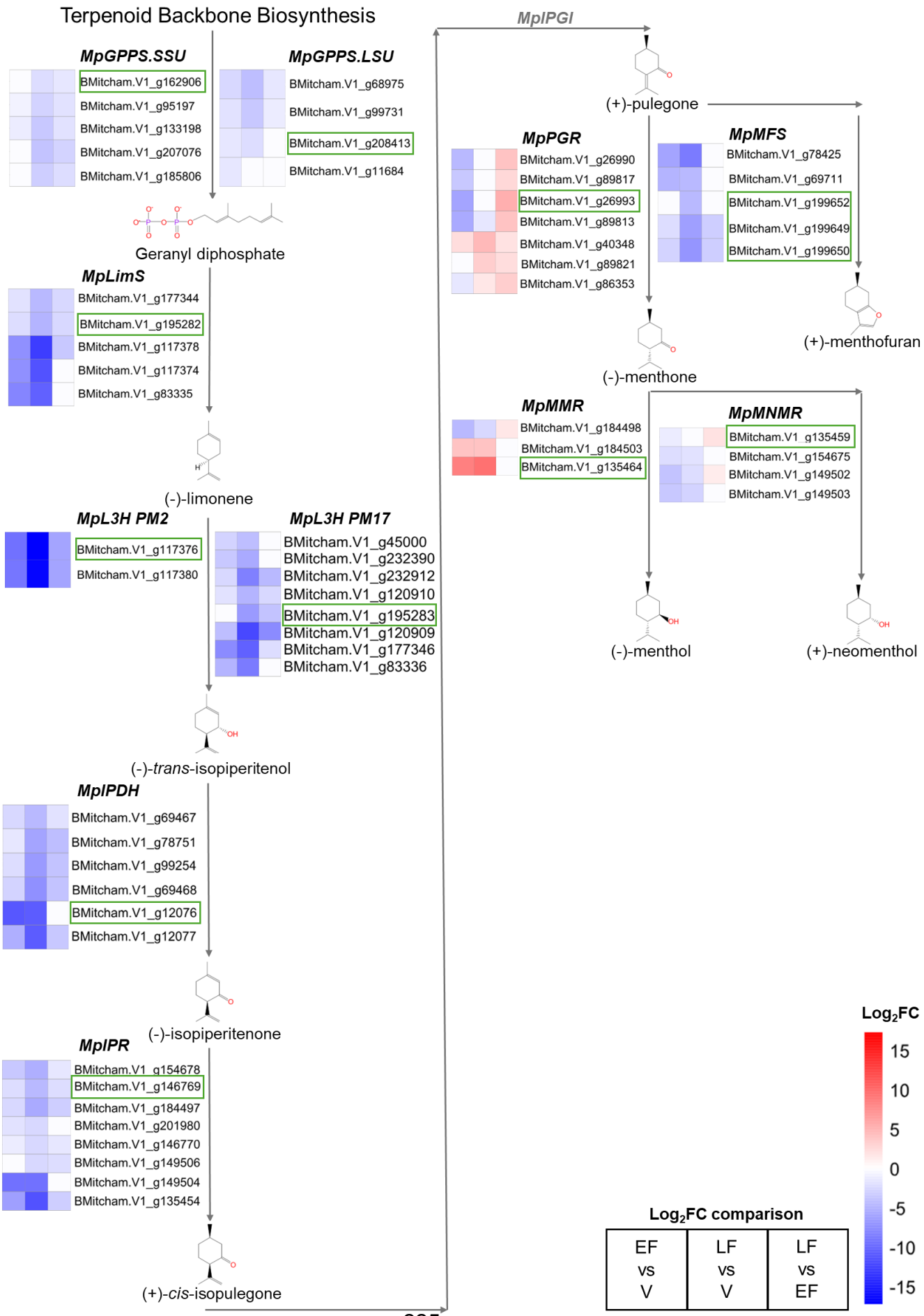
Terpenoid Backbone Biosynthesis
MpGPPS.SSU
BMitcham.V1_g162906
BMitcham.V1_g95197
BMitcham.V1_g133198
BMitcham.V1_g207076
BMitcham.V1_g185806
MpGPPS.LSU
BMitcham.V1_g68975
BMitcham.V1_g99731
BMitcham.V1_g208413
BMitcham.V1_g11684
Geranyl diphosphate
MpLimS
BMitcham.V1_g177344
BMitcham.V1_g195282
BMitcham.V1_g117378
BMitcham.V1_g117374
BMitcham.V1_g83335
(-)-limonene
MpL3H PM2
BMitcham.V1_g117376
BMitcham.V1_g117380
MpL3H PM17
BMitcham.V1_g45000
BMitcham.V1_g232390
BMitcham.V1_g232912
BMitcham.V1_g120910
BMitcham.V1_g195283
BMitcham.V1_g120909
BMitcham.V1_g177346
BMitcham.V1_g83336
(-)-trans-isopiperitenol
MpIPDH
BMitcham.V1_g69467
BMitcham.V1_g78751
BMitcham.V1_g99254
BMitcham.V1_g69468
BMitcham.V1_g12076
BMitcham.V1_g12077
(-)-isopiperitenone
MpIPR
BMitcham.V1_g154678
BMitcham.V1_g146769
BMitcham.V1_g184497
BMitcham.V1_g201980
BMitcham.V1_g146770
BMitcham.V1_g149506
BMitcham.V1_g149504
BMitcham.V1_g135454
(+)-cis-isopulegone
MpIPGI
(+)-pulegone
MpPGR
BMitcham.V1_g26990
BMitcham.V1_g89817
BMitcham.V1_g26993
BMitcham.V1_g89813
BMitcham.V1_g40348
BMitcham.V1_g89821
BMitcham.V1_g86353
MpMFS
BMitcham.V1_g78425
BMitcham.V1_g69711
BMitcham.V1_g199652
BMitcham.V1_g199649
BMitcham.V1_g199650
(+)-menthofuran
(-)-menthone
MpMMR
BMitcham.V1_g184498
BMitcham.V1_g184503
BMitcham.V1_g135464
MpMNMR
BMitcham.V1_g135459
BMitcham.V1_g154675
BMitcham.V1_g149502
BMitcham.V1_g149503
(-)-menthol
(+)-neomenthol
Log2FC
15
10
5
0
-5
-10
-15
Log2FC comparison
EF vs V
LF vs V
LF vs EF

Figure 5.20. Heatmaps of the DEGs associated with the menthol biosynthesis pathway. Heatmaps for each gene represent the log2fc associated with the comparison points. The comparison points are shown in empty boxes. EF = early flowering. LF = late flowering. V = vegetative. A red colour indicates a positive log_2fc. A blue colour indicates a negative log_2fc. Green boxes indicate the associated gene which had the best similarity score compared to the biochemically characterised gene, as determined by blastx. For *MpMNMR,* the highest matching gene was not included after a $p < 0.05$ cutoff point, so the next highest matching gene is indicated. *Mp: M. x piperita. GPPS.SSU: Geranyl diphosphate synthase small subunit. GPPS.LSU: Geranyl diphosphate synthase large subunit. LimS: Limonene synthase. L3H: Limonene-3-hydroxylase. IPDH: trans-Isopiperitenol dehydrogenase. IPR: Isopiperitenone reductase. IPGI: Isopulegone isomerase. PGR: Pulegone reductase. MFS: Menthofuran synthase. MMR: Menthone reductase. MNMR: Menthone neomenthol reductase*

Overall, *MpGPPS.SSU, MpGPPS.LSU, MpLimS, MpL3H PM2, MpL3H PM17, MpIPDH, MpIPR, MpMFS and MpMNMR* showed a decrease in expression in both early flowering vs vegetative and late flowering vs vegetative comparisons (Figure 5.20).

There were five genes associated with the canonical *MpGPPS.SSU*, of which all showed a negative log2fc in the late flowering vs vegetative comparison, suggesting there is the highest level of expression of all *MpGPPS.SSU* genes in the vegetative sample. In the late flowering vs early flowering comparison, all 5 genes show a negative log2fc, suggesting a decrease in *MpGPPS.SSU* expression. There were four genes associated with *MpGPPS.LSU,* of which one gene (Bmitcham.V1_g11684) showed a significant difference in log2fc only in the early flowering vs vegetative comparison, suggesting a role of this specific *MpGPPS.LSU* in the transitionary stage between vegetative stage plants and flowering plants. The *MpGPPS.LSU* with the greatest match to the canonical gene showed the largest negative log2fc in the late flowering vs vegetative comparison, followed by the early flowering vs vegetative, with no significant change detected in the early flowering vs late flowering comparison. This suggests its high activity in vegetative plants, which is then shut off at the transition into flowering stage plants, and is not reactivated in late flowering stage plants.

Five genes were associated with *MpLimS*, with the largest negative log2fc being shown in the late flowering vs vegetative comparison, indicating high expression of the *MpLimS* genes in the vegetative stage. *MpLimS* is downregulated in the early flowering stage, and this downregulation persists into the late flowering stage, as

indicated by the log2fc values in the early flowering vs vegetative, and late flowering vs early flowering comparisons.

Comparing the canonical genes for *MpL3H* PM2 and PM17, PM2 showed the largest negative log2fc in the late flowering vs vegetative comparison, followed by early flowering vs vegetative, and finally late flowering vs early flowering, which suggests it was most highly upregulated in the vegetative samples. The PM17 variant showed the largest negative log2fc in the late flowering vs vegetative comparison, followed by late flowering vs early flowering, and finally early flowering vs vegetative. This suggests that the PM17 variant is upregulated in the vegetative tissue, and shows a downregulation only in the late vegetative stages.

Six genes were associated with *MpIPDH*, which all showed high expression in the vegetative stages, as shown by the late flowering vs vegetative comparison. For the gene which most closely matched the canonical *MpIPDH*, there is a sudden downregulation in the early flowering stages, as indicated by the log2fc values in the early flowering vs vegetative, and late flowering vs early flowering comparisons. As there is little change in the late flowering vs early flowering, it can be assumed that this gene is essential switched off upon the transitioning to flowering.

Eight genes were associated with *MpIPR*, which all showed high upregulation in the vegetative stages, as indicated by the log2fc values in the late flowering vs vegetative and early flowering vs vegetative comparisons. Downregulation of the genes start to occur once the plant enters the flowering stage, as indicated by the early flowering vs vegetative, and late flowering vs early flowering comparisons.

For *MpPGR* genes, there were seven total associated genes, with two different gene expression profiles observed. Five genes, which included the gene with the highest similarity to the canonical *MpPGR*, were highly expressed in vegetative tissue. Expression declined during the transition to early flowering, followed by upregulation in the late flowering stage. In contrast, the *MpPGR* genes Bmitcham.V1_g40348 and Bmitcham.V1_g89821 showed the opposite trend, where expression increased during the transition from vegetative to early flowering, and remained elevated in late flowering tissue. This highlights two potential subfamilies of *MpPGR* like genes, which have separate roles in the oil profile changes throughout development.

For *MpMFS* genes, there were five associated genes, where three of these genes had an equally high similarity match to the canonical *MpMFS* gene. The overall expression pattern showed a gradual downregulation from vegetative, to early flowering, and through to late flowering.

Three genes were associated with *MpMMR* where the gene with the closest similarity to the canonical *MpMMR* (BMitcham.V1_g135464) and BMitcham.V1_g184503 showed a strong upregulation in the early flowering stage, with further upregulation in the late flowering stage, as indicated by the early flowering vs vegetative and late flowering vs vegetative comparisons. This highlights these two genes being activated only after the transitioning to flowering tissue has occurred. The other *MpMMR* like gene (BMitcham.V1_g184498) showed upregulation in vegetative tissues, followed by a downregulation in early flowering tissue, and further slight upregulation in late flowering tissue. This expression profile matched those of the four *MpPGR* genes, and may be implicated in late flowering stage changes to oil profiles.

Four genes were associated with *MpMNMR*, which relative to the other MBP genes, did not show large log_2fc changes throughout the different developmental stages. For the gene that showed highest similarity to the canonical *MpMNMR* gene, a slight upregulation in the vegetative stage, followed by upregulation in the early flowering and late flowering stage can be observed.

Overall, the early MBP genes (*MpGPPS.SSU, MpGPPS.LSU, MpLimS, MpL3H* PM2, *MpL3H* PM17, *MpIPDH, MpIPR*) all show a general trend of higher expression in the vegetative stage, which is downregulated upon the transition into flowering. *MpPGR* and *MpMMR* showed two distinct expression patterns, which may group them into separate subfamilies. *MpMFS* catalyses the conversion of (+)-pulegone to the side product (+)-menthofuran, and production of (+)-menthofuran is believed to be a stress related metabolite (Croteau et al. 2005). As the levels of (+)-menthofuran showed a slight increase throughout plant maturation, and the gene expression profiles showed a decrease in expression, there appears to be no correlation between these two factors, suggesting alternative regulator mechanisms may be more influential. The next stage of analysis was to elucidate potential TFs that may be controlling the changes in gene expression of MBP genes throughout

developmental stages as observed so far. The first step was to determine putative TFBS in the promoters of the MBP related genes.

5.2.6 Transcription factor binding site prediction in the promoters of menthol biosynthesis pathway genes

Promoters of the MBP genes were classed as the intergenic regions between a MBP genes transcriptional start site (TSS) and the next upstream gene. If this distance exceeded 2000 bp, then a region of 2000 bp upstream from the TSS was chosen. The promoter regions were then analysed for putative binding sites using plantTFDB using the *Salvia miltiorriza* database (which is the most closely related species available), and the counts of each binding site were visualised in a heatmap (Jin et al. 2017) (

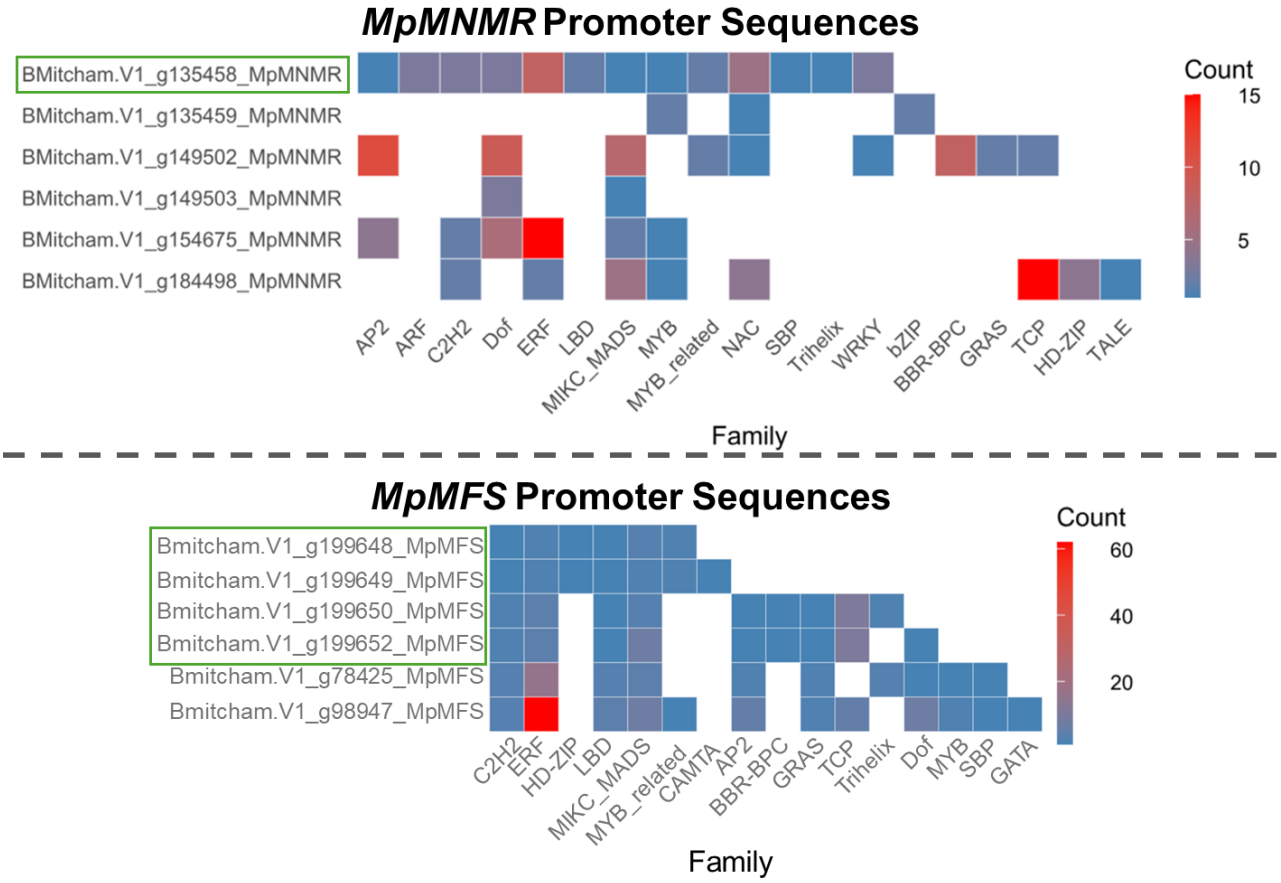

Figure 5.21).

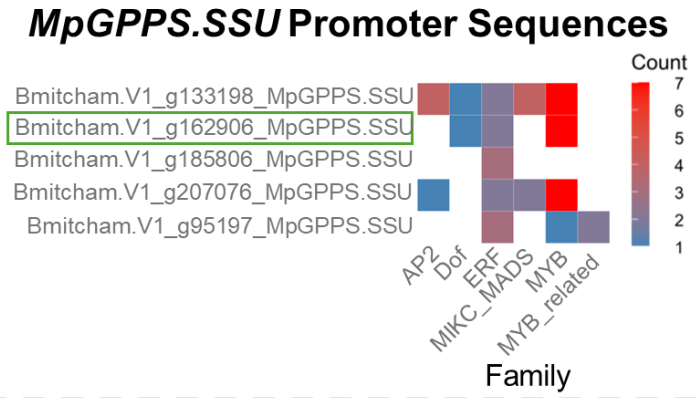
MpGPPS.SSU Promoter Sequences
Bmitcham.V1_g133198_MpGPPS.SSU
Bmitcham.V1_g162906_MpGPPS.SSU
Bmitcham.V1_g185806_MpGPPS.SSU
Bmitcham.V1_g207076_MpGPPS.SSU
Bmitcham.V1_g95197_MpGPPS.SSU
AP2
Dof
ERF
MIKC_MADS
MYB
MYB_related
Family
Count
7
6
5
4
3
2
1

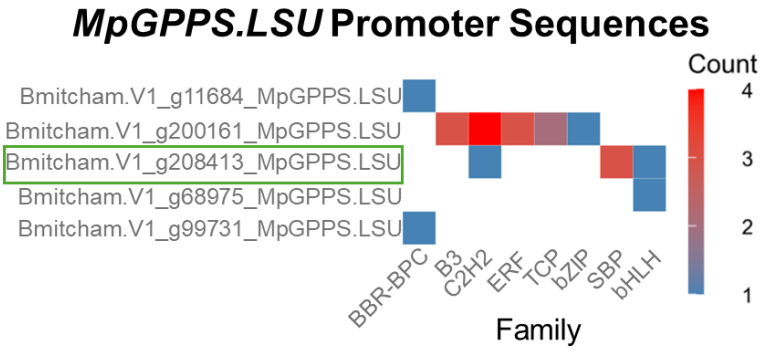
MpGPPS.LSU Promoter Sequences
Bmitcham.V1_g11684_MpGPPS.LSU
Bmitcham.V1_g200161_MpGPPS.LSU
Bmitcham.V1_g208413_MpGPPS.LSU
Bmitcham.V1_g68975_MpGPPS.LSU
Bmitcham.V1_g99731_MpGPPS.LSU
BBR-BPC
B3
C2H2
ERF
TCP
bZIP
SBP
bHLH
Family
Count
4
3
2
1

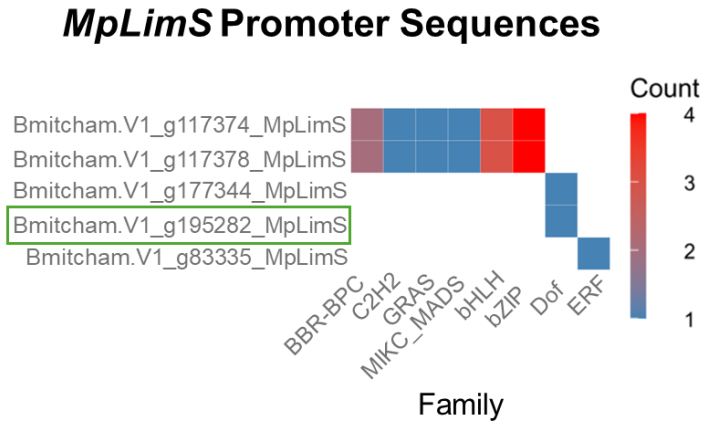
MpLimS Promoter Sequences
Bmitcham.V1_g117374_MpLimS
Bmitcham.V1_g117378_MpLimS
Bmitcham.V1_g177344_MpLimS
Bmitcham.V1_g195282_MpLimS
Bmitcham.V1_g83335_MpLimS
BBR-BPC
C2H2
GRAS
MIKC_MADS
bHLH
bZIP
Dof
ERF
Family
Count
4
3
2
1

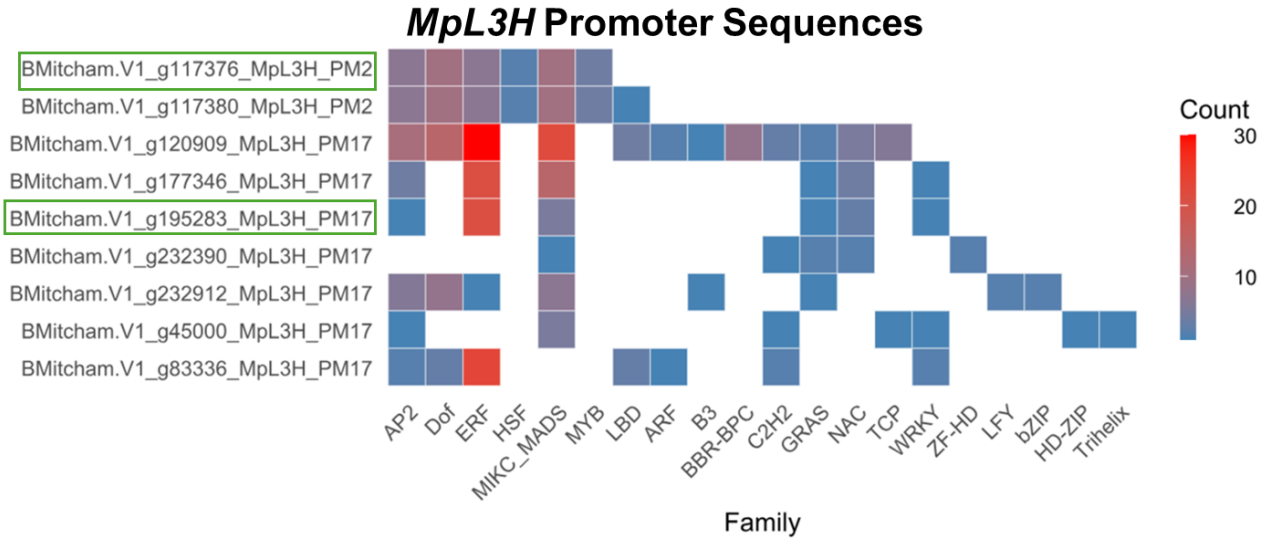
MpL3H Promoter Sequences
BMitcham.V1_g117376_MpL3H_PM2
BMitcham.V1_g117380_MpL3H_PM2
BMitcham.V1_g120909_MpL3H_PM17
BMitcham.V1_g177346_MpL3H_PM17
BMitcham.V1_g195283_MpL3H_PM17
BMitcham.V1_g232390_MpL3H_PM17
BMitcham.V1_g232912_MpL3H_PM17
BMitcham.V1_g45000_MpL3H_PM17
BMitcham.V1_g83336_MpL3H_PM17
AP2
Dof
ERF
HSF
MIKC_MADS
MYB
LBD
ARF
B3
BBR-BPC
C2H2
GRAS
NAC
TCP
WRKY
ZF-HD
LFY
bZIP
HD-ZIP
Trihelix
Family
Count
30
20
10

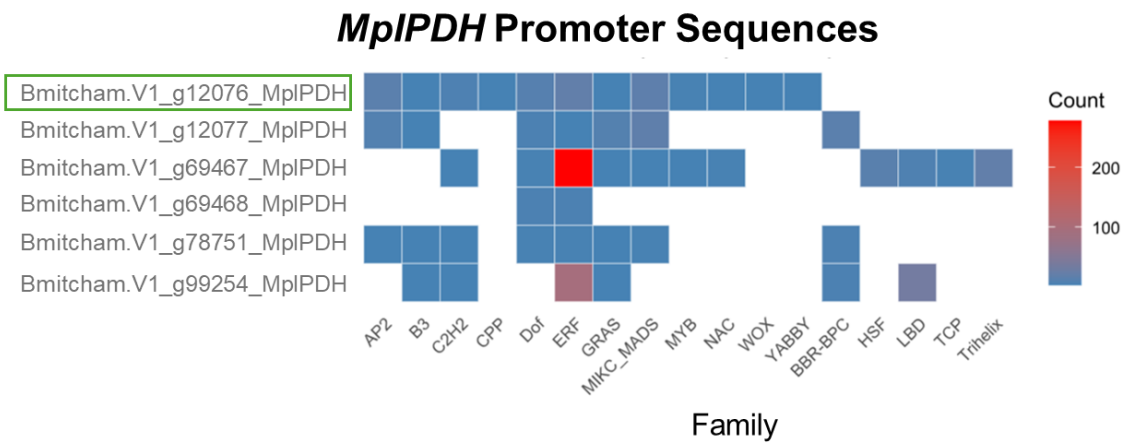
MpIPDH Promoter Sequences
Bmitcham.V1_g12076_MpIPDH
Bmitcham.V1_g12077_MpIPDH
Bmitcham.V1_g69467_MpIPDH
Bmitcham.V1_g69468_MpIPDH
Bmitcham.V1_g78751_MpIPDH
Bmitcham.V1_g99254_MpIPDH
AP2
B3
C2H2
CPP
Dof
ERF
GRAS
MIKC_MADS
MYB
NAC
WOX
YABBY
BBR-BPC
HSF
LBD
TCP
Trihelix
Family
Count
200
100

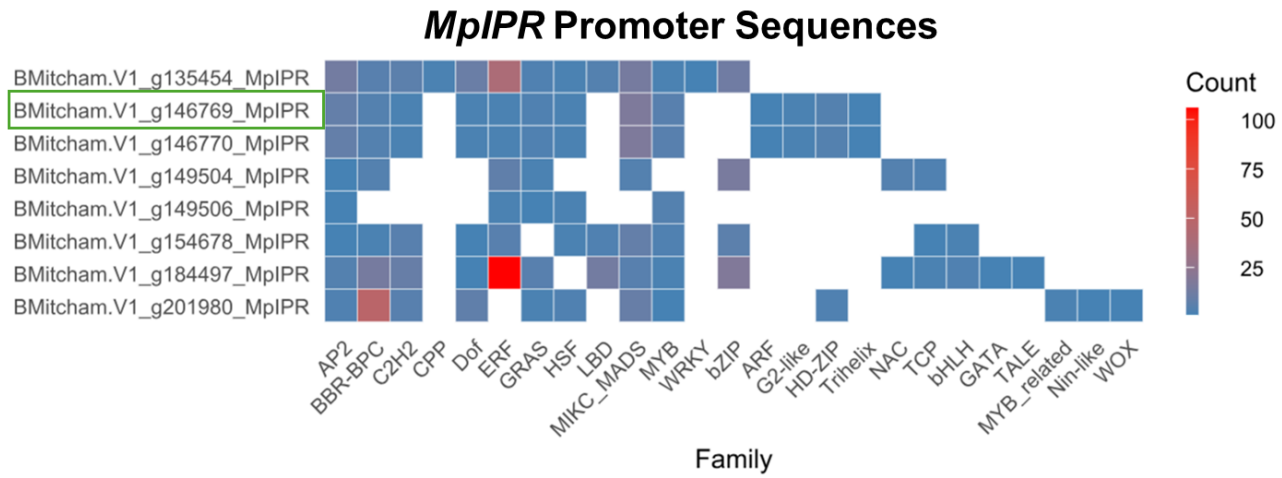
MpIPR Promoter Sequences
BMitcham.V1_g135454_MpIPR
BMitcham.V1_g146769_MpIPR
BMitcham.V1_g146770_MpIPR
BMitcham.V1_g149504_MpIPR
BMitcham.V1_g149506_MpIPR
BMitcham.V1_g154678_MpIPR
BMitcham.V1_g184497_MpIPR
BMitcham.V1_g201980_MpIPR
AP2
BBR-BPC
C2H2
CPP
Dof
ERF
GRAS
HSF
LBD
MIKC_MADS
MYB
WRKY
bZIP
ARF
G2-like
HD-ZIP
Trihelix
NAC
TCP
bHLH
GATA
TALE
MYB_related
Nin-like
WOX
Family
Count
100
75
50
25

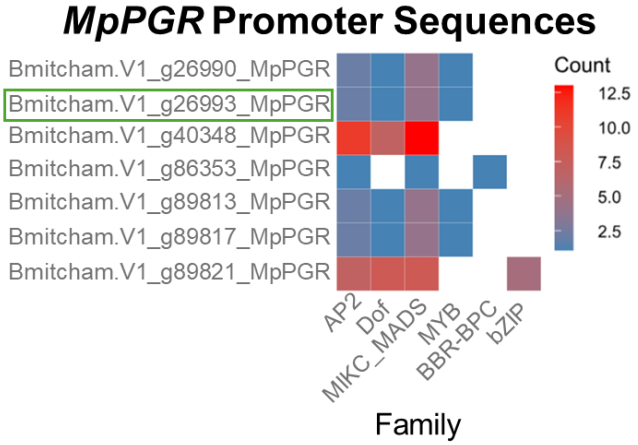
MpPGR Promoter Sequences
Bmitcham.V1_g26990_MpPGR
Bmitcham.V1_g26993_MpPGR
Bmitcham.V1_g40348_MpPGR
Bmitcham.V1_g86353_MpPGR
Bmitcham.V1_g89813_MpPGR
Bmitcham.V1_g89817_MpPGR
Bmitcham.V1_g89821_MpPGR
AP2
Dof
MIKC_MADS
MYB
BBR-BPC
bZIP
Family
Count
12.5
10.0
7.5
5.0
2.5

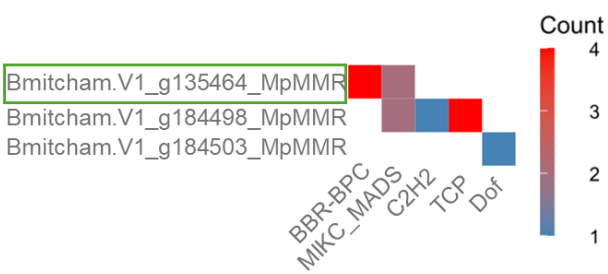
MpMMR Promoter Sequences
Bmitcham.V1_g135464_MpMMR
Bmitcham.V1_g184498_MpMMR
Bmitcham.V1_g184503_MpMMR
BBR-BPC
MIKC_MADS
C2H2
TCP
Dof
Count
4
3
2
1

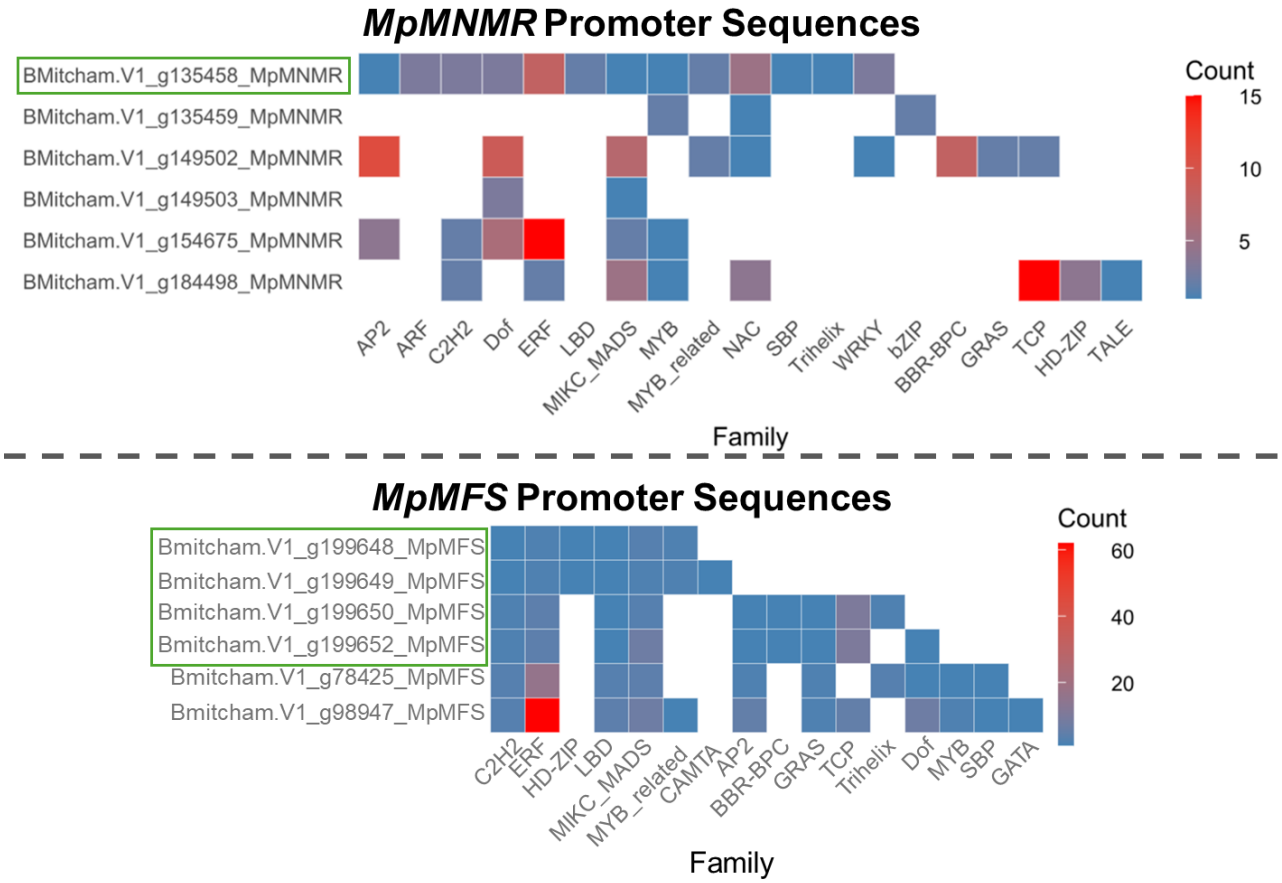

Figure 5.21. Heatmap representing putative TFBS in the promoters of menthol biosynthesis pathway genes. The y axis indicates the corresponding gene ID from the Black Mitcham genome annotation. The x axis indicates transcription factor family. The heatmap represents the counts of the TFBS, where blue shows a low number, while red shows a high number of counts. A green box highlights the gene which showed the highest similarity match to its respective biochemically characterised gene, known as the “canonical” gene.

For all the *MPGPPS.SSU* promoters, the presence of AP2, Dof, ERF, MADS, MIKC_MADS, MYB and MYB_related TFBS were detected (

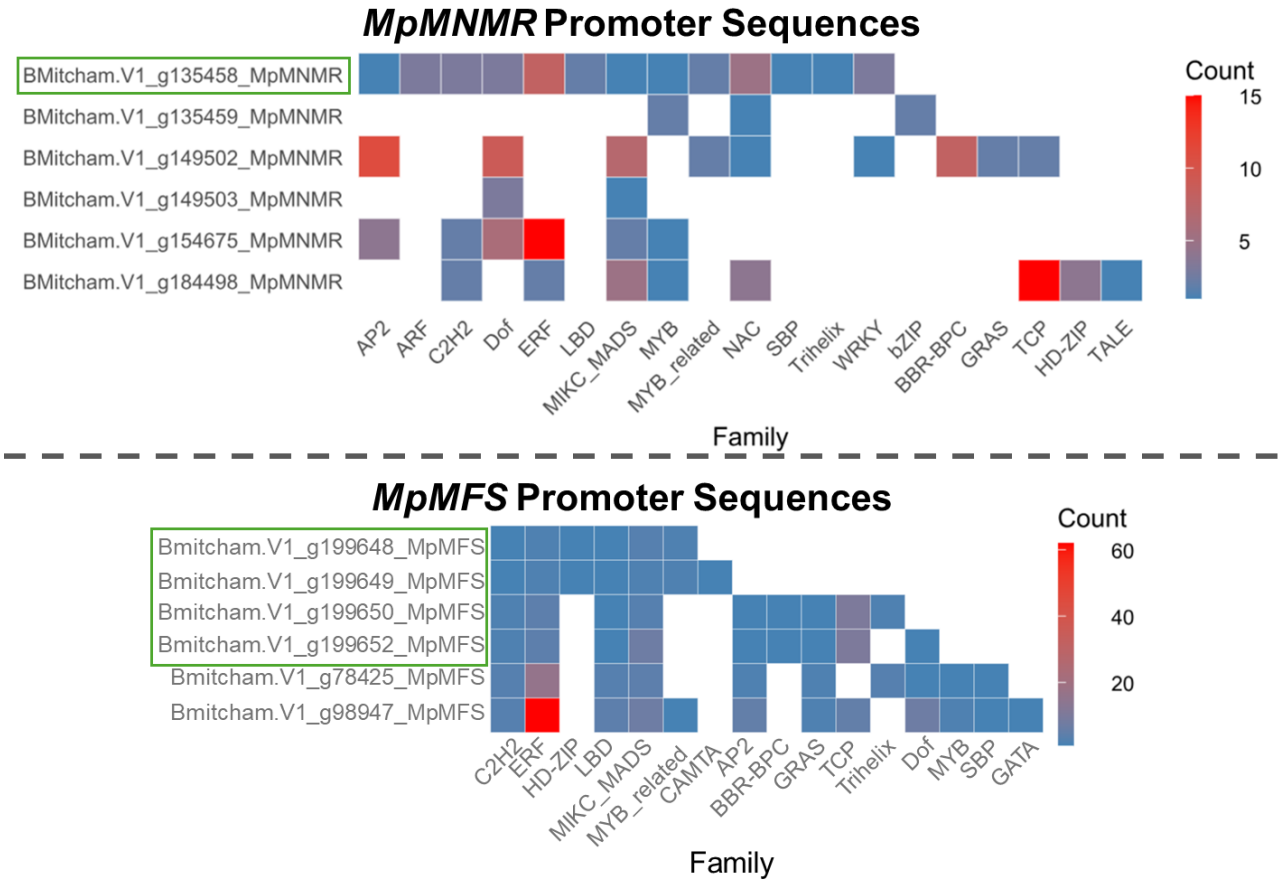

Figure 5.21). For the canonical *MpGPPS.SSU* promoter, only Dof, ERF and MYB TFBS were present. The partner *MpGPPS.LSU* promoters showed the presence of BBR-BPC, B3, C2H2, ERF, TCP, bZIP, SBP and bHLH. The canonical *MpGPPS.LSU* showed only C2H2, SBP and bHLH. *MpGPPS.SSU and MpGPPS.LSU* code for subunits which form a heterodimeric enzyme. Looking at only the canonical promoters, there are no shared TFBS between the promoters. Looking at all the promoters from both *MpGPPS.SSU* and *MpGPPS.LSU*, the only common TFBS is from the ERF family. This suggests that regulation of these genes is controlled by distinct TF families, despite coding for two parts of the same enzyme.

The *MpLimS* promoters showed the presence of BBR-BPC, C2H2, GRAS, MIKC_MADS, bHLH, bZIP, Dof and ERF TFBS. The canonical promoter only had Dof TFBS. The two *MpLimS* genes (Bmitcham.V1_g117374 and Bmitcham.V1_g117378) which have a 99.94% sequence similarity in the coding sequence, and a 99.55% sequence similarity in the promoter sequence, were the

only promoters which contained BBR-BPC, C2H2, GRAS, MIKC_MADS, bHLH and bZIP TFBS. This suggests that each *MpLimS* gene may be under transcriptional control of distinct TF families.

The *MpL3H* PM2 variant had two promoter sequences associated with them, Bmitcham.V1_g117376 and Bmitcham.V1_g117380. Bmitcham.V1_g117376 was the canonical PM2 promoter, and contained TFBS from the AP2, Dof, ERF, HSF, MIKC_MADS and MBD families. Bmitcham.V1_g117380, also classed as a PM2 variant, had the same TFBS, with the addition of the LBD binding site. The *MpL3H* PM17 variant promoters contained AP2, Dof, ERF, MIKC_MADS, LBD, ARF, B3, BBR-BPC, C2H2, GRAS, NAC, TCP, WRKY, ZF-HD, LFY, bZIP, HD-ZIP and Trihelix family TFBS. The canonical *MpL3H* PM17 promoter contained only AP2, ERF, MIKC_MADS, GRAS, NAC and WRKY TFBS, with ERF TFBS being the most abundant. Common TFBS between the canonical *MpL3H* PM17 and PM2 promoters were AP2, ERF and MIKC_MADS, highlighting that these TF families may play a role in the regulation of both *MpL3H* variants.

TFBS families in the *MpIPDH* promoters were the AP2, B3, C2H2, CPP, Dof, ERF, GRAS, MIKC_MADS, MYB, NAC, WOX, YABBY, BBR-BPC, HSF, LBD, TCP and Trihelix. The canonical *MpIPDH* promoter contained only AP2, B3, C2H2, CPP, Dof, ERF, GRAS, MIKC_MADS, MYB, NAC, WOX and YABBY TFBS. The ERF TFBS was common between all of the *MpIPDH* promoters, suggesting a role in regulation of all *MpIPDH* genes.

TFBS for the *MpIPR* promoters were from the AP2, BBR-BPC, C2H2, CPP, Dof, ERF, GRAS, HSF, LBD, MIKC_MADS, MYB, WRKY, bZIP, ARF, G2-like, HD-ZIP, Trihelix, NAC, TCP, bHLH, GATA, TALE, MYB_related, Nin-like and WOX TF families. The canonical *MpIPR* promoter contained only the AP2, BBR-BPC, C2H2, Dof, ERF, GRAS, HSF, MIKC_MADS, MYB, ARF, G2-like, HD-ZIP and Trihelix family TFBS. The AP2 family TFBS was common between all *MpIPR* promoters, suggesting a role in regulation of all *MpIPR* genes.

The MpPGR promoters had TFBS for the AP2, Dof, MIKC_MADS, MYB, BBR-BPC and bZIP TF families. Grouping the *MpPGR* promoters by the subfamilies observed in Figure 5.20, Bmitcham.V1_g40348 and Bmitcham.V1_g89821 showed a different expression pattern compared to the other *MpPGR* genes. The promoters for these

genes included the TFBS for the AP2, Dof and MIKC_MADS, with Bmitcham.V1_g89821 containing the bZIP TFBS family as well, and is the only *MpPGR* promoter to contain this TFBS. In all the *MpPGR* promoters, the AP2 TFBS was commonly found between them all. The *MpPGR* promoters from Bmitcham.V1_g26990, Bmitcham.V1_g26993, Bmitcham.V1_g89813 and Bmitcham.V1_g89817 all shared the same AP2, Dof, MIKC_MADS and MYB family TFBS, suggesting these TF families may be involved in the regulation of these *MpPGR* genes specifically.

The *MpMMR* promoters had the TFBS from the BBR-BPC, MIKC_MADS, C2H2, TCP and Dof TF families. The canonical *MpMMR* promoter Bmitcham.V1_g135464 and Bmitcham.V1_g184503 had similar expression patterns as determined in Figure 5.20. The canonical *MpMMR* promoter Bmitcham.V1_g135464 had a high number of BBR-BPC TFBS, and also the presence of MIKC_MADS TFBS, whilst Bmitcham.V1_g184503 only had Dof TFBS. This suggests that there is no common TF regulating both the *MpMMR* genes, even though they share a similar expression pattern. The last *MpMMR* which showed a different expression pattern (Bmitcham.V1_g184498) had the presence of MIKC_MADS, C2H2 and TCP TFBS, where C2H2 and TCP TFBS were unique to this *MpMMR* gene. As this gene only has the presence of C2H2 and TCP TFBS, this may suggest these TF families have a role in independently controlling the expression of this *MpMMR* gene.

The canonical *MpMNMR* promoter had the presence of AP2, ARF, C2H2, Dof, ERF, LBD, MIKC_MADS, MYB, MYB_related, NAC, SBP, Trihelix and WRKY family TFBS. The other putative *MpMNMR* gene promoters included the bZIP, BBR-BPC, GRAS, TCP, HD-ZIP and TALE family TFBS. There was no common TFBS between all the *MpMNMR* gene promoters.

The *MpMFS* genes had 4 genes which showed an equally high sequence similarity to the canonical *MpMFS* gene. The promoter sequences however, had different TFBS detected. All 4 promoter sequences contained the C2H2, ERF, LBD and MADS family TFBS. Bmitcham.V1_g199646 and Bmitcham.V1_g199649 both had the HD-ZIP and MYB_related family TFBS. Bmitcham.V1_g199649 also had the presence of an additional CAMTA family TFBS. Both Bmitcham.V1_g199650 and Bmitcham.V1_g199652 had the additional presence of the AP2, BBR-BPC, GRAS

and TCP family TFBS. Only Bmitcham.V1_g199650 had the additional presence of the Trihelix family TFBS, whilst only Bmitcham.V1_g199652 had the additional presence of the Dof family TFBS. Other TF family TFBS detected in the other *MpMFS* gene promoters were the MYB, SBP and GATA family TFBS.

Overall, the AP2 and ERF TFBS appear in almost every gene family (*MpGPPS*.SSU*, MpGPPS.LSU, MpL3H, MpIPDH, MpIPR, MpPGR, MpMNMR, MpMFS*), suggesting a general role in monoterpene metabolism in Black Mitcham. This is consistent with the AP2/ERF family of TFs having broader functions in other plants, including regulation of terpenoid biosynthesis (Chen et al. 2025). The MIKC_MADS family TFBS frequently co-occurs with AP2 and ERF (present in *MpGPPS.SSU, MpL3H, MpIPDH, MpIPR, MpPGR, MpMMR, MpMNMR* and *MpMFS*), suggesting a synergistic role in transcriptional regulation. Overall, the canonical gene promoters are associated with fewer TF families. For example, the canonical *MpL3H* PM17 variant only has AP2, ERF, MADS, GRAS, NAC and WRKY, compared to the 16 families detected in the other variants. To further elucidate these potential regulators, the MBP genes were clustered together with any gene that was associated with a TF (as determined by gene ontology analysis), by k-means clustering.

5.2.7 K-means clustering of menthol biosynthesis pathway genes and transcription factor genes to determine putative regulators

K-means clustering was performed on the MBP genes, and any TF related genes to look for co-expression profiles, and therefore putative regulators of the MBP genes. To first determine the optimal number of clusters, three statistical tests were performed: (1) Elbow method, (2) Silhouette method and (3) Gap statistic method. All three methods determined 3 clusters as the optimal method (Appendix Figure 16), however upon visual inspection of the clusters, the shapes of the expression profiles did not cluster tightly enough (Appendix Figure 17). Therefore, cluster numbers of 6 (Appendix Figure 17) and 9 were tested, with 9 clusters showing a tight clustering after visual inspection (Figure 5.22).

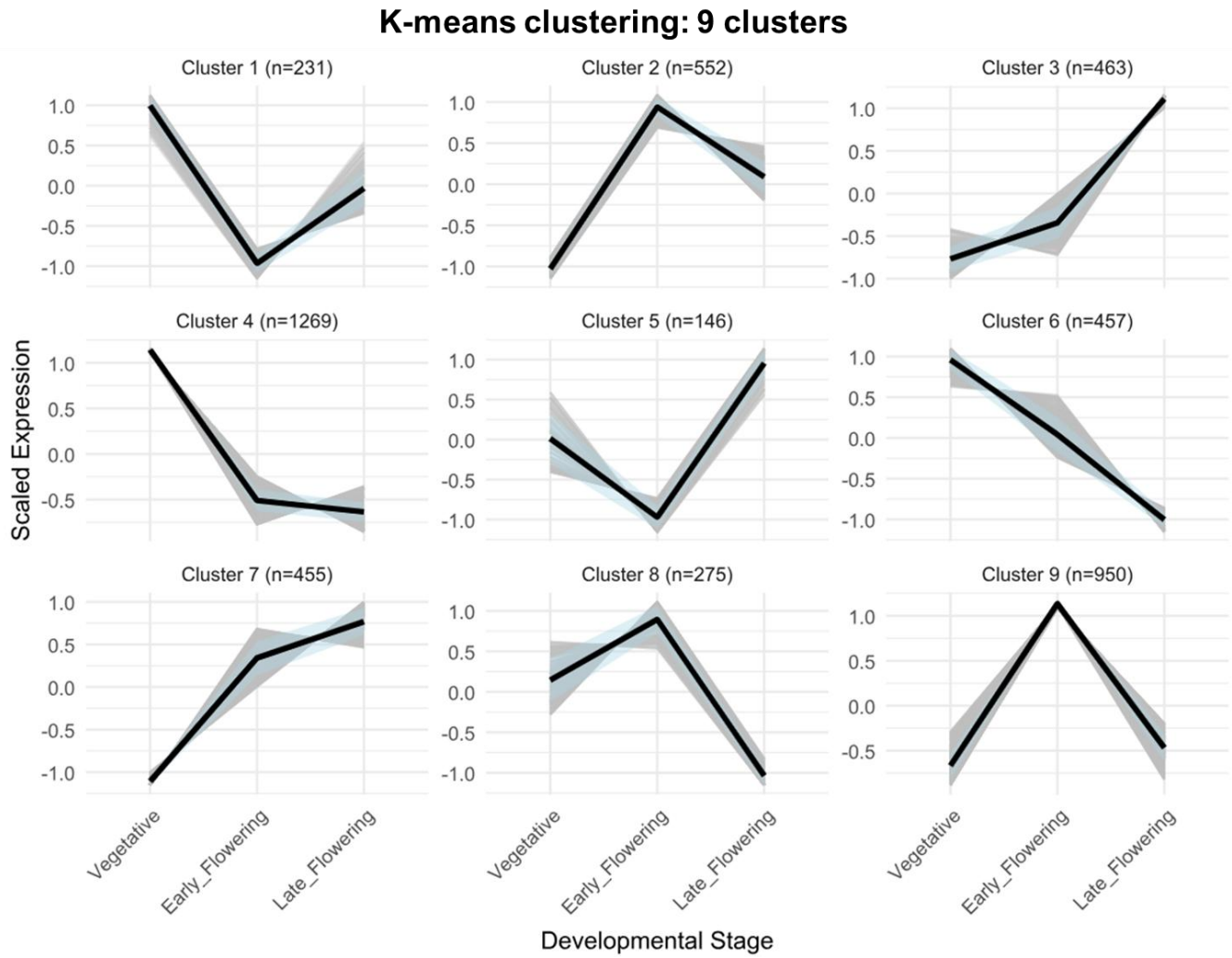

Figure 5.22. k-means clustering of menthol biosynthesis pathway genes and transcription factor genes with 9 clusters. The black line is the cluster centroid, which represents the mean profile of all genes in the cluster. The grey lines represent the individual genes in the cluster. The light blue shading indicates the standard deviation around the mean. Y-axis shows the scaled expression of the mean of normalised counts from 3 biological replicates. X-axis shows the developmental stages. The number of DEGs (n) is shown above each graph.

Clustering into 9 clusters showed distinct gene expression profile shapes for each cluster (Figure 5.22). In terms of genes per cluster, cluster 1 had 231 genes, cluster 2 had 552 genes, cluster 3 had 463 genes, cluster 4 had 1269 genes, cluster 5 had 146 genes, cluster 6 had 457 genes, cluster 7 had 455 genes, cluster 8 had 275 genes, and cluster 9 had 950 genes. To distinguish which TFs were co-expressing with which MBP genes, the clusters where the MBP genes were located were extracted, and the TFs in the same cluster were characterised according to their respective TF family (Figure 5.23).

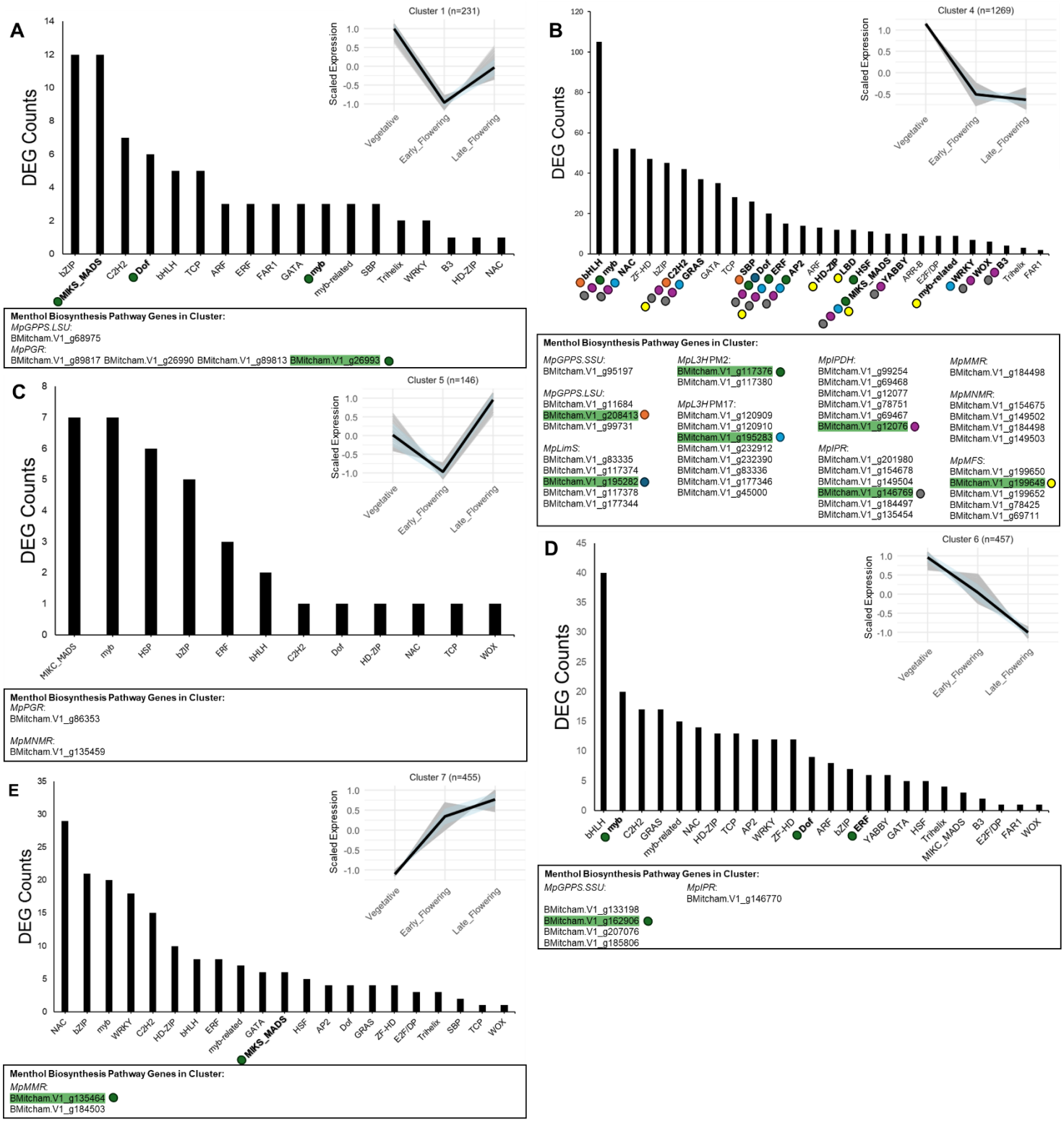

Figure 5.23. k-means cluster information after separation into 9 clusters. Clusters 1, 4, 5, 6 and 7, where menthol biosynthesis genes were located are shown. A. Cluster 1. B. Cluster 4. C. Cluster 5. D. Cluster 6. E. Cluster 7. Cluster expression profiles are shown to illustrate overall expression trends. In each bar graph, the x-axis represents transcription factor families and the y-axis represents the number of differentially expressed genes (DEGs) within the cluster. Canonical menthol biosynthesis genes are highlighted in green. Coloured dots adjacent to transcription factor family labels indicate canonical genes whose promoters contain predicted binding sites for that transcription factor family as identified in Figure 5.21.

The majority of MBP genes, including the canonical genes, clustered into cluster 4 (Figure 5.23 B). Of the canonical genes, these were *MpGPPS.LSU, MpLimS, MpL3H* PM2, *MpL3H* PM17, *MpIPDH, MpIPR* and *MpMFS*. Comparing the TFBS identified in

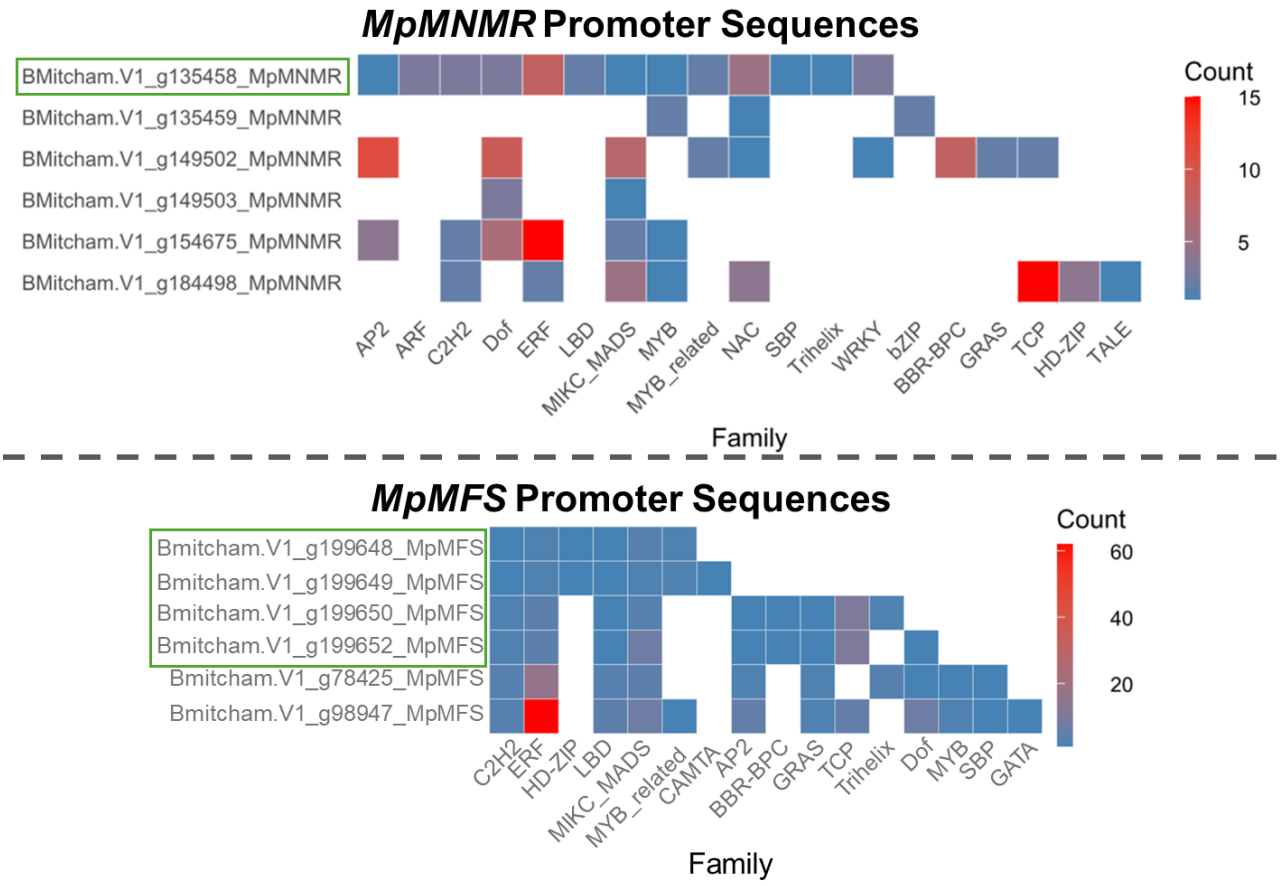

Figure 5.21, with the TF DEGs identified in Figure 5.23, *MpGPPS.LSU* contains the C2H2, SBP and bHLH TFBS. *MpLimS* contains the Dof TFBS. *MpL3H* PM2 contains the AP2, Dof, ERF, HSF, MIKC-MADS and MYB TFBS. *MpL3H* PM17 contains the AP2, ERF, MIKC-MADS, GRAS, NAC and WRKY TFBS. *MpIPDH* contains the AP2, B3, C2H2, Dof, ERF, GRAS, MIKC-MADS, MYB, NAC, WOX and YABBY TFBS. *MpIPR* contains the AP2, C2H2, Dof, ERF, GRAS, HSF, MIKC-MADS, MYB, ARF, HD-ZIP and Trihelix TFBS. Finally, the *MpMFS* contains the C2H2, ERF, HD-ZIP, LBD, MIKC-MADS and MYB-related TFBS. The canonical *MpPGR* gene clustered into cluster 1, which co-expressed with 18 TF DEG families, of which only Dof, MIKC-MADS and MYB promoter binding sites are found on the caonical *MpPGR* promoter (Figure 5.23 A). The canonical *MpGPPS.SSU* gene clustered into cluster 6,

which was co-expressed with the Dof, MYB and ERF TF DEGs, with the corresponding TFBS being detected in the promoter (Figure 5.23 D). The canonical *MpMMR* gene clustered into cluster 7, which was co-expressed with the MIKC-MADS TF, and the promoter had the corresponding TFBS (Figure 5.23 E). This cluster analysis can also be used to identify TF DEGs which anti-correlate with MBP genes. An example of this would be to find TF DEGs in cluster 7 which shows the opposite expression profile to the MBP genes in cluster 4 and 6.

Overall, by matching co-expressing TF DEGs with the TFBS in the promoters of the MBP genes, has narrowed down potential TFs which may have a role in the transcriptional regulation of the MBP. The final stage of the transcriptome analysis performed in this chapter, was identifying a potential *MpIPGI* gene, which has been previously uncharacterised to date.

5.2.8 K-means clustering to identify putative *MpIPGI* genes

The IPGI enzyme function is thought to be synonymous with KSI enzyme function from bacteria, and KSI enzymes are part of the larger NTF2 protein family (Currin et al. 2018; Li et al. 2018; Yang et al. 2024a). To identify putative *MpIPGI* genes from the transcriptome generated in this chapter, k-means clustering was performed as above (5.2.7), with the inclusion of any genes that could be classed as a NTF2 or NTF2-like gene, and re-clustering into 9 clusters was performed. The cluster information of clusters which contained both MBP and NTF2 genes were then extracted to identify putative NTF2 genes co-expressing with MBP genes (Figure 5.24).

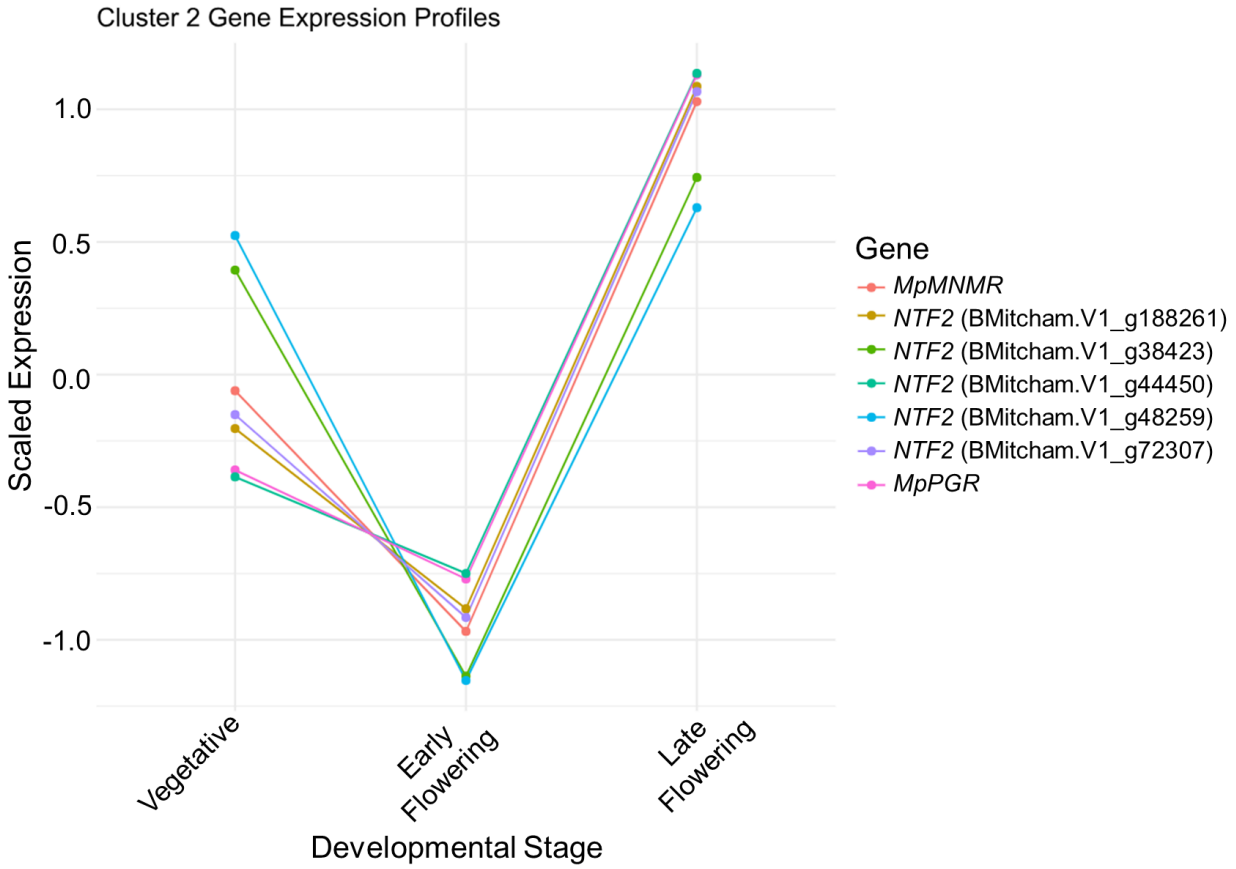

Family	Gene ID	Best Match
MpPGR	BMitcham.V1_g86353	ABR15426.1 (+)-pulegone reductase [Mentha canadensis]
MpMNMR	BMitcham.V1_g135459	ABC88670.1 (-)-menthone:(+)-neomenthol reductase
NTF2	BMitcham.V1_g44450	XP_057793722.1 uncharacterized protein LOC131010288 isoform X1 [Salvia miltiorrhiza]
NTF2	BMitcham.V1_g188261	XP_057810514.1 uncharacterized protein LOC131024952 isoform X2 [Salvia miltiorrhiza]
NTF2	BMitcham.V1_g38423	XP_057805680.1 uncharacterized protein LOC131020706 [Salvia miltiorrhiza]
NTF2	BMitcham.V1_g72307	XP_057805680.1 uncharacterized protein LOC131020706 [Salvia miltiorrhiza]
NTF2	BMitcham.V1_g48259	XP_047976084.1 uncharacterized protein LOC125218454 [Salvia hispanica]

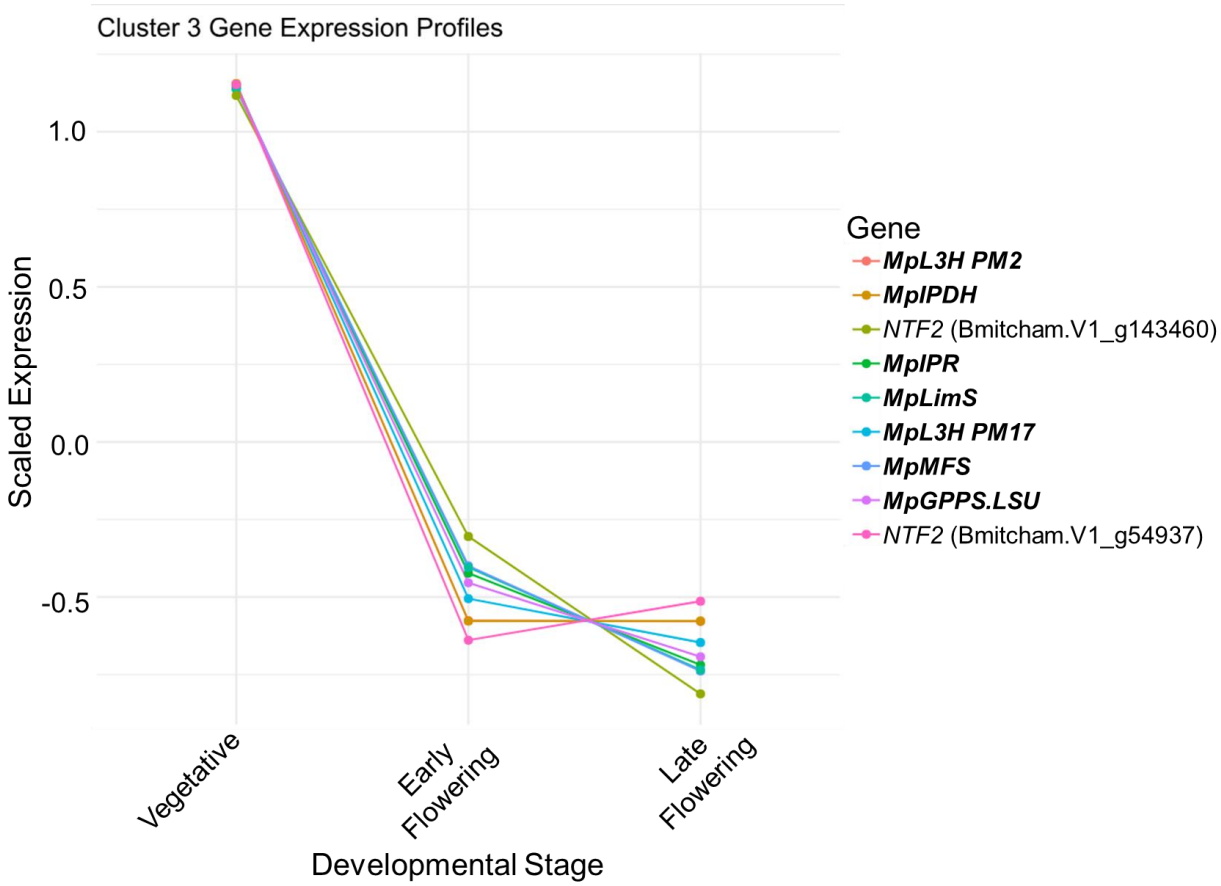

Family	Gene ID	Best Match
MpGPPS.LSU	BMitcham.V1_g208413	AAF08793.1 geranyl diphosphate synthase large subunit [Mentha x piperita]
MpLimS	BMitcham.V1_g195282	AAC37366.1 4S-limonene synthase [Mentha spicata]
MpL3H_PM2	BMitcham.V1_g117376	Q9XHE6.1 RecName: Full=Cytochrome P450 71D15; AltName: Full=(-)-(4S)-Limonene-3-hydroxylase; AltName: Full=Cytochrome P450 isoform PM2
MpL3H_PM17	BMitcham.V1_g195283	Q9XHE7.1 RecName: Full=Cytochrome P450 71D13; AltName: Full=(-)-(4S)-Limonene-3-hydroxylase; AltName: Full=Cytochrome P450 isoform PM17
MpIPDH	BMitcham.V1_g12076	Q5C9I9.1 RecName: Full=(-)-isopiperitenol/(-)-carveol dehydrogenase, mitochondrial; Flags: Precursor
MpIPR	BMitcham.V1_g146769	Q6WAU1.1 RecName: Full=(-)-isopiperitenone reductase
MpMFS	BMitcham.V1_g199649	Q947B7.1 RecName: Full=(+)-menthofuran synthase; AltName: Full=(+)-pulegone 9-hydroxylase
NTF2	BMitcham.V1_g54937	KAG6396422.1 hypothetical protein SASPL_142572 [Salvia splendens]
NTF2	BMitcham.V1_g143460	XP_057769714.1 nuclear transport factor 2-like isoform X1 [Salvia miltiorrhiza]

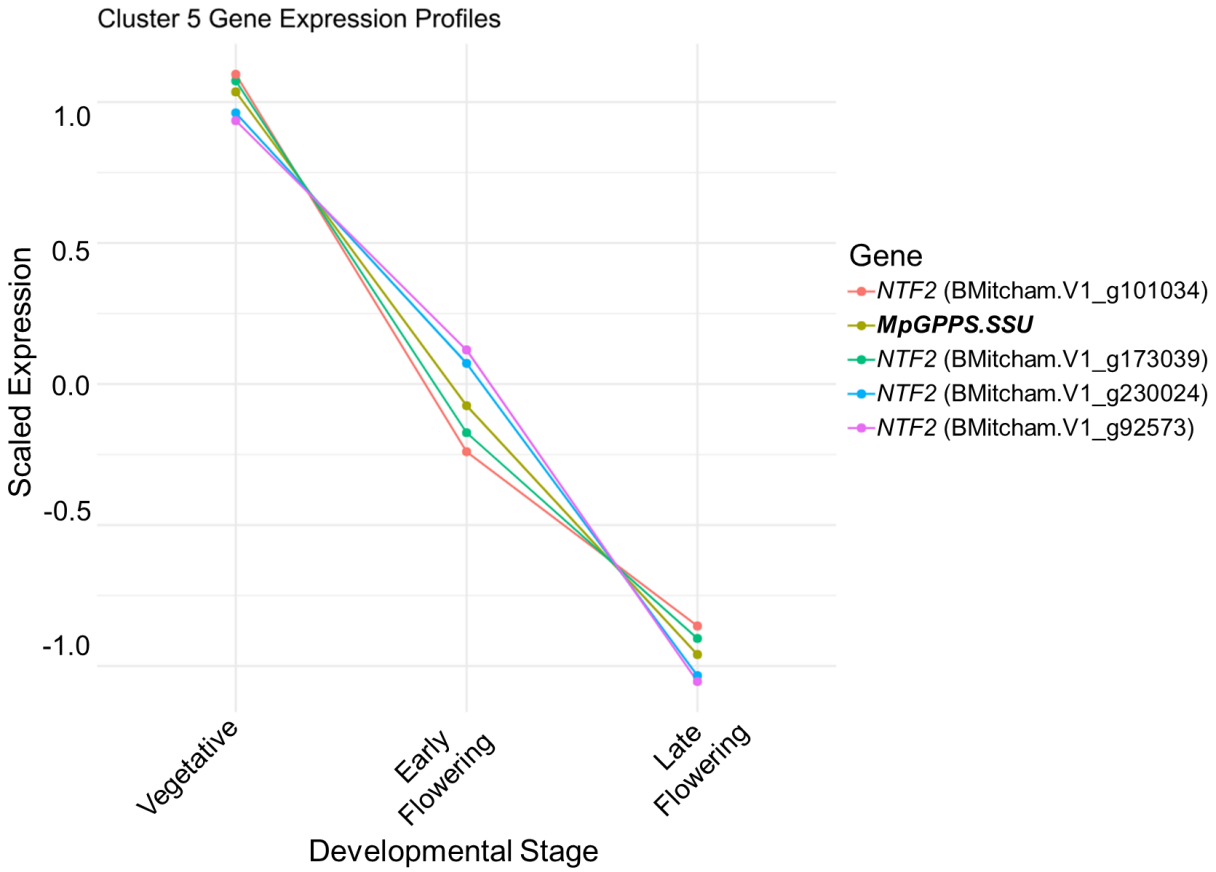

Family	Family	Best Match
MpGPPS.SSU	BMitcham.V1_g162906	AAF08792.1 geranyl diphosphate synthase small subunit [Mentha x piperita]
NTF2	BMitcham.V1_g173039	KAH6757130.1 hypothetical protein C2S53_007968 [Perilla frutescens var. hirtella]
NTF2	BMitcham.V1_g230024	KAH6757130.1 hypothetical protein C2S53_007968 [Perilla frutescens var. hirtella]
NTF2	BMitcham.V1_g101034	KAH6757130.1 hypothetical protein C2S53_007968 [Perilla frutescens var. hirtella]
NTF2	BMitcham.V1_g92573	KAG6396422.1 hypothetical protein SASPL_142572 [Salvia splendens]

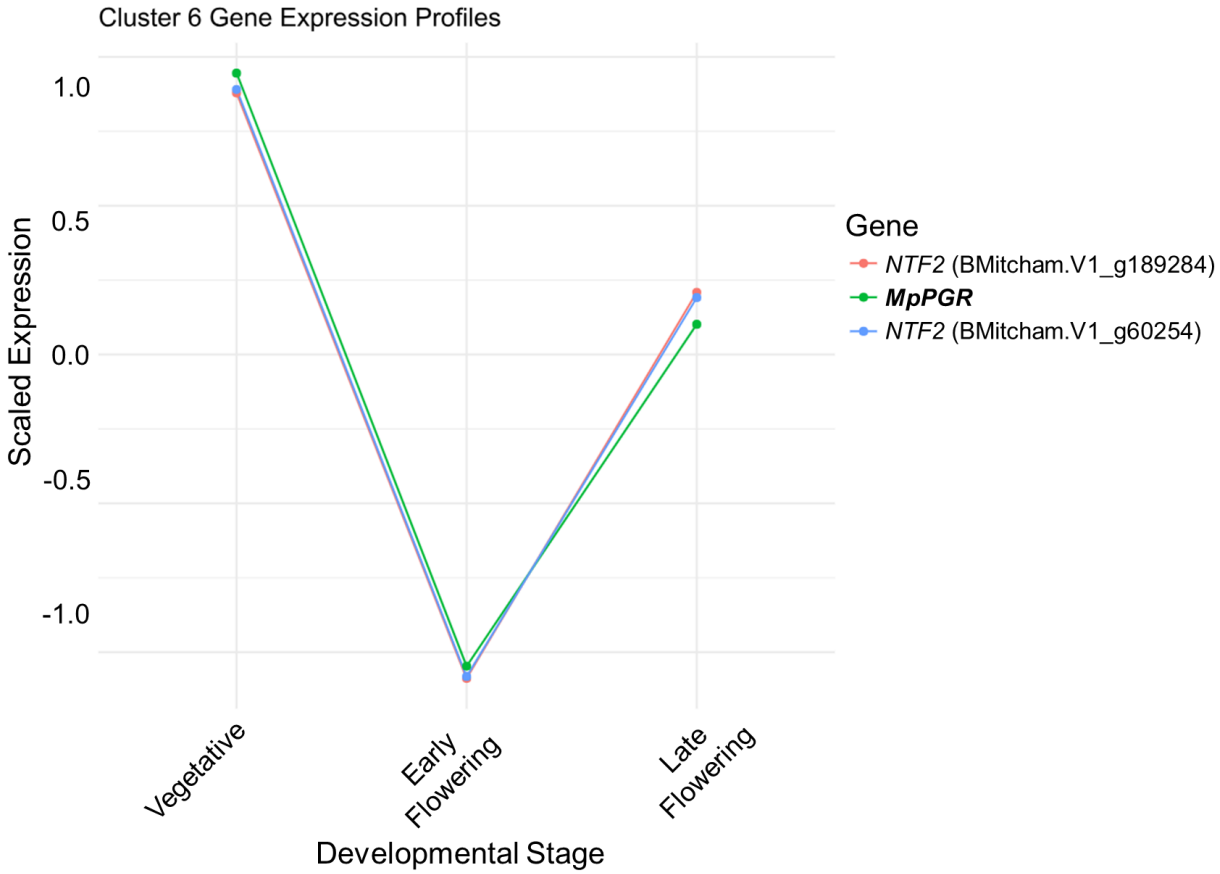

Family	Family	Best Match
MpPGR	BMitcham.V1_g26993	Q6WAU0.1 RecName: Full=(+)-pulegone reductase
NTF2	BMitcham.V1_g189284	XP_057805680.1 uncharacterized protein LOC131020706 [Salvia miltiorrhiza]
NTF2	BMitcham.V1_g60254	XP_057805680.1 uncharacterized protein LOC131020706 [Salvia miltiorrhiza]

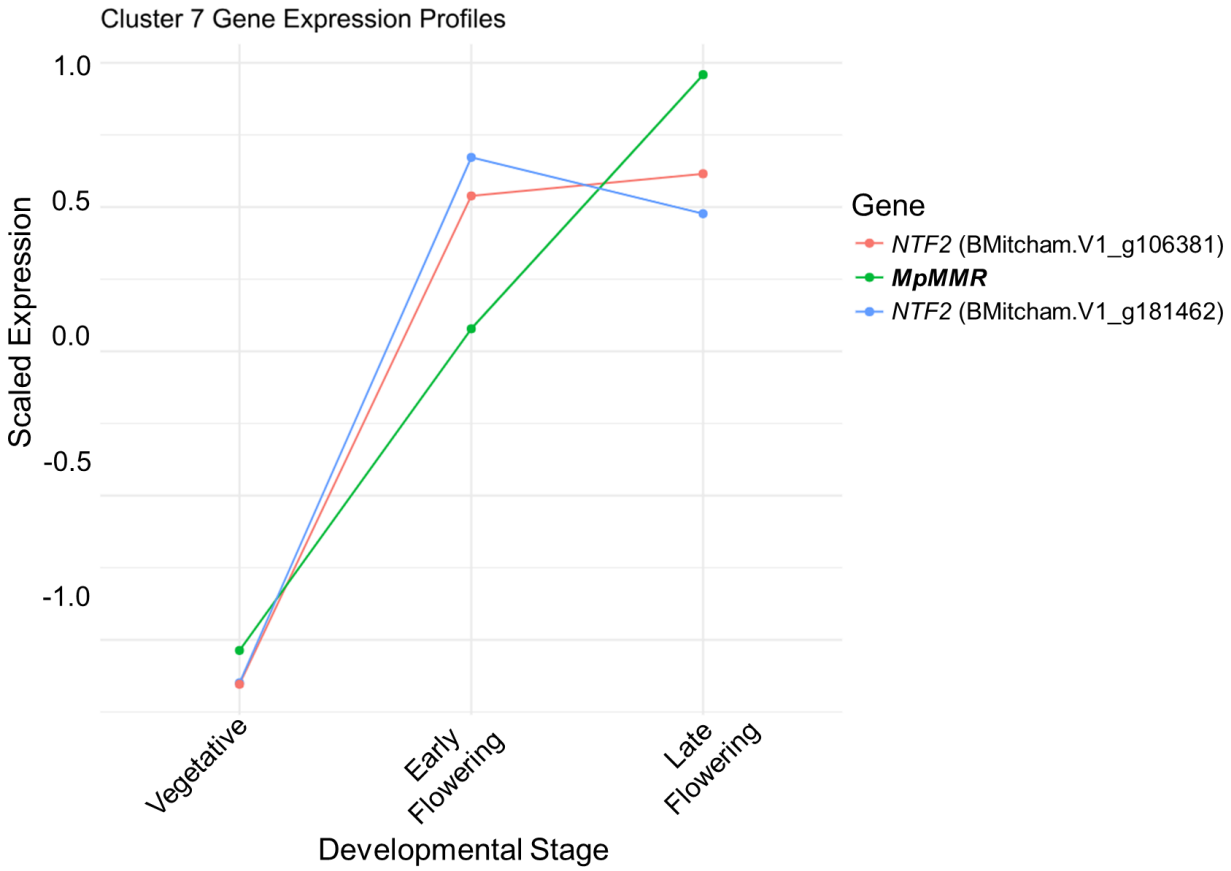

Family	Family	Best Match
MpMMR	BMitcham.V1_g135464	AAQ55960.1 menthol dehydrogenase [Mentha x piperita]
NTF2	BMitcham.V1_g181462	KAH6757130.1 hypothetical protein C2S53_007968 [Perilla frutescens var. hirtella]
NTF2	BMitcham.V1_g106381	XP_057808888.1 nuclear transport factor 2-like [Salvia miltiorrhiza]

Figure 5.24. k-means clustering of menthol biosynthesis pathway genes, transcription factors and nuclear transport factor 2 genes into 9 clusters. Individual cluster graphs where menthol biosynthesis and nuclear transport factor 2 genes co-clustered together are shown. Y-axis shows the scaled expression of the mean of normalised counts, from 3 biological replicates. X-axis shows the developmental stages. Below each cluster graph is a table showing the gene family, gene ID and the best blastx match shown against the lamiaceae protein database. Gene family was determined by first analysing the blastx match results for the lamiaceae. Where this was uninformative, the blastx match results from the Arabidopsis database was used. The canonical menthol biosynthesis pathway genes are shown in **bold** text for clarity. For clarity, where multiple menthol biosynthesis genes for the same gene exist in a cluster, only the canonical gene is shown.

Of the 9 clusters, 5 clusters showed co-clustering of both MBP and NTF2 genes (Figure 5.24). Cluster 2 contained 5 putative NTF2 genes, which also contained non-canonical *MpPGR* and *MpMNMR* genes. Cluster 3 contained 2 putative NTF2 genes, together with the canonical *MpGPPS.LSU, MpLimS, MpL3H* PM2, *MpL3H* PM17, *MpIPDH, MpIPR* and *MpMFS* genes. Cluster 5 contained 4 putative NTF2 genes, together with the canonical *MpGPPS.SSU* gene. Cluster 6 contained 2 putative NTF2 genes, together with the canonical *MpPGR* gene. Cluster 7 contained 2 putative NTF2 genes, together with the canonical *MpMMR* gene. As *MpIPGI* (putative NTF2 family) is located between *MpIPR* and *MpPGR* in the MBP, the NTF2 genes in clusters containing those MBP genes are likely candidates for putative *MpIPGI* genes. Overall, this clustering analysis has identified a range of putative NTF2 family genes, which may correspond to the only uncharacterised gene in the MBP – *MpIPGI*.

5.2.9 RT-qPCR validation of RNAseq dataset

To validate the gene expression profiles observed in the RNAseq dataset, RT-qPCR was performed on a subset of genes from the MBP (*MpGPPS.SSU*, *MpGPPS.LSU*, *MpLimS*, *MpL3H* PM2, *MpL3H* PM17, *MpPGR*, *MpMMR*) and putative NTF2 genes from cluster 3 (BMitcham.V1_g143460) and cluster 6 (BMitcham.V1_g189284) (Figure 5.25).

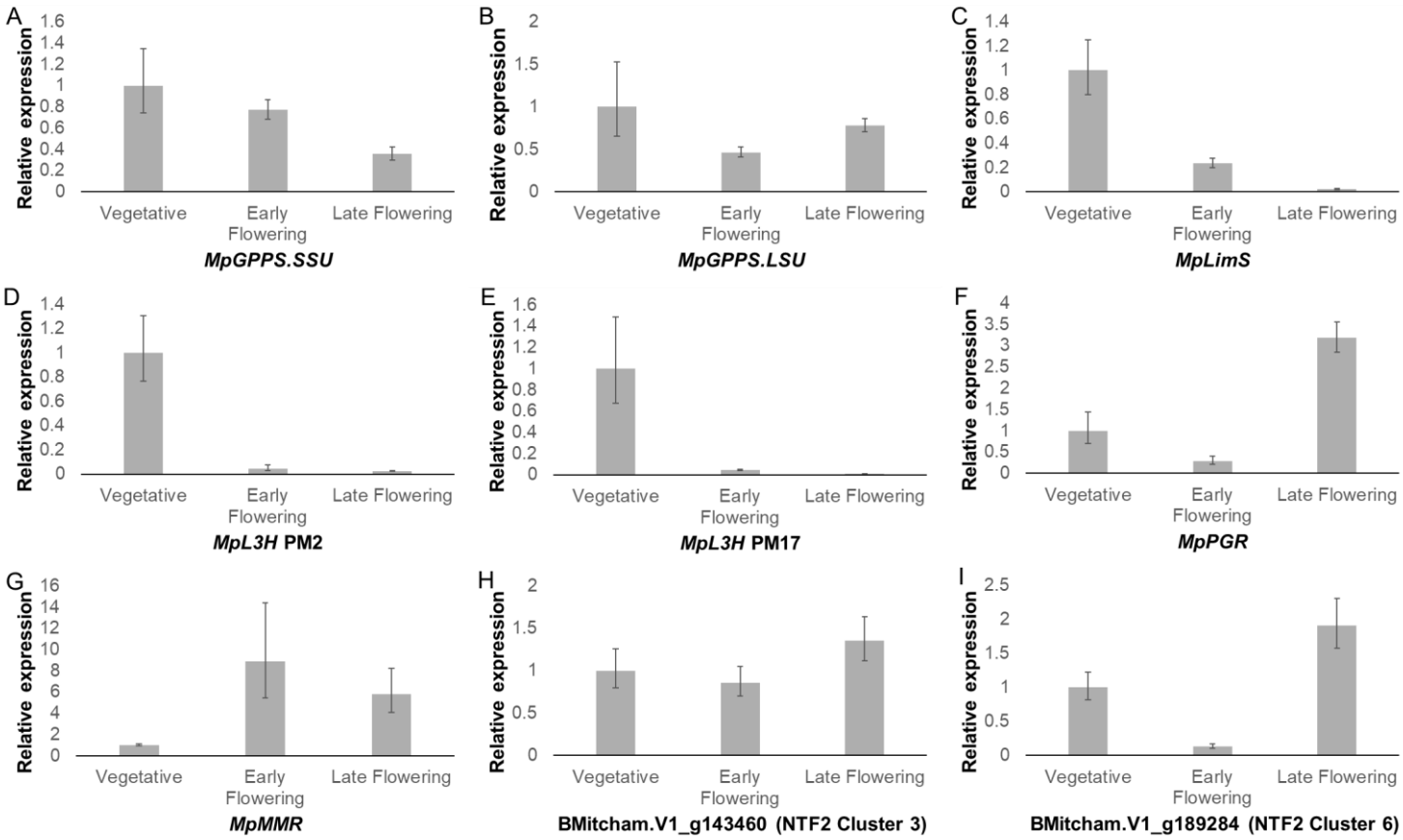

Figure 5.25. RT-qPCR validation of RNAseq data of nine genes in the vegetative, early flowering and late flowering samples. A. *MpGPPS.SSU*. B. *MpGPPS.LSU*. C. *MpLimS*. D. *MpL3H* PM2. E. *MpL3H* PM17. F. *MpPGR* .G. *MpMMR*. H. Putative *NTF2* gene (BMitcham.V1_g143460) from cluster 3. I. Putative *NTF2* (BMitcham.V1_g189284) from cluster 6. Bars are the mean of three technical replicates, and error bars are ± SD.

The expression profile for *MpGPPS.SSU, MpLimS, MpL3H* PM2, *MpL3H* PM17 and *MpPGR* are similar to that of the expression profiles observed from RNA-seq normalised count data (

Figure 5.15, Figure 5.16). The expression profile of *MpGPPS.LSU* is more similar to the BMitcham.V1_g68975 homolog (gene expression drops in early flowering, and increases in late flowering), than to that of the canonical BMitcham.V1_g208413 (

Figure 5.15). *MpMMR* shows a trend of increasing in the early flowering stage, and slightly decreases in the late flowering stage, but overall can be seen as highly expressed in flowering stage tissue (Figure 5.25). This expression profile deviates from that seen in the RNA-seq normalised count expression data, which shows progressive increase in expression in early flowering and late flowering stage tissue. This may be attributed to the variation seen between the biological replicates of the RNA-seq expression data. This is confirmed when manually inspecting the normalised count data from the biological replicate the RT-qPCR is derived from (Vegetative: 103.5671657, Early Flowering: 2340.746155, Late Flowering: 2757.823061). The expression of BMitcham.V1_g143460 (NTF2-like gene from cluster 3) does not match the expression profile of the scaled expression shown in Figure 5.24, as there does not appear to be much change in expression between developmental stages. The expression of BMitcham.V1_g189284 (NTF2 from cluster 6) is in line with the scaled expression shown in Figure 5.24, and also shows a similar expression profile to *MpPGR* which is in the same cluster (Figure 5.25). Overall, the RT-qPCR gene expression is mostly in line with the observed expression profiles derived from RNA-seq data.

5.3 Conclusions

This chapter generated a high-quality RNA-seq dataset aligned to the *M. x piperita* cv. Black Mitcham genome and integrated transcriptomic data with essential oil analysis across leaf developmental stages. Correlating essential oil profiles with gene expression revealed coordinated regulation of the menthol biosynthetic pathway during leaf maturation and flowering.

Multiple genes (and putative homologs) encoding enzymes in the pathway were identified, and their expression patterns were examined in detail. The core pathway genes from *MpGPPS.SSU* to *MpIPR* displayed high expression in vegetative tissue, which declined following the transition to flowering. *MpPGR* showed a distinctive profile, with strong expression in vegetative tissue, a sharp switch-off during the onset of flowering, and reactivation in late flowering tissue. For *MpMMR*, three homologs were identified: two were only expressed after the transition to flowering, while one showed high expression in vegetative leaves, repression during flowering, and re-induction in late flowering tissue.

To investigate regulatory mechanisms, k-means clustering and TFBS analysis identified several candidate TF families potentially involved in regulating menthol biosynthesis genes. Co-expression analysis also highlighted putative NTF2 family genes, which may correspond to the currently uncharacterised *MpIPGI* gene.

Together, these findings provide new insight into the developmental regulation of menthol biosynthesis in peppermint and highlight potential regulatory nodes that may be exploited in future metabolic engineering approaches. The broader implications of these results will be discussed in the general discussion chapter (Chapter 6).

Chapter 6 – Discussion and Conclusions

6.1 Optimisation of *in vitro* regeneration methods and exploration of novel transformation methods in Black Mitcham

A. tumefaciens co-cultivation of Black Mitcham is the most widely reported method for genetic transformation but still suffers from low transformation efficiencies (Niu et al. 2000; Yu et al. 2022). Chapter 3 aimed to address this by optimising the *in vitro* regeneration of Black Mitcham explants, which is a key factor to generate whole transgenic plants following transformation. This optimised regeneration protocol was then used to transform Black Mitcham by *A. tumefaciens*, but after multiple rounds of troubleshooting was unsuccessful. This prompted the exploration of alternative and novel transformation methods for Black Mitcham.

6.1.1 *In vitro* regeneration from Black Mitcham is most optimally produced from young internode segments cultured on NAA and TDZ

The establishment of a stable transformation protocol utilizing infection of explants requires a reliable and efficient *in vitro* regeneration system. While numerous regeneration protocols have been described in the literature, due to the qualitative nature of explant regeneration it is often unclear which protocol is the most efficient (Niu et al. 1998; Wang et al. 2009; Yu et al. 2022). Variability has also been seen between published protocols, stemming from the lack of standardization of explant type, age, media composition and potentially the variant of Black Mitcham clones used in the studies.

To bridge this gap in the literature, a systematic re-evaluation of the optimal explant source and PGR combinations for regeneration of Black Mitcham was performed. A key component in the methodology of this chapter was the omission of coconut water from the medium due to the natural kinetin content. Although a commonly used additive in TC protocols, the inherent biological variability makes it hard to attribute regeneration responses to specific plant growth regulators (PGRs) (George and Sherrington 1984). Its exclusion allowed a clearer assessment of the regenerative potential of the different PGRs tested in this chapter by directly controlling cytokinin levels.

A comparison of different explant sources showed that in general, young internode explants responded more favourably compared to leaf explants, to PGR treatments both in terms of initial callus development and shoot regeneration. This contradicts previous studies which identified leaves as the most morphogenetically responsive explant for shoot regeneration (Niu et al. 1998; Niu et al. 2000). The location of callus formation observed in chapter 3 was consistent with Niu et al (1998), where it was primarily at the sites of dissection, and hence wounding, where callus formation occurred. The use of internode segments as an explant source has also been previously explored in the literature, and their findings were consistent with the work done in this chapter (Wang et al. 2009; Yu et al. 2022). Only Wang et al. (2009) investigated internode position, and found that the position (2) (the 2nd internode section from the shoot apex of the plant) was optimal. However, a direct comparison with this study cannot be made as they tested this on medium supplemented with coconut water, which again makes systematic evaluation difficult due to the inherent variability of coconut water composition. Furthermore, from a logistical perspective, internode segments are more abundant from a donor plant compared to leaf explants and can provide a greater area of regenerative cells per experiment.

In this study, the cytokinins thidiazuron (TDZ), 6-Benzylaminopurine (BAP) and kinetin (KIN) were evaluated for their regenerative induction capacity in Black Mitcham. In internode tissue, both TDZ and BAP performed equally well in shoot regeneration. However, explants cultured with TDZ showed an overall higher regeneration capacity (induction of callus) in the experimental time frame. Although not recorded, and this is a caveat in the experiment performed here, TDZ qualitatively showed a greater number of well-defined shoots per callus compared to BAP. KIN showed the lowest regenerative capacity, and although shoots were still capable of being regenerated, the frequency of callus induction was dramatically lower. Taken together, this shows that TDZ was the PGR of choice for regeneration induction in Black Mitcham. Curiously, varying the concentration range (4.5 µM, 9 µM or 13.62 µM) had no obvious effect on callus induction, as all concentrations showed a 100% callus induction rate. It would be an interesting further study to quantify the number of shoots per explant in the varying TDZ concentrations.

The genotype-specific nature of regeneration was also explored in different *Mentha* species, using the optimised regeneration protocol developed in this chapter. Each

Mentha species showed a varied response when cultured on shoot induction medium (SIM), with *Mentha longifolia* being completely unresponsive to PGR mediated regeneration. This is in agreement with the prior findings that different plant species can use distinct mechanisms to influence regenerative capacity (Chen et al. 2024).

Overall, a PGR regime of 0.5 µM 1-Naphthaleneacetic acid (NAA) and 9 µM TDZ was shown to be effectively to induce shoot-like callus, and upon transfer to HF medium, whole regenerated plants could be obtained (Figure 3.13). Further optimisation of the work performed here would be to quantify shoots per explant, measurement of shoot elongation rates and quantifying the proportion of shoots that successfully root.

6.1.2 Black Mitcham callus can be induced by 2,4-Dichlorophenoxyacetic acid (2,4-D), but are non-regenerative

An alternative approach to directly producing shoot-like callus through SIM, was trialled by the use of 2,4-Dichlorophenoxyacetic acid (2,4-D), which has been commonly used to induce somatic embryogenesis in previous studies (Horstman et al. 2017). 2,4-D has not previously been used for *in vitro* regeneration of Black Mitcham, so this was largely an exploratory approach. The observed phenotype of non-green, friable callus was similar to that observed in other plant species induced with 2,4-D (Krishnan and Siril 2017; Gan et al. 2023; Huang et al. 2023). There appeared to be a change in colour of the callus as concentrations of 2,4-D increased, where lower concentrations showed a darker phenotype, which got progressively lighter with increasing concentration. This concentration dependent phenotype has been observed in 2,4-D induced sorghum seeds, where both a loose white callus (Type 1) and friable, creamy callus (Type 2) were observed, highlighting the unpredictability of somatic embryogenesis induction (Wu et al. 2024). The authors also noted that only callus induced from high concentrations of 2,4-D were capable of regenerating into whole plants (Wu et al. 2024). Black Mitcham explants induced on 2,4-D in this study differed only by callus colour, as both had a loose, non-compact characteristic. It was the difference in colour which informed the decision the take forward callus induced on 9 µM 2,4-D, as it was assumed that the darker coloured callus had begun necrosis and browning. However, the callus

induced through 2,4-D appeared to be recalcitrant to regeneration on SIM used in this study.

A potential future direction for this experiment would be to try alternative combinations of PGRs specific to induction of shooting from 2,4-D induced callus from Black Mitcham. Indeed, both the type and combination and PGRs used can vary wildly when inducing shoot regeneration from embryogenic callus (Kumlay and Ercisli 2015). The browning and subsequent necrosis observed could be tackled by including a period of darkness treatment during TC, as this has been shown to inhibit the activity of phenolic formation associated with callus browning (Permadi et al. 2024). The addition of chemical additives such as activated charcoal (AC) to the growth medium has also been shown to inhibit callus browning (Mensuali-Sodi et al. 1993). Furthermore, callus browning has also been linked to high levels of secondary metabolite production in plants, where AC has been shown to inhibit this (Aliyu 2005). However, in the context of regeneration including an *A. tumefaciens* co-cultivation step, the use of AC in this study was shown to cause an overgrowth of *A. tumefaciens*. Nonetheless, this could be circumvented by the addition of AC in subsequent steps of TC steps following *A. tumefaciens* co-cultivation. For example, including AC in only the TC medium only after residual *A. tumefaciens* has been removed from the co-cultivated explants. The addition of PVPP could also act as an adsorbent to the potential chemicals involved in callus browning (Tang et al. 2004). PVPP is thought to act as a polyphenol binding agent to prevent the browning of callus tissue (Chen et al. 2022). Overall, the investigation of 2,4-D induced callus of Black Mitcham in chapter 3 has laid the groundwork for developing an alternative *in vitro* regeneration protocol for Black Mitcham.

6.1.3 Fipexide (FPX) shows a propensity to induce rhizome-like structures from Black Mitcham explants

Fipexide (FPX) is a novel PGR which has shown versatile applications for the *in vitro* regeneration of both monocot and dicot plant species (Nakano et al. 2018). It has also been used successful in-tandem with *A. tumefaciens*-mediated in poplar and *Brachypodium* (Nakano et al. 2018). FPX has also been shown to outperform typically used PGR combinations in both *in vitro regeneration* and *A. tumefaciens*-mediated transformations in *Brachypodium distachyon* and *Matthiola incana* (Yu et al. 2019; Tanahara et al. 2022). This made FPX an attractive option for its use in

Black Mitcham. As the phenotype of callus induced through FPX can vary between plant species, this was largely an exploratory approach in Black Mitcham as there have been no similar reports on the literature. FPX treated internode explants of Black Mitcham showed the development of hairy root-like callus at lower concentrations (10 μM), whilst at higher concentrations bulbous and friable like callus was observed. Interestingly, the callus was seen to originate throughout the internode tissue, as opposed to originating at the wound sites seen with TDZ, BAP and KIN. Leaf explant tissue at lower concentrations (10 μM) showed friable callus developing throughout the leaf tissue, as opposed to just at the leaf petiole which was typically seen with other PGRs. At higher concentrations (50 μM), the entire leaf morphology was overtaken with friable callus growth. As the callus does not solely originate from the wounded ends of the explants (cut ends of internode explants, leaf petiole of leaf explants), this suggests that FPX induced callus may not be induced by cambium cell exposure which are exposed during wounding (Ikeuchi et al. 2013). Both FPX and 2,4-D induced friable callus in Black Mitcham explants, however FPX induced callus appeared a darker brown at higher concentrations, whilst 2,4-D induced callus showed the opposite effect.

In a similar manner to 2,4-D-induced callus, FPX-induced callus was used as starting material to be transferred to SIM to determine if shoot regeneration could be observed from the potentially regenerative callus. Explants originating from callus induced on lower concentrations (10 μM) of FPX appeared healthier when transferred to SIM. In both leaf and internode explants from explants originating from 10 μM FPX, the callus appears to be a mix of brown and green tissue. Interestingly, rhizome-like structures appear be protruding from the callus masses. A similar trend can be seen with 20 μM FPX induced callus, where there is a mix of brown and green tissue, with rhizome-like structures protruding from the callus mass. In the internode tissue, rhizome-like structures predominantly appear from throughout the internode tissue, as opposed to just at the cut ends. Explants originating from 50 μM FPX concentrations have a higher degree of browning and possible necrosis. However, shorter, possibly rhizome-like structures can be observed developing in both internode and leaf explants. This is the first preliminary study of the use of FPX on Black Mitcham, a plant which propagates vegetatively through rhizomes (Lawrence 2006). It should be noted that prolonged exposure of explants on FPX

eventually led to tissue necrosis (data not shown), hence the decision to first induce explants on FPX and then transfer to SIM. It was hypothesized that shoot development would occur, unexpectedly however, the first documented case of rhizome-like callus was observed. Future work to build on this finding, would be to perform whole genome transcriptomics analysis to reveal key genes involved in FPX induced rhizome formation in Black Mitcham. Indeed, a recent study on FPX induced *Medicago sativa* revealed the involvement of *SMALL AUXIN UPREGULATED RNA (SAUR)* genes, and it would be interesting to elucidate a similar mechanism in Black Mitcham (Zhao et al. 2025). Although it is unknown if FPX is metabolised by the explants, a study in liver microsomes revealed that FPX is readily hydrolysed into methylenedioxybenzylpiperazine and 4-CPA (Sleno et al. 2007). Curiously, 4-CPA is a PGR typically used to inhibit rooting in legumes and used to prevent flower and fruit drop (Yang et al. 2024b). It would be interesting to see if there is indeed a link between FPX, 4-CPA and the rhizome inducing effects observed in Black Mitcham explants. Finally, another avenue for future work would be to transfer the rhizome induced callus onto soil and observe if whole plants could be regenerated. Taken together, this represents a potential new tool to study rhizome development in Black Mitcham.

6.1.4 Stable Black Mitcham transformation is unfeasible through *A. tumefaciens*-mediated transformation utilizing Modular Cloning derived parts and vectors

A multitude of *A. tumefaciens*-mediated transformation of Black Mitcham procedures with varying protocol and effectiveness have been reported in the literature (Caissard et al. 1996; Diemer et al. 1998; Niu et al. 1998; Krasnyanski et al. 1999; Niu et al. 2000; Mahmoud and Croteau 2001; Yu et al. 2022). One of the original goals of this thesis was to utilize the MoClo plant cloning system to introduce large multi-gene vectors into Black Mitcham as a single mendelian inheritance unit to modify gene expression of essential oil related genes (Engler et al. 2014). To achieve this, the main bottleneck to resolve was the development of an optimised transformation method to deliver the multi-gene constructs into Black Mitcham. As there were many reported protocols to do so, inspiration was taken from the literature to outline a set of parameters to optimise this procedure.

One of the key aspects of an *A. tumefaciens*-mediated transformation protocol using explants is the ability to distinguish between transformed and non-transformed tissue. Typically, this is achieved through a selection agent in the form of an antibiotic to prevent the growth of non-transformed tissue that does not harbour an endogenous resistance gene. Although the antibiotics kanamycin and hygromycin, as well as the herbicide phosphinothricin have been used as selective markers in the literature, kanamycin was chosen for this thesis as this was the most commonly used (Li et al. 2001; Mahmoud and Croteau 2001; Yu et al. 2022). Most reported concentration ranges of kanamycin were between 20-50 µg/mL, however in this study, concentrations as low as 10 µg/mL appeared sufficient to either halt or severely impede the development of healthy green callus. This is in agreement with a pioneering paper on Black Mitcham transformation studies, where the authors found a concentration of 1 µg/mL Kanamycin was sufficient to prevent callus development (Caissard et al. 1996). Therefore, a Kanamycin concentration of 20 µg/mL was used in the SM to strike a balance between maintaining a high enough selection pressure to prevent escapes, and not being too high to prevent growth of even resistant callus.

Another major consideration was the *A. tumefaciens* strain used, as different strains are known to yield varying transformation efficiencies depending on the plant (Sheikh et al. 2014). This variation in transformation efficiency can even be observed at the level of plant cultivar (De Saeger et al. 2021). In Black Mitcham, the *A. tumefaciens* strains GV3101::pMP90 and EHA105 have been reported to be effective in transformation, with the latter having been used more frequently in the literature (Diemer et al. 1998; Krasnyanski et al. 1999; Niu et al. 2000; Yu et al. 2022). The *A. tumefaciens* strain LBA4404 was also trialled in the literature, but was shown to be incapable of infecting Black Mitcham (Diemer et al. 1998; Niu et al. 1998; Niu et al. 2000). GV3101::pMP90 and EHA105 are derived from C58 *A. tumefaciens* background strains, whilst LBA4404 is derived from Ach5 (Ooms et al. 1982; Koncz and Schell 1986; Hood et al. 1993). However, a direct comparison of transformation efficiency under exact experimental conditions had not been previously performed, and was therefore another factor that this thesis aimed to address. It was expected that LBA4404 would not transform Black Mitcham tissue, however the fact that Black Mitcham tissue co-cultivated with either GV3101::pMP90 or EHA105 did not lead to

transformation from more than 100 explants was not in line with the successful transformations reported in previous studies (Niu et al. 1998; Krasnyanski et al. 1999; Diemer et al. 2001). Going forward with further potential optimisations, EHA105 was used as the standard, due to it being the more widely cited strain used in the literature (GV3101::pMP90 is only mentioned in a single publication). Additionally, prior to starting the work of this thesis, researchers from the Scofield lab had only used GV3101::pMP90, and similarly could not recover any verified transformants (unpublished). Further optimisation parameters of varying *A. tumefaciens* liquid co-cultivation time, solid co-cultivation time, temperature or addition of chemical additives did not show any change in transformability of Black Mitcham. When AC was added to the medium to supress the callus browning that was sometimes observed in the cultures, it appeared to cause an overgrowth of *A. tumefaciens* around the explants. The addition of AC may have inhibited the cefotaxime added to the SM plates which is used to prevent the overgrowth of *A. tumefaciens* (Alsheikh et al. 2002). This definitively ruled out the use of AC as a potential chemical additive to use in SM.

These findings led to the pL2Kan:GUS plasmid used for transformation optimisation to be called into question, as all other experimental factors used have been successfully used in the literature. Although Kanamycin has been widely used as a selection agent with respect to Black Mitcham, the promoter used in this study may have been non-functional in Black Mitcham. The promoter used to drive Kanamycin expression was the *A. thaliana ACT2* gene promoter sequence which is known to drive strong, constitutive expression in vegetative tissues at all stages of development (An et al. 1996). It is also known to drive transient expression in *N. benthamiana,* as well as drive stable expression as shown in the next chapter (Engler et al. 2014).However, there has been no evidence in the literature of the *ACT2* gene promoter functioning in Black Mitcham, so this could have been a possible reason for the transformation failures observed. The *A. tumefaciens nos* promoter driving expression of the *uidA* gene in pL2Kan:GUS has been shown to function in Black Mitcham (Li et al. 2001). It should be noted that the well characterised driver of strong overexpression CaMV 35S promoter sequence was excluded from the design of pL2Kan:GUS as it was wanted to be used for driving expression of a menthol biosynthesis gene in later construct designs (Guilley et al.

1982; Ow et al. 1987). The rationale for this was to reduce the repetitive use of a single promoter type to circumvent the possibility of transgene silencing occurring (Yasmeen et al. 2023). With this in mind, one hypothesis was that transformation may have been successful, but due to the possible non-expression of the Kanamycin resistance gene, putative transformant explants were unable to regenerate on SM. To test this hypothesis, transformation was repeated without the use of Kanamycin in the selection medium, and the majority of co-cultivated callus were able to generate elongated shoots and subsequently whole plants. However, when stained for *uidA* expression, no GUS activity could be observed from either the developing callus or the elongated shoots. Staining for GUS activity at both callus development and shoot development was to ensure various stages of tissue maturity were captured, and that GUS activity at a particular developmental or temporal stage was missed. When the same pL2Kan:GUS in EHA105 was tested in the model plant species *A. thaliana* and *N. benthamiana* by stable transformation, the *nptII* gene was expressed at a sufficient level to allow selection of both *A. thaliana* seeds and *N. benthamiana* callus on SM containing kanamycin. Furthermore, there was clear expression of the *uidA* gene showing strong GUS staining in both *A. thaliana* young plants, and in both the developing callus and whole plants of *N. benthamiana*. This result highlighted that although *A. thaliana* and *N. benthamiana* are distant relatives to Black Mitcham, both the *A. tumefaciens* strain and the pL2Kan:GUS plasmid were completely functional in these species, but not in Black Mitcham.

Overall, it is still unclear as to why transformation of Black Mitcham was not attainable after the troubleshooting steps performed in chapter 3. One explanation could be that the Black Mitcham used in this study was maintained and propagated *in vitro* and thus underwent somaclonal variation to generate a recalcitrance to *A. tumefaciens*-mediated transformation (Bhatia and Sharma 2015). Indeed, it is known that even between cultivars, transformation efficiencies can vary, and some may even show a complete recalcitrance to transformation (De Saeger et al. 2021). Therefore, perhaps somaclonal variation occurred in the Black Mitcham strain used in this study to an extent where it could be classed as a new cultivar completely recalcitrant to transformation. Another possibility could be that there is intraspecific variation between the Black Mitcham cultivars reported in the literature that had undergone successful transformation. These authors do not state explicitly that the

Black Mitcham cultivar used was sourced from a standardized plant gene bank. Furthermore, the Black Mitcham variety used in this study was established at Cardiff University prior to the start of work on this chapter, and had to be used for consistency. A possible future avenue to troubleshoot the transformation failure of the Black Mitcham used in this study would be to source Black Mitcham from various sources, including the USDA plant gene bank to fully rule out transformation recalcitrance from inter or intraspecific variation.

The plasmid backbone used for transformation is also an important point to consider, as the work in this chapter is the first to make use of the MoClo system to transform Black Mitcham. Previous reports from the literature have successfully used vectors derived from pGPTV, pCAMBIA and pGA (Krasnyanski et al. 1999; Li et al. 2001; Mahmoud and Croteau 2001; Yu et al. 2022). Both pGPTV and pGA derived plasmids contain *A. tumefaciens* origin of replication elements from RK2, whilst pCAMBIA is derived from pVS1 (An 1987; Becker 1990; Komori et al. 2007). The MoClo plasmid backbone pAGM4673 used in this thesis contains RK2 replication elements (Weber et al. 2011). Although the MoClo vector pAGM4673 has not been previously used in Black Mitcham in the past, it is unlikely that the difference in backbone is the cause for transformation failure as the *A. tumefaciens* origin of replication elements are identical. Nonetheless, the nucleotide sequences of the backbones do still differ, and there could be uncharacterised elements causing the inability of the MoClo pAGM4673 vector to transform Black Mitcham. The type IIS restriction enzyme based cloning method of MoClo is still an attractive option for introducing multi-gene constructs in Black Mitcham and a possible future avenue for study may be to create an identical backbone as those from the pGPTV, pGA or pCAMBIA backbones and adapt this to a MoClo system.

The route to generating stable transformants in Black Mitcham and the subsequent host of optimisation and troubleshooting attempts showed that implementing genetic changes in Black Mitcham is not as straightforward as originally thought. The relatively long timelines reported for successful transformations have been between 5-8 weeks for callus initiation and 10-14 weeks for shoot formation to occur on antibiotic selection (Niu et al. 1998; Niu et al. 2000; Yu et al. 2022). This made troubleshooting in this chapter a long and arduous endeavour, as plates of explants had to be maintained and observed over a 14 week period for each experimental

variation. This highlighted the need for a different transformation procedure without the need for explant mediated regeneration in TC to be explored.

6.1.5 RAPID transformation of Black Mitcham highlights potential use in genetic engineering studies

A. tumefaciens-mediated transformation is typically the most commonly used method to deliver exogenous DNA into plant genomes (Azizi-Dargahlou and pouresmaeil 2024). A logistical downside of this process is the need for multiple TC manipulations which require specialist equipment and increased risk of infection during explant handling. There is also the risk of somaclonal variation induced from the explant regeneration process which further complicates the process (Hwang et al. 2017). In this chapter, even after thorough troubleshooting of *A. tumefaciens*-mediated transformation of Black Mitcham, regenerative callus could still not be recovered. Taken together, this lead to the exploration of a novel technique known as the RAPID transformation protocol, which has never been used for Black Mitcham transformations (Mei et al. 2023). As Black Mitcham propagates vegetatively through rhizomes, this represented the perfect opportunity to observe if injection of *A. tumefaciens* solution into rhizome, stem and nodal tissue would be able to regenerate transgenic plants. GUS activity was observed primarily at the sites of injection, whilst a widespread GUS staining pattern was observed in certain rhizome segments and regenerating roots. A much clearer GUS activity was observed in certain root tissue originating from the rhizome injection sites. Although stable, whole transgenic plants were not yet able to be generated as part of the work for this thesis, this still represents a novel and promising result for future research. A potential caveat of the observed GUS activity could be that as the experiment was performed in non-sterile conditions, it could be argued that the GUS activity may have been endogenous activity from the soil microorganisms or surrounding environment. However, this is highly unlikely, as the *uidA* gene used contained two plant introns to ensure that any transcription of the gene would only be capable by plant transcriptional machinery. Additionally, the control plants treated with just the injection solution showed no evidence of GUS activity. Logistically, injection of the *A. tumefaciens* solution required a lot of pressure and it was questioned whether a sufficient volume of solution entered the plant tissue. Overall, this exploratory preliminary experiment into the use of RAPID transformation of Black Mitcham is

extremely promising for both stable and transient studies, and additional studies should look to further optimise this approach.

6.1.6 Biolistic bombardment of Black Mitcham tissue can be a used to rapidly prototype plasmids before committing to stable transformation

A limitation exposed by the extensive troubleshooting of *A. tumefaciens* transformation performed in this chapter is the long regeneration time. Validating if a particular plasmid, or the containing genetic elements would be functional in Black Mitcham through stable transformation is not feasible. Although the MoClo system affords the rapid cloning of different genetic parts into a plasmid, the number of possible permutations and combinations to test require a more rapid approach, before committing to stable transformations. There has only been a single mention in the literature of the use of biolistic bombardment to transform Black Mitcham, and no stable transformants were recovered even after bombarding >22000 explants (Niu et al. 1998). Transient expression was observed however, and this led to a preliminary exploration of using biolistic bombardment to test if MoClo derived plasmids would be functional in Black Mitcham tissue. To this end, Black Mitcham leaf disc tissue was bombarded with the pL2Kan:GUS plasmid, and GUS activity can be observed. This shows that, at least transient expression can be conferred by the pL2Kan:GUS plasmid. These findings collectively indicate that plasmid delivery and short-term transgene expression is achievable in Black Mitcham tissue, whereas stable transformation is likely limited by inefficient genomic integration, selection or regeneration of transformed cells/explants. Interestingly, it appears that the GUS activity may be originating from a glandular peltate trichome, suggesting that targeting expression in just the trichomes is also a possibility. This represents another promising result to utilize biolistic bombardment to rapidly prototype MoClo derived vectors for use in Black Mitcham transformation. A future study should investigate utilizing a large host of different genetic elements and testing them through biolistic bombardment, which would prove as a quality control step prior to committing to stable transformations.

6.2 Heterologous expression of menthol biosynthesis pathway genes in non-native plant hosts

Chapter 4 aimed to develop methods for the transient and stable heterologous expression of MBP genes outside of its native host plant, *M. x piperita*, to evaluate the potential of producing high value compounds such as menthol in plants more amenable to genetic engineering approaches.

To this end, a method to rapidly test and validate the expression of MBP genes was developed in *N. benthamiana*, by use of *A. tumefaciens* leaf infiltration to transiently express genes of interest, and static HS-SPME to detect any resulting volatile terpenes produced. The early genes of the MBP, *MpGPPS.SSU, PaLimS* and *MpL3H* were co-infiltrated into *N. benthamiana* leaves, resulting in the production of limonene and (-)-*trans*-isopiperitenol which was detectable in the headspace of the detached leaves. Further co-infiltration of additional downstream MBP genes of *MpIPDH, MpIPR, PpKSI, MpPGR* and *MpMMR* did not result in the production of the expected downstream products. *In planta* substrate feeding assays were performed to determine *MpPGR and MpMMR* functionality in a transient expression system, where menthone was produced.

As limonene was produced by co-infiltration, had the clearest peak pattern on the chromatogram, and (-)-limonene was readily available as an analytical standard, a method for detection and quantification was developed. This was done by testing liquid solvent extractions, dynamic HS-SPME and static HS-SPME, where only static HS-SPME was able to detect limonene from co-infiltrated *N. benthamiana* leaves. Quantification in this system was enabled by use of an external (-)-limonene standard curve. This enabled the co-infiltration of downstream MEP pathway genes together with *MpGPPS.SSU* + *PaLimS* to determine if a change in limonene production could be observed. Only the addition of *NtDXS* caused an increase in limonene production.

The successfully assayed gene combinations of *MpGPPS.SSU* + *PaLimS* and *MpGPPS.SSU* + *PaLimS* + *MpL3H* were combined into multi gene constructs (pL2_LimS) and (pL2_L3H), which were also able to confer the production of limonene and (-)-*trans*-isopiperitenol in *N. benthamiana* leaves. The pL2_L3H construct was stably transformed into both *N benthamiana* and *A. thaliana*.

Transformation into *N. benthamiana* resulted in the expected products of (-)-limonene and (-)-*trans*-isopiperitenol. Transformation into *A. thaliana* resulted in the production if limonene, (-)-*trans*-isopiperitenol, Isopiperitenone and Piperitenone. Finally, to develop tools for future trichome targeted metabolic engineering studies, a suite of MoClo compatible trichome-specific promoters were characterised in *N. benthamiana* and *A. thaliana*, where the *NtMald1* promoter and *MpPGR* promoter conferred trichome-specific expression in both species.

6.2.1 Reconstitution of the early MBP to produce limonene and (-)-*trans*-isopiperitenol in *N. benthamiana*

The work in this chapter has demonstrated the first report of using MoClo derived vectors to produce limonene and (-)-*trans*-isopiperitenol in *N. benthamiana*. This was done by co-infiltration of *MpGPPS.SSU* + *PaLimS* + *MpL3H* for transient expression studies in *N. benthamiana*. The *p19*-harbouring *A. tumefaciens* was included in all transient expression experiments to increase gene expression by the action of p19 supressing post transcriptional gene silencing (Jay et al. 2023). Resulting chromatograms from co-infiltrated samples were compared against samples infiltrated with only *A. tumefaciens* transformed with the *p19* gene, acting as the control. This control was chosen as it would account for the mechanical stress and defence responses resulting from the physical act of infiltrating a solution into the leaf tissue, the effect of *A. tumefaciens* infection which can lead to a heightened immune response, and the action of the p19 protein itself which can promote salicylic acid signalling (Grosse-Holz et al. 2018b; Chincinska 2021; Hamel et al. 2023).

The production of limonene in *N. benthamiana* has been reported previously in the literature both transiently and stably using a combination of *MpGPPS.SSU* + *PaLimS* (Yin et al. 2017). The authors surmised that the co-expression of *MpGPPS.SSU* with *PaLimS* was necessary to produce limonene. Indeed, one of the proposed mechanisms of heterodimeric GPPS enzymes are their function as “modifiers” to other GPPS enzymes (Wang and Dixon 2009). The GPPS from *M. x piperita* is one such heterodimeric GPPS, and exists as a small sub unit (SSU) and a large subunit (LSU) (Burke et al. 1999). The SSU is believed to be catalytically inactive alone, but can modify the chain length specificity of other hetero or homodimeric GPPS enzymes (Burke and Croteau 2002b). Therefore, when *MpGPPS.SSU* is expressed in other plant species such as *N. benthamiana* or *A. thaliana,* it can modify the

endogenous GPPS/GGPPS of the host plant to favour the production of the C_{10} geranyl diphosphate, which is the monoterpene precursor for limonene. This is why *MpGPPS.SSU* was chosen to be co-expressed with *PaLimS* in both this chapter and in work reported by (Yin et al. 2017). Previous work of this chapter showed that limonene could be reliably detected in the headspace of *MpGPPS.SSU* + *PaLimS* co-infiltrated *N. benthamiana* leaves. An important distinction between the work of this chapter and previous work in the literature, was the use of MoClo vectors and genetic elements to drive expression.

The use of *PaLimS* was chosen over the characterised and *Mentha* derived *Mentha spicata* limonene synthase (*MsLimS*) as Yin et al. (2017) showed that *MsLimS,* either alone or co-infiltrated with *MpGPPS.SSU* was unable to produce limonene in transiently expressing *N. benthamiana* leaves. However, for the purposes of producing MBP intermediates, both *PaLimS* and *MsLimS* favour the production of the (-)-limonene enantiomer, and therefore should be suitable for producing the early (-)-menthol precursor (Colby et al. 1993; Martin et al. 2004). Although enantiomeric determination of which limonene ((+)-limonene or (-)-limonene) was not shown in this chapter, it is highly likely that (-)-limonene was the dominant enantiomer being formed based on previous characterization of the PaLimS enzyme. However, future experiments should involve repeating this experiment and analysing the headspace of limonene-producing *N. benthamiana* leaves on a GC fitted with a chiral column, as this would provide further evidence for the correct identification of the (-)-limonene enantiomer being produced.

Following on from this preliminary work, the next step-wise co-expression was the combination of *MpGPPS.SSU* + *PaLimS* + *MpL3H*. In this chapter, this yielded an isopiperitenol in the headspace when co-expressed in *N. benthamiana* leaves, identified by the NIST database as (-)-*trans*-isopiperitenol. Once again, although enantiomeric determination was not possible in this chapter, the isopiperitenol produced is highly like to be (-)-*trans*-isopiperitenol, as the *MpL3H* used in this chapter has been previously characterised to cause the C3-allylic hydroxylation of (-)-limonene in *M. x piperita*, to produce (-)-*trans*-isopiperitenol (Lupien et al. 1999). The production of the enantiomer (+)-*trans*-isopiperitenol has been previously reported in the literature, in transgenic *N. tabacum* stably expressing three *Citrus limon* L. Burm. f. monoterpene synthases, including (+)-limonene cyclase 1 (*ClLimS*)

(Lücker et al. 2004b), and an additional *Mentha spicata* L. *'Crispa'* L3H (*MsL3H*) (Lücker et al. 2004a). The authors reported the production of (+)-limonene and (+)-*trans*-isopiperitenol, caused by the hydroxylation of (+)-limonene by the introduced MsL3H enzyme (Lücker et al. 2004a). However, the work of this chapter used PaLimS to produce (-)-limonene, and converted it into (-)-*trans*-isopiperitenol by the action of MpL3H. Overall, this is the first report of the reconstitution of the early MBP pathway to produce the intermediates limonene and its hydroxylation product (-)-*trans*-isopiperitenol, by transient co-infiltration of *MpGPPS.SSU* + *PaLimS* + *MpL3H* in *N. benthamiana*.

6.2.2 Utility of multi gene MoClo constructs in both transient and stable expression of the early MBP genes

The production of limonene and (-)-*trans*-isopiperitenol in preliminary experiments was performed by step-wise co-infiltration of multiple *A. tumefaciens* transformed with single gene L1 MoClo constructs. To build upon the utility of the MoClo system, the same L1 MoClo constructs were combined into L2 multi-gene constructs and assessed for production of either limonene or (-)-*trans*-isopiperitenol by transient expression. The L2 multi-gene construct pL2_LimS was able to produce limonene, and pL2_L3H was able to produce both limonene and (-)-*trans*-isopiperitenol. This showed that transient expression of multi-gene constructs was able to replicate the results of the previously seen step-wise co-infiltration of single gene constructs, demonstrating the utility of the MoClo system for reconstituting the early MBP genes. This strategy of transient expression of multi-gene constructs to produce plant metabolites through pathway reconstitution has been previously applied to the production of genistein and scutellarin (Yao et al. 2022), or casbene and jolkinol (Forestier et al. 2021b).

Having demonstrated that the early MBP volatiles limonene and (-)-*trans*-isopiperitenol could be produced by pL2_L3H, the replicability in stable transformants of *N. benthamiana* was performed. The headspace of three independently transformed T0 *N. benthamiana* were assayed, and although all three lines showed the production of limonene and (-)-*trans*-isopiperitenol, line 1 showed the clearest peaks on the GC trace. This showed the applicability of pL2_L3H as a construct for both transient and stable production of early MBP products.

This assessment of stable pL2_L3H T0 transformants was only preliminary however, and there are several potential lines of further investigation to be performed. Firstly, although an untransformed *N. benthamiana* was used as a control in chapter 4, an additional *N. benthamiana* control transformed with just the empty vector and antibiotic selection gene could have been performed to ensure the newly produced products were a result of the pL2_L3H construct and not as a consequence of *A. tumefaciens* stable transformation instead. This is unlikely however, as transient expression of *A. tumefaciens* harbouring only *p19* did not yield any additional products. Secondly, only three independent transformant lines in the T0 generation were able to be generated and analysed in this thesis, and to increase the robustness of the analysis of stable transformants, additional lines need to be assayed to account for the effects of insertional position of the integrated genes. Thirdly, subsequent generations of stable transformants should be grown to a generation where the insertion is homozygous, to ensure stable integration and inheritance of the transgenes (Passricha et al. 2016). Fourthly, genotyping of the stable transformants was not performed, and identification relied solely on selection of antibiotic growth medium and subsequent GCMS analysis for the anticipated products, and therefore would need to be performed to confirm the stable integration of the transgenes. Fifthly, RT-qPCR could be used to determine highest expressing lines, and could serve as an additional selection parameter for selecting the best performing lines. Finally, whole genome sequencing of potential lines would confirm integration of the introduced genes, together with screening more lines to find the most optimal transformant. Overall, the work done in this chapter to reconstitute the early pathway steps of the MBP up to the production of (-)-*trans*-isopiperitenol has laid strong foundations for future MBP reconstruction metabolic studies in *N. benthamiana*, which could be further fine-tuned by tissue specific expression or inducible promoter systems.

Stable transformation of the pL2_L3H construct into *A. thaliana* caused the production of limonene and (-)-*trans*-isopiperitenol as observed in *N. benthamiana*, but also the additional production of isopiperitenone and piperitenone. RT-PCR (Appendix Figure 20) confirmed expression of *MpGPPS.SSU, PaLimS* and *MpL3H* as introduced by the pL2_L3H construct. The *PaLimS* gene would be responsible for the presence of limonene, and the *MpL3H* gene would be responsible for the

presence of (-)-*trans*-isopiperitenol. In *Mentha*, isopiperitenone is produced via the allylic oxidation of (-)-*trans*-isopiperitenol, catalysed by IPDH, which requires NAD as a cofactor (Kjonaas et al. 1985). A BLASTx search of *MpIPDH* to *A. thaliana* matches to various NAD-dependent binding Rossman-fold superfamily proteins (InterPro ID: SSF51735). These enzymes endogenously present in *A. thaliana* may be catalysing the formation of isopiperitenone from the newly produced (-)-*trans*-isopiperitenol. The production of piperitenone from isopiperitenone has been noted in a study using *Mentha* leaf extracts derived from the mesophyll tissue, and is thought to involve an isomerisation reaction (Kjonaas et al. 1985; Croteau and Venkatachalam 1986). However, the native enzyme responsible for this putative reaction has yet to be identified, therefore making identification (e.g. through homology based identification) of the enzyme responsible in *A. thaliana* difficult. Lucker et al. (2004) produced *N. tabacum* lines expressing *Citrus limon* L. Burm. f. (lemon) *LimS* and *MsL3H*, which emitted the expected products (+)-limonene and (+)-*trans*-isopiperitenol, but also noted the production of isopiperitenone, which similarly may be due to endogenous enzyme activity. Taken together, introduction of the *MpIPR* gene to produce (+)-*cis*-isopulegone from isopiperitenone should be theoretically possible, and further transformation with *PpKSI* or the other putative IPGI homologs identified in chapter 5 could bridge the gap towards (+)-pulegone production through heterologous expression. Should this be successful, it was already seen from chapter 4 that *MpPGR* was able to function to convert (+)-pulegone to menthone, and therefore completing the entire heterologous expression of the MBP in *A. thaliana* or *N. benthamiana* could be possible.

6.2.3 Reconstitution of subsequent steps of the menthol biosynthesis pathway

Further step-wise reconstitution of genes following from *MpL3H* did not result in the detection of the anticipated monoterpene intermediates. RT-PCR was performed to check for the detection of the transiently expressed transgenes, and all genes appeared to be transcribed in the transient *N. benthamiana* expression system used in this chapter. The 3 dpi time point used for initial analysis was selected based on maximal limonene detection across a time course of 1, 3, 5 and 7 dpi. However, it was possible that accumulation of downstream intermediates from limonene occurred later or required prolonged enzyme activity. To address this, leaves co-infiltrated with all the MBP genes were additionally harvested at 5 and 7 dpi. Despite

this extended sampling window, none of the expected downstream monoterpene products (such as (-)-menthol)) were detected (Appendix Figure 13). Taken together, these findings suggest that while transcription of the MBP genes are detectable in the transient expression system, downstream pathway reconstitution is limited at a post-transcriptional or metabolic level. This may reflect insufficient enzyme activity, improper protein folding or localisation, inadequate metabolic flux, substrate competition or instability of intermediates in the host *N. benthamiana* (Sirirungruang et al. 2022; Kalalagh et al. 2025a)

To address the possibility that enzymes encoded by MBP genes downstream of MpL3H were improperly folded in *N. benthamiana* leaf tissue, thereby preventing efficient conversion of (-)-trans-isopiperitenol to downstream intermediates, substrate feeding assays were performed. Protein functionality could be determined by substrate feeding assays, where a suitable precursor chemical substrate can be co-infiltrated during or a few days after initial infiltration with the genes of interest to test (Fu et al. 2021). With respect to the MBP, the next readily available substrate was (+)-pulegone, and this was therefore used as an infiltrated precursor for *N. benthamiana* leaves co-infiltrated with *MpPGR* and *MpMMR*. MpPGR, if functional in this assay, this should cause the reduction of (+)-pulegone to (-)-menthone, followed by the reduction of (-)-menthone to (-)-menthol (Battaile et al. 1968; Ringer et al. 2003; Davis et al. 2005). The *in planta* substrate feeding assay from this chapter revelated two additional peaks on the chromatogram, identified as menthone by NIST. The two peaks correspond to either menthone or iso-menthone, however the NIST database was not able to accurately distinguish the two. Exact identification of which stereoisomer could be done by comparison to an external standard of (-)-menthone, but this was not done in this case as the goal for the experiment was the confirmation of MpPGR activity, which was shown. Curiously, no evidence for menthol production was observed in the headspace, which if MpMMR was active, should have reduced the observed menthone to menthol. Taken together, this shows that the MpPGR enzyme was active by way of menthone being produced, and therefore, the bottleneck lies somewhere between MpL3H and PpKSI (MpIPGI homolog). Although chemical synthesis of the intermediates between (-)-*trans*-isopiperitenol and (+)-*cis*-isopulegone was outside the scope of this thesis, a future

direction would be to co-infiltrate each enzyme with its respective precursor to determine enzyme activity *in planta*.

A multi-gene construct harbouring the entire menthol biosynthesis pathway, pL2_MBP was also trialled for both transient and stable expression. In transient expression, no detection of any of the expected monoterpene products were detected. This may be due to the use of a homomeric GPPS (*AgGPPS*) being used in place of a heteromeric small subunit (*MpGPPS.SSU*), as not even the previously observed limonene or (-)-*trans*-isopiperitenol were observed. A homomeric GPPS was chosen as it was unknown at the time of producing the stable *N. benthamiana* transformants whether a heteromeric small subunit GPPS would be sufficient to increase flux towards limonene production in a stable expression system. However, even in stable transformants, the presence of any monoterpene products was unable to be detected. Together with the results of transient expression, these results show that the homomeric AgGPPS used in this study is unable to direct flux into the production of limonene, and the subsequent downstream monoterpene products. Overall, this shows the utility of testing constructs in a transient expression system first, before committing to producing stable transformants.

The failure to detect (-)-menthol and any intermediates following reconstitution of the entire MBP pathway suggests several possible underlying causes and avenues for future investigation. The genes *MpIPDH, MpIPR, PpKSI* and *MpMMR* may not be producing functional protein products in *N. benthamiana*, and thus are not producing the associated monoterpene products. To address this, future work should involve purification of the respective proteins from co-infiltrated *N. benthamiana* leaves and detection through western blotting to confirm protein expression. Recombinant protein purification in *N. benthamiana* is a well-established technique, and pre-existing purification tags from the MoClo kit can be readily added to the coding sequence parts used in this chapter (Engler et al. 2014; Lee et al. 2024). This would be especially important for *PpKSI*, as there may be host incompatibility arising from expression of a bacterial protein in a plant host. Follow up experiments of biochemical characterisation of gene sequences used could be performed in yeast or microbial systems, which can build towards further evidence of why full pathway reconstruction was not possible *in-planta* (Lv et al. 2022b; Roque et al. 2025).

Subcellular localisation of the encoded proteins could also be a key factor in the absence of the expected monoterpene products. In the native *Mentha,* the monoterpene biosynthesis enzymes have distinct subcellular localizations (Croteau et al. 2005). Although the MBP genes used in chapter 4 natively contain localisation signals, the localisation of the transcribed proteins was not confirmed. This could be confirmed by the use of fluorescent tags, which are readily available from the MoClo kit, and visualisation could be performed in *N. benthamiana* protoplasts for example (Rolland 2018).

Another hypothesis is that the intermediates may indeed be being produced but are being sequestered away by conversion into unwanted side products by endogenous *N. benthamiana* enzymes. Indeed, in similar pathway reconstitution studies, the target compounds were seen to be acted on by endogenous *N. benthamiana* enzymes, resulting in oxidation, dephosphorylation and even glycosylation being reported (Liu et al. 2011; Khakimov et al. 2015; Wang et al. 2016a). In a study to reconstitute the early iridoid pathway, the volatile monoterpene geraniol was found to be both either glycosylated or oxidised to non-volatile side products (Dudley et al. 2022a). The modification of normally volatile monoterpenes to a non-volatile state would escape detection by GCMS analysis (Godshaw et al. 2019). Therefore, it may be possible that the MBP intermediates may have been produced but could not be detected by the methods used in this thesis. Future work should explore the analysis of MBP expressing *N. benthamiana* leaves by detection suitable for non-volatile compounds, such as ultra-high performance liquid chromatography – mass spectrometry (UPLC/MS) analysis.

The expressed MBP enzymes may have undergone proteolysis by *N. benthamiana* proteases, such as aspartic of cysteine proteases activated during agroinfiltration stress (Zheng et al. 2024). For future work, reduction of proteolysis could be achieved by: addition or co-expression of proteases during the transformation process, or gene silencing/editing to remove the potential proteases acting on the newly introduced MBP enzymes (Grosse-Holz et al. 2018a; Beritza et al. 2024). Many of the MBP pathway enzymes, particularly the oxidoreductases, require cofactors (ATP, NAD(P)H etc.) to function (Croteau et al. 2005). It may be that there is competition for these co-factors by endogenous enzymes, resulting in intermediate accumulation or diversion that were undetectable by the methods used in this thesis

(Kalalagh et al. 2025b). Furthermore, the MBP enzymes may require currently undiscovered ancillary enzymes to function, which when expressed outside the native plant, fail to function due to the lack of partner ancillary enzymes. This need for ancillary enzymes has been reported in the reconstitution of the monoterpene indole alkaloid biosynthesis pathway in *N. benthamiana*, where co-expression of a major latex protein-like enzyme was crucial for producing the intermediate strictosidine (Dudley et al. 2022a). Therefore, it is plausible that an uncharacterised ancillary enzyme is required to be co-expressed with the MBP enzymes to realise entire reconstitution of the MBP in a non-native plant host.

6.2.4 Co-infiltration of *NtDXS* results in increased flux into the early MBP

The development of a quantitative methodology for limonene detection in this chapter enabled the exploration of whether co-infiltration of any of the MEP genes would result in an increased emission of monoterpenes. In the context of the MBP, the MEP pathway feeds in precursor compounds to be metabolised into further monoterpenes products, one of such being limonene. As limonene was both readily produced, and had a commercially available standard, the effects of co-infiltration of MEP genes was assessed based on the increase of limonene. To do so however, required a quantitative method. Initial work on this chapter relied on qualitative analysis of static HS-SPME samples analysed by GCMS. When additional methods were trialled, such as solvent extractions and dynamic HS-SPME, the previously detectable limonene by static HS-SPME was unable to be detected. This highlighted that the limonene being produced by co-infiltrated *N. benthamiana* was at too low an amount to be extracted by these methods, and hence was unable to be detected on the GCMS .Therefore, a quantitative method based on HS-SPME was performed here, by use of an external limonene standard to quantify against. Although there are caveats to this method, and it cannot be called a truly quantitative method. This is due to the emissions from co-infiltrated *N. benthamiana* originating from a leaf sample, whilst the emissions from the limonene standard were in the form of a liquid. This will inherently introduce inaccuracies, as the matrix (solid *N. benthamiana* leaf) is not matched to the limonene standard matrix (liquid solvent) (Aspromonte et al. 2022). Thus, the quantitative method used in this thesis is only semi-quantitative, and the exploration of matrix effects and matrix matching the sample and external

standards needs to be investigated in the future. Nonetheless, the method used in this chapter enabled both the detection and quantification of limonene (Figure 4.10).

This was leveraged to test if the co-infiltration of the MEP genes together with *MpGPPS.SSU* + *PaLimS* into *N. benthamiana* leaves had any effect on emitted limonene. Of all the genes tested only samples co-infiltrated with the first gene in the MEP pathway, *NtDXS* showed the production of ~932 ng/g FW limonene a statistically significant difference ($p < 0.05$) compared to all other gene combinations tested (~25-83 ng/g FW limonene). A similar effect has been observed in studies looking at diterpene production in *N. benthamiana*, where the *DXS* gene from *S. lycopersicum* and *A. thaliana* were shown to increase the emissions of the diterpenes casbene and cembratrien-ol (Brückner and Tissier 2013; Forestier et al. 2021b). It is important to note that the *DXS* genes only showed an increase in their respective diterpene product when co-infiltrated with a *GPPS* gene, further highlighting the synergistic effects. When the same *S. lycopersicum DXS* gene was co-expressed with *PaLimS* in another study, no appreciable change was detected in the monoterpene (-)-limonene emissions (Yin et al. 2017). Therefore, the species of from which the DXS gene was derived, as well as the context of terpenoid production can have an impact on whether the co-expressed gene has any effect. The co-expression of *NtDXS* + *MpGPPS.SSU* + *PaLimS* in this chapter is the first report of a *DXS* used to increase emissions of the monoterpene limonene. However, future work could include the exploration of different MEP genes from different plant species to determine the optimal set of MEP genes to co-express in the context of increase early MBP monoterpene emissions.

6.2.5 Characterization of trichome-specific promoters for use in future metabolic engineering efforts in *N. benthamiana* and *A. thaliana*

In chapter 4, *N. benthamiana* and *A. thaliana* were stably transformed with pL2_L3H, which contained the early MBP up to the production of (-)-*trans*-isopiperitenol. The promoters used in the pL2_L3H were all constitutively expressed, so tissue specificity of expression was not a consideration. To build upon this for future metabolic engineering studies, a selection of trichome-specific promoters were characterised in both *N. benthamiana* and *A. thaliana* (Figure 4.27, Figure 4.28). This was done to assess suitability in both these systems, to confirm if only purely trichome expression was observed. The rationale for choosing trichome-specific

promoters, was to alleviate the potential detrimental effects to the plant when monoterpenes are expressed ubiquitously (Tissier 2012). An example of this was seen in the *A. thaliana* stably transformed with pL2_L3H, where the leaves showed a high degree of chlorosis in comparison to WT plants. Additionally, the overall aim was to reconstitute the menthol biosynthesis pathway in *N. benthamiana* to mimic that of Black Mitcham, where monoterpene biosynthesis occurs in the peltate glandular trichomes (PGTs) (Gershenzon et al. 2000). Therefore, a selection of trichome-specific promoters was selected from the literature from both *N. tabacum* and *M. x piperita* which were compatible with the MoClo system (did not contain internal type IIS restriction sites) were characterised. Of the selected promoters, only *NtMald1* and *MpPGR* promoters showed strong trichome-specific expression in both *A. thaliana* and *N. benthamiana*. In *A. thaliana*, there was also strong expression in the shoot apex and root tissue conferred by the *NtMald1* promoter, and strong expression in the shoot apex conferred by the *MpPGR* promoter. In *N. benthamiana*, both the *NtMadl1* and *MpPGR* promoters showed strong GUS activity confined to the trichomes. The *MpL3H* promoter showed trichome expression in the developing leaf originating from a callus. The other tested promoters either did not show any expression, or showed non trichome-specific expression patterns, highlighting their unsuitability for confining gene expression purely to the trichomes. Qamar et al. (2022) showed that the MBP gene promoters sourced from *M. x piperita* ‘Madhuras’ (*MpLimS, MpL3H, MpIPDH* and *MpPGR*) were all able to confer glandular trichome specific GUS activity in T0 *N. tabacum* transformants. When the same promoters were tested in this thesis by transformation into *N. benthamiana*, only the *MpL3H and MpPGR* promoters were able to confer GUS activity.

This highlights the need for further characterization of these promoters in *N. benthamiana* and *A. thaliana*. However, the work reported in this chapter has identified two potential trichome-specific promoters (*NtMald1* and *MpPGR*) for use in both *A. thaliana* and *N. benthamiana* metabolic engineering, to drive non-glandular and glandular trichomes expression, respectively. The caveats to the characterization in *N. benthamiana* in developing T0 transformants can be addressed by obtaining T1 transformants and characterising the expression pattern at varying developmental stages. This would help predict the expression pattern when driving monoterpene genes such as *MpLimS* or *MpL3H*, as well as assess the

most optimal time to detect monoterpene production based on developmental stage. Furthermore, identification of the regulatory elements within these promoters conferring trichome specific expression could be used to build synthetic trichome specific promoters for future studies. This could be achieved by promoter deletion analysis, to narrow down regions of the promoter responsible for trichome specific expression, and subsequent motif analysis of the deleted promoter region. A summary figure of the metabolic engineering approach, findings and suggested future directions is shown in

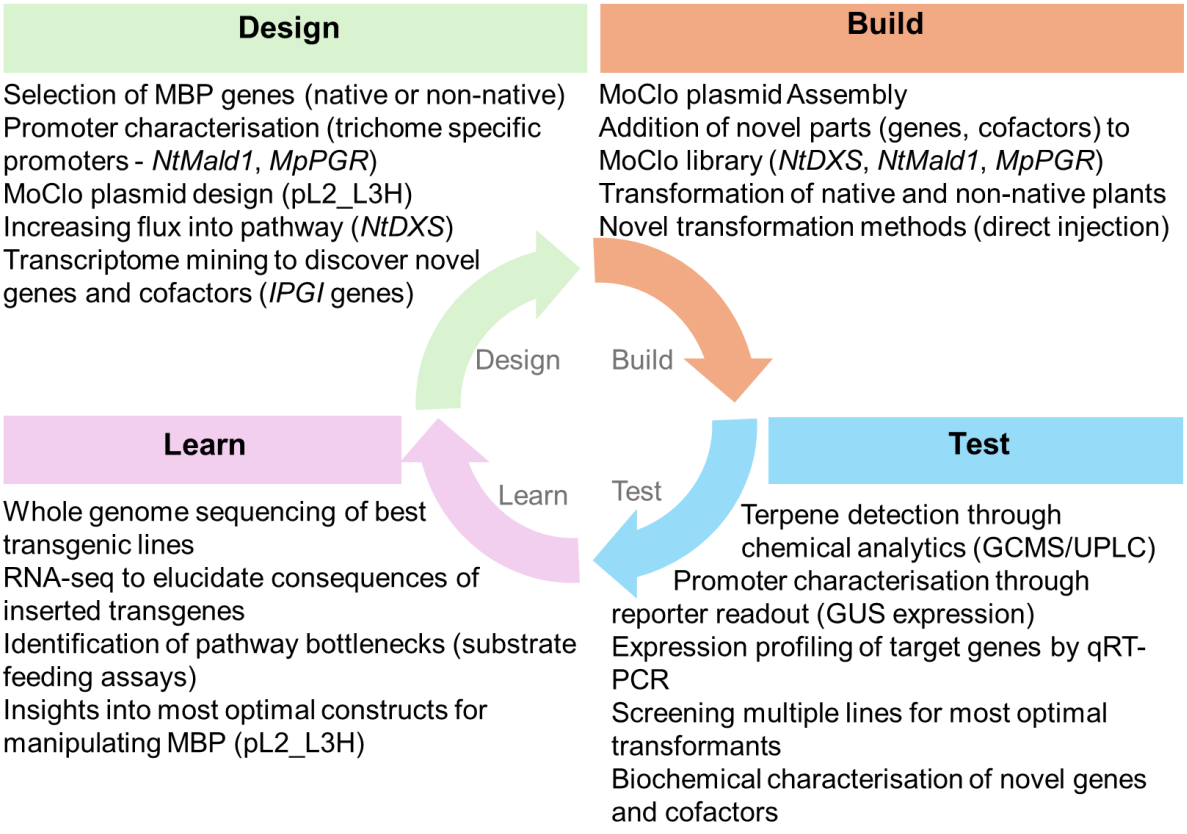

Figure 6.1. Metabolic engineering summary of approaches and findings in this thesis, together with suggested future directions

6.3 Correlation of changing essential oil composition and gene expression in Black Mitcham leaves using transcriptomic methods – a route towards the discovery of novel genes and transcription factors controlling the menthol biosynthesis genes

Chapter 5 aimed to compare the essential oil profile in whole leaves of Black Mitcham from plants at different developmental stages of vegetative, early flowering and late flowering. The leaves which showed the greatest change in the main

essential oil components between developmental stages were chosen to carry out transcriptomic analysis, to correlate the changes in gene expression of the menthol biosynthesis pathway genes with the changes in oil composition. The Black Mitcham genome was recently sequenced and assembled to the chromosome level, although sub-genome resolution was not achieved (Talbot et al. 2024). The last transcriptomics study to be performed in Black Mitcham did not have a reference genome to map against, and instead relied on *de novo* transcriptome assembly (Ahkami et al. 2015). The transcriptome generated in this study is the first of its kind to look at the changes in gene expression profiles over different developmental stages in Black Mitcham, whilst mapping to the newly released reference genome. Mapping to the newly released reference genome overcomes prior studies limitations relying on the diploid *M. longifolia* genome, thereby increasing mapping accuracy and DEG identification by more closely matching the allohexaploid chromosome structure of Black Mitcham (Vining et al. 2022; Talbot et al. 2024). The analysis of this transcriptome was used to identify putative TFs which may be responsible for the changing gene expression profiles of MBP genes which represent the change in essential oil content. Additionally, putative IPGI genes were identified for future study.

6.3.1 Changes in essential oil composition throughout development

In the present study, the solvent extraction method and subsequent GCMS analysis of the leaves from different developmental stages was able to detect the main MBP related monoterpene products pulegone, menthofuran, menthone and menthol. Vegetative leaves had the highest composition of menthone (~70%), which dropped to ~47% in early flowering leaves, and further dropped to ~8% in late flowering leaves. This change in menthone was accompanied by an increase in menthol, where in vegetative leaves menthol is present in trace amount (~0.8%), which then increases to ~23% in early flowering leaves, and a further increase to ~50% in late flowering leaves. A similar trend was observed in a study looking at changes in Black Mitcham essential oil monoterpene composition over time (Gershenzon et al. 2000). The study showed that menthone was highest in 15-day old leaves (75.5%), which steadily decreased to 10% in 55-day old leaves. Appreciable amounts of menthol were only detected in 18-day old leaves (1.6%), which rapidly increased to 54% in 55-day old leaves. Although the growth conditions were not the same as used in this thesis, and the developmental stages of the overall plant were not reported, this

shows that the samples chosen for this thesis accurately represent the transition from an immature essential oil (high in menthone) to a mature essential oil (high in menthol) (Croteau et al. 2005). In this thesis, only trace amounts of limonene were detected in the vegetative samples. Limonene is the first intermediate in the MBP, and has been shown to accumulate in younger leaf tissue (Colby et al. 1993; Gershenzon et al. 2000). Limonene was shown to represent 26.8% of the essential oil in 5 day old leaves, which dropped to 5% in 15 day old leaves, whilst eucalyptol (reported as 1,8-Cineole) was only detectable at appreciable amounts (2.4%) in 15 day old leaves (Gershenzon et al. 2000). However, a similar study showed in their youngest leaf pair, only 0.4% limonene was accumulated, whilst 4% of eucalyptol (reported as 1,8-Cineole) was accumulated (Brun et al. 1991). In their oldest leaf pair, limonene content was relatively unchanged (0.43%), whilst eucalyptol represented 8.8% of the essential oil monoterpene content. In this thesis, between limonene and eucalyptol, only eucalyptol could be reliably detected, and represented ~4% in vegetative stage leaves, ~8.6% in early flowering stage leaves, and finally ~8.2% in late flowering stage leaves, and the difference between vegetative and both early flowering and late flowering leaves was statistically significant ($p<0.05$). Although eucalyptol is not involved in the MBP, the change in content over developmental stages is in agreement with a similar study from the literature (Brun et al. 1991). The lack of detection of limonene in this thesis may be that the vegetative stage samples were too mature, and if trace amounts of limonene were present, may not have been extracted in appreciable amounts by the solvent extraction performed in this thesis. The levels of pulegone did not change appreciably between developmental stages in this thesis, representing only minute amounts in vegetative (~2.4%), early flowering (~2%) and late flowering (~2.3%). However, pulegone has been shown to fluctuate as the leaf ages: 24.9% in 5 day old leaves, decreasing to 7.1% in 15 day old leaves, with another rise to 17.5% in 18 day old leaves, a drop to 11.8% at 21 days, and a rise to 21.1% at 30 days, followed by a sharp decrease to 0.8% in 55 day old leaves (Gershenzon et al. 2000). In another study however, pulegone abundance was not shown to vary, and represented only a small proportion of essential oil content (0.3-2.1%), as observed in this thesis (Brun et al. 1991). These discrepancies may be due to the varied experimental setup or even growth conditions used between these studies (Rohloff et al. 2005). Menthofuran, which is considered to be a stress metabolite and unwanted side product from the

MBP (Burbott and Loomis 1967; Clark and Menary 1980; Voirin et al. 1990; Abdi et al. 2019), was present at ~15.7% in vegetative leaf samples, ~17% in early flowering leaf samples, and ~22% in late flowering leaf samples, showing a slight increase, which was not statistically significant ($p<0.05$). This level of menthofuran is higher than the ranges reported due to variation in growth season and location, suggesting that the growth conditions afforded by the Cardiff University greenhouses at the time of this study may not be optimal for Black Mitcham growth (Pierson and Antoniotti 2025). Finally, menthyl acetate was only detected in the early flowering (~0.08%) and late flowering (~0.6%) stage samples. Menthyl acetate typically only forms in mature leaves, and is found in greater abundance in leaves approaching senescence (Croteau and Hooper 1978; Brun et al. 1991). Therefore, the observation of increasing menthyl acetate content in the leaf samples chosen in this thesis further shows that the leaves represent a transitionary state from an immature to mature essential oil.

Overall, the leaf samples from the vegetative, early flowering and late flowering stages used in this thesis represented the most diverse change in oil composition between all samples tested and represent a transition from an immature oil to a mature oil. However, future work should look to explore a range of earlier vegetative stages, to fully capture the changes in oil composition in more juvenile stages of development, potentially capturing upstream intermediates such as (-)-limonene which were not detected at appreciable levels in this study. Further exploration of alternative extraction methods to increase detection of lower abundance monoterpenes, such as steam distillation or microwave assisted extraction should be performed (Hedayati et al. 2025).

6.3.2 Gene expression changes of menthol biosynthesis genes over developmental stages

For each gene in the MBP, multiple homologs were detected which had distinct expression patterns. The MBP genes were identified by BLASTx sequence similarity to the canonically biochemically characterised genes (Croteau et al. 2005). As each MBP gene had multiple homologs, the homolog with the closest sequence similarity match was termed as the canonical gene (Appendix Table 3). The early MBP genes *MpGPPS.SSU, MpGPPS.LSU, MpLimS, MpL3H* PM2*, MpL3H* PM17*, MpIPDH* and *MpIPR* showed high expression in the vegetative stage leaves, which showed a

progressive decrease in expression in the early flowering and subsequently the late flowering stage leaves. This expression pattern is similar to a previous study which looked at the changes in the expression through RNA-blot analysis of *MpGPPS, MpLimS and MpL3H* in leaves at different ages, whereby it was reported that there was a spike in expression in younger leaves, which tapered off as the leaf matured (McConkey et al. 2000). In a more recent study utilising a transcriptomic approach, the expression of *MpLimS*, *MpL3H* and *MpIPR* were elevated in younger leaves, whilst in mature leaves showed a decrease in expression (Ahkami et al. 2015). There have been two biochemically characterised isoforms for the *MpL3H* gene, the PM2 and PM17 isoform (Schalk and Croteau 2000). From this thesis, the canonical *MpL3H* PM2 showed higher gene expression (8026 normalised counts) in the vegetative stage samples compared to the 7423 normalised counts of *MpL3H* PM17. Expression of recombinant *MpL3H* PM2 and PM17 isoforms in *E. coli* showed that the PM2 isoform showed greater enzyme activity compared to the PM17 isoform (Haudenschild et al. 2000). A transcriptomics study showed that the PM2 isoform was the dominant form in *M. x piperita*, but did not present any data for expression of the PM17 isoform (Ahkami et al. 2015). In this thesis, although both PM17 and PM2 showed relatively high expression in the vegetative stage tissues, the expression of both homologs (BMitcham.V1_g117376 and BMitcham.V1_g117380) for the PM2 isoform could not be detected in early flowering and late flowering stage tissue. The PM17 isoform canonical gene (Bmitcham.V1_g195283) however, maintained expression into the early flowering and late flowering stage tissues, suggesting that the PM17 isoform may have a role during the later maturation of the essential oil profile.

The canonical *MpPGR* gene (BMitcham.V1_g26993) showed high expression in the vegetative stage (754 normalised counts), a drop in expression in the early flowering stage (10 normalised counts), followed by an increase in expression in the late flowering stage (439 normalised counts). The high expression of *MpPGR* in the vegetative stage, coupled with the high expression of the preceding genes (*MpGPPS.SSU, MpGPPS.LSU, MpLimS, MpL3H PM17, MpL3H PM2, MpIPDH* and *MpIPR*) is consistent with the high menthone content observed in the vegetative stage leaves (PGR catalyses the reduction of (+)-pulegone to (-)-menthone) (Battaile et al. 1968; Croteau and Venkatachalam 1986). Furthermore, the leading theory for

essential oil production in *M. x piperita* is characterised by an initial *de-novo* oil synthesis, which is in line with the findings of this this thesis, followed by a later oil maturation, where (-)-menthone is converted to (-)-menthol (Croteau et al. 2005). Ahkami et al. (2015) reported a different expression pattern for *MpPGR,* where it was shown that *MpPGR* expression increased with leaf maturation. A similar expression pattern was seen in the BMitcham.V1_g40348 *MpPGR* homolog, which showed 33 normalised counts in the vegetative stage, increasing to 200 normalised counts in the early flowering stage, and further increasing to 989 normalised counts in the late flowering stage. Direct comparison between the work of Akhami et al. (2015) and this thesis are not possible however, due to the differences in experimental setup and developmental stages used. Furthermore, it is not possible to determine if the transcript (BMitcham.V1_g40348) for *MpPGR* used in this thesis is the same as the one used by Akhami et al. (2015), as the sequence was not reported. With those caveats aside, this could implicate the different homologs of *MpPGR* genes being involved in different stages of (+)-pulegone conversion, however this is with the assumption that transcriptional activity is directly correlated with enzymatic activity, and biochemical characterisation of these *MpPGR* homologs would need to be done.

There were three genes identified as *MpMMR* genes (BMitcham.V1_g184503, BMitcham.V1_g184498 and BMitcham.V1_g135464), with BMitcham.V1_g135464 (canonical gene) showing the greatest homology to the biochemically characterised *MpMMR* (Kjonaas et al. 1982). The canonical *MpMMR* had no expression in the vegetative state tissue, and expression increased in the early flowering stage (60 normalised read counts), and further increased in the late flowering stage (107 normalised read counts). The BMitcham.V1_g184503 had a similar expression pattern, but was expressed in vegetative stage (135 normalised read counts), and rose in expression in the early flowering (2196 normalised read counts) and late flowering (2188 normalised read counts). The action of BMitcham.V1_g184503 may explain the trace menthol amounts detected in the vegetative state leaf samples. The expression pattern of both of these *MpMMR* homologs does match with the increasing menthol composition of the early flowering and late flowering essential oil samples, and is also in line with ‘late maturation’ of essential oil observed in flowering *Mentha* when stored menthone is rapidly converted into menthol (Croteau et al. 2005). The third *MpMMR* homolog (BMitcham.V1_g184498) showed a

separate expression pattern, with high expression (1093 normalised counts) in the vegetative stage, and dropped in the early flowering stage (39 normalised counts), followed by a slight increase in the late flowering stage (154 normalised counts). The high expression in the vegetative stage may be contributing to the trace amounts of menthol observed, however the drop in expression is not conducive to menthol production in the later stage tissues. This homolog may be negatively affected by the expression of the other two homologs, causing a reduction in expression when the other two homologs are expressed. It may even be that the products of the *MpMMR* homologs may produce different menthol isomers, and the formation of these isomers have a role in regulating the expression of the *MpMMR* homologs themselves. A similar feedback mechanism has been speculated for *MpPGR*, where the presence of high levels of menthofuran suppresses the expression of *MpPGR*, to allow pulegone to accumulate (Mahmoud and Croteau 2003). Another explanation is that the three homologs may be under the control of different transcriptional regulators, the possibility of which will be discussed below. In the study by Ahkami et al. (2015), no *MpMMR* expression was observed in the immature leaves, and it was only in mature leaves where *MpMMR* expression was switched on, which is similar to the expression pattern of the canonical *MpMMR* (BMitcham.V1_g135464) identified in this thesis. A transcriptomics study had characterised three *MMR* homologs from *M. x piperita* 'Cim-Madhuras', and found that their expression varied (Akhtar et al. 2017). As the change in developmental stage was not a focus of the above study, the source of plant tissue (age, developmental stage, leaf pair etc.) was not reported. The catalytic activity of the *MpMMR* isoforms did not correlate with expression values, as for example their MPMD1 (MMR isoform 1) showed the lowest expression compared to MPMD2 (MMR isoform 2) and MPMD3 (MMR isoform 3), but had the highest catalytic activity (Akhtar et al. 2017). Conversely MPMD3 had the highest expression but lowest catalytic activity. In the *MpMMR* homologs identified in this thesis (from *M. x piperita* cv. Black Mitcham) distinct expression patterns were also seen, however further biochemical characterisation is needed to determine the catalytic activity. This information could then better explain the different expression patterns observed between the homologs at the different developmental stages shown in this thesis.

There were four *MpMFS* genes which had 100% sequence similarity to the biochemically characterised gene, however only three (BMitcham.V1_g199652, BMitcham.V1_g199649 and BMitcham.V1_g199650) were classified as DEGs after the threshold imposed in this study (log_2fc >1 or <-1, padj<0.05) (Bertea et al. 2001) (Figure 5.17,Figure 5.18). All of the homologs identified showed a similar expression pattern, with high expression in the vegetative state tissue, which gradually decreased in the early flowering and late flowering stage samples (Figure 5.17). This is not consistent with the increasing menthofuran content in the essential oil observed from vegetative to early flowering to late flowering samples (Figure 5.14). It has been shown that suppression through RNAi of *MpMFS* has led to a decrease in menthofuran levels in transgenic Black Mitcham, suggesting a strong correlation between transcriptional activity and menthofuran production (Mahmoud and Croteau 2003). Therefore, based on the menthofuran content observed in this thesis, the transcriptional levels of *MpMFS* would have thought to be elevated (and subsequently the protein, however proteins were not measured) at all developmental stages, however this was not the case. As the menthofuran levels did not dramatically vary however, it could be that menthofuran accumulates in the vegetative stage and is subsequently stored in the PGTs, and that the differences observed in this thesis are purely due to the chemical extraction efficiency methods used. Although in the study done by Ahkami et al (2015), it was shown that *MpMFS* expression was high in immature leaves, and decreased in mature leaves, which is in line with the findings of this thesis. Nonetheless, this requires further investigation, and biochemical characterisation of all the *MpMFS* homologs is needed to confirm their identity.

Overall, a general trend of the early MBP genes (*MpGPPS.SSU*, *MpGPPS.LSU* until *MpPGR*) having high expression in vegetative tissue is in line with the high menthone content observed in the essential oil (Figure 5.4). This is also consistent with the prior observation of a *de-novo* oil synthesis first phase where menthone first accumulates in PGTs (Croteau et al. 2005). The second phase is characterised by a later conversion of menthone to menthol, which is in line with increasing *MpMMR* in early flowering, and peaking in late flowering leaf samples (Figure 5.16), as well as the observed high menthol in the essential oil (Figure 5.4) A summary figure of these

findings is shown in Figure 6.1

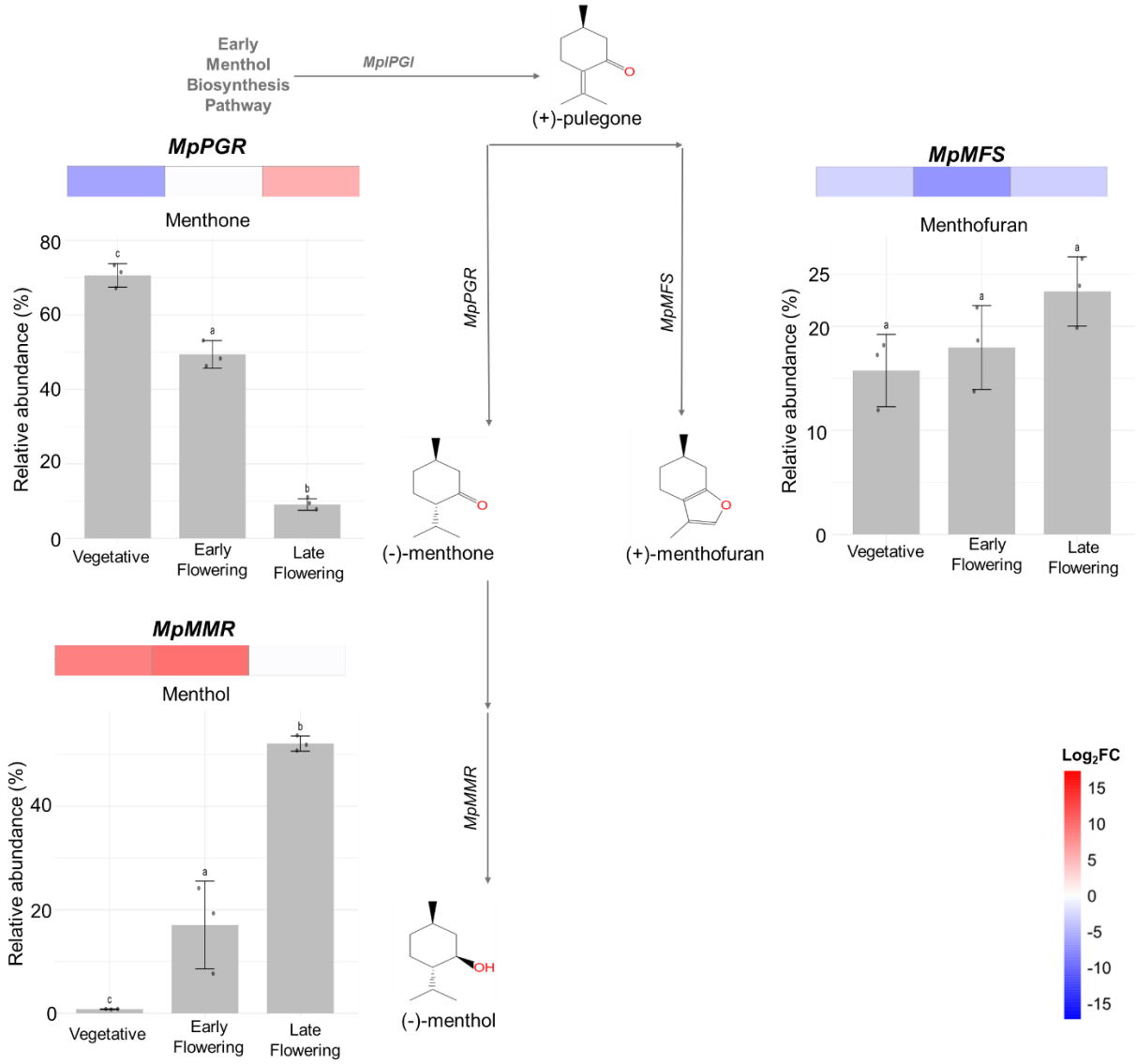

Figure 6.2. Summary of transcript expression and monoterpene composition over different developmental stages. Figure is adapted from data from Figures 5.5 and 5.20. Heatmaps from Figure 5.20 only show the gene expression for the canonical homolog for each respective gene shown. Data is only shown for monoterpenes which were detected, and also had a corresponding gene associated with it.

6.3.3 Functional enrichment analysis of DEGs at the different developmental stages

A comparison of upregulated or downregulated DEGs in the early flowering vs vegetative, late flowering vs vegetative, and late flowering vs early flowering revealed a core set of genes (769 upregulated DEGs, 3087 downregulated DEGs) which were either showing a consistent increase or decrease in expression from vegetative, to early flowering, to late flowering. DEGs which showed a consistent

increase in expression were associated with the carotenoid biosynthesis pathway, strigolactone biosynthetic processes and abscisic acid-activated signalling pathway terms. Carotenoids in photosynthetic green tissue such as leaves are involved in roles such as photosystem assembly, photoprotection and light harvesting (Domonkos et al. 2013). They also serve as precursors in the production of strigolactone and abscisic acid, both of which contribute to plant growth, development and stress responses (Smith 2014; Stra et al. 2023; Mo et al. 2024). Consistently upregulated DEGs were also associated with strigolactone biosynthesis and abscisic acid-activated signalling pathways. Downregulated DEGs included the biosynthesis of secondary metabolites and metabolic pathways. Taken together, the progressive upregulation of carotenoid, strigolactone, and ABA-related genes from vegetative through early to late flowering likely reflects increasing demands for photoprotection and photosynthetic efficiency in developing source tissues, alongside the need to coordinate shoot architecture, flowering time, and stress resilience during reproductive development (Riboni et al. 2016; Zhang et al. 2020; Cholin et al. 2024; Visentin et al. 2024). In contrast, the concurrent downregulation of broader metabolic pathways suggests a developmental shift in resource allocation away from general metabolism and towards reproductive investment (Huang et al. 2024; Khan et al. 2024; Liu et al. 2025).

As secondary metabolite production and general metabolic pathways require a sugar source derived from primary metabolism, the downregulation of these pathways could lead to an accumulation of sugars (Aharoni and Galili 2011). The accumulation of sugars has been linked to leaf aging, where older leaves show a greater accumulation of sugars compared to younger leaves, and this may explain why there is a progressive downregulation of DEGs associated with secondary metabolite production and metabolic pathways (Asim et al. 2023).

Functional enrichment analysis of DEGs in the early flowering vs vegetative comparison showed that the KEGG pathway term ‘biosynthesis of secondary metabolites’ was an enriched term (Figure 5.12). These terms were shared in both upregulated and downregulated genes, and may represent the downregulation of the early MBP genes, and upregulation of *MpMMR* genes as the shift towards oil maturation occurs, whereby (-)-menthone is converted into (-)-menthol. This is further accompanied by an upregulation of DEGs associated with isoprenoid

metabolic processes, which provides precursors to metabolic pathways such as the MBP (Lange et al. 2001). This is same trend is seen in the late flowering vs early flowering comparison, and may further indicate the downregulation of more early MBP genes and further upregulation of *MpMMR* genes as oil maturation continues (Figure 5.13). This may also be reflected in the late flowering vs vegetative comparison, where although there is a high proportion of downregulated DEGs associated with the biosynthesis of secondary metabolites, there are a subset of upregulated DEGs associated with secondary metabolite biosynthetic process and terpenoid biosynthetic process, which may reflect the transcriptional reprogramming required for essential oil maturation during later developmental stages. Additionally seen in the late flowering vs vegetative comparison is a combination of upregulated and downregulated DEGs associated with pyruvate metabolism, and may further be implicated in the change in gene expression associated with essential oil maturation. However, as the samples for RNAseq derived from whole leaf tissue, a whole range of different changes in the leaf are reflected in the GO analysis, many of which are interconnected pathways, making it difficult to distinguish which changes are related to menthol biosynthesis. Furthermore, a caveat of the functional enrichment analysis performed in this thesis is that it uses DEGs which had an annotation from *A. thaliana*, which may not reflect the true nature of the DEG in *Mentha*, and therefore may not accurately capture the changes related to the MBP.

6.3.4 Promoter analysis and putative transcriptional regulators of menthol biosynthesis pathway genes

Previous genetic engineering approaches in Black Mitcham have relied on perturbation of the MBP genes themselves to influence both composition and yield of the essential oil (Lange et al. 2011). The work presented in chapter 5 of this thesis to identify new MBP homologs for genetic engineering approaches is an attractive option for future study, both in stable and transient transformation approaches. An alternative approach is to modify the expression of TFs that regulate the MBP genes, ideally multiple genes at once. Terpene synthesis in plants is regulated by various TF families, such as the AP2/ERF, bHLH, MYB, NAC, YABBY, WRKY and bZIP families (Wang et al. 2016b; Reddy et al. 2017; Xu et al. 2019b; Singh et al. 2024) Examples of these TFs have been most notably reported in the artemisin biosynthesis pathway from *Artemisia annua*, such as *AaWRKY1, AaERF1* and *AaERF2* (Ma et al. 2009; Yu

et al. 2012). To elucidate potential TF families that may be involved in the regulation of the MBP genes, promoter analysis was performed to find putative TFBS using plantTFDB (Jin et al. 2017), combined with k-means clustering to find which TF families shared the same expression patterns as the MBP genes (Figure 5.21).

The *MpGPPS.SSU* canonical gene (BMitcham.V1_g162906) did not cluster with any other of the canonical MBP genes (Cluster 6). The promoter contained TFBS for Dof, ERF and MYB TF families, and those same families of TFs were found to be co-expressed in the same cluster. In the *Torreya grandis* GPPS (a homomeric GPPS), the *TgERF2* TF was found to bind to the *TgGPPS* promoter in yeast 1-hybrid assays (Zhang et al. 2023b). The ERF TF family gene *LcERF134* from *Litsea cubeba* has also been shown to directly bind to the promoter of *LcGPPS.SSU*, which resulted in its upregulation and subsequent increase in the synthesis of monoterpenes such as limonene or and geranial (Zhao et al. 2023). Taken together, this would make the ERF TFs identified to cluster with *MpGPPS.SSU* in this thesis a promising target as potential regulators. The *MpGPPS.LSU* canonical gene (BMitcham.V1_g208413) clustered in cluster 4, together with the canonical genes for *MpLimS* (BMitcham.V1_g195282), *MpL3H* PM2 (BMitcham.V1_g117376), *MpL3H* PM17 (BMitcham.V1_g195283), *MpIPDH* (BMitcham.V1_g12076), *MpIPR* (BMitcham.V1_g146769) and *MpMFS* (BMitcham.V1_g199649/g199650/g199652). The promoter of *MpGPPS.LSU* contained TFBS for the C2H2, SBP and bHLH which also had the corresponding TF families in the same cluster. In *M. spicata*, the *MsGPPS.LSU* promoter is bound by the *MsMYB* TF and represses its activity (Reddy et al. 2017). Although no MYB TFBS could be detected in any of the *MpGPPS.LSU* homologs here by computational prediction (plantTFDB), manual searching of the MYB TFBS as determined by Reddy et al. (2017) revealed MYB TFBS in the canonical *MpGPPS.LSU* (BMitcham.V1_g208413), as well as in the homologs BMitcham.V1_g99731, BMitcham.V1_g68975 and BMitcham.V1_g200161 (Appendix Figure 14). Due to the negative regulatory effect of *MsMYB* on the *MsGPPS.LSU* promoter, an equivalent candidate for Black Mitcham would probably be found in a cluster that shows the opposite co-expression pattern to cluster 4. Cluster 7 matches this description, and ~20 MYB family TFs can be found in this cluster, and these may be targets for further characterisation and future metabolic engineering studies.

The *MpLimS* canonical gene (BMitcham.V1_g208413) contained only Dof TFBS, and subsequently ~20 Dof TF were co-expressed in cluster 4. In a study characterising the *M. canadensis LimS* promoter, the *McDof4.2* TF was found to co-express with the *McLimS*, and contained four putative Dof TFBS (Li et al. 2025b). Putative DOF TFBS were also observed in the *MpLimS* promoter from the Madhuras variety of *M. x piperita* (Qamar et al. 2022). In *Salvia miltiorrhiza*, the *SmDof32* TF is known to enhance salvianolic acid production, through upregulation of the salvianolic acid biosynthesis pathway genes lipoxygenase and rosmarinic acid synthases (Lv et al. 2025). Therefore, the Dof TF family may play a role in the regulation of the canonical *MpLimS* gene identified in this thesis. Furthermore, putative TFBS (computationally determined) for the MYB, bHLH, WRKY, AP2/ERF and bZIP TF families were detected in *McLimS*, and of these, bHLH and bZIP TFBS were detected in the *MpLimS* homologs BMitcham.V1_g117374 and BMitcham.V1_g117378. The *McbZIP1* TF has further been shown experimentally to bind directly to the *McLimS* promoter (Yu et al. 2024). Overexpression of *McbZIP1* in transgenic *M. x piperita* lines also showed an increase in the expression of *MpGPPS.LSU, MpLimS, MpIPDH, MpIPR* and *MpPGR*.

The canonical *MpL3H* PM2 gene (BMitcham.V1_g117376) contains the AP2, Dof, ERF, HSF, MIKC-MADS and MYB TFBS, whilst the canonical *MpL3H PM17* gene (BMitcham.V1_g195283) contains the AP2, ERF, MIKC-MADS, GRAS, NAC and WRKY TFBS, as determined by co-expression and promoter analysis. Common TFBS are AP2, ERF and MIKC-MADS, and these TFBS are present in most of the homologs of *MpL3H* promoters (Figure 5.19). In *M. haplocalyx* Briq, the expression of *MhL3H* was highly correlated with ERF TF family genes, and the authors surmised that ERF plays a role in the regulation of *MhL3H* (An et al. 2023).

The regulatory mechanisms of *MpIPDH* and even general *IPDH* enzymes in other plants have not been a subject of much study. However this thesis has identified potential regulators from the AP2, B3, C2H2, Dof, ERF, GRAS, MIKC-MADS, MYB, NAC, WOX and YABBY TF families, by co-expression and promoter analysis. In *M. spicata,* the *MsYABBY5* TF is known to be general suppressor of monoterpene production, and in *Ocimum basilicum* and *Nicotiana sylvestris* was shown to be a suppressor of secondary metabolite production (Wang et al. 2016b). Alternatively, in *Artemisa annua, the AaYABBY5* was shown to directly bind to the promoters of two

artemisinin biosynthesis genes to cause upregulation, and overexpression of *AaYABBY5* led to an increase of artemisinin and intermediate products (Kayani et al. 2019). Therefore the role of YABBY TFs in regulation of *MpIPDH* requires further study, and potential YABBY DEG TFs have been elucidated by this thesis.

The *MpIPR* gene has not been a subject of much study with regards to its regulation. The canonical *MpIPR* (BMitcham.V1_g146769) contained AP2, C2H2, Dof, ERF, GRAS, HSF, MIKC-MADS, MYB, ARF, HD-ZIP and Trihelix TFBS (Figure 5.19), and corresponding co-expressed DEG TFs (Figure 5.21). As discussed above, the *MsMYB* TF plays a role in the negative regulation of monoterpene biosynthesis in *M. spicata*, and could have a similar role in regulation of *MpIPR* (Reddy et al. 2017). In *Dendrobium officinale*, the biosynthesis of the terpene (E)-caryophyllene is controlled by the *(E)-β-caryophyllene synthase (DoECS)* gene (Lv et al. 2022a). The DoMYB26, DoMYB29 and DoMYB31 TFs have been shown to bind to the promoter of *DoECS* and regulate its expression, where DoMYB26 and DoMYB31 positively regulate it, whilst DoMYB29 negatively regulates it. Therefore, MYB TFs may have a similar effect in the regulation of *MpIPR*. The work of this thesis have narrowed down potential TFs that may be regulating this gene, but there are no obvious candidates as of yet and the regulation of *MpIPR* requires further study. However, as previously discussed, the bZIP TF family (specifically a homolog of *McbZIP1* in *M. x piperita*) may influence the expression of both *MpIPDH* and *MpIPR* (Yu et al. 2024).

The canonical *MpPGR* gene (BMitcham.V1_g26993) clustered into cluster 1, which was co-expressed with the Dof, MIKC-MADS and MYB TF families, and the promoter contained putative TFBS for these families. In *M. haplocalyx* Briq, the MYB family TFs *MhMYB1* and *MhMYB2* are known to directly bind to the *MhPGR* promoter, and downregulation of *MhMYB1/2* led to a decrease in the (-)-menthone and (-)-menthol content of the essential oil (An et al. 2024). Therefore, it is possible that *M. x piperita* MYB TFs may play a similar role in the regulation of *MpPGR*. Furthermore, in *S. lycopersicum*, the *SlMYB75* TF is known to directly bind the promoters of genes involved in anthocyanin production, leading to upregulation and an increase in anthocyanin accumulation (Jian et al. 2019). Of the 7 *MpPGR* homologs identified, BMitcham.V1_g26993 (canonical), BMitcham.V1_g89813, BMitcham.V1_g26990 and BMitcham.V1_g89817 all clustered in cluster 1, and all have the MYB TFBS and all co-cluster with MYB TF DEGs (Figure 5.21). Furthermore, the bZIP TF family may

influence the *MpPGR*, as the *MpPGR* homolog BMitcham.V1_g89821 contains bZIP TFBS (Yu et al. 2024). Additionally, An et al. (2023) speculated that the bHLH, bZIP, MYB and WRKY TF families were involved in the regulation of *PGR* in *M. haplocalyx* Briq, based on co-expression inference. Taken together with the findings of this thesis, it is possible that the MYB and bZIP TF families play a key role in *MpPGR* regulation in Black Mitcham.

The canonical *MpMMR* gene (BMitcham.V1_g135464) only contained TFBS for BBR-BPC and MIKC-MADS (Figure 5.19), and only MIKC-MADS DEG TFs were identified in the same cluster 7 (Figure 5.21). There is currently no information available on the role of MIKC-MADS TFs in the regulation of *MpMMR*, and the work of this thesis have identified potential targets for future study. The *MhMYB1* and *MhMYB2* MYB TFs from *M. haplocalyx* Briq are known to interact with the *MhMMR* gene, and cause upregulation leading to an increase in (-)-menthone and (-)-menthol (An et al. 2024). Although no MYB TFBS could be detected by the computational methods of this thesis (plantTFDB), ~20 MYB DEG TFs were co-expressed in the same cluster 7 (Figure 5.21). Therefore, it could be possible that a *MpMYB* TF may be involved in the regulation of *MpMMR*. The other *MpMMR* homolog which was in cluster 7 (BMitcham.V1_g184503) only contained Dof TFBS (Figure 5.19), and was also co-expressed with Dof DEG TFs (Figure 5.21). The *A. thaliana Dof4;2* TF is known to be a negative regulator of flavonoid biosynthesis genes (Skirycz et al. 2007). Therefore, the Dof DEG TFs in cluster 4, which show an opposite expression pattern to cluster 7, may be involved in the negative regulation of *MpMMR* homolog BMitcham.V1_g184503. Conversely, as TFs can act as both activators or repressors, Dof DEG TFs located in cluster 7 may be acting as positive regulators (Martinez-Corral et al. 2024).

The canonical *MpMFS* genes BMitcham.V1_g199650, BMitcham.V1_g199649 and BMitcham.V1_g199652 were clustered into cluster 4, where the majority of MBP genes were also located (Figure 5.21). Taking into account both TFBS and DEG TFs which co-expressed in the same cluster, the C2H2, ERF, LBD, MIKC-MADS TFs were common, whilst BMitcham.V1_g199649 were associated with additional HD-ZIP and myb-related TFs (Figure 5.19). As *MpMFS* codes for the production of (+)-menthofuran, which is an undesirable side product in the essential oil, downregulation of this gene is typically desired (Bertea et al. 2001). In *Artemisia*

annua, the C2H2 TF *AaZFP1* is known to increase the expression of *AaIDI* (IDI catalyses the interconversion of precursor terpenes isopentenyl diphosphate and dimethylallyl diphosphate which feed into the artemisinin biosynthesis pathway) and lead to an increase in artemisinin content (Deng et al. 2022). As TFs can both negatively and positively regulate genes, it could be possible that a C2H2 TF in the opposite cluster 7 could have a negative regulatory effect on the *MpMFS* genes. A C2H2 TF that negatively regulates *MpMFS* would also be ideal as C2H2 TFBS are present on all copies of the *MpMFS* genes.

Overall, by combining TFBS promoter analysis with the identification of co-expressing DEG TFs with MBP genes, the findings of this thesis have identified a whole host of potential TFs for further study, such as the YABBY TF family in regulating *MpIPDH,* in relation to the regulation of MBP genes.

6.3.5 Discovery of putative IPGI genes – the missing link in the menthol biosynthesis pathway?

The conversion of (+)-*cis*-isopulegone to (+)-pulegone is thought to be carried out by IPGI, however the isolation and characterisation of *Mentha IPGI* has eluded researchers since its role was first proposed (Croteau and Venkatachalam 1986). The enzymatic mechanism resembles that of a bacterial ketosteroid isomerase (KSI), and this has led to the discovery of the microbial derived *PpKSI* being able to carry out the aforementioned conversion in *E. coli* (Talalay and Benson 1972; Currin et al. 2018). Since then, the utilisation of *PpKSI* has been utilised in the *de-novo* menthol biosynthesis in *Saccharomyces cerevisiae*, highlighting the possibility of its use in a plant system (Lv et al. 2022b). Attempts to do so in chapter 4 of this thesis by heterologous expression of *PpKSI* with the remaining MBP genes were unsuccessful (Figure 4.16). This prompted the need to discover the endogenous IPGI, however sequence based homology attempts to discover KSI genes in plants has been unsuccessful to date (Meitinger et al. 2015). Indeed, similar attempts performed in this thesis against the Black Mitcham genome using microbial KSI sequences did not yield any matches (data not shown). However, KSI enzymes are part of the larger NTF2 protein family, and putative *IPGI* genes were identified in *Mentha suaveolens* ‘Variegata’ by using a co-expression analysis approach (Li et al. 2018; Yang et al. 2024a). This encouraged a similar approach in this thesis, and a k-means clustering approach was used to look for potential NTF2 genes which co-

expressed with the MBP genes (Figure 5.23). Cluster 3 revealed two putative NTF2 genes (BMitcham.V1_g54937 and BMitcham.V1_g143460) which co-expressed with the canonical MBP genes for *MpGPPS.LSU, MpLimS, MpL3H* PM2, *MpL3H* PM17, *MpIPDH*, *MpIPR* and *MpMFS*. Cluster 6 revealed an additional two putative NTF2 genes (BMitcham.V1_g189284 and BMitcham.V1_g60254) which co-expressed with the canonical *MpPGR* gene. As IPGI is located between the IPR and PGR enzymes in the MBP, the NTF2s in cluster 3 and 6 are ideal targets for biochemical characterisation, and could lead to the discovery of the *MpIPGI* that has to this date eluded researchers (Croteau et al. 2005).

6.3.6 Limitations and future directions of transcriptomic analysis performed in chapter 5

The MBP homologs identified in this study would still need biochemical characterisation to confirm their identity as MBP genes, validate enzymatic activity and to confidently group them together in gene families. This would also further narrow down potential targets for future genetic engineering studies, as determining which transcripts (and subsequent enzymes) have what level of effect on monoterpene composition would help gain better understanding to fine tune metabolic engineering efforts. These same limitations apply to the putatively identified *IPGI* genes.

The lack of known ancillary enzymes required for MBP enzymes to function outside of their native plant host was a proposed limitation as to why full MBP reconstitution was not possible in this thesis. Further clustering analysis on the transcriptome produced in this thesis could be leveraged to find genes that have roles as electron transfer partners (e.g. cytochrome P450s), modifiers (glycotransferases, acyltransferases etc.) or transport/localisation (plastid-targeted proteins, endoplasmic reticulum (ER) membrane proteins etc.) (da Fonseca-Pereira et al. 2023). This could be further refined by findings genes which share the same sub cellular localisation with the MBP genes of interest, which could be identified by ER or plastid targeting peptides. This could be further supplemented by future experimental work involving single cell RNA sequencing of Black Mitcham glandular trichome tissue, to further reduce the dataset to tissue responsible for the majority of essential oil biosynthesis (Moskal et al. 2025)

To elucidate potential TFs regulating the MBP genes, TFBS were computationally identified in putative promoter sequences, and k-means clustering was performed to identify TFs which co-expressed with MBP genes. Combining the results of these two analysis has revealed a variety of putative TFs which may be involved in regulating the MBP genes and control the changes in expression seen over the different developmental stages. However, functional validation of the TF-promoter interactions will require assays such as chromatin immunoprecipitation sequencing (ChIP-seq), electrophoretic mobility shift assay (EMSA) and yeast one-hybrid (Y1H) (Gray and Grotewold 2025).

6.4 Overall conclusions and future directions

Although stable transformants of Black Mitcham explants were unable to be produced in this thesis, the application of the novel RAPID technique showed promise as a future avenue for introducing genetic changes into an otherwise difficult to transform plant. Whether or not stable integration of the transgene into the nuclear genome of the transformed Black Mitcham was not established in this work, so it remains to be seen if the GUS activity conferred was a result of transient or stable expression. The method for assaying transformation was by measure of GUS activity, which is inherently a destructive method as the plant tissue is killed during the assay. This could be circumvented by the use of non-destructive methods, such as using green fluorescent protein (GFP) or the belatain biosynthesis pathway derived RUBY system, which would allow transformed tissue to be identified without the need to destroy the tissue (Yang et al. 2019a; Tabara et al. 2024). Furthermore, these fluorescent protein/dye based methods would also be applicable to *A. tumefaciens*-mediated transformation, as the developing callus could be tracked as the tissue differentiates, which would reduce the number of false positive transformants observed. The applicability of biolistic bombardment to test construct activity in Black Mitcham tissue was shown through the use of a constitutive promoter to drive GUS expression, which was observed in the glandular trichomes of bombarded leaf tissue. This system could be applied to the testing of trichome specific promoters directly into Black Mitcham tissue, which would circumvent the need to produce stable transformants to determine trichome specificity.

A host of MBP gene homologs were identified through transcriptomic methods, each having varying levels of expression, and in the case of *MpPGR* and *MpMMR*, having

different expression profiles. Biochemical characterisation of these homologs to confirm their activity as MBP genes, and subsequent enzymatic activity assays would identify novel targets for metabolic engineering studies, which could be applied in Black Mitcham itself, or through heterologous expression in *N. benthamiana* or *A. thaliana*. Putative IPGI homologs were also identified in the form of NTF2 protein family genes, which could be tested by co-infiltration with the other MBP genes in *N. benthamiana* (in place of *PpKSI*) to elucidate if full MBP reconstruction can be achieved *in-planta*. Furthermore, the activity of *MpGPPS.SSU*, *PaLimS* and *MpL3H* could be determined *in-planta* through the production of limonene and (-)-*trans*-isopiperitenol in co-infiltration assays of *N. benthamiana*. The additional co-infiltration of the identified DEG TFs together with the above mentioned genes could serve as a platform to determine if they would have an effect on their expression. Doing so in a transient system to identify potential regulators would speed up the identification process, and ideal targets could then be used in stable transformation studies. To further fine tune the expression of MBP genes and potential co-regulators, the use of the trichome specific promoters identified in this thesis (*NtMald1* and *MpPGR*) to function in both glandular and non-glandular trichomes could be used to compartmentalise expression to trichomes. This could prevent phenotypes which negatively impact the plant, as seen in the stable *A. thaliana* lines which produced limonene, (-)-*trans*-isopiperitenol, isopiperitenone and piperitenone in this thesis, which showed a high degree of leaf chlorosis. Finally, the co-infiltration of *NtDXS* with *MpGPPS.SSU* and *PaLimS* was shown to dramatically increase limonene yields from transient expression. It remains to be seen if the addition of overexpressing *NtDXS* together with other MBP genes would have a similar synergistic effect in stable transformants.

Overall, the findings of this thesis have laid the foundations for a whole host of potential targets for MBP engineering in both the native Black Mitcham, as well as for reconstitution of the entire MBP in non-native plants such as *N. benthamiana* and *A. thaliana*. The applications of which could lead to higher essential oil quality and yield in Black Mitcham plants through genetic engineering approaches, and the possibility of producing specific MBP intermediate compounds (such as limonene and (-)-*trans*-isopiperitenol) in other plant species. All of which, are of great importance both from an academic and industrial standpoint.

More broadly, this work constitutes to the expanding field on reconstituting specialised metabolic pathways in tractable hosts, where the aim is to move from pathway discovery in native plants to functional reconstruction and engineering in non-native hosts. Studies on triterpene and diterpenoid gene clusters in model and crop plants, including work from the Graham and Osborne labs, have shown that physically linked sets of biosynthetic genes can often be transferred as modular units into heterologous systems, enabling complete or near complete pathway reconstitution and revealing key branchpoints and tailoring steps (Mugford et al. 2013; Dudley et al. 2022b; Schotte et al. 2025). By defining and testing a minimal set of MBP genes in *N. benthamiana* and *A. thaliana*, together with characterisation of trichome specific promoters, and the preliminary analysis and mining of the transcriptome revealing putative *IPGI* genes, this thesis follows a similar modular logic and provides a case study in reconstituting the *M x piperita* MBP across different plant backgrounds. In doing so, this thesis aligns with a wider body of work that uses transient expression, stable transformation and combinatorial assemblies to interrogate how enzyme stoichiometry, host metabolism and cellular context shape flux through specialised pathways (Medema and Osbourn 2016; Zhu et al. 2021). The work of this thesis also highlights several challenges that are increasingly recognised in the pathway reconstitution literature. Complete pathway reconstitution was not achievable here, and may gave been due to the competition for precursors, promiscuous host enzymes and feedback regulation, all of which can result in flux being directed away from the intended products, or generate unexpected intermediates (as seen in the stable *A. thaliana* transformants) (Reed and Osbourn 2018). Trichome localised pathways (such as the MBP) appear particularly sensitive to expression context, as misexpression outside of the appropriate cell types can impose physiological penalties, such as the chlorosis observed in the engineered *A. thaliana* lines from this thesis, consisted with observations from other reconstituted plant pathways (Li et al. 2019; Schuurink and Tissier 2020). These observations mirror the broader findings from plant metabolic gene cluster and pathway studies, where network context and spatial organisation prove as important as the core biosynthetic genes themselves (Ji et al. 2024). Therefore, the work towards full MBP reconstitution in this thesis, offers a platform to explore the general principles of pathway robustness, plasticity and regulation in specialised metabolic pathways.

However, further broader refinements and future directions could be implemented to this work.

Further analysis of the transcriptome generated in this thesis could also reveal the existence of gene clusters in the MBP pathway, which could identify additional genes which may be required for reconstitution outside of the native host. A more systematic control of the pathway flux could be achieved by assembling the MBP pathway genes under a panel of standardised promoters and terminators, which could influence the regulation strength of each gene introduced (Brooks et al. 2023). This could be further refined by integrating single MBP pathway genes of clusters of genes at defined genomic loci, rather than relying solely on random insertion, thereby reducing positional effects and allowing a more direct comparison of different gene combinations (McLaughlin et al. 2025). More extensive use of multi-omics approaches (transcriptomics, proteomics and targeted metabolomics) in the engineered lines produced by this thesis could further clarify how introduction of the MBP genes perturbs the native pathways and networks in the non-native host, and help identify additional partner genes/enzymes that could be co-engineered to further control pathway flux (Zhang et al. 2022). Looking forward to continuing the work of this thesis. One aim could focus on developing an optimised plant chassis for monoterpene pathway reconstitution, using refined transformation methods, modular trichome-specific expression cassettes, and genome editing to install MBP modules at pre-characterised genomic locations using CRISPR approaches (Medema and Osbourn 2016; Schuurink and Tissier 2020; McLaughlin et al. 2025). A second aim could couple this with quantitative flux analysis, using isotope labelling and computational modelling to predict how changes in enzyme expression, precursor supply and pathway branching affect yields of limonene, (-)-trans-isopiperitenol and downstream products (Medema and Osbourn 2016; Koley et al. 2024). A third aim could extend the approach to additional menthol-related or broader terpenoid pathways identified through comparative genomics and gene cluster mining in other species (eg. related *Mentha* species with different chemotype profiles), testing whether the design principles derived from MBP (promoter choice, cellular compartmentation, regulatory co-factors) are generalisable. Together, these directions would position the thesis not just as a standalone case study in Black

Mitcham improvement, but as a springboard for competitive funding at the interface of plant specialized metabolism, pathway reconstitution and industrial biotechnology.

References

Abdel-Ghany, S.E., Day, I., Heuberger, A.L., Broeckling, C.D. and Reddy, A.S.N. 2013. Metabolic engineering of Arabidopsis for butanetriol production using bacterial genes. *Metabolic Engineering* 20, pp. 109–120. doi: 10.1016/j.ymben.2013.10.003.

Abdi, G., Shokrpour ,Majid and and Salami, S.A. 2019. Essential Oil Composition at Different Plant Growth Development of Peppermint (Mentha x piperita L.) Under Water Deficit Stress. *Journal of Essential Oil Bearing Plants* 22(2), pp. 431–440. doi: 10.1080/0972060X.2019.1581095.

Aboofazeli, N., Khosravi, S., Bagheri, H., Chandler, S.F., Pan, S.Q. and Azadi, P. 2024. Conquering Limitations: Exploring the Factors that Drive Successful Agrobacterium-Mediated Genetic Transformation of Recalcitrant Plant Species. *Molecular Biotechnology*. Available at: https://doi.org/10.1007/s12033-024-01247-x [Accessed: 30 June 2025].

Adal, A.M. and Mahmoud, S.S. 2020. Short-chain isoprenyl diphosphate synthases of lavender (Lavandula). *Plant Molecular Biology* 102(4), pp. 517–535. doi: 10.1007/s11103-020-00962-8.

Afkar, S. 2023. Optimization of RNA extraction protocol for Mentha piperita. *Iranian Journal of Plant Physiology* 2(2), p. 4535. doi: 10.30495/ijpp.2023.704669.

Aharoni, A. and Galili, G. 2011. Metabolic engineering of the plant primary–secondary metabolism interface. *Current Opinion in Biotechnology* 22(2), pp. 239–244. doi: 10.1016/j.copbio.2010.11.004.

Ahkami, A., Johnson, S.R., Srividya, N. and Lange, B.M. 2015. Multiple Levels of Regulation Determine Monoterpenoid Essential Oil Compositional Variation in the Mint Family. *Molecular Plant* 8(1), pp. 188–191. doi: 10.1016/j.molp.2014.11.009.

Akhtar, M.Q., Qamar, N., Yadav, P., Kulkarni, P., Kumar, A. and Shasany, A.K. 2017. Comparative glandular trichome transcriptome-based gene characterization reveals reasons for differential (−)-menthol biosynthesis in *Mentha* species. *Physiologia Plantarum* 160(2), pp. 128–141. doi: 10.1111/ppl.12550.

Aliyu, O.M. 2005. Application of tissue culture to cashew (Anacardium occidentale L.) breeding: An appraisal. *African Journal of Biotechnology* 4(13). Available at: https://www.ajol.info/index.php/ajb/article/view/116551 [Accessed: 7 July 2025].

Alonso, W.R., Rajaonarivony, J.I., Gershenzon, J. and Croteau, R. 1992. Purification of 4S-limonene synthase, a monoterpene cyclase from the glandular trichomes of peppermint (Mentha x piperita) and spearmint (Mentha spicata). *The Journal of Biological Chemistry* 267(11), pp. 7582–7587.

Alsheikh, M., Suso, H.-P., Robson, M., Battey, N. and Wetten, A. 2002. Appropriate choice of antibiotic and Agrobacterium strain improves transformation of antibiotic-sensitive Fragaria vesca and F. v. semperflorens. *Plant Cell Reports* 20(12), pp. 1173–1180. doi: 10.1007/s00299-002-0453-0.

Amelunxen, F. 1965. ELEKTRONENMIKROSKOPISCHE UNTERSUCHUNGEN AN DEN DRÜSENSCHUPPEN VON MENTHA PIPERITA L.1. *Planta Medica* 13, pp. 457–473. doi: 10.1055/s-0028-1100141.

Amente, G. and Chimdessa, E. 2021. Control of browning in plant tissue culture: A review. *Journal of Scientific Agriculture*, pp. 67–71. doi: 10.25081/jsa.2021.v5.7266.

An, G. 1987. [17] Binary ti vectors for plant transformation and promoter analysis. In: *Methods in Enzymology*. Recombinant DNA Part D. Academic Press, pp. 292–305. Available at: https://www.sciencedirect.com/science/article/pii/0076687987530609 [Accessed: 9 July 2025].

An, X. et al. 2023. Transcriptome analysis of transcription factors and enzymes involved in monoterpenoid biosynthesis in different chemotypes of Mentha haplocalyx Briq. *PeerJ* 11, p. e14914. doi: 10.7717/peerj.14914.

An, X., Liao, Y., Yu, Y., Fan, J., Wan, J., Wei, Y. and Ouyang, Z. 2024. Effects of MhMYB1 and MhMYB2 transcription factors on the monoterpenoid biosynthesis pathway in l-menthol chemotype of Mentha haplocalyx Briq. *Planta* 260(1), p. 3. doi: 10.1007/s00425-024-04441-y.

An, Y.Q., McDowell, J.M., Huang, S., McKinney, E.C., Chambliss, S. and Meagher, R.B. 1996. Strong, constitutive expression of the Arabidopsis ACT2/ACT8 actin

subclass in vegetative tissues. *The Plant Journal: For Cell and Molecular Biology* 10(1), pp. 107–121. doi: 10.1046/j.1365-313x.1996.10010107.x.

Ascensão, L. and Pais, M.S. 1998. The Leaf Capitate Trichomes ofLeonotis leonurus: Histochemistry, Ultrastructure and Secretion. *Annals of Botany* 81(2), pp. 263–271. doi: 10.1006/anbo.1997.0550.

Ashrafi-Dehkordi, E., Alemzadeh, A., Tanaka, N. and Razi, H. 2021. Effects of vacuum infiltration, Agrobacterium cell density and acetosyringone concentration on Agrobacterium-mediated transformation of bread wheat. *Journal of Consumer Protection and Food Safety* 16(1), pp. 59–69. doi: 10.1007/s00003-020-01312-y.

Asim, M. et al. 2023. Leaf senescence attributes: the novel and emerging role of sugars as signaling molecules and the overlap of sugars and hormones signaling nodes. *Critical Reviews in Biotechnology* 43(7), pp. 1092–1110. doi: 10.1080/07388551.2022.2094215.

Aspromonte, J., Lancioni, C. and Purcaro, G. 2022. Solid-Phase Microextraction—Gas Chromatography Analytical Strategies for Pesticide Analysis. *Methods and Protocols* 5(5), p. 82. doi: 10.3390/mps5050082.

Aydın Akbudak, M. and Srivastava, V. 2017. Effect of gene order in DNA constructs on gene expression upon integration into plant genome. *3 Biotech* 7(2), p. 94. doi: 10.1007/s13205-017-0729-2.

Azizi-Dargahlou, S. and pouresmaeil, M. 2024. Agrobacterium tumefaciens-Mediated Plant Transformation: A Review. *Molecular Biotechnology* 66(7), pp. 1563–1580. doi: 10.1007/s12033-023-00788-x.

Bach, S.S., Bassard, J.-É., Andersen-Ranberg, J., Møldrup, M.E., Simonsen, H.T. and Hamberger, B. 2014. High-Throughput Testing of Terpenoid Biosynthesis Candidate Genes Using Transient Expression in Nicotiana benthamiana. In: Rodríguez-Concepción, M. ed. *Plant Isoprenoids: Methods and Protocols*. Methods in Molecular Biology. New York, NY: Springer, pp. 245–255. Available at: https://doi.org/10.1007/978-1-4939-0606-2_18 [Accessed: 19 January 2024].

References

Battaile, J., Burbott, A.J. and Loomis, W.D. 1968. Monoterpene interconversions: Metabolism of pulegone by a cell-free system from *Mentha piperita*. *Phytochemistry* 7(7), pp. 1159–1163. doi: 10.1016/S0031-9422(00)88264-3.

Battaile, J. and Loomis, W.D. 1961. Biosynthesis of terpenes. II. The site and sequence of terpene formation in peppermint. *Biochimica Et Biophysica Acta* 51, pp. 545–552. doi: 10.1016/0006-3002(61)90612-6.

Becker, D. 1990. Binary vectors which allow the exchange of plant selectable markers and reporter genes. *Nucleic Acids Research* 18(1), p. 203. doi: 10.1093/nar/18.1.203.

Beigi, M., Torki-Harchegani, M. and Ghasemi Pirbalouti, A. 2018. Quantity and chemical composition of essential oil of peppermint (*Mentha* × *piperita* L.) leaves under different drying methods. *International Journal of Food Properties* 21(1), pp. 267–276. doi: 10.1080/10942912.2018.1453839.

Bélanger, J.G., Copley, T.R., Hoyos-Villegas, V., Charron, J.-B. and O'Donoughue, L. 2024. A comprehensive review of in planta stable transformation strategies. *Plant Methods* 20(1), p. 79. doi: 10.1186/s13007-024-01200-8.

Bennur, P.L., O'Brien, M., Fernando, S.C. and Doblin, M.S. 2025. Improving transformation and regeneration efficiency in medicinal plants: insights from other recalcitrant species. *Journal of Experimental Botany* 76(1), pp. 52–75. doi: 10.1093/jxb/erae189.

Bergman, M.E. and Phillips, M.A. 2021. Structural diversity and biosynthesis of plant derived p-menthane monoterpenes. *Phytochemistry Reviews* 20(2), pp. 433–459. doi: 10.1007/s11101-020-09726-0.

Beritza, K., Watts, E.C. and van der Hoorn, R.A.L. 2024. Improving transient protein expression in agroinfiltrated Nicotiana benthamiana. *New Phytologist* 243(3), pp. 846–850. doi: 10.1111/nph.19894.

Bernula, D. et al. 2020. Timely removal of exogenous cytokinin and the prevention of auxin transport from the shoot to the root affect the regeneration potential of Arabidopsis roots. *Plant Cell, Tissue and Organ Culture (PCTOC)* 140(2), pp. 327–339. doi: 10.1007/s11240-019-01730-3.

References

Berry, C., Van Eck, J.M., Kitto, S.L. and Smigocki, A. 1996. Agrobacterium-mediated transformation of commercial mints. *Plant Cell, Tissue and Organ Culture* 44(2), pp. 177–181. doi: 10.1007/BF00048197.

Bertea, C.M., Schalk, M., Karp, F., Maffei, M. and Croteau, R. 2001. Demonstration That Menthofuran Synthase of Mint (Mentha) Is a Cytochrome P450 Monooxygenase: Cloning, Functional Expression, and Characterization of the Responsible Gene. *Archives of Biochemistry and Biophysics* 390(2), pp. 279–286. doi: 10.1006/abbi.2001.2378.

Bhat, S., Maheshwari, P., Kumar, S. and Kumar, A. 2002. Mentha species: In vitro Regeneration and Genetic Transformation. *Molecular Biology Today* 3(1), pp. 11–23.

Bhatia, S. and Sharma, K. 2015. Chapter 13 - Technical Glitches in Micropropagation. In: Bhatia, S., Sharma, K., Dahiya, R., and Bera, T. eds *Modern Applications of Plant Biotechnology in Pharmaceutical Sciences*. Boston: Academic Press, pp. 393–404. Available at: https://www.sciencedirect.com/science/article/pii/B9780128022214000133 [Accessed: 9 July 2025].

Bhatt, R., Asopa, P.P., Jain, R., Kothari-Chajer, A., Kothari, S.L. and Kachhwaha, S. 2021. Optimization of Agrobacterium Mediated Genetic Transformation in Paspalum scrobiculatum L. (Kodo Millet). *Agronomy* 11(6), p. 1104. doi: 10.3390/agronomy11061104.

Booth, J.K., Page, J.E. and Bohlmann, J. 2017. Terpene synthases from Cannabis sativa. Hamberger, B. ed. *PLOS ONE* 12(3), p. e0173911. doi: 10.1371/journal.pone.0173911.

Bourtsoukidis, E. et al. 2024. High temperature sensitivity of monoterpene emissions from global vegetation. *Communications Earth & Environment* 5(1), p. 23. doi: 10.1038/s43247-023-01175-9.

Brooks, E.G. et al. 2023. Plant Promoters and Terminators for High-Precision Bioengineering. *Biodesign Research* 5, p. 0013. doi: 10.34133/bdr.0013.

Brown, J.T., Hegarty, P.K. and Charlwood, B.V. 1987. The toxicity of monoterpenes to plant cell cultures. *Plant Science* 48(3), pp. 195–201. doi: 10.1016/0168-9452(87)90090-2.

Brückner, K. and Tissier, A. 2013. High-level diterpene production by transient expression in Nicotiana benthamiana. *Plant Methods* 9(1), p. 46. doi: 10.1186/1746-4811-9-46.

Brun, N., Colson, M., Perrin, A. and Voirin, B. 1991. Chemical and morphological studies of the effects of ageing on monoterpene composition in Mentha ×piperita leaves. *Canadian Journal of Botany* 69(10), pp. 2271–2278. doi: 10.1139/b91-285.

Buntru, M., Gärtner, S., Staib, L., Kreuzaler, F. and Schlaich, N. 2013. Delivery of multiple transgenes to plant cells by an improved version of MultiRound Gateway technology. *Transgenic Research* 22(1), pp. 153–167. doi: 10.1007/s11248-012-9640-0.

Burbott, A.J. and Loomis, W.D. 1967. Effects of Light and Temperature on the Monoterpenes of Peppermint 1. *Plant Physiology* 42(1), pp. 20–28. doi: 10.1104/pp.42.1.20.

Burke, C. and Croteau, R. 2002a. Geranyl diphosphate synthase from Abies grandis: cDNA isolation, functional expression, and characterizationq,qq. *Archives of Biochemistry and Biophysics*, p. 7.

Burke, C. and Croteau, R. 2002b. Interaction with the Small Subunit of Geranyl Diphosphate Synthase Modifies the Chain Length Specificity of Geranylgeranyl Diphosphate Synthase to Produce Geranyl Diphosphate. *Journal of Biological Chemistry* 277(5), pp. 3141–3149. doi: 10.1074/jbc.M105900200.

Burke, C., Klettke, K. and Croteau, R. 2004. Heteromeric geranyl diphosphate synthase from mint: construction of a functional fusion protein and inhibition by bisphosphonate substrate analogs. *Archives of Biochemistry and Biophysics* 422(1), pp. 52–60. doi: 10.1016/j.abb.2003.12.003.

Burke, C.C., Wildung, M.R. and Croteau, R. 1999. Geranyl diphosphate synthase: Cloning, expression, and characterization of this prenyltransferase as a heterodimer.

Proceedings of the National Academy of Sciences 96(23), pp. 13062–13067. doi: 10.1073/pnas.96.23.13062.

Burnett, M.J.B. and Burnett, A.C. 2020. Therapeutic recombinant protein production in plants: Challenges and opportunities. *PLANTS, PEOPLE, PLANET* 2(2), pp. 121–132. doi: 10.1002/ppp3.10073.

Caissard, J.-C., Faure, O., Jullien, F., Colson, M. and Perrin, A. 1996. Direct regenerationin vitro and transient GUS expression inMentha xpiperita. *Plant Cell Reports* 16(1), pp. 67–70. doi: 10.1007/BF01275452.

Caputi, L. et al. 2018. Missing enzymes in the biosynthesis of the anticancer drug vinblastine in Madagascar periwinkle. *Science (New York, N.Y.)* 360(6394), pp. 1235–1239. doi: 10.1126/science.aat4100.

Chakrabarty, R., Viswakarma, N., Bhat, S.R., Kirti, P.B., Singh, B.D. and Chopra, V.L. 2002. Agrobacterium-mediated transformation of cauliflower: Optimization of protocol and development of Bt-transgenic cauliflower. *Journal of Biosciences* 27(5), pp. 495–502. doi: 10.1007/BF02705046.

Chalhoub, B. et al. 2014. Early allopolyploid evolution in the post-Neolithic Brassica napus oilseed genome. *Science* 345(6199), pp. 950–953. doi: 10.1126/science.1253435.

Chang, M.C.Y., Eachus, R.A., Trieu, W., Ro, D.-K. and Keasling, J.D. 2007. Engineering Escherichia coli for production of functionalized terpenoids using plant P450s. *Nature Chemical Biology* 3(5), pp. 274–277. doi: 10.1038/nchembio875.

Chang, T.-H., Hsieh, F.-L., Ko, T.-P., Teng, K.-H., Liang, P.-H. and Wang, A.H.-J. 2010. Structure of a Heterotetrameric Geranyl Pyrophosphate Synthase from Mint (*Mentha piperita*) Reveals Intersubunit Regulation. *The Plant Cell* 22(2), pp. 454–467. doi: 10.1105/tpc.109.071738.

Chen, A., Kroon, P.A. and Poulter, C.D. 1994. Isoprenyl diphosphate synthases: protein sequence comparisons, a phylogenetic tree, and predictions of secondary structure. *Protein Science : A Publication of the Protein Society* 3(4), pp. 600–607. doi: 10.1002/pro.5560030408.

Chen, C. et al. 2024. Plant regeneration in the new era: from molecular mechanisms to biotechnology applications. *Science China Life Sciences* 67(7), pp. 1338–1367. doi: 10.1007/s11427-024-2581-2.

Chen, Q., Lai, H., Hurtado, J., Stahnke, J., Leuzinger, K. and Dent, M. 2013. Agroinfiltration as an Effective and Scalable Strategy of Gene Delivery for Production of Pharmaceutical Proteins. *Advanced techniques in biology & medicine* 1(1), p. 103. doi: 10.4172/atbm.1000103.

Chen, Q., Li, N., Cui, X. and Ge, F. 2025. AP2/ERF transcription factors regulate the biosynthesis of terpenoids, phenolics, and alkaloids in plants. *Horticulture Research* 13(1), p. uhaf280. doi: 10.1093/hr/uhaf280.

Chen, Q.-J., Zhou, H.-M., Chen, J. and Wang, X.-C. 2006. A Gateway-based platform for multigene plant transformation. *Plant Molecular Biology* 62(6), pp. 927–936. doi: 10.1007/s11103-006-9065-3.

Chen, S., Zhou, Y., Chen, Y. and Gu, J. 2018. fastp: an ultra-fast all-in-one FASTQ preprocessor. *Bioinformatics* 34(17), pp. i884–i890. doi: 10.1093/bioinformatics/bty560.

Chen, X. et al. 2022. The Effect of Anti-browning Agent Activated Carbon and Polyvinyl Pyrrolidone on the Rooting of Embryo Seedlings of “FengDan” and Its Transcriptome Analysis. *Frontiers in Plant Science* 13. Available at: https://www.frontiersin.org/journals/plant-science/articles/10.3389/fpls.2022.832619/full [Accessed: 7 July 2025].

Cheng, S. et al. 2019. Orthogonal Engineering of Biosynthetic Pathway for Efficient Production of Limonene in Saccharomyces cerevisiae. *ACS Synthetic Biology* 8(5), pp. 968–975. doi: 10.1021/acssynbio.9b00135.

Chhangawala, S., Rudy, G., Mason, C.E. and Rosenfeld, J.A. 2015. The impact of read length on quantification of differentially expressed genes and splice junction detection. *Genome Biology* 16(1), p. 131. doi: 10.1186/s13059-015-0697-y.

Chincinska, I.A. 2021. Leaf infiltration in plant science: old method, new possibilities. *Plant Methods* 17, p. 83. doi: 10.1186/s13007-021-00782-x.

Cholin, S.S. et al. 2024. Deciphering Carotenoid and Flowering Pathway Gene Variations in Eastern and Western Carrots (Daucus carota L.). *Genes* 15(11), p. 1462. doi: 10.3390/genes15111462.

Chou, J., Huang, J. and Huang, Y. 2020. Simple and efficient genetic transformation of sorghum using immature inflorescences. *Acta Physiologiae Plantarum* 42(3), p. 41. doi: 10.1007/s11738-020-3023-6.

Christianson, D.W. 2017. Structural and Chemical Biology of Terpenoid Cyclases. *Chemical Reviews* 117(17), pp. 11570–11648. doi: 10.1021/acs.chemrev.7b00287.

Clark, R.J. and Menary, R.C. 1980. Environmental Effects on Peppermint (Mentha piperita L.). I. Effect of Daylength, Photon Flux Density, Night Temperature and Day Temperature on the Yield and Composition of Peppermint Oil. *Functional Plant Biology* 7(6), pp. 685–692. doi: 10.1071/pp9800685.

Clough, S.J. and Bent, A.F. 1998. Floral dip: a simplified method forAgrobacterium-mediated transformation ofArabidopsis thaliana: Floral dip transformation of Arabidopsis. *The Plant Journal* 16(6), pp. 735–743. doi: 10.1046/j.1365-313x.1998.00343.x.

Colby, S.M., Alonso, W.R., Katahira, E.J., McGarvey, D.J. and Croteau, R. 1993. 4S-limonene synthase from the oil glands of spearmint (Mentha spicata). cDNA isolation, characterization, and bacterial expression of the catalytically active monoterpene cyclase. *The Journal of Biological Chemistry* 268(31), pp. 23016–23024.

Colinas, M. and Goossens, A. 2018. Combinatorial Transcriptional Control of Plant Specialized Metabolism. *Trends in Plant Science* 23(4), pp. 324–336. doi: 10.1016/j.tplants.2017.12.006.

Compeau, P.E.C., Pevzner, P.A. and Tesler, G. 2011. How to apply de Bruijn graphs to genome assembly. *Nature Biotechnology* 29(11), pp. 987–991. doi: 10.1038/nbt.2023.

Croteau, R. and Hooper, C.L. 1978. Metabolism of Monoterpenes: Acetylation of (-)-Menthol by a Soluble Enzyme Preparation from Peppermint (Mentha piperita) Leaves. *Plant Physiology* 61(5), pp. 737–742. doi: 10.1104/pp.61.5.737.

Croteau, R., Karp, F., Wagschal, K.C., Satterwhite, D.M., Hyatt, D.C. and Skotland, C.B. 1991. Biochemical Characterization of a Spearmint Mutant That Resembles Peppermint in Monoterpene Content. *Plant Physiology* 96(3), pp. 744–752. doi: 10.1104/pp.96.3.744.

Croteau, R. and Venkatachalam, K.V. 1986. Metabolism of monoterpenes: demonstration that (+)-cis-isopulegone, not piperitenone, is the key intermediate in the conversion of (-)-isopiperitenone to (+)-pulegone in peppermint (Mentha piperita). *Archives of Biochemistry and Biophysics* 249(2), pp. 306–315. doi: 10.1016/0003-9861(86)90007-x.

Croteau, R.B., Davis, E.M., Ringer, K.L. and Wildung, M.R. 2005. (−)-Menthol biosynthesis and molecular genetics. *Naturwissenschaften* 92(12), p. 562. doi: 10.1007/s00114-005-0055-0.

Currin, A. et al. 2018. Engineering the “Missing Link” in Biosynthetic (−)-Menthol Production: Bacterial Isopulegone Isomerase. *ACS Catalysis* 8(3), pp. 2012–2020. doi: 10.1021/acscatal.7b04115.

Dafny-Yelin, M. and Tzfira, T. 2007. Delivery of Multiple Transgenes to Plant Cells. *Plant Physiology* 145(4), pp. 1118–1128. doi: 10.1104/pp.107.106104.

van Dam, S., Võsa, U., van der Graaf, A., Franke, L. and de Magalhães, J.P. 2018. Gene co-expression analysis for functional classification and gene–disease predictions. *Briefings in Bioinformatics* 19(4), pp. 575–592. doi: 10.1093/bib/bbw139.

Davis, A.M., Hall, A., Millar, A.J., Darrah, C. and Davis, S.J. 2009. Protocol: Streamlined sub-protocols for floral-dip transformation and selection of transformants in Arabidopsis thaliana. *Plant Methods* 5, p. 3. doi: 10.1186/1746-4811-5-3.

Davis, E.M. and Croteau, R. 2000. Cyclization Enzymes in the Biosynthesis of Monoterpenes, Sesquiterpenes, and Diterpenes. In: Leeper, F. J. and Vederas, J. C. eds *Biosynthesis: Aromatic Polyketides, Isoprenoids, Alkaloids*. Berlin, Heidelberg: Springer, pp. 53–95. Available at: https://doi.org/10.1007/3-540-48146-X_2 [Accessed: 4 September 2025].

Davis, E.M., Ringer, K.L., McConkey, M.E. and Croteau, R. 2005. Monoterpene Metabolism. Cloning, Expression, and Characterization of Menthone Reductases

from Peppermint. *Plant Physiology* 137(3), pp. 873–881. doi: 10.1104/pp.104.053306.

De Saeger, J. et al. 2021. *Agrobacterium* strains and strain improvement: Present and outlook. *Biotechnology Advances* 53, p. 107677. doi: 10.1016/j.biotechadv.2020.107677.

Deng, Y.-A., Li, L., Peng, Q., Feng, L.-F., Yang, J.-F., Zhan, R.-T. and Ma, D.-M. 2022. Isolation and characterization of AaZFP1, a C2H2 zinc finger protein that regulates the AaIPPI1 gene involved in artemisinin biosynthesis in Artemisia annua. *Planta* 255(6), p. 122. doi: 10.1007/s00425-022-03892-5.

Deshpande, D. et al. 2023. RNA-seq data science: From raw data to effective interpretation. *Frontiers in Genetics* 14. Available at: https://www.frontiersin.org/journals/genetics/articles/10.3389/fgene.2023.997383/full [Accessed: 21 August 2025].

Dhar, U. and Joshi, M. 2005. Efficient plant regeneration protocol through callus for Saussurea obvallata (DC.) Edgew. (Asteraceae): effect of explant type, age and plant growth regulators. *Plant Cell Reports* 24(4), pp. 195–200. doi: 10.1007/s00299-005-0932-1.

Dhifi, W., Bellili, S., Jazi, S., Bahloul, N. and Mnif, W. 2016. Essential Oils' Chemical Characterization and Investigation of Some Biological Activities: A Critical Review. *Medicines* 3(4), p. 25. doi: 10.3390/medicines3040025.

Diemer, F., Caissard, J.-C., Moja, S., Chalchat, J.-C. and Jullien, F. 2001. Altered monoterpene composition in transgenic mint following the introduction of 4S-limonene synthase. *Plant Physiology and Biochemistry* 39(7–8), pp. 603–614. doi: 10.1016/S0981-9428(01)01273-6.

Diemer, F., Jullien, F., Faure, O., Moja, S., Colson, M., Matthys-Rochon, E. and Caissard, J.C. 1998. High efficiency transformation of peppermint (*Mentha* × *piperita* L.) with *Agrobacterium tumefaciens*. *Plant Science* 136(1), pp. 101–108. doi: 10.1016/S0168-9452(98)00107-1.

Dobin, A. et al. 2013. STAR: ultrafast universal RNA-seq aligner. *Bioinformatics* 29(1), pp. 15–21. doi: 10.1093/bioinformatics/bts635.

Domonkos, I., Kis, M., Gombos, Z. and Ughy, B. 2013. Carotenoids, versatile components of oxygenic photosynthesis. *Progress in Lipid Research* 52(4), pp. 539–561. doi: 10.1016/j.plipres.2013.07.001.

Dragumilo, A., Pejčev, R.Đ., Božić, D., Sarić-Krsmanović, M., Vrbničanin, S., Rajković, M. and Marković, T. 2025. Impact of synthetic films and organic mulches on yield and quality of *Mentha piperita* L. essential oil. *Industrial Crops and Products* 224, p. 120356. doi: 10.1016/j.indcrop.2024.120356.

Du, C., Chai, L., Liu, C., Si, Y. and Fan, H. 2022. Improved Agrobacterium tumefaciens-mediated transformation using antibiotics and acetosyringone selection in cucumber. *Plant Biotechnology Reports* 16(1), pp. 17–27. doi: 10.1007/s11816-021-00734-w.

Dudley, Q.M. et al. 2022a. Reconstitution of monoterpene indole alkaloid biosynthesis in genome engineered Nicotiana benthamiana. *Communications Biology* 5(1), pp. 1–12. doi: 10.1038/s42003-022-03904-w.

Dudley, Q.M. et al. 2022b. Reconstitution of monoterpene indole alkaloid biosynthesis in genome engineered Nicotiana benthamiana. *Communications Biology* 5(1), p. 949. doi: 10.1038/s42003-022-03904-w.

Eapen, S. 2011. Pollen grains as a target for introduction of foreign genes into plants: an assessment. *Physiology and Molecular Biology of Plants* 17(1), pp. 1–8. doi: 10.1007/s12298-010-0042-6.

Eftekhari, A., Khusro, A., Ahmadian, E., Dizaj, S.M., Hasanzadeh, A. and Cucchiarini, M. 2021. Phytochemical and nutra-pharmaceutical attributes of *Mentha* spp.: A comprehensive review. *Arabian Journal of Chemistry* 14(5), p. 103106. doi: 10.1016/j.arabjc.2021.103106.

Eisenreich, W., Sagner, S., Zenk, M.H. and Bacher, A. 1997. Monoterpenoid essential oils are not of mevalonoid origin. *Tetrahedron Letters* 38(22), pp. 3889–3892. doi: 10.1016/S0040-4039(97)00761-2.

Engler, C. et al. 2014. A Golden Gate Modular Cloning Toolbox for Plants. *ACS Synthetic Biology* 3(11), pp. 839–843. doi: 10.1021/sb4001504.

Ewels, P., Magnusson, M., Lundin, S. and Käller, M. 2016. MultiQC: summarize analysis results for multiple tools and samples in a single report. *Bioinformatics* 32(19), pp. 3047–3048. doi: 10.1093/bioinformatics/btw354.

Fallah, S., Ghanbari-Odivi, A., Rostaei, M., Maggi, F. and Shahbazi, E. 2024. Improvement of production and quality of essential oils in multi-cut peppermint (*Mentha* x *piperita* L.) through eco-friendly fertilizers in the semi-arid highlands. *Industrial Crops and Products* 216, p. 118801. doi: 10.1016/j.indcrop.2024.118801.

Farré, G., Blancquaert, D., Capell, T., Straeten, D.V.D., Christou, P. and Zhu, C. 2014. Engineering Complex Metabolic Pathways in Plants. *Annual Review of Plant Biology* 65(Volume 65, 2014), pp. 187–223. doi: 10.1146/annurev-arplant-050213-035825.

Fazal, H., Akram, M., Ahmad, N., Qaisar, M., Kanwal, F., Rehman, G. and Ullah, I. 2023. Nutritionally rich biochemical profile in essential oil of various Mentha species and their antimicrobial activities. *Protoplasma* 260(2), pp. 557–570. doi: 10.1007/s00709-022-01799-2.

Fejér, J., Gruľová, D., De Feo, V., Ürgeová, E., Obert, B. and Preťová, A. 2018. *Mentha* × *piperita* L. nodal segments cultures and their essential oil production. *Industrial Crops and Products* 112, pp. 550–555. doi: 10.1016/j.indcrop.2017.12.055.

Ferretti, M. et al. 2025. Accurate and robust method for plant volatilome analysis by GC-MS. *Talanta Open* 12, p. 100578. doi: 10.1016/j.talo.2025.100578.

Fischer, R. and Buyel, J.F. 2020. Molecular farming – The slope of enlightenment. *Biotechnology Advances* 40, p. 107519. doi: 10.1016/j.biotechadv.2020.107519.

da Fonseca-Pereira, P., Monteiro-Batista, R. de C., Araújo, W.L. and Nunes-Nesi, A. 2023. Harnessing enzyme cofactors and plant metabolism: an essential partnership. *The Plant Journal* 114(5), pp. 1014–1036. doi: 10.1111/tpj.16167.

Forestier, E.C.F., Brown, G.D., Harvey, D., Larson, T.R. and Graham, I.A. 2021a. Engineering Production of a Novel Diterpene Synthase Precursor in Nicotiana benthamiana. *Frontiers in Plant Science* 12. Available at: https://www.frontiersin.org/journals/plant-science/articles/10.3389/fpls.2021.757186/full [Accessed: 21 July 2025].

Forestier, E.C.F., Czechowski, T., Cording, A.C., Gilday, A.D., King, A.J., Brown, G.D. and Graham, I.A. 2021b. Developing a Nicotiana benthamiana transgenic platform for high-value diterpene production and candidate gene evaluation. *Plant Biotechnology Journal* 19(8), pp. 1614–1623. doi: 10.1111/pbi.13574.

Frame, B.R. et al. 2006. Improved Agrobacterium-mediated transformation of three maize inbred lines using MS salts. *Plant Cell Reports* 25(10), pp. 1024–1034. doi: 10.1007/s00299-006-0145-2.

Frank, A. and Groll, M. 2017. The Methylerythritol Phosphate Pathway to Isoprenoids. *Chemical Reviews* 117(8), pp. 5675–5703. doi: 10.1021/acs.chemrev.6b00537.

Fu, R. et al. 2021. Versatility in acyltransferase activity completes chicoric acid biosynthesis in purple coneflower. *Nature Communications* 12, p. 1563. doi: 10.1038/s41467-021-21853-6.

Fuchs, L.K. et al. 2022. Genetic Manipulation of Biosynthetic Pathways in Mint. *Frontiers in Plant Science* 13, p. 928178. doi: 10.3389/fpls.2022.928178.

Gan, Z., Shu, M., Yang, F., Wang, G., Zhang, W. and Pan, X. 2023. Somatic embryo induction and plantlet regeneration of Canna × generalis from immature zygotic embryo. *Plant Cell, Tissue and Organ Culture (PCTOC)* 155(3), pp. 681–692. doi: 10.1007/s11240-023-02588-2.

Garcia-Perez, E., Vazquez-Vilar, M. and Orzaez, D. 2026. Engineering Conditional Transgene Expression in Nicotiana benthamiana. *Plant Biotechnology Journal* 24(1), pp. 18–30. doi: 10.1111/pbi.70350.

Gelvin, S.B. 2017. Integration of *Agrobacterium* T-DNA into the Plant Genome. *Annual Review of Genetics* 51(1), pp. 195–217. doi: 10.1146/annurev-genet-120215-035320.

George, E.F. and Sherrington, Paul.D. 1984. *Plant propagation by tissue culture*. 1st ed. Eversley, Basingstoke, Hampshire, England: Exegetics Ltd.

Gershenzon, J. and Dudareva, N. 2007. The function of terpene natural products in the natural world. *Nature Chemical Biology* 3(7), pp. 408–414. doi: 10.1038/nchembio.2007.5.

Gershenzon, J., Maffei, M. and Croteau, R. 1989. Biochemical and Histochemical Localization of Monoterpene Biosynthesis in the Glandular Trichomes of Spearmint (Mentha spicata) 12. *Plant Physiology* 89(4), pp. 1351–1357.

Gershenzon, J., McConkey, M.E. and Croteau, R.B. 2000. Regulation of Monoterpene Accumulation in Leaves of Peppermint. *Plant Physiology* 122(1), pp. 205–214. doi: 10.1104/pp.122.1.205.

Ghawana, S. et al. 2011. An RNA isolation system for plant tissues rich in secondary metabolites. *BMC Research Notes* 4, p. 85. doi: 10.1186/1756-0500-4-85.

Gobert, V., Moja, S., Colson, M. and Taberlet, P. 2002. Hybridization in the section Mentha (Lamiaceae) inferred from AFLP markers. *American Journal of Botany* 89(12), pp. 2017–2023. doi: 10.3732/ajb.89.12.2017.

Gobert, V., Moja, S., Taberlet, P. and Wink, M. 2006. Heterogeneity of three molecular data partition phylogenies of mints related to M. x piperita (Mentha; Lamiaceae). *Plant Biology (Stuttgart, Germany)* 8(4), pp. 470–485. doi: 10.1055/s-2006-924043.

Godshaw, J., Hjelmeland, A.K., Zweigenbaum, J. and Ebeler, S.E. 2019. Changes in glycosylation patterns of monoterpenes during grape berry maturation in six cultivars of *Vitis vinifera*. *Food Chemistry* 297, p. 124921. doi: 10.1016/j.foodchem.2019.05.195.

Golubova, D., Tansley, C., Su, H. and Patron, N.J. 2024. Engineering *Nicotiana benthamiana* as a platform for natural product biosynthesis. *Current Opinion in Plant Biology* 81, p. 102611. doi: 10.1016/j.pbi.2024.102611.

Grabherr, M.G. et al. 2011. Full-length transcriptome assembly from RNA-Seq data without a reference genome. *Nature Biotechnology* 29(7), pp. 644–652. doi: 10.1038/nbt.1883.

Gray, J. and Grotewold, E. 2025. Decoding complexity: tackling the challenge of how many transcription factors regulate a plant gene. *Transcription* 16(2–3), pp. 261–283. doi: 10.1080/21541264.2025.2521767.

Grosse-Holz, F. et al. 2018a. Three unrelated protease inhibitors enhance accumulation of pharmaceutical recombinant proteins in Nicotiana benthamiana. *Plant Biotechnology Journal* 16(10), pp. 1797–1810. doi: 10.1111/pbi.12916.

Grosse-Holz, F., Kelly, S., Blaskowski, S., Kaschani, F., Kaiser, M. and van der Hoorn, R.A.L. 2018b. The transcriptome, extracellular proteome and active secretome of agroinfiltrated Nicotiana benthamiana uncover a large, diverse protease repertoire. *Plant Biotechnology Journal* 16(5), pp. 1068–1084. doi: 10.1111/pbi.12852.

Grotewold, E. 2008. Transcription factors for predictive plant metabolic engineering: are we there yet? *Current Opinion in Biotechnology* 19(2), pp. 138–144. doi: 10.1016/j.copbio.2008.02.002.

Grover, C.E., Gallagher, J.P., Szadkowski, E.P., Yoo, M.J., Flagel, L.E. and Wendel, J.F. 2012. Homoeolog expression bias and expression level dominance in allopolyploids. *New Phytologist* 196(4), pp. 966–971. doi: 10.1111/j.1469-8137.2012.04365.x.

Grützner, R., König, K., Horn, C., Engler, C., Laub, A., Vogt, T. and Marillonnet, S. 2024. A transient expression tool box for anthocyanin biosynthesis in Nicotiana benthamiana. *Plant Biotechnology Journal* 22(5), pp. 1238–1250. doi: 10.1111/pbi.14261.

Guerrieri, A., Dong, L. and Bouwmeester, H.J. 2019. Role and exploitation of underground chemical signaling in plants. *Pest Management Science* 75(9), pp. 2455–2463. doi: 10.1002/ps.5507.

Guilley, H., Dudley, R.K., Jonard, G., Balàzs, E. and Richards, K.E. 1982. Transcription of Cauliflower mosaic virus DNA: detection of promoter sequences, and characterization of transcripts. *Cell* 30(3), pp. 763–773. doi: 10.1016/0092-8674(82)90281-1.

Guzmán, E. and Lucia, A. 2021. Essential Oils and Their Individual Components in Cosmetic Products. *Cosmetics* 8(4), p. 114. doi: 10.3390/cosmetics8040114.

Gwak, Y.S., Han, J.Y., Adhikari, P.B., Ahn, C.H. and Choi, Y.E. 2017. Heterologous production of a ginsenoside saponin (compound K) and its precursors in transgenic

tobacco impairs the vegetative and reproductive growth. *Planta* 245(6), pp. 1105–1119. doi: 10.1007/s00425-017-2668-x.

Haliloglu, K. and Aydin, M. 2016. Efficient regeneration system from rye leaf base segments. *SpringerPlus* 5(1), p. 2005. doi: 10.1186/s40064-016-3689-9.

Hamel, L. et al. 2023. Molecular responses of agroinfiltrated Nicotiana benthamiana leaves expressing suppressor of silencing P19 and influenza virus-like particles. *Plant Biotechnology Journal* 22(5), pp. 1078–1100. doi: 10.1111/pbi.14247.

Hao, S., Zhang, Y., Li, R., Qu, P. and Cheng, C. 2024. *Agrobacterium*-mediated *in planta* transformation of horticultural plants: Current status and future prospects. *Scientia Horticulturae* 325, p. 112693. doi: 10.1016/j.scienta.2023.112693.

Harley, R.M. and Brighton, C.A. 1977. Chromosome numbers in the genus Mentha L. *Botanical Journal of the Linnean Society* 74(1), pp. 71–96. doi: 10.1111/j.1095-8339.1977.tb01168.x.

Haudenschild, C., Schalk, M., Karp, F. and Croteau, R. 2000. Functional Expression of Regiospecific Cytochrome P450 Limonene Hydroxylases from Mint (Mentha spp.) in Escherichia coli and Saccharomyces cerevisiae. *Archives of Biochemistry and Biophysics* 379(1), pp. 127–136. doi: 10.1006/abbi.2000.1864.

Hedayati, S., Tarahi, M., Baeghbali, V., Tahsiri, Z. and Hashempur, M.H. 2025. Mint (Mentha spp.) essential oil extraction: from conventional to emerging technologies. *Phytochemistry Reviews* 24(4), pp. 3157–3178. doi: 10.1007/s11101-024-10020-6.

Heidari Japelaghi, R., Haddad, R., Valizadeh, M., Dorani Uliaie, E. and Jalali Javaran, M. 2018. High-Efficiency Agrobacterium-Mediated Transformation of Tobacco (Nicotiana tabacum). *Journal of Plant Molecular Breeding* 6(2), pp. 38–50. doi: 10.22058/jpmb.2019.92266.1170.

Heinig, U., Gutensohn, M., Dudareva, N. and Aharoni, A. 2013. The challenges of cellular compartmentalization in plant metabolic engineering. *Current Opinion in Biotechnology* 24(2), pp. 239–246. doi: 10.1016/j.copbio.2012.11.006.

Hill, K. and Schaller, G.E. 2013. Enhancing plant regeneration in tissue culture: a molecular approach through manipulation of cytokinin sensitivity. *Plant Signaling & Behavior* 8(10), p. doi: 10.4161/psb.25709. doi: 10.4161/psb.25709.

Holland, C.K. and Jez, J.M. 2018. Arabidopsis: the original plant chassis organism. *Plant Cell Reports* 37(10), pp. 1359–1366. doi: 10.1007/s00299-018-2286-5.

Hood, E.E., Gelvin, S.B., Melchers, L.S. and Hoekema, A. 1993. NewAgrobacterium helper plasmids for gene transfer to plants. *Transgenic Research* 2(4), pp. 208–218. doi: 10.1007/BF01977351.

Horstman, A., Bemer, M. and Boutilier, K. 2017. A transcriptional view on somatic embryogenesis. *Regeneration* 4(4), pp. 201–216. doi: 10.1002/reg2.91.

Huang, M. et al. 2023. Somatic embryogenesis and plant regeneration of Litchi chinensis Sonn. cv. 'Zili' from immature zygotic embryos. *Plant Cell, Tissue and Organ Culture (PCTOC)* 156(2), p. 39. doi: 10.1007/s11240-023-02660-x.

Huang, T., Men, W., Myanganbayar, A. and Davaasambuu, U. 2025. Transcriptome analysis reveals regulatory mechanism of methyl jasmonate-induced monoterpenoid biosynthesis in Mentha arvensis L. *Frontiers in Plant Science* 15, p. 1517851. doi: 10.3389/fpls.2024.1517851.

Huang, X., Zhu, Y., Su, W., Song, S. and Chen, R. 2024. Widely-targeted metabolomics and transcriptomics identify metabolites associated with flowering regulation of Choy Sum. *Scientific Reports* 14(1), p. 10682. doi: 10.1038/s41598-024-60801-4.

Huchelmann, A., Boutry, M. and Hachez, C. 2017. Plant Glandular Trichomes: Natural Cell Factories of High Biotechnological Interest1[OPEN]. *Plant Physiology* 175(1), pp. 6–22. doi: 10.1104/pp.17.00727.

Hudz, N. et al. 2023. Mentha piperita: Essential Oil and Extracts, Their Biological Activities, and Perspectives on the Development of New Medicinal and Cosmetic Products. *Molecules* 28(21), p. 7444. doi: 10.3390/molecules28217444.

Hwang, H.-H., Yu, M. and Lai, E.-M. 2017. Agrobacterium-mediated plant transformation: biology and applications. *The Arabidopsis Book* 15, p. e0186. doi: 10.1199/tab.0186.

Hwang, H.-S., Adhikari, P.B., Jo, H.-J., Han, J.Y. and Choi, Y.E. 2020. Enhanced monoterpene emission in transgenic orange mint (Mentha × piperita f. citrata)

overexpressing a tobacco lipid transfer protein (NtLTP1). *Planta* 252(3), p. 44. doi: 10.1007/s00425-020-03447-6.

Hyatt, D.C., Youn, B., Zhao, Y., Santhamma, B., Coates, R.M., Croteau, R.B. and Kang, C. 2007. Structure of limonene synthase, a simple model for terpenoid cyclase catalysis. *Proceedings of the National Academy of Sciences* 104(13), pp. 5360–5365. doi: 10.1073/pnas.0700915104.

Ikeuchi, M., Sugimoto, K. and Iwase, A. 2013. Plant Callus: Mechanisms of Induction and Repression. *The Plant Cell* 25(9), pp. 3159–3173. doi: 10.1105/tpc.113.116053.

Illumina. 2024. *Considerations for RNA Seq read length and coverage | Illumina Knowledge*. Available at: https://knowledge.illumina.com/library-preparation/rna-library-prep/library-preparation-rna-library-prep-reference_material-list/000001243 [Accessed: 24 September 2025].

Isah, T. 2019. Stress and defense responses in plant secondary metabolites production. *Biological Research* 52. Available at: http://www.scielo.cl/scielo.php?script=sci_abstract&pid=S0716-97602019000100236&lng=es&nrm=iso&tlng=en [Accessed: 22 September 2025].

Iwase, A., Matsui, K. and Ohme-Takagi, M. 2009. Manipulation of plant metabolic pathways by transcription factors. *Plant Biotechnology* 26(1), pp. 29–38. doi: 10.5511/plantbiotechnology.26.29.

Jay, F., Brioudes, F. and Voinnet, O. 2023. A contemporary reassessment of the enhanced transient expression system based on the tombusviral silencing suppressor protein P19. *The Plant Journal* 113(1), pp. 186–204. doi: 10.1111/tpj.16032.

Jeleń, H.H., Obuchowska, M., Zawirska-Wojtasiak, R. and Wąsowicz, E. 2000. Headspace Solid-Phase Microextraction Use for the Characterization of Volatile Compounds in Vegetable Oils of Different Sensory Quality. *Journal of Agricultural and Food Chemistry* 48(6), pp. 2360–2367. doi: 10.1021/jf991095v.

Ji, F. and Sadreyev, R.I. 2018. RNA-seq: Basic Bioinformatics Analysis. *Current protocols in molecular biology* 124(1), p. e68. doi: 10.1002/cpmb.68.

Ji, W., Osbourn, A. and Liu, Z. 2024. Understanding metabolic diversification in plants: branchpoints in the evolution of specialized metabolism. *Philosophical Transactions of the Royal Society B: Biological Sciences* 379(1914), p. 20230359. doi: 10.1098/rstb.2023.0359.

Jian, W. et al. 2019. SlMYB75, an MYB-type transcription factor, promotes anthocyanin accumulation and enhances volatile aroma production in tomato fruits. *Horticulture Research* 6, p. 22. doi: 10.1038/s41438-018-0098-y.

Jiang, Z., Kempinski, C. and Chappell, J. 2016. Extraction and Analysis of Terpenes/Terpenoids. *Current protocols in plant biology* 1, pp. 345–358. doi: 10.1002/cppb.20024.

Jin, J., Tian, F., Yang, D.-C., Meng, Y.-Q., Kong, L., Luo, J. and Gao, G. 2017. PlantTFDB 4.0: toward a central hub for transcription factors and regulatory interactions in plants. *Nucleic Acids Research* 45(D1), pp. D1040–D1045. doi: 10.1093/nar/gkw982.

Jongedijk, E. et al. 2020. Novel routes towards bioplastics from plants: elucidation of the methylperillate biosynthesis pathway from Salvia dorisiana trichomes. Takahashi, H. ed. *Journal of Experimental Botany* 71(10), pp. 3052–3065. doi: 10.1093/jxb/eraa086.

Kajla, M., Roy, A., Singh, I.K. and Singh, A. 2023. Regulation of the regulators: Transcription factors controlling biosynthesis of plant secondary metabolites during biotic stresses and their regulation by miRNAs. *Frontiers in Plant Science* 14. Available at: https://www.frontiersin.org/journals/plant-science/articles/10.3389/fpls.2023.1126567/full [Accessed: 23 February 2026].

Kalalagh, K.F., Papon, N., Courdavault, V., van der Krol, S., Kappers, I.F. and Kashkooli, A.B. 2025a. Metabolic engineering in Nicotiana benthamiana. *aBIOTECH* 6(4), pp. 638–662. doi: 10.1007/s42994-025-00234-3.

Kalalagh, K.F., Papon, N., Courdavault, V., van der Krol, S., Kappers, I.F. and Kashkooli, A.B. 2025b. Metabolic engineering in Nicotiana benthamiana. *aBIOTECH* 6(4), pp. 638–662. doi: 10.1007/s42994-025-00234-3.

Kamatou, G.P.P., Vermaak, I., Viljoen, A.M. and Lawrence, B.M. 2013. Menthol: A simple monoterpene with remarkable biological properties. *Phytochemistry* 96, pp. 15–25. doi: 10.1016/j.phytochem.2013.08.005.

Karp, F., Mihaliak, C.A., Harris, J.L. and Croteau, R. 1990. Monoterpene biosynthesis: specificity of the hydroxylations of (-)-limonene by enzyme preparations from peppermint (Mentha piperita), spearmint (Mentha spicata), and perilla (Perilla frutescens) leaves. *Archives of Biochemistry and Biophysics* 276(1), pp. 219–226. doi: 10.1016/0003-9861(90)90029-x.

Kayani, S.-I. et al. 2019. The YABBY Family Transcription Factor AaYABBY5 Directly Targets Cytochrome P450 Monooxygenase (CYP71AV1) and Double-Bond Reductase 2 (DBR2) Involved in Artemisinin Biosynthesis in Artemisia Annua. *Frontiers in Plant Science* 10, p. 1084. doi: 10.3389/fpls.2019.01084.

Kellogg, B.A. and Poulter, C.D. 1997. Chain elongation in the isoprenoid biosynthetic pathway. *Current Opinion in Chemical Biology* 1(4), pp. 570–578. doi: 10.1016/s1367-5931(97)80054-3.

Khakimov, B. et al. 2015. Identification and genome organization of saponin pathway genes from a wild crucifer, and their use for transient production of saponins in Nicotiana benthamiana. *The Plant Journal: For Cell and Molecular Biology* 84(3), pp. 478–490. doi: 10.1111/tpj.13012.

Khan, A., Tian, R., Bean, S.R., Yerka, M. and Jiao, Y. 2024. Transcriptome and metabolome analyses reveal regulatory networks associated with nutrition synthesis in sorghum seeds. *Communications Biology* 7, p. 841. doi: 10.1038/s42003-024-06525-7.

Killiny, N. and Jones, S.E. 2017. Profiling of volatile organic compounds released from individual intact juvenile and mature citrus leaves. *Journal of Plant Physiology* 208, pp. 47–51. doi: 10.1016/j.jplph.2016.11.001.

Kippes, N., Culp, D., Wilson, R.G., Dowd, E., Comai, L. and Henry, I.M. 2025. Velvet: An alternative high-yielding peppermint clone for oil production. *Crop Science* 65(1), p. e21421. doi: 10.1002/csc2.21421.

Kjonaas, R. and Croteau, R. 1983. Demonstration that limonene is the first cyclic intermediate in the biosynthesis of oxygenated *p*-menthane monoterpenes in *Mentha piperita* and other *Mentha* species. *Archives of Biochemistry and Biophysics* 220(1), pp. 79–89. doi: 10.1016/0003-9861(83)90389-2.

Kjonaas, R., Martinkus-Taylor, C. and Croteau, R. 1982. Metabolism of Monoterpenes: Conversion of l-Menthone to l-Menthol and d-Neomenthol by Stereospecific Dehydrogenases from Peppermint (Mentha piperita) Leaves 12. *Plant Physiology* 69(5), pp. 1013–1017. doi: 10.1104/pp.69.5.1013.

Kjonaas, R.B., Venkatachalam, K.V. and Croteau, R. 1985. Metabolism of monoterpenes: oxidation of isopiperitenol to isopiperitenone, and subsequent isomerization to piperitenone by soluble enzyme preparations from peppermint (Mentha piperita) leaves. *Archives of Biochemistry and Biophysics* 238(1), pp. 49–60. doi: 10.1016/0003-9861(85)90139-0.

Koley, S., Jyoti, P., Lingwan, M. and Allen, D.K. 2024. Isotopically nonstationary metabolic flux analysis of plants: recent progress and future opportunities. *New Phytologist* 242(5), pp. 1911–1918. doi: 10.1111/nph.19734.

Komori, T., Imayama, T., Kato, N., Ishida, Y., Ueki, J. and Komari, T. 2007. Current Status of Binary Vectors and Superbinary Vectors. *Plant Physiology* 145(4), pp. 1155–1160.

Koncz, C. and Schell, J. 1986. The promoter of TL-DNA gene 5 controls the tissue-specific expression of chimaeric genes carried by a novel type of Agrobacterium binary vector. *Molecular and General Genetics MGG* 204(3), pp. 383–396. doi: 10.1007/BF00331014.

Krasnyanski, S., May, R.A., Loskutov, A., Ball, T.M. and Sink, K.C. 1999. Transformation of the limonene synthase gene into peppermint (Mentha piperita L.) and preliminary studies on the essential oil profiles of single transgenic plants. *Theoretical and Applied Genetics* 99(3–4), pp. 676–682. doi: 10.1007/s001220051284.

Krishnan, S.R.S. and Siril, E.A. 2017. Auxin and nutritional stress coupled somatic embryogenesis in Oldenlandia umbellata L. *Physiology and Molecular Biology of Plants* 23(2), pp. 471–475. doi: 10.1007/s12298-017-0425-z.

Kumari, M., Checker, V.G., Kathpalia, R., Srivastava, V., Singh, I.K. and Singh, A. 2024. Metabolic engineering for enhanced terpenoid production: Leveraging new horizons with an old technique. *Plant Physiology and Biochemistry* 210, p. 108511. doi: 10.1016/j.plaphy.2024.108511.

Kumlay, A.M. and Ercisli, S. 2015. Callus induction, shoot proliferation and root regeneration of potato (Solanum tuberosum L.) stem node and leaf explants under long-day conditions. *Biotechnology & Biotechnological Equipment* 29(6), pp. 1075–1084. doi: 10.1080/13102818.2015.1077685.

Lackus, N.D., Petersen, N.P., Nagel, R., Schmidt, A., Irmisch, S., Gershenzon, J. and Köllner, T.G. 2019. Identification and Characterization of trans-Isopentenyl Diphosphate Synthases Involved in Herbivory-Induced Volatile Terpene Formation in Populus trichocarpa. *Molecules* 24(13), p. 2408. doi: 10.3390/molecules24132408.

Lange, B.M. et al. 2011. Improving peppermint essential oil yield and composition by metabolic engineering. *Proceedings of the National Academy of Sciences* 108(41), pp. 16944–16949. doi: 10.1073/pnas.1111558108.

Lange, B.M. 2015. Biosynthesis and Biotechnology of High-Value p-Menthane Monoterpenes, Including Menthol, Carvone, and Limonene. In: Schrader, J. and Bohlmann, J. eds *Biotechnology of Isoprenoids*. Advances in Biochemical Engineering/Biotechnology. Cham: Springer International Publishing, pp. 319–353. Available at: http://link.springer.com/10.1007/10_2014_289 [Accessed: 18 October 2021].

Lange, B.M. and Ahkami, A. 2013. Metabolic engineering of plant monoterpenes, sesquiterpenes and diterpenes-current status and future opportunities. *Plant Biotechnology Journal* 11(2), pp. 169–196. doi: 10.1111/pbi.12022.

Lange, B.M., Ketchum, R.E.B. and Croteau, R.B. 2001. Isoprenoid Biosynthesis. Metabolite Profiling of Peppermint Oil Gland Secretory Cells and Application to Herbicide Target Analysis. *Plant Physiology* 127(1), pp. 305–314. doi: 10.1104/pp.127.1.305.

Lange, B.M., Wildung, M.R., Stauber, E.J., Sanchez, C., Pouchnik, D. and Croteau, R. 2000. Probing essential oil biosynthesis and secretion by functional evaluation of

expressed sequence tags from mint glandular trichomes. *Proceedings of the National Academy of Sciences* 97(6), pp. 2934–2939. doi: 10.1073/pnas.97.6.2934.

Langenheim, J.H. 1994. Higher plant terpenoids: A phytocentric overview of their ecological roles. *Journal of Chemical Ecology* 20(6), pp. 1223–1280. doi: 10.1007/BF02059809.

Larsen, B. et al. 2017. Identification of Iridoid Glucoside Transporters in Catharanthus roseus. *Plant and Cell Physiology* 58(9), pp. 1507–1518. doi: 10.1093/pcp/pcx097.

Lawrence, B.M. 1978. *A study of the monoterpene interrelationships in the genus mentha with special reference to the origin of pulegone and menthofuran*. Print Three Inc. Canada.

Lawrence, B.M. ed. 2006. *Mint: The Genus Mentha*. Boca Raton: CRC Press. doi: 10.1201/9780849307980.

Lee, J., Lee, K.-R., Kim, N.-S., Lee, J., Lee, S.-K. and Lee, S. 2024. High-Level Production of a Recombinant Protein in Nicotiana benthamiana Leaves Through Transient Expression Using a Double Terminator. *International Journal of Molecular Sciences* 25(21), p. 11573. doi: 10.3390/ijms252111573.

Lee, L.-Y. and Gelvin, S.B. 2008. T-DNA Binary Vectors and Systems. *Plant Physiology* 146(2), pp. 325–332. doi: 10.1104/pp.107.113001.

Lee, M.H. et al. 2020. Temporal and Spatial Expression Analysis of Shoot-Regeneration Regulatory Genes during the Adventitious Shoot Formation in Hypocotyl and Cotyledon Explants of Tomato (CV. Micro-Tom). *International Journal of Molecular Sciences* 21(15), p. 5309. doi: 10.3390/ijms21155309.

Leonelli, S. 2007. Growing Weed, Producing Knowledge An Epistemic History of Arabidopsis thaliana. *History and Philosophy of the Life Sciences* 29(2), pp. 193–223.

Li, F. et al. 2024. Characterization of a vacuolar importer of secologanin in Catharanthus roseus. *Communications Biology* 7(1), p. 939. doi: 10.1038/s42003-024-06624-5.

Li, H., Chen, N., Zhang, H. and Xu, D. 2025a. Multidimensional regulation of transcription factors: decoding the comprehensive signals of plant secondary metabolism. *Frontiers in Plant Science* 16. Available at: https://www.frontiersin.org/journals/plant-science/articles/10.3389/fpls.2025.1522278/full [Accessed: 23 February 2026].

Li, J., Mutanda, I., Wang, K., Yang, L., Wang, J. and Wang, Y. 2019. Chloroplastic metabolic engineering coupled with isoprenoid pool enhancement for committed taxanes biosynthesis in Nicotiana benthamiana. *Nature Communications* 10(1), p. 4850. doi: 10.1038/s41467-019-12879-y.

Li, S. et al. 2025b. The promoter sequence of (-)-limonene synthase in Mentha Canadensis and its strong activity in the glandular trichome and in the stomatal guard cells. Available at: https://www.researchsquare.com/article/rs-6702558/v1 [Accessed: 7 July 2025].

Li, T., Li, S., Liang, C., Zhu, J., Liu, M. and Yang, Y. 2018. Chemical shift assignments of RHE_RS02845, a NTF2-like domain-containing protein from Rhizobium etli. *Biomolecular NMR Assignments* 12(2), pp. 249–252. doi: 10.1007/s12104-018-9817-4.

Li, X. et al. 2001. Bar-expressing peppermint (Mentha × Piperita L. var. Black Mitcham) plants are highly resistant to the glufosinate herbicide Liberty. *Molecular Breeding* 8(2), pp. 109–118. doi: 10.1023/A:1013316816955.

Liu, C. et al. 2023. The NAC Transcription Factor PgNAC41-2 Gene Involved in the Regulation of Ginsenoside Biosynthesis in Panax ginseng. *International Journal of Molecular Sciences* 24(15), p. 11946. doi: 10.3390/ijms241511946.

Liu, Q. et al. 2011. Reconstitution of the Costunolide Biosynthetic Pathway in Yeast and Nicotiana benthamiana. *PLoS ONE* 6(8), p. e23255. doi: 10.1371/journal.pone.0023255.

Liu, X. et al. 2025. Integrated transcriptomic and metabolomic analysis reveals developmental stage-specific molecular responses to phosphorus deficiency in soybean. *Frontiers in Plant Science* 16. Available at: https://www.frontiersin.org/journals/plant-science/articles/10.3389/fpls.2025.1692661/full [Accessed: 24 February 2026].

Livak, K.J. and Schmittgen, T.D. 2001. Analysis of relative gene expression data using real-time quantitative PCR and the 2(-Delta Delta C(T)) Method. *Methods (San Diego, Calif.)* 25(4), pp. 402–408. doi: 10.1006/meth.2001.1262.

Lombardi, R. et al. 2009. High-level HIV-1 Nef transient expression in Nicotiana benthamiana using the P19 gene silencing suppressor protein of Artichoke Mottled Crinckle Virus. *BMC biotechnology* 9, p. 96. doi: 10.1186/1472-6750-9-96.

Long, Y., Yang, Y., Pan, G. and Shen, Y. 2022. New Insights Into Tissue Culture Plant-Regeneration Mechanisms. *Frontiers in Plant Science* 13. Available at: https://www.frontiersin.org/journals/plant-science/articles/10.3389/fpls.2022.926752/full [Accessed: 30 June 2025].

López-Hernández, F. and Cortés, A.J. 2022. Whole Transcriptome Sequencing Unveils the Genomic Determinants of Putative Somaclonal Variation in Mint (Mentha L.). *International Journal of Molecular Sciences* 23(10), p. 5291. doi: 10.3390/ijms23105291.

Love, M.I., Huber, W. and Anders, S. 2014. Moderated estimation of fold change and dispersion for RNA-seq data with DESeq2. *Genome Biology* 15(12), p. 550. doi: 10.1186/s13059-014-0550-8.

Low, L.-Y. et al. 2018. Transgenic Plants: Gene Constructs, Vector and Transformation Method. In: *New Visions in Plant Science*. IntechOpen. Available at: https://www.intechopen.com/chapters/63134 [Accessed: 30 June 2025].

Lücker, J., Schwab, W., Franssen, M.C.R., Van Der Plas, L.H.W., Bouwmeester, H.J. and Verhoeven, H.A. 2004a. Metabolic engineering of monoterpene biosynthesis: two-step production of (+)-trans-isopiperitenol by tobacco. *The Plant Journal* 39(1), pp. 135–145. doi: 10.1111/j.1365-313X.2004.02113.x.

Lücker, J., Schwab, W., van Hautum, B., Blaas, J., van der Plas, L.H.W., Bouwmeester, H.J. and Verhoeven, H.A. 2004b. Increased and Altered Fragrance of Tobacco Plants after Metabolic Engineering Using Three Monoterpene Synthases from Lemon. *Plant Physiology* 134(1), pp. 510–519. doi: 10.1104/pp.103.030189.

Ludwiczuk, A., Kiełtyka-Dadasiewicz, A., Sawicki, R., Golus, J. and Ginalska, G. 2016. Essential Oils of some Mentha Species and Cultivars, their Chemistry and

Bacteriostatic Activity. *Natural Product Communications* 11(7), p. 1934578X1601100736. doi: 10.1177/1934578X1601100736.

Ludwiczuk, A., Skalicka-Woźniak, K. and Georgiev, M.I. 2017. Chapter 11 - Terpenoids. In: Badal, S. and Delgoda, R. eds *Pharmacognosy*. Boston: Academic Press, pp. 233–266. Available at: https://www.sciencedirect.com/science/article/pii/B9780128021040000111 [Accessed: 2 September 2025].

Lupien, S., Karp, F., Wildung, M. and Croteau, R. 1999. Regiospecific Cytochrome P450 Limonene Hydroxylases from Mint (Mentha) Species: cDNA Isolation, Characterization, and Functional Expression of (−)-4S-Limonene-3-hydroxylase and (−)-4S-Limonene-6-hydroxylase. *Archives of Biochemistry and Biophysics* 368(1), pp. 181–192. doi: 10.1006/abbi.1999.1298.

Lv, B. et al. 2025. The transcription factor Dof32 coordinates salvianolic acid biosynthesis and drought tolerance in Salvia miltiorrhiza. *Plant Physiology* 198(2), p. kiaf221. doi: 10.1093/plphys/kiaf221.

Lv, M. et al. 2022a. Terpenoid biosynthesis in *Dendrobium officinale*: Identification of (*E*)-*β*-caryophyllene synthase and the regulatory *MYB* genes. *Industrial Crops and Products* 182, p. 114875. doi: 10.1016/j.indcrop.2022.114875.

Lv, X. et al. 2022b. Engineered Saccharomyces cerevisiae for the De Novo Biosynthesis of (−)-Menthol. *Journal of Fungi* 8(9), p. 982. doi: 10.3390/jof8090982.

Lytovchenko, A. et al. 2009. Application of GC-MS for the detection of lipophilic compounds in diverse plant tissues. *Plant Methods* 5, p. 4. doi: 10.1186/1746-4811-5-4.

Ma, C. et al. 2021. Heterologous expression and metabolic engineering tools for improving terpenoids production. *Current Opinion in Biotechnology* 69, pp. 281–289. doi: 10.1016/j.copbio.2021.02.008.

Ma, D. et al. 2009. Isolation and characterization of AaWRKY1, an Artemisia annua transcription factor that regulates the amorpha-4,11-diene synthase gene, a key gene of artemisinin biosynthesis. *Plant & Cell Physiology* 50(12), pp. 2146–2161. doi: 10.1093/pcp/pcp149.

Ma, L., Lukasik, E., Gawehns, F. and Takken, F.L.W. 2012. The Use of Agroinfiltration for Transient Expression of Plant Resistance and Fungal Effector Proteins in Nicotiana benthamiana Leaves. In: Bolton, M. D. and Thomma, B. P. H. J. eds *Plant Fungal Pathogens: Methods and Protocols*. Totowa, NJ: Humana Press, pp. 61–74. Available at: https://doi.org/10.1007/978-1-61779-501-5_4 [Accessed: 12 September 2025].

Mad' Atari, M.F. bin and Folta, K.M. 2019. Transformation improvement with the Standardized Pressure Agrobacterium Infiltration Device (SPAID). *BMC Research Notes* 12, p. 144. doi: 10.1186/s13104-019-4117-3.

Maffei, M., Chialva, F. and Sacco, T. 1989. Glandular trichomes and essential oils in developing peppermint leaves: I. Variation of peltate trichome number and terpene distribution within leaves. *The New Phytologist* 111(4), pp. 707–716. doi: 10.1111/j.1469-8137.1989.tb02366.x.

Mahmoud, S. 2004. Cosuppression of limonene-3-hydroxylase in peppermint promotes accumulation of limonene in the essential oil. *Phytochemistry* 65(5), pp. 547–554. doi: 10.1016/j.phytochem.2004.01.005.

Mahmoud, S.S. and Croteau, R.B. 2001. Metabolic engineering of essential oil yield and composition in mint by altering expression of deoxyxylulose phosphate reductoisomerase and menthofuran synthase. *Proceedings of the National Academy of Sciences* 98(15), pp. 8915–8920. doi: 10.1073/pnas.141237298.

Mahmoud, S.S. and Croteau, R.B. 2003. Menthofuran regulates essential oil biosynthesis in peppermint by controlling a downstream monoterpene reductase. *Proceedings of the National Academy of Sciences* 100(24), pp. 14481–14486. doi: 10.1073/pnas.2436325100.

Mahood, H.E., Sarropoulou, V. and Tzatzani, T.-T. 2022. Effect of explant type (leaf, stem) and 2,4-D concentration on callus induction: influence of elicitor type (biotic, abiotic), elicitor concentration and elicitation time on biomass growth rate and costunolide biosynthesis in gazania (Gazania rigens) cell suspension cultures. *Bioresources and Bioprocessing* 9(1), p. 100. doi: 10.1186/s40643-022-00588-2.

Malik, T.G. et al. 2023. Environmental Factors Affecting Monoterpene Emissions from Terrestrial Vegetation. *Plants* 12(17), p. 3146. doi: 10.3390/plants12173146.

Marillonnet, S. and Grützner, R. 2020. Synthetic DNA Assembly Using Golden Gate Cloning and the Hierarchical Modular Cloning Pipeline. *Current Protocols in Molecular Biology* 130(1), p. e115. doi: 10.1002/cpmb.115.

Marillonnet, S. and Werner, S. 2025. Golden Gate Cloning of Multigene Constructs Using the Modular Cloning System MoClo. In: Schindler, D. ed. *Golden Gate Cloning: Methods and Protocols*. New York, NY: Springer US, pp. 21–39. Available at: https://doi.org/10.1007/978-1-0716-4220-7_2 [Accessed: 12 September 2025].

Markus Lange, B. and Turner, G.W. 2013. Terpenoid biosynthesis in trichomes-current status and future opportunities. *Plant Biotechnology Journal* 11(1), pp. 2–22. doi: 10.1111/j.1467-7652.2012.00737.x.

Martin, D.M., Fäldt, J. and Bohlmann, J. 2004. Functional Characterization of Nine Norway Spruce TPS Genes and Evolution of Gymnosperm Terpene Synthases of the TPS-d Subfamily. *Plant Physiology* 135(4), pp. 1908–1927. doi: 10.1104/pp.104.042028.

Martinez-Corral, R., Friedrich, D., Frömel, R., Velten, L., Gunawardena, J. and DePace, A.H. 2024. Emergence of activation or repression in transcriptional control under a fixed molecular context. *bioRxiv*, p. 2024.05.29.596388. doi: 10.1101/2024.05.29.596388.

Matsuo, K., Fukuzawa, N. and Matsumura, T. 2016. A simple agroinfiltration method for transient gene expression in plant leaf discs. *Journal of Bioscience and Bioengineering* 122(3), pp. 351–356. doi: 10.1016/j.jbiosc.2016.02.001.

McCaskill, D. and Croteau, R. 1995. Monoterpene and sesquiterpene biosynthesis in glandular trichomes of peppermint (Mentha x piperita) rely exclusively on plastid-derived isopentenyl diphosphate. *Planta* 197(1), pp. 49–56. doi: 10.1007/BF00239938.

McCaskill, D., Gershenzon, J. and Croteau, R. 1992. Morphology and monoterpene biosynthetic capabilities of secretory cell clusters isolated from glandular trichomes of peppermint (Mentha piperita L.). *Planta* 187(4), pp. 445–454. doi: 10.1007/BF00199962.

McConkey, M.E., Gershenzon, J. and Croteau, R.B. 2000. Developmental Regulation of Monoterpene Biosynthesis in the Glandular Trichomes of Peppermint. *Plant Physiology* 122(1), pp. 215–224. doi: 10.1104/pp.122.1.215.

McLaughlin, J.E., Kue Foka, I.C., Lawton, M.A. and Di, R. 2025. CRISPR activation: identifying and using novel genes for plant disease resistance breeding. *Frontiers in Genome Editing* 7. Available at: https://www.frontiersin.org/journals/genome-editing/articles/10.3389/fgeed.2025.1596600/full [Accessed: 1 March 2026].

Medema, M.H. and Osbourn, A. 2016. Computational genomic identification and functional reconstitution of plant natural product biosynthetic pathways. *Natural Product Reports* 33(8), pp. 951–962. doi: 10.1039/c6np00035e.

Mei, G., Chen, A., Wang, Y., Li, S., Wu, M., Liu, X. and Hou, X. 2023. A simple and efficient in planta transformation method based on the active regeneration capacity of plants. p. 2023.01.02.522521. Available at: https://www.biorxiv.org/content/10.1101/2023.01.02.522521v1 [Accessed: 30 June 2025].

Meitinger, N., Geiger, D., Augusto, T.W., Maia de Pádua, R. and Kreis, W. 2015. Purification of Δ5-3-ketosteroid isomerase from *Digitalis lanata*. *Phytochemistry* 109, pp. 6–13. doi: 10.1016/j.phytochem.2014.10.025.

Mensuali-Sodi, A., Panizza, M., Serra, G. and Tognoni, F. 1993. Involvement of activated charcoal in the modulation of abiotic and biotic ethylene levels in tissue cultures. *Scientia Horticulturae* 54(1), pp. 49–57. doi: 10.1016/0304-4238(93)90082-2.

Minutolo, M., Chiaiese, P., Di Matteo, A., Errico, A. and Corrado, G. 2020. Accumulation of Ascorbic Acid in Tomato Cell Culture: Influence of the Genotype, Source Explant and Time of In Vitro Cultivation. *Antioxidants (Basel, Switzerland)* 9(3), p. 222. doi: 10.3390/antiox9030222.

Mo, W., Zheng, X., Shi, Q., Zhao, X., Chen, X., Yang, Z. and Zuo, Z. 2024. Unveiling the crucial roles of abscisic acid in plant physiology: implications for enhancing stress tolerance and productivity. *Frontiers in Plant Science* 15, p. 1437184. doi: 10.3389/fpls.2024.1437184.

Mołdoch, J., Agacka-Mołdoch, M., Jóźwiak, G. and Wojtunik-Kulesza, K. 2025. Biological Activity of Monoterpene-Based Scaffolds: A Natural Toolbox for Drug Discovery. *Molecules* 30(7), p. 1480. doi: 10.3390/molecules30071480.

Molina-Hidalgo, F.J. et al. 2021. Engineering Metabolism in Nicotiana Species: A Promising Future. *Trends in Biotechnology* 39(9), pp. 901–913. doi: 10.1016/j.tibtech.2020.11.012.

Molina-Risco, M., Ibarra, O., Faion-Molina, M., Kim, B., Septiningsih, E.M. and Thomson, M.J. 2021. Optimizing Agrobacterium-Mediated Transformation and CRISPR-Cas9 Gene Editing in the tropical japonica Rice Variety Presidio. *International Journal of Molecular Sciences* 22(20), p. 10909. doi: 10.3390/ijms222010909.

Moreno, L., Bello, R., Primo-Yúfera, E. and Esplugues, J. 2002. Pharmacological properties of the methanol extract from Mentha suaveolens Ehrh. *Phytotherapy Research* 16(S1), pp. 10–13. doi: 10.1002/ptr.744.

Moskal, K. et al. 2025. Why “Where” Matters as Much as “How Much”: Single-Cell and Spatial Transcriptomics in Plants. *International Journal of Molecular Sciences* 26(24), p. 11819. doi: 10.3390/ijms262411819.

Mosquera, M.E.G. et al. 2021. Terpenes and Terpenoids: Building Blocks to Produce Biopolymers. *Sustainable Chemistry* 2(3), pp. 467–492. doi: 10.3390/suschem2030026.

Mugford, S.T. et al. 2013. Modularity of Plant Metabolic Gene Clusters: A Trio of Linked Genes That Are Collectively Required for Acylation of Triterpenes in Oat[W][OA]. *The Plant Cell* 25(3), pp. 1078–1092. doi: 10.1105/tpc.113.110551.

Muntean, D. et al. 2019. Evaluation of essential oil obtained from Mentha×piperita L. against multidrug-resistant strains. *Infection and Drug Resistance* 12, pp. 2905–2914. doi: 10.2147/IDR.S218141.

Muppala, S., Gudlavalleti, P.K., Malireddy, K.R., Puligundla, S.K. and Dasari, P. 2021. Development of stable transgenic maize plants tolerant for drought by manipulating ABA signaling through *Agrobacterium*-mediated transformation. *Journal*

of Genetic Engineering and Biotechnology 19(1), p. 96. doi: 10.1186/s43141-021-00195-2.

Murray, M.J. and Todd, W.A. 1972. Registration of Todd's Mitcham Peppermint (Reg. No. 1). *Crop Science* 12(1), p. cropsci1972.0011183X001200010056x. doi: 10.2135/cropsci1972.0011183X001200010056x.

Nair, B. 2001. Final report on the safety assessment of Mentha Piperita (Peppermint) Oil, Mentha Piperita (Peppermint) Leaf Extract, Mentha Piperita (Peppermint) Leaf, and Mentha Piperita (Peppermint) Leaf Water. *International Journal of Toxicology* 20 Suppl 3, pp. 61–73.

Nakano, T. et al. 2018. FPX is a Novel Chemical Inducer that Promotes Callus Formation and Shoot Regeneration in Plants. *Plant and Cell Physiology* 59(8), pp. 1555–1567. doi: 10.1093/pcp/pcy139.

Niedbała, G., Niazian, M. and Sabbatini, P. 2021. Modeling Agrobacterium-Mediated Gene Transformation of Tobacco (Nicotiana tabacum)—A Model Plant for Gene Transformation Studies. *Frontiers in Plant Science* 12. Available at: https://www.frontiersin.org/journals/plant-science/articles/10.3389/fpls.2021.695110/full [Accessed: 10 September 2025].

NIST. 2014. *NIST/EPA/NIH Mass Spectral Library (NIST 14), NIST Standard Reference Database 1A v2.2*. Gaithersburg, MD: National Institute of Standards and Technology. Available at: https://www.nist.gov/srd/nist-standard-reference-database-1a.

Niu, X., Li, X., Veronese, P., Bressan, R.A., Weller, S.C. and Hasegawa, P.M. 2000. Factors affecting Agrobacterium tumefaciens -mediated transformation of peppermint. *Plant Cell Reports* 19(3), pp. 304–310. doi: 10.1007/s002990050017.

Niu, X., Lin, K., Hasegawa, P.M., Bressan, R.A. and Weller, S.C. 1998. Transgenic peppermint (Mentha × piperita L.) plants obtained by cocultivation with Agrobacterium tumefaciens. *Plant Cell Reports* 17(3), pp. 165–171. doi: 10.1007/s002990050372.

Norkunas, K., Harding, R., Dale, J. and Dugdale, B. 2018. Improving agroinfiltration-based transient gene expression in Nicotiana benthamiana. *Plant Methods* 14, p. 71. doi: 10.1186/s13007-018-0343-2.

Ohara, K., Ujihara, T., Endo, T., Sato, F. and Yazaki, K. 2003. Limonene production in tobacco with Perilla limonene synthase cDNA. *Journal of Experimental Botany* 54(393), pp. 2635–2642. doi: 10.1093/jxb/erg300.

Ooms, G., Hooykaas, P.J.J., Van Veen, R.J.M., Van Beelen, P., Regensburg-Tuïnk, T.J.G. and Schilperoort, R.A. 1982. Octopine Ti-plasmid deletion mutants of *Agrobacterium tumefaciens* with emphasis on the right side of the T-region. *Plasmid* 7(1), pp. 15–29. doi: 10.1016/0147-619X(82)90023-3.

Orlova, I. et al. 2009. The Small Subunit of Snapdragon Geranyl Diphosphate Synthase Modifies the Chain Length Specificity of Tobacco Geranylgeranyl Diphosphate Synthase in Planta. *The Plant Cell* 21(12), pp. 4002–4017. doi: 10.1105/tpc.109.071282.

Ow, D.W., Jacobs, J.D. and Howell, S.H. 1987. Functional regions of the cauliflower mosaic virus 35S RNA promoter determined by use of the firefly luciferase gene as a reporter of promoter activity. *Proceedings of the National Academy of Sciences of the United States of America* 84(14), pp. 4870–4874. doi: 10.1073/pnas.84.14.4870.

Park, S., Mani, V., Kim, J.A., Lee, S.I. and Lee, K. 2022. Combinatorial transient gene expression strategies to enhance terpenoid production in plants. *Frontiers in Plant Science* 13. Available at: https://www.frontiersin.org/articles/10.3389/fpls.2022.1034893 [Accessed: 11 August 2023].

Park, Y.D., Papp, I., Moscone, E.A., Iglesias, V.A., Vaucheret, H., Matzke, A.J. and Matzke, M.A. 1996. Gene silencing mediated by promoter homology occurs at the level of transcription and results in meiotically heritable alterations in methylation and gene activity. *The Plant Journal: For Cell and Molecular Biology* 9(2), pp. 183–194. doi: 10.1046/j.1365-313x.1996.09020183.x.

Passricha, N., Saifi, S., Khatodia, S. and Tuteja, N. 2016. Assessing zygosity in progeny of transgenic plants: current methods and perspectives. *Journal of Biological Methods* 3(3), p. e46. doi: 10.14440/jbm.2016.114.

Paszkowski, J., Shillito, R.D., Saul, M., Mandák, V., Hohn, T., Hohn, B. and Potrykus, I. 1984. Direct gene transfer to plants. *The EMBO Journal* 3(12), pp. 2717–2722. doi: 10.1002/j.1460-2075.1984.tb02201.x.

Patel, T., Ishiuji, Y. and Yosipovitch, G. 2007. Menthol: A refreshing look at this ancient compound. *Journal of the American Academy of Dermatology* 57(5), pp. 873–878. doi: 10.1016/j.jaad.2007.04.008.

Pathi, K.M., Tula, S. and Tuteja, N. 2013. High frequency regeneration via direct somatic embryogenesis and efficient Agrobacterium- mediated genetic transformation of tobacco. *Plant Signaling & Behavior* 8(6), p. e24354. doi: 10.4161/psb.24354.

Patterson, J. et al. 2019. Impact of sequencing depth and technology on de novo RNA-Seq assembly. *BMC Genomics* 20(1), p. 604. doi: 10.1186/s12864-019-5965-x.

Pawar, B.D., Jadhav, A.S., Kale, A.A., Chimote, V.P. and Pawar, S.V. 2013. Effect of explants, bacterial cell density and overgrowth-control antibiotics on transformation efficiency in tomato (*Solanum lycopersicum* L.). *Journal of Applied Horticulture* 15(2), pp. 95–99.

Payá-Milans, M., Olmstead, J.W., Nunez, G., Rinehart, T.A. and Staton, M. 2018. Comprehensive evaluation of RNA-seq analysis pipelines in diploid and polyploid species. *GigaScience* 7(12), p. giy132. doi: 10.1093/gigascience/giy132.

Peng, R. et al. 2014. Metabolic engineering of Arabidopsis for remediation of different polycyclic aromatic hydrocarbons using a hybrid bacterial dioxygenase complex. *Metabolic Engineering* 26, pp. 100–110. doi: 10.1016/j.ymben.2014.09.005.

Permadi, N. et al. 2024. Traditional and next-generation methods for browning control in plant tissue culture: Current insights and future directions. *Current Plant Biology* 38, p. 100339. doi: 10.1016/j.cpb.2024.100339.

Petrie, J.R. et al. 2010. Rapid expression of transgenes driven by seed-specific constructs in leaf tissue: DHA production. *Plant Methods* 6(1), p. 8. doi: 10.1186/1746-4811-6-8.

Petrie, J.R. et al. 2012. Metabolic Engineering Plant Seeds with Fish Oil-Like Levels of DHA. *PLoS ONE* 7(11), p. e49165. doi: 10.1371/journal.pone.0049165.

Phillips, M.A., León, P., Boronat, A. and Rodríguez-Concepción, M. 2008. The plastidial MEP pathway: unified nomenclature and resources. *Trends in Plant Science* 13(12), pp. 619–623. doi: 10.1016/j.tplants.2008.09.003.

Piasecka, A., Jedrzejczak-Rey, N. and Bednarek, P. 2015. Secondary metabolites in plant innate immunity: conserved function of divergent chemicals. *New Phytologist* 206(3), pp. 948–964. doi: 10.1111/nph.13325.

Pierson, M. and Antoniotti, S. 2025. Metadata review of variation in published chemical compositions of Mentha piperita essential oils. *Journal of Essential Oil & Plant Composition*, pp. 45–59. doi: 10.58985/jeopc.2025.v03i01.65.

Poormassalehgoo, A., Kaniecka, E., Mirzaei, M. and Goto-Yamada, S. 2025. Optimization of selection agent concentrations and expanding G418 utility for gentamicin resistance in Marchantia polymorpha. *Scientific Reports* 15(1), p. 26836. doi: 10.1038/s41598-025-11801-5.

Pottier, M., Laterre, R., Van Wessem, A., Ramirez, A.M., Herman, X., Boutry, M. and Hachez, C. 2020. Identification of two new trichome-specific promoters of Nicotiana tabacum. *Planta* 251(3), p. 58. doi: 10.1007/s00425-020-03347-9.

Poulter, C.D. and Rilling, H.C. 1978. The prenyl transfer reaction. Enzymic and mechanistic studies of the 1’-4 coupling reaction in the terpene biosynthetic pathway. *Accounts of Chemical Research* 11(8), pp. 307–313. doi: 10.1021/ar50128a004.

Qamar, N., Pandey, M., Vasudevan, M., Kumar, A. and Shasany, A.K. 2022. Glandular trichome specificity of menthol biosynthesis pathway gene promoters from Mentha × piperita. *Planta* 256(6), p. 110. doi: 10.1007/s00425-022-04029-4.

Qasim, M. et al. 2024. Impact of plant monoterpenes on insect pest management and insect-associated microbes. *Heliyon* 10(20), p. e39120. doi: 10.1016/j.heliyon.2024.e39120.

Qi, X. et al. 2018. Transcriptome Analysis of JA Signal Transduction, Transcription Factors, and Monoterpene Biosynthesis Pathway in Response to Methyl Jasmonate Elicitation in Mentha canadensis L. *International Journal of Molecular Sciences* 19(8), p. 2364. doi: 10.3390/ijms19082364.

Qi, X., Chen, Z., Yu, X., Li, L., Bai, Y., Fang, H. and Liang, C. 2022. Characterisation of the Mentha canadensis R2R3-MYB transcription factor gene McMIXTA and its involvement in peltate glandular trichome development. *BMC Plant Biology* 22(1), p. 219. doi: 10.1186/s12870-022-03614-9.

Radivojac, A. et al. 2021. Extraction of Peppermint Essential Oils and Lipophilic Compounds: Assessment of Process Kinetics and Environmental Impacts with Multiple Techniques. *Molecules* 26(10), p. 2879. doi: 10.3390/molecules26102879.

Rai, A., Smita, S.S., Singh, A.K., Shanker, K. and Nagegowda, D.A. 2013. Heteromeric and Homomeric Geranyl Diphosphate Synthases from Catharanthus roseus and Their Role in Monoterpene Indole Alkaloid Biosynthesis. *Molecular Plant* 6(5), pp. 1531–1549. doi: 10.1093/mp/sst058.

Rajput, R. et al. 2025. Multigene engineering in plants: Technologies, applications, and future prospects. *Biotechnology Advances* 85, p. 108697. doi: 10.1016/j.biotechadv.2025.108697.

Reddy, V.A. et al. 2017. Spearmint R2R3-MYB transcription factor MsMYB negatively regulates monoterpene production and suppresses the expression of geranyl diphosphate synthase large subunit (MsGPPS.LSU). *Plant Biotechnology Journal* 15(9), pp. 1105–1119. doi: 10.1111/pbi.12701.

Reed, J. and Osbourn, A. 2018. Engineering terpenoid production through transient expression in Nicotiana benthamiana. *Plant Cell Reports* 37(10), pp. 1431–1441. doi: 10.1007/s00299-018-2296-3.

Riboni, M., Robustelli Test, A., Galbiati, M., Tonelli, C. and Conti, L. 2016. ABA-dependent control of GIGANTEA signalling enables drought escape via up-regulation of FLOWERING LOCUS T in Arabidopsis thaliana. *Journal of Experimental Botany* 67(22), pp. 6309–6322. doi: 10.1093/jxb/erw384.

Rieu, I. and Powers, S.J. 2009. Real-Time Quantitative RT-PCR: Design, Calculations, and Statistics. *The Plant Cell* 21(4), pp. 1031–1033. doi: 10.1105/tpc.109.066001.

Ringer, K.L., Davis, E.M. and Croteau, R. 2005. Monoterpene Metabolism. Cloning, Expression, and Characterization of (−)-Isopiperitenol/(−)-Carveol Dehydrogenase of

Peppermint and Spearmint. *Plant Physiology* 137(3), pp. 863–872. doi: 10.1104/pp.104.053298.

Ringer, K.L., McConkey, M.E., Davis, E.M., Rushing, G.W. and Croteau, R. 2003. Monoterpene double-bond reductases of the (−)-menthol biosynthetic pathway: isolation and characterization of cDNAs encoding (−)-isopiperitenone reductase and (+)-pulegone reductase of peppermint. *Archives of Biochemistry and Biophysics* 418(1), pp. 80–92. doi: 10.1016/S0003-9861(03)00390-4.

Rios-Estepa, R., Lange, I., Lee, J.M. and Lange, B.M. 2010. Mathematical Modeling-Guided Evaluation of Biochemical, Developmental, Environmental, and Genotypic Determinants of Essential Oil Composition and Yield in Peppermint Leaves. *Plant Physiology* 152(4), pp. 2105–2119. doi: 10.1104/pp.109.152256.

Rohloff, J., Dragland, S., Mordal, R. and Iversen, T.-H. 2005. Effect of Harvest Time and Drying Method on Biomass Production, Essential Oil Yield, and Quality of Peppermint (Mentha × piperita L.). *Journal of Agricultural and Food Chemistry* 53(10), pp. 4143–4148. doi: 10.1021/jf047998s.

Rolland, V. 2018. Determining the Subcellular Localization of Fluorescently Tagged Proteins Using Protoplasts Extracted from Transiently Transformed Nicotiana benthamiana Leaves. In: Covshoff, S. ed. *Photosynthesis: Methods and Protocols*. New York, NY: Springer, pp. 263–283. Available at: https://doi.org/10.1007/978-1-4939-7786-4_16 [Accessed: 5 August 2025].

Roque, R., Rodriguez, V. and Santos, P.M. 2025. Microbial Production of Menthol. In: *Microbial Production of Food Bioactive Compounds*. Springer, Cham, pp. 1–26. Available at: https://link.springer.com/rwe/10.1007/978-3-030-81403-8_59-1 [Accessed: 24 February 2026].

Rosati, D., Palmieri, M., Brunelli, G., Morrione, A., Iannelli, F., Frullanti, E. and Giordano, A. 2024. Differential gene expression analysis pipelines and bioinformatic tools for the identification of specific biomarkers: A review. *Computational and Structural Biotechnology Journal* 23, pp. 1154–1168. doi: 10.1016/j.csbj.2024.02.018.

Ruiz-Hernández, V., Roca, M.J., Egea-Cortines, M. and Weiss, J. 2018. A comparison of semi-quantitative methods suitable for establishing volatile profiles. *Plant Methods* 14(1), p. 67. doi: 10.1186/s13007-018-0335-2.

Ruiz-Lopez, N., Haslam, R.P., Usher, S.L., Napier, J.A. and Sayanova, O. 2013. Reconstitution of EPA and DHA biosynthesis in Arabidopsis: Iterative metabolic engineering for the synthesis of n−3 LC-PUFAs in transgenic plants. *Metabolic Engineering* 17, pp. 30–41. doi: 10.1016/j.ymben.2013.03.001.

Salas, M., Park, S., Srivatanakul, M. and Smith, R. 2001. Temperature influence on stable T-DNA integration in plant cells. *Plant Cell Reports* 20(8), pp. 701–705. doi: 10.1007/s002990100374.

Saxena, B., Subramaniyan, M., Malhotra, K., Bhavesh, N.S., Potlakayala, S.D. and Kumar, S. 2014. Metabolic engineering of chloroplasts for artemisinic acid biosynthesis and impact on plant growth. *Journal of Biosciences* 39(1), pp. 33–41. doi: 10.1007/s12038-013-9402-z.

Sayanova, O., Ruiz-Lopez, N., Haslam, R.P. and Napier, J.A. 2012. The role of Δ6-desaturase acyl-carrier specificity in the efficient synthesis of long-chain polyunsaturated fatty acids in transgenic plants. *Plant Biotechnology Journal* 10(2), pp. 195–206. doi: 10.1111/j.1467-7652.2011.00653.x.

Schalk, M. and Croteau, R. 2000. A single amino acid substitution (F363I) converts the regiochemistry of the spearmint (−)-limonene hydroxylase from a C6- to a C3-hydroxylase. *Proceedings of the National Academy of Sciences* 97(22), pp. 11948–11953. doi: 10.1073/pnas.97.22.11948.

Schmidt, A., Waؾchtler, B., Temp, U., Krekling, T., Seۨguin, A. and Gershenzon, J. 2010. A Bifunctional Geranyl and Geranylgeranyl Diphosphate Synthase Is Involved in Terpene Oleoresin Formation in Picea abies. *Plant Physiology* 152(2), pp. 639–655. doi: 10.1104/pp.109.144691.

Schmidt, E. et al. 2009. Chemical composition, olfactory evaluation and antioxidant effects of essential oil from Mentha x piperita. *Natural Product Communications* 4(8), pp. 1107–1112.

Schotte, C. et al. 2025. Identification of BAHD-acyltransferase enzymes involved in ingenane diterpenoid biosynthesis. *The New Phytologist* 247(6), pp. 2591–2600. doi: 10.1111/nph.70388.

Schultz, B.J., Kim, S.Y., Lau, W. and Sattely, E.S. 2019. Total Biosynthesis for Milligram-Scale Production of Etoposide Intermediates in a Plant Chassis. *Journal of the American Chemical Society* 141(49), pp. 19231–19235. doi: 10.1021/jacs.9b10717.

Schuurink, R. and Tissier, A. 2020. Glandular trichomes: micro-organs with model status? *New Phytologist* 225(6), pp. 2251–2266. doi: 10.1111/nph.16283.

Schwarz, O.J. and Beaty, R.M. 2000. Organogenesis. In: *Plant Tissue Culture Concepts and Laboratory Exercises*. 2nd edn Routledge.

Sheikh, A.H., Raghuram, B., Eschen-Lippold, L., Scheel, D., Lee, J. and Sinha, A.K. 2014. Agroinfiltration by Cytokinin-Producing Agrobacterium sp. Strain GV3101 Primes Defense Responses in Nicotiana tabacum. *Molecular Plant-Microbe Interactions*® 27(11), pp. 1175–1185. doi: 10.1094/MPMI-04-14-0114-R.

Sheikholeslam, S.N. and Weeks, D.P. 1987. Acetosyringone promotes high efficiency transformation of Arabidopsis thaliana explants by Agrobacterium tumefaciens. *Plant Molecular Biology* 8(4), pp. 291–298. doi: 10.1007/BF00021308.

Shen, Q., Yan, T., Fu, X. and Tang, K. 2016. Transcriptional regulation of artemisinin biosynthesis in Artemisia annua L. *Science Bulletin* 61(1), pp. 18–25. doi: 10.1007/s11434-015-0983-9.

Shiboleth, Y. and Tzfira, T. 2012. *Agrobacterium*-mediated plant genetic transformation. In: Altman, A. and Hasegawa, P. M. eds *Plant Biotechnology and Agriculture*. San Diego: Academic Press, pp. 99–116. Available at: https://www.sciencedirect.com/science/article/pii/B9780123814661000079 [Accessed: 30 June 2025].

Shou, C., Zheng, Y.-C., Zhan, J.-R., Li, C.-X. and Xu, J.-H. 2022. Removing the Obstacle to (−)-Menthol Biosynthesis by Building a Microbial Cell Factory of (+)-cis-Isopulegone from (−)-Limonene. *ChemSusChem* 15(9), p. e202101741. doi: 10.1002/cssc.202101741.

Singh, G. 2007. *Chemistry of Terpenoids and Carotenoids*. Discovery Publishing House.

Singh, S., Chhatwal, H. and Pandey, A. 2024. Deciphering the Complexity of Terpenoid Biosynthesis and Its Multi-level Regulatory Mechanism in Plants. *Journal of Plant Growth Regulation* 43(10), pp. 3320–3336. doi: 10.1007/s00344-024-11347-2.

Sirirungruang, S., Markel, K. and Shih, P.M. 2022. Plant-based engineering for production of high-valued natural products. *Natural Product Reports* 39(7), pp. 1492–1509. doi: 10.1039/D2NP00017B.

Skirycz, A., Jozefczuk, S., Stobiecki, M., Muth, D., Zanor, M.I., Witt, I. and Mueller-Roeber, B. 2007. Transcription factor AtDOF4;2 affects phenylpropanoid metabolism in Arabidopsis thaliana. *New Phytologist* 175(3), pp. 425–438. doi: 10.1111/j.1469-8137.2007.02129.x.

Skoog, F. and Miller, C.O. 1957. Chemical regulation of growth and organ formation in plant tissues cultured in vitro. *Symposia of the Society for Experimental Biology* 11, pp. 118–130.

Sleno, L., Staack, R.F., Varesio, E. and Hopfgartner, G. 2007. Investigating the in vitro metabolism of fipexide: characterization of reactive metabolites using liquid chromatography/mass spectrometry. *Rapid communications in mass spectrometry: RCM* 21(14), pp. 2301–2311. doi: 10.1002/rcm.3092.

Smith, S.M. 2014. Q&A: What are strigolactones and why are they important to plants and soil microbes? *BMC Biology* 12(1), p. 19. doi: 10.1186/1741-7007-12-19.

Soltanbeigi, A., Özgüven, M. and Hassanpouraghdam, M.B. 2021. Planting-date and cutting-time affect the growth and essential oil composition of *Mentha* × *piperita* and *Mentha arvensis*. *Industrial Crops and Products* 170, p. 113790. doi: 10.1016/j.indcrop.2021.113790.

Song, G., Walworth, A. and Hancock, J.F. 2012. Factors influencing Agrobacterium-mediated transformation of switchgrass cultivars. *Plant Cell, Tissue and Organ Culture (PCTOC)* 108(3), pp. 445–453. doi: 10.1007/s11240-011-0056-y.

Song, Z. et al. 2013. Screening Chinese soybean genotypes for Agrobacterium-mediated genetic transformation suitability. *Journal of Zhejiang University. Science. B* 14(4), pp. 289–298. doi: 10.1631/jzus.B1200278.

Stachel, S.E., Messens, E., Van Montagu, M. and Zambryski, P. 1985. Identification of the signal molecules produced by wounded plant cells that activate T-DNA transfer in Agrobacterium tumefaciens. *Nature* 318(6047), pp. 624–629. doi: 10.1038/318624a0.

Stephenson, M., Reed, J., Patron, N.J., Lomonossoff, G.P. and Osbourn, A. 2020. Engineering Tobacco for Plant Natural Product Production. In: Hung-Wen, B. and Begley, T. P. eds *Comprehensive Natural Products III*. Elsevier, pp. 244–262. doi: 10.1016/B978-0-12-409547-2.14724-9.

Stephenson, M.J., Reed, J., Brouwer, B. and Osbourn, A. 2018. Transient Expression in Nicotiana Benthamiana Leaves for Triterpene Production at a Preparative Scale. *Journal of Visualized Experiments : JoVE* (138), p. 58169. doi: 10.3791/58169.

Stra, A., Almarwaey, L.O., Alagoz, Y., Moreno, J.C. and Al-Babili, S. 2023. Carotenoid metabolism: New insights and synthetic approaches. *Frontiers in Plant Science* 13. Available at: https://www.frontiersin.org/journals/plant-science/articles/10.3389/fpls.2022.1072061/full [Accessed: 28 September 2025].

Su, W., Xu, M., Radani, Y. and Yang, L. 2023. Technological Development and Application of Plant Genetic Transformation. *International Journal of Molecular Sciences* 24(13), p. 10646. doi: 10.3390/ijms241310646.

Sutradhar, M. and Mandal, N. 2023. Reasons and riddance of Agrobacterium tumefaciens overgrowth in plant transformation. *Transgenic Research* 32(1), pp. 33–52. doi: 10.1007/s11248-023-00338-w.

Sweetlove, L.J., Ratcliffe, R.G. and Fernie, A.R. 2025. Non-canonical plant metabolism. *Nature Plants* 11(4), pp. 696–708. doi: 10.1038/s41477-025-01965-3.

Tabara, M., Matsumoto, A., Kibayashi, Y., Takeda, A. and Motomura, K. 2024. Straightforward and affordable agroinfiltration with RUBY accelerates RNA silencing research. *Plant Molecular Biology* 114(3), p. 61. doi: 10.1007/s11103-024-01463-8.

Talalay, P. and Benson, A.M. 1972. 18 Δ5-3-Ketosteroid Isomerase. In: Boyer, P. D. ed. *The Enzymes*. Academic Press, pp. 591–618. Available at:

https://www.sciencedirect.com/science/article/pii/S1874604708600530 [Accessed: 21 July 2025].

Talbot, S.C., Pandelova, I., Lange, B.M. and Vining, K.J. 2024. A first look at the genome structure of hexaploid “Mitcham” peppermint (Mentha × piperita L.). *G3 Genes|Genomes|Genetics* 14(12), p. jkae195. doi: 10.1093/g3journal/jkae195.

Tanahara, Y., Yamanaka, K., Kawai, K., Ando, Y. and Nakatsuka, T. 2022. Establishment of an efficient transformation method of garden stock (Matthiola incana) using a callus formation chemical inducer. *Plant Biotechnology* 39(3), pp. 273–280. doi: 10.5511/plantbiotechnology.22.0602a.

Tang, W., Harris, L.C., Outhavong, V. and Newton, R.J. 2004. Antioxidants enhance in vitro plant regeneration by inhibiting the accumulation of peroxidase in Virginia pine (Pinus virginiana Mill.). *Plant Cell Reports* 22(12), pp. 871–877. doi: 10.1007/s00299-004-0781-3.

Telci, İ. et al. 2011. The effect of ecological conditions on yield and quality traits of selected peppermint (*Mentha piperita* L.) clones. *Industrial Crops and Products* 34(1), pp. 1193–1197. doi: 10.1016/j.indcrop.2011.04.010.

Teoh, E.S. 2015. Secondary Metabolites of Plants. *Medicinal Orchids of Asia*, pp. 59–73. doi: 10.1007/978-3-319-24274-3_5.

Tholl, D., Boland, W., Hansel, A., Loreto, F., Röse, U.S.R. and Schnitzler, J.-P. 2006. Practical approaches to plant volatile analysis. *The Plant Journal* 45(4), pp. 540–560. doi: 10.1111/j.1365-313X.2005.02612.x.

Tholl, D., Kish, C.M., Orlova, I., Sherman, D., Gershenzon, J., Pichersky, E. and Dudareva, N. 2004. Formation of Monoterpenes in Antirrhinum majus and Clarkia breweri Flowers Involves Heterodimeric Geranyl Diphosphate Synthases. *The Plant Cell* 16(4), pp. 977–992. doi: 10.1105/tpc.020156.

Thul, S.T. and Kukreja, A.K. 2010. An Efficient Protocol for High-frequency Direct Multiple Shoot Regeneration from Internodes of Peppermint (Mentha x piperita). *Natural Product Communications* 5(12), p. 1934578X1000501223. doi: 10.1177/1934578X1000501223.

Tissier, A. 2012. Trichome Specific Expression: Promoters and Their Applications. In: Ozden ifti, Y. ed. *Transgenic Plants - Advances and Limitations*. InTech. Available at: http://www.intechopen.com/books/transgenic-plants-advances-and-limitations/trichome-specific-expression-promoters-and-their-applications [Accessed: 18 October 2021].

Todd, W.A., Green Jr., R.J. and Horner, C.E. 1977. Registration of Murray Mitcham Peppermint (Reg. No. 2). *Crop Science* 17(1), p. cropsci1977.0011183X001700010054x. doi: 10.2135/cropsci1977.0011183X001700010054x.

Tremblay, R., Wang, D., Jevnikar, A.M. and Ma, S. 2010. Tobacco, a highly efficient green bioreactor for production of therapeutic proteins. *Biotechnology Advances* 28(2), pp. 214–221. doi: 10.1016/j.biotechadv.2009.11.008.

Tucker, A.O. 2012. Genetics and Breeding of the Genus Mentha: a Model for Other Polyploid Species with Secondary Constituents. Available at: http://scholarworks.umass.edu/jmap/vol1/iss1/7/ [Accessed: 18 October 2021].

Tucker, A.O., Harley, R.M. and Fairbrothers, D.E. 1980. The Linnaean Types of Mentha (lamiaceae). *TAXON* 29(2–3), pp. 233–255. doi: 10.2307/1220285.

Tucker, A.O. and Naczi, R.F.C. 2006. Mentha: An overview of its classification and relationships. In: *Mint: The Genus Mentha*. pp. 1–39.

Turner, G., Gershenzon, J., Nielson, E.E., Froehlich, J.E. and Croteau, R. 1999. Limonene Synthase, the Enzyme Responsible for Monoterpene Biosynthesis in Peppermint, Is Localized to Leucoplasts of Oil Gland Secretory Cells1. *Plant Physiology* 120(3), pp. 879–886. doi: 10.1104/pp.120.3.879.

Turner, G.W. and Croteau, R. 2004. Organization of Monoterpene Biosynthesis in Mentha. Immunocytochemical Localizations of Geranyl Diphosphate Synthase, Limonene-6-Hydroxylase, Isopiperitenol Dehydrogenase, and Pulegone Reductase. *Plant Physiology* 136(4), pp. 4215–4227. doi: 10.1104/pp.104.050229.

Turner, G.W., Gershenzon, J. and Croteau, R.B. 2000a. Development of Peltate Glandular Trichomes of Peppermint. *Plant Physiology* 124(2), pp. 665–680. doi: 10.1104/pp.124.2.665.

Turner, G.W., Gershenzon, J. and Croteau, R.B. 2000b. Distribution of Peltate Glandular Trichomes on Developing Leaves of Peppermint. *Plant Physiology* 124(2), pp. 655–664. doi: 10.1104/pp.124.2.655.

Upton, R.N., Correr, F.H., Lile, J., Reynolds, G.L., Falaschi, K., Cook, J.P. and Lachowiec, J. 2023. Design, execution, and interpretation of plant RNA-seq analyses. *Frontiers in Plant Science* 14. Available at: https://www.frontiersin.org/journals/plant-science/articles/10.3389/fpls.2023.1135455/full [Accessed: 13 September 2025].

Vaidya, B.N., Asanakunov, B., Shahin, L., Jernigan, H.L., Joshee, N. and Dhekney, S.A. 2019. Improving micropropagation of Mentha × piperita L. using a liquid culture system. *In Vitro Cellular & Developmental Biology - Plant* 55(1), pp. 71–80. doi: 10.1007/s11627-018-09952-4.

Van Schie, C.C.N., Ament, K., Schmidt, A., Lange, T., Haring, M.A. and Schuurink, R.C. 2007. Geranyl diphosphate synthase is required for biosynthesis of gibberellins: Gibberellin precursor biosynthesis. *The Plant Journal* 52(4), pp. 752–762. doi: 10.1111/j.1365-313X.2007.03273.x.

Vining, K.J. et al. 2017. Draft Genome Sequence of Mentha longifolia and Development of Resources for Mint Cultivar Improvement. *Molecular Plant* 10(2), pp. 323–339. doi: 10.1016/j.molp.2016.10.018.

Vining, K.J. et al. 2022. Chromosome-level genome assembly of Mentha longifolia L. reveals gene organization underlying disease resistance and essential oil traits. *G3 Genes|Genomes|Genetics* 12(8), p. jkac112. doi: 10.1093/g3journal/jkac112.

Vining, K.J., Hummer, K.E., Bassil, N.V., Lange, B.M., Khoury, C.K. and Carver, D. 2020. Crop Wild Relatives as Germplasm Resource for Cultivar Improvement in Mint (Mentha L.). *Frontiers in Plant Science* 11, p. 1217. doi: 10.3389/fpls.2020.01217.

Visentin, I. et al. 2024. Strigolactones promote flowering by inducing the miR319-LA-SFT module in tomato. *Proceedings of the National Academy of Sciences* 121(19), p. e2316371121. doi: 10.1073/pnas.2316371121.

Voinnet, O., Rivas, S., Mestre, P. and Baulcombe, D. 2003. An enhanced transient expression system in plants based on suppression of gene silencing by the p19

protein of tomato bushy stunt virus. *The Plant Journal: For Cell and Molecular Biology* 33(5), pp. 949–956. doi: 10.1046/j.1365-313x.2003.01676.x.

Voirin, B., Brun, N. and Bayet, C. 1990. Effects of daylength on the monoterpene composition of leaves of *Mentha x piperita*. *Phytochemistry* 29(3), pp. 749–755. doi: 10.1016/0031-9422(90)80012-6.

Voshall, A. and Moriyama, E.N. 2020. Next-generation transcriptome assembly and analysis: Impact of ploidy. *Methods* 176, pp. 14–24. doi: 10.1016/j.ymeth.2019.06.001.

Wang, B. et al. 2016a. Transient production of artemisinin in Nicotiana benthamiana is boosted by a specific lipid transfer protein from A. annua. *Metabolic Engineering* 38, pp. 159–169. doi: 10.1016/j.ymben.2016.07.004.

Wang, C., Liwei, M., Park, J.-B., Jeong, S.-H., Wei, G., Wang, Y. and Kim, S.-W. 2018. Microbial Platform for Terpenoid Production: Escherichia coli and Yeast. *Frontiers in Microbiology* 9. Available at: https://www.frontiersin.org/journals/microbiology/articles/10.3389/fmicb.2018.02460/full [Accessed: 11 September 2025].

Wang, G. and Dixon, R.A. 2009. Heterodimeric geranyl(geranyl)diphosphate synthase from hop (Humulus lupulus) and the evolution of monoterpene biosynthesis. *Proceedings of the National Academy of Sciences of the United States of America* 106(24), pp. 9914–9919. doi: 10.1073/pnas.0904069106.

Wang, Q. et al. 2016b. Metabolic engineering of terpene biosynthesis in plants using a trichome-specific transcription factor *MsYABBY5* from spearmint (*Mentha spicata*). *Plant Biotechnology Journal* 14(7), pp. 1619–1632. doi: 10.1111/pbi.12525.

Wang, X., Chen, X., Cheng, Q., Zhu, K., Yang, X. and Cheng, Z. 2019. *Agrobacterium*–mediated Transformation of *Kalanchoe laxiflora*. *Horticultural Plant Journal* 5(5), pp. 221–228. doi: 10.1016/j.hpj.2019.07.001.

Wang, X., Gao, Z., Wang, Y., Bressan, R.A., Weller, S.C. and Li, X. 2009. Highly efficient in vitro adventitious shoot regeneration of peppermint (Mentha x piperita L.) using internodal explants. *In Vitro Cellular & Developmental Biology - Plant* 45(4), pp. 435–440. doi: 10.1007/s11627-008-9170-x.

Weber, E., Engler, C., Gruetzner, R., Werner, S. and Marillonnet, S. 2011. A Modular Cloning System for Standardized Assembly of Multigene Constructs. Peccoud, J. ed. *PLoS ONE* 6(2), p. e16765. doi: 10.1371/journal.pone.0016765.

Webster, B., Bruce, T., Dufour, S., Birkemeyer, C., Birkett, M., Hardie, J. and Pickett, J. 2008. Identification of Volatile Compounds Used in Host Location by the Black Bean Aphid, Aphis fabae. *Journal of Chemical Ecology* 34(9), pp. 1153–1161. doi: 10.1007/s10886-008-9510-7.

Werker, E., Ravid, U. and Putievsky, E. 1985. STRUCTURE OF GLANDULAR HAIRS AND IDENTIFICATION OF THE MAIN COMPONENTS OF THEIR SECRETED MATERIAL IN SOME SPECIES OF THE LABIATAE. Available at: https://brill.com/view/journals/ijps/34/1/article-p31_5.xml [Accessed: 3 September 2025].

Wiebke, B., Ferreira, F., Pasquali, G., Bodanese-Zanettini, M.H. and Droste, A. 2006. Influence of antibiotics on embryogenic tissue and Agrobacterium tumefaciens suppression in soybean genetic transformation. *Bragantia* 65, pp. 543–551. doi: https://doi.org/10.1590/S0006-87052006000400002.

Williams, A.G., Thomas, S., Wyman, S.K. and Holloway, A.K. 2014. RNA-seq Data: Challenges in and Recommendations for Experimental Design and Analysis. *Current protocols in human genetics / editorial board, Jonathan L. Haines ... [et al.]* 83, p. 11.13.1-11.13.20. doi: 10.1002/0471142905.hg1113s83.

Williams, D.C., McGarvey, D.J., Katahira, E.J. and Croteau, R. 1998. Truncation of limonene synthase preprotein provides a fully active ‘pseudomature’ form of this monoterpene cyclase and reveals the function of the amino-terminal arginine pair. *Biochemistry* 37(35), pp. 12213–12220. doi: 10.1021/bi980854k.

Wise, M.L. and Croteau, R. 1999. Monoterpene Biosynthesis. In: Barton, S. D., Nakanishi, K., and Meth-Cohn, O. eds *Comprehensive Natural Products Chemistry*. Oxford: Pergamon, pp. 97–153. Available at: https://www.sciencedirect.com/science/article/pii/B9780080912837000382 [Accessed: 3 September 2025].

Wong, Y.F., Yan, D., Shellie, R.A., Sciarrone, D. and Marriott, P.J. 2019. Rapid Plant Volatiles Screening Using Headspace SPME and Person-Portable Gas

Chromatography–Mass Spectrometry. *Chromatographia* 82(1), pp. 297–305. doi: 10.1007/s10337-018-3605-2.

Wood, D.W. et al. 2001. The genome of the natural genetic engineer Agrobacterium tumefaciens C58. *Science* 294(5550), pp. 2317–2323. doi: 10.1126/science.1066804.

Woodhouse, M.R., Cheng, F., Pires, J.C., Lisch, D., Freeling, M. and Wang, X. 2014. Origin, inheritance, and gene regulatory consequences of genome dominance in polyploids. *Proceedings of the National Academy of Sciences of the United States of America* 111(14), pp. 5283–5288. doi: 10.1073/pnas.1402475111.

Woodward, A.W. and Bartel, B. 2018. Biology in Bloom: A Primer on the Arabidopsis thaliana Model System. *Genetics* 208(4), pp. 1337–1349. doi: 10.1534/genetics.118.300755.

Wu, H. et al. 2024. Somatic embryogenesis from mature sorghum seeds: An underutilized genome editing recipient system. *Heliyon* 10(1), p. e23638. doi: 10.1016/j.heliyon.2023.e23638.

Wydro, M., Kozubek, E. and Lehmann, P. 2006. Optimization of transient Agrobacterium-mediated gene expression system in leaves of Nicotiana benthamiana. *Acta Biochimica Polonica* 53(2), pp. 289–298.

Xu, H., Li, W., Schilmiller, A.L., van Eekelen, H., de Vos, R.C.H., Jongsma, M.A. and Pichersky, E. 2019a. Pyrethric acid of natural pyrethrin insecticide: complete pathway elucidation and reconstitution in Nicotiana benthamiana. *New Phytologist* 223(2), pp. 751–765. doi: 10.1111/nph.15821.

Xu, Y., Zhu, C., Xu, C., Sun, J., Grierson, D., Zhang, B. and Chen, K. 2019b. Integration of Metabolite Profiling and Transcriptome Analysis Reveals Genes Related to Volatile Terpenoid Metabolism in Finger Citron (C. medica var. sarcodactylis). *Molecules* 24(14), p. 2564. doi: 10.3390/molecules24142564.

Yamamoto, T. et al. 2018. Improvement of the transient expression system for production of recombinant proteins in plants. *Scientific Reports* 8(1), p. 4755. doi: 10.1038/s41598-018-23024-y.

Yang, H. et al. 2024a. A haplotype-resolved gap-free genome assembly provides novel insight into monoterpenoid diversification in Mentha suaveolens ‘Variegata’. *Horticulture Research* 11(3), p. uhae022. doi: 10.1093/hr/uhae022.

Yang, H., Liu, S., Chen, S., Lu, P., Huang, J., Sun, L. and Liu, H. 2024b. Novel 4-chlorophenoxyacetate dioxygenase-mediated phenoxyalkanoic acid herbicides initial catabolism in *Cupriavidus* sp. DL-D2. *Journal of Hazardous Materials* 478, p. 135427. doi: 10.1016/j.jhazmat.2024.135427.

Yang, S. et al. 2019a. An efficient Agrobacterium-mediated soybean transformation method using green fluorescent protein as a selectable marker. *Plant Signaling & Behavior* 14(7), p. 1612682. doi: 10.1080/15592324.2019.1612682.

Yang, W., Zhang, D., Cai, X., Xia, L., Luo, Y., Cheng, X. and An, S. 2019b. Significant alterations in soil fungal communities along a chronosequence of *Spartina alterniflora* invasion in a Chinese Yellow Sea coastal wetland. *Science of The Total Environment* 693, p. 133548. doi: 10.1016/j.scitotenv.2019.07.354.

Yang, X., Yu, X., Zhou, Z., Ma, W.-J. and Tang, G. 2016. A high-efficiency Agrobacterium tumefaciens mediated transformation system using cotyledonary node as explants in soybean (Glycine max L.). *Acta Physiologiae Plantarum* 38(3), p. 60. doi: 10.1007/s11738-016-2081-2.

Yao, X. et al. 2022. Engineering the expression of plant secondary metabolites-genistein and scutellarin through an efficient transient production platform in Nicotiana benthamiana L. *Frontiers in Plant Science* 13. Available at: https://www.frontiersin.org/articles/10.3389/fpls.2022.994792 [Accessed: 11 August 2023].

Yasmeen, E., Wang, J., Riaz, M., Zhang, L. and Zuo, K. 2023. Designing artificial synthetic promoters for accurate, smart, and versatile gene expression in plants. *Plant Communications* 4(4), p. 100558. doi: 10.1016/j.xplc.2023.100558.

Yin, J., Wong, W., Jang, I. and Chua, N. 2017. Co-expression of peppermint geranyl diphosphate synthase small subunit enhances monoterpene production in transgenic tobacco plants. *New Phytologist* 213(3), pp. 1133–1144. doi: 10.1111/nph.14280.

Yong, J.W.H., Ge, L., Ng, Y.F. and Tan, S.N. 2009. The Chemical Composition and Biological Properties of Coconut (Cocos nucifera L.) Water. *Molecules* 14(12), pp. 5144–5164. doi: 10.3390/molecules14125144.

Yu, G., Wang, J., Miao, L., Xi, M., Wang, Q. and Wang, K. 2019. Optimization of Mature Embryo-Based Tissue Culture and Agrobacterium-Mediated Transformation in Model Grass Brachypodium distachyon. *International Journal of Molecular Sciences* 20(21), p. 5448. doi: 10.3390/ijms20215448.

Yu, X. et al. 2021. Transcriptome Analysis of Light-Regulated Monoterpenes Biosynthesis in Leaves of Mentha canadensis L. *Plants* 10(5), p. 930. doi: 10.3390/plants10050930.

Yu, X. et al. 2022. A stable method for Agrobacterium-mediated transformation of Mentha piperita and Mentha canadensis using internodal explants. *In Vitro Cellular & Developmental Biology - Plant*. Available at: https://doi.org/10.1007/s11627-022-10294-5 [Accessed: 12 October 2022].

Yu, X. et al. 2024. Transcriptional regulation and functional validation analysis of the *McbZIP1 in Mentha canadensis* L. *Plant Science* 348, p. 112212. doi: 10.1016/j.plantsci.2024.112212.

Yu, Z.-X., Li, J.-X., Yang, C.-Q., Hu, W.-L., Wang, L.-J. and Chen, X.-Y. 2012. The jasmonate-responsive AP2/ERF transcription factors AaERF1 and AaERF2 positively regulate artemisinin biosynthesis in Artemisia annua L. *Molecular Plant* 5(2), pp. 353–365. doi: 10.1093/mp/ssr087.

Zambre, M. et al. 2003. Light strongly promotes gene transfer from Agrobacterium tumefaciens to plant cells. *Planta* 216(4), pp. 580–586. doi: 10.1007/s00425-002-0914-2.

Zhang, H. et al. 2020. Carotenoid metabolite and transcriptome dynamics underlying flower color in marigold (Tagetes erecta L.). *Scientific Reports* 10, p. 16835. doi: 10.1038/s41598-020-73859-7.

Zhang, R., Zhang, C., Yu, C., Dong, J. and Hu, J. 2022. Integration of multi-omics technologies for crop improvement: Status and prospects. *Frontiers in Bioinformatics* 2, p. 1027457. doi: 10.3389/fbinf.2022.1027457.

Zhang, Z. et al. 2023a. Transcription factors TgbHLH95 and TgbZIP44 cotarget terpene biosynthesis gene TgGPPS in Torreya grandis nuts. *Plant Physiology* 193(2), pp. 1161–1176. doi: 10.1093/plphys/kiad385.

Zhang, Z. et al. 2023b. Transcription factors TgbHLH95 and TgbZIP44 cotarget terpene biosynthesis gene TgGPPS in Torreya grandis nuts. *Plant Physiology* 193(2), pp. 1161–1176. doi: 10.1093/plphys/kiad385.

Zhao, H. et al. 2022. *Peppermint* essential oil: its phytochemistry, biological activity, pharmacological effect and application. *Biomedicine & Pharmacotherapy* 154, p. 113559. doi: 10.1016/j.biopha.2022.113559.

Zhao, L., Chang, W., Xiao, Y., Liu, H. and Liu, P. 2013. Methylerythritol Phosphate Pathway of Isoprenoid Biosynthesis. *Annual review of biochemistry* 82, pp. 497–530. doi: 10.1146/annurev-biochem-052010-100934.

Zhao, W., Li, S., Lan, B., Gai, Y., Du, F.K. and Yin, K. 2025. Fipexide Rapidly Induces Callus Formation in Medicago sativa by Regulating Small Auxin Upregulated RNA (SAUR) Family Genes. *Crops* 5(3), p. 28. doi: 10.3390/crops5030028.

Zhao, Y., Wang, M., Chen, Y., Gao, M., Wu, L. and Wang, Y. 2023. *LcERF134* increases the production of monoterpenes by activating the terpene biosynthesis pathway in *Litsea cubeba*. *International Journal of Biological Macromolecules* 232, p. 123378. doi: 10.1016/j.ijbiomac.2023.123378.

Zheng, K. et al. 2024. The proteome of Nicotiana benthamiana is shaped by extensive protein processing. *The New Phytologist* 243(3), pp. 1034–1049. doi: 10.1111/nph.19891.

Zheng, M.Y. and Konzak, C.F. 1999. Effect of 2,4-dichlorophenoxyacetic acid on callus induction and plant regeneration in anther culture of wheat (Triticum aestivum L.). *Plant Cell Reports* 19(1), pp. 69–73. doi: 10.1007/s002990050712.

Zhu, Q., Wang, B., Tan, J., Liu, T., Li, L. and Liu, Y.-G. 2019. Plant Synthetic Metabolic Engineering for Enhancing Crop Nutritional Quality. *Plant Communications* 1(1), p. 100017. doi: 10.1016/j.xplc.2019.100017.

Zhu, X., Liu, X., Liu, T., Wang, Y., Ahmed, N., Li, Z. and Jiang, H. 2021. Synthetic biology of plant natural products: From pathway elucidation to engineered

biosynthesis in plant cells. *Plant Communications* 2(5), p. 100229. doi: 10.1016/j.xplc.2021.100229.

Zielińska-Błajet, M. and Feder-Kubis, J. 2020. Monoterpenes and Their Derivatives—Recent Development in Biological and Medical Applications. *International Journal of Molecular Sciences* 21(19), p. 7078. doi: 10.3390/ijms21197078.

Zlobin, N.E., Lebedeva, M.V. and Taranov, V.V. 2020. CRISPR/Cas9 genome editing through in planta transformation. *Critical Reviews in Biotechnology* 40(2), pp. 153–168. doi: 10.1080/07388551.2019.1709795.

Appendix

Appendix Table 1. List of concentrations in both µM and µg/mL for *Mentha* tissue cultures. Conversions are performed by the formula C = M * MW * 10^{-3}, where C is concentration in µg/mL, M is molarity in µM, and MW is molecular weight in g/mol.

Plant Growth Regulator	Molecular Weight (g/mol)	Concentration in µM	Concentration in ug/mL
1-Naphthaleneacetic acid (NAA)	186.2066	0.5	0.0931
Thidiazuron (TDZ)	220.251	4.5	0.9911
		9	1.9823
		13.62	2.9998
6-Benzylaminopurine (BAP)	225.2492	13.32	3.0003
		17.76	4.0004
		22.2	5.0005
Kinetin (KIN)	215.21	4.65	1.0007
		9.3	2.0015
		13.95	3.0022
2,4-Dichlorophenoxyacetic acid (2,4-D)	221.038	2.6	0.4995
		4.52	0.9991
		9.05	2.0004
Fipexide (FPX)	388.85	10	3.8885
		20	7.777
		50	19.4425

Appendix Table 2. List of primers used in this study.

Primer	Purpose	Sequence (5'-3')	Expected Product Size (bp)
E3	*MpGPPS.SSU* RT-PCR partial sequence	GCCGTTCTTCTTCCGCGC	443
I4		TGACCCGGCCAGCAACTCAAAC	

Appendix

MxP GPPS.SSU F	*MpGPPS.SSU* RT-PCR full length	ATGGCCATTAATCTCTCCCATATCAACTCC	942
MxP GPPS.SSU R		CTAAGCCGCGTAAAGGCTCGG	
C3	pL1MpGPPS.SSU *A. tumefaciens* PCR	CTGGTGGCAGGATATATTGTGGTG	2357
C4		GAACCCTGTGGTTGGCATGCACATAC	
I18	*PaLimS* RT-PCR partial sequence	CTTGCATTGCGACTGACCCCAA	336
I19		AACCACTGGCGATCCACTTTGC	
PaLimS F	*PaLimS* RT-PCR full length	ATGTCTCCTGTTTCTGTCATACCGTTGG	1905
PaLimS R		TTACAAAGGCACAGGTTCAAGGACCATTC	
C3	pL1PaLimS *A.tumefaciens* PCR	CTGGTGGCAGGATATATTGTGGTG	2828
C4		GAACCCTGTGGTTGGCATGCACATAC	
MxP L3H F	*MpL3H* RT-PCR full length	ATGGAGCTCCTCCAGCTTTGGTC	1497
MxP L3H R		TCATGATGAAGGATCGTAGGGTGTGG	
C3	pL1MpL3H PM2 *A.tumefaciens* PCR	CTGGTGGCAGGATATATTGTGGTG	2456
C4		GAACCCTGTGGTTGGCATGCACATAC	
MxP IPDH F	*MpIPDH* RT-PCR full length	ATGGCAAGCGTGAAGAAGCTCG	798
MxP IPDH R		TCACTTGGCCACGGCCAC	
C3	pL1MpIPDH *A. tumefaciens* PCR	CTGGTGGCAGGATATATTGTGGTG	1733
C4		GAACCCTGTGGTTGGCATGCACATAC	
MxP IPR F	*MpIPR* RT-PCR full length	ATGGCAGAAGTACAGAGGTATGCATTGG	945
MxP IPR R		TTAATAGAGAGCCAAAGCTTTGTCTCGAGG	
C3	pL1MpIPR *A. tumefaciens* PCR	CTGGTGGCAGGATATATTGTGGTG	2379
C4		GAACCCTGTGGTTGGCATGCACATAC	
PpKSI F	*PpKSI* RT-PCR full length	ATGAATCTCCCTACCGCCCAGGA	396
PpKSI R		CTATTGTGGTTCTCTTACGCTTAGGTTTACTTC	

C3	pL1PpKSI *A. tumefaciens* PCR	CTGGTGGCAGGATATATTGTGGTG	1811
C4		GAACCCTGTGGTTGGCATGCACATAC	
MxP PGR F	*MpPGR* RT-PCR full length	ATGGTGATGAACAAGCAAATTGTACTCAACAAC	1029
MxP PGR R		TTACTCGCGAGAAACGGCAACAAC	
C3	pL1MpPGR *A. tumefaciens* PCR	CTGGTGGCAGGATATATTGTGGTG	1988
C4		GAACCCTGTGGTTGGCATGCACATAC	
MxP MMR F	*MpMMR* RT-PCR full length	ATGGCAGATACGTTTACCCAAAGGTATGC	936
MxP MMR R		TTAGTACAAGGACAAGGCTTCCTCTCG	
C2	pL1MpMMR *A. tumefaciens* PCR	GTCTCATGAGCGGATACATATTTGAATG	2737
C3		GAACCCTGTGGTTGGCATGCACATAC	
C3	pL1TBSVp19 *A. tumefaciens* PCR	CTGGTGGCAGGATATATTGTGGTG	1934
C4		GAACCCTGTGGTTGGCATGCACATAC	
NtCPS2_Pro_5U_F	Amplification of *NtCPS2* promoter with golden gate cloning overhangs for insertion into L0 acceptor vector pICH41295	TTGAAGACAAGGAGCTGCAAATCTCCC	1476
NtCPS2_Pro_5U_R		TTGAAGACAACATTTTTCTAATTTAATTTTTGTTTTATTCTTCCAATGAGAATTG	
NtMald1_Pro_5U_F	Amplification of *NtMadl1* promoter with golden gate cloning overhangs for insertion into L0 acceptor vector pICH41295	TTGAAGACAAGGAGAATTTTGATTACTTTAAAACTGTGGC	1995
NtMald1_Pro_5U_R		TTGAAGACAACATTTTTTTTTTTCCTCTAAAAAAACTTGGAGTG	
MpBActinF1	RT-qPCR for *MpBetaActin* (BMitcham.V1_g90804)	GAGAAGCTGGCCTACATTGC	178
MpBActinR1		CAGCAGCTTCCATTCCGATC	
MpGPPS.SSUF2	RT-qPCR for *MpGPPS.SSU* (BMitcham.V1_g162906)	GCTGAGGAATTTCGGGCTTT	154
MpGPPS.SSUR2		CATCAGCTCAGCGTTCTTCC	
MpGPPS.LSUF1	RT-qPCR for *MpGPPS.LSU* (BMitcham.V1_g208413)	GACCACCTCGAGTTCATCCA	223
MpGPPS.LSUR1		TATCCGCCACCAGATCCTTC	

MpLimSF1	RT-qPCR for *MpLimS* (BMitcham.V1_g195282)	AGAGACCGTCGACAGTTTGT	211
MpLimSR1		CTTCTTCCACACCTCCGCTA	
MpL3HPM2F2	RT-qPCR for *MpL3H* PM2 (BMitcham.V1_g117376)	AACGTTGAGGTTCCATTGGC	157
MpL3HPM2R2		AGGAAGGATCGTAGGGTGTG	
MpL3HPM17F1	RT-qPCR for *MpL3H* PM17 (BMitcham.V1_g195283)	TCGGGTTGGCAAATGTTGAG	155
MpL3HPM17R1		GGGTGTGGGAACGAGTAGAA	
MpPGRF1	RT-qPCR for *MpPGR* (BMitcham.V1_g26993)	GGCGTCCACAACTTGCTTAA	215
MpPGRR1		TGATTGCCAACGTTACGACC	
MpMMRF2	RT-qPCR for *MpMMR* (BMitcham.V1_g135464)	TGCAACAAAACAACTGGCCT	240
MpMMRR2		AGAAGAAGGATCCTGAGGGC	
NTF2Cluster3F2	RT-qPCR for NTF2 Cluster 3 XP_057769714.1 nuclear transport factor 2-like isoform X1 [Salvia miltiorrhiza] (BMitcham.V1_g143460)	GCTCCTTTCTCATCAACACGG	218
NTF2Cluster3R2		CCCCATTGAAGTTTCCACGG	
NTF2Cluster6F1	RT-qPCR for NTF2 Cluster 6 XP_057805680.1 uncharacterized protein LOC131020706 [Salvia miltiorrhiza] (BMitcham.V1_g189284)	GGTACGGATCAGAGCTCCTC	213
NTF2Cluster6R1		CGAACTCGCACTTGTCTTCA	

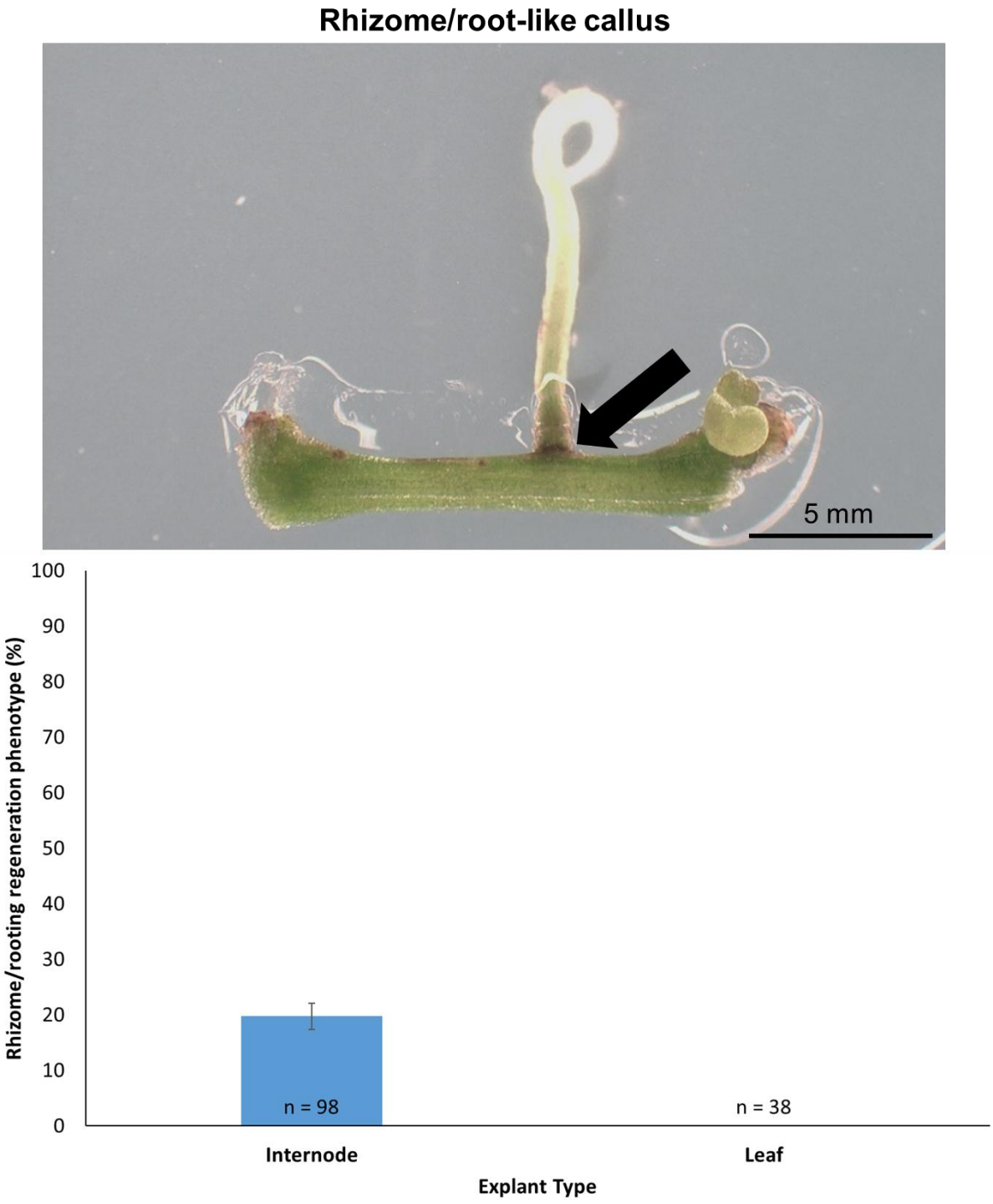

Appendix Figure 1. Rhizome/root like callus phenotype of Black Mitcham internode cultured on growth medium supplemented with 0.5 µM NAA and 4.65 µM KIN. The rhizome/root-like callus phenotype was only observed in internode explants cultured on growth medium supplemented with KIN. Red arrows highlight areas of shoot-like callus formation. Black bar is the scale at 5mm.

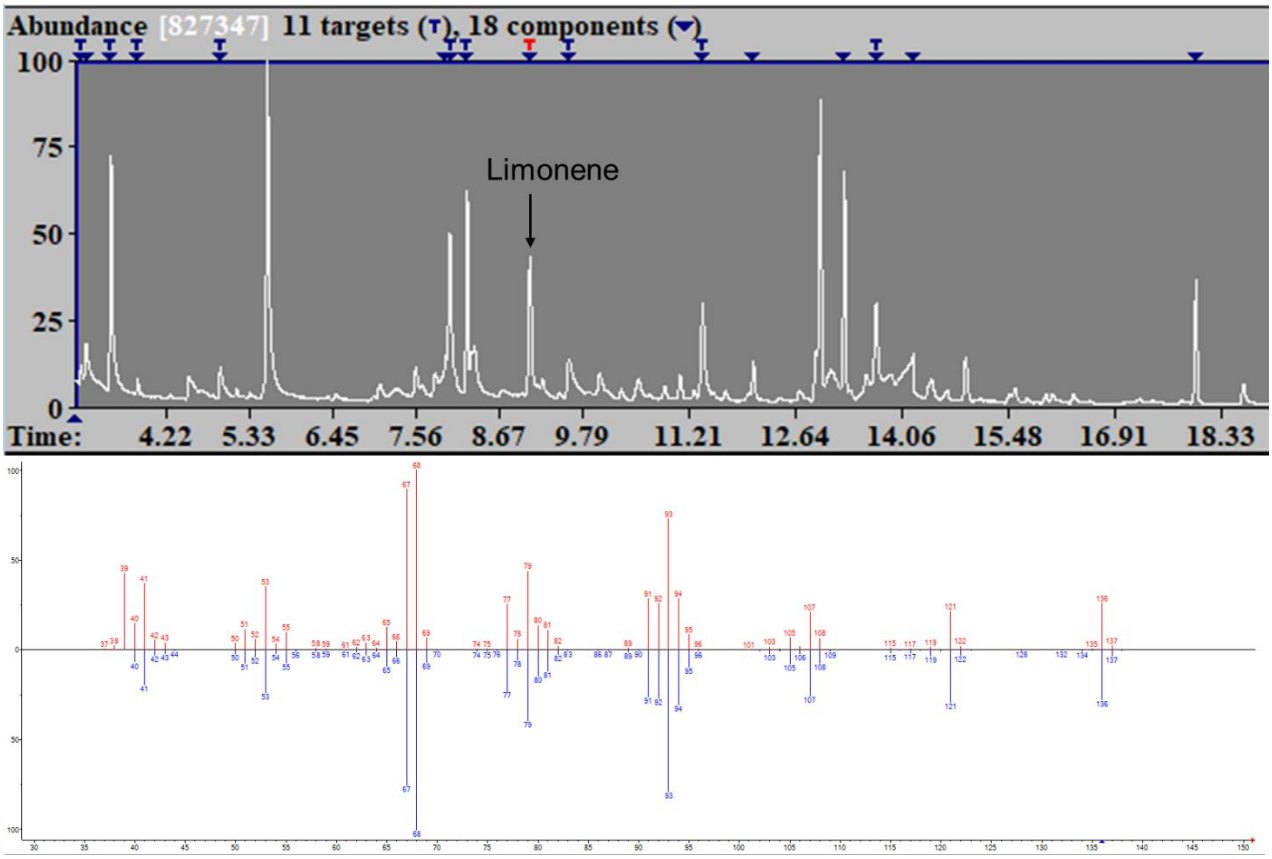

Appendix Figure 2. Chromatogram from AMDIS showing preliminary results from co-infiltration of *MpGPPS.SSU* + *PaLimS* + *p19* in *N. benthamiana* leaves. The peak corresponding to a putatively identified limonene is shown by a black arrow. A head-to-tail m/z plot of the putative limonene (red) against the NIST library limonene (blue) is shown.

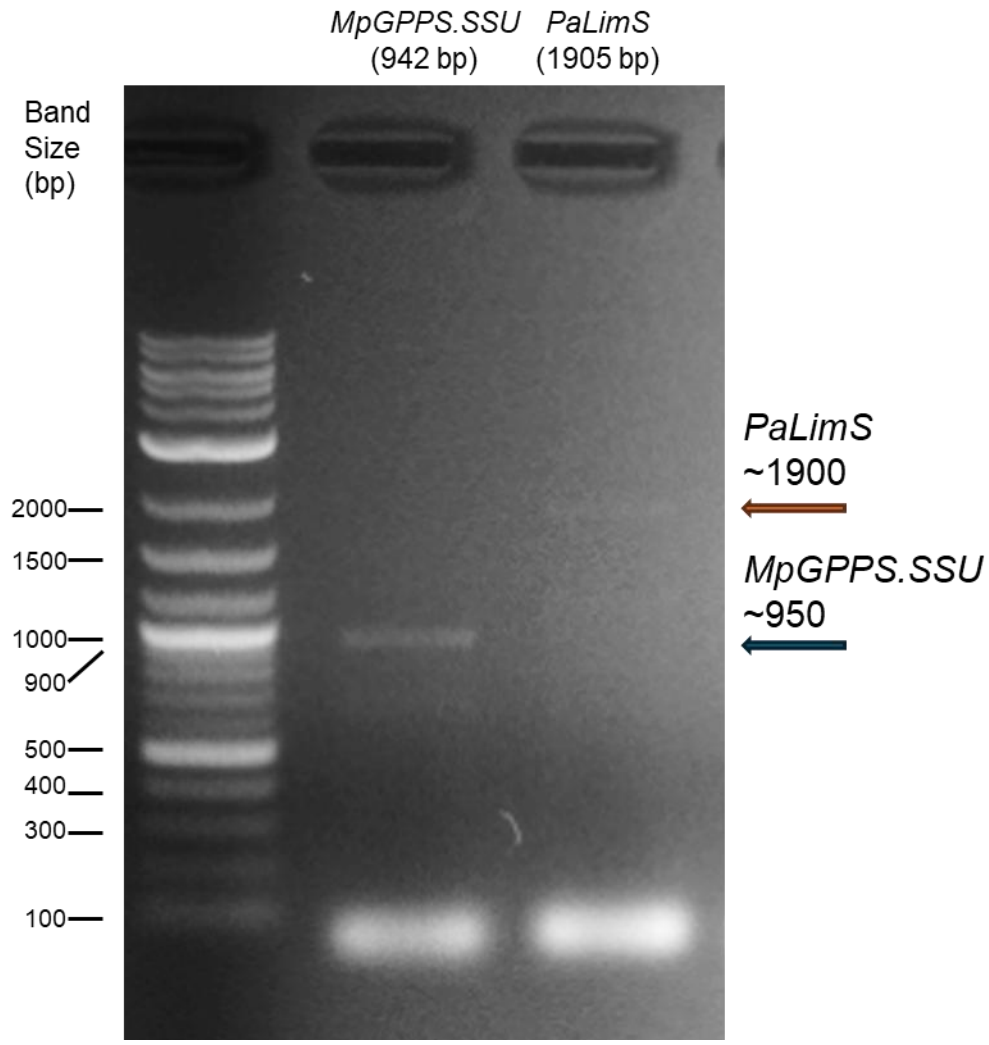

Appendix Figure 3. Image adjusted gel from Figure 4.17 to show band for *PaLimS* and *MpGPPS.SSU* clearer. Adjustment was performed in Microsoft Powerpoint (+40% brightness; +40% contrast)

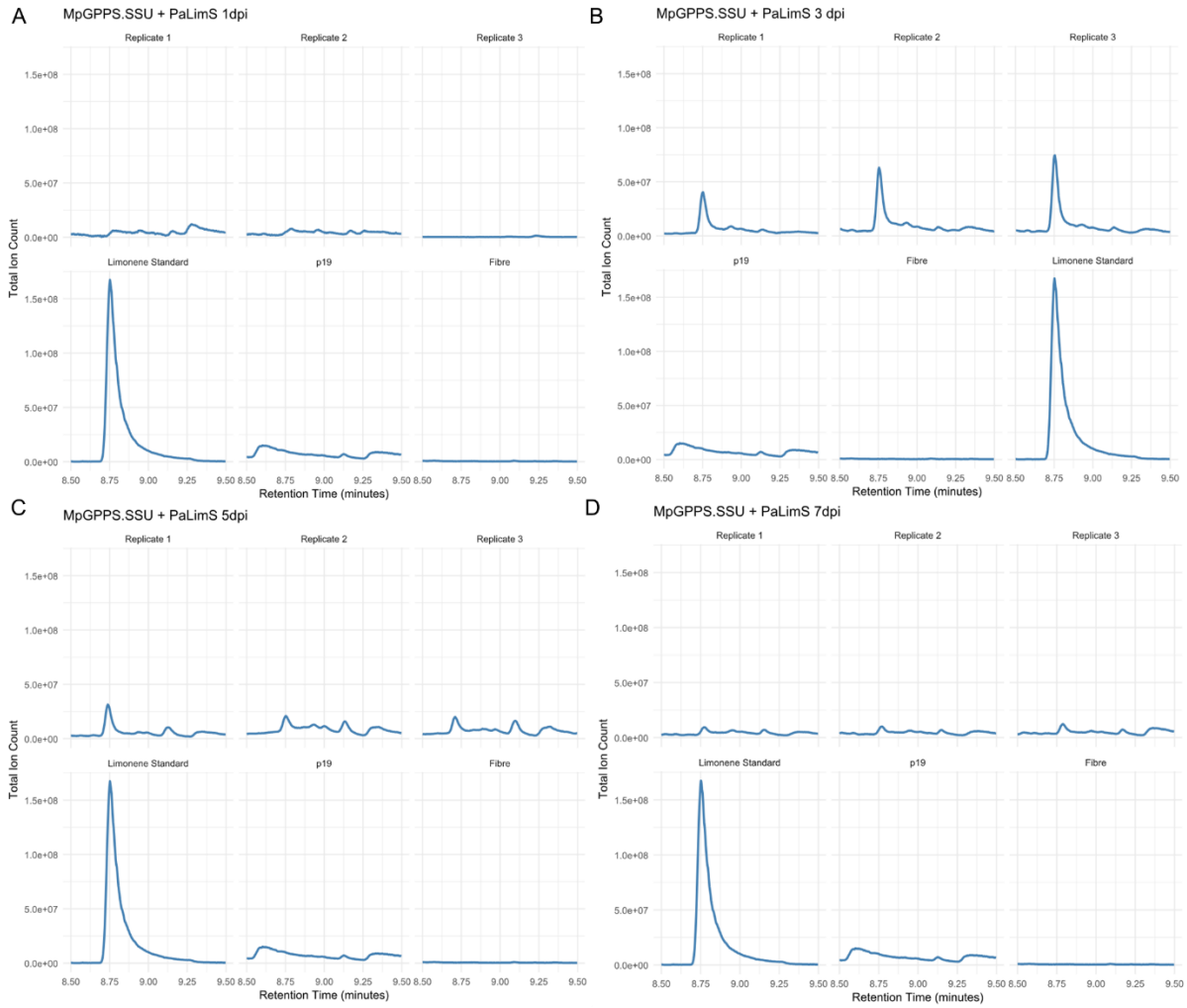

Appendix Figure 4. Co-infiltration of *MpGPPS.SSU* + *PaLimS* + *p19 in N. benthamiana* at A: 1, B: 3, C: 5 and D: 7 dpi. Three replicates are shown, in comparison with a (-)-limonene standard, a *p19* only infiltrated control, and the SPME fibre used for volatile extraction. Total ion count is on the Y-axis, retention time (minutes) is on the x-axis. This figure is to accompany Figure 4.6, 4.7, 4.8 and 4.9.

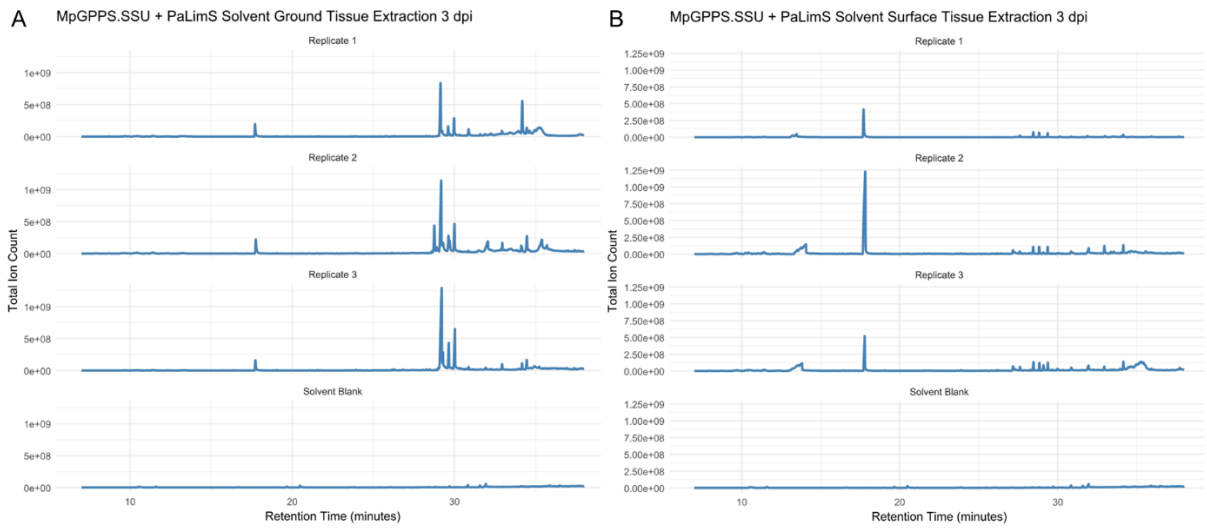

Appendix Figure 5. GCMS traces for *N. benthamiana* co-infiltrated with *MpGPPS.SSU* + *PaLimS* + *p19*, and extracted by A: Leaf tissue ground in liquid nitrogen and extracted with dichloromethane, or B: Leaf tissue surface extracted with dichloromethane. Three replicates are shown for each. Y-axis shows the total ion count. X-axis shows retention time (minutes). This figure is to accompany Figures 4.11 and 4.12.

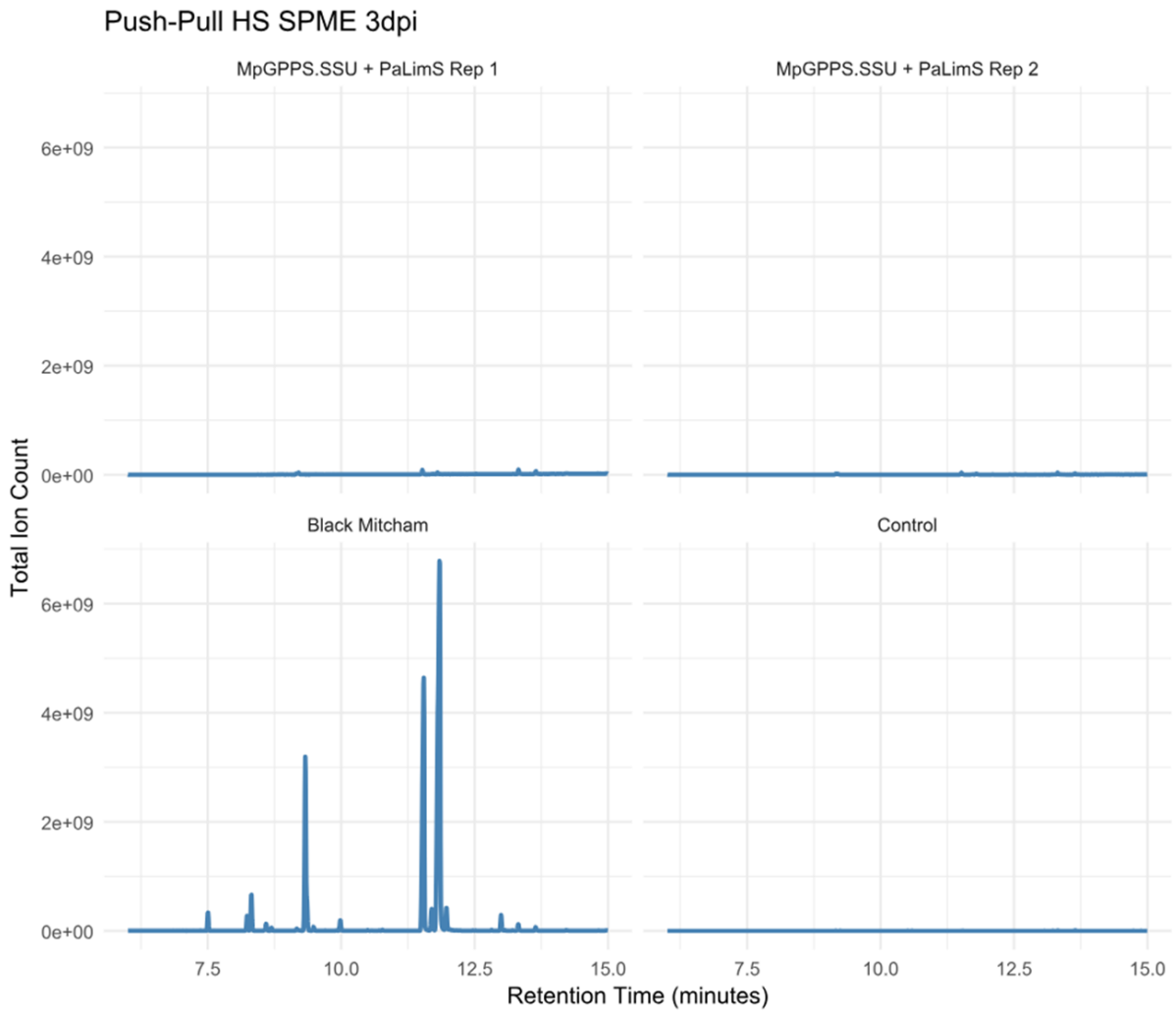

Appendix Figure 6. Dynamic HS-SPME *of N. benthamiana* leaf tissue co-infiltrated with *MpGPPS.SSU* + *PaLimS* + *p19* at 3dpi. Two replicates are shown. Y-axis shows the total ion count . X-axis shows the retention time (minutes). This figure is to accompany figure 4.13.

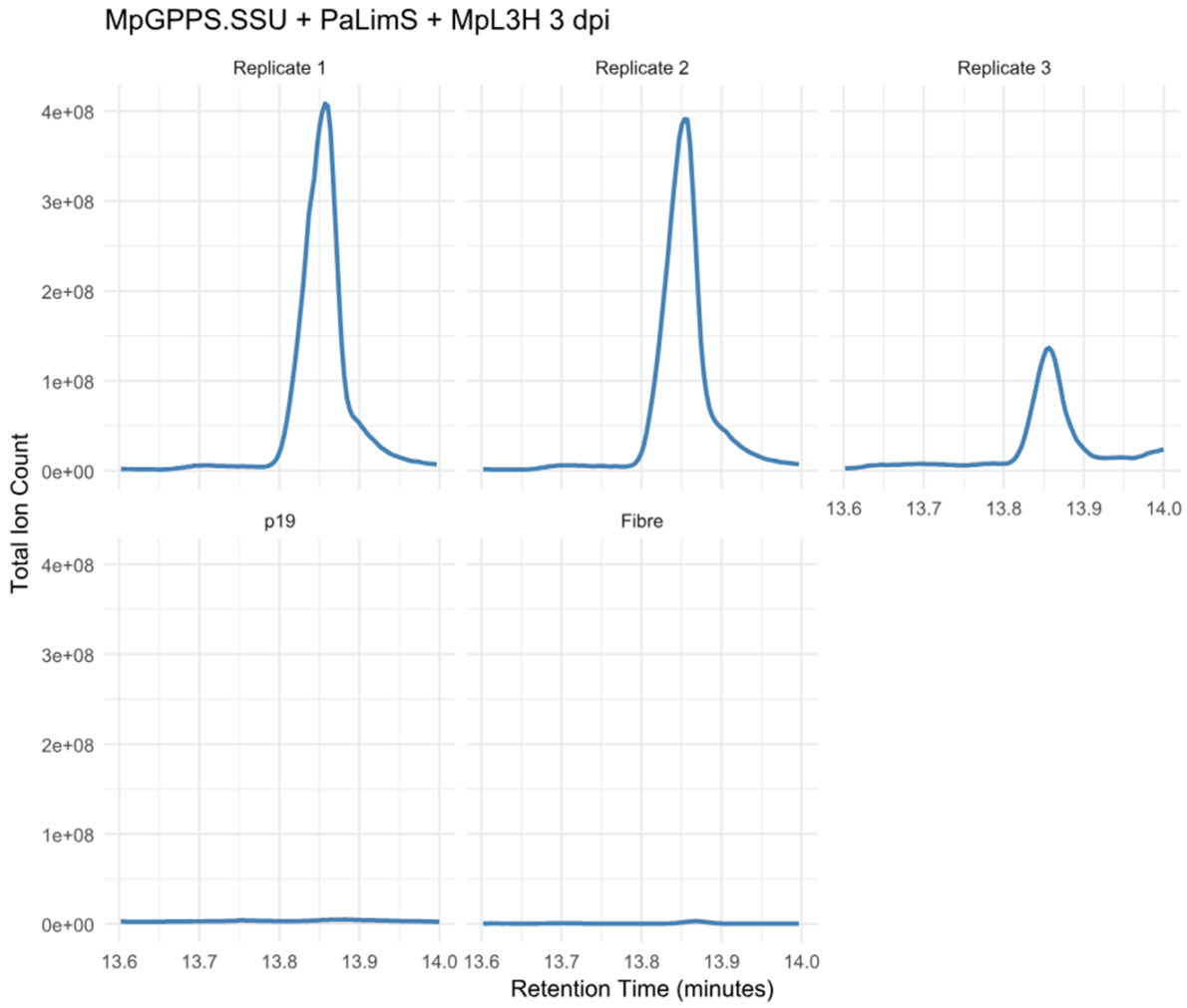

Appendix Figure 7. Co-infiltration of *MpGPPS.SSU* + *PaLimS* + *MpL3H* + *p19* in *N. benthamiana*. Chromatogram highlights the (-)-*trans*-isopiperitenol peak. Three replicates are shown. Y-axis shows the total ion count . X-axis shows the retention time (minutes). This is to accompany Figure 4.14.

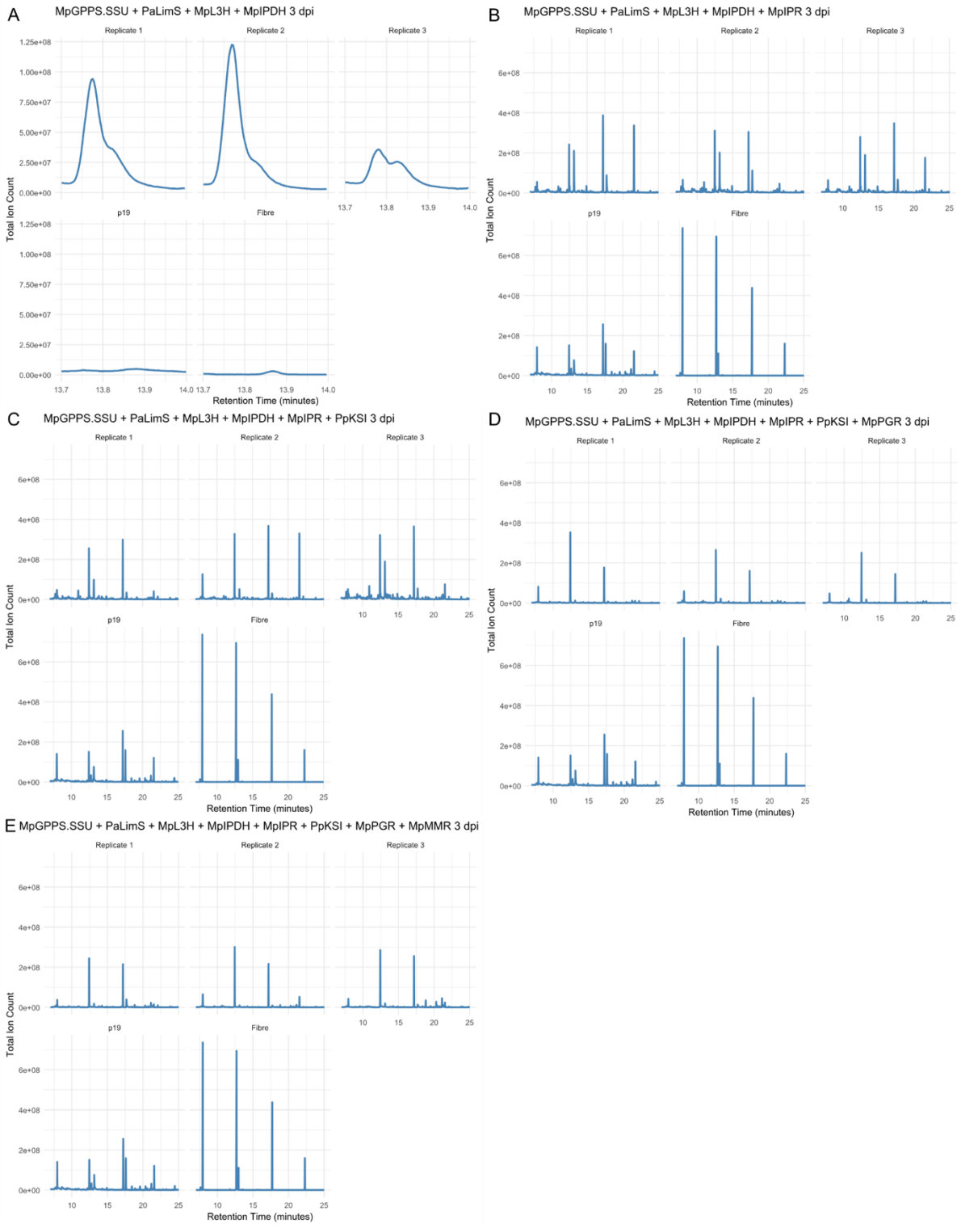

Appendix Figure 8. Chromatograms from three replicates of *N. benthamiana* co-infiltrated with A: *MpGPPS.SSU* + *PaLimS* + *MpL3H* + *MpIPDH* + *p19*, B: *MpGPPS.SSU* + *PaLimS* + *MpL3H* + *MpIPDH* + *MpIPR* + *p19,* C: *MpGPPS.SSU* + *PaLimS* + *MpL3H* + *MpIPDH* + *MpIPR* + *PpKSI* + *p19*. D: *MpGPPS.SSU* + *PaLimS* + *MpL3H* + *MpIPDH* + *MpIPR* + *PpKSI* + *MpPGR* + *p19*, E: *MpGPPS.SSU* + *PaLimS* + *MpL3H* + *MpIPDH* + *MpIPR* + *PpKSI* + *MpPGR* + *MpMMR* + *p19*. Y-axis shows the total ion count . X-axis shows the retention time (minutes). This is to accompany Figure 4.16.

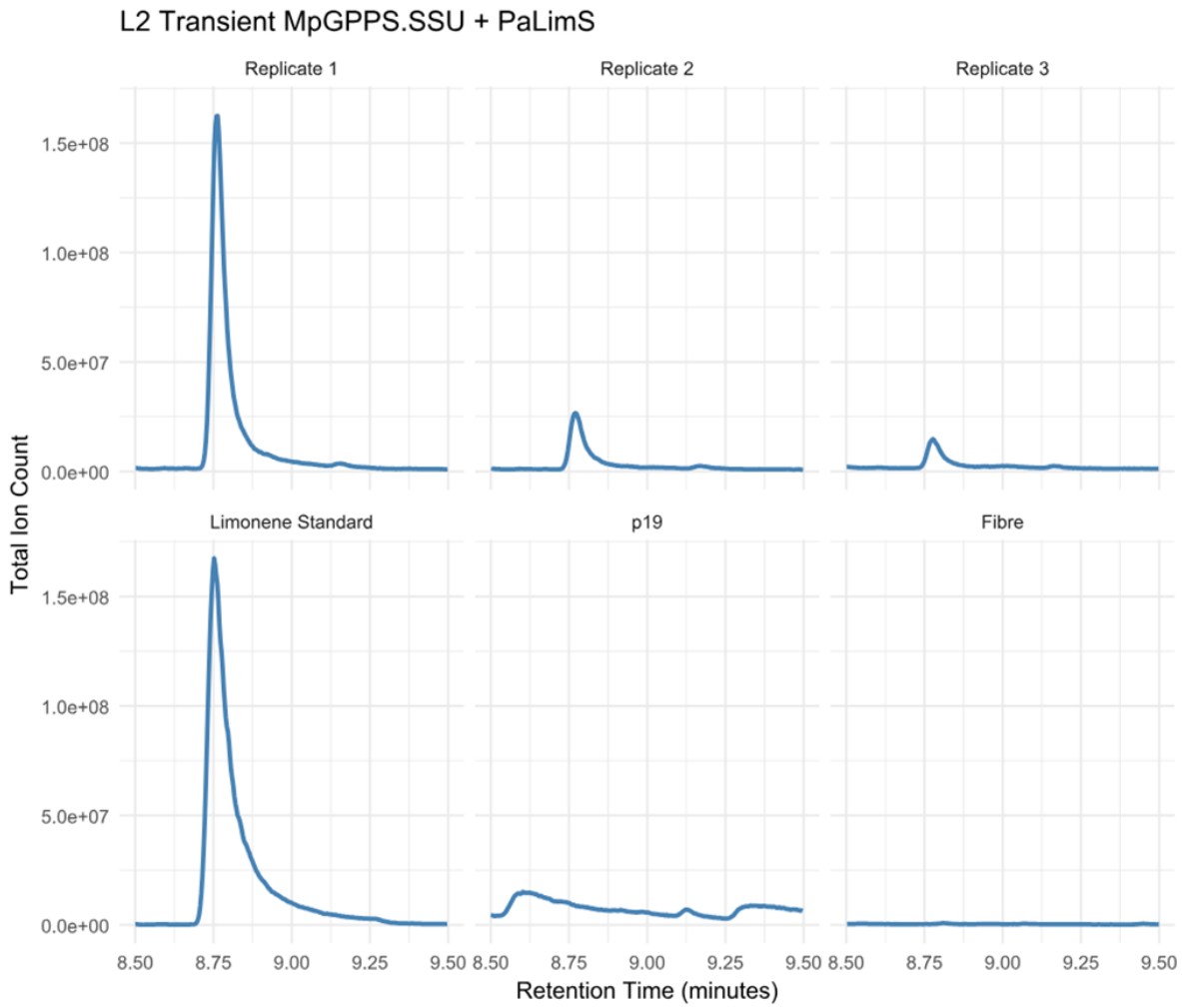

Appendix Figure 9. Infiltration of *N. benthamiana* leaves with the pL2_LimS construct and assayed at 3dpi. Y-axis shows the total ion count . X-axis shows the retention time (minutes). This is to accompany Figure 4.20.

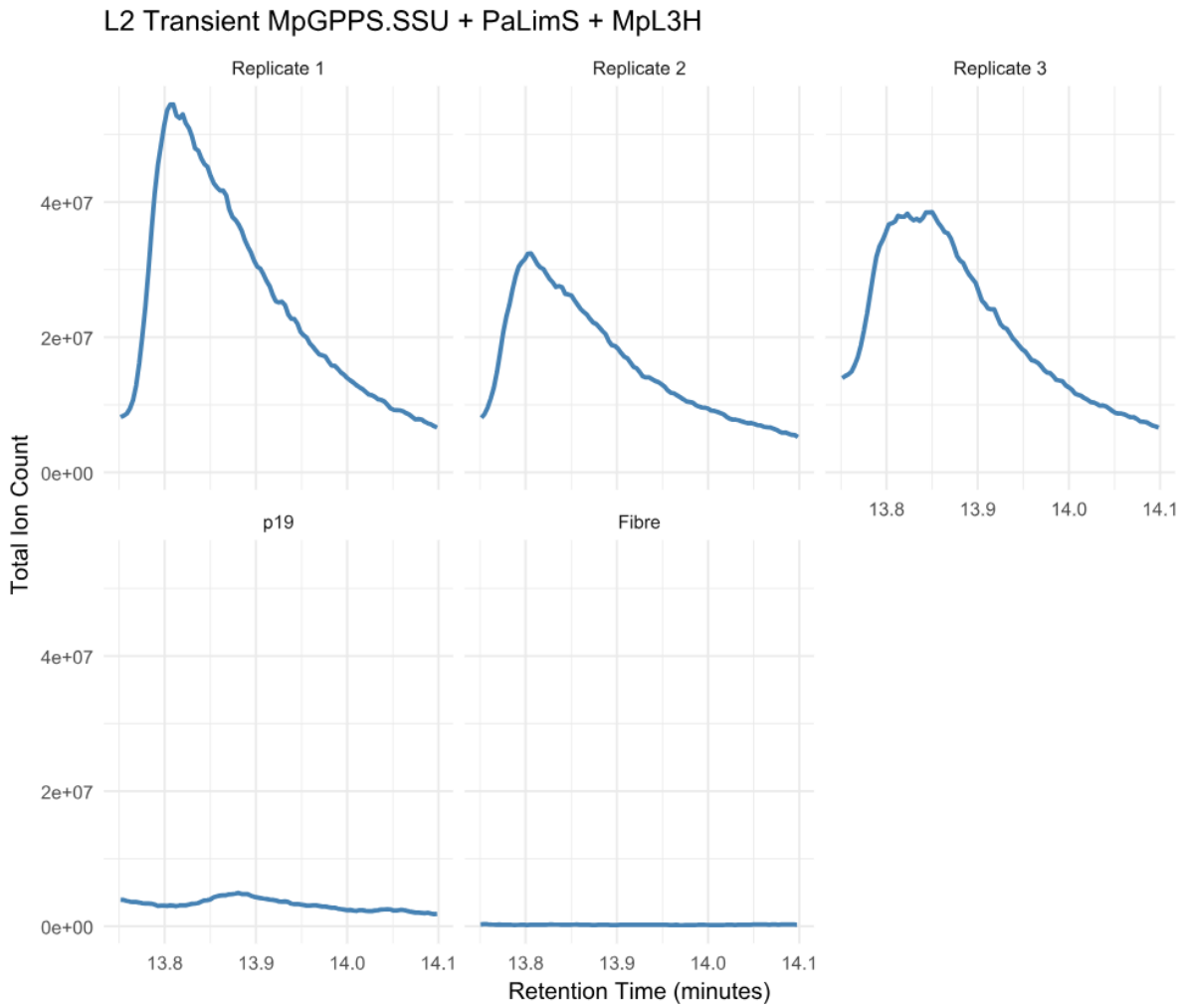

Appendix Figure 10. Infiltration of *N. benthamiana* leaves with the pL2_L3H construct and assayed at 3dpi. Y-axis shows the total ion count . X-axis shows the retention time (minutes). This is to accompany Figure 4.21.

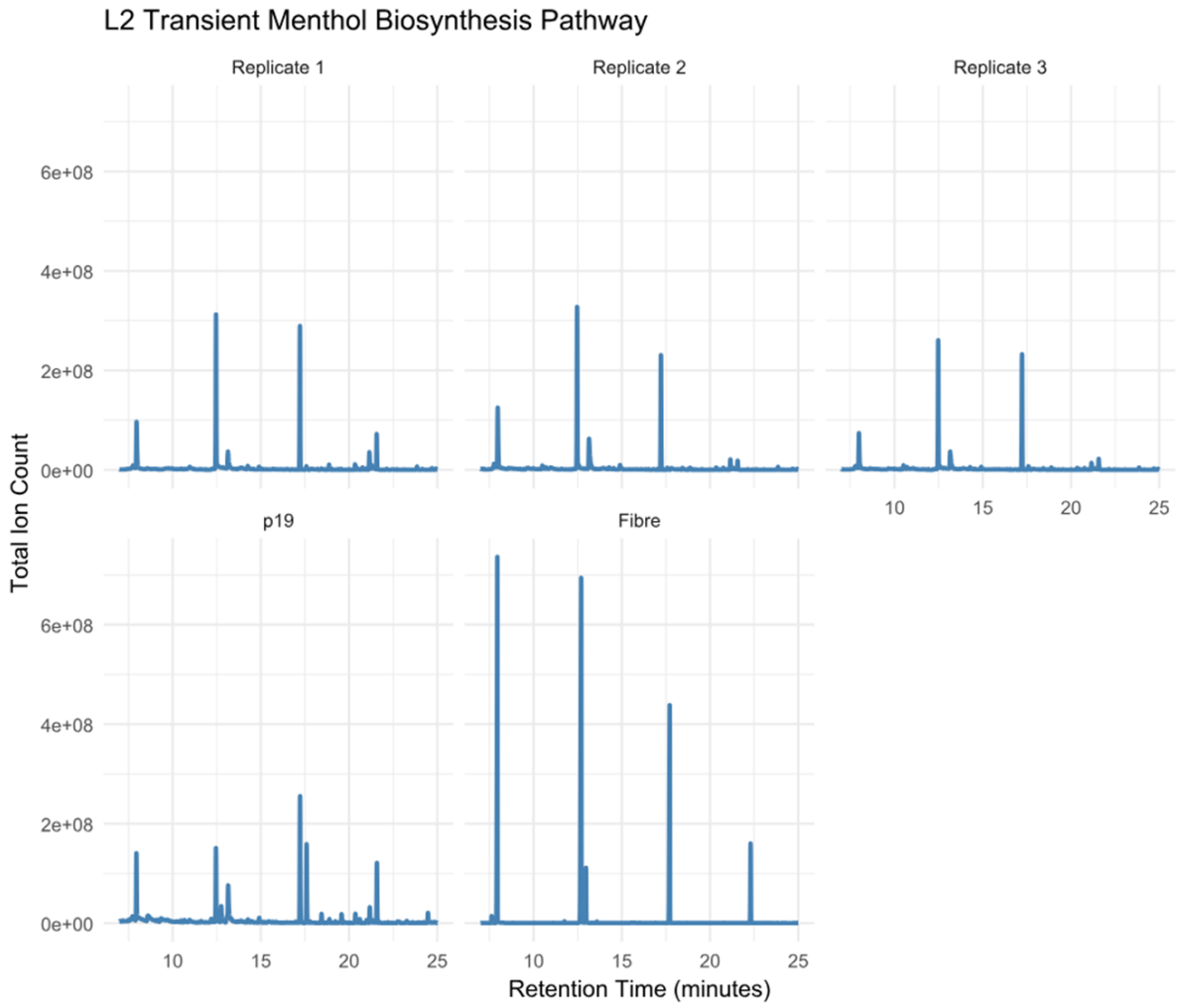

Appendix Figure 11. Infiltration of *N. benthamiana* leaves with the pL2_MBP construct and assayed at 3dpi. Y-axis shows the total ion count . X-axis shows the retention time (minutes). This is to accompany Figure 4.22.

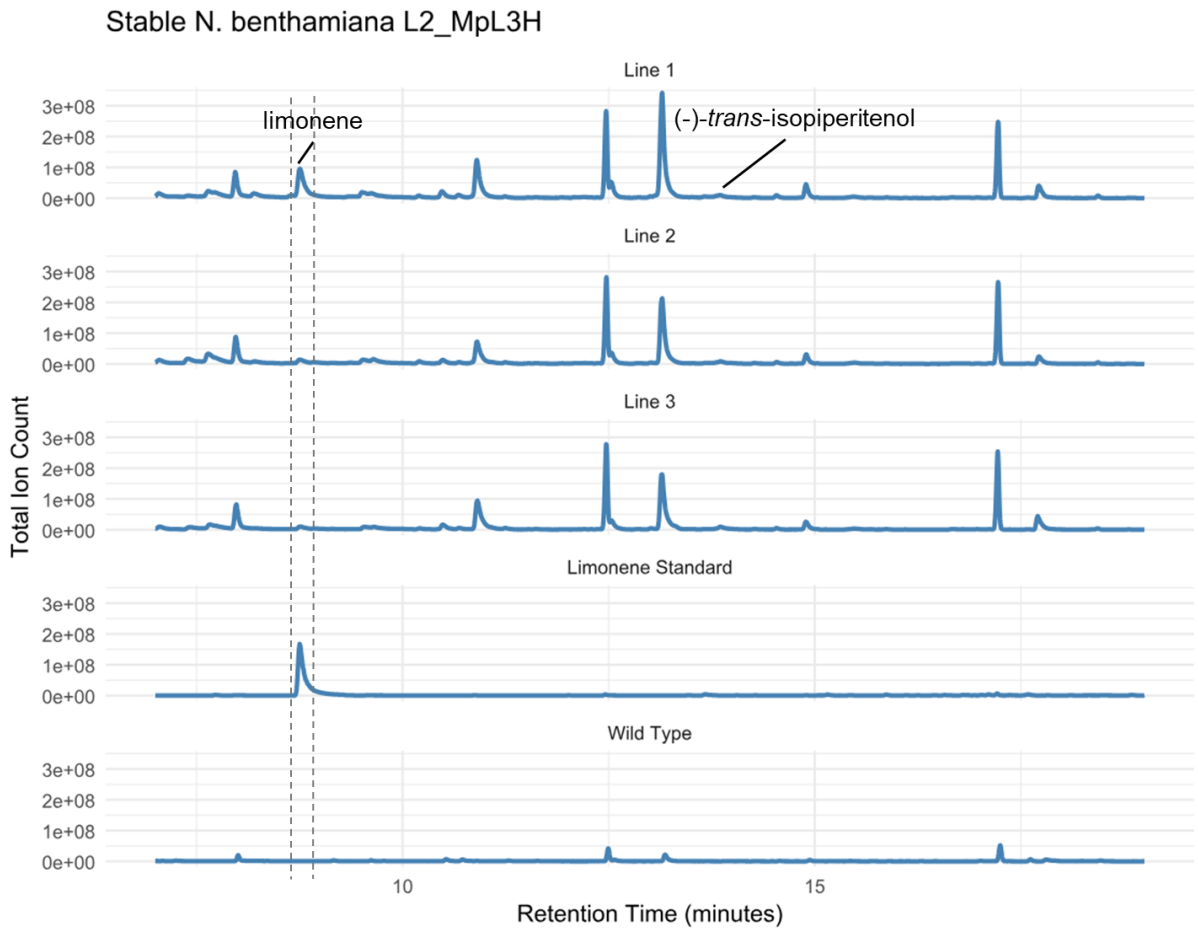

Appendix Figure 12. Stable transformation of pL2_L3H in *N. benthamiana*. Independent T0 transformant lines 1-3 are shown. Limonene and (-)-*trans*-isopiperitenol peaks are highlighted. Y-axis shows the total ion count . X-axis shows the retention time (minutes). This is to accompany Figure 4.23.

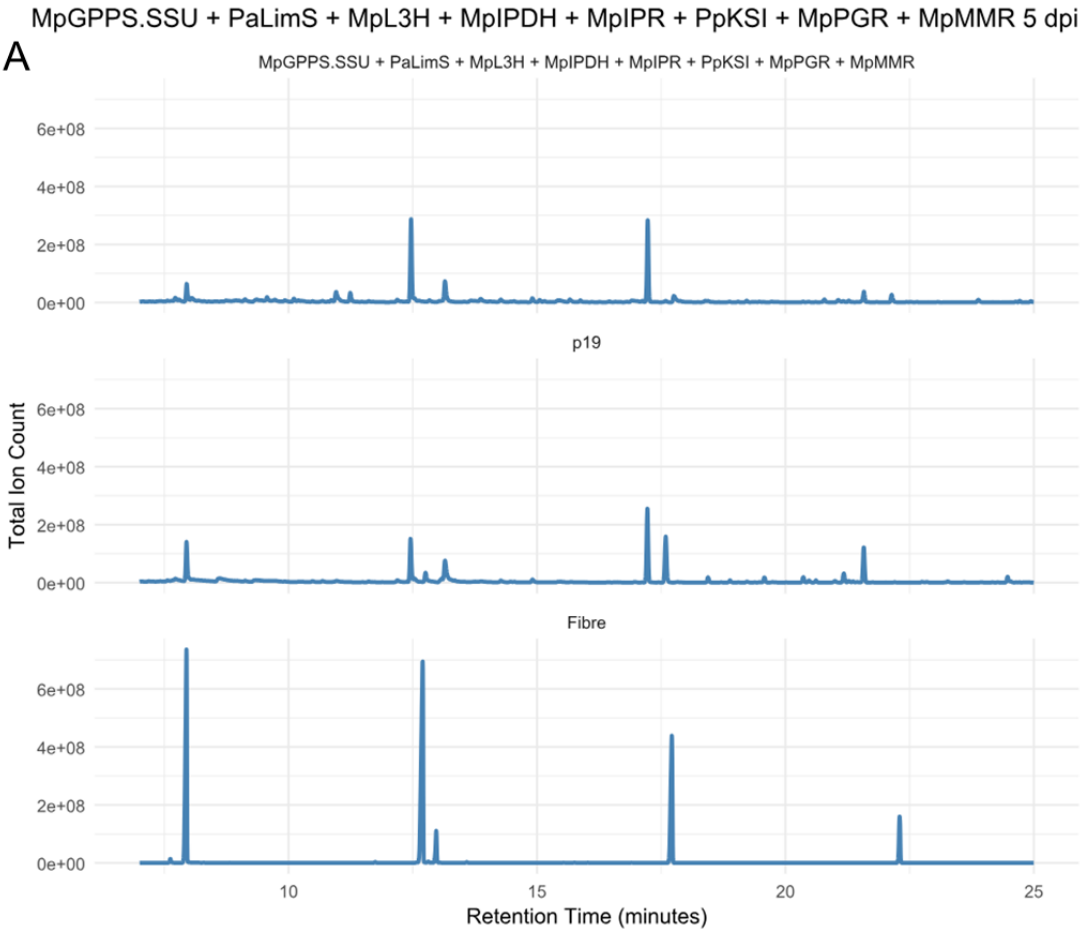
MpGPPS.SSU + PaLimS + MpL3H + MpIPDH + MpIPR + PpKSI + MpPGR + MpMMR 5 dpi
A
MpGPPS.SSU + PaLimS + MpL3H + MpIPDH + MpIPR + PpKSI + MpPGR + MpMMR
p19
Fibre
Total Ion Count
6e+08
4e+08
2e+08
0e+00
10
15
20
25
Retention Time (minutes)

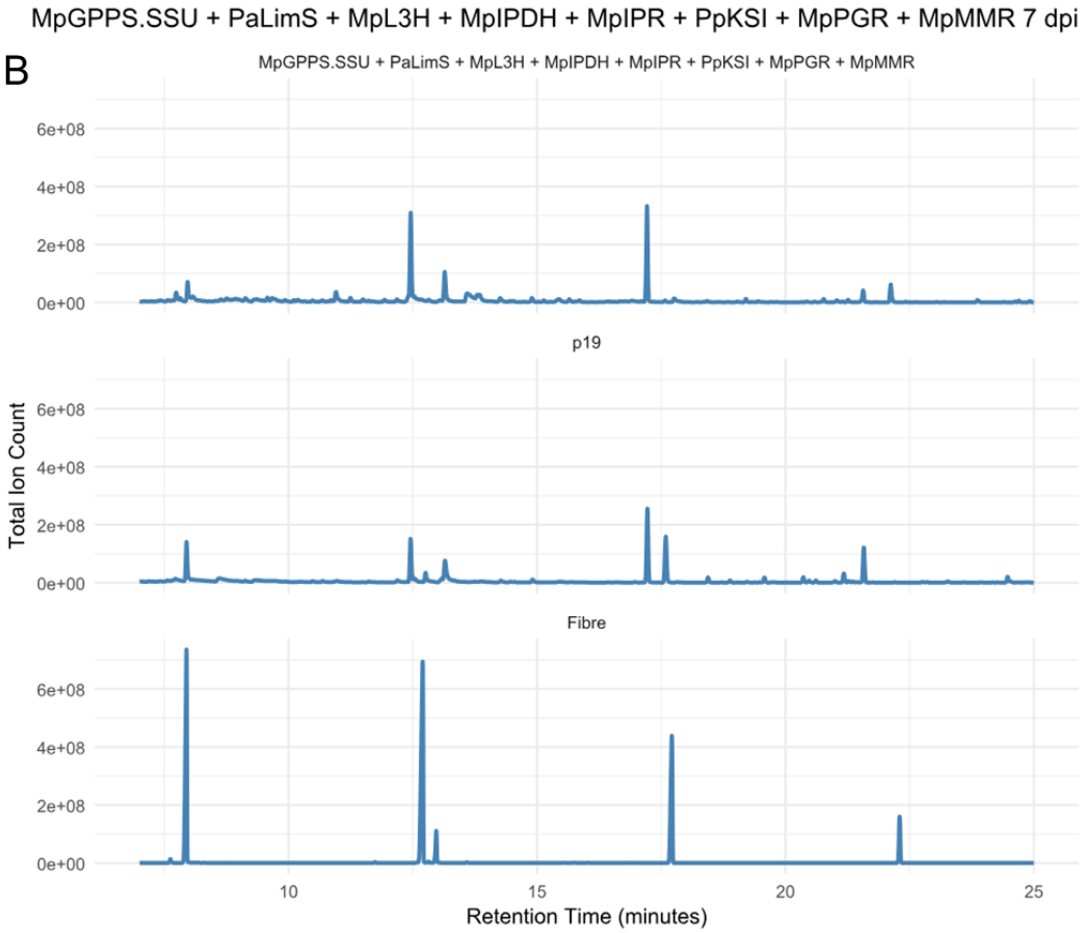
MpGPPS.SSU + PaLimS + MpL3H + MpIPDH + MpIPR + PpKSI + MpPGR + MpMMR 7 dpi
B
MpGPPS.SSU + PaLimS + MpL3H + MpIPDH + MpIPR + PpKSI + MpPGR + MpMMR
p19
Fibre
Total Ion Count
6e+08
4e+08
2e+08
0e+00
10
15
20
25
Retention Time (minutes)

Appendix Figure 13. Representative chromatogram of *N. benthamiana* leaves co-infiltrated with *MpGPPS.SSU* + *PaLimS* + *MpL3H* + *MplPDH* + *MplPR* + *PpKSI* + *MpPGR* + *MpMMR* at (A) 5 dpi and (B) 7 dpi. Y-axis is the total ion count. X-axis is retention time (minutes)

>BM.chr65:3582573-3584572_BMitcham.V1_g208413_MpGPPS.LSU

ACTCTAATTGCATTGCTACTTGAAACACGTGACCATTACATTAAGTGTAGCTGTAA
GATTTAAGAACAATTTTGGGCCATGGAAAGAGAATAGTTGACTTCAGTCTCCACA
TTTTAACTTTTCTTTATCATGATTAATTGTTGTACTTGTAGAATATCATTTACTTATAT
TTTTTTTTTGTCGGGCAAGAAAATATTTTATTAGAAAACAAAGGCACAAGCCGTGC
CAAAGCAGTACAACTTCAAAACGGCAGTTGAATGTTTGTAAAGAAAAAACCGGTT
ATCATTTACTTATATTGGACTCCAATGTTTTTTTTTACGAGTTAAAAAAAAGGAAAA
AATCTTATACTGTTTTTTCCCCTTCTTTTGTGCCTTCTGCCATTATCAACTACTAGT
ATTTATTAATTTATTCGATTATTTTGTCTTTGCCATTATCAACTACTAGTACTATATAG
CGATTTTACATAAATAAATATTTAGAGGGGGGATTTAGGCGTGATCGAAGCTTTTG
GTTACTTCAATACTCAATTTTTTTTATCATATTGCTTGTTTCCTTCCAAGTTTATTTT
ACAACTTGTTCAAGTCTTGTATTTTACGCTATACTATTATATTTTTTCTTCATGATGT
ATTGAGTTTATGGGCTTTTCACGATTTTCCAAGGATTTCTTTTAGTTCTTATTAGTC
AGAATCAGATAGAGAAGTTTAAGGGGGTCGCTACCCGGCTTATGAATTTAATAATT
GGATATCGATTTGTTCTTTTCCCAAATATTAGTATAATCGGATAGACAAAAACTTAG
GTCAGCCGGAAACACCGTGCGGCCGGGCTCAAAATGTCATTTTTTATACAGAAA
AGTGTCAATCTATATGAATAAAAGTGTCAATCTTTAACATAAGTATTTTACGAATAAA
ATGCCAATTTTTTAAAAGTATTAATCTTTATACATAAAAGTGTCAATCTATATGAATAA
AAGTGTCAGTGTTTTAGCTCGGCCGTACGGTGCCTCCGACTGACCCAAGTGTAT
CCCAATTGGATATCAATTTGTTCTTTTCCTGTTAAAAAAGCAGTTGTAGCCATGCG
GATAAGATCCTCTATTGCATTTCCGTATAGAATATTTCTACGCGTAGAATATTTCTG
ATGGCAAAATTAAATGAACAATTTGACGCACTTGACTATTTATTGCAGCACGCTAG
AAATGGATAAATTCAAGATAAATGTCATGTCATTGCTTTATTAATAAGTGGTAATTAT
GAAGCTATTTATAATATACTACTTCCTCTTTCCTCTGTTTTTTTCAAGTGACTCACT
TATATTCAAGTGTTGTAATATCCAGTAAAAAAAAATATATTTAAAAGTCATTATCAAA
AGGCTCGAAAAAACTTGCCATAAATCCTAAAAAAATATAACAACTTCAAAAAGACG
GAGAAAATATAAAATATATAAGTGAGCCGTTTAAAAAAAATAAAAATAGAGGGAGTA
CTAATACTCCTGTTCAATAGTTGAATCTTGATGGTTCGTAATTAGTAGCTGATATAG
CCCACACACTGAAGAATTTTGGAATCTCATGCAAATTCATTTATTATTTTTACTTGT
TCGCATCAAAATTCTAAGAATGAAATCACTGAATTGTATAGAAATGGTGGTCCATA
AATCACCGATTTTTAGATCTTTTATTGTATTTTTAGATAAAATGTTTTCATAATCAGTA
ATAATTAAAGAATTTTATAAATAGAAATATTGAATTTTATAAATAAAAGATATTTATTTA
GAGCTTTAAAAGAAGACTAAGATGTTAGGCGTTAAACTGCCAAACTCTCCCAATC
AAACAAAATCTCCACTCTTTAATTTGCACATCACATACTATATTCATTCACCTAATCT
CCTTCTTCACCTGAAATGAAGCTGCCAAATTAAAACAATTCTGACGTTGTTGTTTC
TTGGCACAGATTTCCAGTTGCAGTGCTGGGTTAATATTTACTAATATATCTTTTTTT
GAGGGAAAA

>BM.chr12:1240464-1242261_BMitcham.V1_g11684_MpGPPS.LSU

TTTTACCAACAGAAATATATATATATATATAAATACACGAGATTATATATATATCAACCC
AGCACTGCAACTGGAAATCTGTGCGAAGAAACAACGTCAGAATTGTTTTGGCAA
TTAGGTGAATGAATATATGTGATGTTGCAATAAAAGAGCGGAGATTTTGATTGGGA
GAGTTTGGCAGTTTAACGCCTAACTGCTTTTAAAGCCCTAAACTGCTTTAAATAAT
AATTCAATAAACACAATTACATTAAATACATGACGATCATCCCACGGTGTAACAAG
GAAATGTAATAGATGATCTGAATCGCTAGTTTATGCACCACCATCAATGGATTCTT

GAATCGGATCCTCAATTGCATTTCCGTGTTGCATCTTTTATTGCAATGACGGTTGA
TTAACAAGTGCTAAAAATATTTTTAAATCTAGTATTTTTTGTTTGTTTGTTTATGATTT
TTTTTAATCTATGGCTGGTTTTGGAAACATTTTTAACACGCGTCAATCATTCCTCG
TTGCAATAGAAGATGCAATACGGAAATGTATCAGAGGATTCCATTCGACAGATTTC
ATTTTGATTCACAAGTAAAAATAATACTCTTTCTTGAATTTTTTTTATTTAAACTGAG
TTTATTATAATAATAAAATATGTCGAGATATGAAGAATAAATGAATTCGTATGAGCTT
CCATTATTCTTTTAAGTGCGGGCTATATCAGCTACTAAGTACTAACCATCCAGATTC
AACTATATTATAAATAGCATCATAATTACCACTTATTATTAAAGTAATAACATGAGATT
TAATTTGAATTTATCCATGTGTAATGTGCTTCAATACATAGTGCGAATGCGTCAAAT
TGTTAATTTAATTTTGCCATCAGATTCGACACGACTAAAGTTGATTTTTTAACAAGC
GAAGAATAAATCGATATCCAATTATAGTAATAGTTGGGGAAAAAAAAATAAATTCTT
CCTCACTAATTAAATTCTTATAAAACGGGTAGCGACCCCCTTACACTTCTCTCTCT
GTCCTTAGAAAAACGTGAAAAGCCCGAAAACTCAATTAATCATAAATAAAAACTAA
TACTAACGTAAAATACAAGACTTGAAAAAGTTAAAGGAAACAAACAATATGTTAAA
GGAAACAAGCAATATGATAAAAATTTGAGTAATTAAGTAACCAAAAGCTTCCATCA
CGTCTAAATCTTCCCCCTAAATATTTATTCTTTGTAGTTCGGAAGCCTTTATCAAAC
AACCAAAACAGGCACTGCACAATTTAACAAGTACTCCCTCCGTCCCGTCGAAATT
GCCCTGTTTCTATATTTTATACCTCACATATATTCAAGAAACAGGGCCATTTCGAC
GGGACGGAAGGAGTACTAGTTTGTGTGTGTGTGTGTGTGTGTGCAAGTGCTA
GTAGTTGATAATGGCAGAAGGCATAAATGAAGGGGAAAAAACAGTACTATAAGGT
TTTTTTTTTTTCCCTAACAACAGTAAGGAAAAATTTGGAGTCCAATATAACTATATA
AGTAAATGATGTATTCTACAAGTACAACAATAAATCATACTGTAATAAAGAAAAGTG
AAATGTGGAGACTAAAGTCAACTATTCTGGCTCTTTCTCTTTCCCTGGCCCAAAA
TTGTTCTTAAATCTTTCAGCTACAATTAATGTAATGGTCCCGTGTTTCAAGTATGAA
TTTATCTATGTATTCAACAAGATTTTGGAGAATTTTTTACCATCTCCTTCCAGAATG
GAATACTACCGTTTAGAAGCTTGGAGCAAAATCGATCGATAGGGTT

>BM.chr31:28188571-28190167_BMitcham.V1_g99731_MpGPPS.LSU

AACCCTATTGATCGATTTTGCTTCAAGCATCTAAACGGTAGTATTCCATTCTGGAA
AGAGATGGTAAAAAATTCTCCAAAATCTTGTTGAATACATAGATAAATTCATACTTG
AAACACGGGACCATTACATTAATTGTAGCTGTAAGATTTAAGAACAATTTTGGGCC
AGGGAAAGAGAAAGAGCCAGAATAGTTGACTTTAGTCTCCACATTTCACTTTTCT
TTATCATGATATATTGTTGTACTTGTGGAATACATCATTTACTTATATGGTAATATTGG
ACTCCAAATTTTTCCTTACTGTTAGGGAAAAAAAAAAACTTATAGTAGTACTGTTTT
TTCCCCTTCATTTATGCCTTCTGCCATTATCAACTACTAGTACTTGTTAAATTGTGC
AGTGCCTGTTTTGGTTGTTTGATAAAGGCTTCTGAACTACACAGAATAAATATTTA
GGGGGGAGATTTAGACGTGATGGAAGCTTTTGGTTACTTCATTACTCAAATTTTTA
TCATATTGTTTGTTTCCTCTAACTTGTTCAAGTCTTGTATTTTACGTTATATTATAGT
TTTTCTTTATAATGGTTTATTGAGTTTTCGGGCTTTTCACGATTTTCTAAGGACAGA
TAGAGAAGTGTAAGGGGGTCGCTGCCCGTTTTATAAGAATTTAATTAGTGAGGGA
GAAATAATTTTATTCTTCTCTTGTTAAAAAAATCAACTGTAGTCGTGCCGAATATTT
CTGATGGCAAAATTAAATTAACAATTTGACGCATTCGCACTATGTATTGAAGCACA
TTACAAATGGACAAATTCAAATTAAATCTCATGTTATTACTTTATTAATAAGTGGTAA
TTATGATGCTATTTATAATATAGTTGAATCTGGATGGTTAGTACTTAGTAGCTGATAT
AGCCCGCACTTAAAAGAATTATGGAAGCTCATACAAGTTCATTTATTCTTCCTATC
TCGACATATTTTATTATTATAATAAACTCAGTTTAAATTAAAAAAAAATCAAGAAAGA
GTATTATTTTTACTTGTGAATCAAAATGAAATATGTCAAATCGGATCCTCTGATACA
TTTTCGTGTTGCATTTTCTATTGCAACGACGAATGATTGACGTGTGTTAAAAATGT
TTCAAAAACTAGCAATAATCAAAAAGTTTCATAAACAAAAATACTAGACTTAAAAAA
ATTTTAGCACTTGTAAATCATCCGTCCTTGCAATAAAGATGCAACACGGAAATGCA

ATAGAGGATTCGATTCGAGAATCCGTTGATGGTGGTGCATAAACTAGCGATTCGG
ATCCTCTATTACATTTCCTTGTTGCACCGTGGCATGATAGTCATGTATTTCTGTAAT
TGTGTTTATTGAATTATTATTTAAAGCAGATTAGGGCTTTAAAAGCAGTTAGGCGTT
AAACTGCCAAACTATCCCAATCAAAATCTCCACTCGTTTATTGCAACATCACATAT
ATTCATTCACCTAATTGCCTAAACAATTCTGACGTTGTTTCTTCGCATAGATTTCCA
GTTGCAGTGCTGGGTTGATATACATATAATCTTGTGTATTTATATATATATATCTGT
TGGTAAAA

>BM.chr24:15731910-15733349-rev-comp_BMitcham.V1_g68975_MpGPPS.LSU

AACCCTAGTGACCGATTTCGCTCCAAGCGTCTAAACGGTAGTATTCCATTCTGGA
AAGAGATAAAAATTCTCCAAAGTCTTGTTGAATACATAGATAAATTCATAGTTGAAA
CACGTGACCTTTACATTAATTGTAGCTGAAAGATTTGAGAGCAATTTTGGGCCAG
GGAAAGAGAAAGAACCAGAATAGTCTACTTTAGTCTCCACACTTCACTTTTCTTTA
TCATGATTTATTGTTGTACTTGTAGAATACATCATTTACTTATGTTGGACTCCAAATT
TTTCCTTACTGATGTTTCCCCTTCGCCATTATCAACTACTAGTATTTGTTAAATTGT
GCAGTGCTTGTTTTGGTTTGTTTGATAAAAGGCTTCTGAACTACACAGAATAAATA
TTTAGGGGGAAGATTTAGACGTGATGGGAGCTTTTGGTTACTTCATTACTCAAGT
TTTTGTTTGTTTCCTTTAACTTGTTCATGTCTTGTATTTTACGTTATATTATAGTTTTT
CTTTATTGTGATGTATTGAGTTTTCAGGCTTTTCACGATTTTCTAAGGACAAGTGT
AAGGGGGTCGCTACCCGTTTTTAAGAATTTAATTATTGAGGTAGAAATATTTTTTTC
CCCAACTATTACGATAATTGGATATCAATTTATTTTTCCCCTATTTAAAAAAGCAACT
GTAGCCGTGTCGAAAATTTCTGATGACAAGATTAAATTAATTTGTATTGCAGCATA
CTACAAATGGATAAAATTCAAATAAAATGCCATGTTATTCTTTATTAATAAGTGGTAA
TTATTATGCTATTTATAATATAGTAGACTCATTGTTCAAAAGTTGAATCTGGATGGTT
AGTAGAGTACTTAGTAGCTAATATGGCCCGCGCTGAAGAATTATGGAAGCTCAAA
CCAATTCATTTATTCCCTATATCTCGACATAGTATCTTATAGTATTATTATAATAGACT
CAATTTAAATAAAAATATATGAAGCTAGATAAAATATGGTGAATATTATTTTTACTTGT
TCACATCAAAATTCTAAGAATGAAAACATTAAATTGAATCGAACTGGAATTTGTTG
ATCGTGGATTCGTGGTGTATAAACTAGCGATTCAGGTCATCTGTTGCATTTCCTTG
TTGCACAGTCGCGCTTGCTATCTTCATGCTTTAAAAATATTTTCAAAATGAATAATT
TTGTAATTCTGATTATTGAATTATTTAAAGCAGTTTAGGGCTTTTAAAGCAGTTAGG
CGTTAAACTGCCAAACTCTCTCAATTAAAATATCCACTCTTAATTGCAAAATATCAC
ATATATTCATTCACCTACTAATTCCTTCTTCACCTCAAATGAAACTGCCAAAATAAT
TCCGACGTTGTTTCTTCGCACAGATTTTCCAGTTGCAGTGGTGGGTTTTGATATA
TATAATCTTGTGTTGGTAAAA

>BM.chr61:22271573-22273572-rev-comp_BMitcham.V1_g200161_MpGPPS.LSU

TTTTTCGTGTATTCAACGAATTTCGTGAATTGATGAATTTCAATCCGTGTATTGTAG
AACAAACGACAAAAAATTTCATGAATAATTTTTTCGTGTATATGTATTGTGCGTGCG
TATGATTGTTGTGTGTGTGTGATAGAGGGGTGTTGTGTATGCTGTGAGTTGTGTG
ATGTGTGCGTGAGTTATGTGTATGTGTGTGCGTGAGTTGCTGTGTATGTGTGTGT
TTTGCTGTGCATGTGCATGAGTGTGTGCATTTTGCTGTGAGTGTGTATGCATGCG
TGAGTGTGTGTTTGCATGCGTGGGTGTGTGTGTTTGCATGTGTGTGTGTTTCTG
TGTGCGTGAGTGCGTGTCAATTGCTGAGGTGTGTGTGTTTGAGTGGGTGCGTG
AGTGTGTGTTTGAGGGTGAGTTTTGGGGAAGAAGAAAATGAGTTAATTTTATTAA
GGTAGCAATGTAATTACTTTTAAAAGTGGTTAGTTTTTATTTTTTTTATTTTAGTGAC
TACTTTTTTATTTTACTATCTCAAAATAACTATTTTACTAGTTGTCCCAATTTTTAATG
TATTTATATAACTTTCATATATTAAATTACTATATGCTTGATTGAAGTAATTCACTAGT
TAATATATATAGGTAGCAGTAGTACCTGTATATTTATCAATGTTCGTGAGGTGATATT
AAAGAATTGTAACGAAATAATAATATTTTGTATCGGTATATTGGCATGTGAATAAGC

TAGTAGTGATGCAAAACCTTTTAAACATAGCTAAACAAAACCACAGAATTTGATTT
TTACGGTGATAAAATTGAGTTGAATAATTAGTAAAAAAATGTACAATTTTACATGTAT
ATGCATAGGATAAGGTACAAATATCTTCTAACGTTTTTATGAAAAACAAATTGAGCT
CTGAACTTTGTTTTAATACAAATAGGACACCCATCTTCATTTTTAGGTACAAATACC
CCTTAACGTTTTTATGAAAAAAATAAATTGTCTCCTAAACTTTGTTTTGGTATGAAA
AGGACCATCATCTTTATTTTTAGTCATACTCTATCTCTTCGATAACAAATTGTCCCC
TAAATATTTAGAAACCTAATTTTCAAAAAAATGAAATCTCTAATCTGCTCACCTTTAT
CTCTTGAACCGACGACGTCATCGGTGACTTTGCTATTTCAATATCGGCACCGCCT
CCTTGTTATACCTCAAATTCGTCCTGTCGACCACTTCTTGCACGAGCTTGATTGT
TGGAGGCGGAGAGAAACACTCGGTCCTTATGCTCACCGTTGTGCTTGTTTGTAT
AAAAAAAAATCAAAGAAGACGGTTGTGAGTGTTTCGTTAGTTGGTTTGGTGAATT
GTTCCTAAAAATGAAGATAATGGTCCTTTTCGTACCAAAACAAAGTTGAAGGGCA
ATTTGTGTTTTTTTTTTTCGTAAAAACGTTAGGAGTATTTGTACCTAAAAATGAAGA
TGCTAGTTCTATTTGTACCAAAACAAAATTTAGGGGTCAATTTATTTTTTTTTTGTA
AAAACGTTCGAAGGGTATTTGTTCCTTGTCCCATATACATATCACATGATTGCATC
ACAAATGGAATTAGATGTATTTATGAGGTTGTATAAGAAAAGAGGAGCAAGAGTAA
TTATTAATGATTGGGAGGTGGAACCCACGCAGGGAGGTGGGAAAAAAAACGTGA
GGTGAGTTCACAGCTCATCTTTACCTTGGCATCTTTGTACAGTAGTGTGCACCTT
CCCCCCCCTTCGCCTTCACCACGTCCTGTCATTTCCACCATAAATCTGACTCAAC
GCGATTTTTCTAGAGATACTGTTACCCCCTACAGTGAAGTTCACGATCAAAACTC
GTGATTTTTCTCTCCCCCACTACCACTATATAATCTTTTCCTCTTCCTCTACTCACC
ATTCCCATATACCAACAGTAAACAGTAACTCTTCCTCTTTCTCTGGTCGGCATTTT
CACAAACAGTTGGGGGGCGGGTGCGATGACTGTGAG

CAGTTG = MYB binding site 1

CAGTTA = MYB binding site 2

BMitcham.V1_g208413 = Canonical *MpGPPS.LSU*

Appendix Figure 14. Manual detection of MYB TFBS in the *MpGPPS.LSU* promoter sequences. MYB binding sites are as determined by Reddy et al. (2017).

```
#
#
#  Percent Identity  Matrix - created by Clustal2.1
#
#
```

1: MpLimS_Madhuras_OP527754.1	100.00	98.74	98.74	54.95	54.56	52.70	55.30
2: MpLimS_BMitcham.V1_g117374	98.74	100.00	99.55	47.60	47.19	45.87	53.16
3: MpLimS_BMitcham.V1_g117378	98.74	99.55	100.00	47.92	47.57	46.19	53.16
4: MpLimS_BMitcham.V1_g177344	54.95	47.60	47.92	100.00	98.90	54.25	60.13
5: MpLimS_BMitcham.V1_g195282	54.56	47.19	47.57	98.90	100.00	54.22	60.40
6: MpLimS_BMitcham.V1_g83335	52.70	45.87	46.19	54.25	54.22	100.00	67.11
7: McLimS_OR428312.1	55.30	53.16	53.16	60.13	60.40	67.11	100.00

Appendix Figure 15. Percent identity matrix from promoter sequence alignment of *MpLimS* (cv. Black Mitcham) promoters identified in this thesis, together with the *MpLimS* (cv. Madhuras) promoter identified from Qamar et al. (2022), and *Mentha canadensis LimS* promoter identified from Li et al (2025). Canonical promoter for *MpLimS* identified in this thesis is highlighted by a green box. *MpLimS* cv. Madhuras promoter is highlighted by a red box. *McLimS* is highlighted by a yellow box.

Appendix Table 3. Menthol biosynthesis genes annotation table. Genes with highest homology based matching to the biochemically characterised gene is highlighted in green.

Black Mitcham Chromosome #	Chromosome co-ordinates	Black Mitcham Gene ID #	Query Cover (%)	Identities (%)	Canonical Gene ID #	Canonical Gene Name
50	17173082..17174189	BMitcham.V1_g162906	94	100	AAF08792.1	*MpGPPS.SSU*
41	8166679..8165546	BMitcham.V1_g133198	94	98.72	AAF08792.1	*MpGPPS.SSU*
64	17435131..17436264	BMitcham.V1_g207076	94	98.5	AAF08792.1	*MpGPPS.SSU*
58	6802090..6801011	BMitcham.V1_g185806	100	90.79	AAF08792.1	*MpGPPS.SSU*
30	22780598..22781539	BMitcham.V1_g95197	100	85.94%	AAF08792.1	*MpGPPS.SSU*
65	3584492..3585814	BMitcham.V1_g208413	100	100	AAF08793.1	*MpGPPS.LSU*
12	1240558..1239257	BMitcham.V1_g11684	100	90.98	AAF08793.1	*MpGPPS.LSU*
31	28190077..28191377	BMitcham.V1_g99731	100	90.98	AAF08793.1	*MpGPPS.LSU*
24	15731979..15730736	BMitcham.V1_g68975	100	89.68	AAF08793.1	*MpGPPS.LSU*
55	10495910..10496547	BMitcham.V1_g177344	100	97.16	AAC37366.1	*MpLimS*
60	10111652..10112298	BMitcham.V1_g195282	100	97.83	AAC37366.1	*MpLimS*
37	6254339..6254722	BMitcham.V1_g117374	100	93.16	AAC37366.1	*MpLimS*
37	6278421..6278804	BMitcham.V1_g117378	100	93.32	AAC37366.1	*MpLimS*
28	7262395..7262778	BMitcham.V1_g83335	100	93.82	AAC37366.1	*MpLimS*
37	6264647..6265535	BMitcham.V1_g117376	100	100	Q9XHE6.1	*MpL3H PM2*
37	6288460..6289348	BMitcham.V1_g117380	100	98.8	Q9XHE6.1	*MpL3H PM2*
60	10128683..10129577	BMitcham.V1_g195283	100	99.2	Q9XHE7.1	*MpL3H PM17*
55	10518649..10519543	BMitcham.V1_g177346	100	99.8	Q9XHE7.1	*MpL3H PM17*
28	7278388..7279282	BMitcham.V1_g83336	100	96.8	Q9XHE7.1	*MpL3H PM17*
19	10179069..10179925	BMitcham.V1_g45000	100	97.55	Q9XHE7.1	*MpL3H PM17*
9	7762407..7763286	BMitcham.V1_g232390	100	91.8	Q9XHE7.1	*MpL3H PM17*
9	11523998..11524787	BMitcham.V1_g232912	97	71.29	Q9XHE7.1	*MpL3H PM17*
38	11496789..11497402	BMitcham.V1_g120910	99	96.91	Q9XHE7.1	*MpL3H PM17*
38	11495775..11496839	BMitcham.V1_g120909	93	84.45	Q9XHE7.1	*MpL3H PM17*
12	3362390..3363187	BMitcham.V1_g12076	100	100	Q5C9I9.1	*MpIPDH*
12	3365188..3365952	BMitcham.V1_g12077	99	72.41	Q5C9I9.1	*MpIPDH*
26	28216652..28217449	BMitcham.V1_g78751	100	98.11	Q5C9I9.1	*MpIPDH*
31	25534243..25535046	BMitcham.V1_g99254	100	97	Q5C9I9.1	*MpIPDH*
24	19811047..19811832	BMitcham.V1_g69467	99	90.46	Q5C9I9.1	*MpIPDH*
24	19816058..19816822	BMitcham.V1_g69468	97	73.05	Q5C9I9.1	*MpIPDH*
		BMitcham.V1_g208088	97	84	Q5C9I9.1	*MpIPDH*

45	23224861..23225242	BMitcham.V1_g146769	100	100	Q6WAU1.1	*MpIPR*
45	23229338..23229714	BMitcham.V1_g146770	100	95.75	Q6WAU1.1	*MpIPR*
46	23096722..23097103	BMitcham.V1_g149504	100	97.45	Q6WAU1.1	*MpIPR*
46	23,112,687..23,114,544	BMitcham.V1_g149506	100	93.31	Q6WAU1.1	*MpIPR*
49	2350203..2350584	BMitcham.V1_g154678	100	98.73	Q6WAU1.1	*MpIPR*
42	2102786..2103162	BMitcham.V1_g135454	100	96.73	Q6WAU1.1	*MpIPR*
57	21360925..21361306	BMitcham.V1_g184497	100	94.9	Q6WAU1.1	*MpIPR*
62	18329142..18329523	BMitcham.V1_g201980	100	85.99	Q6WAU1.1	*MpIPR*
15	5,102,399..5,104,045	BMitcham.V1_g26993	100	100	Q6WAU0.1	*MpPGR*
15	5,082,483..5,084,132	BMitcham.V1_g26990	100	99.42	Q6WAU0.1	*MpPGR*
15	5,058,073..5,059,737	BMitcham.V1_g26986	99	97.95	Q6WAU0.1	*MpPGR*
15	5,153,093..5,154,715	BMitcham.V1_g27003	98	93.26	Q6WAU0.1	*MpPGR*
15	5,155,564..5,157,191	BMitcham.V1_g27004	98	94.12	Q6WAU0.1	*MpPGR*
3	6,210,629..6,212,282	BMitcham.V1_g89813	100	99.42	Q6WAU0.1	*MpPGR*
3	6,230,367..6,232,020	BMitcham.V1_g89817	100	98.83	Q6WAU0.1	*MpPGR*
3	6,270,422..6,272,040	BMitcham.V1_g89821	98	94.41	Q6WAU0.1	*MpPGR*
3	6,278,942..6,279,823	BMitcham.V1_g89824	98	93.37	Q6WAU0.1	*MpPGR*
3	6,277,330..6,278,821	BMitcham.V1_g89823	100	95.02	Q6WAU0.1	*MpPGR*
18	6,003,847..6,004,234	BMitcham.V1_g40348	99	91.43	Q6WAU0.1	*MpPGR*
29	5,160,314..5,160,700	BMitcham.V1_g86353	60	92.06	Q6WAU0.1	*MpPGR*
26	18,057,137..180,57,520	BMitcham.V1_g77385	68	91.27	Q6WAU0.1	*MpPGR*
31	13,079,735..130,80,115	BMitcham.V1_g97746	99	90.48	Q6WAU0.1	*MpPGR*
28	14,882,092..14,882,479	BMitcham.V1_g84158	99	88.07	Q6WAU0.1	*MpPGR*
28	15,059,235..15,059,622	BMitcham.V1_g84183	99	85.32	Q6WAU0.1	*MpPGR*
61	11,255,787..11,256,170	BMitcham.V1_g198865	98	90.03	Q6WAU0.1	*MpPGR*
12	14,087,094..14,087,447	BMitcham.V1_g13640	99	87.16	Q6WAU0.1	*MpPGR*
12	14,087,477..14,088,993	BMitcham.V1_g13641	76	88.94	Q6WAU0.1	*MpPGR*
19	17,968,215..17,968,594	BMitcham.V1_g45954	91	81.18	Q6WAU0.1	*MpPGR*
19	18,201,440..18,202,967	BMitcham.V1_g45985	99	86.51	Q6WAU0.1	*MpPGR*
60	20,385,800..20,386,179	BMitcham.V1_g196499	91	81.18	Q6WAU0.1	*MpPGR*
57	21399075..21399529	BMitcham.V1_g184503	100	77.49	AAQ55960.1	*MpMMR**
57	21376161..21376541	BMitcham.V1_g184498	96	76.6	AAQ55960.1	*MpMMR*
42	2306369..2306830	BMitcham.V1_g135464	100	87.3	AAQ55960.1	*MpMMR***
42	2185089..2185597	BMitcham.V1_g135458	100	100	AAQ55959.1	*MpMNMR*
	2194737..2195238	BMitcham.V1_g135459	100	74.69	AAQ55959.1	*MpMNMR*
49	2317656..2318060	BMitcham.V1_g154675	98	74.53	AAQ55959.1	*MpMNMR*
46	23085827..23086089	BMitcham.V1_g149502	99	88.24	AAQ55959.1	*MpMNMR*
46	23087028..23087410	BMitcham.V1_g149503	99	77.25	AAQ55959.1	*MpMNMR*
57	21376173..21376534	BMitcham.V1_g184498	100	81.54	AAQ55959.1	*MpMNMR*

61	18998949..18999825	BMitcham.V1_g199648	92	100	Q947B7.1	*MpMFS*
61	19010446..19011322	BMitcham.V1_g199649	92	100	Q947B7.1	*MpMFS*
61	19018767..19019643	BMitcham.V1_g199650	92	100	Q947B7.1	*MpMFS*
61	19046010..19046886	BMitcham.V1_g199652	92	100	Q947B7.1	*MpMFS*
26	26237295..26238177	BMitcham.V1_g78425	92	88.16	Q947B7.1	*MpMFS*
24	21351015..21351886	BMitcham.V1_g69711	67	92.77	Q947B7.1	*MpMFS*

* Highest overall match is to *Mentha arvensis MMR* (100% Querry Cover, 95.26% Identity, NCBI ID: ANA95864)
** Highest overall match is to *Mentha x piperita* cv. Madhuras *MMR* (100% Querry Cover, 99.05% Identity, NCBI ID: ANA95860

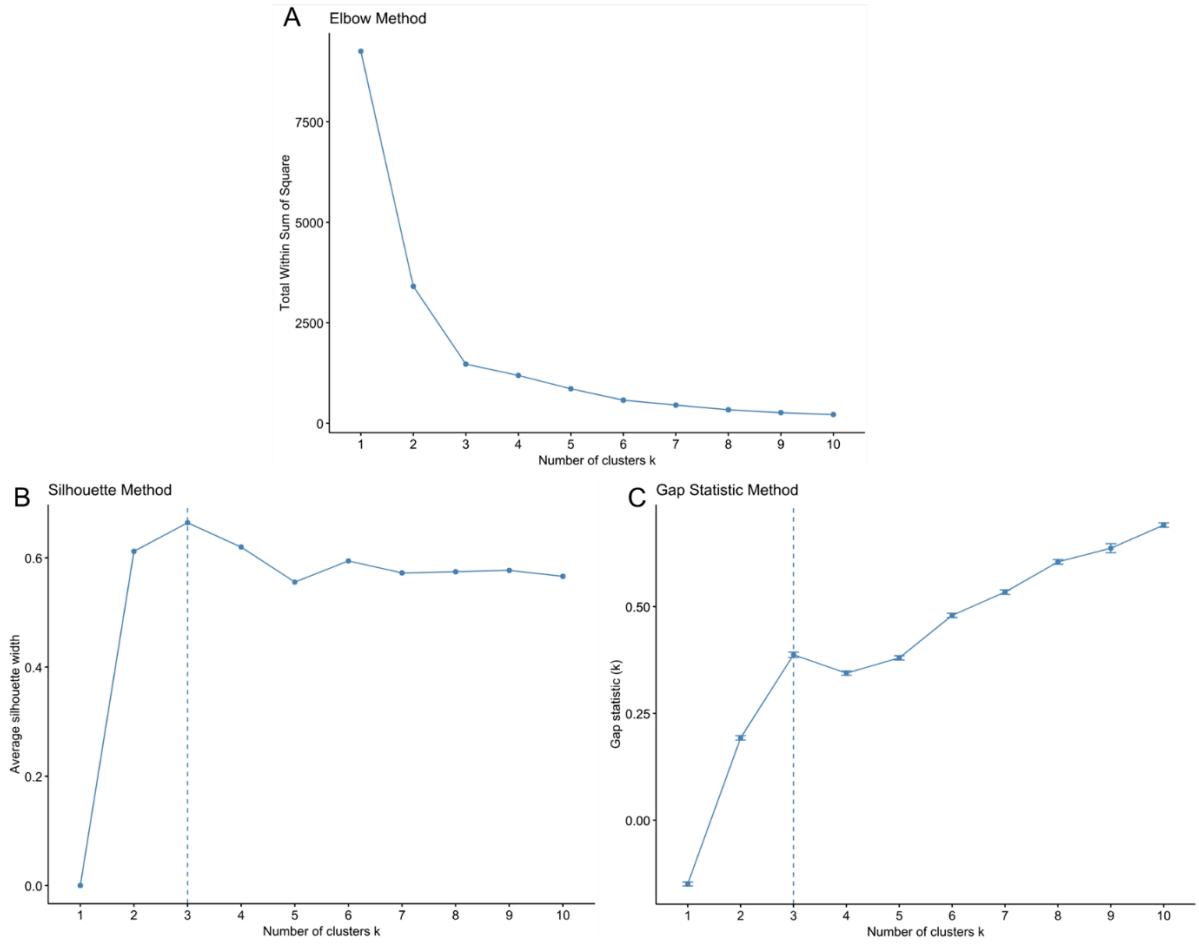

Appendix Figure 16. Statistical methods to determine optimal number of clusters for k-means clustering. A. Elbow method. B. Silhouette method. C. Gap statistic method.

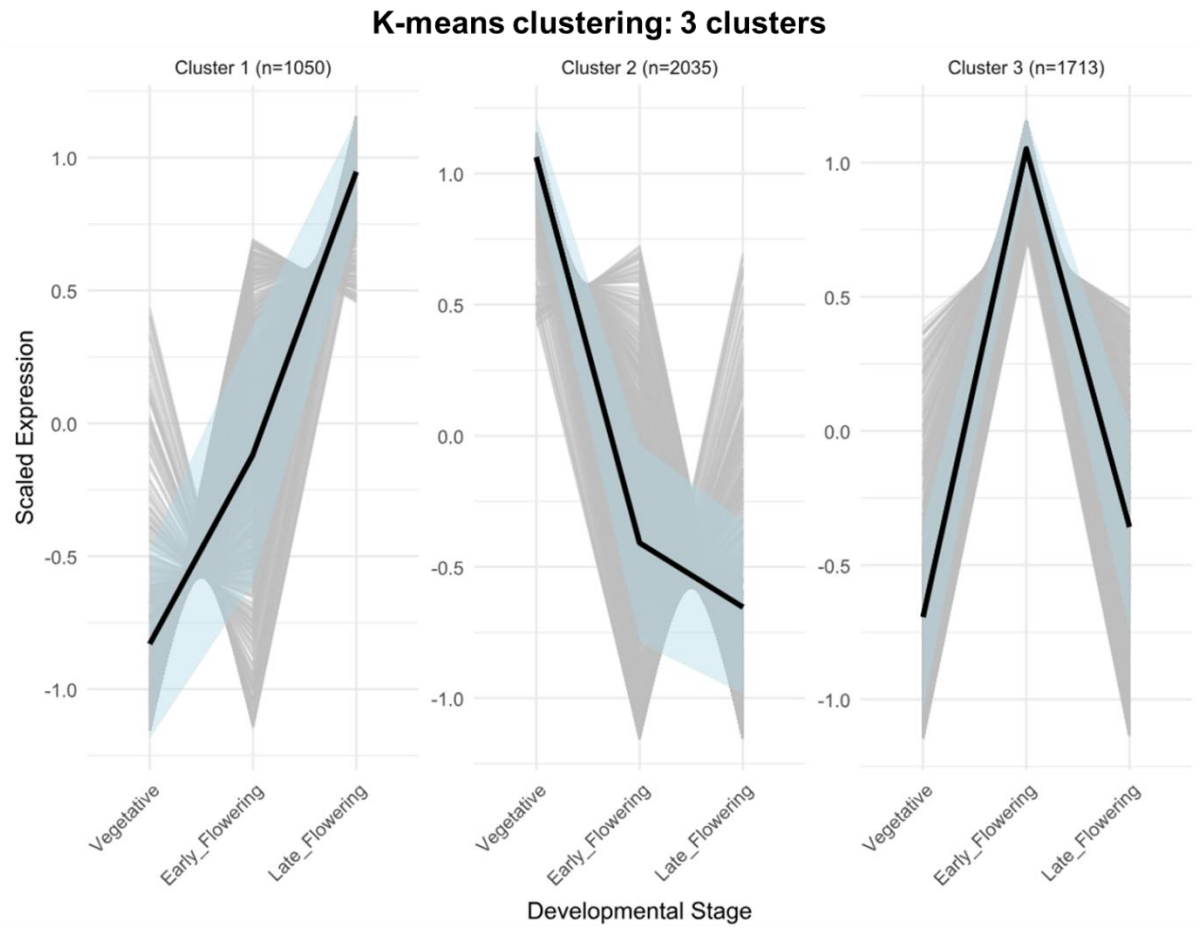
K-means clustering: 3 clusters
Cluster 1 (n=1050)
Cluster 2 (n=2035)
Cluster 3 (n=1713)
Scaled Expression
1.0
0.5
0.0
-0.5
-1.0
Vegetative
Early_Flowering
Late_Flowering
Developmental Stage

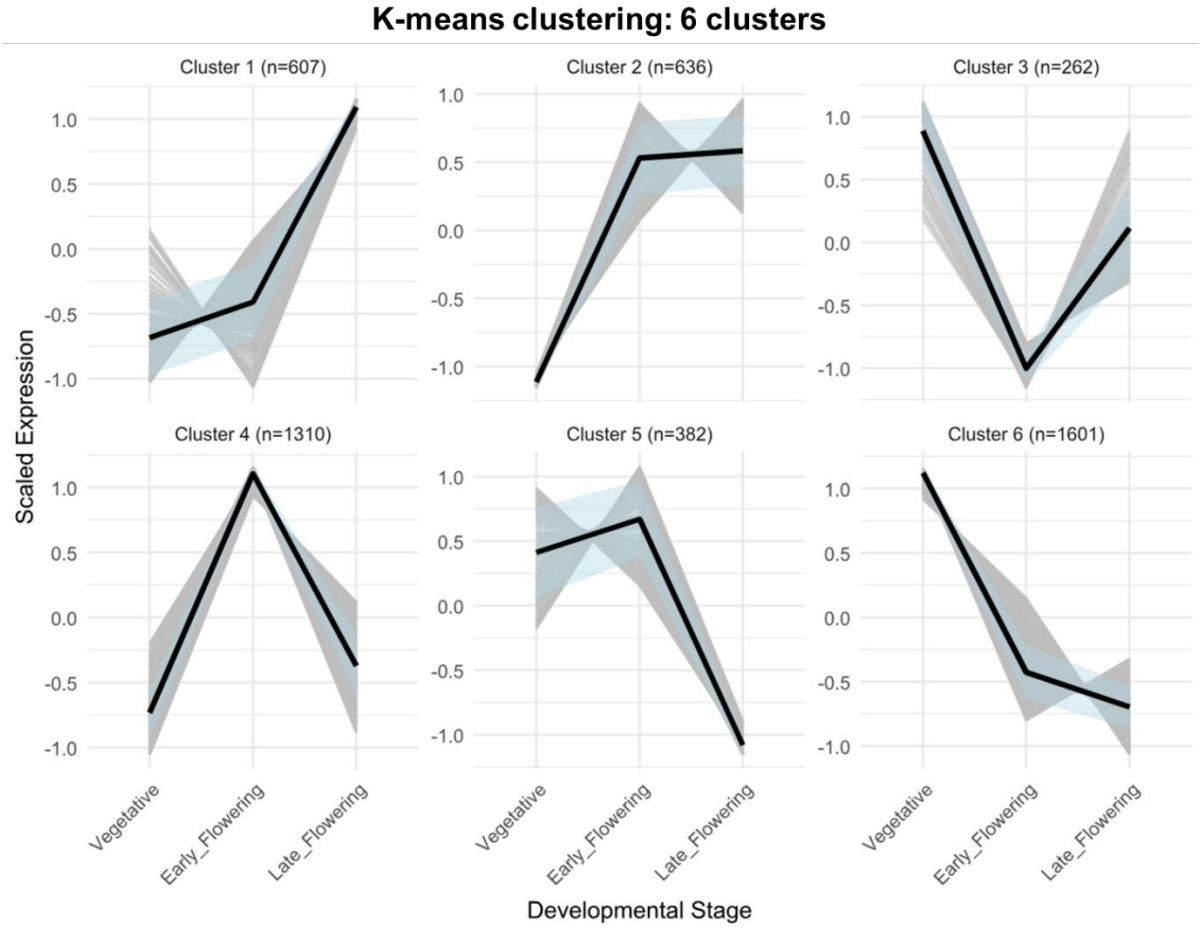
K-means clustering: 6 clusters
Cluster 1 (n=607)
Cluster 2 (n=636)
Cluster 3 (n=262)
Cluster 4 (n=1310)
Cluster 5 (n=382)
Cluster 6 (n=1601)
Scaled Expression
1.0
0.5
0.0
-0.5
-1.0
Vegetative
Early_Flowering
Late_Flowering
Developmental Stage

Appendix Figure 17. K-means clustering for 3 and 6 clusters. These cluster numbers were trialled before deciding on 9 clusters as shown in Figure 5.21.

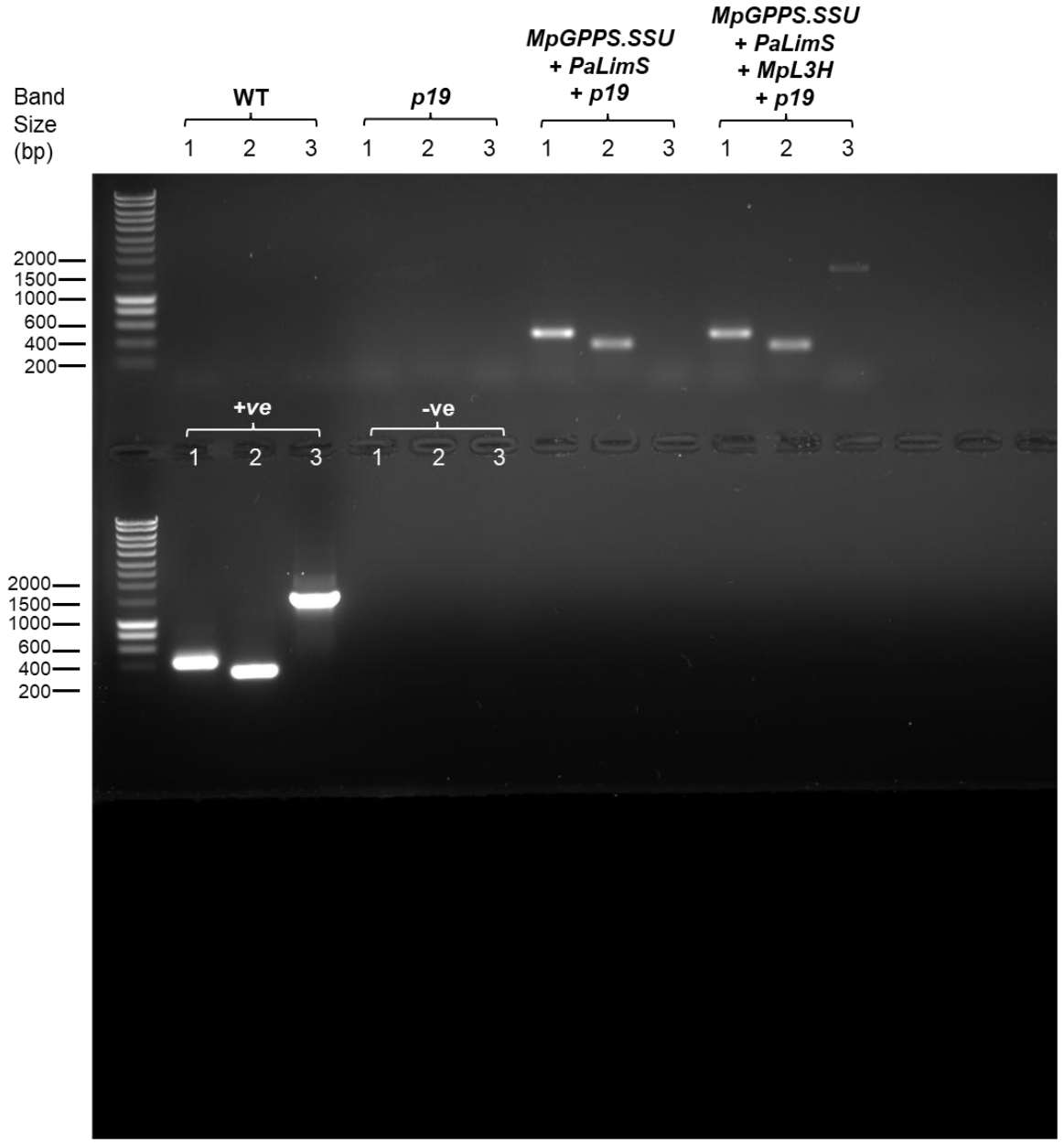

Legend:		
1: *MpGPPS.SSU* primer pair (443bp)	+ve : Positive plasmid control	Bp: base pairs
2: *PaLimS* primer pair (336bp)	-ve: No template negative control	
3: *MpL3H* primer pair (1497bp)	WT: Wild type	

Appendix Figure 18. Uncropped image of Figure 4.15.

Appendix

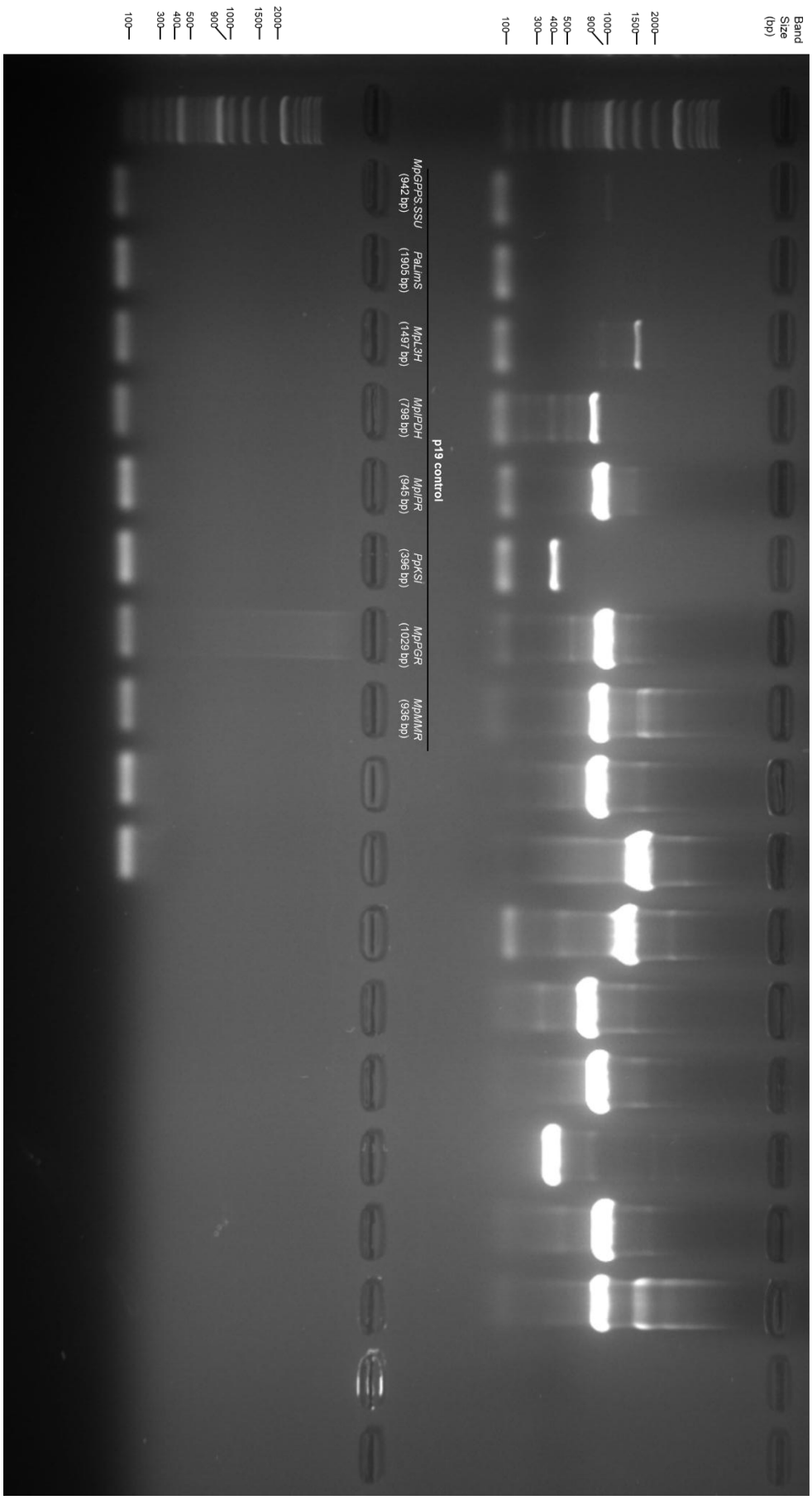
N. benthamiana co-infiltrated with:
MpGPPS.SSU + PaLimS + MpL3H + MpIPDH + MpIPR + PpKSI + MpPGR + MpMMR + p19
MpGPPS.SSU (942 bp)
PaLimS (1905 bp)
MpL3H (1497 bp)
MpIPDH (798 bp)
MpIPR (945 bp)
PpKSI (396 bp)
MpPGR (1029 bp)
MpMMR (936 bp)
p19 control
MpGPPS.SSU (942 bp)
PaLimS (1905 bp)
MpL3H (1497 bp)
MpIPDH (798 bp)
MpIPR (945 bp)
PpKSI (396 bp)
MpPGR (1029 bp)
MpMMR (936 bp)
Positive plasmid control
MpGPPS.SSU (942 bp)
PaLimS (1905 bp)
MpL3H (1497 bp)
MpIPDH (798 bp)
MpIPR (945 bp)
PpKSI (396 bp)
MpPGR (1029 bp)
MpMMR (936 bp)
Band Size (bp)
2000
1500
1000
900
500
400
300
100
2000
1500
1000
900
500
400
300
100

Appendix Figure 19. Uncropped image of Figure 4.17

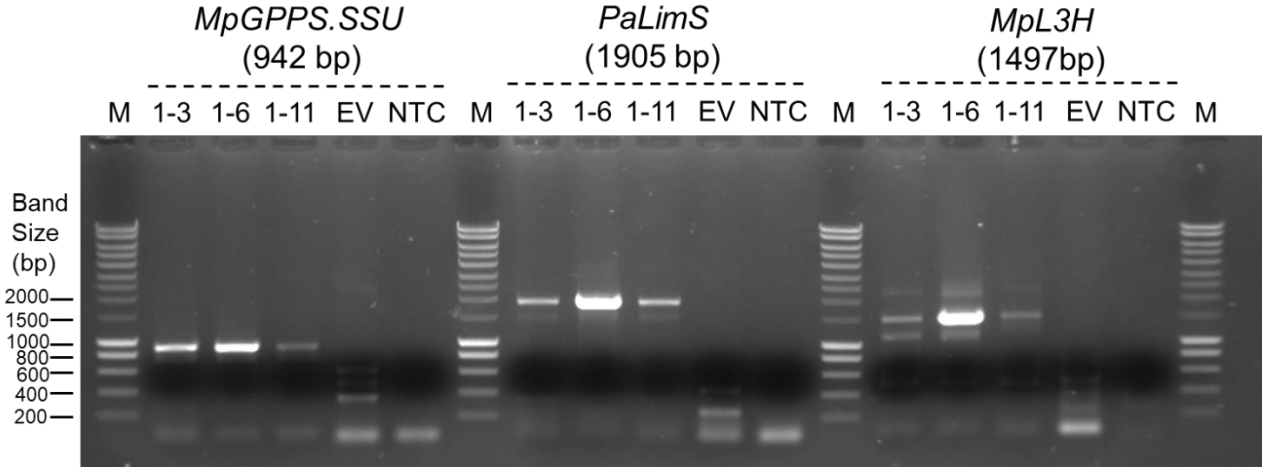

Appendix Figure 20. RT-PCR analysis of *MpGPPS.SSU*, *PaLimS* and *MpL3H* expression in transgenic *Arabidopsis thaliana* lines 1-3, 1-6 and 1-11. RT-PCR was performed using cDNA from transgenic *Arabidopsis thaliana* lines 1-3, 1-6 and 1-11, which were stably transformed with the pL2_L3H construct. EV = Wild type empty vector control, NTC = No template control, M = Marker.